

3AC



EARLY TO MIDDLE PROTEROZOIC GRANITIDS, BASALTIC DYKES AND
ASSOCIATED LAYERED ROCKS OF S.E. EYRE PENINSULA, SOUTH AUSTRALIA.

By Graham E. Mortimer B.Sc.(Hons)
(University of Adelaide)

A thesis submitted in partial fulfilment of the
requirements for the degree of Doctor of Philosophy.

UNIVERSITY OF ADELAIDE.

Awarded 3/12/84

TABLE OF CONTENTS

	<u>PAGE</u>
<u>TABLE OF CONTENTS</u>	I
<u>LIST OF TABLES</u>	V
<u>LIST OF FIGURES</u>	VII
<u>SUMMARY</u>	X
<u>STATEMENT OF ORIGINALITY</u>	XIV
<u>ACKNOWLEDGEMENTS</u>	XV
<u>CHAPTER 1</u> <u>INTRODUCTION AND GENERAL GEOLOGY</u>	1
1.1 INTRODUCTION	1
1.2 METHOD OF INVESTIGATION	1
1.3 REGIONAL TECTONIC FRAMEWORK	2
1.4 PREVIOUS INVESTIGATIONS	2
1.5 ROCK UNITS AND GENERAL GEOLOGY	6
1.5.1 Rock units in study area	6
1.5.2 Structural and metamorphic outline	7
<u>CHAPTER 2</u> <u>DONINGTON GRANITOID SUITE</u>	11
2.1 INTRODUCTION	11
2.2 PETROGRAPHY AND FIELD RELATIONS	12
2.2.1 Rock types	12
2.2.2 Petrography	13
2.3 MINERAL CHEMISTRY, IGNEOUS CRYSTALLISATION	20
2.3.1 Pyroxenes	20
2.3.2 Feldspars	22
2.3.3 Iron-titanium oxides	22
2.3.4 Amphiboles	23
2.3.5 Biotites	23
2.3.6 Conditions of metamorphism	24
2.3.7 Conditions of igneous recrystallisation	24
2.3.8 Intrusive analogues	26
2.4 GEOCHRONOLOGY	27
2.4.1 Rb-Sr total-rock geochronology	27
2.4.2 U-Pb zircon geochronology	34
2.5 GEOCHEMISTRY OF THE DGS	36
2.5.1 Introduction	36
2.5.2 Opx-granitoids	36
2.5.3 Granite Gneisses	43

<u>CHAPTER 3</u>	<u>COLBERT GRANITOID SUITE</u>	47
3.1	INTRODUCTION AND FIELD GEOLOGY	47
3.2	PETROGRAPHY AND MINERAL CHEMISTRY	47
3.2.1	Colbert hornblende granite gneiss A	48
3.2.2	Colbert hornblende granite gneiss B	49
3.2.3	Colbert alkali feldspar granite gneiss	49
3.2.4	Mineral chemistry	49
3.2.5	Summary and discussion	51
3.3	RB-SR GEOCHRONOLOGY	51
3.3.1	Results	52
3.3.2	Discussion	53
3.4	GEOCHEMISTRY	56
3.4.1	Geochemical classification	56
3.4.2	Major element geochemistry	56
3.4.3	Trace element geochemistry	57
3.4.4	REE geochemistry	57
3.4.5	Summary	58
3.5	SUMMARY	59
<u>CHAPTER 4</u>	<u>MOODY GRANITOID SUITE</u>	60
4.1	INTRODUCTION	60
4.2	PETROGRAPHY AND MINERAL CHEMISTRY	61
4.2.1	Yunta Well Leucogranite	61
4.2.2	Moody Tank Adamellite	62
4.2.3	Chinmina Syenite	62
4.2.4	Mineral Chemistry	62
4.2.5	Discussion and summary	62
4.3	GEOCHEMISTRY	65
4.3.1	Geochemical classification	65
4.3.2	Major element geochemistry	66
4.3.3	Trace element geochemistry	66
4.3.4	REE geochemistry	67
4.3.5	Discussion	67
4.4	RB-SR GEOCHRONOLOGY	69
4.4.1	Results	69
4.4.2	Discussion	71
4.5	SUMMARY	72

	<u>PAGE</u>
<u>CHAPTER 5</u> <u>MASSENA BAY GNEISSES</u>	74
5.1 INTRODUCTION	74
5.2 PETROGRAPHY AND MINERAL CHEMISTRY	75
5.2.1 Quartzofeldspathic gneisses	75
5.2.2 Garnet + sillimanite gneisses	76
5.2.3 Calc-silicate gneisses	77
5.2.4 Granitic gneisses	77
5.2.5 Amphibolitic "dykes"	78
5.2.6 Mineral chemistry	79
5.2.7 Discussion	81
5.3 GEOCHEMISTRY	82
5.3.1 Introduction	82
5.3.2 Geochemical classification	83
5.3.3 Major element geochemistry of QF gneisses	84
5.3.4 Trace element geochemistry	85
5.3.5 REE geochemistry	86
5.3.6 Discussion and summary	86
5.4 RB-SR GEOCHRONOLOGY	86
5.4.1 Introduction	86
5.4.2 Previous dating of QF gneisses	88
5.4.3 Rb-Sr geochronology	88
5.4.4 Summary	91
5.5 COMPARISON WITH THE HUTCHISON GROUP	91
5.5.1 Stratigraphy	91
5.5.2 Metamorphism	92
5.5.3 Isotopic constraints	92
5.6 SUMMARY OF CONCLUSIONS	93
 <u>CHAPTER 6</u> <u>BASALTIC AND ULTRAMAFIC ROCKS</u>	 94
6.1 INTRODUCTION	94
6.2 PETROGRAPHY AND MINERAL CHEMISTRY	95
6.2.1 Petrography of DK2 dykes	95
6.2.2 Petrography of DK1 dykes	98
6.2.3 Mineral chemistry	99
6.2.4 Constraints on Kimban metamorphism	101
6.3 GEOCHEMISTRY	102
6.3.1 Sampling and alteration	102
6.3.2 Basaltic geochemical groups	103
6.3.3 Geochemistry of Group A	106

	PAGE
6.3.4 Geochemistry of Group B	116
6.3.5 Geochemistry of Group C	121
6.3.6 Summary of enrichment history of sources	127
6.3.7 Comparable basaltic rock suites	128
6.3.8 Tectonic environment of tholeiites	131
6.4 SR-ISOTOPE GEOCHEMISTRY	132
6.4.1 Introduction	132
6.4.2 Group A	132
6.4.3 Group B	134
6.4.4 Group C	135
6.4.5 Summary	135
<u>CHAPTER 7</u> <u>EARLY TO MIDDLE PROTEROZOIC CRUSTAL EVOLUTION</u>	137
7.1 INTRODUCTION	137
7.2 PETROGENESIS OF BASALTIC AND GRANITOID MAGMAS	139
7.2.1 Bimodal magmatism	139
7.2.2 Petrogenesis of basaltic magmas	140
7.2.3 Petrogenesis of granitoid magmas	145
7.3 CONSTRAINTS IMPOSED BY ISOTOPIC DATA	157
7.3.1 Sr-isotopic constraints on I-type source	157
7.3.2 Sm-Nd isotopic constraints - review	159
7.3.3 Comparison of Sr-isotopes	161
7.3.4 Concluding statement	162
7.4 PROTEROZOIC TECTONIC MODELS	163
7.4.1 Introduction	163
7.4.2 Tectonic pattern of the study area	163
7.4.3 Tectonic review of Arunta-Gawler Province	164
7.4.4 Brief review of global Proterozoic tectonics	165
7.4.5 Brief review of crustal development models	169
7.4.6 Tectonic model of study area	170
7.5 CONCLUDING DISCUSSION	172
7.6 SUGGESTIONS FOR FURTHER WORK	173
<u>REFERENCES CITED</u>	175
<u>APPENDIX A1</u> <u>EXPERIMENTAL TECHNIQUES</u>	A1
(1) RB-SR GEOCHRONOLOGY	A1
(2) ZIRCON U-PB GEOCHRONOLOGY	A4

(3)	MAJOR AND TRACE ELEMENT GEOCHEMISTRY	A6
(4)	REE GEOCHEMISTRY	A7
<u>APPENDIX A2</u>	<u>RECONNAISSANCE FLUID INCLUSION STUDY OF DGS</u>	A8
<u>APPENDIX A3</u>	<u>SAMPLE LOCATIONS</u>	A10

APPENDIX TABLES

Appendix Table 1.1	Previously published Rb-Sr data
Appendix Table 1.2	Calculated Sr-isotope evolution curves
Appendix Table 2.1	Donington Granitoid Suite mineral analyses
Appendix Table 2.2	Donington Granitoid Suite major elements
Appendix Table 2.3	Donington Granitoid Suite trace elements
Appendix Table 3.1	CGS, MGS and MBG mineral analyses
Appendix Table 3.2	Colbert Granitoid Suite major elements
Appendix Table 3.3	Colbert Granitoid Suite trace elements
Appendix Table 4.1	Moody Granitoid Suite major elements
Appendix Table 4.2	Moody Granitoid Suite trace elements
Appendix Table 5.1	Massena Bay Gneisses major elements
Appendix Table 5.2	Massena Bay Gneisses trace elements
Appendix Table 6.1	Basaltic dykes mineral analyses
Appendix Table 6.2	Basaltic dykes major elements
Appendix Table 6.3	Basaltic dykes trace elements
Appendix Table 6.4	Basaltic dykes elemental ratios
Appendix Table 6.5(a)	Additional trace element data
	(b) Previously analysed amphibolites
Appendix Table 6.6	Partition coefficient data
Appendix Table 6.7	Hutchison Group amphibolites major elements
Appendix Table 7.1	Calculated model source compositions

Follows pag

LIST OF TABLES

1.1	Previous stratigraphic terminology, Gawler domain	4
1.2	Previous structural and metamorphic histories, Gawler domain	6
1.3	Main rock units in present study area	7
1.4	Structural and metamorphic history of present study	9
2.1	Donington Granitoid Suite - rock types	11
2.2	Donington Granitoid Suite - petrographic summary	12
2.3	Donington Granitoid Suite - geothermometry, geobarometry	22
2.4	Opx-granitoids - Rb-Sr isotopic data	27
2.5	Rb-Sr isochron regressions	28
2.6	Granite gneisses - Rb-Sr isotopic data	29

LIST OF TABLES (cont'd)

2.7	Quartz gabbro-norite Gneiss - Zircon U-Pb data	34
2.8	Opx-granitoids compared with I-, S-, and A-types granitoids	35
2.9	Opx-granitoids - average chemical compositions	37
2.10	Opx-granitoids - selected geochemical indicators	40
2.11	Least squares modelling of opx-granitoids	41
2.12	Granite gneisses - average chemical compositions	43
2.13	Comparison of opx-granitoids and retrogressive gneisses	45
3.1	Colbert Granitoid Suite - modal and textural summary	49
3.2	Colbert Granitoid Suite - geothermometry	51
3.3	Colbert Granitoid Suite - Rb-Sr data	52
3.4	Colbert Granitoid Suite - Rb-Sr isochron regressions	53
3.5	Geochemical comparison with I- and A-type granitoids	55
4.1	Moody Granitoid Suite - modal and textural summary	61
4.2	Moody Granitoid Suite - geothermometry	62
4.3	Geochemical comparison with I-, S- and A-type granitoids	64
4.4	Geochemical data for Moody Granitoid Suite	65
4.5	Moody Granitoid Suite - Rb-Sr data	69
4.6	Moody Granitoid Suite - Rb-Sr isochron regressions	70
4.7	Estimates of timing of D ₃	71
5.1	Massena Bay Gneisses - modal and textural summary	74
5.2	Massena Bay Gneisses - geothermometry	79
5.3	Geochemical comparison with I-type granitoids	82
5.4	QF gneisses - Rb-Sr data	87
5.5	QF gneisses - Rb-Sr isochron regressions	88
6.1	Tholeiitic dykes - petrographic and metamorphic summary	94
6.2	Tholeiitic dykes - geothermometry and geobarometry	99
6.3	Least squares modelling of cumulates 739, 785 and 786	106
6.4	Least squares modelling of fractionated liquids B16 and B26	107
6.5	Estimates of degree of partial melting from model pyrolite	110
6.6	Model Sc, V and Y in pyrolite partial melts	111
6.7	Model La/Sm, Yb/Gd, Ti/Zr, Ti/Y, Zr/Y, Zr/Nb and Rb/Sr fractionation	112
6.8	Least squares modelling of fractionated liquid B82	117
6.9	Trace element modelling of fractionated liquid B82	120
6.10	Least modelling of cumulate 756 and fractionated 1351 and 1354	122
6.11	Trace element modelling of fractionated liquids 1351 and 1354	124
6.12	Rb-Sr isotopic data for selected tholeiitic dykes	131

LIST OF TABLES (cont'd)

7.1	Geochemical comparison of Gawler domain granitoids and volcanics	145
7.2	Estimated lower crustal compositions	151
7.3	Least squares modelling of I-type melt compositions	153
7.4	Least squares modelling of silicic volcanic melts	154
7.5	Least squares modelling of I-type granitoids	155
7.6	Least squares modelling of silicic volcanic melts	156
7.7	Least squares modelling from Taylor & McLennan source	157
7.8	Calculated Ni and Cr in model sources	158

LIST OF FIGURES

	Faces page	
1.1	Generalised geological map of Gawler domain	2
1.2	Geological map of present study area	5
1.3	Contact relationship of Colbert and Donington Granitoid Suites	7
1.4	Orthogneissic layering developed in D ₃ shear zone	8
1.5	Field geological photographs, intrusive contacts	11
1.6	Field geological photographs, D ₁ and D ₂	11
1.7	Field geological photographs, D ₃	11
1.8	Field geological photographs, D ₃ and D ₄	11
1.9	Microtextural features	11
2.1	Geological map of Cape Donington and Cape Colbert	12
2.2	Sketch map of zonation of facies in retrogressive gneisses	13
2.3	Microtextural features of opx, cpx and plagioclase phenocrysts	14
2.4	Microtextural features of alkali feldspar megacrysts	15
2.5	Microtextural features of subsolidus facies variation	18
2.6	Ferromagnesian and feldspar mineral compositions	21
2.7	P-T diagram for Fe-opx	23
2.8	Fe-Ti oxide and biotite temperature - oxygen fugacity	24
2.9	Amphibole compositions of subsolidus facies	25
2.10	Experimental solidus of alkali granite + H ₂ O + CO ₂	26
2.11	Locality diagram for geochronology samples	27
2.12	Isochron diagrams for retrogressive granite gneisses	28
2.13	Isochron diagrams for opx-granitoids	29
2.14	Isochron and Rb-Sr diagrams for selected gneisses	30
2.15	Sr-isotope evolution of opx-granitoids and possible source rocks	33
2.16	Zircon U-Pb concordia diagram	35
2.17	AFM and K-Na-Ca diagrams for opx-granitoids	36
2.18	Alkali-silica-lime index of opx-granitoids	37
2.19	Major element variation diagrams - opx-granitoids	38

LIST OF FIGURES (cont'd)

2.20	Trace element variation diagrams - opx-granitoids	39
2.21	Trace element variation diagrams - opx-granitoids	40
2.22	Chondrite-normalised REE- opx-granitoids	41
2.23	Summary of rock relationships - opx-granitoids	42
2.24	Major element variation diagrams - granite gneisses	43
2.25	Trace element variation diagrams - granite gneisses	44
2.26	Trace element variation diagrams - granite gneisses	45
2.27	Chondrite-normalised REE - granite gneisses	46
3.1	Geological map of Colbert Granitoid Suite	47
3.2	Ferromagnesian and feldspar mineral compositions	50
3.3	Amphibole mineral compositions	51
3.4	Fe-Ti oxide and biotite temperature-oxygen fugacity	52
3.5	Isochron diagrams for Colbert Granitoid Suite	53
3.6	Comparison with Sr-isotopes of Middlecamp Granite	54
3.7	Sr-isotope evolution diagram for Colbert Granitoid Suite	55
3.8	AFM and K-Na-Ca diagrams for Colbert Granitoid Suite	56
3.9	Major element variation diagrams - Colbert Granitoid Suite	57
3.10	Trace element variation diagrams - Colbert Granitoid Suite	58
3.11	Chondrite-normalised REE - Colbert Granitoid Suite	59
4.1	Geological map of Moody Granitoid Suite	60
4.2	Ferromagnesian and feldspar mineral compositions	62
4.3	Fe-Ti oxide and biotite temperature-oxygen fugacity	63
4.4	AFM and K-Na-Ca diagrams - Moody Granitoid Suite	65
4.5	Major element variation diagrams - Moody Granitoid Suite	66
4.6	Trace element variation diagrams - Moody Granitoid Suite	67
4.7	Chondrite-normalised REE plots - Moody Granitoid Suite	68
4.8	Isochron diagrams - Moody Granitoid Suite	70
4.9	Sr-isotope evolution diagram - Moody Granitoid Suite	71
5.1	Geological map of portion of Massena Bay	75
5.2	Ferromagnesian and feldspar mineral compositions	79
5.3	Amphibole mineral compositions - QF gneisses	80
5.4	Fe-Ti oxide and biotite temperature - oxygen fugacity	81
5.5	AFM and K-Na-Ca diagrams - Massena Bay Gneisses	83
5.6	Major element variation diagrams - Massena Bay Gneisses	84
5.7	Trace element variation diagrams - Massena Bay Gneisses	85
5.8	Chondrite-normalised REE plots - QF gneisses	86
5.9	Isochron diagrams - QF gneisses	88

LIST OF FIGURES (cont'd)

5.10	Sr-isotope evolution diagram - QF gneisses	90
5.11	Stratigraphy of Massena Bay Gneisses and Hutchison Group	91
5.12	Hutchison Group amphibolite geochemistry	92
6.1	Schematic microtextural features in tholeiitic dykes	95
6.2	Ferromagnesian minerals, Fe-Ti oxide and biotite T-log a_{O_2}	100
6.3	Shear zones, faults, garnet granulites and magnetic anomalies	101
6.4	Ti-Zr-Y and Ti-Zr-Sr - tholeiitic dykes	106
6.5	MgO-Ni and MgO-Cr - tholeiitic dykes	107
6.6	Al_2O_3/TiO_2 - TiO_2 and CaO/TiO_2 - TiO_2 - tholeiitic dykes	108
6.7	Ti-Zr, Ti-Y, Ti- K_2O , Ti-Sc - tholeiitic dykes	111
6.8	Zr-Y, Zr-Nb, Zr-Ba, Zr-Sr, Zr-Rb, Zr-Sc	112
6.9	Chondrite-normalised REE - tholeiitic dykes	113
6.10	Ce-Ti, Ce-Y, Ce- P_2O_5 ; Ce- K_2O , Ce-Rb, Ce-Nb	114
6.11	Extended REE plot - komatiite, MORB and Victorian tholeiites	115
6.12	Extended REE plot - tholeiitic dykes	116
6.13	Extended REE plot - kimberlite, basanite, olivine melilitite	117
6.14	MgO-CaO, MgO- Al_2O_3 , MgO- SiO_2 , MgO- TiO_2 -tholeiitic dykes	118
6.15	Extended REE plots - tholeiites of various ages	128
6.16	Zr-Zr/Y and Zr-Zr/Nb plots - tholeiitic dykes	131
6.17	Isochron and Sr-isotope evolution diagram - tholeiite dykes	132
7.1	SiO_2 histograms for Gawler domain igneous rocks	139
7.2	Extended REE plots - tholeiites of various ages	141
7.3	Geochemical comparison - I-type granitoids and volcanics	146
7.4	Major element geochemical comparison - I-type granitoids	147
7.5	Trace element geochemical comparison - I-type granitoids	148
7.6	REE comparison of I-type granitoids and volcanics	149
7.7	Extended REE comparison I-type granitoids and tholeiite dykes	150
7.8	SiO_2 - P_2O_5 , SiO_2 - K_2O of I-type granitoids and volcanics	151
7.9	SiO_2 -Zr, SiO_2 -Y, SiO_2 -Sr, SiO_2 -Ba I-type rocks	152
7.10	Model REE of sources based on Taylor & McLennan Model	155
7.11	Model REE of sources based on pyroxene granulite	155
7.12	Model REE of sources based on (amph + gt) granulite	156
7.13	Model REE of sources based on (parg + gt) granulite	156
7.14	Model extended REE of preferred sources and tholeiite dykes	157
7.15	Model Sr-isotope evolution of preferred sources	159
7.16	Nd-isotope systematics of Colorado 1.8 Ga crust	160
7.17	Sr-isotope comparison of Gawler domain and Colorado crust	161
7.18	Model and measured P-T of crustal rocks	169

THESIS SUMMARY

Integrated field, petrographic, Sr-isotopic and geochemical studies of portion of south eastern Eyre Peninsula, South Australia, have sought to define the nature of the geochemical and structural evolution of Proterozoic crust in the Gawler orogenic domain. Six suites of Proterozoic orthogneisses, paragneisses, and granitoid and basaltic plutonic rocks were emplaced sequentially throughout the major Kimban Orogeny, and constitute the previously defined Lincoln Complex.

Four deformations have been recognised in the Kimban Orogeny of which the first two are high-grade and probably flat-lying, the third is lower grade and upright and the fourth resulted in only minor warping. Metamorphism locally attained granulite facies with calculated pyroxene temperatures suggesting 800°C - 900°C at greater than 8 kbar confining pressure.

The characteristics of the six rock suites are ;

- (1) The Massena Bay Gneisses (MBG) are interpreted as an original mixed sequence of silicic volcanic rocks and basaltic dykes and/or sills and subordinate calc-silicate and pelitic sediments, approximately coeval with, and forming at least in part the provenance of, the westerly Hutchison Group (which is not exposed in the study area).

Rb-Sr total-rock isotopic data show that the quartzofeldspathic (QF) gneisses of the MBG have suffered considerable disturbance.

- (2) The Donington Granitoid Suite (DGS) of opx-granitoids was emplaced into the MBG prior to D_1 and suffered prolonged batholithic crystal fractionation. Rb-Sr total-rock and U-Pb zircon data suggest an emplacement age of 1841 ± 7 Ma with an IR range of 0.7041 - 0.7053.

Hornblende + biotite granite gneisses of the DGS are spatially disposed adjacent to the major Kalinjala Mylonite Zone (KMZ), contain retrograde S_{1-2} fabrics, and have similar, although slightly disturbed, Rb-Sr total-rock systematics, but slightly different geochemical characteristics, to the opx-granitoids. The granite gneisses are believed to be the result of retrogressive fluid flow along the KMZ.

- (3) Type 1 basaltic dykes (DK1) have granoblastic textures manifesting amphibolite and granulite facies conditions and were emplaced prior to D_2 and in some cases D_1 . Geochemical changes associated with amphibolisation are spatially controlled by the KMZ.
- (4) The Colbert Granitoid Suite (CGS) of hornblende granitoids was emplaced as narrow dykes between D_2 and D_3 at 1757 ± 10 Ma with an IR of 0.7087 ± 10 , and has experienced only moderate local metamorphism in local D_3 shear zones.
- (5) The Moody Granitoid Suite (MGS) comprising I-type hornblende granitoids and S-type muscovite leucogranites, was emplaced into the metasedimentary Hutchison Group west of the main study area during or after D_3 .
The I-types are unfoliated and produce an isochron age of 1709 ± 14 Ma with IR of 0.7070 ± 4 .
The S-types are foliated and produce an isochron age of 1675 ± 22 Ma with IR of 0.7163 ± 233 .
- (6) Type 2 basaltic dykes (DK2) have doleritic textures with variable degrees of sub-solidus recrystallisation and amphibolisation. The dominant phenocrysts are plagioclase, opx and cpx, with olivine occurring only rarely. Sub-solidus corona textures manifest pyroxene granulite, hornblende granulite and garnet granulite assemblages.

The metamorphic and structural features outlined above are suggested to be those produced by early crustal extension and ductile spreading coupled with addition to the lower crust (and sub-crust) of basaltic and I-type granitoid magma, followed by later compression and near-isobaric cooling.

Geochemical studies of the intrusive rocks show that calc-alkaline intermediate rocks are absent, the magmatism being bimodal basaltic and silicic. There are regular temporal petrochemical changes within the the granitoid suites, but the DK1 and DK2 basaltic dykes, although falling into three main geochemical divisions, do not show any igneous temporal variation.

Geochemical group A basaltic dykes contain primitive, high MgO liquids with low TiO_2 , but show LREE and some other LIL element enrichment and Ti/Zr less than chondritic, and are interpreted to represent fractionation from a high degree partial melt of enriched upper mantle peridotite.

Geochemical group B basaltic dykes are more evolved, contain less MgO but greater TiO_2 than Group A, and are LREE and MREE and some other LIL element enriched but have near chondritic Ti/Zr . They are interpreted to be derived by fractionation of a melt of upper mantle peridotite of enrichment character different in detail from Group A.

Geochemical group C basaltic dykes are LREE and some other LIL-element enriched, but Al_2O_3 , CaO , TiO_2 relationships suggest that the upper mantle peridotite source had suffered a melt extraction and depletion event prior to LIL-element enrichment and partial melting.

The enriched source of Proterozoic Gawler domain basaltic dykes was probably produced by mantle metasomatism by a LREE-, LIL-, Co_2 -rich fluid phase, and may reflect mantle outgassing at this time.

Within the granitoid rocks the younging sequence from MBG to MGS I-types shows a regular increase in level of elements such as P_2O_5 , Nb, LREE and except for the MGS I-types an increase in K_2O , TiO_2 , Zr. The MGS I-types are displaced towards the fields of the MGS S-types and probably reflect the mixing of S-type and I-type materials. Otherwise the enrichment sequence is similar to the character of the proposed enriching component of the basaltic magma source. It is suggested that progressive enrichment of the granitoid source region by a similar component to that which metasomatised the upper mantle peridotite may have occurred in the following way.

Upper mantle metasomatism and basaltic melt production and mobilisation may have been localised by a major zone of weakness which may be represented within the crust by the Kalinjala Mylonite Zone. (Fluid flow along the Kalinjala Zone has caused extensive retrogressive metasomatism in the crust.) Basaltic melt underplated at the mantle - lower crust interface suffered high crustal pressure fractionation, crystallisation and metamorphism, and in a tensional tectonic regime formed dykes within the lower

crust and intermediate crust. Deep crustal and sub-crustal isobaric cooling of the underplated mafic material resulted in the garnet granulite corona textures.

Continued transfer of heat to the lower crust and sub-crust by ascending basaltic melts and fluids and possibly mantle diapirism may have raised the prevailing geotherm to a level where the accreted mafic material may have been periodically partially melted, thus producing the granitoid magmas.

Based on Sr IR's and geochemical considerations the Proterozoic Gawler domain lower crust and sub-crust are proposed to have consisted of mafic granulite material which yielded initial silicic, LIL element poor melts (MBG), but was progressively enriched with time to yield subsequent LIL-element enriched melts (DGS, CGS and MGS I-types). The MGS S-types are proposed to be due to near-in-situ melting of pelitic metasediments at shallower crustal depth, triggered by the diapiric intrusion of the MGS I-types.

Major and trace element least squares mathematical modelling is consistent with these interpretations.

This model may be applied to the bimodal post-tectonic Gawler Range Volcanic province 250 km to the north of the study area, and to other Proterozoic bimodal, plutonovolcanic complexes of Australia and other continents.

The absence of calc-alkaline intermediate igneous rocks suggests that Proterozoic magmatism in the study area was probably not subduction related, but more consistent with an ensialic tensional environment. A close coupling of mantle and lower crustal thermal and geochemical events, especially of a metasomatic character, is suggested. This may be linked to mantle degassing at this time.

The nature of temporal geochemical evolution has allowed a petrogenetic model of Proterozoic magmatism to be erected, which, it is proposed, has regional, and possibly intercontinental, application.

ACKNOWLEDGEMENTS

This project was initiated at the suggestion of my supervisors Dr. J.A. Cooper and Dr. R.L. Oliver, to whom I am grateful for their continual interest and helpful advice.

Discussions with Shen-Su Sun, Chris Giles, Mark Fanning, Peter Cohen, Graham Teale, Mark Hochman, and Robert Lawrence were helpful, and the encouragement of colleagues in the Geology Department was welcome.

Technical support by David Bruce, John Stanley, Wayne Mussared, Geoff Trevelyan, Rick Barrett and Evert Bleys was invaluable.

I thank Robyn Mortimer for her skillful typing of the body of the text and Bronwyn Hosking, Sandra Storer and Joan Brumby for their contributions.

Many thanks to the Low family for their generous and most enjoyable field accommodation.

To my wife Julie and two boys, thank you for helping me to keep a perspective and thank you for your sacrifices.

Humble thanks to praying friends for their solid and consistent support, particularly during the latter stages of preparation of this thesis. A sincere tribute to the influence of John Byrnes, in memoriam.

All praise to the Lord Jesus.

The research on which this thesis is based was funded by a Commonwealth Postgraduate Research Scholarship.

CHAPTER 1INTRODUCTION AND GENERAL GEOLOGY1.1 INTRODUCTION

The project, on which this thesis reports, was initiated subsequent to the discovery of Archaean crustal rocks on southern Eyre Peninsula (Cooper et al. 1976; Webb & Thomson 1977), for the following reasons;

- (1) to delineate the present day westerly extent of Archaean crustal rocks
- (2) to establish the relationship between the Archaean rocks and later Early to Middle Proterozoic supracrustal and metabasaltic and granitoid gneisses
- and (3) to investigate in detail the petrogenesis of the Early to Middle Proterozoic metabasaltic and granitoid gneisses.

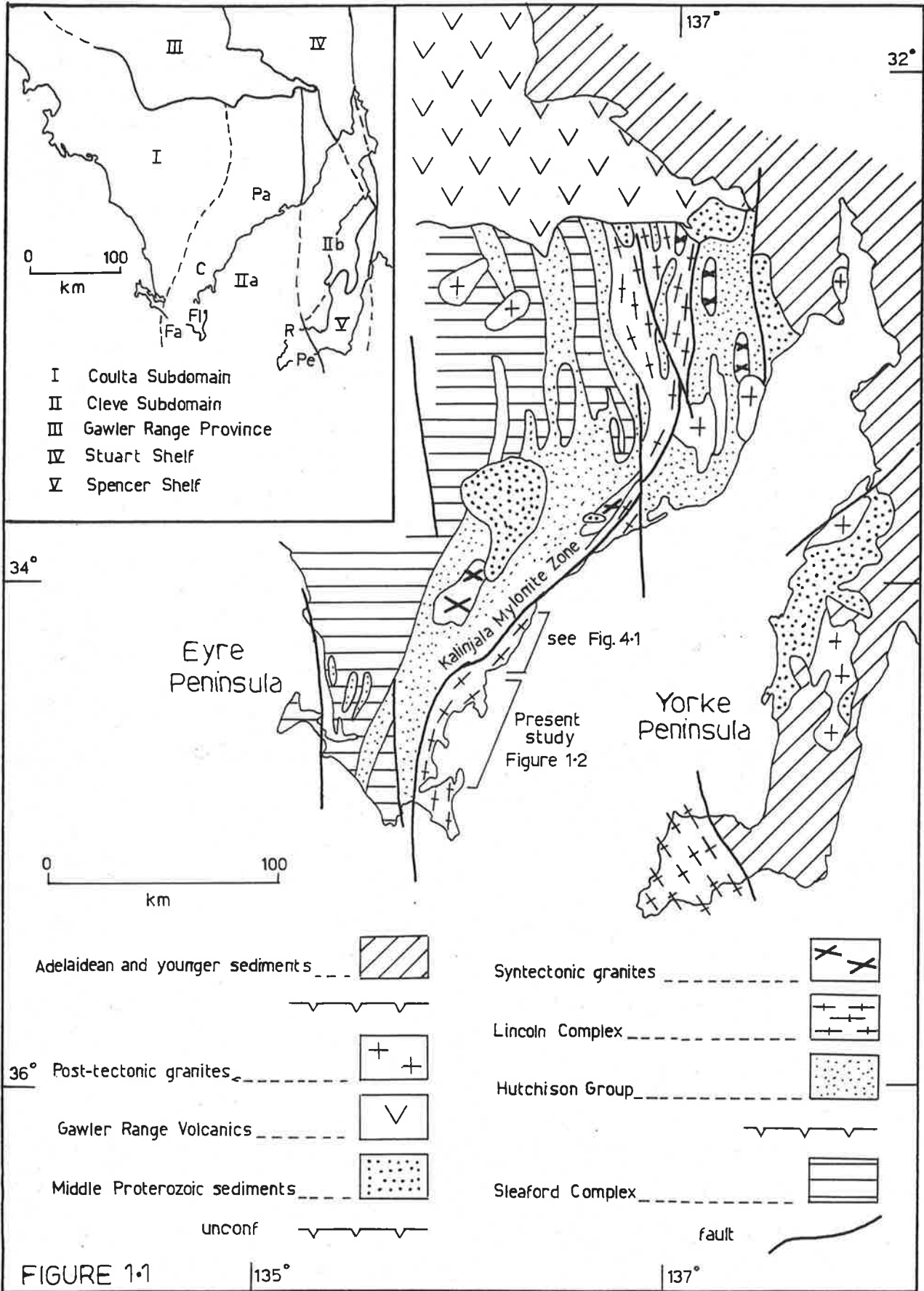
In this way it was expected to be able to comment on the nature of Proterozoic orogenesis and crustal growth, and the extent to which pre-existing Archaean sial may be involved in them. These then constitute the fundamental aims of this thesis.

In this chapter a review of the prior geological work is given first. This is followed by an overview of the rock units and structural relationships encountered in the study area in relation to the overall region. Subsequent chapters will describe in detail the rock units delineated and the final chapter will draw these observations together into a tectonic and petrogenetic framework for the study area, which will be generalised to comment on Proterozoic geology on a global scale.

1.2 METHOD OF INVESTIGATION

This study proceeded from the basis of extensive field observation and detailed mapping of small key areas resulting in the definition of the rock units and interpretation of the sequence of events described below. The rock units were examined in detail petrographically and subsequently suites of samples believed to represent the diversity within the units were prepared for geochemical and isotopic study. The analytical methods employed are described in Appendix A1.

The plutonic rock nomenclature of Streckeisen (1976) has been adopted. Metamorphic textural descriptions follow the scheme of Moore (1970).



Generalised geological map of eastern Eyre Peninsula and Yorke Peninsula, with inset showing tectonic subdomains and areas studied by previous workers.

(C = Coin 1976; Fa = Fanning 1975; Fl = Flook 1975; Pa = Parker 1980; Pe = Pedler 1976; R = Richardson 1978)
modified after Rutland et al. 1981; Parker & Lemon 1982.

1.3 REGIONAL TECTONIC FRAMEWORK

The high-grade gneisses of southern Eyre Peninsula (Fig. 1.1) constitute the most southerly, best exposed rocks of the Gawler orogenic domain of Rutland (1976). Rutland et al. (1981) include the Gawler orogenic domain in the Gawler Province which is characterised by Early Proterozoic orogenic evolution, subsequent transitional tectonism and cratonisation and Middle Proterozoic platform cover. The present author's study area occurs within the Cleve subdomain (Fig. 1.1) of the Gawler orogenic domain. No comprehensive tectonic interpretation of the Gawler orogenic domain has as yet been published, although Rutland (1976) suggested that the orogenic activity was of a continental interior type. Furthermore in a review of the Precambrian tectonic evolution of the Australian continent Rutland (1981) proposed that the orogenic belts "were probably developed in back-arc environments adjacent to continental margins". More particularly he suggested the Early Proterozoic orogenic belts were developed on Archaean protocontinental crust, resulting in vertical accretion of continental crust, and the orogenic trends "can probably be attributed to the operation of a new plate system".

Northern Australia contains numerous Proterozoic orogenic domains included within the linked Arunta - Gawler Province of Rutland (1976), and for which Rossiter & Ferguson (1980) have evolved a unified model related to mantle plume activity and associated continental rifting. In their model, early orogenic sequences, transitional tectonism, cratonisation and post-tectonic magmatism and platform cover are explained as the result of initiation, development and cessation of shallowly rising mantle plumes. The abundant similarities between the Gawler orogenic domain and the orogenic domains of northern Australia invite comparison, and the model of Rossiter & Ferguson will be examined in more detail in Chapter 7.

1.4 PREVIOUS INVESTIGATIONS

Within the Gawler orogenic domain outcrop occurs largely on narrow coastal platforms and some discontinuous areas adjacent to the coast. The bulk of Eyre Peninsula is covered by Cainozoic sediments. The discontinuity of outcrop over most of the domain has hindered regional correlations so that until recent years the stratigraphy has been only poorly understood.

The pioneering work of Tilley (1920; 1921 a,b,c) suggested the sequence depicted in Table 1.1. He believed that the oldest rocks exposed consisted of a metasedimentary sequence, the Hutchison Series, intruded by a younger complex of igneous rocks, the Flinders Series. Furthermore he maintained that the relationship of the Flinders Series to the Hutchison Series "is always of an intrusive kind" (Tilley 1921c).

Within the Flinders Series Tilley recognised two main lithological groupings, the Sleaford Gneisses characterised by the ubiquitous presence of garnet, and the Lincoln Gneisses characterised by the augen granitic gneisses of Kirton Point and pyroxene granitoid gneisses (charnockites). The Lincoln Gneisses are chiefly exposed on the eastern side of southern Eyre Peninsula and constitute the bulk of the present author's study area.

Tilley found difficulty in relating the large thicknesses of metaquartzite on the western side of the peninsula to the Hutchison Series but believed them to be younger and named them the Warrow Series. Later massive granites he assigned to his Dutton Series.

Later workers encountered difficulty in applying these stratigraphic concepts to rocks away from the type areas studied by Tilley, and considerable confusion arose. Johns (1961) attempted to simplify the scheme of Tilley, and erected a simple two-fold subdivision (Table 1.1), consisting of "older gneissose rocks" the Flinders Group and "younger schistose rocks" the Hutchison Group. His Warrow Quartzite was placed within the Flinders Group. In doing this Johns attributed to all the rocks a metasedimentary origin and effectively inverted a large part of Tilley's stratigraphic succession. This scheme, however, has also proved inadequate and confusing.

Reconnaissance Rb-Sr studies on Eyre Peninsula by Compston et al. (1966) aimed to define the minimum age of the metamorphic basement rocks so that a maximum age limit could be placed on the overlying Adelaidean sediments. A relatively precise Rb-Sr total rock isochron age of 1503 ± 25 Ma was determined for the Gawler Range Volcanics which unconformably overlie the Flinders and Hutchison Groups. Furthermore granitoids and granitoid gneisses underlying the volcanics suggested the basement may range in age between ca. 1600 Ma and ca. 1800 Ma.

Compston & Arriens (1968) reported an imprecise regional Rb-Sr total rock isochron from Eyre Peninsula gneisses and granitoids giving an age of 1740 ± 120 Ma. Additional data reported by Arriens (1975)

did not improve the precision of the isochron but suggested that a range in ages between ca. 1600 Ma and greater than 2000 Ma may exist in the basement gneisses.

The regional geochemical study of Bradley (1972) on the southern and southeastern coasts of the Peninsula did not clarify the age relationships of the rock units, but revealed a diversity of bulk rock and mineralogical composition. He was able to constrain the conditions of granulite grade metamorphism observed to 800° - 950° C at 7-9 Kbar, and confirm the presence of metasedimentary, metagranitoid and pyroxene granitoid rocks as well as dykes of amphibolite, pyroxene granulite and dolerite, as originally reported by Tilley. In addition he pointed out a major zone of retrogression ca. 5 km wide adjacent to Port Lincoln, which forms a major subject of the discussion of this thesis.

In an effort to more closely define the Precambrian polar wander curve for Australia, Giddings & Embleton (1976) studied mafic dykes from the Eyre Peninsula and adjacent Yorke Peninsula (Fig. 1.1). They reported two distinct groups of dykes, which were imprecisely dated by Compston & Crawford (unpublished) at 1700 ± 100 Ma and 1500 ± 200 Ma.

Stratigraphic concepts on Eyre Peninsula have recently been revised extensively following an intensive period of field mapping and Rb-Sr geochronological investigations by officers of the South Australian Department of Mines and Energy and researchers in the Department of Geology and Mineralogy, University of Adelaide. It has become apparent that a long and complex history of evolution exists for the Gawler domain, which has been summarised by Webb (1980) and Thomson (1980) and presented in Table 1.1.

Investigations of southern Eyre Peninsula by Fanning (1975), Cooper et al. (1976) and Webb & Thomson (1977) demonstrated that there was a period of extensive generation and emplacement of granitoids into high-grade metasedimentary gneisses at ca. 2400 Ma. Model calculations suggest that the metasedimentary gneisses probably have an Archaean pre-history (Fanning 1975). This complex of Archaean metasedimentary and granitic gneisses has been named the Sleaford Complex by Thomson (1980), in which Fanning et al. (1981) proposed the Carnot Gneisses as a "sub-complex" (Table 1.1).

Similar gneisses outcrop in the northwestern portion of the Peninsula where they have been named the Mulgathing Complex (Daly et al. 1980) and have yielded total rock Rb-Sr ages between ca. 2300 Ma

Table 1.1 Comparison of pre-existing stratigraphic terminologies for the Gawler orogenic domain.

<u>Tilley 1920;1921 a,b,c</u>	<u>Johns 1961</u>	<u>Thomson 1980</u>
<u>DUTTON SERIES</u> "granites" intrusive into Warrow Series	<u>HUTCHISON GROUP</u> "youngest schistose rocks" metasediments and undigested sediments	<u>LINCOLN COMPLEX</u> Granitic gneisses e.g. Lincoln Gneisses reworked older basement complexes
<u>WARROW SERIES</u> "metamorphosed sequence of sediments" mainly quartzite		<u>HUTCHISON GROUP</u> metasediments including Warrow Quartzite unconformably overlies Sleaford Complex
<u>FLINDERS SERIES</u> "complex of igneous rocks" intrusive into Hutchison Series (a) "Lincoln Gneisses" (b) "Sleaford Gneisses"	<u>FLINDERS GROUP</u> "oldest gneissose rocks" metasediments metasomatized to granitoid types	<u>SLEAFORD COMPLEX</u> ≡ MULGATHING COMPLEX * Whidbey Granite Kiana Granite (gneissic) Carnot Gneisses **
<u>HUTCHISON SERIES</u> "sedimentary origin" "oldest group of rocks"		* after Daly et al. 1980 ** after Fanning et al. 1981

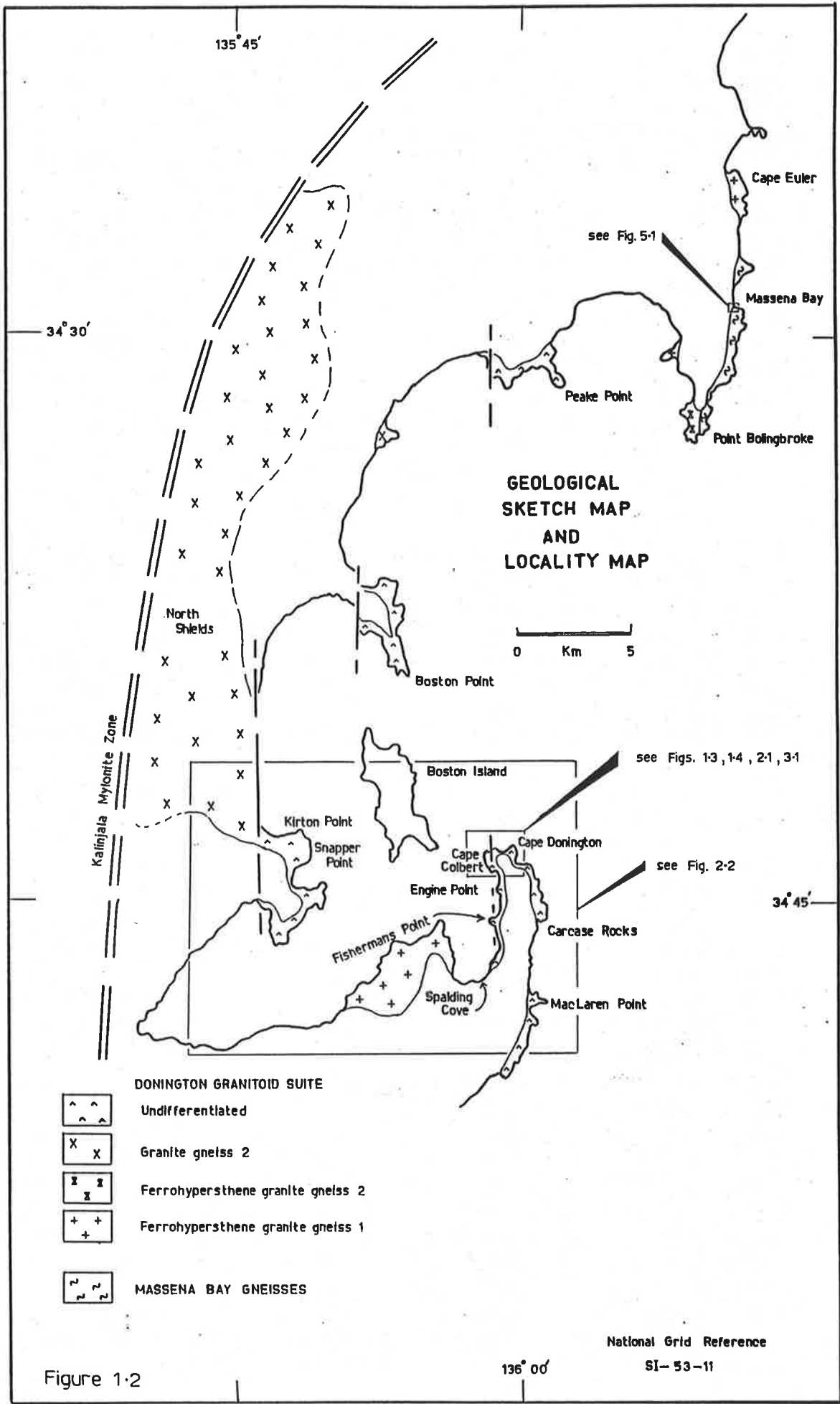



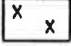
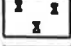
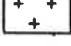
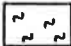
Figure 1-2

136° 00'

135° 45'

34° 30'

34° 45'

- DONINGTON GRANITOID SUITE**
-  Undifferentiated
 -  Granite gneiss 2
 -  Ferrohypersthene granite gneiss 2
 -  Ferrohypersthene granite gneiss 1
- MASSENA BAY GNEISSES**
- 

see Fig. 5-1

see Figs. 1-3, 1-4, 2-1, 3-1

see Fig. 2-2

Kalinjala Mylonite Zone

North Shields

Boston Point

Boston Island

Kirton Point

Snapper Point

Engine Point

Fishermans Point

Spalding Cove

Peake Point

Point Bolingbroke

Cape Euler

Massena Bay

GEOLOGICAL SKETCH MAP AND LOCALITY MAP

and ca. 2500 Ma (Daly et al. 1978). Daly et al. (1978) demonstrated that the Mulgathing Complex experienced granulite facies metamorphism in this age bracket.

In the south the Sleaford Complex is in tectonic contact with, but believed to be unconformably overlain by, the basal Warrow Quartzite of the Hutchison Group (Glen et al. 1977; Parker & Lemon 1982). In the north, Hutchison Group correlatives overlie unconformably the Mulgathing Complex (Daly et al. 1980). The Early Proterozoic mixed clastic and chemical sediments of the Hutchison Group have been metamorphosed, multiply deformed and intruded by various suites of basaltic dykes and granitoids during the Kimban Orogeny (Thomson 1969) which extended from ca. 1820 Ma to ca. 1580 Ma (Webb 1980). A later but much weaker deformation, the Wartakan Event (Thomson 1969), is recognised locally throughout the craton and this occurred ca. 1500-1450 Ma (Parker & Lemon 1982).

The complex of granitoid gneisses, migmatites, pyroxene granitoid gneisses and basic intrusives, largely exposed on the southeastern coast of the Peninsula and produced by the Kimban Orogeny, has been named the Lincoln Complex (Thomson 1980). It includes the original Lincoln Gneisses of Tilley, and comprises the bulk of the present author's study area (Figs. 1.1, 1.2). Without specifying which particular outcrops are intended, Thomson (1980) has included within the Lincoln Complex gneisses believed to be "quartzofeldspathic gneiss relics of older basement complexes reworked by Kimban tectonism". A similar theme has been presented by Rutland et al. (1981) and Parker et al. (1981). The present author will show below that in the study area of this report no reworked Archaean gneisses occur in the Lincoln Complex, but that the Complex is composed entirely of Early Proterozoic supracrustal rocks and more commonly intrusives. The notion of Johns (1961) that the rocks of the Lincoln Complex, as well as the other major rock units, "are metasediments which have responded to metasomatism on a regional scale" is rejected in favour of a largely meta-igneous origin.

Three major deformation events have been recognised for the Kimban Orogeny on Eyre Peninsula (Parker 1978, 1980; Glen et al. 1977; Cooper et al. 1976; Rutland et al. 1981) followed by the weaker Wartakan Event (Table 1.2). These authors demonstrate the existence of a layer parallel S_1 schistosity, only rarely associated with F_1 folds but associated with high grade metamorphism, followed by a tight to isoclinal group of major F_2 folds also accompanied by high

grade metamorphism and a prominent S_2 schistosity. The third deformation appears to be significantly younger and to have produced upright F_3 folds, retrogressive metamorphism and ductile shear zones represented particularly by the major Kalinjala Mylonite Zone (Fig. 1.1) of Parker (1980) and Clarke (1976). These observations correlate well with events on Yorke Peninsula recorded by Richardson (1978), and Pedler (1976) and are summarised in Table 1.2.

The subsolidus recrystallisation and deformation of granitoid gneisses in the Lincoln Complex emplaced prior to D_1 of the Kimban Orogeny locally occurred under granulite facies conditions (Mortimer et al. 1980). The granitoid gneisses have been dated by the Rb-Sr total-rock method at ca. 1820 Ma (Cooper et al. 1976; Mortimer et al. 1980). The Gawler orogenic domain has thus experienced granulite facies metamorphism at ca. 2400 Ma (Daly et al. 1978; 1980) and again at ca. 1820 Ma. Further constraints on the age of Kimban deformation have been proposed by Rutland et al. (1981) who report an isochron age of 1650 ± 35 Ma (Webb 1978) for the syn - D_2 Middle Camp Granite.

1.5 ROCK UNITS AND GENERAL GEOLOGY

1.5.1 Rock units in the present study area

The area mapped in detail by the present author occurs exclusively within the Lincoln Complex (Figs. 1.1, 1.2). However it is the present author's contention that the Lincoln Complex, as defined by Thomson (1980), inadequately represents the variety of rock types present in the study area, and does not convey their geological relationships.

For the purposes of the present discussion, six discrete rock units have now been recognised by the present author (Table 1.3), viz,

- (1) Massena Bay Gneisses (MBG)
- (2) Donington Granitoid Suite (DGS)
- (3) Metabasaltic dykes; amphibolite and granulite facies (DK1)
- (4) Colbert Granitoid Suite (CGS)
- (5) Moody Granitoid Suite (MGS)
- (6) Basaltic dykes; unmetamorphsed (DK2)

Of these the Moody Granitoid Suite and basaltic dykes have already been differentiated from the Lincoln Complex by Thomson (1980) but the interrelationship of the other groups has not been described. Each of these rock units is characterised briefly in Table 1.3, where it can be seen that each has been generated prior to, during or soon

Table 1.2 Summary of previously published structural and metamorphic histories of the Gawler orogenic domain.

WARTAKAN EVENT	M ₅	kinks	
	D ₄	crenulations	
		Pegmatite	
KIMBAN OROGENY	M ₄	S ₃ mica, weak	
	D ₃	F ₃ upright open Kalinjala Mylonite Zone	
			Narridy Creek Granite
	M ₃	S ₂ sillimanite, biotite	
	D ₂	F ₂ isoclinal locally overturned to east co-axial lineation	
			Middlecamp Granite, (1650 ± 35 Ma)
			Pegmatite
	M ₂	S ₁ sillimanite, biotite, hornblende layer parallel	
	D ₁	F ₁ rare isoclinal to tight	
			migmatites, gabbro, granitoids, dolerite
	M ₁	Possible andalusite or staurolite	
		HUTCHISON GROUP sedimentation	
		unconformity	
		SLEAFORD COMPLEX	

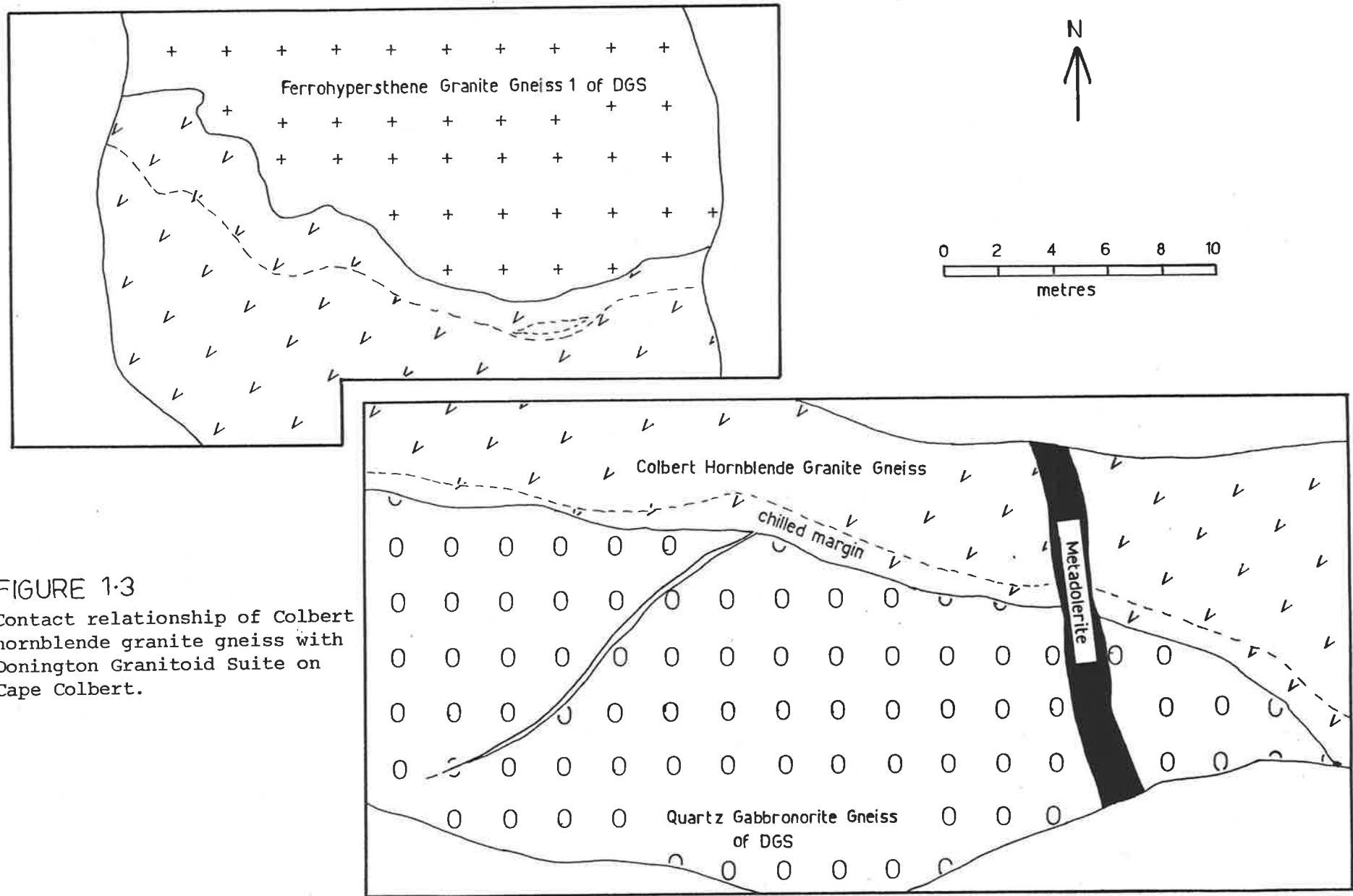


FIGURE 1.3
 Contact relationship of Colbert
 hornblende granite gneiss with
 Donington Granitoid Suite on
 Cape Colbert.

after the Kimban Orogeny or Wartakan event

1.5.2 Structural and metamorphic outline

In order to constrain adequately the relative temporal importance of Kimban petrogenetic processes preserved in the rocks of the study area, it is necessary to tie together the sequence of structural events, metamorphic events, and the episodes of emplacement of granitoid and basaltic magma.

Comparison of the present author's qualitative observations with previous detailed structural studies in other parts of the Gawler orogenic domain (e.g. Parker & Lemon 1982; Richardson 1978; Glen et al. 1977) has allowed a relative chronology to be erected (Table 1.4). Each of the main intrusive, metamorphic and structural events will also be described in more detail below.

(1) Pre-D₁ features

Within the MBG there is a fine-scale, discontinuous, migmatitic layering that has apparently developed prior to the first deformation (Fig. 1.6A). This migmatitic layering is cut by a suite of basaltic "dykes" which also were emplaced prior to D₁ (Fig. 1.6B). Porphyroblasts in the garnet - sillimanite and quartzofeldspathic gneisses of the MBG tend to be poikiloblastic, the inclusions tending to be randomly oriented, suggesting growth prior to the well-developed early fabrics in the rocks (Figs. 1.9 D,E). It is thought likely that metamorphism in the MBG prior to, or early in, the first deformation caused growth of poikiloblasts and in situ development of migmatitic segregations.

One specimen, at least, of pre-D₁ basaltic "dyke" or sill in the MBG preserves a granulite facies assemblage, suggesting the MBG itself has experienced early granulite facies metamorphism.

Richardson (1978) recognised a similar migmatitic development and basaltic "dyke" emplacement prior to D₁ on Yorke Peninsula, and Glen et al. (1977) suggest pre-D₁ growth of poikiloblasts is common throughout the Gawler domain. Richardson, furthermore, recognised a pre-D₁ intrusive suite of gabbros and megacrystic granite sheets, which the present author correlates with elements of the DGS.

Table 1.3 Characterisation of main rock units in present study area.

Rock unit and type locality	Brief Description	Field Relations
Basaltic dykes (DK2) Cape Donington	unmetamorphosed dolerites	dykes intruding all of previous rock units after main metamorphism and deformation
Moody Granitoid Suite (MGS) west of Tumby Bay	differentiated granitoids some hornblende - bearing some muscovite - bearing	massive granitoids intruding Hutchison Group
Colbert Granitoid Suite (CGS) Cape Colbert	differentiated granitoid gneisses hornblende - bearing	narrow dykes intruding DGS chilled margins
Metabasaltic dykes (DK1)	metabasaltic amphibolites and pyroxene granulites	dykes intruding DGS before main D_{1-2} metamorphism and deformation
Donington Granitoid Suite (DGS) Cape Donington Kirton Point	differentiated granitoids opx-bearing variable retrogression	batholith intruding MBG before main D_{1-2} metamorphism and deformation retrogression pre D_{1-2}
Massena Bay Gneisses (MBG) Massena Bay Cape Donington	-dominant biotite + hornblende quartzofeldspathic gneisses -subordinate metasediments -semiconcordant metabasaltic dykes	emplaced prior to D_1

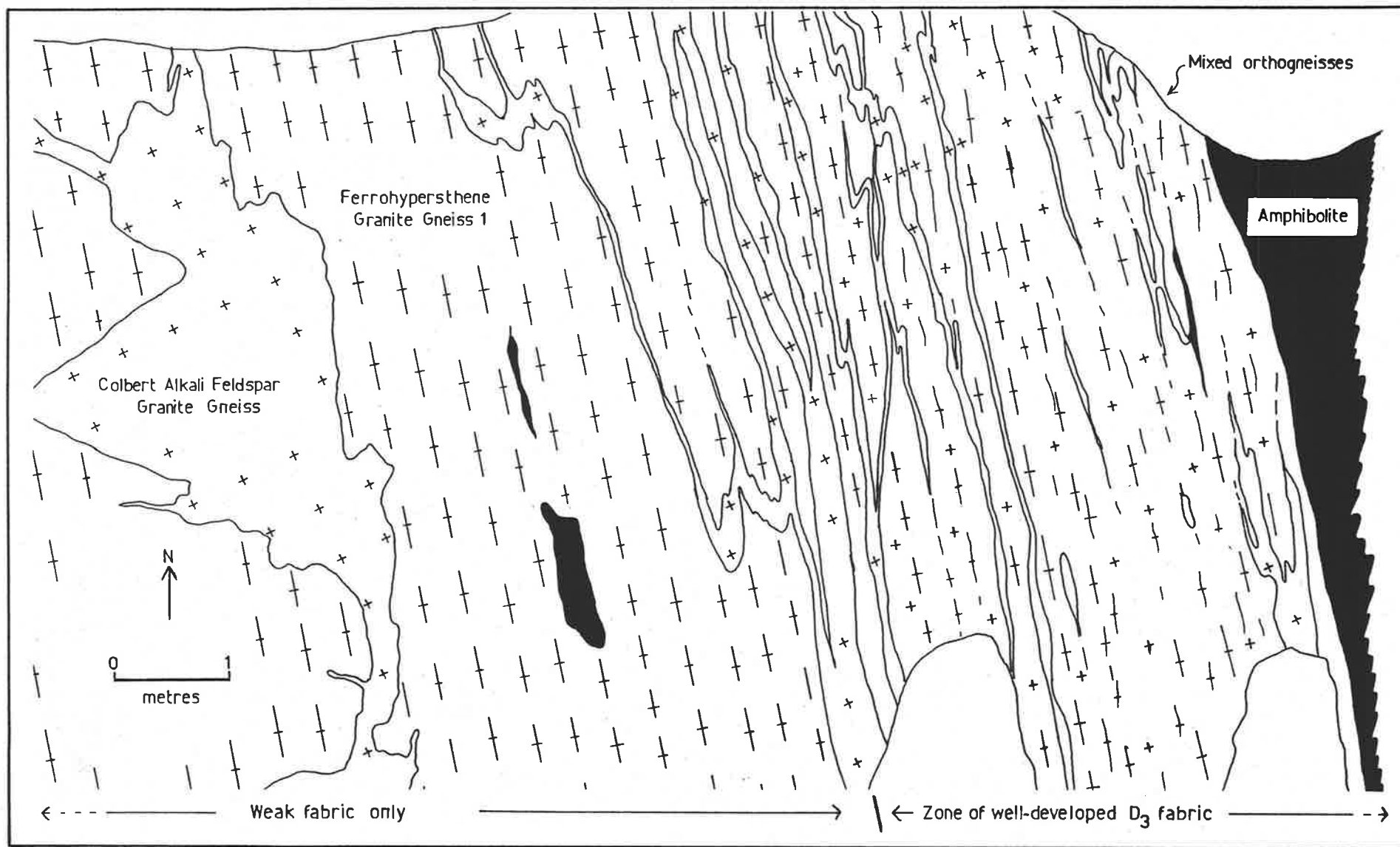


Figure 1.4 Orthogneissic layering developed in D₃ shear zone at contact of Colbert Granitoid Suite and Donington Granitoid Suite, Cape Colbert.

(2) Event 1 (D_1)

F_1 folds are rare throughout the Cleve Subdomain and the present author tentatively recognises only one occurrence. However, it is clear that many F_2 folds are folding a fabric of earlier Kimban age. Most commonly this earlier S_1 fabric is high-grade, planar, layer-parallel and flat-lying and is defined in rocks of appropriate composition by the alignment of hornblende, biotite, elongate garnet porphyroblasts and clinopyroxene.

Richardson (1978) observed F_1 isoclinal folds in correlatives of the MBG on Yorke Peninsula, whereas Parker & Lemon (1982) suggest that S_1 in the Hutchison Group formed during burial and compaction of the sedimentary pile.

Elsewhere in the Gawler Province, D_1 may be associated with nappe tectonics (Glen et al. 1977).

(3) Event 2 (D_2)

Prior to D_2 , but post-dating D_1 , a suite of coarse-grained pegmatitic veins intruded the MBG, cross-cutting the pre- D_1 migmatitic layering. These pegmatites were deformed in D_2 and exhibit F_2 isoclinal folds and well developed fabrics (Figs. 1.6C,D; 1.8C,D).

In the pegmatites and elsewhere, the S_2 foliation is parallel to S_1 , so that in most outcrops the main foliation is a combination of S_1 and S_2 and is designated S_{1-2} . Quartz ribbon fabrics are common in S_{1-2} , and are particularly well-developed in the MBG at Cape Donington and DGS near Carcase Rock (Fig. 1.2). Here the quartz ribbon fabrics can be seen to wrap around feldspar porphyroblasts and relict phenocrysts (Fig. 1.9 A,B) and also they may be folded with new quartz ribbons formed in an axial planar orientation (Fig. 1.9C).

This S_{1-2} fabric is also present elsewhere in members of the DGS, where it is expressed by parallel hornblende and biotite (Fig. 1.7 A,B), although those rocks in the DGS containing primary igneous orthopyroxene or recrystallised subsolidus orthopyroxene tend not to have developed tectonite fabrics. In the MBG mineral assemblages with the S_{1-2} fabric are generally of amphibolite facies. Hence it is suggested that DGS and MBG during development of the S_{1-2} fabric have suffered high-grade metamorphism locally attaining granulite facies, but in areas where hydrated rocks are present assemblages manifest the amphibolite facies. This observation will be discussed in more detail in Chapter 2 dealing with the DGS.

Richardson (1978) and Parker & Lemon (1982) also recognised tight to isoclinal F_2 folds, with high-grade metamorphic assemblages and strong fabric on both Yorke Peninsula and Eyre Peninsula respectively, and Richardson recognised pre- D_2 pegmatite intrusions.

(4) Event 3 (D_3)

F_3 folds are common throughout the study area and may be symmetric or asymmetric (Figs. 1.7A,B) and may have associated displacement on limbs in which pegmatitic veins may occur in an axial planar orientation (Figs. 1.7D; 1.8C,D). Similar pegmatitic veins have been noted by Glen et al. (1977) and Richardson (1978). S_3 fabrics are not commonly well developed in F_3 folds.

Fabrics are more strongly developed in D_3 shear zones, (Fig. 1.7C), some of which are mylonitic. A number of narrow mylonitic zones occur throughout the present study area (Fig. 1.2) and the major Kalinjala Mylonite Zone of Parker (1980) has been assigned by him to D_3 . In most of these zones the mineral assemblages are of amphibolite facies, but on Yorke Peninsula (Pedler 1976) and in northern central Eyre Peninsula lower grade conditions are represented by D_3 .

D_3 strain commonly is localised at contacts between different rock units, presumably because of inhomogeneity of rheological properties. One such zone, less than 20m wide, occurs on Cape Colbert where the CGS intrudes the DGS and a tectonic layering has formed (Figs. 1.7C; 1.4). Elsewhere the CGS is little deformed. However, adjacent to the zone on Cape Colbert another D_3 zone in alkali feldspar granite gneiss of the CGS contains mafic inclusions which appear to have been involved in at least two fabric-forming events (Fig. 1.5C). It is problematical at this outcrop whether the mafic inclusions intrude the CGS or whether they represent xenoliths and hence it is uncertain whether the earlier fabric represents S_{1-2} developed in situ, or is inherited from the source of the inclusion. The presence of xenoliths of DGS material with S_{1-2} fabrics in hornblende granite gneiss of the CGS, also on Cape Colbert, argues for a xenolithic origin for the mafic inclusions.

In addition, the CGS chilled contacts against the DGS (Fig. 1.5B; 1.3) suggests emplacement into relatively cool country rocks after the peak of D_{1-2} metamorphism.

(5) Event 4 (D_4) Wartakan Event

The D_4 event post-dates the later suite of essentially unmetamorphosed basaltic dykes (DK2, Table 1.2) and is expressed in F_4 flexures

Table 1.4 Comparison of structural and metamorphic history of this study with previous studies summarised in Table 1.2.

M ₅	S ₄	biotite, pegmatitic segregations in kinks
D ₄	F ₄	kinks and shears

DK2 Dolerite dykes
MGS emplacement (?)

M ₄	S ₃	hornblende, biotite pegmatites in axial planar displacements
D ₃	F ₃	open to tight upright local shear zones

CGS emplacement

M ₃	S ₂	sillimanite, biotite, hornblende, opx (?) axial plane
D ₂	F ₂	isoclinal, recumbent (?)

DK1 dolerites
Pegmatite

M ₂	S ₁	sillimanite, biotite, opx, hornblende layer parallel
D ₁	F ₁	rare isoclinal

metabasaltic "dykes" in MBG
DGS emplaced and retrogressed

M ₁		migmatites in MBG developed hornblende, garnet poikiloblasts in MBG
----------------	--	--

MASSENA BAY GNEISSES
protolith

lateral equivalent (?)
of HUTCHISON GROUP

(Fig. 1.5D), which may have diffuse pegmatitic patches developed in the axial planar orientation (Figs. 1.8A,B).

A summary of these structural and intrusive events is presented in Table 1.4 and may be compared with the observations of previous authors in Table 1.2.

The discussion of the individual rock suites in following chapters will enlarge upon some of the more significant features described in brief above.

Figure 1.5 Photographs of aspects of field geology,
south eastern Eyre Peninsula.

- A. Tectonically interlayered, original intrusive relationship between megacrystic granite gneiss of the Donington Granitoid Suite and host quartzofeldspathic gneisses of the Massena Bay Gneisses, Point Bolingbroke.
Scale : ball point pen ca. 12 cm
- B. Chilled intrusive contact and apophyse of hornblende granite gneiss of the Colbert Granitoid Suite against quartz gabbro-norite gneiss of the Donington Granitoid Suite, Cape Colbert.
Scale : lens cap ca. 4 cm diameter
- C. Metabasaltic inclusion within alkali feldspar granite gneiss of the Colbert Granitoid Suite, showing S3 fabric in host gneiss and earlier folded fabric in inclusion, Cape Colbert.
Scale : inclusion ca. 40 cm long
- D. Metabasaltic dyke in granite gneiss offset by F4 kink, Point Boston.
Scale : dyke in fore ground ca. 1.5 m wide



Figure 1.6 Photographs of aspects of field geology,
south eastern Eyre Peninsula.

- A. Pre-D1 migmatitic layering in quartzofeldspathic gneisses of the Massena Bay Gneisses, Massena Bay.
Scale : hammer head ca. 8 cm wide
- B. Pre-D1 metabasaltic "dykes" in quartzofeldspathic gneisses of the Massena Bay Gneisses, Massena Bay.
Scale : ball point pen ca. 12 cm
- C. F2 isoclinal fold in discordant pegmatite vein in quartzofeldspathic gneisses of the Massena Bay Gneisses, Massena Bay.
Scale : lens cap ca. 4 cm diameter
- D. F2 isoclinal fold in discordant pegmatite vein in quartzofeldspathic gneisses of the Massena Bay Gneisses, Massena Bay.
Scale : ball point pen ca. 12 cm

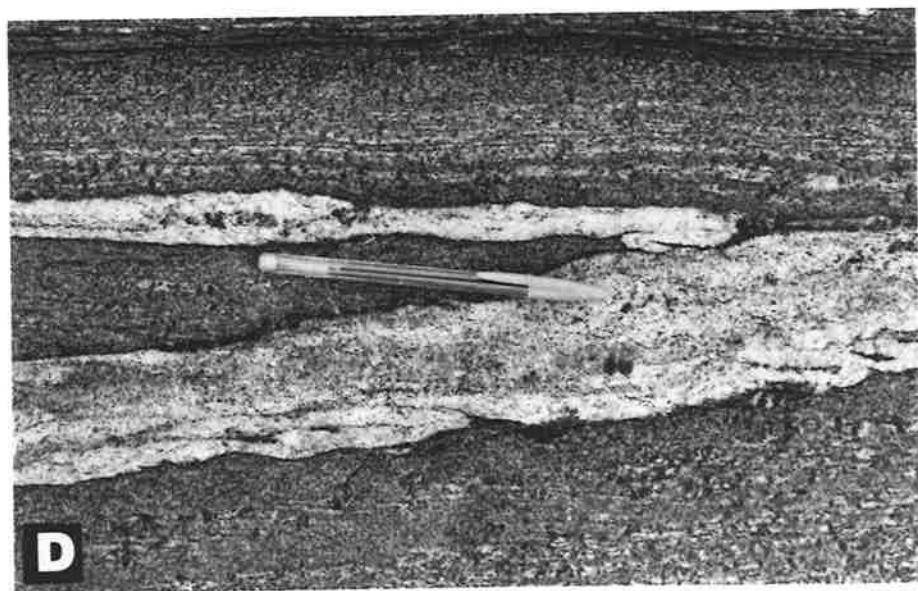
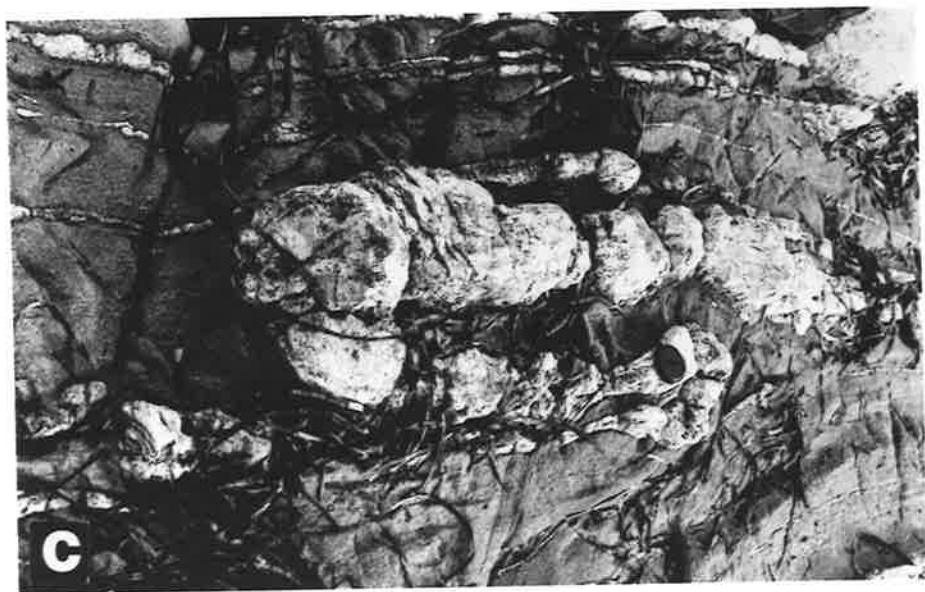
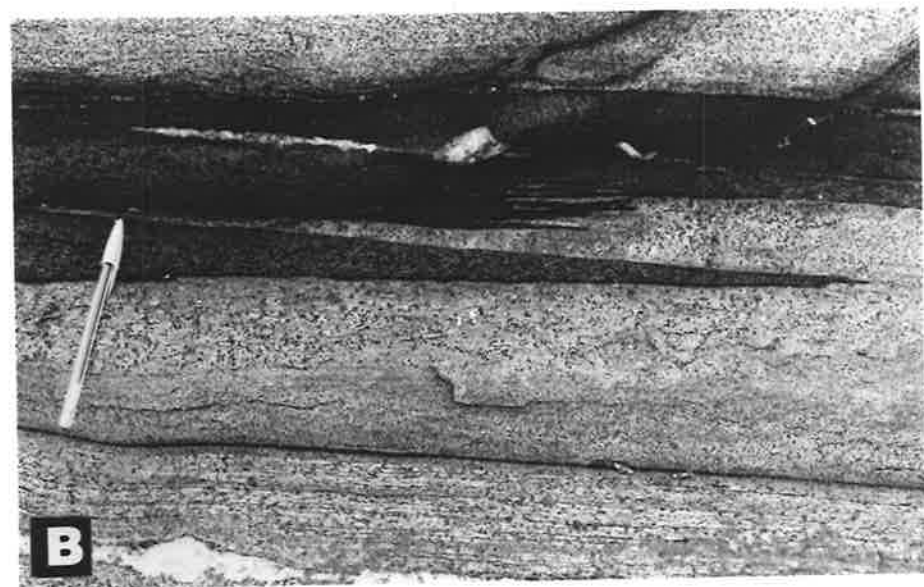


Figure 1.7 Photographs illustrating D₃ features,
south eastern Eyre Peninsula.

- A. Centre of field of view (FOV): F3 crenulations of S1-2 fabric in megacrystic granite gneiss of Donington Granitoid Suite.
Bottom left of FOV: S3 fabric well developed.
Top right of FOV: S1-2 fabric almost unmodified by F3; some of augen may be folded by F2.
Kirton Point.
Scale : coin ca. 3 cm diameter
- B. Close up view of F3 crenulations and S3 development in granite gneisses of Donington Granitoid Suite, Kirton Point.
Scale : lens cap ca. 4 cm diameter
- C. Orthogneiss layering developed in D3 shear zone at contact of Colbert Granitoid Suite (light-coloured), Cape Colbert.
Scale : lens cap ca. 4 cm diameter
- D. F3 folds in metabasaltic dykes in quartzofeldspathic gneisses of Massena Bay Gneisses, Massena Bay.
Note: pegmatitic veins in displacement zones parallel to F3 fold axial plane.
Scale : coin ca. 3 cm diameter

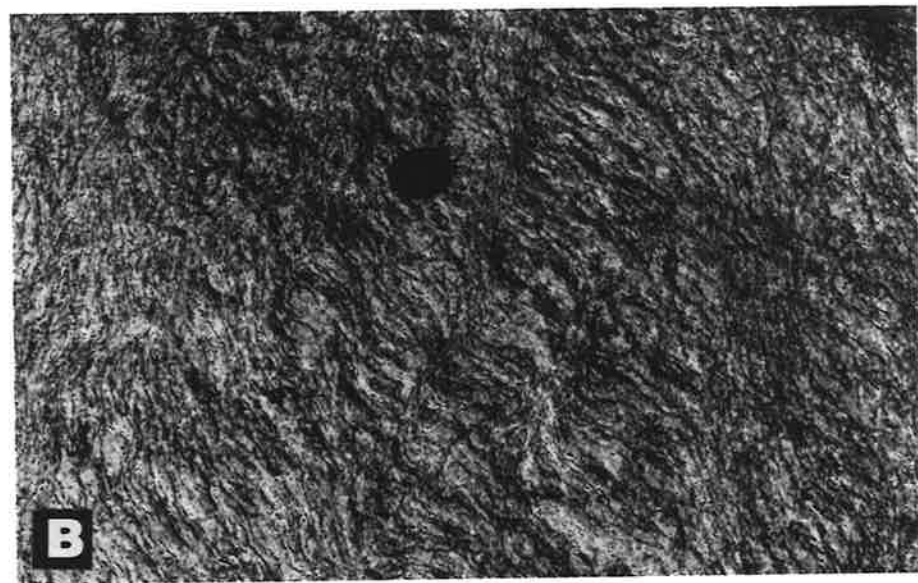


Figure 1.8 Photographs of aspects of D_3 and D_4 ,
south eastern Eyre Peninsula.

- A. F4 kink with diffuse pegmatite in axial plane in megacrystic granite gneisses of Donington Granitoid Suite, Peake Point.
Scale : pen ca. 12 cm long
- B. F4 kink with diffuse pegmatite in axial plane in quartzofeldspathic gneisses of Massena Bay Gneisses, Massena Bay.
Scale : coin ca. 3 cm diameter
- C. and D. Different views of same F3 fold in quartzofeldspathic gneisses of Massena Bay Gneisses, Massena Bay, with sheared limb and pegmatite vein in shear. Also discordant pegmatite veins folded by F2 and F3.
Scale : ball point pen ca. 12 cm

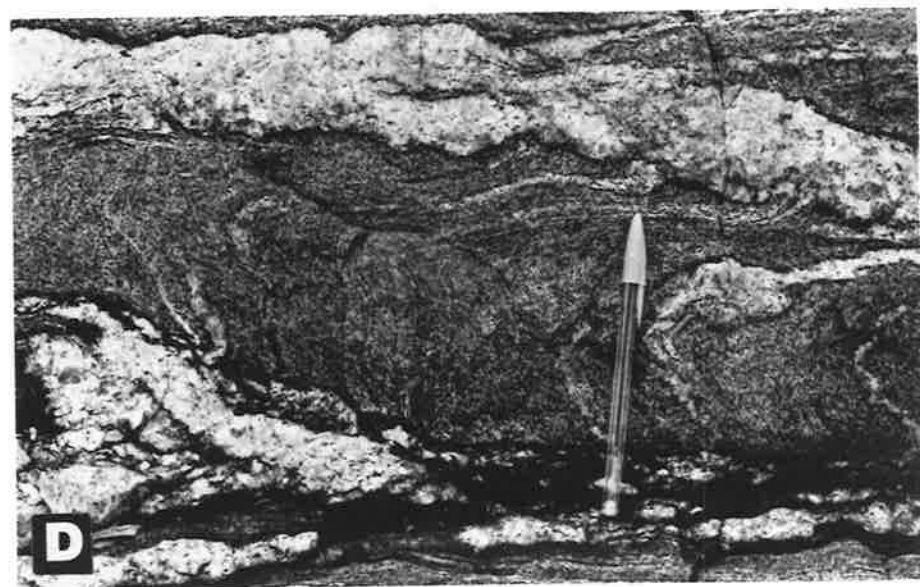
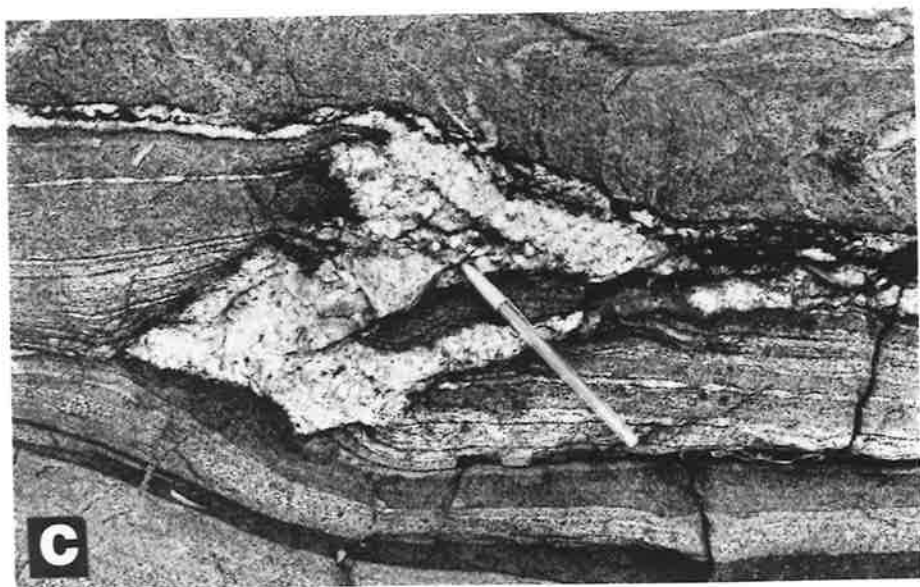
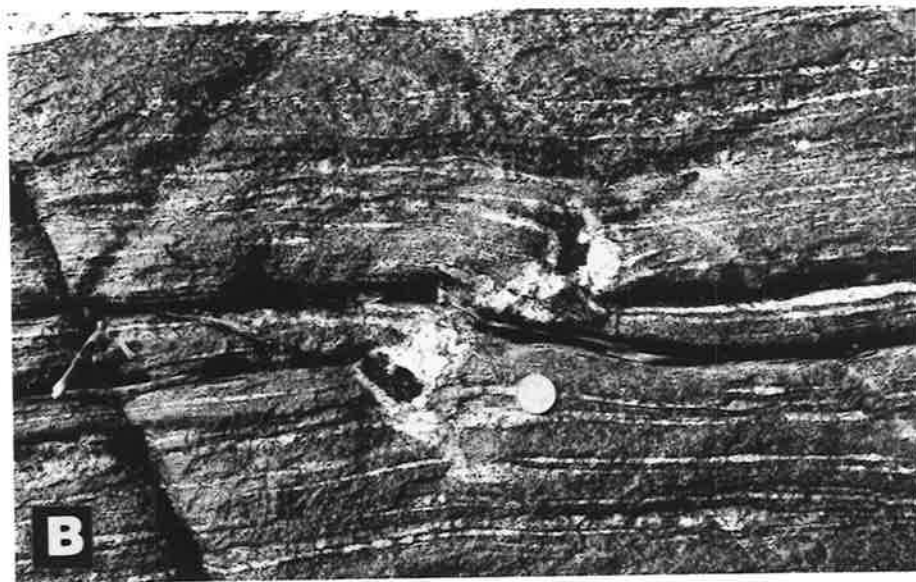


Figure 1.9 Line drawings from thin sections illustrating microtextural aspects of structure and metamorphism, south eastern Eyre Peninsula.

- A. Feldspar megacrysts with quartz ribbon fabric wrapping around in granite gneisses of the Donington Granitoid Suite, Cape Donington.
- B. S1-2 quartz ribbon fabric wrapped around relict plagioclase phenocryst in alkali feldspar granite gneiss of the Donington Granitoid Suite, north of Carcase Rock.
- C. S1-2 quartz ribbon fabric folded by F2 fold and with new S1-2 quartz ribbon fabric, Cape Donington.
- D. Hornblende M1 poikiloblast with sub-random quartz and opaque oxide inclusions, possibly pre-D1, in quartzofeldspathic gneisses of the Massena Bay Gneisses; Yorke Peninsula.
- E. Garnet M1 poikiloblast in garnet-sillimanite gneisses of the Massena Bay Gneisses with sub-random inclusions of biotite, quartz and opaque oxides possibly pre-D1, Cape Donington.

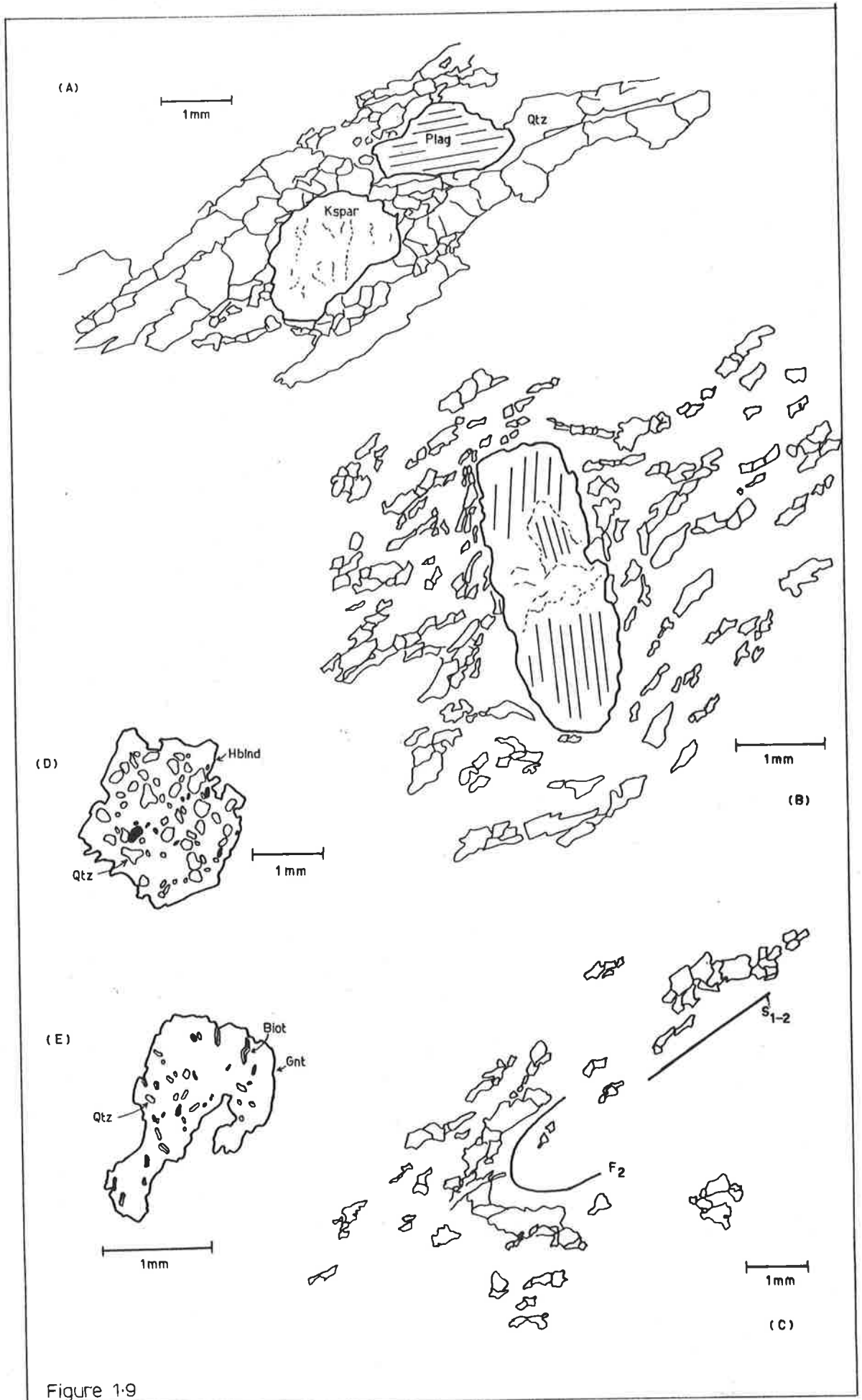


Figure 1-9

CHAPTER 2DONINGTON GRANITOID SUITE2.1 INTRODUCTION

The Donington Granitoid Suite (DGS), as defined here and in Mortimer et al. (1980), includes rocks containing pyroxene as the major ferromagnesian mineral, as well as rocks containing hornblende and biotite to the exclusion of pyroxene. It is the present author's major contention that these two different groups of rocks originally had a common magmatic origin as pyroxene granitoids (or charnockites; Tobi 1971), and that the hornblende-biotite bearing rocks were derived by subsequent retrogression from the primary pyroxene granitoids.

Previous authors have recognised and described aspects of the two groups of rocks, but largely because the pyroxene granitoids are dark coloured and massive and the hornblende-biotite granitic rocks are light-coloured and gneissic, and because the two are not commonly seen in contact have not recognised the primary interrelationship. For instance, Tilley (1921C) recorded without further comment that variation existed within his Lincoln Gneisses from hornblende-biotite granite gneisses at the type locality, Kirton Point, to charnockites on Boston Island. Subsequently Bradley (1972;1980) described a "high-potassium garnet-free charnockite" which he proposed was unrelated to the hornblende-biotite granite gneisses around Port Lincoln which he attributed to a zone of retrogression ca. 5km wide. Bradley suggested that the charnockite may be part of a water undersaturated intrusive batholith and that the gneisses may represent reworked and updated elements of the Sleaford Complex.

On the basis of qualitative structural observations the present author has implied that the granite gneisses of the DGS were emplaced and retrogressed prior to, or during D_1 (Table 1.3, Table 1.4; Chapter 1). The following sections of this chapter will document the petrographic geochemical and Sr-isotopic bases for the contention that the opx-granitoids and granite gneisses of the DGS constitute an original comagmatic suite of differentiated granitoids.

The importance of this conclusion lies in the fundamental question as to the nature of the Proterozoic Kimban Orogeny i.e. whether the extensive tracts of granite gneiss represent new magmatic additions to the crust or tectonically reworked and updated Archaean crustal rocks.

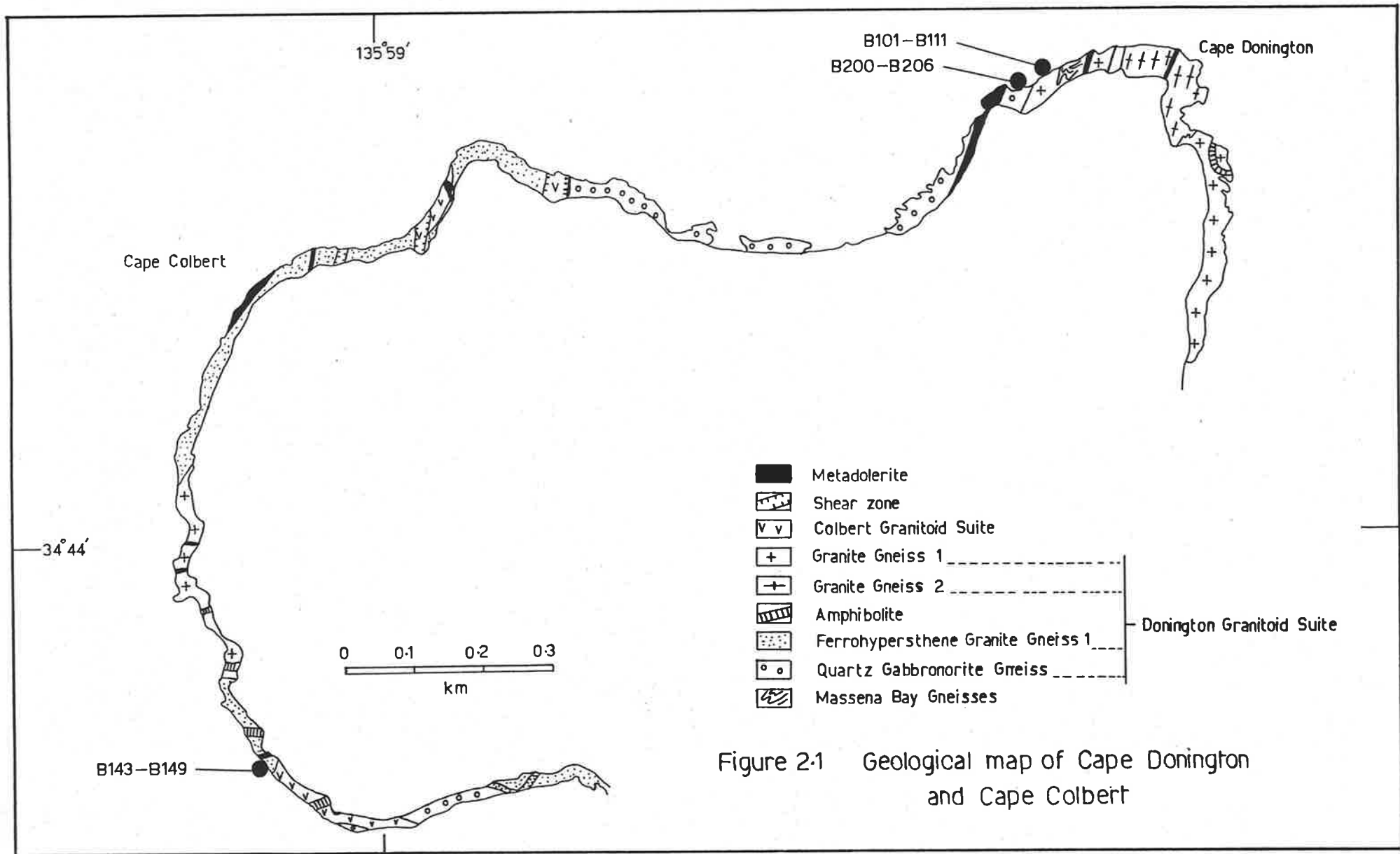


Figure 2-1 Geological map of Cape Donington and Cape Colbert

If it can be demonstrated that the granite gneisses were derived by retrogression from primary opx-granitoids, and if the petrogenesis of the primary magma can be adequately constrained, the ensialic or otherwise nature of Proterozoic orogenesis will be characterised for this portion of the Gawler domain.

A more generalised discussion of Proterozoic orogenesis will be included in Chapter 7.

2.2 PETROGRAPHY AND FIELD RELATIONS WITHIN THE DGS

2.2.1 Rock types within the DGS

Detailed field and petrographic studies have resulted in the recognition of a number of different rock-types within the DGS. The main rock types are,

- (1) Quartz gabbro-norite gneiss, (QGNG)
- (2) Ferrohypersthene granite gneiss 1, (FGG1)
- (3) Ferrohypersthene granite gneiss 2, (FGG2)
- (4) Eulitic alkali feldspar granite gneiss, (EAGG)
- (5) Hornblende biotite granite gneiss 1, (GG1)
- (6) Hornblende biotite granite gneiss 2, (GG2)
- (7) Alkali feldspar granite gneiss, (AGG).

The field relationships and major minerals of the different rock-types are summarised in Table 2.1 and Figure 2.1, and in addition some qualifying statements are included in this section.

Relative intrusive relationships among the opx-granitoids (Table 2.1) show that the QGNG is the earliest intrusive phase of the DGS. At the type locality Flook (1975) suggested it intrudes meta-sediments (included in the MBG by the present author). However, it will be proposed in Chapter 5 that the metasedimentary gneisses at Cape Donington are strongly tectonised xenolithic inclusions within both QGNG and GG1-type material, so that although the QGNG is considered by the present author to intrude the MBG, it is nowhere seen in contact with extensive tracts of metasedimentary country rocks.

The dark colouration of all the opx-granitoids, even those that are predominantly composed of quartz and feldspar, is a common feature of charnockitic rocks and has been attributed elsewhere to the presence of chloritic micro-veinlets (e.g. Oliver & Schultz 1968; Bhattacharyya 1977).

The local gradations observed between opx-granitoids and granitic gneisses result in marked petrographic changes which will be described below in detail. The local variations can then be applied to the

Table 2.2 Donington Granitoid Suite - petrographic summary

Rock type	Primary igneous minerals and texture	Secondary metamorphic minerals and texture	Brief Interpretation
Quartz gabbronorite gneiss (QGNG)	Phenocrysts plag + opx + cpx interstitial Qtz + Kspar biot in part replacing pyroxene accessory zircon, apatite	polygonal mosaic plag + opx + cpx (Type 1) coronas of hblnd around px (Type 2)	Accumulated framework of plag + opx + cpx interstitial residual liquid
Ferrohypersthene granite gneiss 1 (FGG1)	Phenocrysts plag + opx + Kspar Groundmass Kspar + Qtz (+ plag) some biot + ilm + hblnd accessory zircon, apatite	polygonal mosaic plag + Kspar + Qtz (Type 1) coronas of hblnd around px (Type 2) some microcline twinning	Opx - granitoid intrusive
Ferrohypersthene granite gneiss 2 (FGG2)	Phenocrysts plag + opx + Kspar Megacrysts Kspar- <i>rapakivi</i> -like Groundmass Kspar + Qtz rare biot + hblnd + ilm accessory zircon, apatite	polygonal mosaic plag + opx + Kspar (Type 1) coronas of hblnd around px (Type 2)	Accumulative feldspar late stage Kspar replacement of plag
Eulitic alkali feldspar granite gneiss (EAGG)	Phenocrysts (plag +) Kspar + Qtz Groundmass (plag +) Kspar + Qtz accessory zircon, apatite (probable fayalite pseudomorphs)	polygonal mosaic opx + mag + feldspar (Type 1) microcline twinning common	Highly fractionated silicic potassic residual liquid
Granite gneisses 1 and 2 (GG1, GG2)	Relict phenocrysts plag + Kspar Relict megacrysts Kspar (<i>rapakivi</i> -like)	inequigranular, interlobate to polygonal plag + Kspar + Qtz + hblnd + biot microcline twinning sphenes coronas around opaque oxides metamorphic tectonite fabric (Type 3)	Retrogressed FGG1, FGG2
Alkali feldspar granite gneiss (AGG)	Relict phenocrysts plag + Kspar	inequigranular, interlobate to polygonal plag + Kspar + Qtz + biot + hm (Type 4) microcline twinning common metamorphic tectonite fabrics (Type 3)	Retrogressed EAGG

Note: Mineral abbreviations as in Table 2.1 plus,

ilm = ilmenomagnetite mag = magnetite hm = haematite

regional variations within the DGS to formulate a regional metamorphic model.

Regionally, in accord with the observation of Mortimer et al. (1980), the prevalence of granitic gneisses of GG1 and GG2 types increases markedly as the Kalinjala Mylonite Zone (KMZ) of Parker (1980) is approached from the east (Fig. 2.2). It is suggested below that the KMZ is the major control on the distribution of retrogressive metamorphism and that this structural control is the strongest argument against the possibility of the mineralogical variation between opx-granitoids and granite gneisses being controlled by primary magmatic processes.

It is important to realise that the main fabric in the granite gneisses, defined by parallel hornblende and biotite, is S_{1-2} (Tables 1.3, 1.4; Chapter 1) and hence, that if the contention argued in this thesis that the granite gneisses were derived by retrogression from the opx-granitoids is accepted, this retrogression must have occurred at least as early as D_2 . This conflicts with the interpretation of Parker (1980) that the KMZ is a D_3 feature. This point will be re-examined in the Rb-Sr geochronological discussion below.

2.2.2 Petrography

The petrography of the rock-types within the DGS will be described in detail in this section, because it is crucial to establish well the petrographic link between the opx-granitoids and the granite gneisses. It is convenient to describe the petrography in two sections,

- (a) primary igneous mineral assemblages and textures
- and (b) subsolidus metamorphic assemblages and textures.

This is possible because despite ubiquitous tectonothermal overprinting, in areas of lesser deformation near-primary mineralogical features and textures are preserved.

The key petrographic observations and interpretations are summarised in Table 2.2 and described below in detail.

2.2.2.1 Primary igneous features

(1) Quartz gabbro-norite gneiss, QGNG

Relict zoned phenocrysts of opx, cpx and plagioclase occur in QGNG. The two pyroxenes contain cores with abundant exsolved platelets of opaque oxide, apparently ilmenite (Fig. 2.3A), surrounded by an opaque-free rim which sometimes shows optical zoning. In addition, the

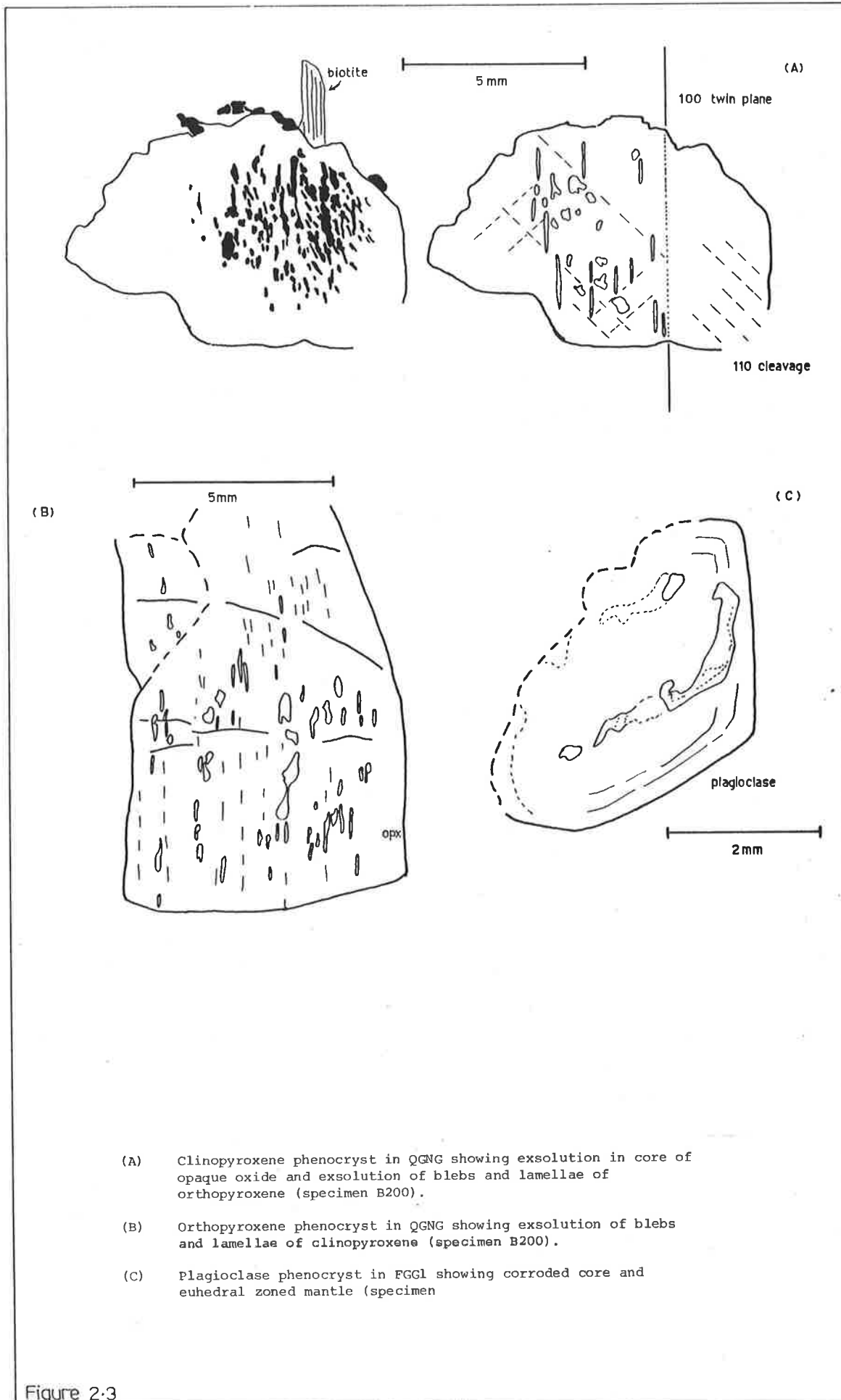


Figure 2.3

opx phenocrysts contain coarse blebs of exsolved cpx elongate parallel to (100) of the host, with another generation of fine cpx lamellae also exsolved parallel to (100) (Fig. 2.3B). Similarly cpx phenocrysts contain coarse and fine generations of exsolved opx parallel to the (100) twin plane of the host (Fig. 2.3A). In both cases the coarse blebby exsolved material tends to be concentrated in the cores of phenocrysts.

Relict plagioclase phenocrysts preserve internal zoning, which is often euhedral. One analysed grain shows oscillatory zoning from a core of composition An_{54} , through an intermediate zone ranging at least to An_{62} into an outer zone of An_{48} (Appendix Table 2.1).

Biotite is a major constituent of QGNG, and forms coarse flakes often apparently moulded onto, and in part replacing pyroxene, and sometimes containing corroded pyroxene relics.

Quartz and alkali feldspar occur only in interstitial patches between the dominant plagioclase, pyroxene and biotite grains.

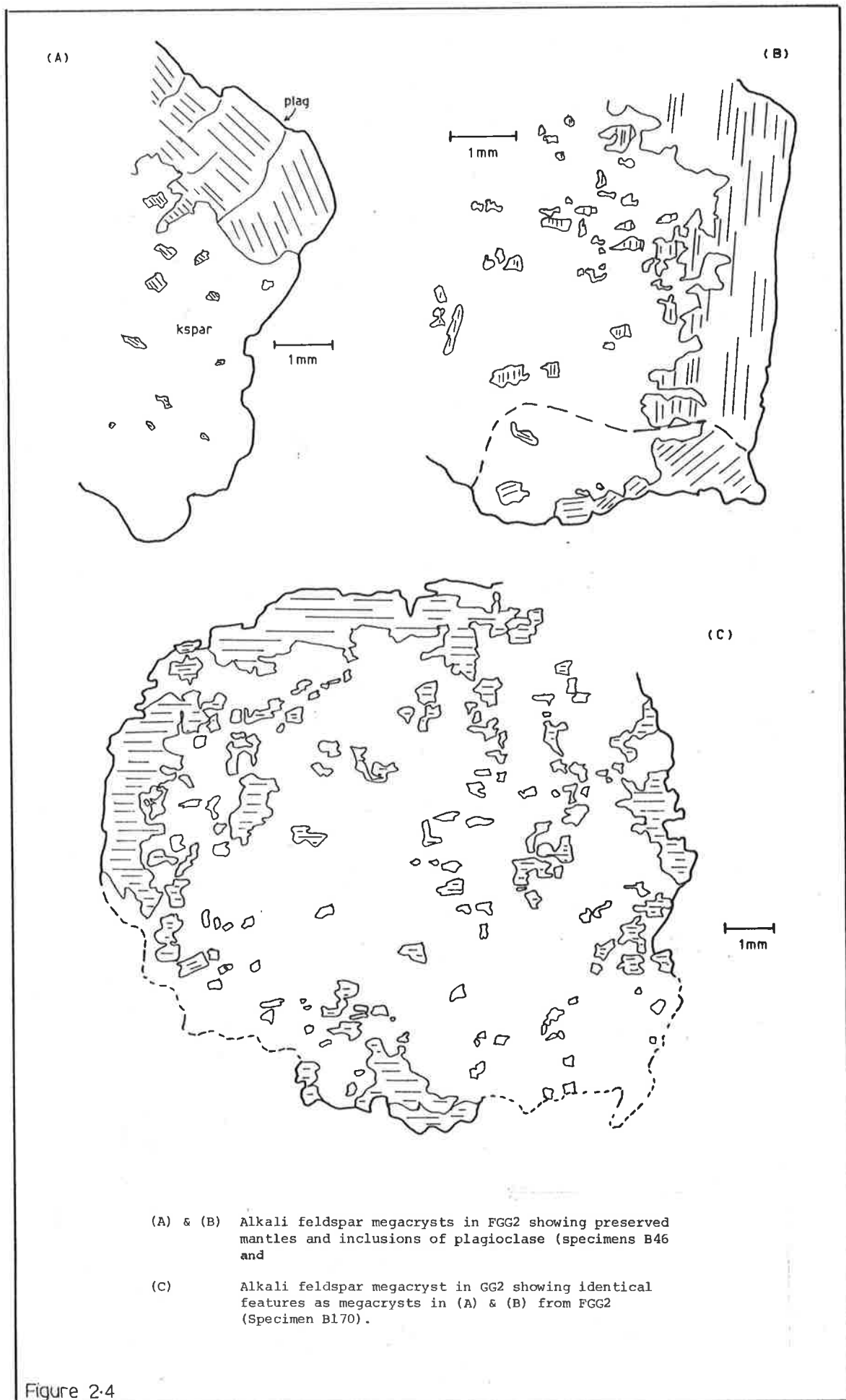
These primary mineral relationships suggest the accumulation of early formed plagioclase and pyroxene phenocrysts, with the crystallisation of quartz and alkali feldspar from trapped intercumulus residual liquid. The biotite is interpreted to have crystallised partly at the expense of pyroxene, possibly in part subsolidus and possibly in part by reaction between pyroxene cumulus phases and trapped interstitial liquid. The implication that the minerals of QGNG were crystallised from a melt is important for the petrogenesis of the DGS opx-granitoids.

Hornblende is a minor component of QGNG and is thought to be largely secondary, developing as coronas to the pyroxene grains. Apatite and zircon are accessory phases, some of the apatite stumpy prisms occurring within pyroxene phenocrysts.

The exsolution textures in the pyroxene phenocrysts will be discussed below in more detail.

(2) Ferrohypersthene granite gneiss 1, FGGL

Relict zoned phenocrysts of plagioclase, orthoclase and opx of ferrohypersthene composition occur in FGGL, set in a matrix of quartz and feldspar. The oligoclase to andesine phenocrysts may have corroded, altered cores with euhedral, zoned mantles (Fig. 2.3C). The orthoclase phenocrysts usually are zoned, and microperthitic and many contain corroded cores of plagioclase. The opx phenocrysts are less well preserved and do not show the exsolution features observed in



QGNG phenocrysts, other than the later fine lamellar set parallel to (100).

Biotite and Fe - Ti oxide tend to occur as discrete grains, often in association with the opx, and often with minor hornblende in some specimens which may in part be of igneous origin. Some specimens contain minor cpx.

Zircon and apatite are common, discrete, accessory phases.

The presence of orthoclase phenocrysts is in distinct contrast to QGNG, as is the rarity of cpx, suggesting a significant compositional difference between the liquids crystallising QGNG and FGGL. In addition the occasional distinctive plagioclase phenocrysts with altered, corroded cores may represent a minor proportion of solid phases in FGGL residual from the source of melting (cf. Chappell & White 1974).

(3) Ferrohypersthene granite gneiss 2 FGG2

Although the mineralogy of FGG2 is similar to FGGL, its texture is quite dissimilar. Phenocrysts of plagioclase and subordinate opx occur in an interpreted cumulate texture, and are accompanied by megacrysts of orthoclase not clearly of phenocryst origin. Both plagioclase and opx phenocrysts are large (up to 3 cm diameter) and the plagioclase is ovoidal and only minimally zoned and probably crystallised slowly under near-equilibrium conditions (Philpotts 1966). Opx phenocrysts show some fine scale exsolution lamellae of cpx parallel to (100).

Some alkali feldspar megacrysts may represent phenocrysts, but most are considered to have a more complex origin. Most occur in contact with the alkali feldspar-rich matrix and may have a partial or nearly complete rim of plagioclase, resembling rapakivi texture (cf. Vorms 1976). In detail a core of alkali feldspar of uniform composition now exists, containing raft-like inclusions of plagioclase generally in optical (and possibly physical) continuity with each other (Fig. 2.4). This core may be partly or almost completely surrounded by a relatively sodic rim of plagioclase which tends to be in optical continuity with the plagioclase inclusions in the core (Fig. 2.4).

Alkali feldspar megacrysts with zonal, euhedral dimensionally oriented plagioclase inclusions have been interpreted to be of early magmatic phenocryst origin (Hibbard 1965; Kerrich 1969; Higgins & Kawachi 1977). However, the plagioclase inclusions in FGG2 alkali

feldspar megacrysts are not euhedral and are not dimensionally oriented. Conversely mantled alkali feldspar megacrysts have been attributed to low pressure (ca. 2 Kbar) pressure quench (Cherry & Trembath 1978), decompression crystallisation (Whitney 1975) or H_2O - activity controlled sequential crystallisation (Tuttle & Bowen 1958). However the rapakivi-like rims of this study, in detail do not have the appearance of mantles, but rather are interpreted to be the result of late - stage disequilibrium replacement reactions. The textural relations are interpreted to suggest disequilibrium between early formed plagioclase phenocrysts and residual alkali feldspar-rich liquid so that a replacement reaction took place. It is thought likely that the potential for reaction and replacement was greater for the less sodic cores of plagioclase phenocrysts so that they were replaced in preference to the rims, leading to the preservation of the rim with its now rapakivi like appearance.

The feldspar relations thus suggest an early period of near-equilibrium crystallisation of plagioclase from the melt, followed by a later period of disequilibrium reaction between plagioclase phenocrysts and residual potassic liquid. It is interesting to note that Giles (1980b) interprets the petrography and geochemistry of some post-tectonic rhyodacites in the Gawler Range Volcanics of the Gawler domain in terms of "mixing of a high- K_2O residual liquid with cumulate crystals of plagioclase, cpx and magnetite".

The quartz + feldspar matrix of FGG2 and the occurrence of minor phases such as biotite, hornblende, Fe - Ti oxide, zircon and apatite are similar to those in FGGL.

(4) Eulitic alkali feldspar granite gneiss, EAGG

Most specimens of EAGG show advanced subsolidus recrystallisation but relict phenocrysts of orthoclase microperthite, oligoclase, and quartz are recognised. The subordinate ferromagnesian minerals are present in small clot-like aggregates of eulite + magnetite + feldspar + quartz, the significance of which is discussed below.

The EAGG is interpreted to represent a highly evolved and fractionated residual liquid consisting dominantly of alkali feldspar and quartz.

(5) Granite gneisses 1 and 2, and Alkali feldspar granite gneiss

Because of their ubiquitous subsolidus recrystallisation, these rocks exhibit only rare relict igneous mineralogical or textural features. In all three however, relict feldspar phenocrysts may be observed.

In particular moderately deformed GG2 at Fisherman's Point (Fig. 1.2) contains alkali feldspar megacrysts up to 1.5 cm diameter, with partially preserved plagioclase rims and raft-like inclusions (Fig. 2.4), identical to those observed in FGG2 elsewhere. At other localities GG2 shows these alkali feldspar megacrysts much more poorly preserved. This observation is one of the crucial petrographic links relating the opx-granitoids to the granite gneisses of the study area.

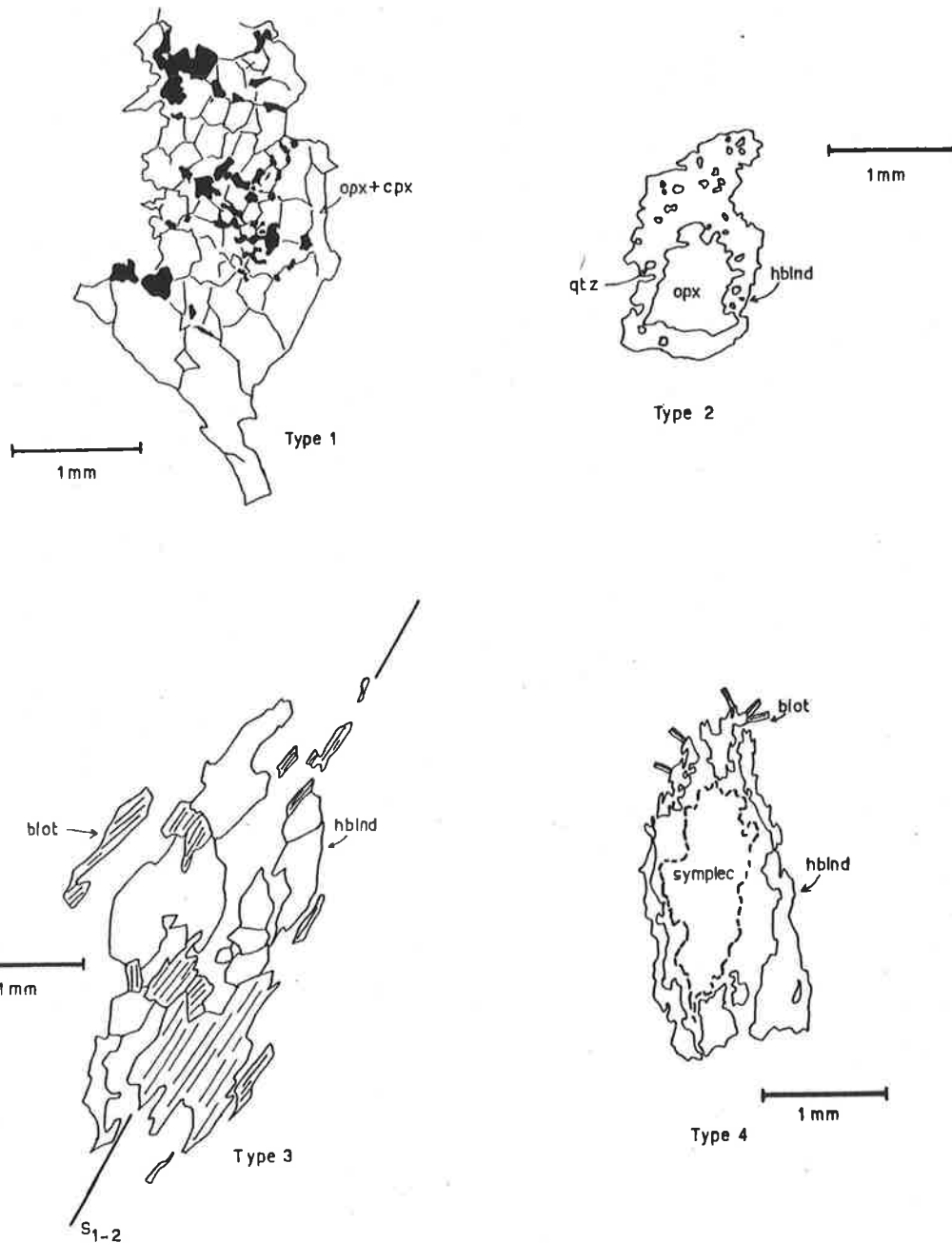
(6) Summary

The intrusive sequence from QGNG to FGG1 and FGG2, and to EAGG is reflected in regular petrographic and mineralogical trends towards a higher content of quartz and alkali feldspar suggestive of fractional crystallisation of plagioclase, pyroxene and latterly alkali feldspar from a liquid initially not saturated in alkali feldspar. Such a liquid would necessarily be a non-minimum granitoid melt, possibly of approximately quartz dioritic composition. This model will be refined as more information is derived in following sections.

2.2.2.2 Secondary metamorphic features

Subsolidus metamorphic textural features are ubiquitous throughout the DGS. Detailed petrographic studies have revealed that considerable variation exists within the recrystallised rocks, some of local and some of regional importance. It will be shown below that in some localities recrystallisation involved considerable growth of new minerals due to the influx of retrogressive fluids, but that elsewhere no retrogression occurred during recrystallisation. These variations are conveniently described under four main headings which are summarised in Table 2.2, and described below in detail.

It is important to recognise that these four main types are somewhat arbitrary and erected principally for ease of description. The boundaries between Types 1, 2 and 3 are gradational, and each may overprint the preceding type so that some specimens and localities show poly-type textures. In addition Type 4 is of local extent only at



Characteristic features of sub-solidus texture types in Donington Granitoid Suite.

- Type 1: recrystallised aggregates opx + cpx (specimen B200)
- Type 2: partial marginal replacement of opx by amphibole corona (specimen D24)
- Type 3: complete replacement of opx by amphibole and development of tectonite fabric (specimen S₁₋₂)
- Type 4: symplectitic pseudomorphing of opx by actinolite and quartz (specimen A88)

Figure 2.5

MacLaren Point where it overprints Type 2.

Regionally, there is a general gradation from east to west, from category 1 to category 3 as the KMZ is approached (Fig. 2.2). This has been interpreted above to suggest that the mylonite zone exerts a strong control on the distribution and extent of retrogression.

(1) Type 1

Rocks illustrating petrographic type 1 have recrystallised polygonal mosaic opx + cpx without the prominent development of either hornblende or metamorphic tectonite fabrics (Table 2.2).

In QGNG considerable nucleation and growth of sub-grains within the pyroxene phenocrysts has resulted in mosaics preserving the approximate outline of the phenocrysts. During this polygonisation the exsolved ilmenite platelets have coalesced into aggregates and discrete grains interstitial to the recrystallised pyroxenes (Fig. 2.5). In addition the polygonal opx grains often exhibit fine scale lamellae of exsolved cpx parallel to (100) suggesting this feature observed in the relict phenocrysts may have developed during late metamorphic cooling, rather than initial cooling from the solidus to the prevailing regional geotherm.

Plagioclase phenocrysts may show similar sub-grain development.

In FGG1 and FGG2 recrystallised polygonal mosaic aggregates of feldspar, quartz and opx are common. In addition microperthitic relict alkali feldspar phenocrysts may show enhanced development of exsolution blebs and stringers.

In EAGG the clot-like aggregates of opx, magnetite, feldspar and quartz with polygonal mosaic textures are interpreted to have developed at a similar time and under similar conditions as the features above. These aggregates will be re-examined below in the light of experimental data on the pressure-sensitive relationship between iron-rich olivine and opx.

These features are considered to point to a period of high-temperature, granulite facies, recrystallisation of the DGS. Rocks in the Cape Donington to Spalding Cove section and the Boston Point locality are particularly illustrative of this petrographic type. The only minor development of hornblende and tectonite fabrics at these localities suggests that there was limited access of fluids, in particular H₂O, and limited deformation manifested in these localities, and it will be suggested below that these two factors are related.

(2) Type 2

Rocks illustrating petrographic type 2 have developed abundant hastingsitic hornblende partially replacing opx, but without the development of prominent metamorphic tectonite fabrics (Table 2.2, Fig. 2.5).

In FGG1 well crystallised hornblende may occur, poikiloblastic with respect to quartz and containing relict corroded inclusions of opx (Fig. 2.5). In many cases the hornblende forms only narrow rims or small patches in or around opx grains. Biotite may be associated with the hornblende. In addition relict alkali feldspar phenocrysts may show prominent perthitic exsolution and development of microcline twinning and sphene coronas may surround Fe - Ti oxide.

These features are interpreted to manifest the retrogressive influx of fluids, but in the absence of strong deformation, and are particularly well illustrated by rocks from the Cape Euler locality.

(3) Type 3

Rocks illustrating petrographic type 3 have developed hornblende and biotite to the total exclusion of pyroxene, and have prominent metamorphic tectonite fabrics (Table 2.2, Fig. 2.5).

In GG1, GG2 and to a lesser extent AGG, the secondary metamorphic minerals and textures give only few clues to the pre-metamorphic nature of the rock. In GG2 at Kirton Point ovoidal, recrystallised aggregates of feldspar (+ quartz) and hornblende and biotite lie in a prominent S_{1-2} fabric which is crenulated by F_3 with some S_3 development (Fig. 1.7A,B; Chapter 1). However in GG2 at Fisherman's Point (Fig. 1.2) rapakivi - like alkali feldspar megacrysts (Fig. 2.4C) occur, very similar to those in FGG2, and suggest that the protolith of GG2 gneisses was FGG2. Whereas the lower degree of deformation at Fisherman's Point allowed preservation and recognition of the megacrysts, at Kirton Point total D_{1-2} recrystallisation has obliterated the relict textures.

Rocks typical of type 3 are well developed at Kirton Point and in outcrop adjacent to the Kalinjala Mylonite Zone and are interpreted to demonstrate the spatial control of both retrogression and deformation adjacent to the mylonite zone. Furthermore it has been shown that the S_{1-2} fabric is manifested by retrogressive mineral assemblages indicating retrogression occurred early in the Kimban Orogeny. This in turn ties the spatial control of retrogression by the KMZ into the

chronology of events and suggests the mylonite was a zone of activity from at least as early as D_2 and probably D_1 .

This last conclusion is in contrast to Parker (1980) who states that the KMZ is a D_3 structure.

The conclusion crucial to later geochronological and geochemical arguments that emerge from this discussion is that the KMZ exerted a major spatial and temporal control on deformation and the influx of retrogressive fluids from at least as early as D_2 (and probably D_1).

(4) Type 4

Rocks illustrating petrographic type 4 have decussate biotite and symplectitic aggregates of ferroactinolite and quartz as the main ferromagnesian minerals, and have no tectonite fabrics (Table 2.2).

In FGG1 at MacLaren Point symplectitic ferroactinolite and quartz replace opx and are surrounded by hastingsitic hornblende coronas relict from type 2 (Fig. 2.5). In addition decussate biotite is present and prominent microcline twinning in alkali feldspar relict phenocrysts.

In AGG at Carcase Rock diffuse patchy retrogradation has resulted in the conversion of the opx + magnetite + feldspar aggregates of EAGG into haematite + feldspar + ragged decussate biotite aggregates.

These features are interpreted to post-date the main metamorphic and deformational events represented by Types 1, 2 and 3 and are thought to be due to local contact retrogression induced by intrusion of a late granitoid similar in appearance to the Moody Granitoid Suite, in the MacLaren Point area (Fig. 1.2).

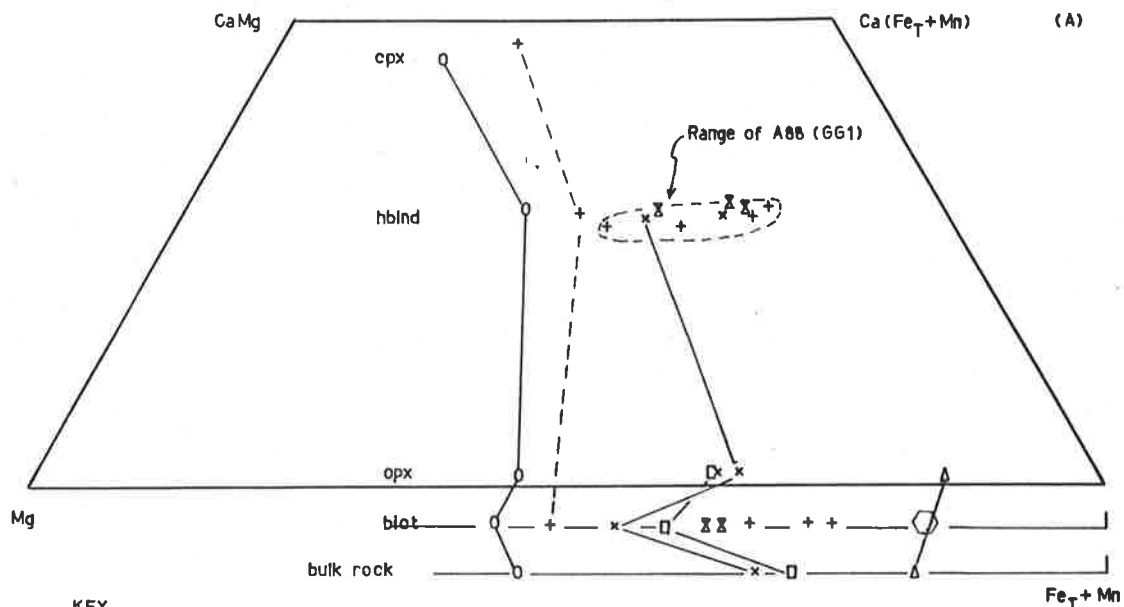
(5) Summary

The thrust of this description of subsolidus variation within the DGS has been to establish that after initial consolidation of the differentiated suite of opx-granitoids, early in the Kimban Orogeny a zonal distribution of retrogressive assemblages was produced in temporal coexistence with recrystallised pyroxenic assemblages. The retrogressive assemblages have been proposed to be due to the influx of fluids, principally H_2O , adjacent to (and along) the Kalinjala Mylonite Zone.

2.3 MINERAL CHEMISTRY, IGNEOUS CRYSTALLISATION AND METAMORPHISM

2.3.1 Pyroxenes

Pyroxenes within the DGS occur either as extensively exsolved relict phenocrysts or recrystallised polygonal mosaic aggregates, both



- KEY**
- QGGG
 - × FGG1
 - FGG2
 - △ EAGG
 - +
 - ⊗ GG2
 - ⬡ AGG

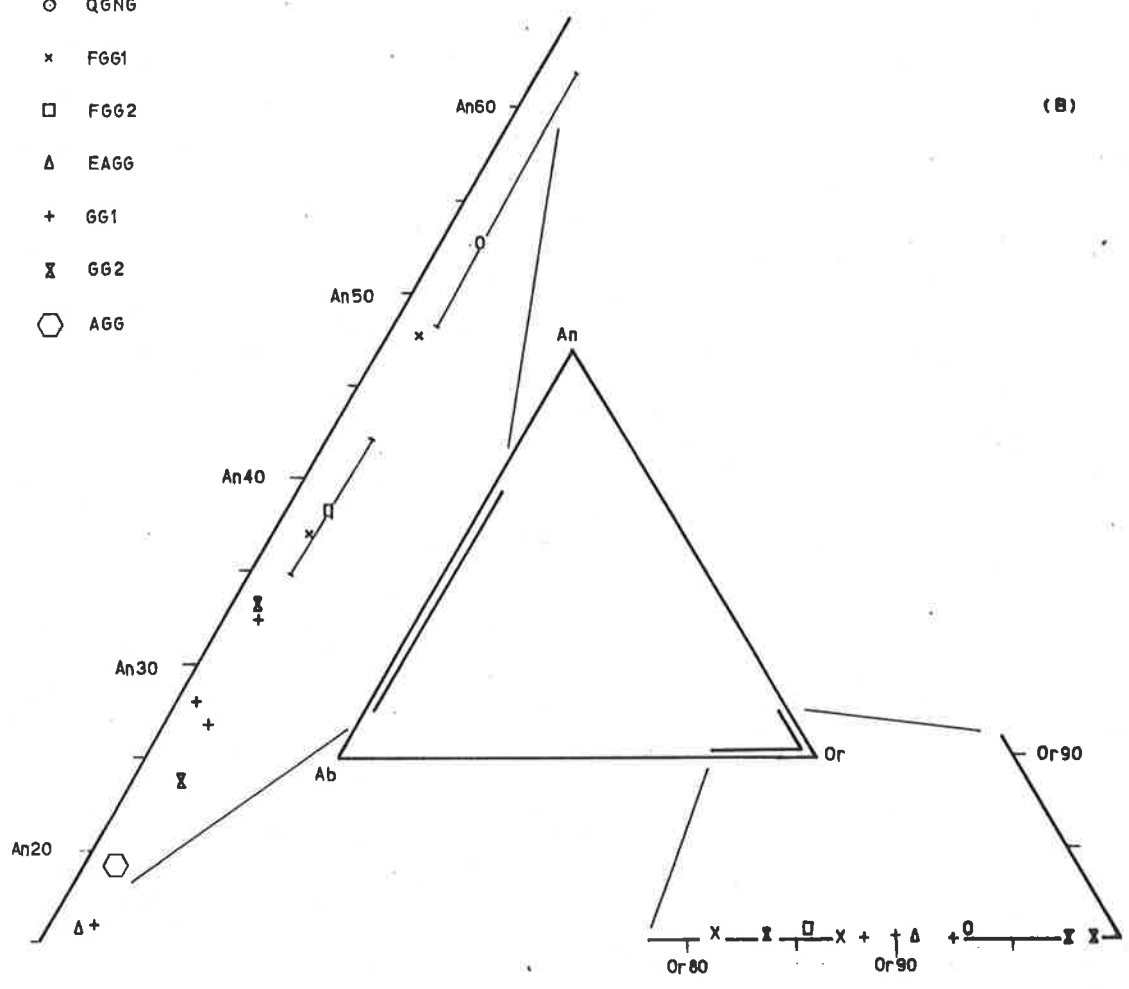


FIGURE 2-6
 Donington Granitoid Suite minerals.
 (A) Ferromagnesian minerals and bulk rocks plotted on Ca-Mg-Fe+Mn quadrilateral.
 (B) Feldspars plotted on An-Ab-Or diagram.

types frequently occurring within the same thin section. The fine scale lamellar exsolution was not resolved by the electron microprobe, so that analyses presented in Appendix Table 2.1 and Fig. 2.6 represent recrystallised mosaic grains, relict phenocryst hosts to coarse exsolved blebs or a combination of host and fine scale lamellae.

Pyroxenes within the DGS become more iron-rich from QGNG through to EAGG (Fig. 2.6), paralleling the changing bulk rock composition (see later). The pyroxenes plot in the fields of metamorphic pyroxenes as indicated in the literature for selected granulite facies terrains (viz., Broken Hill, N.S.W., Binns 1962; Madras, Leelanandam 1967; Weaver et al. 1978; Adirondacks, Bohlen & Essene 1978). The compositions of DGS pyroxenes thus suggest equilibration during initial exsolution and recrystallisation under granulite facies conditions of metamorphism.

The pyroxene geothermometers of Wood & Banno (1973) and Wells (1977), have been applied to coexisting opx and cpx in QGNG, resulting in calculated temperatures of ca. 845°C and ca. 885°C by the respective methods (Table 2.3). Not only are these values very similar to those calculated for other granulite terrains (see compilation in Weaver et al. 1978), but they are identical to calculations made on mafic granulitic rocks included in the DGS and intruding the DGS as dykes (Chapter 6).

Accuracy of the pyroxene geothermometers is limited by inexact knowledge of the pyroxene solvus, especially with respect to the effect of minor elements. Wood (1975), Hewins (1975) and Wilson (1976) suggest that the Wood & Banno (1973) method overestimates temperatures by ca. 60°C, and Wood & Banno (1973) suggest that accuracy is limited to ca. 50°C. Hence the temperature of subsolidus equilibration of QGNG coexisting pyroxenes can be constrained approximately at 800°C - 900°C.

Further constraints on the conditions of metamorphic equilibration of DGS pyroxenes are suggested by the polygonal mosaic aggregates of opx + magnetite + feldspar in EAGG. Wheeler (1965), Nilsen (1973) and Ormaasen (1977) suggest that the intimate association of opx + magnetite in silicic charnockitic rocks is due to the decomposition of original fayalitic olivine. In a quartz-bearing rock at high pressure and temperature eulitic opx and fayalitic olivine may be involved in a pressure sensitive equilibrium (Smith 1971, 1972). Furthermore, based on the compilation of experimental data by Jaffe et al. (1978; Fig. 2.7), the absence of pigeonite and the absence of

fayalite + quartz in favour of opx + magnetite, where the opx has the composition Fs_{85} (Appendix Table 2.1), requires pressure in excess of 8 Kbars at the temperatures suggested above (Table 2.3).

Thus metamorphic pyroxenes in the DGS in the Cape Donington to Carcase Rock area suggest equilibration at temperatures of $800^{\circ}C$ - $900^{\circ}C$ at pressures in excess of 8 Kbars. These results were obtained from rocks of subsolidus petrographic Type 1 not showing prominent metamorphic tectonite fabrics and are suggested to represent early metamorphic conditions coeval with D_{1-2} .

2.3.2 Feldspars

Microprobe analyses of relict plagioclase phenocrysts show that average compositions become less calcic from QGNG through to EAGG (Appendix Table 2.1, Fig. 2.6), paralleling the bulk rock geochemical compositional variation (see later). Furthermore original igneous zoning is preserved.

Relict alkali feldspar phenocrysts are perthitic, and although the exsolution blebs and lamellae are not fully resolved by the microprobe, the compositions tend to reflect subsolidus temperature conditions (Table 2.3, Fig. 2.6).

Neglecting the zoning within the feldspar phenocrysts and recrystallised grains, it is possible to calculate approximate temperatures for coexisting plagioclase and alkali feldspar (Table 2.3). These range from ca. $505^{\circ}C$ to $790^{\circ}C$ for the opx-granitoids and ca. $505^{\circ}C$ to $571^{\circ}C$ for the granite gneisses. Specimen A107 from a D_3 shear zone records a temperature of ca. $550^{\circ}C$. From these results it would appear that averaged feldspar compositions may be giving a guide generally to late stage subsolidus equilibration, at least in one instance in D_3 .

2.3.3 Iron-titanium oxides

Magnetite and ilmenite occur throughout the DGS as discrete grains, or with other ferromagnesian phases, sometimes with textures suggesting the oxide was exsolved from e.g. pyroxene phenocrysts (see above). Textures in reflected light suggest subsolidus metamorphic equilibration reflecting external granule exsolution (Buddington & Lindsley 1964) from a primary ilmenomagnetite solid solution.

The compositions of coexisting magnetite and ilmenite, recalculated from microprobe data by the method of Carmichael (1967),

Table 2.3: Donington Granitoid Suite geothermometry and geobarometry

Method	T ^o C	P Kbar	Comments
<u>opx-granitoids</u>			
opx + cpx Wood & Banno (1973)	845		Type 1 texture
biot + kspar + mag Wones & Eugster (1965)	800-925	(?)	-log a ₀ ₂ = 12-17
plag + kspar Powell & Powell (1977)	505-790	(10)	zoning neglected
mag + ilm Powell & Powell (1977)	435-615		-log a ₀ ₂ = 18.2-26.9
Fe-opx	(800-900)	>8	type 1 texture
<u>Granite gneisses</u>			
biot + kspar + mag Wones & Eugster (1965)	750-880	(?)	-log a ₀ ₂ = 12-18
plag + kspar Powell & Powell (1977)	505-570	(10)	
mag + ilm Powell & Powell (1977)	510		-log a ₀ ₂ = 21

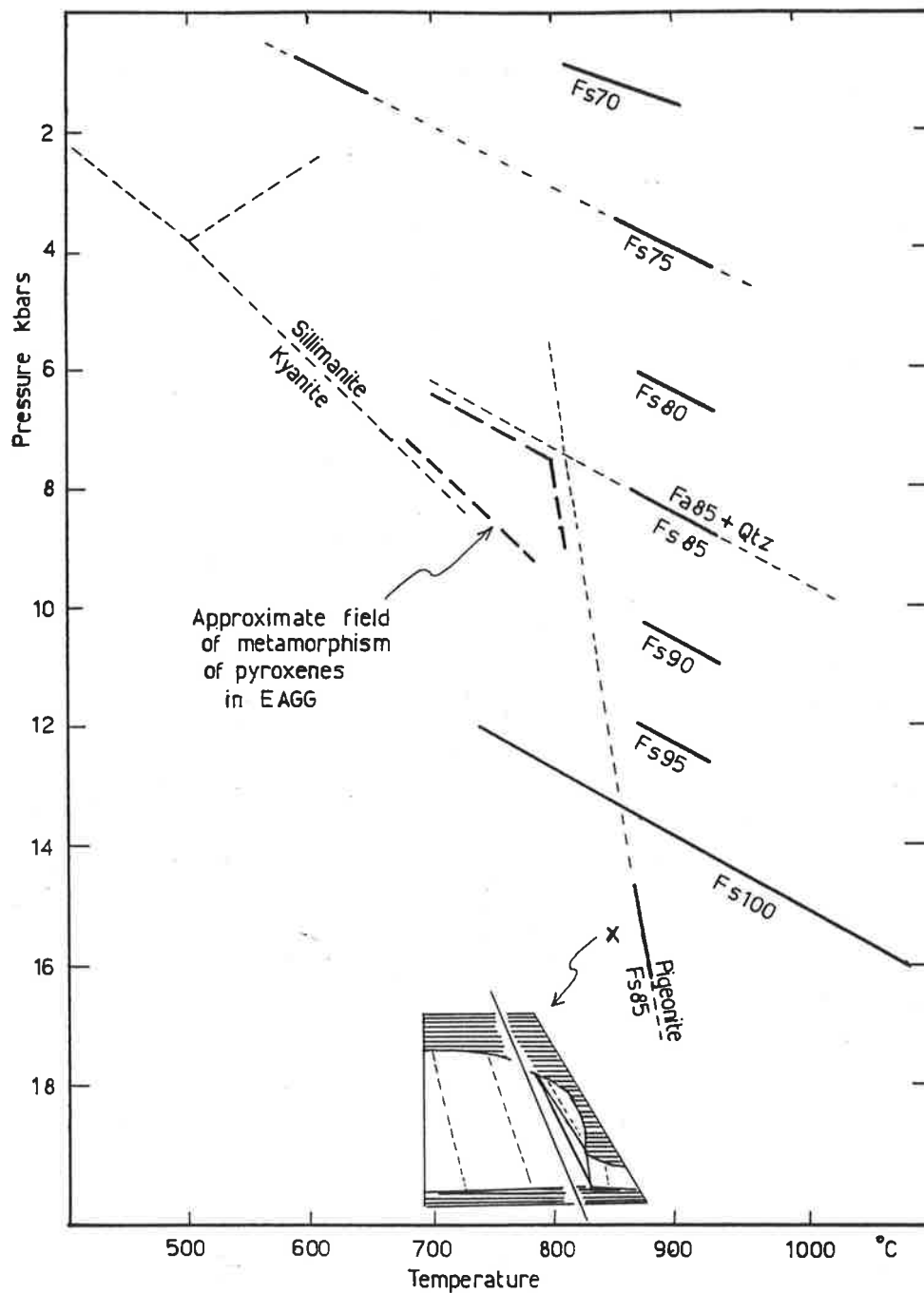


Figure 2.7

Constraints placed on subsolidus recrystallisation of eulitic opx in EAGG by experimental data on Fe-rich pyroxene-olivine system; modified after Jaffe et al. (1978).

are presented in Appendix Table 2.1. The oxygen fugacity and temperature of equilibration has been calculated by the method of Powell & Powell (1977) and plotted on Fig. 2.8. The magnetite-ilmenite pairs in DGS rocks from the Spalding Cove to Carcase Rock section have equilibrated down to very low temperatures of 400°C - 600°C (Table 2.3) at oxygen fugacities around the NNO and FMQ buffers (Eugster & Wones 1962). These results are similar to those for plutonic igneous and metamorphic rocks in many geological situations (cf. Whitney & Stormer 1976; Himmelberg & Ford 1977; Weaver et al. 1978), and illustrate the susceptibility of opaque oxides to low temperature equilibration.

2.3.4 Amphiboles

Amphiboles occur in almost all DGS rock types and range from magnesian hastingsitic hornblende in QGNG, GGL & GG2 through magnesian hastingsite in FGGL and GGL, and hastingsitic hornblende in GGL to edenitic hornblende, ferrohornblende and ferroactinolite in GGL (Fig. 2.6, 2.9; Appendix Table 2.1).

FGGL and QGNG amphiboles exhibit clear correlation in Mg/Mg + Fe with the bulk rock composition. The Type 1 and Type 2 subsolidus textures in these rocks suggest the amphibole compositions manifest either late magmatic or high-grade subsolidus conditions.

Amphiboles in GGL and GG2 Type 3 subsolidus textures show a similar range in Mg/Mg + Fe but lower $(Na + K + Al)/4$ (Fig. 2.9) and are suggested to manifest slightly lower grade retrograde D_{1-2} conditions not grossly different from QGNG and FGGL Type 1 and Type 2 textures.

Specimen A88 (GGL) also shows Type 4 subsolidus textures and amphiboles manifesting these (Fig. 2.9) are ferrohornblende to ferroactinolite and clearly of lower grade composition. These lower grade conditions may either be due to contact retrogression (see above) or late tectonic decompression during uplift.

2.3.5 Biotites

Biotites in the DGS show a compositional correlation with the bulk rock compositional variation (Fig. 2.6; Appendix Table 2.1). Comparison with the experimental results of Wones & Eugster (1965) suggests the biotites may have crystallised at temperatures ranging from ca. 750°C to 925°C at $\log a_{O_2}$ ranging from -13 to -17 (Fig. 2.8; Table 2.3). These conditions are appropriate for the early high-grade subsolidus equilibration of the DGS.

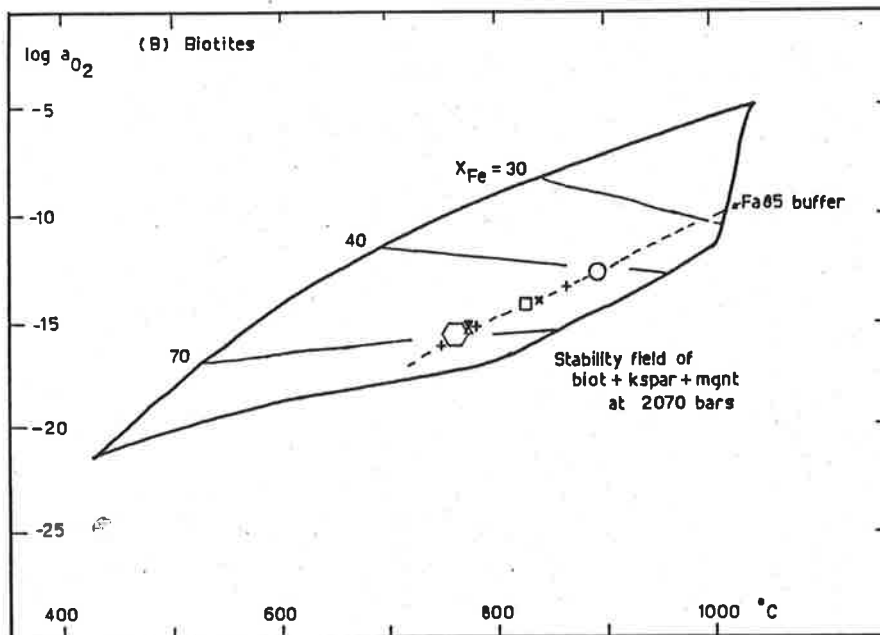
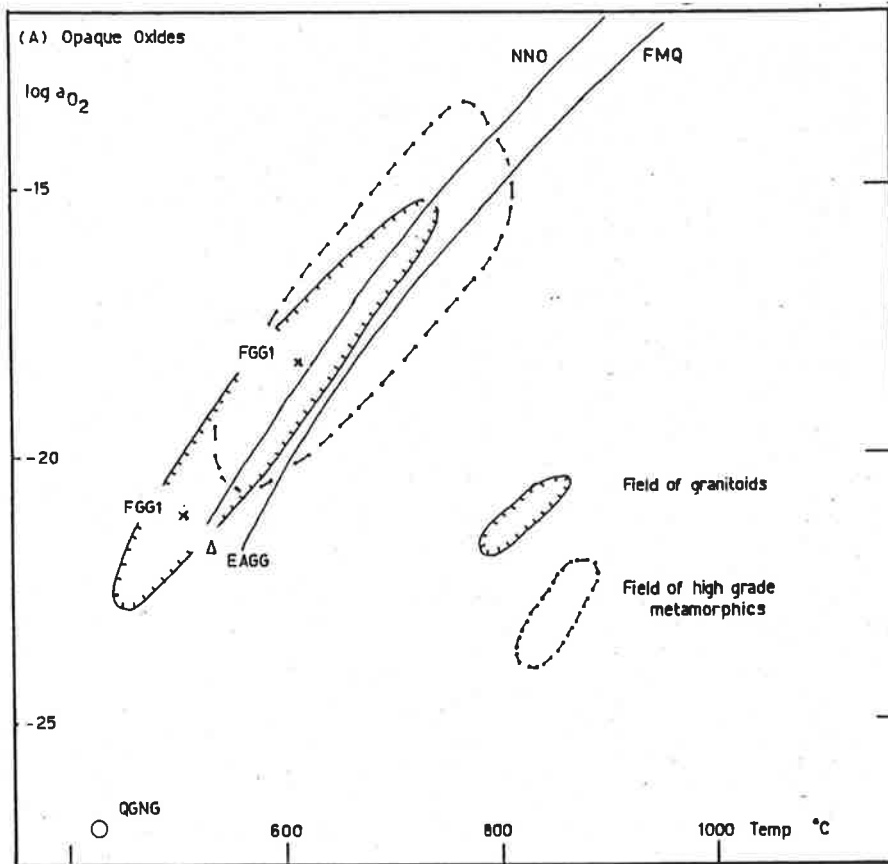


Figure 2.8 Upper: Comparison of coexisting magnetite and ilmenite $\log a_{O_2}$ - T data from DGS with fields of granitoids and high-grade metamorphic rocks.

Lower: Fe-content of biotites in DGS compared with experimental data of Wones & Eugster (1965).

Mineral symbols as in Figure 2.6.

2.3.6 Conditions of metamorphism

Results obtained from coexisting pyroxenes, coexisting feldspars and coexisting opaque oxides, when combined with petrographic and field data, allow some comments to be made concerning Kimban metamorphism on south eastern Eyre Peninsula.

- (1) Petrographic Type 1 rocks recrystallised early in the Kimban Orogeny in the granulite facies, presumably during D_{1-2} , and contain pyroxenes suggesting temperatures of $800^{\circ}\text{C} - 900^{\circ}\text{C}$ at pressures in excess of 8 Kbars.
- (2) Petrographic Type 3 rocks retrogressed early in the Kimban Orogeny, adjacent to the Kalinjala Mylonite Zone, during D_{1-2} manifest amphibolite facies assemblages which are coeval with the adjacent granulite facies assemblages.

Points (1) and (2) combine to suggest that retrogression may be related more to a local control adjacent to a major tectonic lineament, rather than to geothermal gradient variation, analogous to the conclusions of Beach (1976) and Beach & Tarney (1978).

- (3) Coexisting feldspars in a local D_3 shear zone suggest equilibration at ca. 550°C . This may be a true reflection of a decline in geothermal gradient in D_3 , or may indicate that feldspars equilibrate down to lower temperatures during cooling than do pyroxenes.
- (4) Coexisting opaque oxides throughout the opx-granitoids and granite gneisses equilibrated at temperatures of ca. $400^{\circ}\text{C} - 600^{\circ}\text{C}$, irrespective of the subsolidus history of the host rock. This suggests that the oxide phases do not record any specific metamorphic event but simply reflect late cooling of the plutonic complex. However the oxygen fugacities consistent with the NNO and FMQ buffers are similar to a large variety of plutonic and volcanic rocks.
- (5) Late, local, contact retrogressive metamorphism of low grade is recorded in rocks from the MacLaren Point to Carcase Rock section.

2.3.7 Conditions of primary igneous crystallisation

Although many magmatic features of the DGS have been obscured by recrystallisation and retrogression, it is possible to make some inferences concerning the conditions of primary igneous crystallisation.

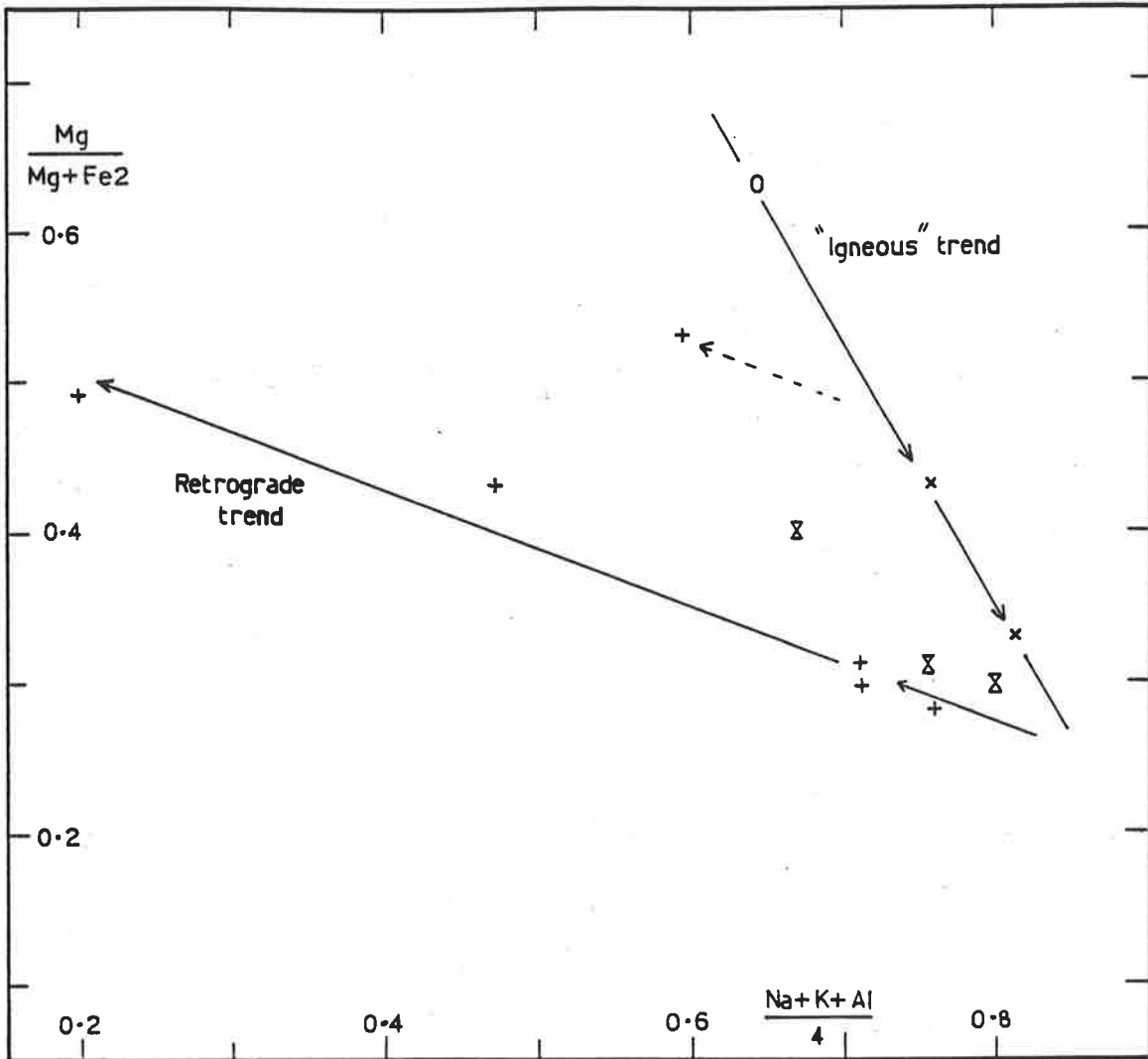


Figure 2.9

Donington Granitoid Suite amphibole compositions showing contrasted high-grade metamorphic or "igneous" trend and retrograde compositional variations. Symbols as in Figure 2.6.

Exsolution features in QGNG pyroxene phenocrysts are instructive viz,

- (1) Exsolved ilmenite platelets in the cores of cpx phenocrysts suggest early Ti-enrichment in cpx, which has been interpreted to indicate rapid crystallisation (e.g. in oceanic volcanics, Coish & Taylor 1979).
- (2) Coexisting subsolidus pyroxenes suggest a minimum temperature of igneous crystallisation of 800°C - 900°C .
- (3) Exsolved cpx blebs sub-parallel to (100) and lamellae parallel to (100) in opx phenocrysts resemble Bushveld - type or Kintoki - San - type of Ishii & Takeda (1974) and suggest primary igneous crystallisation below or just above the pigeonite inversion temperature. Comparison with the data of Ross et al. (1973), Ross & Huebner (1975), Robinson et al. (1977) and Bohlen & Essene (1978) suggests that there is only minimal tie-line rotation on the pyroxene quadrilateral (Fig. 2.6) during exsolution and recrystallisation so that the primary igneous opx in QGNG is estimated to have been ca. Fs_{40-42} . The pigeonite inversion temperature for such an opx is ca. 1050°C (Brown 1972) so that this is an upper temperature limit for primary igneous crystallisation.

Points (1) and (3) combine to suggest that QGNG represents an early rapidly crystallised, possibly chilled phase of the DGS, crystallised from a liquid at temperatures around 1050°C .

Furthermore the opx + magnetite aggregates in EAGG are almost certainly subsolidus breakdown products of a primary igneous fayalitic olivine. Similar features observed by Ormaasen (1977) were used to constrain the maximum pressure of igneous intrusion of charnockitic rocks in Norway by assuming that the $\text{Fe}/(\text{Fe}+\text{Mg})$ of primary fayalite exceeds or is equal to the same ratio in secondary opx. In this way the curve on Fig. 2.7 used to estimate the minimum pressure of subsolidus equilibration of opx in EAGG may also be used to estimate the maximum igneous crystallisation pressure of the primary fayalite, if the upper temperature limit for QGNG opx of 1050°C is assumed. A maximum pressure of igneous intrusion of ca. 11 Kbar is thus estimated.

In addition Ormaasen (1977) cites experimental work by Nowgorodov & Shkodzinsky (1974) on a granite very similar in bulk rock composition to EAGG (Appendix Table 2.2). If the

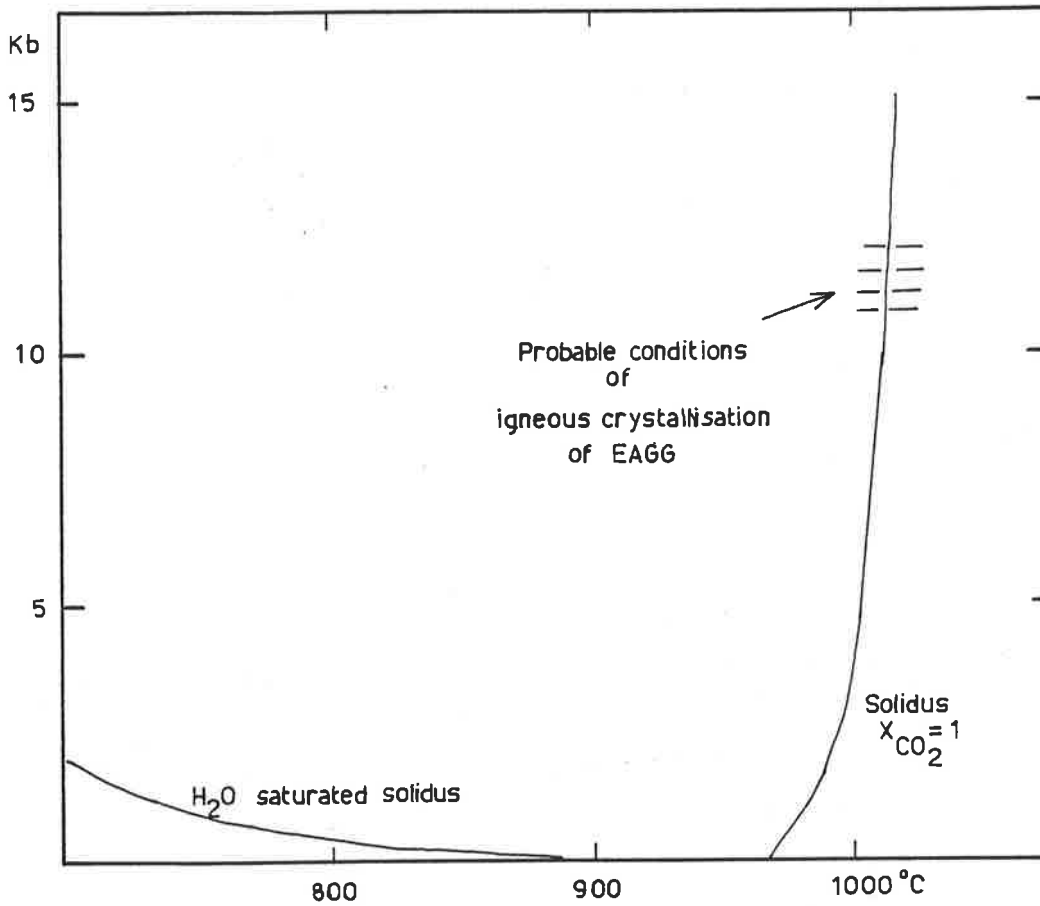


Figure 2.10

Experimentally determined solidus curves for alkali granite similar in composition to EAGG in presence of H₂O and CO₂ fluids, showing estimate of igneous crystallisation conditions for EAGG. Modified from Nowgorodov & Shkodzinsky (1974).

EAGG solidified at ca. 1000°C and 11 Kbar, the experimental solidus curves suggest the likely fluid present to be rich in CO₂ but poor in H₂O (Fig. 2.10). Reconnaissance studies of primary fluid inclusions in FGG2 identified CO₂-rich inclusions, the densities of which suggest original pressures of formation in excess of 10 Kbar at 1000°C (Appendix A2). Hence it is suggested that the DGS opx-granitoids have been poor in H₂O, but relatively rich in CO₂, right throughout their crystallisation interval, which further suggests that the H₂O-rich fluids responsible for the early D₁₋₂ retrogressive activity did not have their origin within the DGS.

It is interesting to note here that both the primary igneous intrusion and subsolidus cooling of the DGS opx-granitoids apparently took place at ca. 8-11 Kbar under near isobaric conditions.

In contrast to the probably chilled QGNG, minimally zoned, large cumulate plagioclase phenocrysts in FGG2 suggest prolonged growth in near equilibrium conditions. In addition, feldspar replacement textures in FGG2 suggest marked late stage disequilibrium conditions.

These observations are combined in a model of igneous crystallisation of the DGS opx-granitoids involving initial intrusion and chilling of a batholithic mass of dry quartz dioritic bulk composition, resulting in an accreted carapace of QGNG. Subsequent thermal insulation by this carapace allowed prolonged near equilibrium crystallisation and accumulation of plagioclase phenocrysts and production of residual progressively more silicic and potassic liquids. Periodic separation of residual liquids (FGG1, EAGG) from crystallised solids (FGG2), possibly by filter pressing (Propach 1976) under the action of tectonic pulses, resulted in upward intrusion of successive phases of the DGS and piercing of the QGNG carapace. Late stage disruption of FGG2 and introduction of residual potassic liquid may have resulted in the development of the feldspar replacement textures.

Some additional support for this model is found in the observation that QGNG only outcrops on Cape Donington where it contains abundant gneissic xenoliths of the MBG which may indicate proximity to an original roof or marginal zone.

This model would ascribe the bulk rock geochemical compositional variations within the DGS opx-granitoids essentially to fractional crystallisation processes.

2.3.8 Intrusive analogues of the opx-granitoids

The Palaeozoic Inlet Quartz Monzonite (Chappell 1978) and Mesozoic

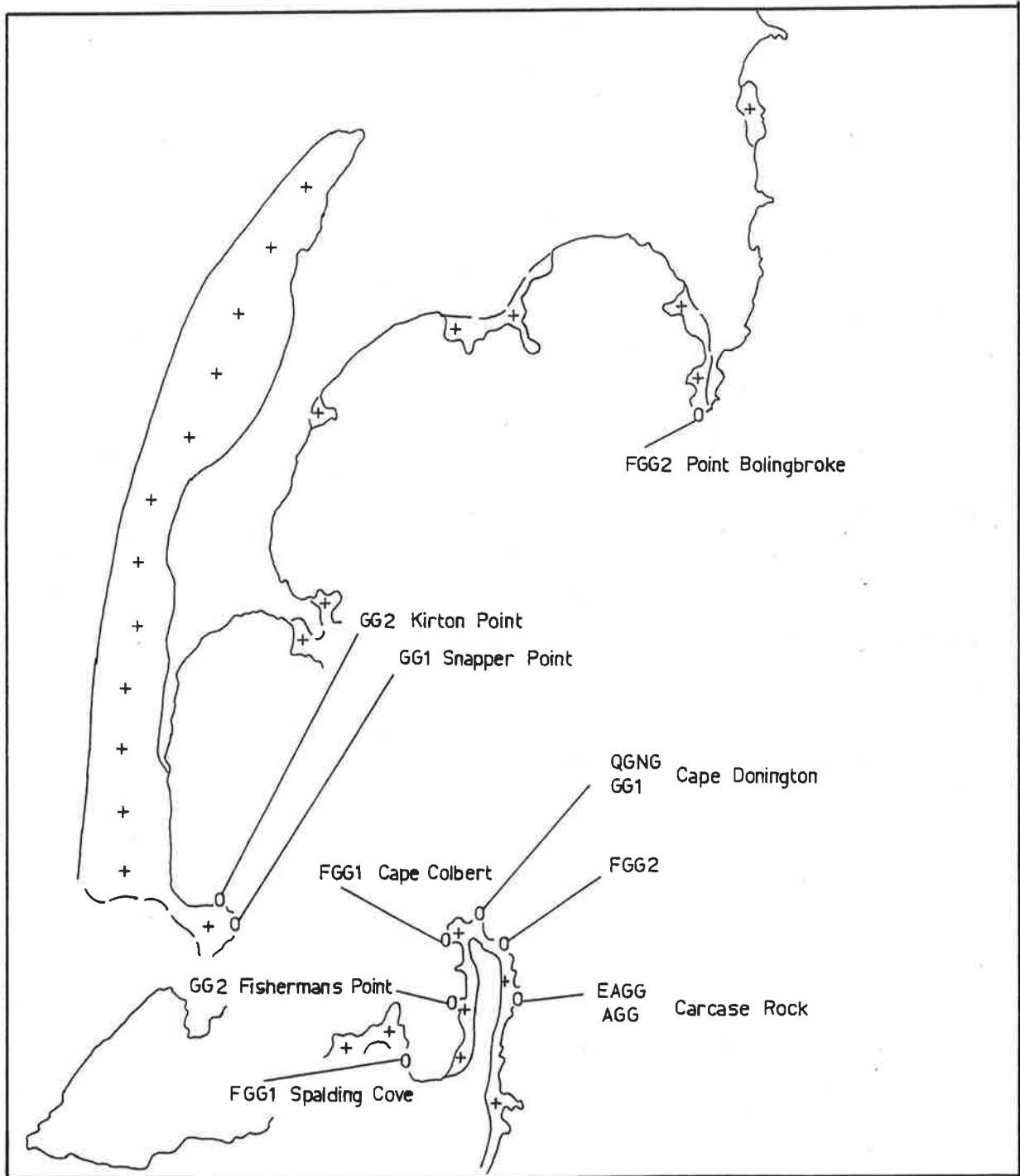


Figure 2.11

Locality diagram for geochronological specimens of Donington Granitoid Suite.

Tuolumne Intrusive Series (Bateman & Chappell 1979) comprise two intrusive analogues of the DGS opx-granitoids. In both of these the respective authors propose that a non-minimum melt has undergone protracted fractional crystallisation, resulting in zoned plutons. The outermost contact zone is most mafic and interpreted to represent an accreted cumulate carapace precipitated during initial chilling. Subsequent intrusive phases show regular mineralogical and compositional variations, and pierce earlier intrusive phases and the mafic carapace. Much of this detail is preserved in the DGS, although tectonism has obscured, in part, the zonation.

Of relevance to this model for the DGS opx-granitoids is experimental work by T.H. Green (1969a, 1969b, 1972) on liquids of quartz dioritic composition. Plagioclase is the major liquidus phase in near anhydrous liquids at pressures ca. 10 Kb, and is joined by pyroxenes at temperatures ca. 30°C lower. The liquidus temperature at this pressure is ca. 1100°C for quartz diorite liquid with ca. 2 wt.%H₂O. Calculated fractionation trends by Green (1969a) are capable of generating plagioclase + pyroxene enriched solids and residual silicic and potassic liquids.

This model for the interrelationship of the opx-granitoids of the DGS will be tested below on the basis of major and trace element geochemical data.

2.4 GEOCHRONOLOGY

2.4.1 Rb-Sr total-rock geochronology

2.4.1.1 Introduction

A previous study of the granite gneisses (GG1) of Snapper Point (Fig. 2.11) has been reported by Flook (1975) and Cooper et al. (1976). (Note: The actual locality of the geochronological samples was misnamed Kirton Point by these authors). Normalisation and regression of their data by the present author yielded a poor fit isochron with Model 2 solution of 1813 ± 23 Ma and initial 87Sr/86Sr ratio (henceforth IR) of 0.7043 ± 17 (regression 6, Table 2.5, Fig. 2.12B). This age was interpreted as an age of primary magmatic crystallisation by Flook (1975) and Cooper et al. (1976).

This result will be compared in the following sections with data from the opx-granitoids and granite gneisses collected by the present author. The sample localities are depicted in Fig. 2.11 and the experimental techniques are described in Appendix A1.

Table 2.4 Donington Granitoid Suite Opx - granitoids
Rb-Sr isotopic data

Sample name	Rb ppm	Sr ppm	Rb/Sr	87Rb/86Sr	*87Sr/86Sr
<u>Quartz gabbro-norite gneiss</u>					
468-B200	93	230	0.39	1.130	0.73470
468-B205	97	240	0.41	1.175	0.73602
468-B203	97	229	0.42	1.231	0.73753
468-B201	102	231	0.44	1.289	0.73871
468-B206	113	217	0.52	1.509	0.74501
468-B202	117	217	0.54	1.561	0.74657
<u>Ferrohypersthene granite gneiss 1</u>					
515-B25	207	167	1.24	3.612	0.79949
515-B143	201	171	1.18	3.439	0.79508
515-B149	211	153	1.38	4.039	0.81060
515-B144	223	155	1.44	4.198	0.81585
515-B146	231	152	1.52	4.443	0.82171
515-B147	237	140	1.69	4.963	0.83474
515-B145	238	140	1.70	4.997	0.83575
<u>Ferrohypersthene granite gneiss 2</u>					
515-A109	135	174	0.78	2.265	0.76575
515-D109	144	228	0.63	1.836	0.75387
515-D107	193	179	1.08	3.144	0.78804
515-D108	185	171	1.08	3.164	0.78881
<u>Eulitic alkali feldspar granite gneiss</u>					
515-B153	397	12	34.2	132.1	4.0985
515-B152	413	12	35.6	140.2	4.3548

Note: *All ratios normalised to E & A standard
 $^{87}\text{Sr}/^{86}\text{Sr} = 0.70800$

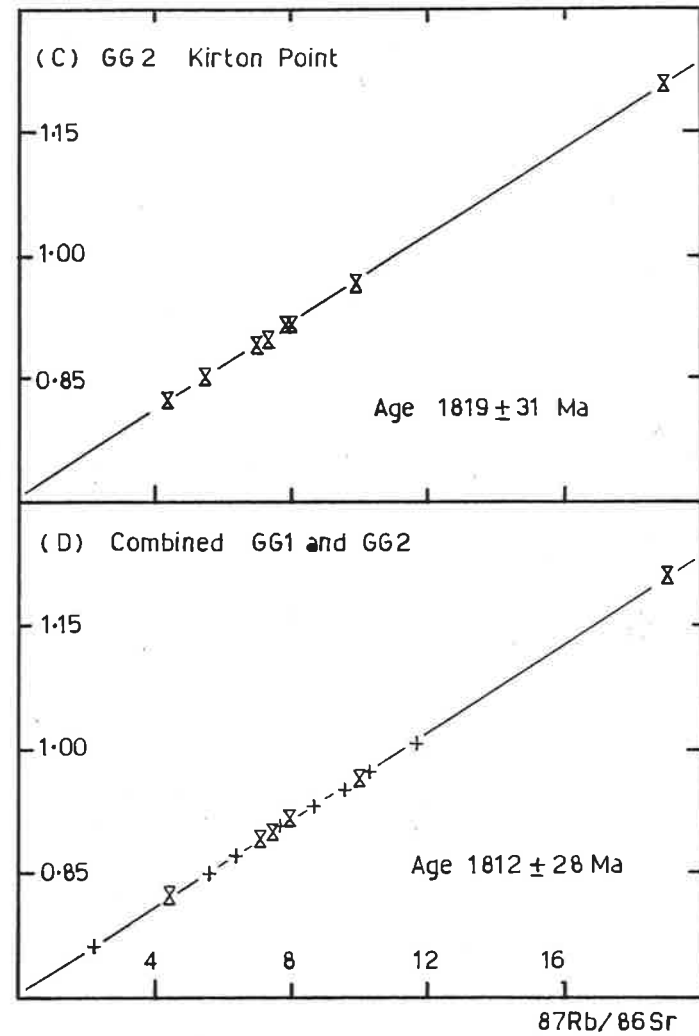
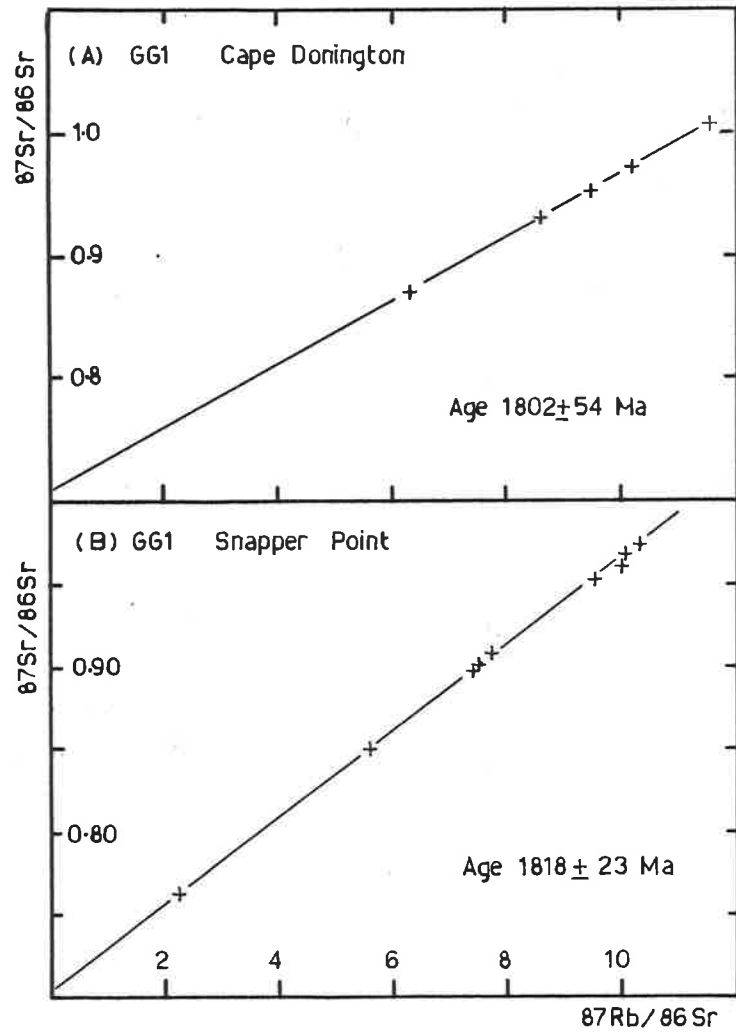


Figure 2.12 Isochron diagrams for GG1 and GG2 gneisses. Symbols as in Figure 2.6.

2.4.1.2 Opx-granitoids

(1) QGNG

Six total-rock samples of QGNG were collected from an outcrop area 15m x 15m at Cape Donington (Fig. 2.11). A low and relatively uniform Rb/Sr ratio (ca. 0.45, Table 2.4), is characteristic of QGNG and hinders precise determination of the isochron slope, although the IR is better defined. A perfect fit isochron results (MSWD = 0.98), with calculated age of 1896 ± 92 Ma and IR of 0.7039 ± 17 (regression 1, Table 2.5; Fig. 2.13B). This result is statistically indistinguishable from the Snapper Point granite gneiss result.

(2) FGG1

Six total-rock samples of FGG1 from Cape Colbert (Fig. 2.11) were supplemented by one from Spalding Cove (Fig. 2.11). An average Rb/Sr ratio of ca. 1.45 is apparent, with a moderate dispersion of ratios (Table 2.4). All seven samples define a perfect fit isochron (MSWD = 0.94) with calculated age of 1823 ± 56 Ma and IR of 0.7050 ± 33 (regression 2, Table 2.5; Fig. 2.13A).

This result is statistically indistinguishable from the previous results for QGNG and from Snapper Point.

(3) FGG2

Three samples of FGG2 from Point Bolingbroke were supplemented by one from 1 km north of Carcase Rock (Fig. 2.11). An Rb/Sr ratio (ca. 0.9) intermediate between QGNG and FGG1 is characteristic of FGG2 (Table 2.4). The four samples define an almost perfect fit isochron (MSWD = 1.58) with Model 3 solution age of 1818 ± 87 Ma and IR of 0.7060 ± 31 (regression 3, Table 2.5; Fig. 2.13C).

This result is indistinguishable from those of the other opx-granitoids and Snapper Point granite gneisses.

(4) Combined data regressions and pooling

In view of the inability to distinguish statistically the three pyroxene granitoid isochrons presented above, it was decided to combine all the data in search of a more precise estimate of age and IR for the DGS. Initially all 17 data points were regressed together resulting in a moderately close fit isochron (MSWD = 2.54) with Model 3 age of 1818 ± 13 Ma and IR of 0.7055 ± 5 (regression 4, Table 2.5; Fig. 2.13D).

The slightly elevated MSWD factor is not considered excessive for statistical perfect fit (Brooks et al. 1972), but the Model 3 solution

Table 2.5: Donington Granitoid Suite Rb-Sr isochron regressions

Regression number and sample group	MSWD*	Model	Age	Initial Ratio
1. Quartz Gabbro-norite Gneiss	0.98(6)	1	1896 \pm 92	0.7039 \pm 17
2. Ferrohypersthene Granite Gneiss 1	0.94(7)	1	1823 \pm 56	0.7050 \pm 33
3. Ferrohypersthene Granite Gneiss 2	1.58(4)	3	1818 \pm 87	0.7060 \pm 31
4. Combined 1, 2, 3	2.54(17)	3	1818 \pm 13	0.7055 \pm 5
5. Averaged outcrops	5.58(5)	3	1807 \pm 63	7061 \pm 26
**Pooled opx-granitoids			1837 \pm 42	0.7041 - 0.7053
6. Granite Gneiss 1, Snapper Point	7.9(10)	2	1818 \pm 23	0.7043 \pm 17
7. Granite Gneiss 1, Cape Donington	1.20(5)	1	1802 \pm 54	0.7054 \pm 67
8. Granite Gneiss 2, Kirton Point	2.86(10)	2	1819 \pm 31	0.7078 \pm 30
9. Granite Gneiss 2, Fisherman's Point	2.26(5)	3	1632 \pm 96	0.7332 \pm 143
10. Combined 6,7,8	11.73(24)	4	1812 \pm 28	0.7061 \pm 31
11. Averaged outcrops	9.54(4)	3	1780 \pm 364	0.7098 \pm 468
**Pooled granite gneisses (excluding Fisherman's Point)			1817 \pm 17	0.7033 - 0.7083

* number in brackets refers to number of data regressed

** pooling procedure after Paradine & Rivett (1960).

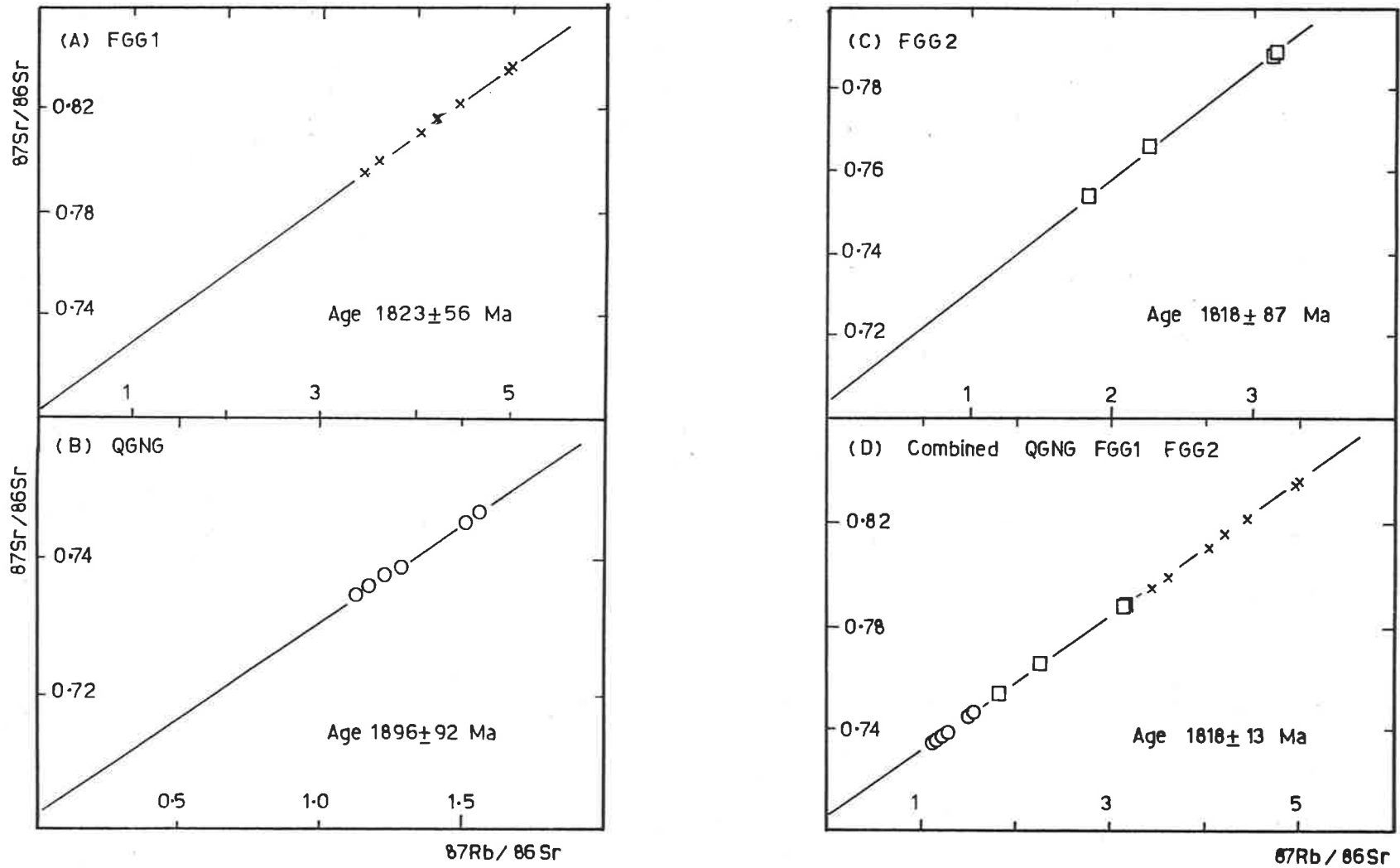


Figure 2.13 Isochron diagrams for QGNG, FGG1 and FGG2 granitoid gneisses. Symbols as in Figure 2.6.

does suggest a small component of regional variation in IR may be present. This is not surprising in view of the wide dispersion of sampling sites and the likelihood of regional variations in IR within large plutons (cf. Roddick & Compston 1977).

As a further test of the probably regional IR variation data points from each sampling site were averaged and then regressed together. The resulting five outcrop regression has MSWD = 5.58 and calculated Model 3 age of 1807 ± 63 Ma and IR of 0.7061 ± 26 (regression 5, Table 2.5). These results suggest that despite the conclusions of Brooks et al. (1972), combined regressions for the DGS are inappropriate due to the regional variation in IR.

A statistically more appropriate treatment of the data from QGNG, FGGL and FGG2 is to accept that IR variation existed within the suite at the time of emplacement and to calculate a weighted mean age (weighting procedure after Paradine & Rivett 1960). This results in a pooled age estimate for the DGS opx-granitoids of 1837 ± 42 Ma (Table 2.5). Zircon U-Pb isotopic data for QGNG (Section 2.4.2) support this age for the DGS.

(5) IR variation in opx-granitoids

If this pooled age is accepted, it is possible to calculate IR's for each of QGNG, FGGL and FGG2 at 1837 ± 42 Ma and thus to constrain the IR variation within the opx-granitoids. These calculations allow a range in IR from ca. 0.7041 to ca. 0.7053 (Table 2.5). Such a range in IR may not be unexpected in a large magma body actively fractionally crystallising feldspars over a prolonged period (e.g. Dickinson & Gibson 1972; McCarthy & Cawthorn 1980). It is more likely that the IR variation developed in this way rather than as an inherited feature of an inhomogeneous source (cf. Roddick & Compston 1977) because of the liquid nature of the DGS parental magma, which apparently contained little solid residual material.

Furthermore it is possible to estimate the period of time over which the opx-granitoids fractionally crystallised based on the Rb/Sr ratios of the rock-types and the IR range. If the average Rb/Sr ratios of QGNG and FGGL are taken as two estimates of the liquid from which the opx-granitoids crystallised, crystallisation periods of ca. 64 Ma and 20 Ma respectively are required to generate the IR change from 0.7041 to 0.7053. McCarthy & Cawthorn (1980) have estimated crystallisation intervals of ca. 20 Ma for large hot bodies of magma emplaced at moderate depth into relatively hot country rocks. The present author concludes that the

Table 2.6 Donington Granitoid Suite

Granite gneisses

Rb-Sr isotopic data

Sample Name	Rb ppm	Sr ppm	Rb/Sr	$^{87}\text{Rb}/^{86}\text{Sr}$	$^{*87}\text{Sr}/^{86}\text{Sr}$
<u>Granite gneiss 1</u>					
468-B111	261	121	2.16	6.355	0.87007
468-B103	296	101	2.93	8.652	0.92993
468-B106	274	85	3.22	9.540	0.95125
468-B107	275	80	3.46	10.259	0.97258
468-B108	257	66	3.91	11.642	1.00672
<u>Granite gneiss 1</u> McLaren Point					
515-A88	235	131	1.79	5.264	0.83589
<u>Granite gneiss 2</u> Kirton Point					
515-F70	229	152	1.51	4.419	0.82482
515-A121	244	129	1.89	5.543	0.85265
515-F76	256	135	1.90	5.551	0.85258
515-F75	263	110	2.39	7.032	0.89158
515-F74	273	113	2.42	7.101	0.89304
515-F73	283	113	2.50	7.409	0.89995
515-F72	271	101	2.68	7.895	0.91446
515-D21	293	109	2.69	7.957	0.91619
515-B500	263	79	3.35	9.949	0.96711
515-D205	371	59	6.25	18.946	1.20906
<u>Granite gneiss 2</u> Fisherman's Point					
515-B164D	323	100	3.23	9.608	0.95982
515-B168	361	108	3.34	9.888	0.96317
515-B164E	370	103	3.59	10.718	0.98468
515-B164C	402	110	3.66	10.899	0.98901
515-B164B	414	99	4.17	12.436	1.02480
<u>Alkali feldspar granite gneiss</u>					
515-B161B	403	11	37.3	154.9	5.1341
515-B154B	442	11	42.1	165.1	4.3802
515-B154A	440	10	42.7	168.7	4.4532
515-B22C	448	10	43.5	182.5	5.3405
515-B157A	459	10	44.1	188.1	5.4578

Note: *All ratios normalised to E & A standard

$$^{87}\text{Sr}/^{86}\text{Sr} = 0.70800$$

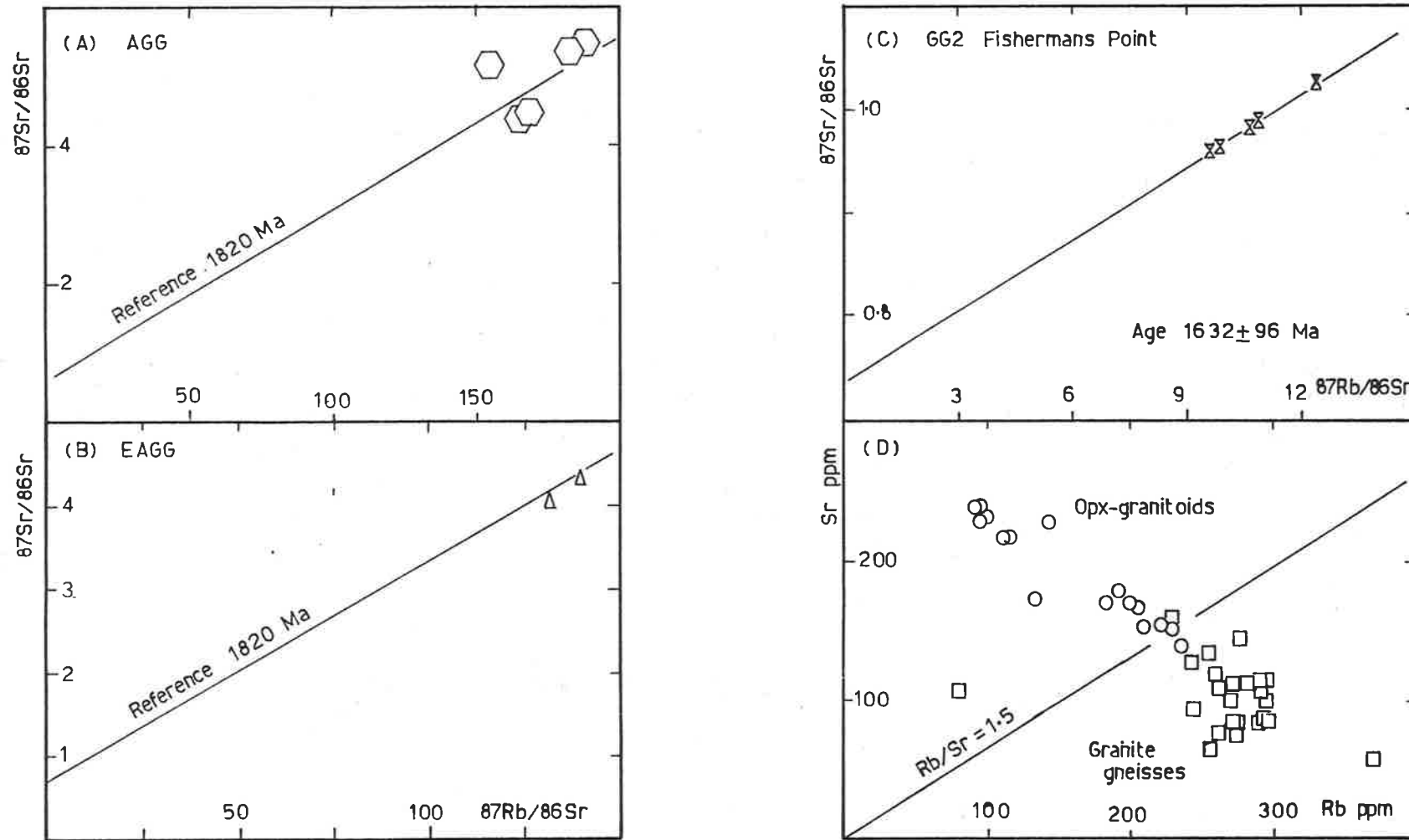


Figure 2.14 Isochron diagram for GG2 from Fisherman's Point and comparison of EAGG and AGG with opx-granitoid isochron and Rb-Sr geochemical comparison of opx-granitoids and granite gneisses.

DGS opx-granitoids have suffered prolonged, deep-seated fractional crystallisation, leading to a within-batholith variation in IR outside the range of experimental error.

(6) EAGG

Two samples of EAGG from Carcase Rock (Fig. 2.11) were analysed (Table 2.4) but not included in the pooled regression since their very high Rb/Sr ratio (ca. 35, Fig. 2.14B) would unduly bias regression calculations. The apparent ages of the two samples, calculated to the IR range of the opx-granitoids are 1810 Ma and 1785 Ma. Both of these total rock specimens appear to have suffered some post-emplacement disturbance (cf. AGG, below).

2.4.1.3 Granite gneisses

(1) GGL

Five medium-grained granite gneiss samples from Cape Donington (Fig. 2.11) were collected over an outcrop length of ca. 20m. The average Rb/Sr ratio (2.6) is almost twice that of FGG1 (Table 2.6).

An almost perfect fit isochron results (MSWD = 1.20) with a calculated Model 1 age of 1802 ± 54 Ma and IR of 0.7054 ± 67 (regression 7, Table 2.5; Fig. 2.12A). This result is indistinguishable from that for both the Snapper Point granite gneiss and the opx-granitoids.

(2) GG2

Ten total-rock samples from Kirton Point (Fig. 2.11) were collected over an outcrop length of 60m. The average Rb/Sr ratio (2.8) is greater than in FGG2 (Table 2.6). A close fit isochron (MSWD = 2.86) results with Model 2 solution age of 1819 ± 31 Ma and IR of 0.7078 ± 30 (regression 8, Table 2.5; Fig. 2.12C). This result is indistinguishable from the previously cited results for granite gneisses and opx-granitoids. The Model 2 solution suggests some variation in Rb/Sr ratio exists greater than expected due to experimental error.

Five total-rock samples were prepared from an outcrop block ca. 0.5m^3 from Fisherman's Point (Fig. 2.11). A small dispersion in Rb/Sr around the average ratio of 3.6 (Table 2.6) is observed, so that only a short isochron results with corresponding uncertainty of estimates of age and IR. The close fit isochron (MSWD = 2.26) has a Model 3 solution age of 1632 ± 96 Ma and IR of 0.7332 ± 143 (regression 9, Table 2.5; Fig. 2.14C). This result is statistically different from the other result for GG2 and from the other granite gneisses and opx-granitoids.

It is most probable that the young age and elevated IR reflect subsolidus redistribution of Rb and/or Sr isotopes within the small volume of rock sampled.

If the model of Black et al. (1978) is applicable, whereby the development of penetrative tectonic fabric leads to resetting of the Rb/Sr clock in small volumes of rock, it is possible that the 1632 ± 96 Ma date represents the age of the prominent S_3 fabric in the Fisherman's Point gneisses. (Further discussion of isotopic constraints on the age of D_3 appears in Chapters 3 and 4).

(3) Combined data regressions and pooling

The Kirton Point GG2 and Cape Donington and Snapper Point GG1 suites individually produce indistinguishable ages and IR's, although the MSWD's and Model 1 and Model 2 solutions suggest more geochemical variation is present than expected from experimental error alone. Furthermore the outcrop average of Fisherman's Point GG2 is close to the Kirton Point GG2 isochron. These results invite attempts to pool the data to constrain the age and IR of the granite gneisses.

Initially all 24 total rock samples (excluding GG2 Fisherman's Point) were regressed together. A poor fit errorchron with MSWD = 11.7 and Model 4 solution age of 1812 ± 28 Ma with IR of 0.7061 ± 13 results (regression 10, Table 2.5; Fig. 2.12D). The elevated MSWD indicates an excess of scatter around the combined errorchron, most of which is supplied by the Snapper Point gneisses. The Model 4 solution suggests that variations in both age and IR may exist between the individual suites.

Each of the four outcrops was then averaged and regressed together, resulting in a poor fit "errorchron" with MSWD = 9.54 and Model 3 solution age of 1780 ± 364 Ma and IR of 0.7098 ± 468 (regression 11, Table 2.5). This result confirms that there is considerable variation between outcrops at least with respect to IR, similar to the opx-granitoids above.

If, excluding Fisherman's Point GG2, the granite gneisses are accepted to contain between outcrop IR variation, but to be the same age, a pooled (weighted) mean age may be calculated (as above for the opx-granitoids). This calculation yields an age for GG1 and GG2 gneisses of 1817 ± 17 Ma, (Table 2.5) statistically indistinguishable from the pooled age of the opx-granitoids. In addition it is possible to calculate the IR of each outcrop, including Fisherman's Point, at ca. 1817 Ma (Table 2.5), the range being ca. 0.7033 to 0.7083, broader than but spanning the range in IR in the

opx-granitoids. On this basis it is impossible to distinguish the granite gneisses from the opx-granitoids.

(4) AGG

The contact retrogressive AGG at Carcase Rock (Fig. 2.11) shows extensive isotopic variability within the outcrop, similar to, but more extreme than that seen in EAGG at the same locality. No isochron can be fitted to these scattered data (Fig. 2.14A). Post-emplacement disturbance by local contact retrogression due to the intrusion of a structurally late granitoid is interpreted to be the cause of the scatter.

2.4.1.4 Discussion

(1) Relationship of opx-granitoids and granite gneisses

The weighted mean age estimates of the opx-granitoids and granite gneisses are statistically indistinguishable at 1837 ± 42 Ma and 1817 ± 17 Ma respectively. Furthermore the regional IR variations within each suite at their respective ages are indistinguishable at 0.7041 - 0.7053 and 0.7033 - 0.7083 respectively. These relationships are taken as strong confirmatory evidence for the original comagmatism, despite widely different subsolidus histories, of the opx-granitoids and granite gneisses. It has been suggested above that the GG1 and GG2 rocks were derived from FGG1 and FGG2 by retrogressive metamorphism.

It is revealing however to examine in more detail the Rb and Sr contents of the respective rocks (Fig. 2.14D) where it can be seen that the retrograded GG1 and GG2 rocks have suffered some decrease in Sr over their FGG1 and FGG2 counterparts but more particularly a marked increase in Rb, resulting in considerably higher Rb/Sr ratios (Table 2.4, 2.6). Moreover there is more scatter in the fields of the higher Rb/Sr rocks. This suggests that the retrogressive process involved the production of bulk Rb and Sr scatter, and probably also accounts for the greater scatter in isotopic composition in the granite gneisses witnessed by the elevated MSWD factors.

(2) Relationship of retrogression to tectonism

The observation that the retrograded rocks have the same Rb-Sr total-rock age and IR variation as the opx-granitoids, yet have considerably higher Rb/Sr ratios suggests that the elevated ratios must have been established at or near the time of original magmatic crystallisation. This is in accord with the petrographic and structural conclusion that retrogression predates (or accompanies)

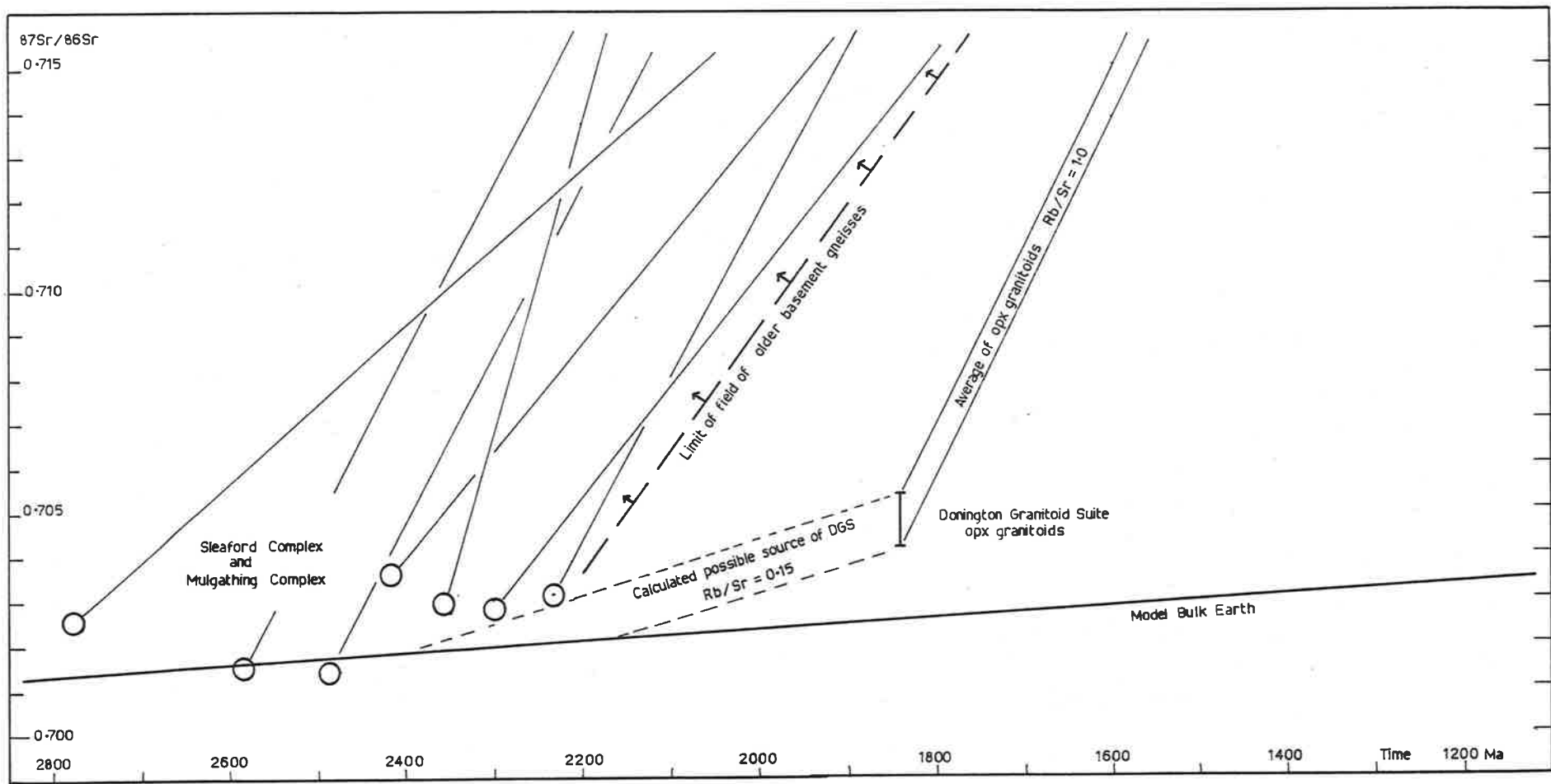


Figure 2-15

Sr-isotope evolution diagram for DGS opx-granitoids compared with Archaean basement gneisses of the Gawler domain and the model bulk earth. Also shown is the possible evolution curve of a model source of the DGS parent magma.

D₁₋₂. Furthermore it was demonstrated that the retrograded rocks are located in and adjacent to the Kalinjala Mylonite Zone (Chapter 1), suggesting localisation of the retrogressive activity along the mylonite zone structure. Thus although Parker (1980) concludes that the Kalinjala Mylonite Zone is a D₃ structure, the present author suggests that retrogressive activity has been present in and adjacent to this zone from as early as 1837 \pm 42 Ma and prior to or during D₁₋₂.

(3) Relationship of DGS to Sleaford Complex

Thomson (1980) and Rutland et al. (1981) suggest that parts of the Lincoln Complex on the east coast of Eyre Peninsula may represent elements of the Sleaford Complex reworked during the Kimban Orogeny. More particularly Bradley (1980) examined opx-granitoids of the DGS and pyroxene granulites of the Sleaford Complex and suggested that "the Lincoln Complex could represent reworked and retrogressed Sleaford Complex". However the present author has calculated Sr-isotope evolution curves for rocks of the Sleaford Complex in the south of Eyre Peninsula (Appendix Table 1.2); and the equivalent Mulgathing Complex in the north of Eyre Peninsula (Appendix Table 1.2), and compared them with similar curves for the DGS (Fig. 2.15). It is immediately apparent that neither the granulites nor the metasediments of the Sleaford Complex form suitable parents for the DGS, either by partial melting or by tectonic reworking, because at 1837 \pm 42 Ma they are grossly enriched in ⁸⁷Sr with respect to the DGS. For Sleaford Complex material to comprise the protolith of the DGS the former would require a markedly different Rb/Sr ratio or IR than is observed in present day exposure, or, alternatively, the Sleaford Complex material so far analysed may be unrepresentative of the complex as a whole. This point will be reexamined in Chapter 7 in connection with a regional Sr-isotope systematic discussion of the Gawler orogenic domain.

Furthermore it is apparent from Fig. 2.15 that the DGS has too high an IR to be derived directly from the presumed upper mantle at 1837 \pm 42 Ma. This point also will be reexamined in Chapter 7, but it is possible here to conclude that the DGS was not derived by partial melting in normal upper mantle at this time nor by partial melting nor tectonic reworking of typical Sleaford Complex material.

(4) Isotopic composition of Sr of possible source rocks

It is possible to speculate on the likely isotopic nature of the source rocks of the DGS parental magma. The liquidus phases of the parental magma, as represented by the phenocrysts in QGNG, are likely to represent the residual phases at the site of partial melting (assuming a crustal origin for the DGS), viz plagioclase, orthopyroxene and clinopyroxene. Using figures published by Hanson (1978) the bulk rock distribution coefficients D_{Rb} and D_{Sr} , for the residue would probably be ca. 0.03 and ca. 3 respectively. If the degree of melting in the source is constrained at 30% (Compston & Chappell 1979) the concentration of Rb in the melt would be ca. 3 times that in the residue and ca. 0.4 times for Sr (Hanson 1978). Thus during partial melting the Rb/Sr ratio would be ca. 7.5 times in the melt that of the source. Hence if the average Rb/Sr ratio of the DGS is estimated to be ca. 1.0 (Appendix Table 1.2) the Rb/Sr of the source would be ca. 0.13. Considering the crudity of the calculation method this has been rounded to 0.15 for the purposes of Fig. 2.15.

Calculation of the Sr-isotope evolution curve for a source of Rb/Sr = 0.15 and which at 1837 ± 42 Ma contained the possible IR range of the opx-granitoids (0.7041 - 0.7053), suggests a probable model age for the source of not greater than ca. 2.4 Ga. It is tempting to speculate that a crustal source area dominated by pyroxenes and plagioclase with a Rb/Sr ratio of ca. 0.15 and of early Proterozoic age may have existed under this portion of the Gawler orogenic domain.

Moreover it is noteworthy that the late Archaean to Early Proterozoic granitoids intruding the Sleaford Complex plot on or near this proposed lower crustal evolution trend (Fig. 2.15) suggesting also their possible derivation from such a source.

The petrogenesis of the DGS opx-granitoid magma is discussed more fully in Chapter 7.

2.4.2 U-Pb zircon geochronology

A suite of zircons from QGNG were prepared for analysis in order to test the Rb-Sr total-rock date of 1837 ± 42 Ma for the opx-granitoids.

2.4.2.1 Description of zircons

The zircon grains extracted from QGNG are predominantly euhedral to fragmented, colourless and transparent. A minor proportion are

Table 2.7 Quartz gabbro-norite gneiss zircon U-Pb isotopic data

Fraction	B11	Q1	Q2	Q3
grain size (microns) colour	100-250 colourless	100-250 colourless	< 100 colourless	100-250 yellow
U ppm	383	366	327	983
Pb ppm	139	132	116	319
Common Pb ppm	0.4	0.4	0.3	0.5
206Pb/238U	0.3217	0.3159	0.3103	0.3094
207Pb/235U	4.9836	4.9060	4.8173	4.7715
206Pb/206Pb	0.1123	0.1126	0.1126	0.1119
206Pb/204Pb	20,106	19,466	24,145	35,717
206Pb/238U Age (Ma)	1798	1770	1742	1738
207Pb/235U Age (Ma)	1817	1803	1788	1780
207Pb/206Pb Age (Ma)	1838	1842	1841	1830

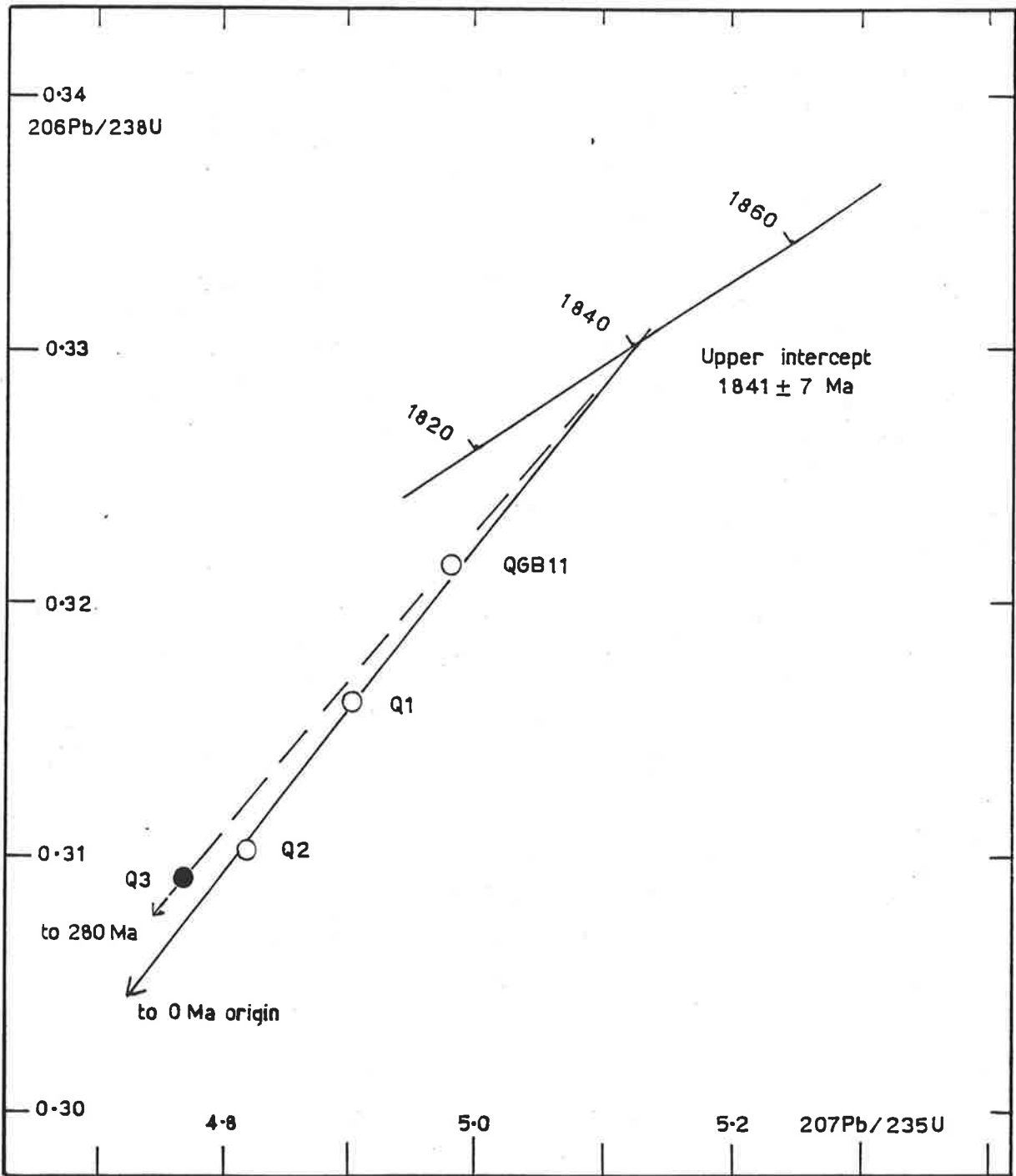


Figure 2.16 Zircon U-Pb data from QGNG displayed on the Concordia diagram. The upper intercept on Concordia has been calculated by forcing the line connecting QGB11, Q1 and Q2 through the 0 Ma origin.

smokey yellow in colour. Four fractions were prepared for analysis (Table 2.7) from the least magnetic fraction of the 100 to 250 micron grain size range. B11 was prepared from this bulk fraction without modification.

Q1, Q2, Q3 were modified using the air-abrasion technique of Krogh (1982). Following air-abrasion the bulk fraction was split into two grain size fractions, greater than and less than 100 microns. Q1 comprised hand-picked colourless to slightly metamict grains greater than 100 microns, and Q2 was similar except for the grain size being smaller than 100 microns. Q3 was prepared by hand-picking smokey yellow, slightly metamict grains from the abraded greater than 100 micron fraction.

2.4.2.2 Results

The experimental technique is described in Appendix A1, and results displayed in Table 2.7. The bulk fraction B11 is very nearly concordant with a $^{207}\text{Pb}/^{206}\text{Pb}$ model age of 1838 Ma. The U-content of 383 ppm is moderate and the common lead amounts to only 0.3% of the total Pb present. Q2 and Q1 have comparable U, Pb, common Pb and calculated ages as B11. Their $^{207}\text{Pb}/^{206}\text{Pb}$ model ages are 1842 and 1841 Ma respectively. Abrasion apparently has modified the zircons only marginally.

The three zircons B11, Q1 and Q2 are collinear almost to within experimental error. The discordia chord has an MSWD = 3.3 with imprecisely defined upper intercept of ca. 1835 Ma and near zero lower intercept on concordia. Constraining the lower intercept to pass exactly through the 0 Ma. origin and regressing B11, Q1 and Q2 maintains collinearity (MSWD = 2.9) and allows a more precise estimate of the upper intercept at 1841^{+7}_{-7} Ma (Fig. 2.16).

Fraction Q3, the smokey yellow zircons, has U content ca. 3 times that of the fractions Q2, Q1 and B11. However it is only marginally more discordant than, although it is not collinear, with, Q2, Q1 and B11 suggesting that it contains a component of partial Pb-loss not evident in the other three. The lower intercept of the join of Q3 with the upper intercept of the Q1, Q2, B11 discordia is ca. 280 Ma suggesting partial Pb-loss in the relatively near-geological past.

2.4.2.3 Discussion

The upper intercept age of QNG is not statistically distinguishable from the pooled opx-granitoid Rb-Sr total-rock age. The concordant

Table 2.8: Geochemical comparison of average opx-granitoids of the Donington Granitoid Suite with typical I-, S- and A-type granitoids.

	1	2	3	4	5	6	7	8
SiO ₂	68.33	67.75	68.48	72.50	72.86	70.19	77.21	73.04
Fe/(Fe+Mg) *	0.70	0.70	0.50	0.64	0.68	0.56	0.94	0.84
Al ₂ O ₃ /(Na ₂ O + K ₂ O + CaO)	0.96	0.99	0.92	1.03	1.07	1.18	1.05	1.03
K ₂ O/Na ₂ O**	1.8	1.9	1.3	1.2	1.5	1.7	1.6	1.1
(La) _N	190	156	98	105	71	93	203	197
(Eu) _N	25	24	-	-	-	-	20	33
(Yb) _N	21	15	-	-	-	-	38	35
Ba	915	1166	985	577	548	448	575	767
Sr	147	169	435	165	142	124	43	148
Zr	305	310	181	147	151	160	170	490
Nb	16	14	11	9	7	-	19	25
Y	41	38	19	29	33	32	90	83
Sc	13	15	9	9	7	-	16	17
V	41	53	53	30	25	63	2	6
Cr	12	18	48	5	8	39	1	2
Ni	21	19	17	6	5	13	1	1
Ga***	18			15			20	21

* molar ratios

** wt.% ratio

*** value for FGG1 from Bradley (1972)

1. Average of 7 FGG1
2. Average of 4 FGG2
3. Average of 10 Moonbi I-types (Chappell 1978)
4. Average of 48 Bega I-types (Collins et al. 1982)
5. Average of 5 Moonbi S-types (Chappell 1978)
6. Average of 20 Kosciusko S-types (Hine et al. 1978)
7. Average of 8 Mumbulla A-types (Collins et al. 1982)
8. Average of 9 Gabo A-types (Collins et al. 1982)

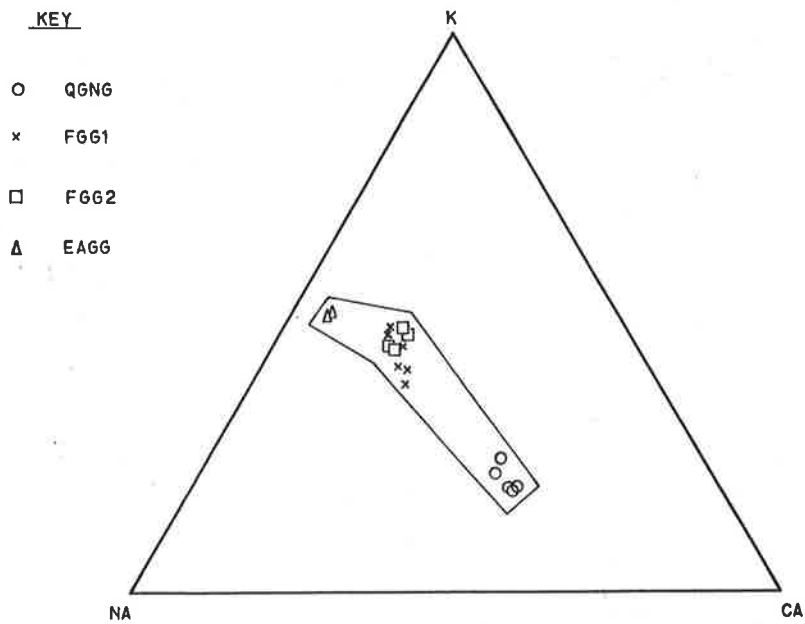
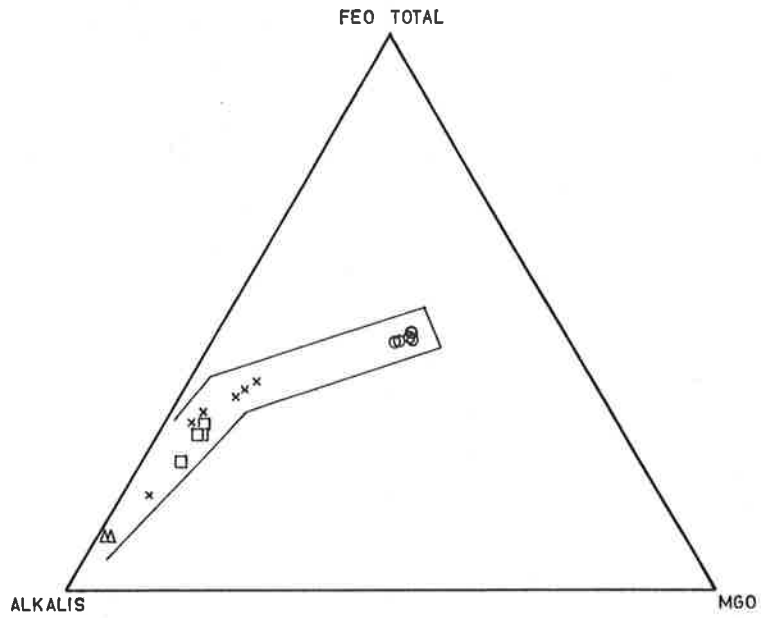


FIGURE 2.17 AFM and K-Na-Ca diagrams for the opx-granitoids of the Donington Granitoid Suite. Outlined field is the approximate envelope of data points.

U-Pb zircon age and Rb-Sr total rock age allows a pooled estimate of the age of the opx-granitoids based on the QGNG U-Pb upper intercept and the three QGNG, FG1 and FG2 Rb-Sr isochrons. The calculated pooled age of 1841 ± 7 Ma is henceforth regarded as the best estimate of the age of the opx-granitoids. Furthermore the concordant dates are interpreted as strong evidence for the pooled age to be representative of primary magmatic crystallisation and emplacement of the opx-granitoids of the DGS.

2.5 GEOCHEMISTRY OF THE DGS

2.5.1 Introduction

On the basis of mineralogical, textural and isotopic criteria, it has been argued that the opx-granitoids constitute an original comagmatic suite related through crystal fractionation. It has further been argued that the granite gneisses have been derived from the opx-granitoids by retrogressive alteration involving the addition of Rb. This raises the question as to whether other geochemical differences may exist.

It is the object of this section to examine separately, and then to compare the opx-granitoids and granite gneisses and to show that retrogression has been accompanied by geochemical alteration.

2.5.2 Opx-granitoids

2.5.2.1 Geochemical classification

Assuming comagmatism of the opx-granitoids the AFM diagram (Fig. 2.17; Barker 1978; Wright 1974) shows a calc-alkaline character (Ringwood 1975) as do both the alkali-silica-lime index (Fig. 2.18; Peacock 1931) and the K-Na-Ca diagram (Fig. 2.16; Barker & Arth 1976). These features suggest the DGS comprises a typical orogenic suite of granitoids.

In terms of the model of granitoid genesis of Chappell & White (1974) the $Al_2O_3/(Na_2O + K_2O + CaO)$ ratio less than 1.1 (Table 2.8), the low IR and low normative corundum (Appendix Table 2.2), coupled with the pyroxene \pm hornblende mafic mineralogy suggest the opx-granitoids are I-type. This model conclusion precludes the involvement, to any significant degree, of pre-existing pelitic sedimentary material in the genesis of the DGS, in favour of an igneous or metaigneous protolith.

However, Emslie (1978) argued that the high K_2O and $Fe_T/(Fe_T + Mg)$ of many Proterozoic and younger granitoid (and volcanic) suites is

more typical of anorogenic magmatism. Subsequently Loiselle & Wones (1979) and Collins et al. (1982) proposed more detailed geochemical criteria to distinguish anorogenic or A-type granitoids, some of which are illustrated in Table 2.8 in comparison with the FGG1 and FGG2 of the DGS. Although the high K_2O/Na_2O , Ga, Zr, Y and $(La)_N$ of the DGS are apparently transitional towards A-type, the moderately high Ni, Cr, V and Ba argue more strongly for I-type. These features coupled with mineralogical criteria cited by Collins et al. lead the present author to conclude that the DGS is a suite of I-type granitoids. The transitional geochemical characteristics alluded to above will be discussed in more detail in Chapter 7.

2.5.2.2 Major element geochemistry

In general terms the major element geochemistry of the opx-granitoids shows these main features, (Appendix Table 2.2, Fig. 2.19, Table 2.9)

- (1) SiO_2 range ca. 55% to ca. 79%
 - (2) SiO_2 gap between ca. 57% and 65%
 - (3) moderate Al_2O_3 ca. 12% to ca. 16%
- and rocks with greater than 65% SiO_2 exhibit
- (4) K_2O between ca. 4.5% and ca. 6%
 - (5) $K_2O/Na_2O > 1.5$
 - (6) $MgO < ca. 1.6\%$
 - (7) $Fe_T / (Fe_T + Mg) > 0.65$.

In the fractionation model proposed in previous sections, opx, cpx and plagioclase were suggested to be early accumulating phenocryst phases resulting in QGNG, whereas subsequent intrusives were suggested to be residual liquids in the case of FGG1 and EAGG, but plagioclase enriched cumulates in FGG2. If this is the case the regular decrease of Fe_2O_{3Tot} , MgO, CaO and Al_2O_3 (Fig. 2.19) for most rocks is easily explicable in terms of pyroxene and feldspar extraction. Similarly it is possible to account for the increases in K_2O and SiO_2 . Moreover minor deviations can be explained on this basis e.g.

- (1) TiO_2 and P_2O_5 in QGNG are below the predicted trends (Fig. 2.19), suggesting in accord with petrographic observation, that ilmenomagnetite and apatite are not liquidus phases initially.
- (2) Al_2O_3 in FGG2 shows a steep increase with increasing SiO_2 (Fig. 2.19), suggesting the accumulation of feldspar.

Table 2.9: Donington Granitoid Suite - Average major and trace element compositions of opx-granitoids.

	QGNG (5) *	FGG1 (7)	FGG2 (4)	EAGG (2)
SiO ₂	56.45	68.33	67.75	76.96
Al ₂ O ₃	14.64	14.67	15.63	11.91
Fe ₂ O ₃ tot	9.85	4.58	3.90	1.04
MnO	0.15	0.07	0.04	0.03
MgO	5.74	0.97	0.83	0.14
CaO	6.71	2.82	2.77	0.75
Na ₂ O	2.44	2.83	2.89	3.00
K ₂ O	2.38	5.07	5.55	5.20
TiO ₂	0.80	0.65	0.63	0.07
P ₂ O ₅	0.21	0.16	0.16	0.00
Total	99.37	100.14	100.15	99.10
Rb	109	229	182	405
Sr	227	147	169	12
Ba	558	915	1166	5
Y	34	41	38	52
Zr	206	305	310	109
Nb	11	16	14	5
Sc	28	13	15	1
V	159	41	53	
Ni	105	21	19	11
Cr		12	18	0
La	33	59	49	
Ce	67	120	101	
Nd	29	49	45	34
Sm	6	9	9	6
Ev	1	2	2	0.2
Gd	5	8	8	6
Dy	5	8	6	7
Er	3	4	4	4
Yb	3	4	3	4

Note: *number in brackets refers to number of samples averaged.

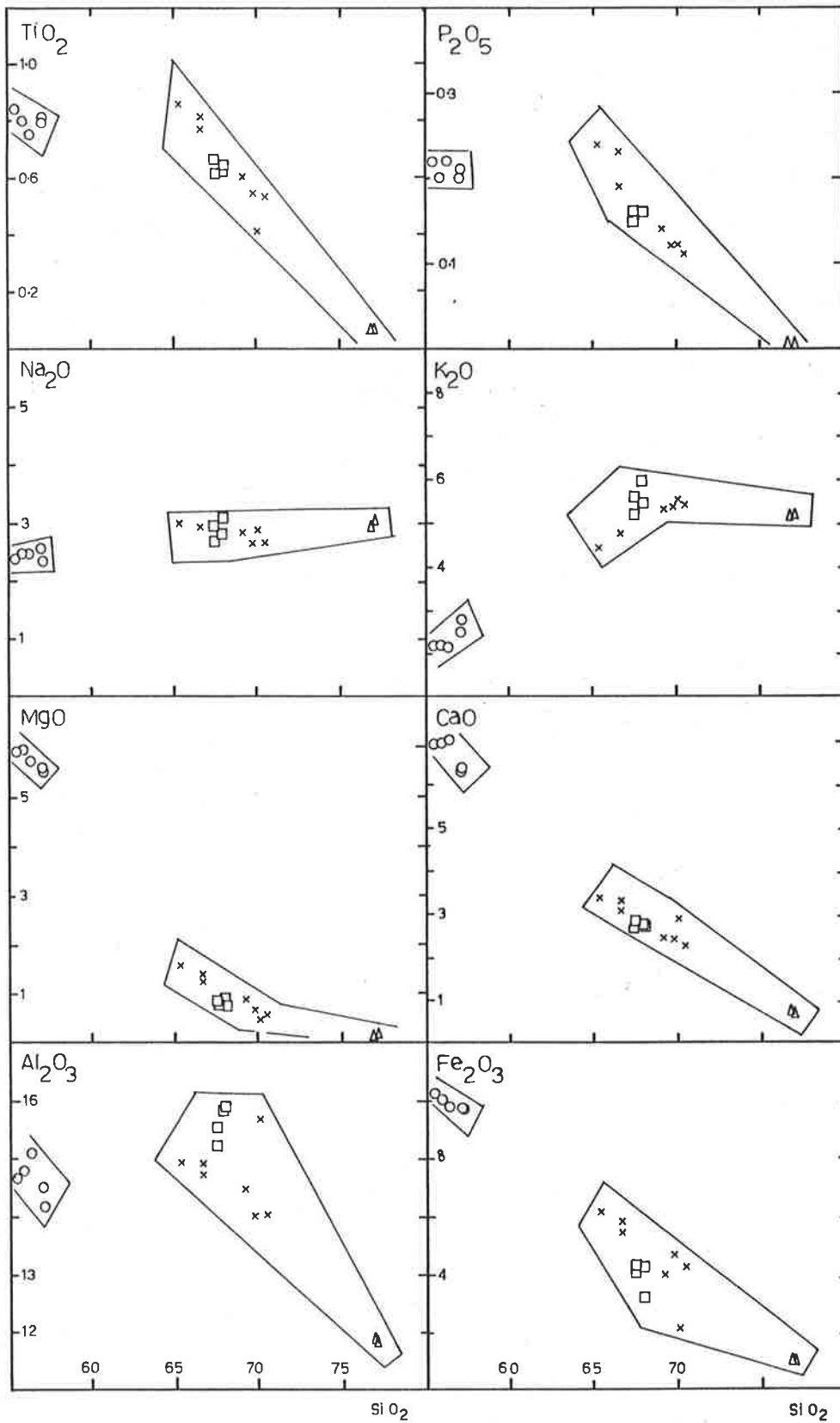


FIGURE 2-19 Major element variation diagrams for opx-granitoids of the Donington Granitoid Suite. Symbols as in Figure 2.17.

2.5.2.3 Trace element geochemistry

The trace element distribution patterns (Table 2.9; Fig. 2.20, 2.21) tend to confirm the conclusions drawn above, although some more detailed information can be extracted, viz,

- (1) Rb increases with SiO_2 over the whole range of compositions suggesting none of the liquidus phases is extracting Rb, i.e. bulk Kd is small. Following discussion by Hanson (1978), the high Kd for Rb in biotite (Arth 1976) would preclude any significant role for biotite phenocrysts in the DGS opx-granitoids including QGNG. This suggests the abundant biotite in QGNG is largely of intercumulus origin (by replacement of pyroxene). However, discussion of the crystal chemical behaviour of Rb by Mason & Moore (1982) weakens this conclusion by partly negating the strong preference of Rb for biotite suggested by Hanson's high Kd values.
- (2) Ba in QGNG is lower than in FGGL, which considering the Kd for Ba in biotite (Arth 1976) again suggests the abundant biotite in QGNG is not of phenocryst origin.
- (3) Ba decreases in rocks with SiO_2 greater than ca. 65% (other than FGG2) suggesting the fractionation of alkali feldspar (Arth 1976).
- (4) Ba in FGG2 shows a sharp increase, suggesting that at least part of the alkali feldspar in this rock may be cumulate.
- (5) Sr decreases almost to zero, over two orders of magnitude, which suggests an efficient process of Sr extraction from the melt has occurred. Mathematical expressions of the partial melting and fractional crystallisation processes (Arth 1976) suggest that such a marked decrease is more likely for fractional crystallisation.
- (6) Sr in FGG2 shows a sharp increase, suggesting feldspar accumulation.
- (7) Zr decreases only in rocks with SiO_2 greater than ca. 70% suggesting that zircon fractionation may have occurred only in the most siliceous rocks.
- (8) Ni in QGNG is much higher than in the more siliceous rocks, reflecting the accumulation of pyroxenes (Gill 1978).

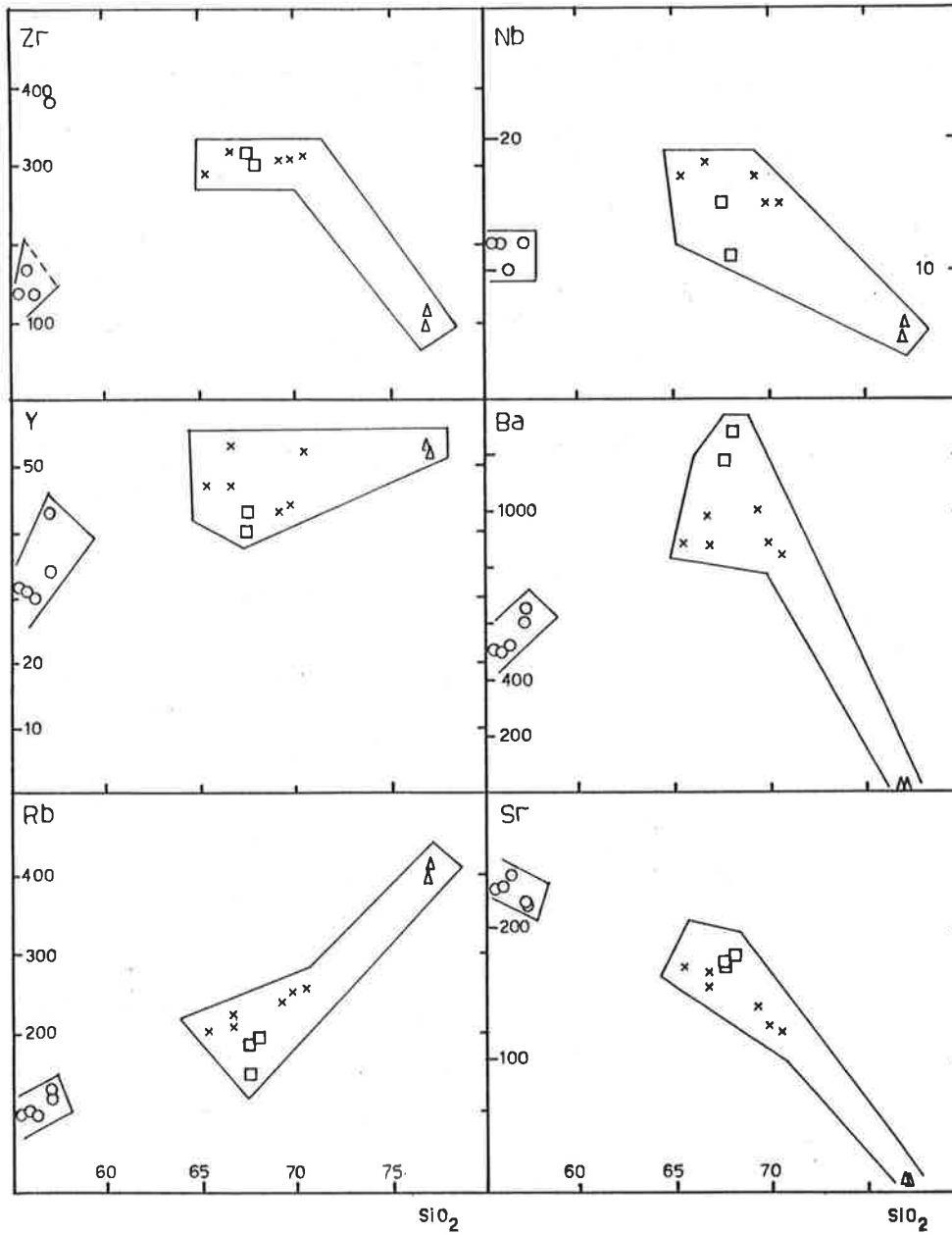


FIGURE 2.20 Trace element variation diagrams for opx-granitoids of the Donington Granitoid Suite. Symbols as in Figure 2.17.

- (9) Ni content in FG1 and FG2 averages ca. 20ppm which argues against derivation of the opx-granitoids by fractionation of basalts (cf. Taylor et al. 1969).
- (10) K/Rb is approximately constant over the whole range of SiO₂ contents, and averages ca. 160, probably precluding the major fractionation of hornblende from the opx-granitoids (Arth 1976).

2.5.2.4 REE geochemistry

Inspection of the REE patterns (Fig. 2.22) and elemental ratios (Table 2.10) of the opx-granitoids shows that,

- (1) All patterns are parallel, but with a progressively increasing negative Eu anomaly from QNG to EAGG, suggesting feldspar fractionation has occurred within the opx-granitoids, but little or no garnet or hornblende fractionation.
- (2) The LREE are enriched and fractionated, $(La/Sm)_N$ ca. 3.52 to ca. 3.74.
- (3) HREE are moderately fractionated, $(Yb/Gd)_N$ ca. 0.48 to ca. 0.78, suggesting major minerals fractionating HREE such as garnet or hornblende (Arth 1976) have been involved in the production of the DGS magma or its source (see Chapter 7).
- (4) The highly fractionated EAGG contains lower total REE than earlier silicic opx-granitoids, suggesting that late fractionation of accessory phases such as zircon and apatite has occurred.

2.5.2.5 Consideration of alternatives to crystal fractionation

All of the previous discussion has been based on the petrographic and mineralogical conclusion that the petrological variation within the DGS opx-granitoids has been developed by prolonged crystal fractionation. At this point, a brief word will be addressed to alternative models of granitoid genesis.

Model 1 Restite-controlled partial fusion

This model, enunciated by Chappell & White (1974), White & Chappell (1977) and Compston & Chappell (1979), and invoked to explain the range in bulk rock compositions in many granitoid suites requires the varying degrees of unmixing of a residual solid

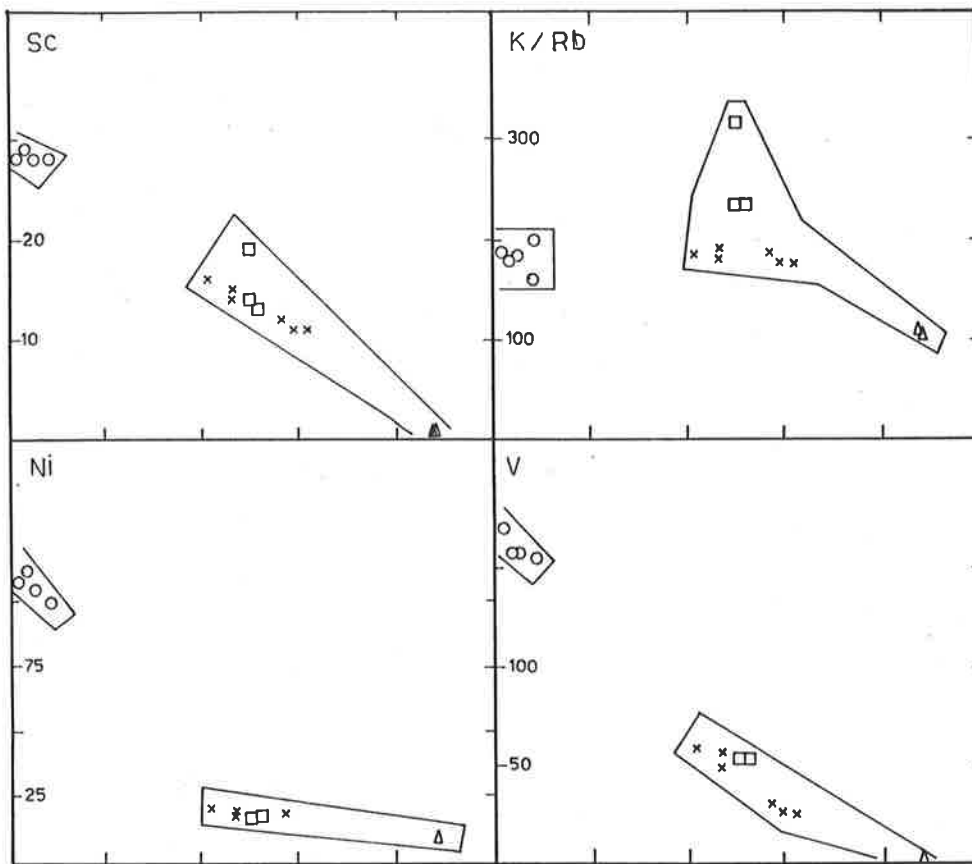


Figure 2-21 Trace element variation diagrams for opx-granitoids of the Donington Granitoid Suite. Symbols as in Figure 2.17.

component (restite) from an interstitial silicic partial melt. Simply speaking felsic granitoids are viewed to contain a high proportion of melt, whereas mafic granitoids contain a high proportion of restite. In its simplest form for a particular granitoid suite, the model requires the restite to be of fixed bulk composition and fixed mineralogical composition and the interstitial melt to be of fixed, commonly near-minimum melt, composition.

The DGS opx-granitoids show a wide range in bulk rock compositional variation and this variation is reflected in sympathetic mineralogical compositional changes (Fig. 2.6). This suggests that the simple end-member unmixing model, or restite-controlled partial fusion model, is not appropriate for the DGS opx-granitoids, but that the minerals crystallised in equilibrium with varying liquid compositions.

Model 2 Hybridisation

Assimilation and disintegration of solid mafic material by granitic liquid has been invoked by de Albuquerque (1971) to explain the variations in Portuguese granitoid composition and Eichelberger (1978) for calc-alkaline magmas. In essence, this model is similar to Model 1, in that the resultant granitoid geochemistry is a result of a physical mixture of solid mafic and liquid felsic material not in chemical equilibrium.

By virtue of its similarity, this model fails for the DGS for the same reasons as Model 1.

Model 3 Progressive partial fusion

In its simpler form such a model allows aggregation, extraction and upward intrusion of successively less silicic magma batches from a common source region resulting in a spectrum of granitoid compositions (e.g. Schwarzwald granitoids; Emmermann 1977). Succeeding liquids have equilibrated with residual solids of progressively evolving compositions, so that a spectrum of mineralogical compositions also results.

Although such a model could perhaps satisfy the major element and mineralogical constraints imposed for the DGS opx-granitoids, it fails for two main reasons.

- (1) The intrusive sequence from QGNG to EAGG is one of increasing SiO_2 , the reverse of that expected for progressive partial fusion.
- (2) The Sr content from QGNG to EAGG decreases by 2 orders

Table 2.10: Selected geochemical ratios for the averaged opx-granitoids of the Donington Granitoid Suite.

	QGNG	FGG1	FGG2	EAGG
K/Rb	183	183	252	109
(La/Sm) _N	3.57	3.74	3.52	
(Yb/Gd) _N	0.68	0.62	0.48	0.78
(Eu/Eu*) _N	0.81	0.57	0.62	0.08

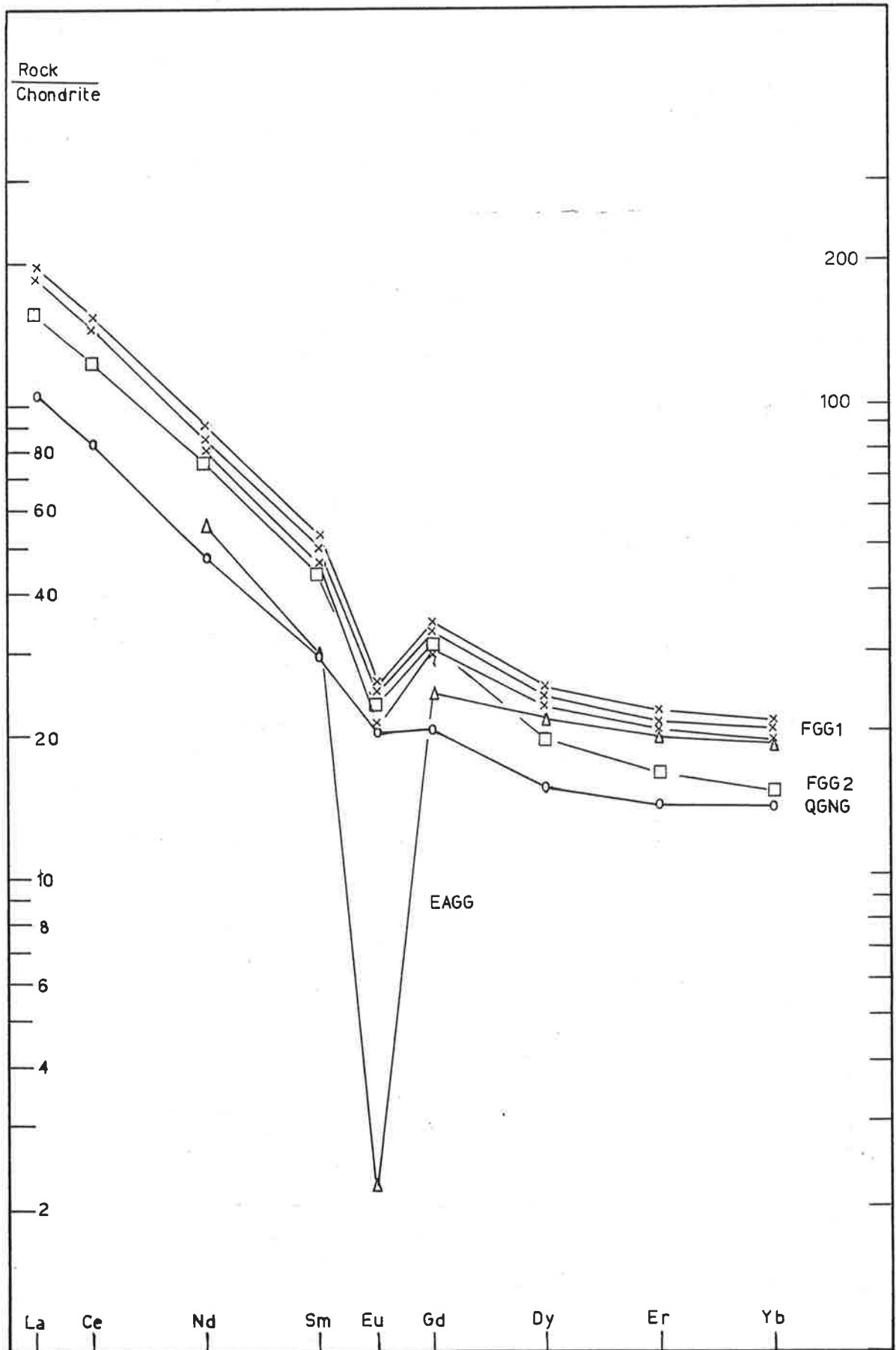


Figure 2.22 Chondrite normalised REE plots for opx-granitoids of the Donington Granitoid Suite. Symbols as in Figure 2.17.

of magnitude. This has been suggested above to argue against a partial melting model for the opx-granitoids.

Model 4 Fractional crystallisation

This model also involves an unmixing process. Initially solids of a fixed composition separate from interstitial melt. Subsequent solids crystallised from the more evolved remaining liquid are of a different composition reflecting the composition of the liquid with which they are in equilibrium. An evolutionary sequence of liquid compositions and mineral compositions is produced, resulting in bulk rock geochemical trends on AFM and Harker diagrams that reflect the nature of the evolutionary path and the crystallising minerals.

Moreover it is apparent that depending on the degree to which solids and residual liquids are unmixed and separated a continuous chemical trend or gaps may be produced.

The evolutionary compositional trends of opx-granitoid phenocrysts in sympathy with bulk rock geochemical variation from QGNG to EAGG (Fig. 2.6) are best explained by this fractional crystallisation model.

2.5.2.6 Fractional crystallisation model for opx-granitoids

A fractional crystallisation model can be formulated for the opx-granitoids on the basis of petrographic, mineralogical and major element geochemical criteria, and is summarised in Fig. 2.23 and Table 2.11.

An unspecified near anhydrous CO₂ buffered quartz dioritic liquid (see next section) is envisaged to intrude and chill against MBG country rocks resulting in QGNG precipitation of liquidus plagioclase, opx and cpx cumulates also trapping a proportion of intercumulus residual liquid. The major element modelling by least squares approximation of QGNG (Table 2.11) demonstrates the possible combination of minerals and residual melt in this process. The small proportion of ilmenite is needed to compensate for ilmenite originally dissolved in the pyroxenes and the small proportion of biotite in the mathematical model suggests some of the biotite in the QGNG may be phenocrystal.

Fractionation of plagioclase, opx, alkali feldspar and ilmenite is capable of generating the geochemical variation within FGGL and EAGG reasonably well (Table 2.11). The moderately large sum of squares residual factor is contributed mainly by Fe, Mg, Ca and Na,

Table 2.11 Donington Granitoid Suite least squares modelling of major element compositions of rock types within the opx-granitoids.

(a) QGNG as cumulate phenocrysts + FGGL intercumulus liquids

	B203	B203*	Residual	Component	Weight Fraction
SiO2	55.53	55.53	-0.00	B143 = FGGL	0.37
TiO2	0.84	0.87	0.03	plag 1	0.28
Al2O3	14.65	14.62	-0.03	cpx	0.12
FeOT	9.12	9.09	-0.03	opx 1	0.17
MnO	0.15	0.17	0.02	biot	0.05
MgO	5.91	5.96	0.05	ilm	0.01
CaO	6.93	6.92	-0.01		
Na2O	2.38	2.60	0.22	Sum of squares of residuals	0.06
K2O	2.20	2.22	0.02		

(b) Fractionation of FGGL = B143 to FGGL = D116

B143	B143*	Residual	Component	Weight Fraction
65.37	65.36	-0.01	D116	0.72
0.86	0.73	-0.13	plag 2	0.16
14.92	15.00	0.08	opx 2	0.07
5.48	5.62	0.14	kspar	0.03
0.10	0.10	0.00	ilm	0.01
1.57	1.14	-0.43		
3.37	2.98	-0.39		
2.98	3.15	0.17	Sum of squares of residuals	0.42
4.43	4.34	-0.09		

(c) Fractionation of FGGL = B143 to EAGG = B153

	B143	B143*	Residual	Component	Weight Fraction
SiO2	65.37	65.35	-0.02	B153	0.51
TiO2	0.86	0.78	-0.08	plag 3	0.24
Al2O3	14.92	15.07	0.15	opx 3	0.12
FeOT	5.48	5.57	0.09	kspar	0.11
MnO	0.10	0.12	0.02	ilm	0.01
MgO	1.57	1.36	-0.21		
CaO	3.37	2.97	-0.40		
Na2O	2.98	3.14	0.16	Sum of squares of residuals	0.28
K2O	4.43	4.31	-0.12		

(d) FGGL = D107 as cumulate of FGGL = B143 phenocrysts and intercumulus residual liquid EAGG = B153

D107	D107*	Residual	Component	Weight Fraction
68.02	68.02	0.00	B143	0.30
0.64	0.62	-0.02	plag 3	0.14
15.90	15.88	-0.02	cpx 3	0.01
2.84	2.86	0.02	kspar	0.13
0.04	0.05	0.01	ilm	0.01
0.75	0.67	-0.08	B153	0.40
2.73	2.78	0.05		
3.08	3.11	0.03	Sum of squares of residuals	0.01
5.45	5.48	0.03		

Note (1) Mineral compositions

	cpx	opx 1	opx 2	opx 3	plag 1	plag 2	plag 3	kspar	biot	ilm
SiO2	52.49	51.07	48.55	48.60	53.90	57.98	55.37	64.86	36.02	0.11
TiO2	0.00	0.00	0.15	0.10	0.00				4.39	48.90
Al2O3	1.17	0.82	0.52	0.62	29.44	26.49	28.38	18.38	14.08	0.54
FeOT	10.06	27.87	37.90	37.12					17.62	48.45
MnO	0.10	0.72	0.94	0.93					0.00	0.35
MgO	13.34	19.00	10.82	10.98					12.90	0.56
CaO	22.27	0.44	0.69	1.00	11.00	7.87	10.07		0.00	0.65
Na2O	0.30	0.09	0.41	0.49	5.25	7.20	5.89	1.27	0.00	0.00
K2O	0.00	0.00	0.00	0.00	0.34	0.32	0.29	15.02	9.78	0.00

Note (2) cpx, opx 1, plag 1, biot, ilm are from QGNG
 opx 2, plag 2, kspar are from FGGL = B143
 plag 3, opx 3 are from FGGL = B143

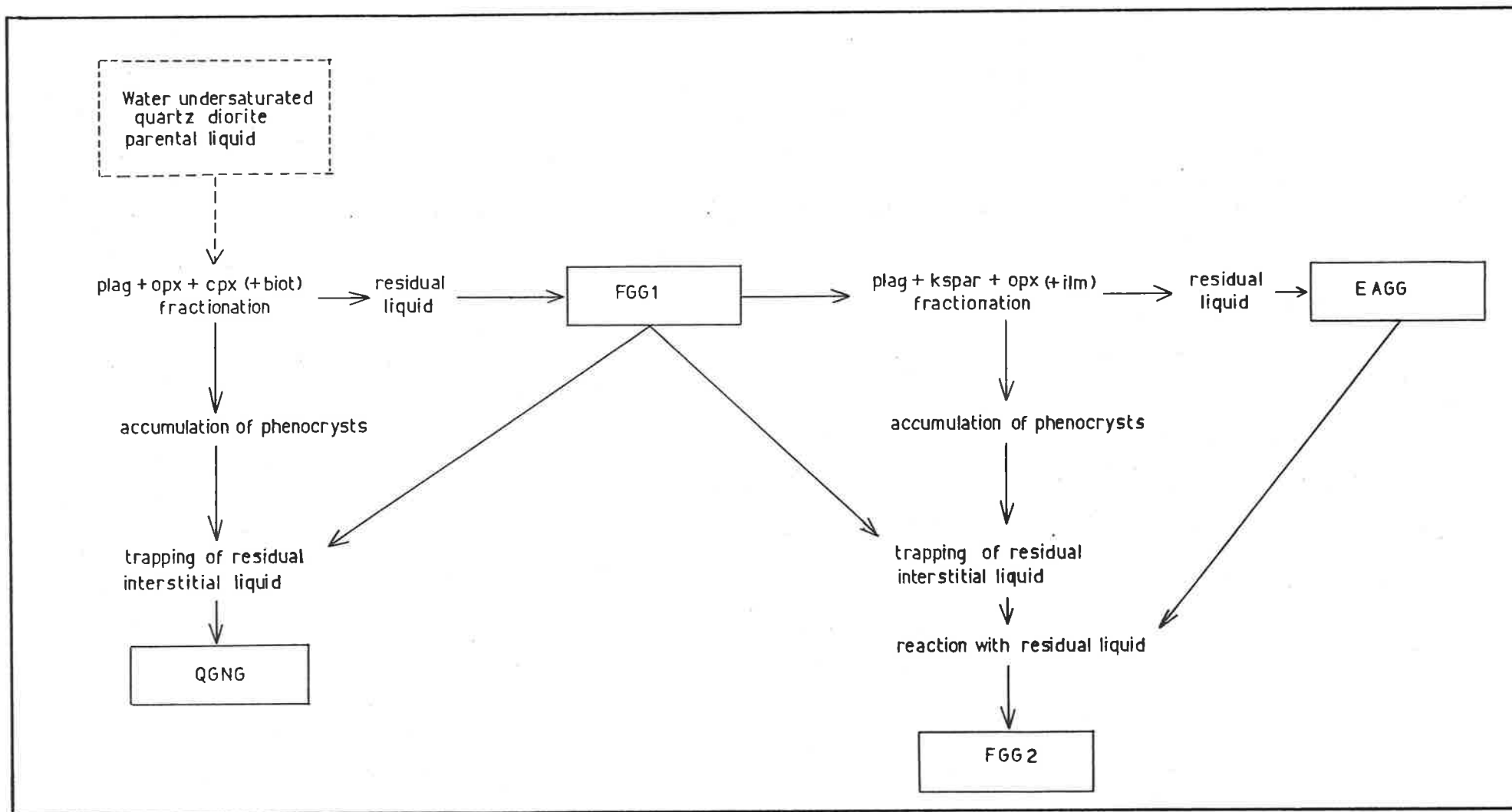


Figure 2.23

Summary chart of relationships of rock units within opx-granitoids of the Donington Granitoid Suite.

possibly reflecting the inappropriateness of the averages used for chemically zoned phenocrysts.

FGG2 can be modelled as a mixture of FGGL parent liquid and opx, plagioclase and alkali feldspar and ilmenite phenocrysts and EAGG residual liquid (Table 2.11).

These mathematical models are supportive of the batholithic fractionation model.

2.5.2.7 Parental magma of DGS opx-granitoids

Assuming that the opx granitoids constitute a comagmatic suite derived from a common parental magma by a fractional crystallisation process, it is possible to place constraints on the nature of the parental magma.

- (1) QGNG cumulate liquidus phases of plagioclase, opx and cpx without amphibole, biotite or alkali feldspar, and CO₂ fluid inclusions suggest a water-undersaturated non-minimum melt.
- (2) QGNG opx phenocrysts show no evidence for pigeonite inversion suggesting a liquidus temperature less than ca. 1050°C.
- (3) Coexisting sub-solidus pyroxenes in QGNG suggest liquidus temperature in excess of 800° - 900°C.
- (4) Predominance of rocks with greater than 65% SiO₂ in exposed outcrop suggests a moderately silicic parental magma.
- (5) Absence of alkali feldspar phenocrysts in QGNG but their presence in FGGL suggest parental magma less siliceous than FGGL.
- (6) Parental magma composition should lie on Harker trends between cumulate QGNG and derivative FGGL.

For these reasons an intermediate to silicic water deficient magma is favoured, perhaps approximately of quartz diorite type.

2.5.2.8 Geochemical analogues of opx-granitoids

It has been pointed out above that despite a general similarity of some geochemical indicators with modern calc-alkaline orogenic rocks, subtle differences in e.g. $Fe_2O_3T, Fe_T/(Fe_T+Mg)$ and K₂O are transitional towards anorogenic magmatism. Thus although a close intrusive parallel has been drawn with the Palaeozoic Inlet Quartz

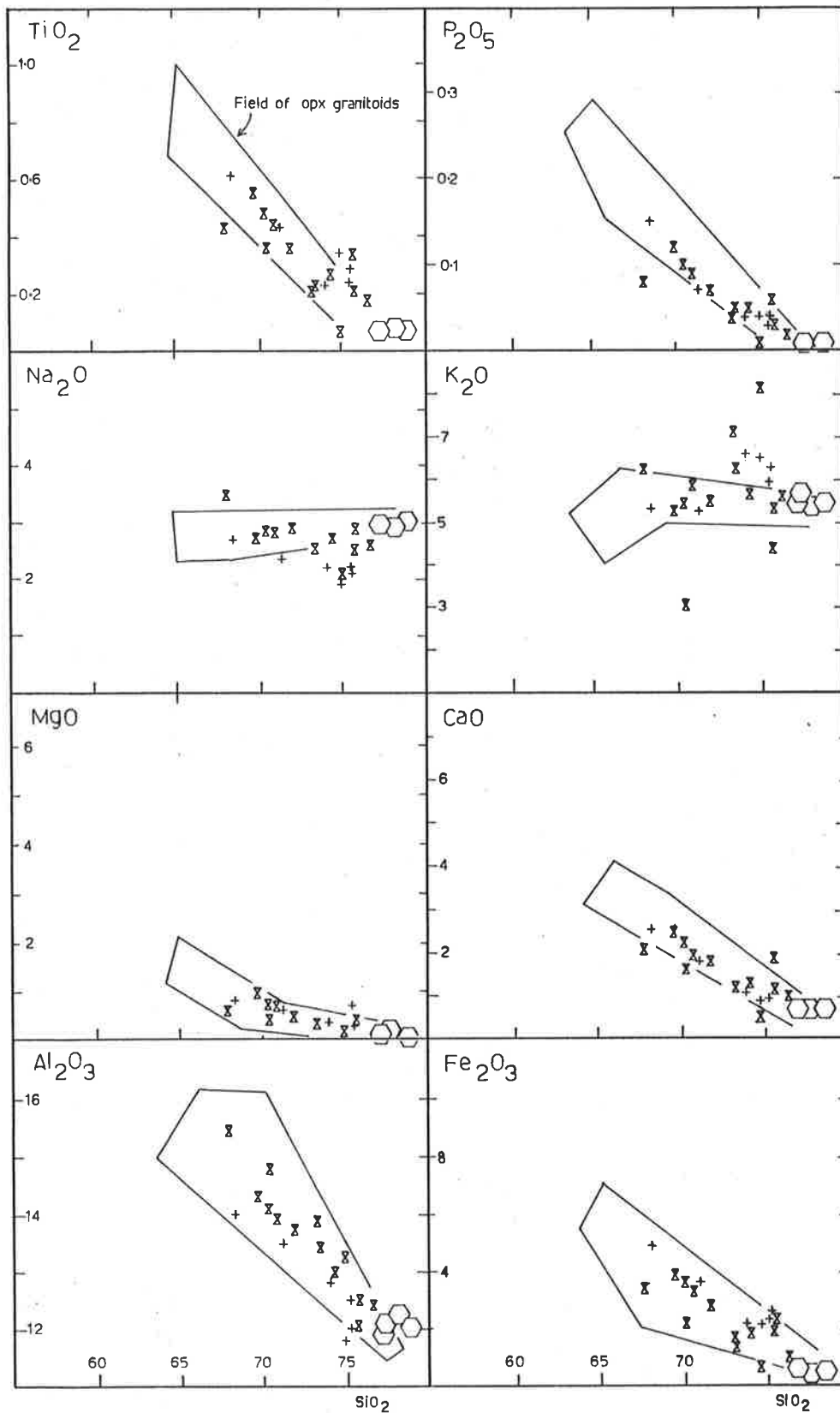


Figure 2-24 Major element variation diagrams for granite gneisses of the Donington Granitoid Suite compared with the fields of opx-granitoids. Symbols as in Figure 2.6.

Monzonite and the Mesozoic Tuolumne Intrusive Series, closer geochemical parallels exist with the silicic complexes cited in Chapter 7. Of these the majority are of Proterozoic age, although some are of Palaeozoic - Mesozoic age.

Rocks of this general geochemical character occur in the charnockitic association, the anorthositic association, the rapakivi granite association and also as widespread volcanics and tuffs.

The significance of magmatism of this type will be re-examined in Chapter 7.

2.5.3 Granite gneisses

2.5.3.1 Major element geochemistry

The granite gneisses, GGI, GG2 and AGG, have a similar range of SiO_2 content as the silicic opx-granitoids (Appendix Table 2.2; Table 2.12) and occupy similar fields on the Harker diagrams for most elements (Fig. 2.24). However relative to the narrowly defined fields of the opx-granitoids on Fig. 2.19, the granite gneisses tend to show more scatter especially for K_2O and $\text{Fe}_2\text{O}_3\text{T}$. This is reminiscent of the scatter in the granite gneiss Rb-Sr isochrons and in their Rb/Sr ratios; and is attributed to the retrogressive process.

2.5.3.2 Trace element geochemistry

The distribution patterns of most trace elements in the granite gneisses, although generally similar to the fields of the opx-granitoids show excessive relative scatter (Fig. 2.25, 2.26). Of particular note is the tendency towards Rb enrichment, wide scatter for Ba and Zr, and the depletion of Y which is particularly evident in the EAGG to AGG transition (Fig. 2.25).

This last feature is reflected also in the REE patterns (Fig. 2.27) where relative to the opx-granitoids the granite gneisses are depleted in MREE and more so the HREE.

2.5.3.3 Genetic model of geochemical distinction from opx-granitoids

The observation, that K_2O (and often other radio active elements such as U, Th, and Rb) and large ion lithophile (LIL) elements are often enriched in rocks bearing hydrated minerals compared with associated anhydrous rock types, is common. A number of authors have attributed these geochemical variations to the primary magmatic intrusive history, e.g.,

Table 2.12: Donington Granitoid Suite. Average major and trace element compositions of granite gneisses.

	GG1(6) *	GG2(13)	AGG(6)
SiO ₂	73.34	72.78	77.85
Al ₂ O ₃	12.80	13.62	12.13
Fe ₂ O ₃ tot	2.91	2.38	0.54
MnO	0.04	0.03	0.01
MgO	0.52	0.48	0.09
CaO	1.44	1.60	0.72
Na ₂ O	2.25	2.72	2.96
K ₂ O	5.98	5.68	5.50
TiO ₂	0.36	0.32	0.07
P ₂ O ₅	0.06	0.06	0.00
Total	99.70	99.67	99.86
Rb	273	299	434
Sr	102	104	11
Ba	608	639	6
Y	30	36	17
Zr	284	195	124
Nb	16	14	7
Sc	8	6	1
V		29	
Ni		15	12
Cr		9	1
La		61	24
Ce		129	34
Nd		37	10
Sm		6	2
Eu		1	0.1
Gd		5	2
Dy		5	2
Er		3	1
Yb		3	2

*number in brackets refers to number of samples averaged.

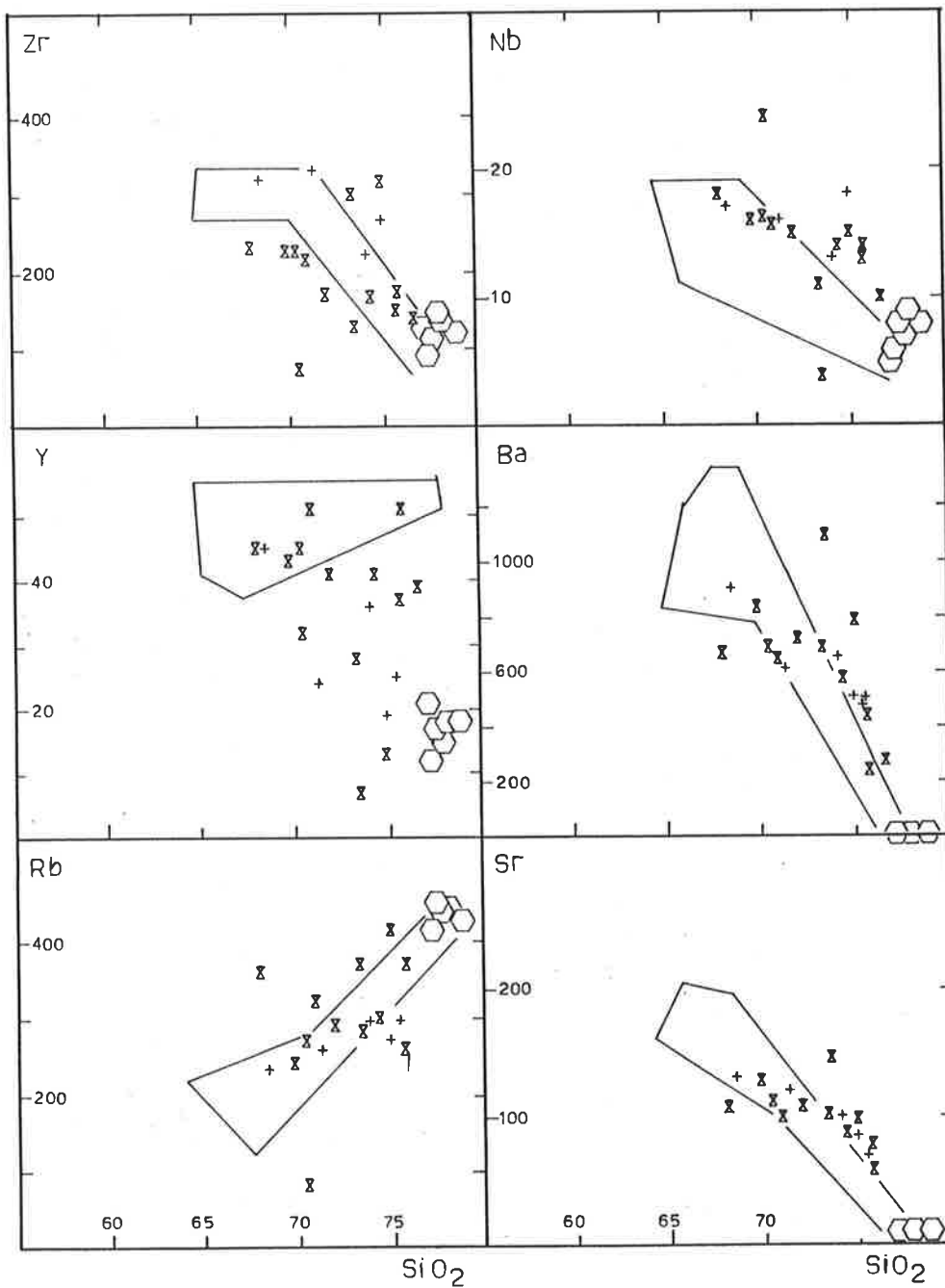


Figure 2.25 Trace element variation diagrams for granite gneisses of the Donington Granitoid Suite compared with the fields of opx-granitoids. Symbols as in Figure 2.6.

- (1) Hubbard & Whitley (1978) suggest that internal differentiation during emplacement, controlled by H_2O aggregation accounts for the association of charnockite and chemically similar granite in the Varberg area of Sweden.
- (2) Kranck (1969) suggested that high-level rapakivi intrusions represent the hydrous facies of lower level anorthositic associations, the rapakivi being also more siliceous and potassic.
- (3) Smithson & Heier (1971) and Smithson & Decker (1973) in two separate instances ascribe radioelement variations in otherwise chemically similar facies of intrusions to the distribution of the fluid phase throughout the magma during intrusion, although here the K_2O content is approximately constant.
- (4) Ormaasen & Raade (1978) show that "wet" and "dry" facies of intrusions contain different LIL element contents, suggestive of primary variations in the distribution of the fluid phase.
- (5) Barker et al. (1975) observe gradations between hydrated and anhydrous intrusive rocks of otherwise similar nature, which they attribute to intrusion of hydrous magma soon after solidification of anhydrous magma.

It is possible that some geochemical variation within the DGS is of a primary nature of the type described by these authors. However the field distribution of the hydrated gneisses has been suggested here to imply a model of retrogressive control in and adjacent to the Kalinjala Mylonite Zone.

A number of previous studies have demonstrated that retrogressive activity in deep crustal rocks is often concentrated in major mylonite shear zones (Burwash & Krupicka 1969; Beach 1976, 1980; Beach & Tarney 1978; Etheridge & Cooper 1981). Similar pervasive chemical changes may occur over larger areas early in the retrogressive cycle but are particularly localised in the shear zone as deformation and strain induced recrystallisation concentrates in them (Beach 1980). These authors and Drury (1973), Wynne-Edwards (1976) and Collerson & Fryer (1978) among others have pointed out the requirement for the passage of a fluid phase through lower crustal rocks pervasively or in shear zones, to accomplish this retrogression. The fluid phase may be H_2O rich or CO_2 rich (Newton et al. 1980; Glassley 1982) and may efficiently

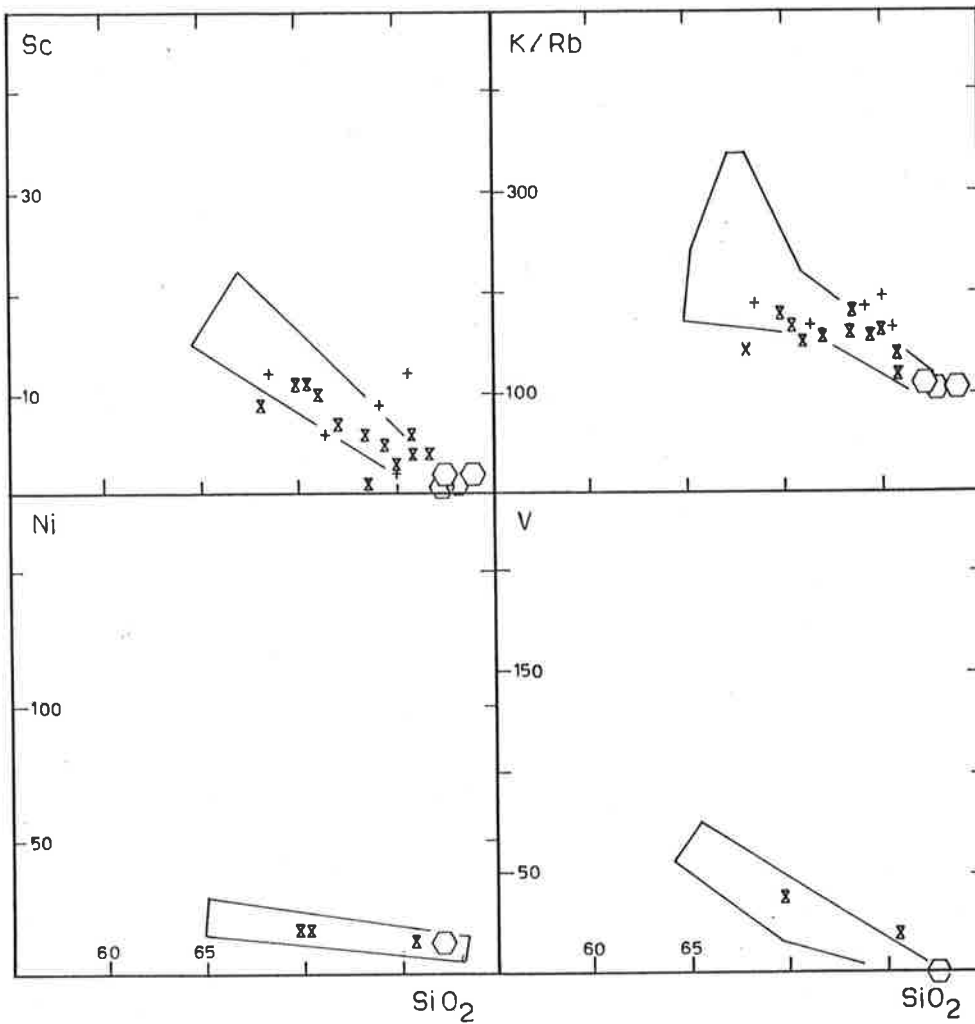


Figure 2-26 Trace element variation diagrams for granite gneisses of the Donington Granitoid Suite compared with the fields of opx-granitoids. Symbols as in Figure 2.6.

complex and transport numerous ionic species. The deep seated shear zones have been suggested to tap mantle fluids (e.g. Beach 1976) and to be associated with mantle melt activity represented by mafic dykes (Beach & Tarney 1978), whereas shallower shear zones have been suggested to tap meteoric water (Etheridge & Cooper 1981). The detailed chemical changes manifested within particular shear zones are a complex function of P, T, PH_2O , PO_2 and the "activities of a whole range of simple and complex species in solution in the fluid, as well as the degree of equilibration between fluid and rock" (Etheridge & Cooper 1981).

A detailed discussion of the specific chemical changes and the nature of the fluids responsible for them is outside the scope of the present study. However it is clear that the transition from FGG1 to GG1 and FGG2 to GG2 involves a significant relative increase in SiO_2 content (Table 2.13). The retrograde mineral reaction series from pyroxene to hornblende to biotite recognised in GG1 and GG2 gneisses is one which involves the release of much SiO_2 which apparently here has been mobilised and deposited in the granite gneisses. All other major elements show a decrease suggestive of SiO_2 dilution except K_2O which shows an increase, suggesting that some K_2O has been added to the retrograde gneisses. Relative to the fields of the opx-granitoids GG1 and GG2 gneisses show more scatter for elements such as K_2O , Na_2O , Rb, Sr, Ba, Y, Zr and Nb with increases for most of these except notably Y (Fig. 2.24, 2.25, 2.26). The REE also show a slight increase in LREE but decrease in HREE (Fig. 2.27). It will be suggested in Chapter 7 that the elements mobile in and added to the retrograde gneisses are similar to elements transported in mantle metasomatising fluids affecting the source areas of the basaltic dyke rocks.

It is the present author's belief that in the Kalinjala shear zone there has been fluid flow up through the crustal rocks possibly from the mantle, effecting mineralogical and geochemical modification and also probably facilitating deformation through hydraulic fracturing.

It is here suggested that the Kalinjala Mylonite Zone on S.E. Eyre Peninsula has acted as a locus of D_{1-2} (as well as D_3 ; Parker 1980) strain, a zone of LIL-enriched fluid flow and extensive retrogressive recrystallisation and metasomatism. The scatter in geochemical and geochronological data in the hydrated gneisses is attributed to this retrogressive, metasomatic process.

Table 2.13: Average composition of opx-granitoids and retrogressive granite gneisses of the Donington Granitoid Suite.

	FGG1 (7) *	GG1 (6)	FGG2 (4)	GG2 (13)
SiO ₂	68.33	73.34	67.75	72.78
Al ₂ O ₃	14.67	12.80	15.63	13.62
Fe ₂ O _{3T}	4.58	2.91	3.90	2.38
MnO	0.07	0.04	0.04	0.03
MgO	0.97	0.52	0.83	0.48
CaO	2.82	1.44	2.77	1.60
Na ₂ O	2.83	2.25	2.89	2.72
K ₂ O	5.07	5.98	5.55	5.68
TiO ₂	0.65	0.36	0.63	0.32
P ₂ O ₅	0.16	0.06	0.16	0.06
Ca	60	-	49	61
Yb	4.4	-	3.1	3.2
Rb	229	273	182	299
Sr	147	102	169	104
Ba	915	608	1166	639
Y	41	30	38	36
Zr	305	284	310	195
Nb	16	16	14	14
Sc	13	8	15	6
V	41	-	53	29
Ni	21	-	19	15
Cr	12	-	18	9
Eu	1.8	-	1.7	1.0

*number of brackets refers to the number of samples averaged.

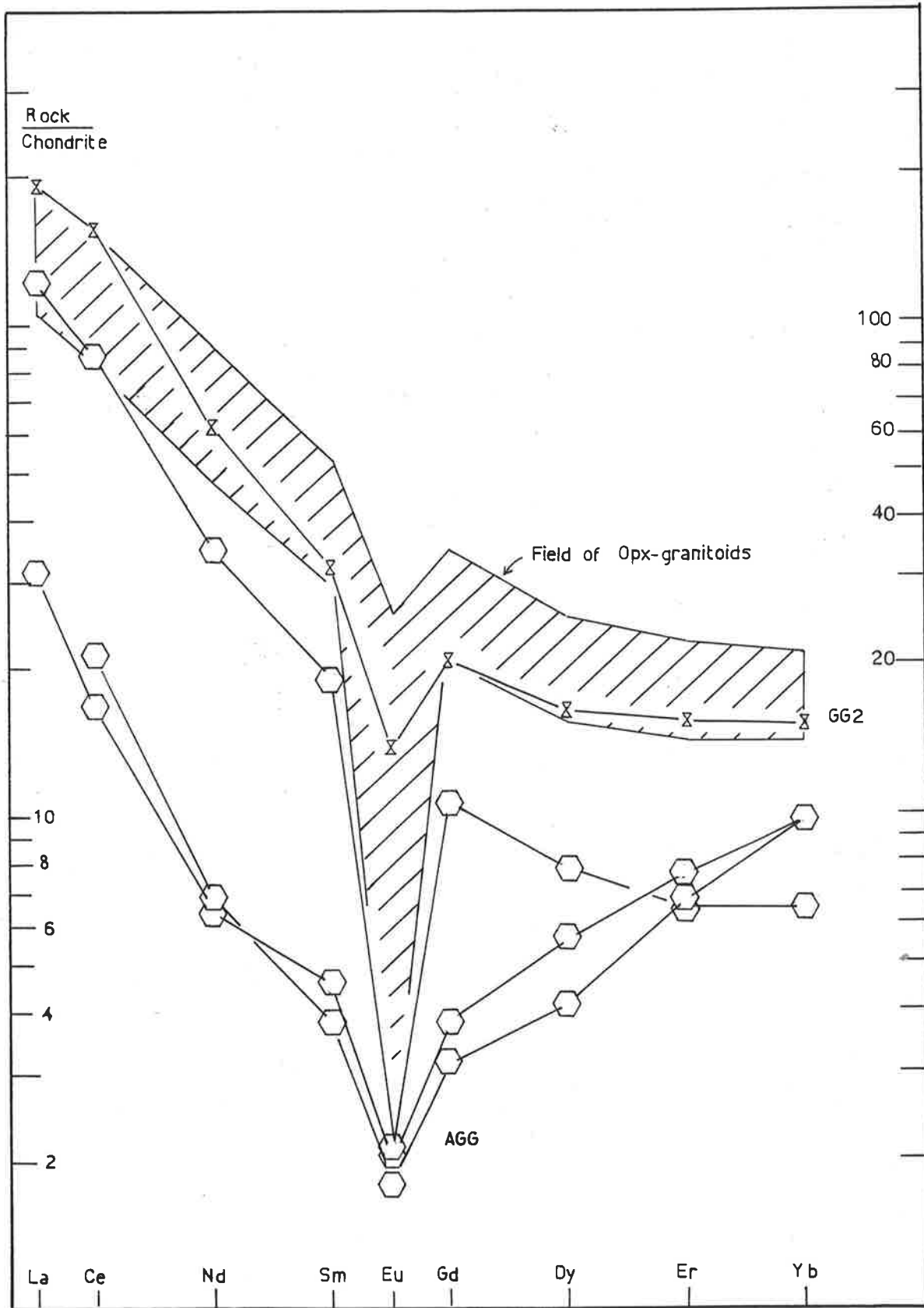


Figure 2.27

Chondrite normalised REE plots of granite gneisses of the Donington Granitoid Suite compared with the field of opx-granitoids. Symbols as in Figure 2.6.

The tracts of granite gneiss in which this retrogressive metasomatic process is suggested to have occurred on south-eastern Eyre Peninsula are extensive and fundamental to the understanding of the development of Proterozoic crust on the Gawler Craton. Collerson & Fryer (1978) envisage Rb-metasomatism of extensive tracts of basement gneisses to account for updating of Rb-Sr isochrons and so suggest that interpretations of crustal evolutionary history in such terrains are worthy of revision. The present author concurs in the recognition of Rb-metasomatic events, but in this particular case is able to show that the metasomatic event is associated spatially with a fundamental tectonic lineament and is approximately coeval with the primary magmatic emplacement of the opx-granitoids.

The implicit fundamental role of the Kalinjala Mylonite Zone in the Proterozoic development of the south eastern Eyre Peninsula will be re-examined in Chapter 7, in conjunction with a petrochemical and tectonic synthesis of data from the other rock suites of this and other studies.

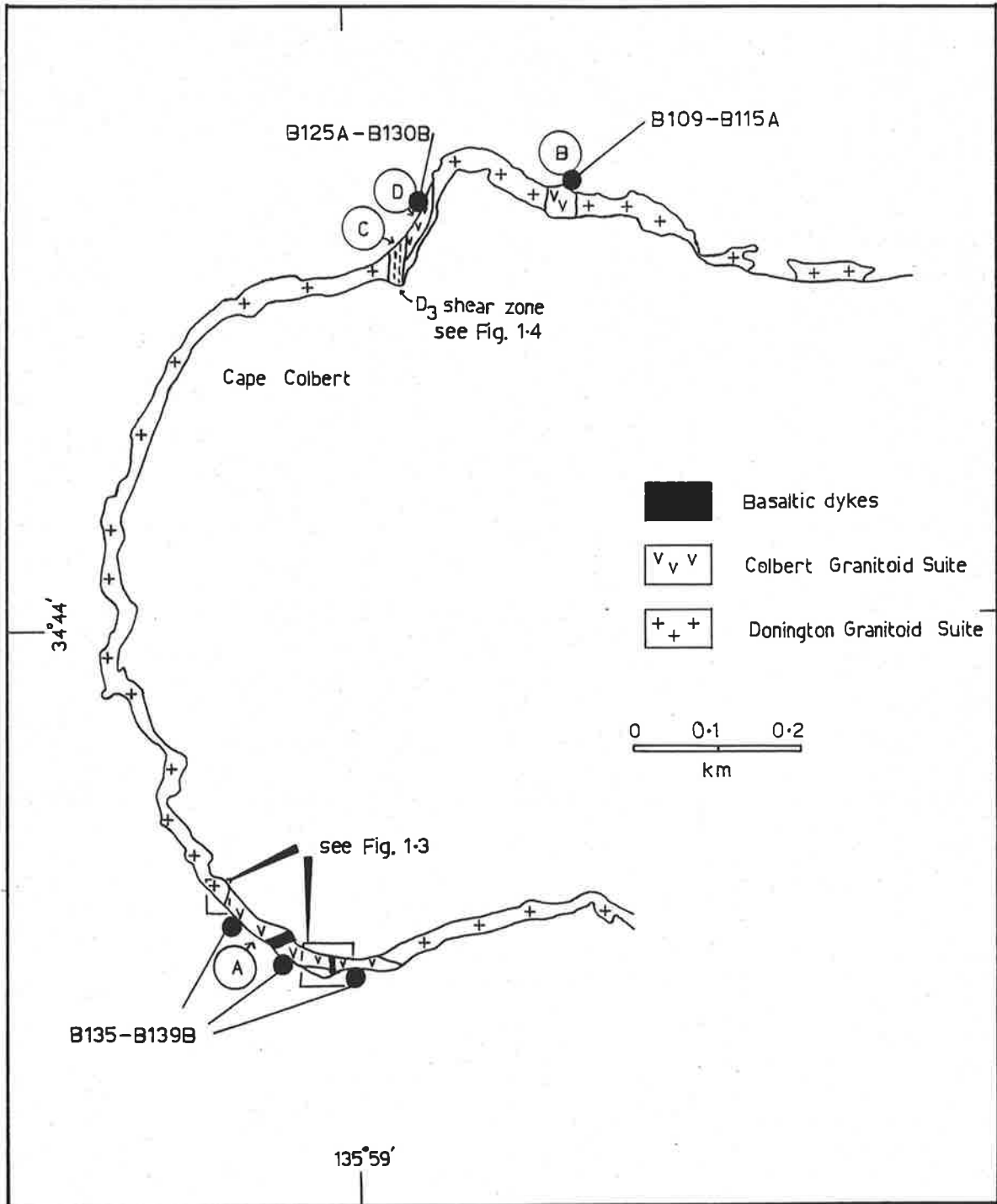


Figure 3.1

Geological map of outcrops of the Colbert Granitoid Suite on Cape Colbert. Refer to Figure 1.2 for the locality of Cape Colbert.

CHAPTER 3.

COLBERT GRANITOID SUITE

3.1 INTRODUCTION AND FIELD GEOLOGY

Prior to this current study no literature account of this suite of granitoid rocks existed. Previously published maps have not differentiated the suite from the gneisses of the Lincoln Complex (Table 1.1) of Thomson (1980).

The Colbert Granitoid Suite (CGS) is composed of two main rock-types,

(1) Colbert hornblende granite gneiss
and (2) Colbert alkali feldspar granite gneiss,
which crop out at four main localities (Fig. 3.1) and locally appear to grade into one another. The hornblende granite gneiss intrudes the DGS with chilled contacts on Cape Colbert at locality A (Fig. 3.1, 1.3). There is only a weak probable S_3 foliation present in the hornblende granite gneiss at this locality whereas the DGS shows abundant D_{1-2} subsolidus recrystallisation. These observations suggest the CGS at this locality has largely escaped strong deformation and was intruded after the peak of high-grade metamorphism and deformation associated with D_{1-2} .

A much more intense, local D_3 shear zone fabric is present in the hornblende granite gneiss at locality B (Fig. 3.1). At locality C (Fig. 3.1) net veins of the alkali feldspar granite gneiss intrude the DGS, and, in a narrow D_3 shear zone, are converted into a tectonic layering (Fig. 1.4, 1.7C). The alkali feldspar granite gneiss also contains well-developed D_3 shear zone fabrics at locality D (Fig. 3.1) where the mafic inclusions described in Chapter 1 occur (Fig. 1.5C).

Amphibolitic dykes intrude the CGS and are involved in D_3 shear zones (Fig. 1.4), and an amphibolitic dyke cross-cuts the hornblende granite gneiss at locality A (Fig. 3.1).

A variety of xenoliths is present in the hornblende granite gneiss at locality A. Most of the xenoliths are rounded, mafic, foliated, amphibole-rich rocks although some are more angular, pink-coloured, quartzofeldspathic, deformed, fine-grained or megacrystic rocks. Many of the mafic xenoliths appear to be residual solid material from the source of melting (Chappell & White 1974) undergoing disaggregation at the time of emplacement, but the quartzofeldspathic xenoliths appear

to be derived from the DGS country rock. The incorporation of pink-coloured xenoliths of DGS material suggests that emplacement of the hornblende granite gneiss post-dated D_{1-2} retrogression of the DGS.

Hence evidence from chilled contacts, shear zones, mafic inclusions, basaltic dykes and xenoliths suggests the CGS was emplaced after the peak of high-grade metamorphism and deformation (D_1 and/or D_2) but before D_3 .

Subsequent sections of this chapter will seek,

- (1) to establish the petrographic, Sr-isotopic, and geochemical character of the CGS,
 - (2) to establish a minimum age for D_2 and a maximum age for D_3
 - (3) to compare the CGS with the DGS
- and (4) to suggest a petrogenetic model for the CGS.

3.2 PETROGRAPHY AND MINERAL CHEMISTRY

3.2.1 Colbert hornblende granite gneiss - Locality A

Locality A (Fig. 3.1, 1.3) constitutes the type locality for the hornblende granite gneiss. The only weak development of S_3 allows a large degree of relict igneous texture to be observed. The rock is grey, medium to coarse grained and porphyritic. Phenocrysts of plagioclase, alkali feldspar and hornblende are visible in hand-specimen.

In thin section the texture is seriate, polygonal to interlobate, with relict phenocrysts of plagioclase, alkali feldspar and hastingsitic hornblende surrounded by a mildly recrystallised matrix. Some ribbon-like quartz aggregates are present and tend to wrap around the relict phenocrysts. The quartz ribbons have developed sub-grains of quartz.

Relict plagioclase phenocrysts are subhedral, moderately zoned with irregular sericitised cores, and often exhibit fine needle-like inclusions of apatite. The alkali feldspar phenocrysts are subhedral to anhedral, sometimes Carlsbad twinned and may contain approximately concentrically arranged, anhedral blebby inclusions of quartz and lesser plagioclase, hornblende, biotite, zircon and apatite. Most grains are perthitic (very fine-grained bead perthite).

Coarse grained, anhedral to subhedral hornblende phenocrysts are often associated in aggregates with quartz, Fe - Ti oxide, biotite and less commonly alkali feldspar and apatite, and may have inclusions

of these same minerals.

Microxenoliths are common in the hornblende granite gneiss, one variety of which is mafic, largely hornblende-bearing, and with inequigranular polygonal to interlobate textures. The amphibole grains in these xenoliths are not dissimilar to the relict phenocrysts in the host.

The amphibole phenocrysts in the bulk rock appear to be in part derived from disaggregation of the xenolith material and hence the xenoliths are thought to be restite, and probably representative of the relict source material of the hornblende granite magma.

These observations are summarised in Table 3.1.

3.2.2 Colbert hornblende granite gneiss - Locality B

The mineralogy of the hornblende granite gneiss at Locality B is similar to that at Locality A. However, the texture is seriate, polygonal to interlobate with a well-developed metamorphic tectonite fabric. This fabric has been developed in a D_3 shear zone at this locality.

Associated with the abundant metamorphic recrystallisation is the development of sphene coronas around ilmenite grains and the development of microcline twinning in alkali feldspar. Minor amounts of subsolidus muscovite are also present.

3.2.3 Colbert alkali feldspar granite gneiss - Locality D

These leucocratic rocks bear close textural similarity to the hornblende granite gneiss at Locality B. Corroded relict phenocrysts of alkali feldspar and lesser plagioclase with sericitised cores are set in a seriate, polygonal to interlobate matrix of microcline, quartz, and lesser plagioclase. Relict hornblende phenocrysts are rare.

These rocks have a well developed S_3 metamorphic tectonite fabric.

3.2.4 Mineral chemistry of the Colbert hornblende granite gneiss

The major minerals from two thin sections of the Colbert hornblende granite gneiss were analysed by electron microprobe. Specimen B135 is from locality A and specimen B114 is from locality B. The averaged compositions are presented in Appendix Table 3.1 and deduced geothermometric data presented in Table 3.2.

(1) Feldspars

The plagioclase phenocrysts in both rocks are broadly similar in composition and average Ab_{60} and Ab_{67} . These compositions are

Table 3.1 Colbert Granitoid Suite model composition and textural summary

Rock unit and locality	Type Specimen	Phenocrysts	Groundmass	Texture and intrusive history
Colbert Hornblende Granite Gneiss Locality A*	515-B135	Plagioclase Alkali Feldspar Hornblende Quartz	Plagioclase Alkali feldspar, Hornblende Quartz biotite, apatite, zircon, Fe-Ti oxide	Relict phenocrysts Chilled margins Seriata, polygonal to interlobate some quartz ribbons mafic restite xenoliths xenoliths of retrogressed DGS rocks intruded post-D ₂
Colbert Hornblende Granite Gneiss Locality B*	515-B114	as above	as above plus sphene coronas on Fe-Ti oxide	Seriata, polygonal to interlobate well developed S ₃ fabric D ₃ shear zone
Colbert Alkali Feldspar Granite Gneiss Locality D*	515-B125	Alkali Feldspar Quartz Plagioclase	Alkali Feldspar Quartz, Plagioclase, (hornblende, biotite, apatite, zircon, Fe-Ti oxide)	Seriata, polygonal to interlobate well developed S ₃ fabric

NOTE: * see Figure 3.1

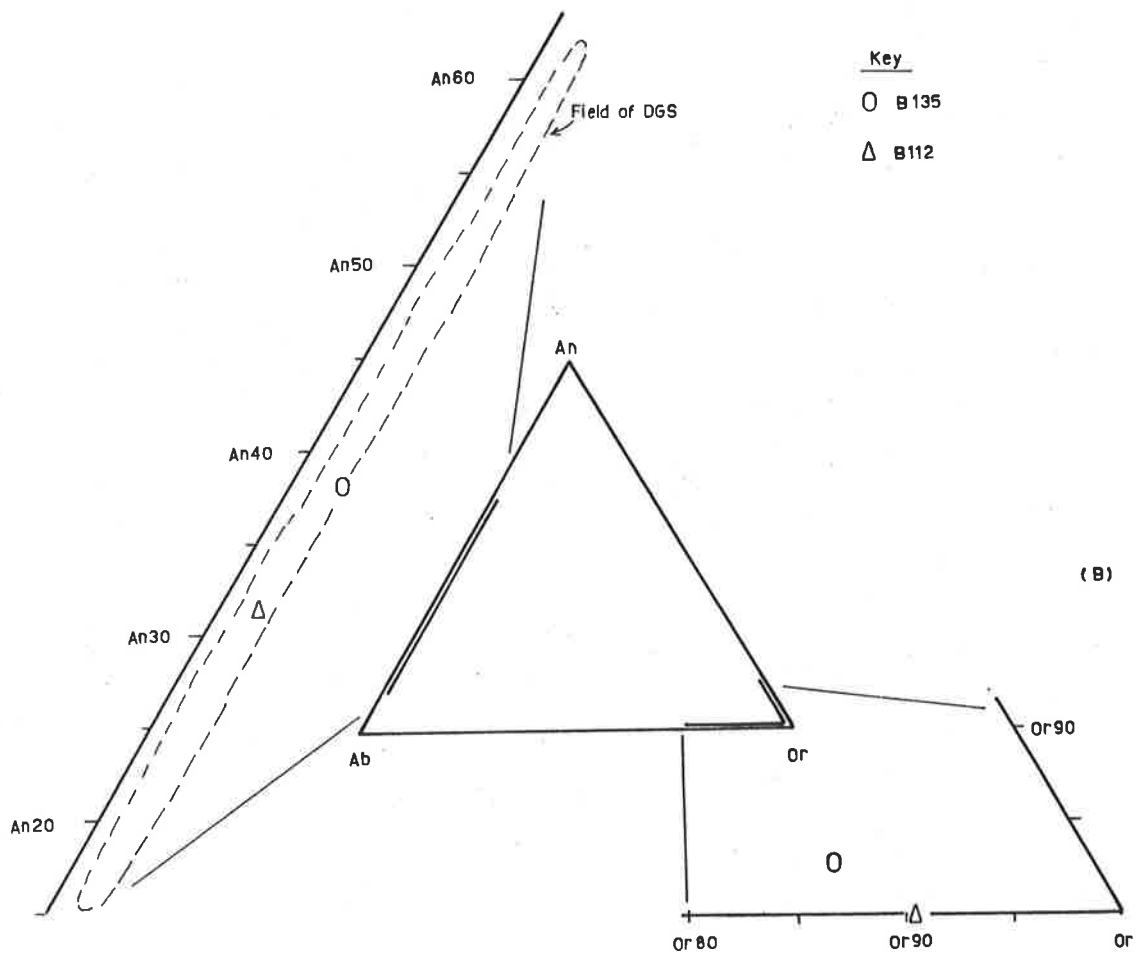
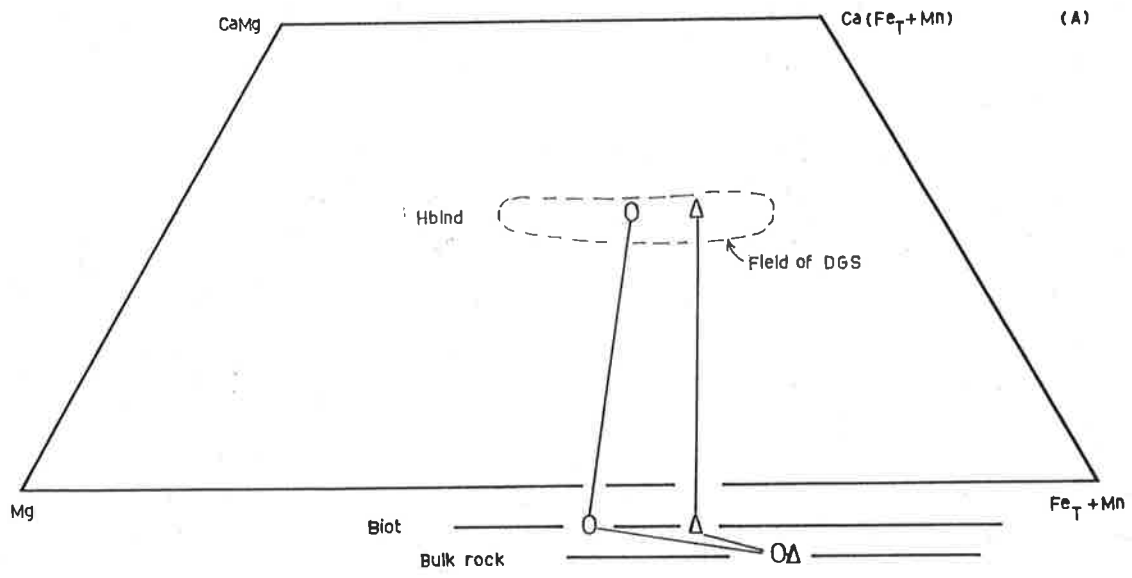


Figure 3.2 Hornblende granite gneiss of the Colbert Granitoid Suite minerals
 (A) Ferromagnesian minerals and bulk rocks on Ca-Mg-Fe + Mn quadrilateral
 (B) Feldspars on An-Ab-Or triangle.

comparable to those in phenocrysts in opx-granitoids of similar SiO_2 content from the DGS (Fig. 3.2). However in the hornblende granite gneiss B135 has the higher SiO_2 content (Appendix Table 3.2) of the two specimens analysed, but the more calcic plagioclase.

The orthoclase phenocrysts in B135 have not exsolved completely and have the composition $\text{Or}_{85} \text{Ab}_{12} \text{An}_3$, whereas the B114 microcline has the composition $\text{Or}_{90} \text{Ab}_{10}$ reflecting subsolidus exsolution.

The relict igneous phenocrysts in B135 allow the calculation of a feldspar temperature (after the method of Powell & Powell (1977) and assuming a pressure of emplacement of 5 Kbar). The calculated temperature of 535°C (Table 3.2) is possibly recording a subsolidus cooling. A similar calculation for B114 yields 495°C (Table 3.2) which may be reflecting D_3 shear zone recrystallisation.

However these temperatures are within the range of feldspar temperatures derived from recrystallised granite gneisses of the DGS (Table 2.3) and may simply be recording a blocking temperature effect during plutonic cooling.

(2) Amphiboles

The amphibole phenocrysts in both B135 and B114 may be classified as magnesian hastingsite (Leake 1978). Their compositions are similar to the igneous or high-grade metamorphic hastingsitic hornblendes in the opx-granitoids of the DGS (Fig. 3.3). However in distinct contrast to the DGS, the more siliceous bulk rock B135 has the amphibole with the higher $\text{Mg}/(\text{Mg} + \text{Fe}_T + \text{Mn})$.

(3) Opaque Oxides

The compositions of magnetite and ilmenite in B114 reflect extensive subsolidus exsolution and recrystallisation during D_3 , whereas B135 contains minimally exsolved and recrystallised phases. The calculated temperature and oxygen fugacity for B135 of 705°C and $\log a_{\text{O}_2} = -13.1$ (Fig. 3.4, Table 3.2) may approximate the conditions of magmatic emplacement, whereas the corresponding values for B114, 440°C and -24.6 (Fig. 3.4, Table 3.2) probably approximate the conditions of D_3 shear zone formation or subsolidus cooling.

These calculated values are similar to, but displaced slightly away from the field of DGS opaque oxides (Fig. 3.4). A buffer more appropriate to primary hornblende + biotite is indicated.

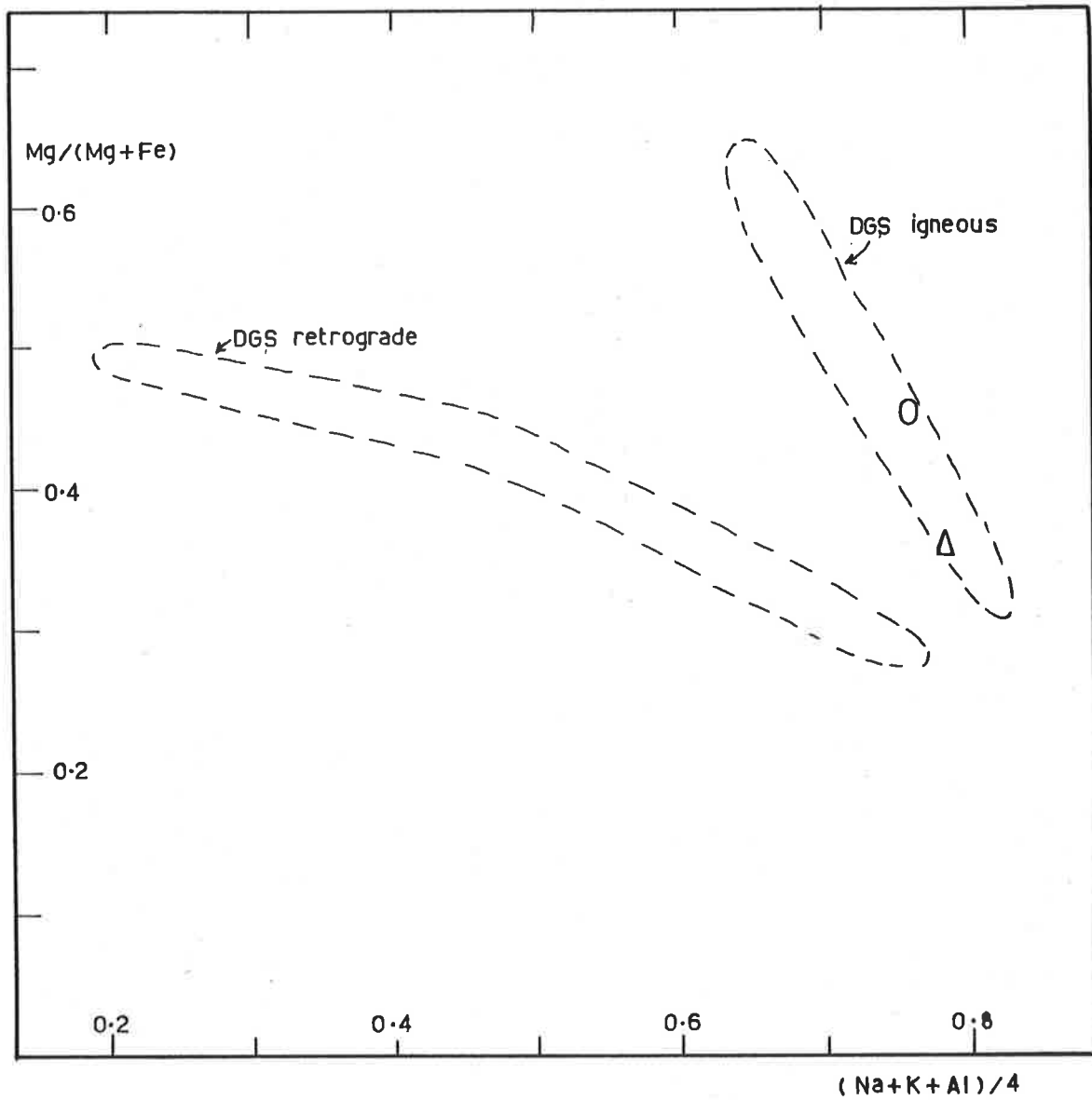


Figure 3.3

Hornblende granite gneiss of the Colbert Granitoid Suite amphiboles compared with amphiboles in high-grade gneisses of the Donington Granitoid Suite. Symbols as in Figure 3.2.

(4) Biotite

The biotite compositions for the hornblende granite gneiss also indicate that the more siliceous bulk rock has the more Mg-rich biotite, similar to the amphiboles (Fig. 3.2). The experimental results of Wones & Eugster (1965) at 2 Kbar total pressure, suggest the hornblende granite gneiss biotites crystallised at 750 C - 850 C at oxygen fugacity of $\log a_{O_2} = -12$ to -15 (Fig. 3.4, Table 3.2) consistent with the opaque oxides.

(5) Discussion and conclusions

The ferromagnesian minerals in the hornblende granite gneiss show a positive correlation between SiO_2 content in the bulk rock and $Mg/(Mg + Fe_T)$ in the mineral. A similar correlation between bulk rock SiO_2 and plagioclase An content exists. These two features are not easily reconcilable with a fractional crystallisation model for the bulk rock variation in composition within the hornblende granite gneiss, but support the observation above that in part the phenocrysts in the gneiss may be derived by disaggregation of the included mafic (restite) xenoliths.

Magmatic emplacement of the hornblende granite gneiss apparently occurred at $750^\circ - 850^\circ C$ at $\log a_{O_2}$ of -12 to -15 with subsequent subsolidus recrystallisation in local D_3 shear zones at $440^\circ - 535^\circ C$ and $\log a_{O_2}$ of ca. -25 .

3.2.5 Summary and discussion

Relict phenocrysts of plagioclase, alkali feldspar and hastingsitic hornblende testify to the primary igneous character of the CGS. There is no evidence for the former presence of orthopyroxene in the granitoids, in contrast to the DGS. However, the pink, alkali feldspar granite gneisses of the CGS and DGS bear superficial resemblance to one another, so that care must be taken in mapping the respective suites. On Cape Colbert this resemblance presents no problem as the pink alkali feldspar granite gneisses of the CGS intrude rocks of the DGS containing primary orthopyroxene.

The well-developed metamorphic tectonite fabrics have been attributed to local narrow D_3 shear zones.

3.3 RB-SR GEOCHRONOLOGY

Rb-Sr geochronology of the rock types within the CGS was undertaken for the following reasons,

Table 3.2: Colbert Granitoid Suite - Geothermometry of the hornblende granite gneiss.

	T°C	- log aO ₂
mag + ilm B135	705	13.1
B114	440	24.6
Powell & Powell (1977)		
plag + Kspar B135	535 (at 5 Kbar)	
B114	495 (at 5 Kbar)	
Powell & Powell (1977)		
biot + Kspar + mag	750-850 (at 2 Kbar)	12-15
Wones & Eugster (1965)		

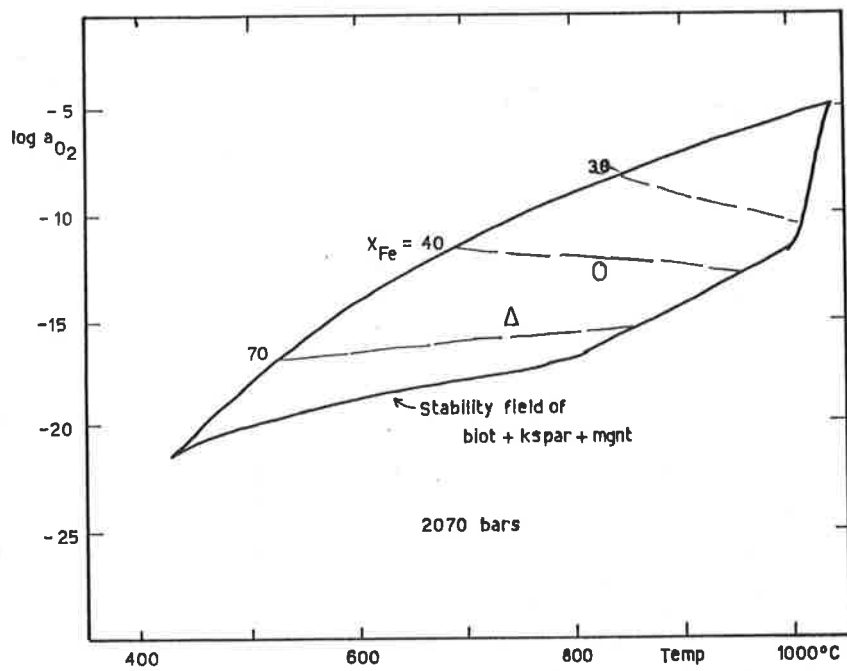
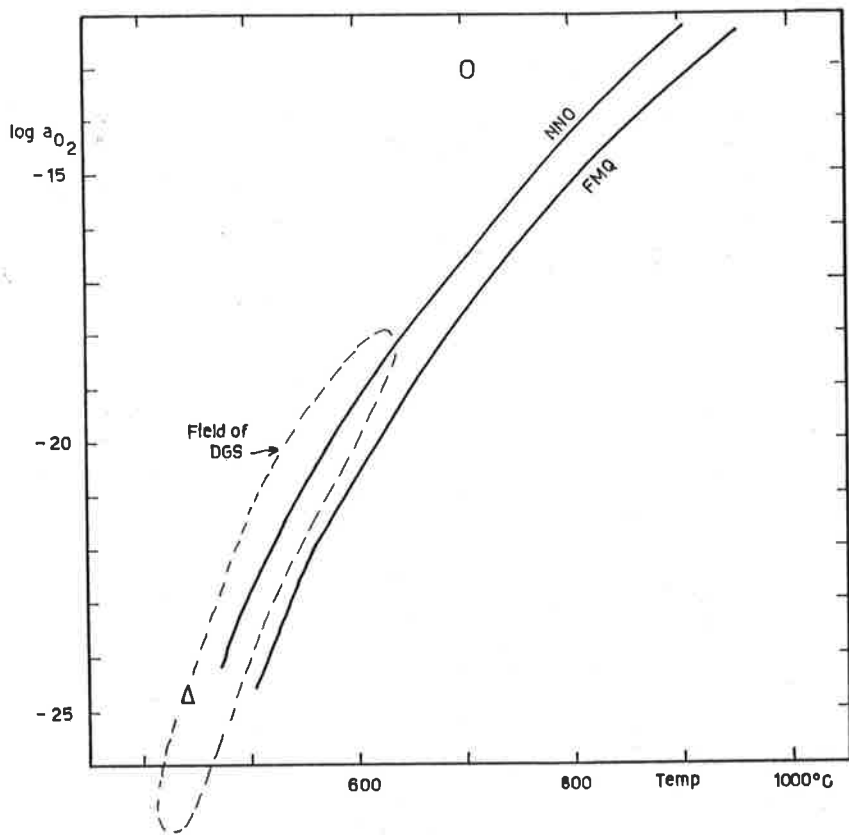


Figure 3.4 Upper: Coexisting magnetite and ilmenite in Colbert Granitoid Suite
 Lower: Biotite in Colbert Granitoid Suite compared with data of Wones & Eugster (1965).
 Symbols as in Figure 3.2.

- (1) to date the intrusion of the CGS
- (2) to test whether the different rock types represent comagmatic intrusions
- (3) to attempt to constrain the age of D_2 and D_3
- (4) to characterise the Sr-isotopic composition of the source of granitoid magma.

3.3.1 Results

(1) Colbert hornblende granite gneiss - Locality A

Seven total-rock samples were collected from Locality A within an area ca 15m x 15m. Only a small dispersion in Rb/Sr exists (Table 3.3) which allows for only poor definition of isochron slope and intercept, despite the perfect fit of data points (Fig. 3.5). The Model 1 solution age is 1789 ± 750 Ma with IR of 0.7066 ± 500 (Regression 1, Table 3.4).

(2) Colbert hornblende granite gneiss - Locality B

A further six total-rock samples were collected from this locality from a smaller area than at Locality A. Samples B112A and B112B were prepared from one block of rock (ca. 6kg) and split into smaller aliquots (ca. 2kg); their Rb/Sr ratios are almost identical (Table 3.3). A low dispersion in Rb/Sr ratio is present in all six samples as at Locality A, although the average Rb/Sr ratios is lower than at Locality A (Table 3.3).

Regression of the six data points indicates a very poor fit to an isochron, with an MSWD = 175 (Table 3.4). The Model 3 solution age is 1833 ± 800 Ma with IR of 0.7048 ± 400 (Fig. 3.5; Regression 2, Table 3.4), and is indistinguishable from the Locality A result although the imprecision allows only limited constraints to be placed.

(3) Combined regression

Combining the 13 samples from both sites results in a near perfect fit isochron of MSWD = 2.22 with Model 3 solution age of 1778 ± 35 Ma and IR of 0.7073 ± 20 (Fig. 3.5; Regression 3, Table 3.4).

(4) Colbert alkali feldspar granite gneiss - Locality D

Sampling of this rock type at Locality D was restricted to an

Table 3.3 Colbert Granitoid SuiteRb-Sr analytical data

Sample	Rb ppm	Sr ppm	Rb/Sr	$^{87}\text{Rb}/^{86}\text{Sr}$	$^{87}\text{Sr}/^{86}\text{Sr}$
<u>Colbert hornblende granite gneiss</u>					
Locality A					
515 - B135	235	145	1.62	4.751	0.82892
515 - B136A	234	143	1.64	4.795	0.83044
515 - B136B	235	143	1.64	4.806	0.83034
515 - B137	232	141	1.65	4.802	0.82945
515 - B138	233	143	1.63	4.763	0.82920
515 - B139A	237	142	1.67	4.886	0.83224
515 - B139B	233	140	1.66	4.867	0.83159
Locality B					
515 - B109	196	187	1.05	3.053	0.78629
515 - B111	198	186	1.06	3.100	0.78569
515 - B112A	197	183	1.08	3.148	0.78834
515 - B112B	199	184	1.08	3.142	0.78802
515 - B114	194	184	1.05	3.062	0.78498
515 - B115A	202	183	1.10	3.234	0.78986
<u>Colbert alkali feldspar granite gneiss</u>					
Locality D					
515 - B125A	276	54.0	5.11	15.380	1.09254
515 - B125B	272	55.8	4.87	14.615	1.07469
515 - B127A	268	57.8	4.64	13.887	1.06449
515 - B127C	278	58.6	4.74	14.221	1.07142
515 - B129A	281	57.0	4.93	14.817	1.08463
515 - B129B	277	56.9	4.87	14.574	1.08041
515 - B130A	300	28.3	10.60	33.098	1.53747
515 - B130B	299	28.1	10.64	33.239	1.55008

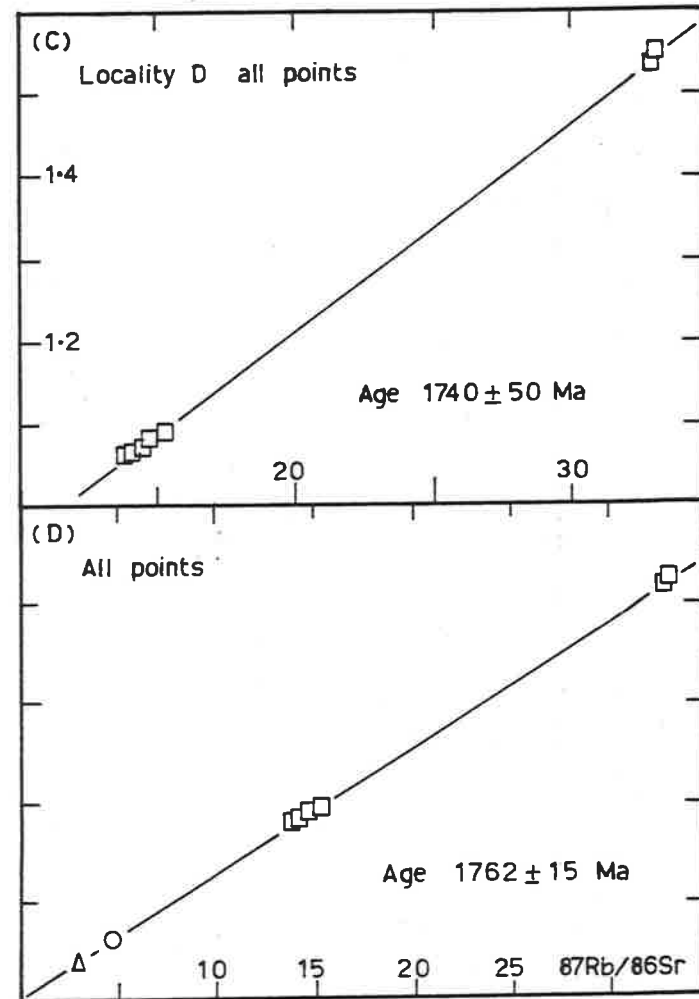
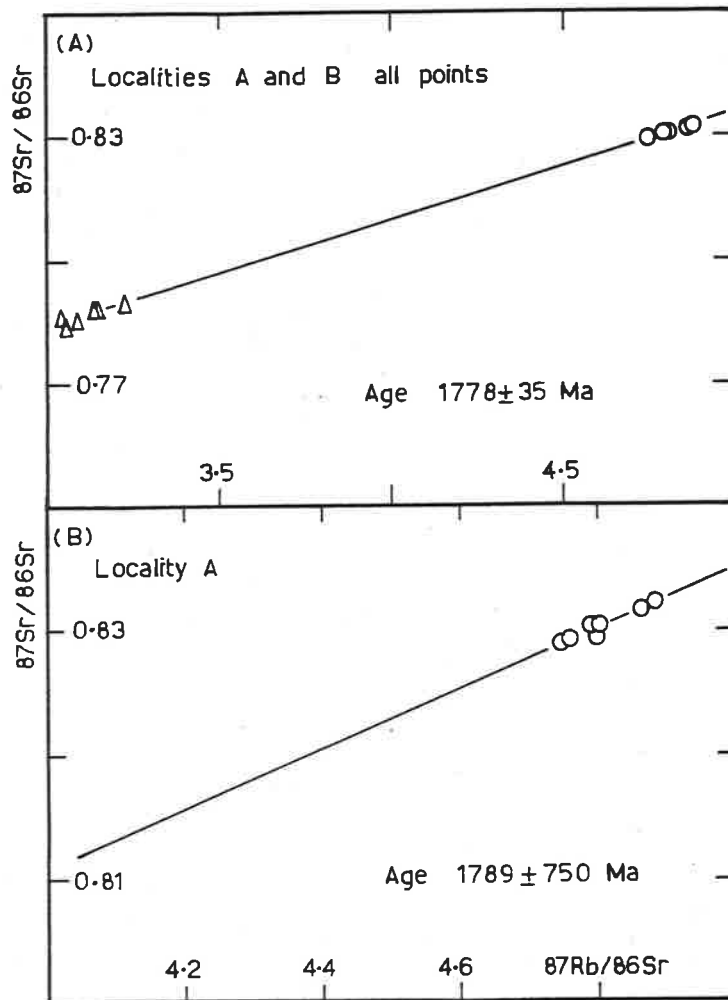


Figure 3.5

Isochron diagrams for rock-types within Colbert Granitoid Suite. Symbols as in Figure 3.2, plus alkali feldspar granite gneiss = open squares.

area ca. 20m x 10m, where four blocks of rock (ca. 6kg) were collected. Each of these blocks were split into aliquots, A, B, and C of ca. 1.5kg, from which B125 (A,B), B127(A,C), B129 (A,B) and B130(A,B) were selected for analysis. The first six of these were sampled from within 5 metres of each other, whereas the last two are more leucocratic and were removed from the others by ca. 10 metres.

The first six samples show a moderate dispersion of Rb/Sr ratio (Table 3.3) and yield a Model 2 solution of MSWD = 5.0 with a calculated age of 1340 ± 350 Ma and IR of 0.7976 ± 700 (Regression 4, Table 3.4). Inclusion of the data for B130(A,B) results in a Model 4 solution of MSWD = 6.3 and calculated age of 1740 ± 50 Ma with IR of 0.7131 ± 90 (Fig. 3.5; Regression 5, Table 3.4). This age and IR are controlled largely by the higher Rb/Sr ratio of B130 (A,B) and are statistically indistinguishable from those calculated for the hornblende granite gneiss.

(5) Combined regression of all Colbert Granitoid Suite samples

The regression of all 21 samples of hornblende granite gneiss and alkali feldspar granite gneiss results in a reasonable fit solution of MSWD = 3.6 with Model 2 solution age of 1762 ± 15 Ma and IR of 0.7082 ± 10 (Fig. 3.5; Regression 6, Table 3.4). This result is indistinguishable from the previous regressions.

3.3.2 Discussion

(1) Emplacement age of the Colbert Granitoid Suite

Inspection of the deviation of data points from the combined isochron shows that all except one of the points from Locality A plot within one standard deviation of the isochron, whereas almost all of the scatter is contained within the data from the other sites B and D. Thus almost all of the scatter is contained in samples which have suffered strong deformation and metamorphic recrystallisation suggesting open system behaviour on the sample size scale.

The effect of isotopic disturbance and redistribution at localities B and D may be minimised by averaging data from these sampling sites to produce an isotopic composition more representative of the site. Combination and regression of these averaged site data with Locality A data points results in a Model 1 isochron of perfect fit (MSWD = 0.65) and calculated age of 1757 ± 14 Ma and IR of 0.7087 ± 10 (Regression 7, Table 3.4). This result strongly suggests that

Table 3.4: Colbert Granitoid Suite
Rb-Sr isochron regression groups

Regression number	Grouping	MSWD*	Model	Age (Ma)	IR
1	Colbert Hornblende Granite Gneiss - Locality A	0.6(7)	1	1789±750	0.7066±500
2	Colbert Hornblende Granite Gneiss - Locality B	175(6)	3	1833±800	0.7048±400
3	All Colbert Hornblende Granite Gneisses	2.2(13)	3	1778± 35	0.7073± 20
4	Colbert Alkali Feldspar Granite Gneiss (selected - Locality D	5.0(6)	2	1340±350	0.7976±700
5	Colbert Alkali Feldspar Granite Gneiss - Locality D	6.3(8)	4	1740± 50	0.7131± 90
6	All samples	3.6(21)	2	1762± 15	0.7082± 10
7	Colbert Hornblende Granite - Locality A plus other sites averaged	0.65(10)	1	1757± 14	0.7087± 10

*number of brackets refers to the number of samples regressed.

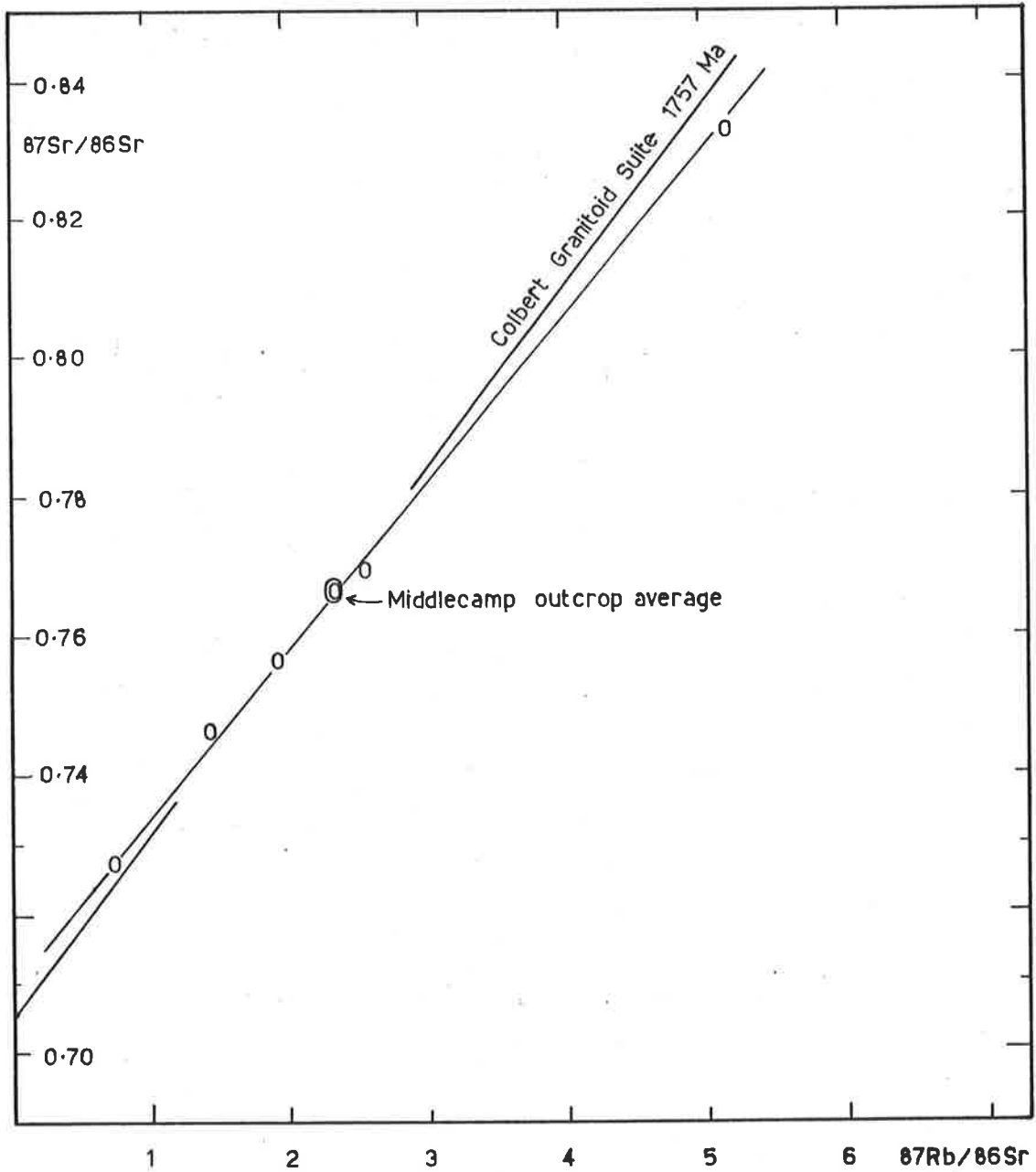


Figure 3-6

Comparison of the Middlecamp Granite data points and outcrop average with the Colbert Granitoid Suite reference isochron.

the comagmatic hornblende granite and alkali feldspar granite crystallised at about the same time at 1757 ± 14 Ma with IR of 0.7087 ± 10 .

(2) Minimum age of D_2

D_2 must have occurred prior to the emplacement of the CGS at 1757 ± 14 Ma.

(3) Time of isotopic disturbance in D_3 shear zones

On the basis of the suggestion that Sr-isotopes may be equilibrated during tectonic episodes over small volumes of rock (e.g. 1m^3 , Black 1977; Black et al. 1978; Roddick & Compston 1977) it is possible to speculate on the time of redistribution of Sr-isotopes at localities B and D. Of all the sample pairs coming from small volumes of rock B125(A & B) is the only pair whose $87\text{Rb}/86\text{Sr}$ ratios differ by more than 5%. Indeed the others are similar to within 2%. Hence a two-point join age for any samples other than B125(A&B) is likely to be meaningless considering analytical uncertainty of the $87\text{Rb}/86\text{Sr}$ ratio is of the order of $\pm 0.5\%$.

The age calculated for B125(A&B) is 1624 ± 190 Ma. Although imprecise, this is very similar to the isochron age of 1632 ± 96 Ma obtained from granite gneiss 2 of the DGS from Fisherman's Point, also obtained on a small volume of rock (Chapter 2). In both these cases the dominant fabric is considered to be S_3 , and it is tentatively suggested that a likely age for D_3 tectonism and metamorphism on S.E. Eyre Peninsula may be ca. 1630 Ma.

Rutland et al. (1981) and Parker et al. (1981) report an age of 1650 ± 35 Ma for their "early D_2 " Middlecamp Granite, but prefer an age ca. 1640 Ma for their interpreted syn- D_3 Carpa Granite (data from Webb 1978). This either suggests that D_2 and D_3 occurred at around the same time or that their structural and geochronological interpretations are at odds. However Rutland et al. (1981) suggest that "the third deformation appears to be significantly younger (than D_1 and D_2) throughout the province and is associated with the intrusion of late tectonic granites".

Webb (1978) in his treatment of the Middlecamp data showed that at least one specimen did not conform to the reported isochron, all six specimens defining a poor fit isochron of 1635 ± 86 Ma with IR of 0.7108 ± 32 . An alternative interpretation of the Middlecamp

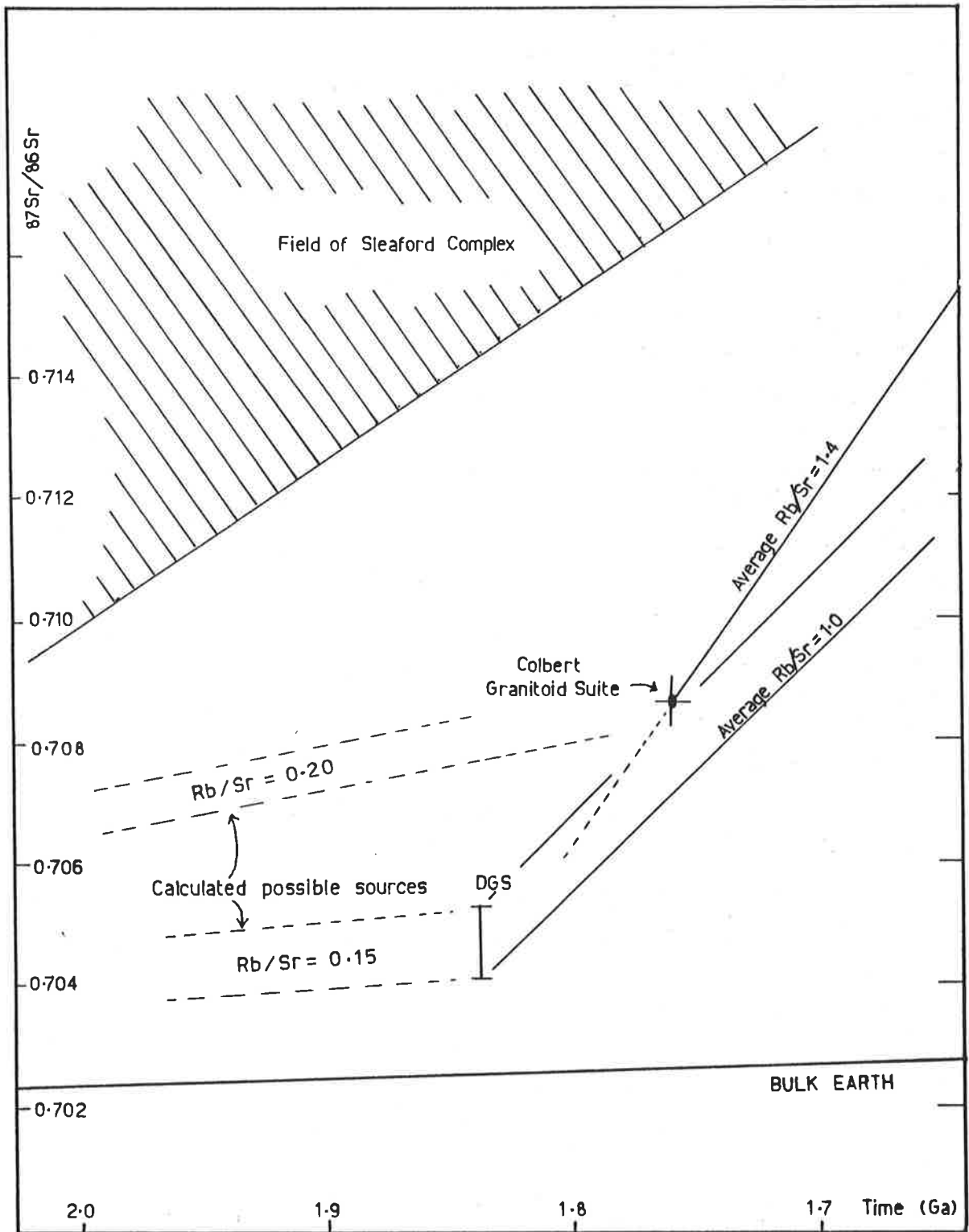


Figure 3.7

Sr-isotope evolution diagram for the Colbert Granitoid Suite compared with the Donington Granitoid Suite and basement gneisses and model bulk earth.

data by the present author would allow the possibility that the foliated granite samples, collected from a small area of outcrop, are recording a subsolidus disturbance of the Sr-isotopes similar to that seen in the locality B and D data above. The original emplacement age for the Middlecamp Granite may be greater than 1635 ± 86 Ma.

The calculated outcrop average for the Middlecamp Granite plots on the CGS averaged outcrops isochron (Fig. 3.6), and the individual data points scatter about the isochron in a manner consistent with there having been a post-emplacement partial redistribution of Sr-isotopes (cf Gray & Compston 1978). Such a model interpretation would also account for the elevated IR of the Middlecamp isochron.

Although not suggesting that the Middlecamp Granite and CGS were originally comagmatic, the thrust of the above discussion is to demonstrate the possibility that the Middlecamp isochron could be attributed to post-emplacement updating. Thus the present author suggests that the age of D_2 is not necessarily constrained to be 1635 ± 86 Ma (nor 1650 ± 35 Ma) as Rutland et al. (1981) and Parker et al. (1981) contend. Furthermore the present author suggests that the Fisherman's Point isochron, the B125(A&B) calculated age, and the Middlecamp isochron may more appropriately constrain the age of D_3 . A weighted mean age of these results is 1629 ± 61 Ma (Paradine & Rivett 1960).

(4) Strontium isotope evolution of the Colbert Granitoid Suite

Comparison of the age and IR of the CGS with the field of "Archaean" gneisses and granitoids of the Sleaford Complex and its equivalents on a Sr-isotope evolution diagram (Fig. 3.7) indicates that the CGS could not have been derived by partial melting of this type of material. Figure 3.7 shows however that the CGS plots very nearly on the curve representing the Sr-isotope evolution of the DGS suggesting it would be possible to partially melt material of DGS isotopic character to produce the CGS at 1757 ± 14 Ma. On the other hand, this model has geochemical objections in that both suites are of similar SiO_2 contents requiring very high degrees of partial melting to produce the CGS from the DGS. On the basis of a calculation involving the Rb/Sr ratios of melt and source similar to that performed for the DGS (Chapter 2), it is likely that a source existed for the CGS of similar age and Sr-isotopic character to that of the DGS.

This source will be discussed more fully in Chapter 7.

Table 3.5 Geochemical comparison of average hornblende granitoid of Colbert Granitoid Suite with Donington Granitoid Suite and typical I-type granitoids.

	1	2	3	4	5	6
SiO ₂	64.42	68.33	67.75	68.48	72.50	73.04
Fe/(Fe + Mg) *	0.70	0.70	0.70	0.50	0.64	0.84
Al ₂ O ₃ /(Na ₂ O+K ₂ O+CaO) *	0.91	0.96	0.99	0.92	1.03	1.03
(La) _N	219	190	156	98	105	197
(Eu) _N	26	25	24	-	-	33
(Yb) _N	20	21	15	-	-	35
Ba	1113	915	1166	985	577	767
Sr	175	147	169	435	165	148
Zr	357	305	310	181	147	490
Nb	21	16	14	11	9	25
Y	49	41	38	19	29	83
Sc	15	13	15	9	9	17
V	-	41	53	53	30	6
Cr	6	12	18	48	5	2
Ni	-	21	19	17	6	1
K ₂ O/Na ₂ O**	1.98	1.8	1.9	1.3	1.2	1.1

* molar ratio

** wt. % ratio

1. Average of 4 Colbert hornblende granite gneiss
2. Average of 7 FGG1, Donington Granitoid Suite
3. Average of 4 FGG2, Donington Granitoid Suite
4. Average of 10 Moonbi I-types (Chappell 1978)
5. Average of 48 Bega I-types (Collins et al. 1982)
6. Average of 9 Gabo A-types (Collins et al. 1982)

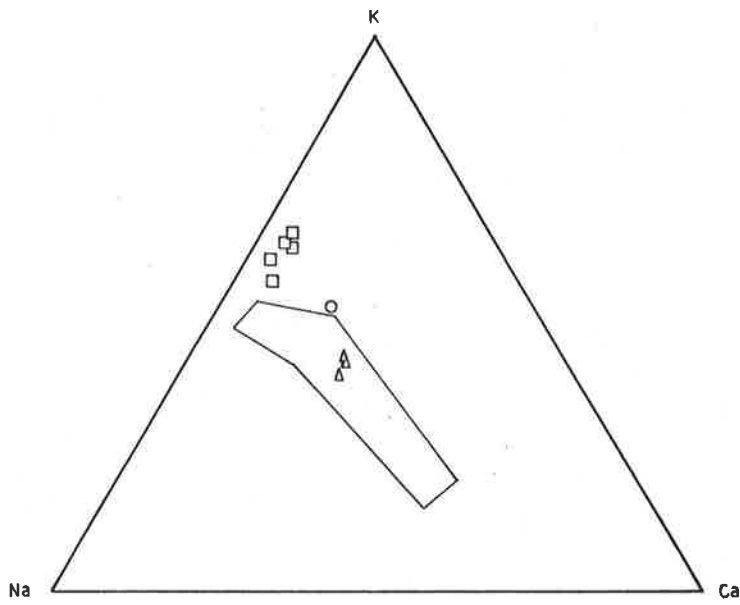
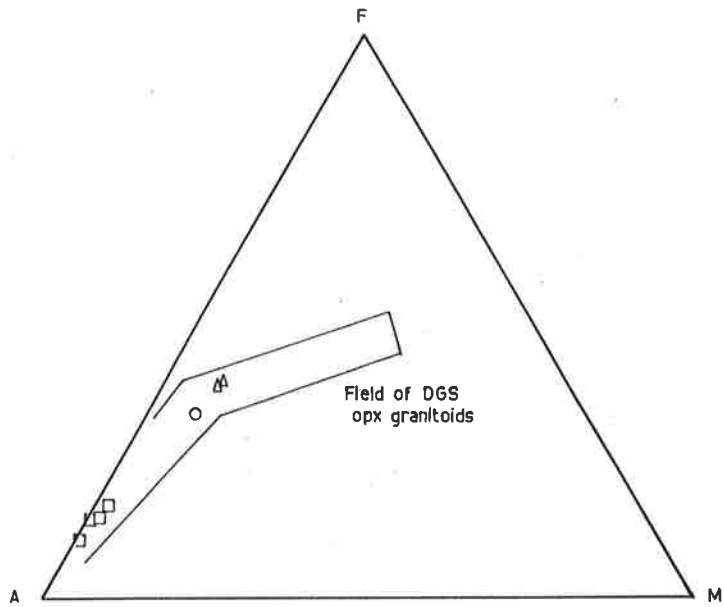


Figure 3.8 AFM and K-Na-Ca diagrams for Colbert Granitoid Suite compared with the fields of the Donington Granitoid Suite opx-granitoids. Symbols as in Figure 3.5.

3.4 GEOCHEMISTRY OF THE COLBERT GRANITOID SUITE

The petrographic and Sr-isotopic evidence presented above strongly suggests that the hornblende granite gneiss and alkali feldspar granite gneiss are indeed a comagmatic suite. It is intended in this section to examine the geochemical relationships of the two rock types and to compare them with the Donington Granitoid Suite.

3.4.1 Geochemical classification

On the AFM and K-Na-Ca diagrams (Fig. 3.8) the CGS shows calc-alkaline trends similar to the DGS, although an enrichment in K over Na is noted. These features suggest the CGS comprises a typical suite of orogenic granitoids.

In terms of the model of orogenic granitoid genesis of Chappell & White (1974) the $Al_2O_3/(Na_2O + K_2O + CaO)$ ratio less than 1.1 (Table 3.5) the moderately low IR and low normative corundum (Appendix Table 3.2), coupled with the presence of hornblende and sphene, suggest the CGS is I-type. This model conclusion precludes the involvement, to any significant degree, of pre-existing pelitic sedimentary material in the genesis of the CGS, in favour of an igneous or meta-igneous protolith.

However, Emslie (1978) argued that the high K_2O and $Fe_T/(Fe_T + Mg)$ of many Proterozoic and younger granitoid (and volcanic) suites is more typical of anorogenic magmatism. Subsequently Loiselle & Wones (1979) and Collins et al. (1982) proposed more detailed geochemical criteria to distinguish anorogenic or A-type granitoids, some of which are illustrated in Table 3.5 in comparison with the CGS, DGS opx-granitoids and typical I-type suites. Although the high K_2O/Na_2O , Zr, Y and $(La)_N$ of the CGS hornblende granites are transitional towards A-type, the moderately high Cr, and Ba argue for I-type.

These features coupled with the mineralogical criteria cited by Collins et al. lead the present author to conclude that the CGS in a suite of I-type granitoids. The transitional geochemical characteristics alluded to above will be discussed in more detail in Chapter 7.

3.4.2 Major element geochemistry

Only a small number of samples has been analysed so that it is

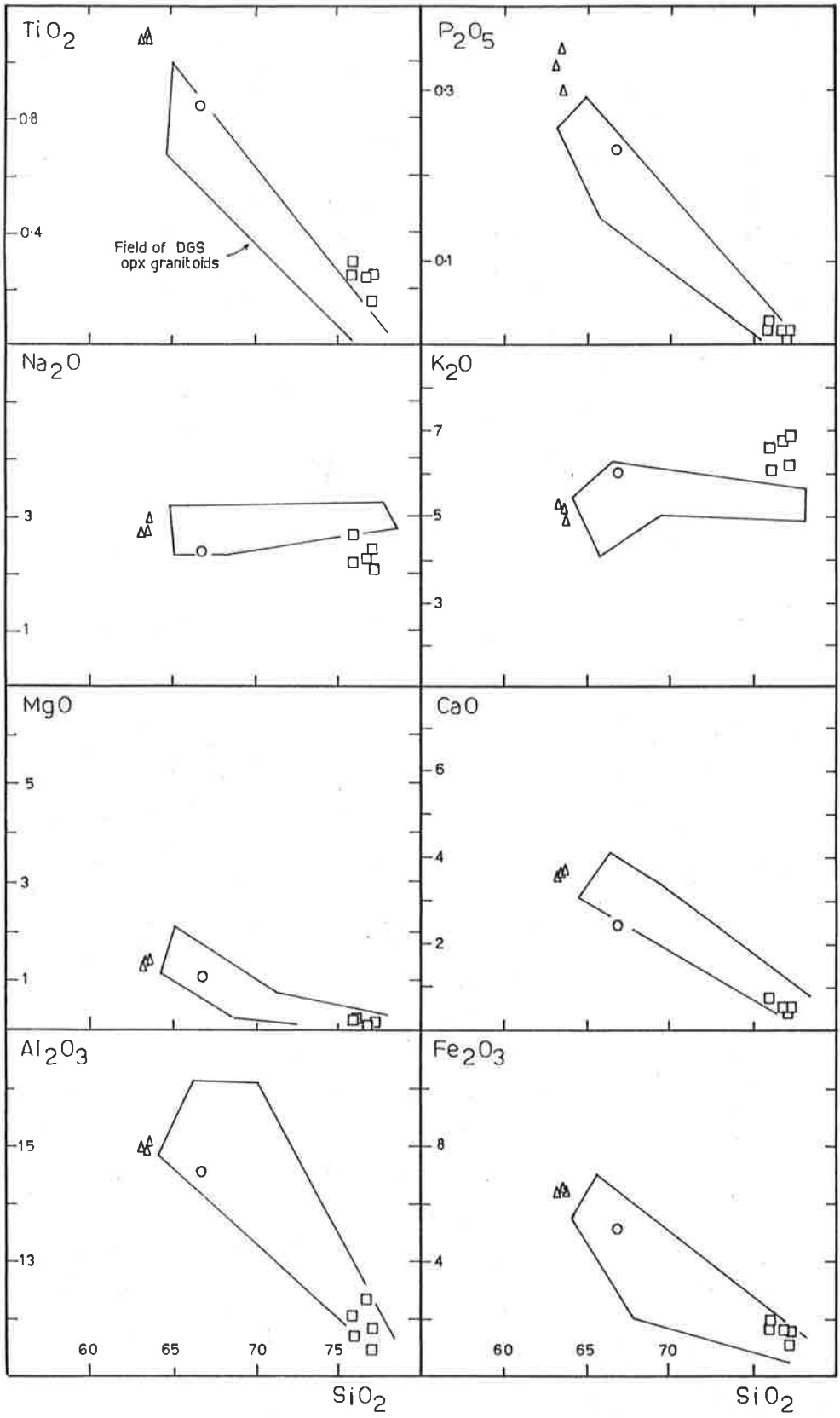


Figure 3-9 Major element variation diagrams for the Colbert Granitoid Suite compared with the fields of the Donington Granitoid Suite opx-granitoids. Symbols as in Figure 3.5.

unlikely that the full spectrum of chemical variation is represented in the data in Appendix Table 3.2. However, a broad range in SiO_2 content from ca. 63% to ca. 77% is spanned although a significant hiatus between ca. 67% to 76% is present (Appendix Table 3.2, Fig. 3.9). The major element variation diagrams are very similar to those of the DGS, with the exception of K_2O and Na_2O where there is a slight K_2O enrichment and Na_2O depletion at SiO_2 greater than 75%.

On this basis of the major element geochemistry, no marked deviations from the DGS interpretative scheme are apparent, other than to note the absence of mafic cumulate rocks. As with the DGS, crystallisation of minerals such as plagioclase, alkali feldspar, biotite, hornblende, Fe - Ti oxide and apatite is considered to control the geochemical evolution of the CGS.

3.4.3 Trace element geochemistry

The trace element geochemistry of the CGS is broadly similar to that of the DGS for most elements (Fig. 3.10, Appendix Table 3.3). Where deviations exist they tend to be most marked for those rocks with greater than 75% SiO_2 . Rb tends to be slightly depleted at high SiO_2 with respect to the DGS opx-granitoids whereas Ba tends to be enriched. For all SiO_2 contents, Zr and Nb tend to be enriched. In the high SiO_2 rocks, Y tends to be markedly depleted.

3.4.4 REE geochemistry

The CGS has fractionated REE patterns (Appendix Table 3.3, Fig. 3.11), with $(\text{La}/\text{Yb})_N$ ranging from 9.3 to 30.1. Whereas the LREE, although strongly fractionated, are subparallel to the field of the DGS (Fig. 3.11), the HREE are fractionated to a greater extent than in the DGS with $(\text{Yb}/\text{Gd})_N$ ranging from 0.49 to ca. 0.3 (cf DGS 0.78 - 0.48). In addition, the absolute levels of abundance of all REE in the CGS tend to be slightly higher than the DGS opx-granitoids for rocks with moderate SiO_2 levels. However, the most siliceous alkali feldspar granite is markedly depleted in HREE with respect to the DGS opx-granitoids (Fig. 3.11).

It is apparent that the REE geochemistry of the CGS requires the involvement of a mineral that actively fractionates the HREE, but which is not involved in the genesis of the DGS opx-granitoids. The petrographic observation that phenocrysts of hornblende occur in the CGS but not in the DGS, leads to the consideration of the role

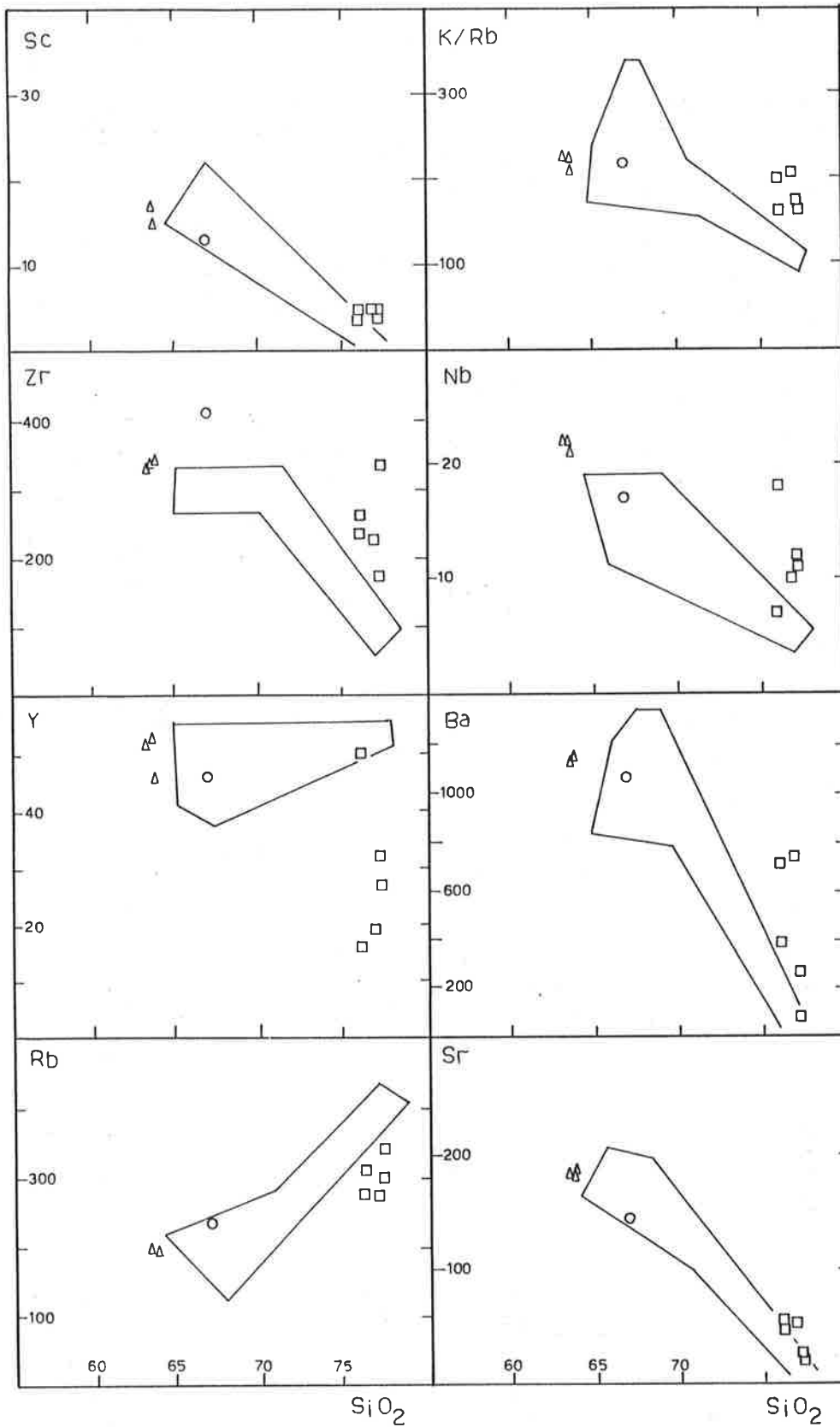


Figure 3.10 Trace element variation diagrams for the Colbert Granitoid Suite compared with the fields of the Donington Granitoid Suite opx-granitoids. Symbols as in Figure 3.5.

of hornblende in REE geochemistry. Partition coefficients for hornblende in dacitic rocks with SiO_2 ca. 67%, range from less than 1 to ca. 3 for the LREE and from ca. 5 to ca. 6 for the HREE (Arth & Barker 1976). Hence fractionation of hornblende alone from the hornblende granite gneiss parental magma would have the effect of slightly depleting the LREE but strongly depleting the HREE. It is thus considered most likely that the variation in REE abundance within the CGS is largely controlled by hornblende fractionation.

It is not clear whether the primary fractionated REE pattern of the least siliceous hornblende granite gneiss (B112A, Fig. 3.11) is inherited from its source region or is due to the presence in the source region of major residual minerals capable of fractionating the HREE (e.g. hornblende or garnet). The presence of hornblende-rich xenoliths (restite) and hornblende phenocrysts in the granite gneiss argues in favour of residual hornblende at the site of magma generation. Major and trace element petrogenetic modelling in Chapter 7 amplifies this discussion.

Furthermore, the progressive fractionation of the HREE within the CGS also suggests that the primary fractionated HREE pattern in the least fractionated specimen of hornblende granite gneiss is probably also due to the role of hornblende. Thus it is likely that hornblende is present and stable at the site of magma production and separation.

3.4.5 Summary

The geochemistry of the CGS is in many respects analogous to that of the DGS, and may suggest a broadly similar petrogenetic history. However, in detail, significant differences exist, viz,

- (1) hornblende is the major precipitating ferromagnesian mineral rather than pyroxene,
 - (2) this is reflected in the HREE patterns,
- and (3) the absolute abundances of K, Zr, LREE and Nb are higher in the CGS.
- (4) Although only a few data exist, the variation within the CGS is suggested to be the result of plagioclase, alkali feldspar, hornblende, apatite, Fe - Ti oxide and zircon crystal fractionation.

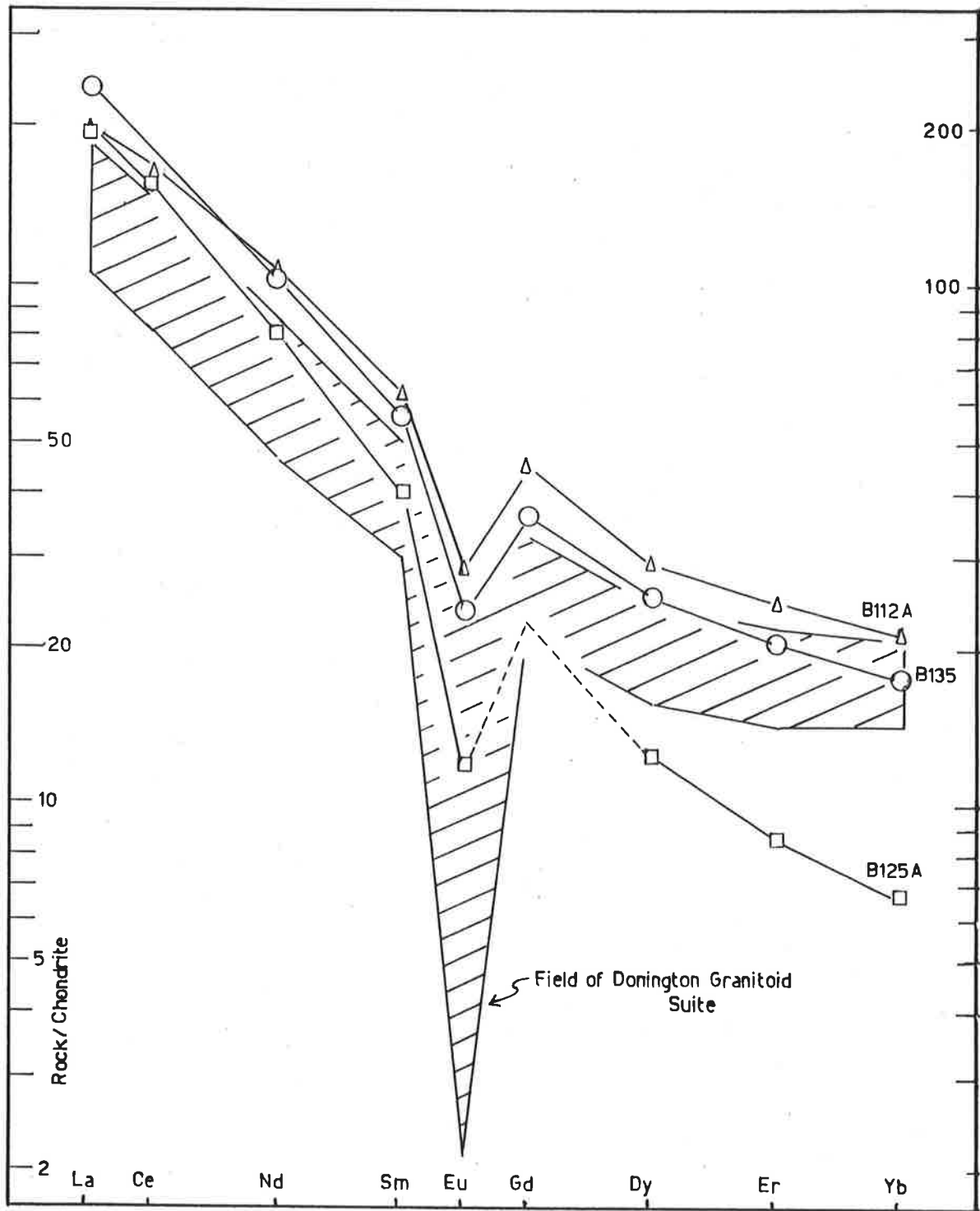


Figure 3.11

Chondrite normalised REE plots for the Colbert Granitoid Suite compared with the field of the Donington Granitoid Suite opx-granitoids. Symbols as in Figure 3.5.

3.5 SUMMARY

The Colbert Granitoid Suite consists of two main rock types, the Colbert hornblende granite gneiss and the Colbert alkali feldspar granite gneiss. These were emplaced after the peak of D_{1-2} granulite facies metamorphism and coeval local D_{1-2} retrogression, but prior to D_3 , and were locally involved in intense D_3 shear zones.

The primary phenocryst assemblage of plagioclase, alkali feldspar and hornblende is different from that in the DGS, although the major and trace element geochemistry of the two suites is broadly similar. In detail, relative to the DGS, the CGS is slightly enriched in K, Zr, LREE and Nb, and the HREE are more fractionated due to the precipitation of hornblende during fractional crystallisation and possible residual mineralogical differences. It is probable that the broad geochemical similarity between the CGS and DGS reflects derivation from compositionally similar sources under broadly similar conditions of partial melting.

Emplacement of the CGS occurred at 1757 ± 14 Ma with an IR of 0.7087 ± 10 .

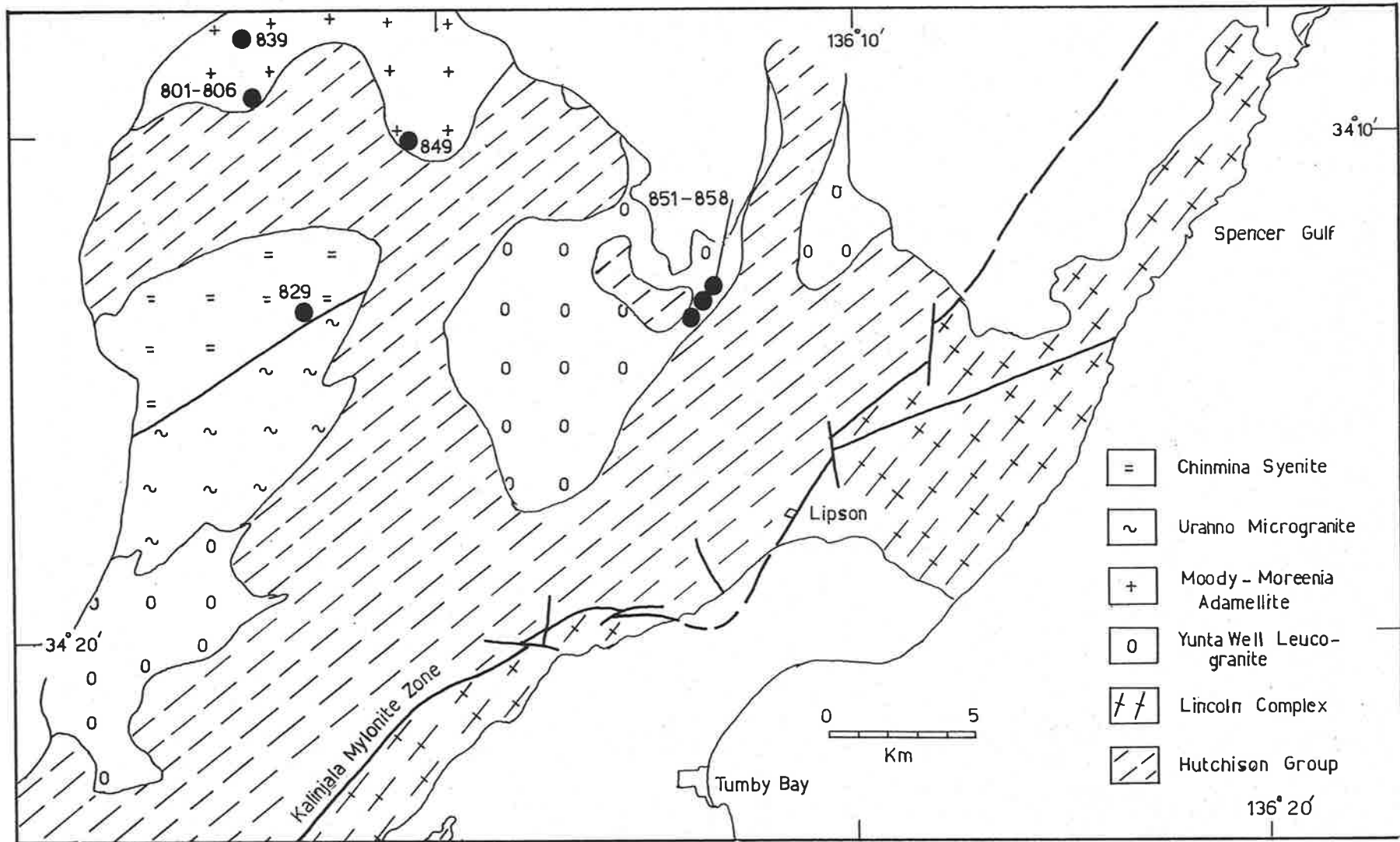


Figure 4.1 Sketch geological map of outcrop of Moody Granitoid Suite near Tumby Bay; see also Figure 1.1. (modified after Coin 1976).

CHAPTER 4.

MOODY GRANITOID SUITE.

4.1 INTRODUCTION

The Moody Granitoid Suite (MGS) was first discussed in detail by Coin (1976). His field and petrographical study of the granitoid and enclosing rocks was supplemented by a small number of major element geochemical analyses. Coin also collected a suite of samples for Rb-Sr geochronology, but did not complete this aspect of his study.

The present author decided to extend the scope of Coin's investigation by completing the Rb-Sr geochronology and collecting a suite of trace element data. In this way it was intended to compare the petrogenetic history of this apparently later syn-tectonic suite of granitoids with the earlier granitoid suites, and to constrain further the crustal evolution in the Gawler orogenic domain at this time.

From Coin's (1976) description of the field geological relationships of the MGS, the following major conclusions may be summarised.

- (1) The MGS was emplaced into the Hutchison Group to the west of the Kalinjala Mylonite Zone (Fig. 4.1).
- (2) The individual rock types appear to have been emplaced in two discrete sequences,
 - (a) foliated Yunta Well Leucogranite (YWL) intruded prior to the last penetrative deformation of the enclosing Hutchison Group (Coin's $D_{2a} = D_3$ of this study).
 - and (b) undeformed Moody Tank Adamellite (MTA) Moody West Adamellite (MWA) Moreenia Adamellite (MOA) and Chinmina Syenite (CHS) all intruded late in D_3 (Coin's D_{2b}).
- (3) The apparent younging sequence of intrusions is YWL, MTA, MWA, MOA and CHS.
- (4) The YWL and numerous pegmatites scattered throughout the metasediments are apparently cogenetic.
- (5) The sillimanite isograd is sub-parallel to the eastern margin of the main body of YWL, suggesting the metamorphism is largely of thermal aureole enhanced regional amphibolite facies.

- (6) The peak of metamorphism attained 490° - 650° C adjacent to YWL, at ca. 3Kbar

None of these inclusions is challenged by the present author. It is the aim of this chapter,

- (1) to describe the petrography, mineralogy, Rb-Sr geochronology and geochemistry of the MGS,
- (2) to compare the MGS with earlier granitoid suites (intrusive into the Lincoln Complex).
- (3) to investigate the discrepancy between the estimates of the timing of D_2 and D_3 by Parker et al. (1981), Rutland et al. (1981) and the present author, (see discussion in Chapter 3). In particular, Rb-Sr dating of the MGS would more adequately constrain D_3 .
- (4) to constrain the petrogenesis of the suite by Sr-isotope and major and trace element geochemistry.

4.2 PETROGRAPHY AND MINERAL CHEMISTRY

Within the MGS the various intrusive phases exhibit considerable petrological and mineralogical variation. These are summarised in Table 4.1. More detailed descriptions of three of the rock units,

- (1) Yunta Well Leucogranite
- (2) Moody Tank Adamellite

and (3) Chinmina Syenite

are presented below, representative of the spectrum of variation throughout the suite.

4.2.1 Yunta Well Leucogranite

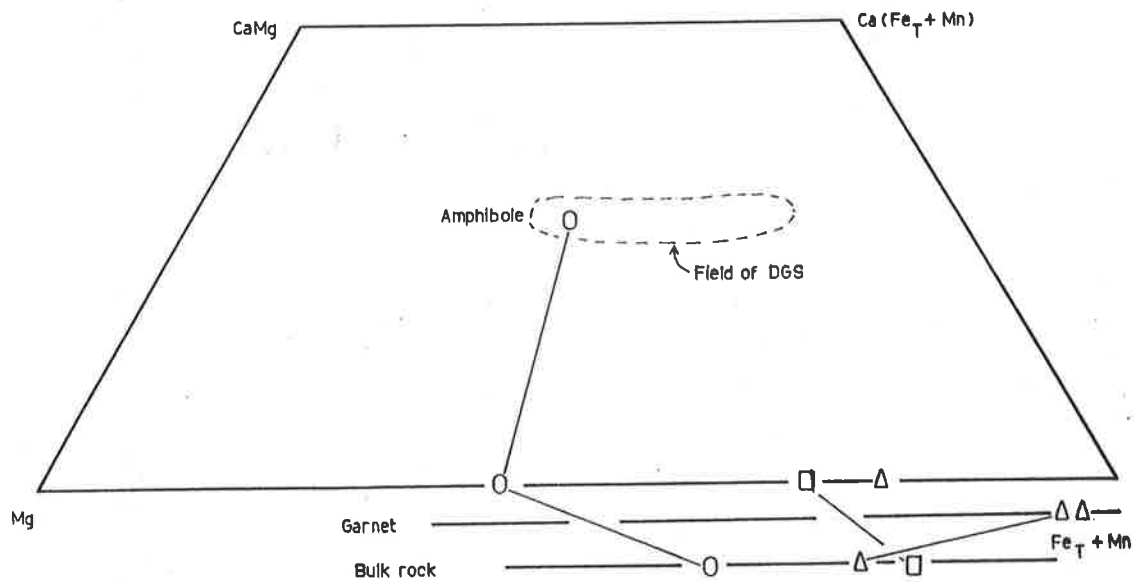
These medium to coarse grained, light coloured rocks generally have allotriomorphic texture, and are foliated. The dominant minerals are quartz, microcline and albite, with common muscovite, tourmaline and spessartine-rich garnet. Some specimens contain a moderate proportion of biotite. Apatite and zircon are accessory minerals.

In some specimens, "chess-board" texture in the feldspar grains suggests late stage albitisation of microcline has occurred.

The foliation, sub-grain development and deformation bands in quartz grains testify to the pre- to syn-tectonic emplacement of this rock unit.

Table 4.1: Moody Granitoid Suite - modal and textural
Summary

Rock unit	Major minerals	Texture
Yunta Well Leucogranite (YWL)	Kspar+qtz+plag+ \pm musc \pm biot	foliated allotriomorphic
Moody Tank Adamellite (MTA)	plag+Kspar+qtz+biot \pm musc	unfoliated hypidiomorphic granula
Moody West Adamellite (MWA)	plag+Kspar+qtz+biot \pm musc (+apatite)	unfoliated hypidiomorphic
Moreenia Adamellite (MOA)	Kspar+plag+qtz+biot \pm musc	unfoliated hypidiomorphic
Chinmina Syenite (CHS)	Kspar+plag+hblnd+biot (+qtz) (+ sphene)	unfoliated hypidiomorphic



- Key
- Chinmina syenite
 - Moody Tank
 - △ Yunta Well

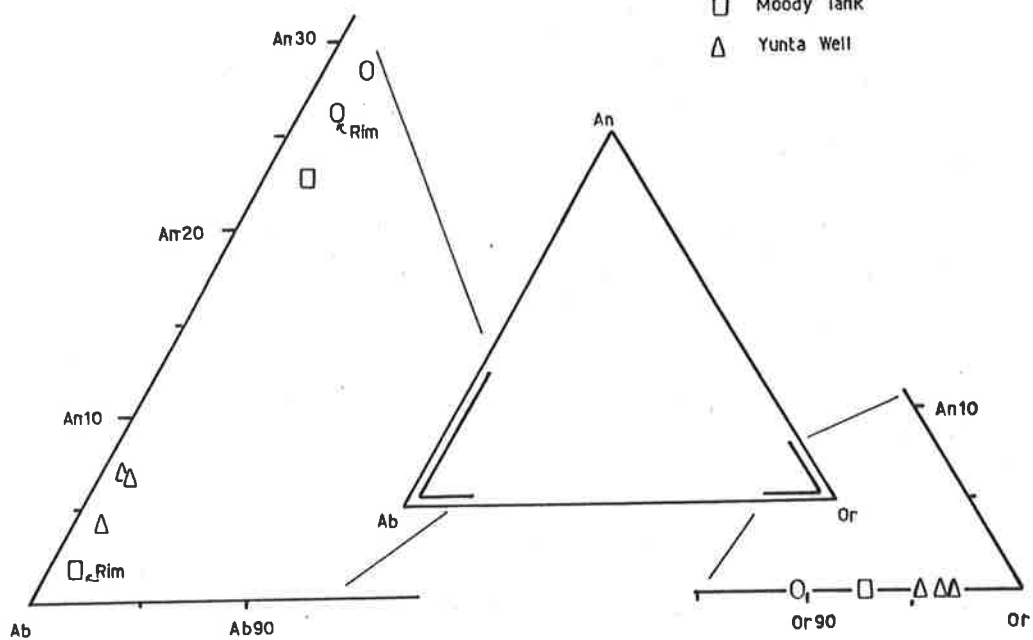


Figure 4-2 Ferromagnesian and feldspar mineral compositions of representative granitoids in the Moody Granitoid Suites.

4.2.2 Moody Tank Adamellite

This medium to coarse grained, light coloured rock has a hypidiomorphic granular texture. The dominant minerals are quartz, microcline, plagioclase and red-brown biotite. Muscovite is commonly intergrown with the biotite or replacing feldspar.

The plagioclase phenocrysts are zoned, often with a sericitised core, and microcline phenocrysts may be Carlsbad twinned and may contain small, randomly oriented plagioclase microphenocrysts which commonly have an albitic rim or overgrowth. Small rounded quartz inclusions may also be present in microcline phenocrysts.

Garnet is present in some specimens, especially adjacent to metasedimentary xenoliths, and may contain biotite and rounded quartz inclusions. Accessory zircon and apatite tend to be associated with biotite, often included within it. Accessory tourmaline may be present in some specimens.

4.2.3 Chinmina Syenite

This coarse grained, dark coloured rock has a hypidiomorphic texture. The major minerals are plagioclase, microcline, quartz, green hornblende and brown biotite. The rock is melanocratic. Fe - Ti oxide is common and has well-developed sphene corona structures. Sphene, apatite and zircon also occur as discrete accessory grains. Large euhedral apatite crystals may be included within biotite and hornblende.

The biotite tends to be moulded onto hornblende grains, and the hornblende may contain some rounded quartz inclusions.

There is virtually no foliation present in the rock, but some recrystallisation is evident in some specimens in the form of quartz deformation bands and sub-grain development. Some of the microcline megacrysts are Carlsbad twinned and contain numerous inclusions of myrmekite, plagioclase and quartz.

Coin's (1976) name for this unit is retained in subsequent discussion although the modal mineralogy suggests it is more correctly a monzonite.

4.2.4 Mineral Chemistry

All the major minerals in the main rock types in the MGS have been analysed by electron microprobe and tabulated in Appendix Table 3.1.

Table 4.2: Moody Granitoid Suite - Geothermometry

	$T^{\circ}\text{C}$	$-\log a_{\text{O}_2}$
mag + ilm Powell & Powell (1977)	510	20.6
plag+Kspar Powell & Powell (1977)	300-480	
biot+Kspar+mag Wones & Eugster (1965)	650-850	12-17

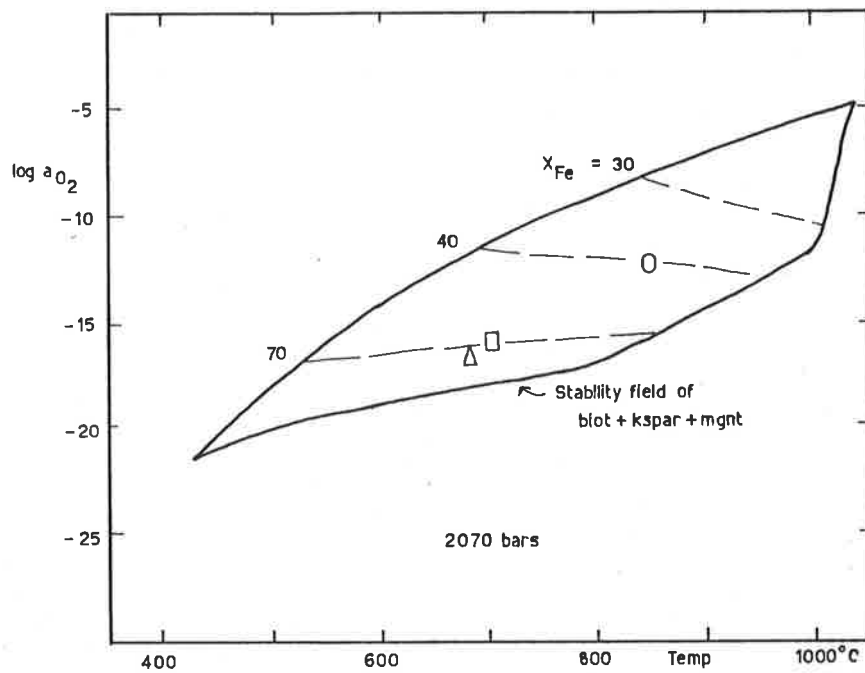
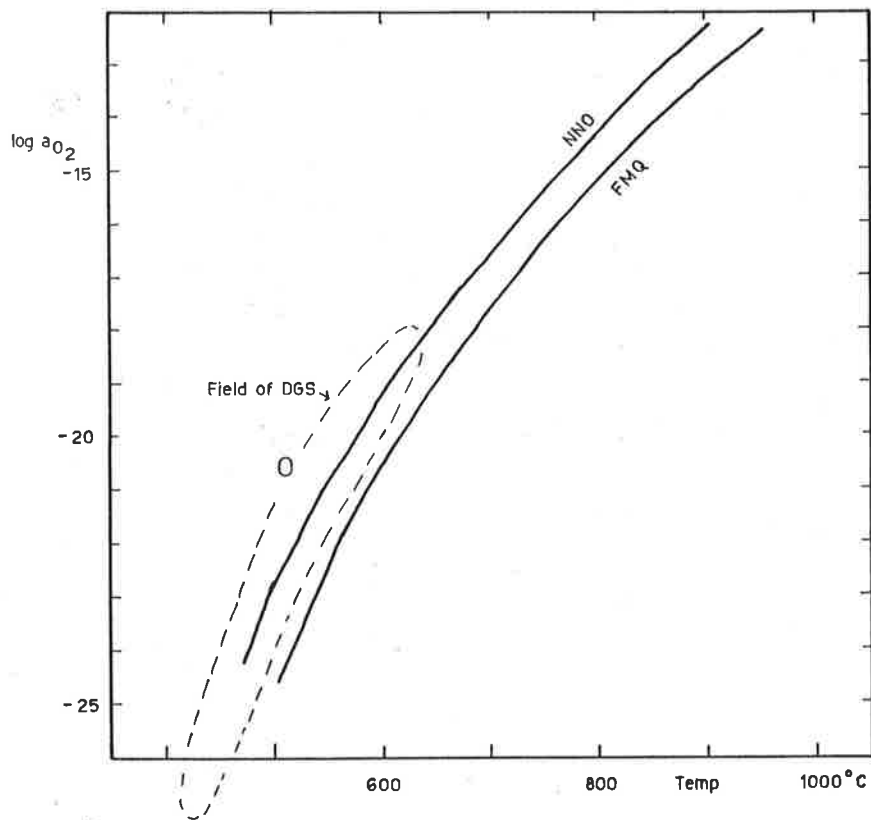


Figure 4.3 Upper: Coexisting magnetite and ilmenite T-log aO₂ plot for Chinmina Syenite
 Lower: Biotites in the Moody Granitoid Suite compared with data of Wones & Eugster (1965)
 Symbols as in Figure 4.2.

(1) Feldspars

The granitoid rocks generally contain two discrete feldspars, usually as phenocrysts, the spot compositions of which indicate only limited solid solution between plagioclase and alkali feldspar (Fig. 4.2). Compositional zoning is present in the feldspars within individual rock types, with the average composition of plagioclase becoming more calcic in the intrusive sequence from YWL through to CHS (Fig. 4.2). Similarly the alkali feldspars become more sodic (Fig. 4.2).

A common feature of the microcline megacrysts, particularly in MTA and CHS, is the presence of plagioclase mantles. In the analysed MTA specimen the mantle is of almost pure albite composition, whereas in the analysed CHS specimen the mantle is of andesine composition (Fig. 4.2) and is almost identical to the exsolved blebs of plagioclase within the megacryst. It is probable that the mantles formed through exsolution and recrystallisation of the plagioclase component during sub-solvus cooling and annealing.

Temperatures calculated after the method of Powell & Powell (1977) range from 385° - 480°C for CHS and MTA, and from 300° - 335°C for YWL (Table 4.2). It is probable that the averaged spot compositions of the feldspars are recording subsolidus equilibration during cooling subsequent to D₃.

(2) Amphibole

Amphibole phenocrysts occur only in CHS and are magnesian hastingsites (after the classification of Leake 1978). They are broadly similar in composition to the more magnesian amphiboles in the DGS (Fig. 4.2).

(3) Opaque oxides

Magnetite and ilmenite coexist in the Chinmina Syenite and show partial subsolidus exsolution. The analysed grains (Appendix Table 3.1) yield a calculated temperature of 510°C and $\log a_{O_2} = -20.55$ (Fig. 4.3, Table 4.2; after method of Powell & Powell 1977) probably reflecting subsolidus conditions.

(4) Biotite

Biotite occurs in addition to alkali feldspar and magnetite in YWL, MTA and CHS. A wide variation in Mg/(Mg+Fe) is present which

correlates with the variation in bulk rock $Mg/(Mg+Fe)$ (Fig. 4.2). Application of the experimental data of Wones & Eugster (1965) to the biotites yields temperatures ranging from ca. $650^{\circ}C$ in YWL to ca. $850^{\circ}C$ in CHS and corresponding $\log a_{O_2}$ ca. -17 to ca. -12 (Fig. 4.3, Table 4.2). These parameters are more likely to correspond to the igneous conditions of crystallisation than to subsolidus equilibration, in contrast to the opaque oxides.

(5) Garnet

Mn-rich garnet is present in some rocks within the YWL, often in association with tourmaline, and almost to the exclusion of biotite (Fig. 4.2). Mn-garnet is possibly replacing biotite in these highly fractionated leucogranites.

(6) Summary

Regular changes in mineralogical composition within the MGS reflect the bulk rock geochemical variation.

The granitoids were probably emplaced at ca. $650^{\circ} - 850^{\circ}C$ deduced from biotite compositions, but considerable subsolidus exsolution and equilibration to temperatures between ca. 300° and $500^{\circ}C$ is recorded in the feldspars and opaque oxides. These latter features may reflect relatively slow cooling at moderate depth (ca. 3 Kbar).

4.2.5 Discussion and Summary

Regular petrographic and mineralogical changes can be discerned throughout the intrusive sequence from YWL through to CHS. The proportion of muscovite decreases markedly, tourmaline and Fe-Mn garnet are present abundantly only in YWL and hornblende and sphene are present only in CHS. Moreover, the plagioclase becomes more calcic and the biotite becomes more magnesian.

These mineralogical trends are quite dissimilar to those in the earlier granitoid suites. In both the DGS and CGS, muscovite, Fe-Mn garnet and tourmaline are absent, whereas plagioclase and biotite become less calcic and less magnesian respectively throughout the younging sequence of intrusive phases. Primary igneous hornblende is present in the CGS in abundance but is only a minor component in the DGS.

The abundant muscovite in YWL is suggestive of an S-type character whereas the hornblende and sphene in CHS is suggestive of I-type

Table 4.3: Geochemical comparison of average granitoids of the
Moody Granitoid Suite with I-, S- and A-type granitoids.

	1	2	3	4	5	6	7
SiO ₂	71.10	68.33	64.42	72.50	74.17	72.86	77.2
Fe/(Fe+Mg) *	0.78	0.70	0.70	0.64	0.64	0.68	0.9
Al ₂ O ₃ /(Na ₂ O+K ₂ O+CaO) *	1.06	0.96	0.91	1.03	1.17	1.07	1.0
K ₂ O/Na ₂ O**	1.6	1.8	2.0	1.2	1.1	1.5	1.6
(La) _N	324	190	219	105	-	71	203
(Eu) _N	19	25	26	-	-	-	20
(Yb) _N	15	21	20	-	-	-	38
Ba	725	915	1113	577	15	548	575
Sr	190	147	175	165	11	142	43
Zr	302	305	357	147	29	151	170
Nb	25	16	21	9	20	7	19
Y	33	41	49	29	10	33	90
Sc	7	13	15	9	2	7	16
V	-	41	-	30	-	25	2
Cr	-	12	6	5	-	8	1
Ni	-	21	-	6	-	5	1

* molar ratio

** wt.% ratio

1. Average of 5 adamellites, Moody Granitoid Suite.
2. Average of 7 FGG1, Donington Granitoid Suite.
3. Average of 4 hornblende granite gneiss, Colbert Granitoid Suite.
4. Average of 48 Bega I-types (Collins et al. 1982).
5. Average of 7 YWL, Moody Granitoid Suite.
6. Average of 5 Moonbi S-types (Chappell 1978).
7. Average of 8 Mumbulla A-types (Collins et al. 1982).

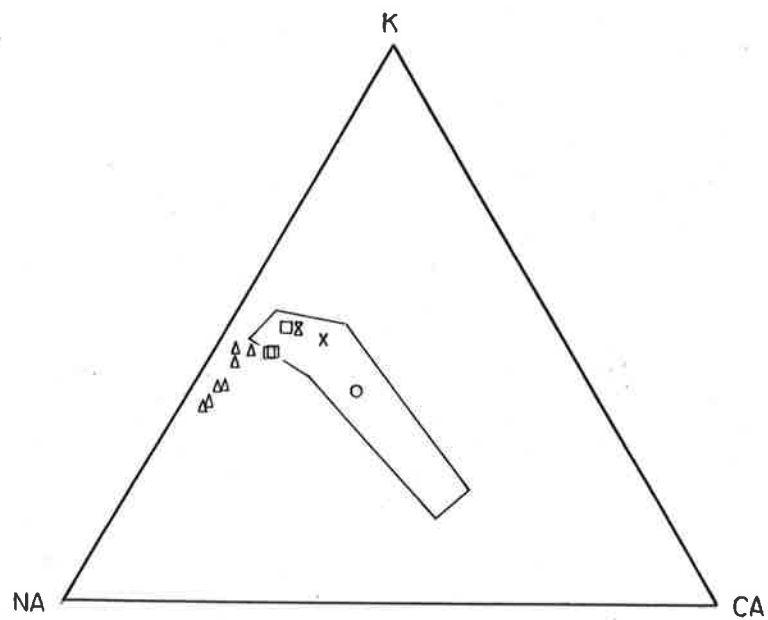
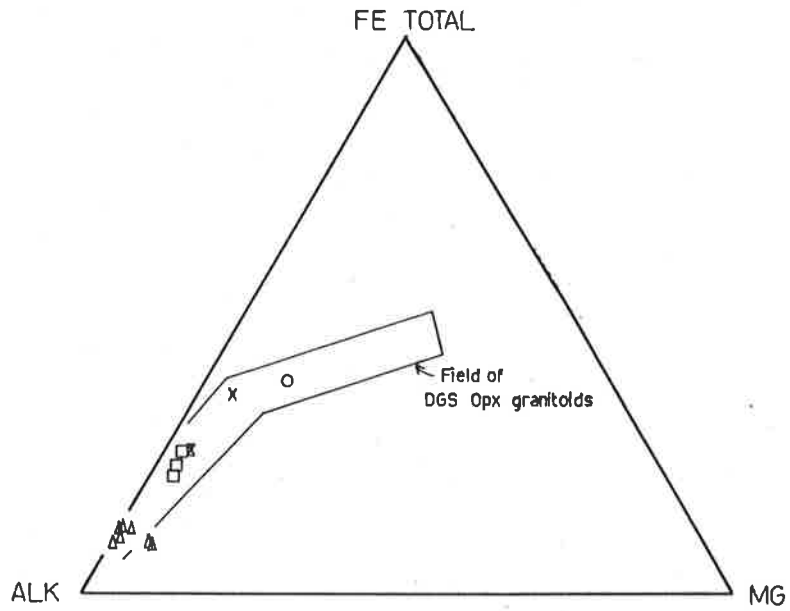


FIGURE 4.4 AFM and K-Na-Ca diagrams for the Moody Granitoid Suite.

Symbols as in Figure 4.2, plus

X = Moreenia Adamellite

\bar{X} = Moody West Adamellite

character (Chappell & White 1974).

Texturally the YWL shows abundant evidence for syn-tectonic emplacement, whereas there is less evidence for this in the adamellites and CHS. For this reason, and because of the distinct mineralogical contrast between the YWL and the other granitoids of the suite, and the disparate outcrop patterns (Fig. 4.1) the present author concurs with the suggestion of Coin (1976) that the MGS comprises two temporally distinct intrusive events, viz

- (1) Yunta Well Leucogranite
 - and (2) Moody Tank Adamellite, Chinmina Syenite
- and other adamellites.

4.3 GEOCHEMISTRY OF THE MOODY GRANITOID SUITE

4.3.1 Geochemical classification

On mineralogical grounds it has been suggested above that the YWL is of S-type character and the CHS and adamellites are of I-type character.

The major element geochemical data (Appendix Table 4.1) when plotted on the AFM diagram (Fig. 4.4) fall within the calc-alkaline field and within the field of the DGS opx-granitoids. Similarly on the K-Na-Ca diagram (Fig. 4.4) the adamellites and CHS show a calc-alkaline trend similar to the DGS, but the YWL is displaced from this trend, reflecting its higher Na/K ratio. These features suggest the MGS comprises a typical suite of orogenic granitoids.

In terms of the model of orogenic granitoid genesis of Chappell & White (1974) the MGS adamellites have $Al_2O_3/(Na_2O + K_2O + CaO)$ less than 1.1 (Table 4.3) suggesting they are I-type, whereas the YWL has a higher value for this indicator (Table 4.3) suggesting the leucogranites are S-types. These model conclusions suggest that the YWL was probably largely derived from pre-existing pelitic sedimentary material whereas the adamellites may have been derived largely from an igneous or meta-igneous protolith.

Emslie (1978) drew attention to the high $Fe_T/(Fe_T + Mg)$ and K_2O of many anorogenic silicic suites and subsequently Loiselle & Wones (1979) and Collins et al. (1982) proposed more detailed geochemical criteria to distinguish anorogenic or A-type granitoids. Application of some of these criteria to the MGS adamellites in comparison with the DGS, and CGS I-types and other well-documented suites (Table 4.3) suggests that although the high $Fe_T/(Fe_T + Mg)$, K_2O/Na_2O , $(La)_N$, Zr,

Table 4.4: Moody Granitoid Suite

Major and trace element geochemical data for averaged granitoids.

	CHS (1) [*]	Adamellites (5)	YWL (6)
SiO ₂	58.88	71.10	74.17
Al ₂ O ₃	15.57	14.17	14.57
Fe ₂ O ₃ tot	7.33	3.53	1.11
MnO	0.12	0.06	0.08
MgO	2.31	0.50	0.31
CaO	4.28	1.47	0.57
Na ₂ O	3.27	3.05	3.96
K ₂ O	5.28	5.23	4.51
TiO ₂	1.40	0.44	0.04
P ₂ O ₅	0.63	0.25	0.29
Total	100.10	99.80	99.61
Rb	164	223	331
Sr	774	190	11
Ba	2471	725	15
Y	40	33	10
Zr	464	302	29
Nb	32	25	20
Sc	12	7	2
La	236	102	
Ce	418	202	5
Nd	169	77	
Sm	23	12	
Eu	4	1.4	
Gd	14	8	
Dy	9	6	
Er	5	3	
Yb	4	3	

*number in brackets refers to number of samples averaged.

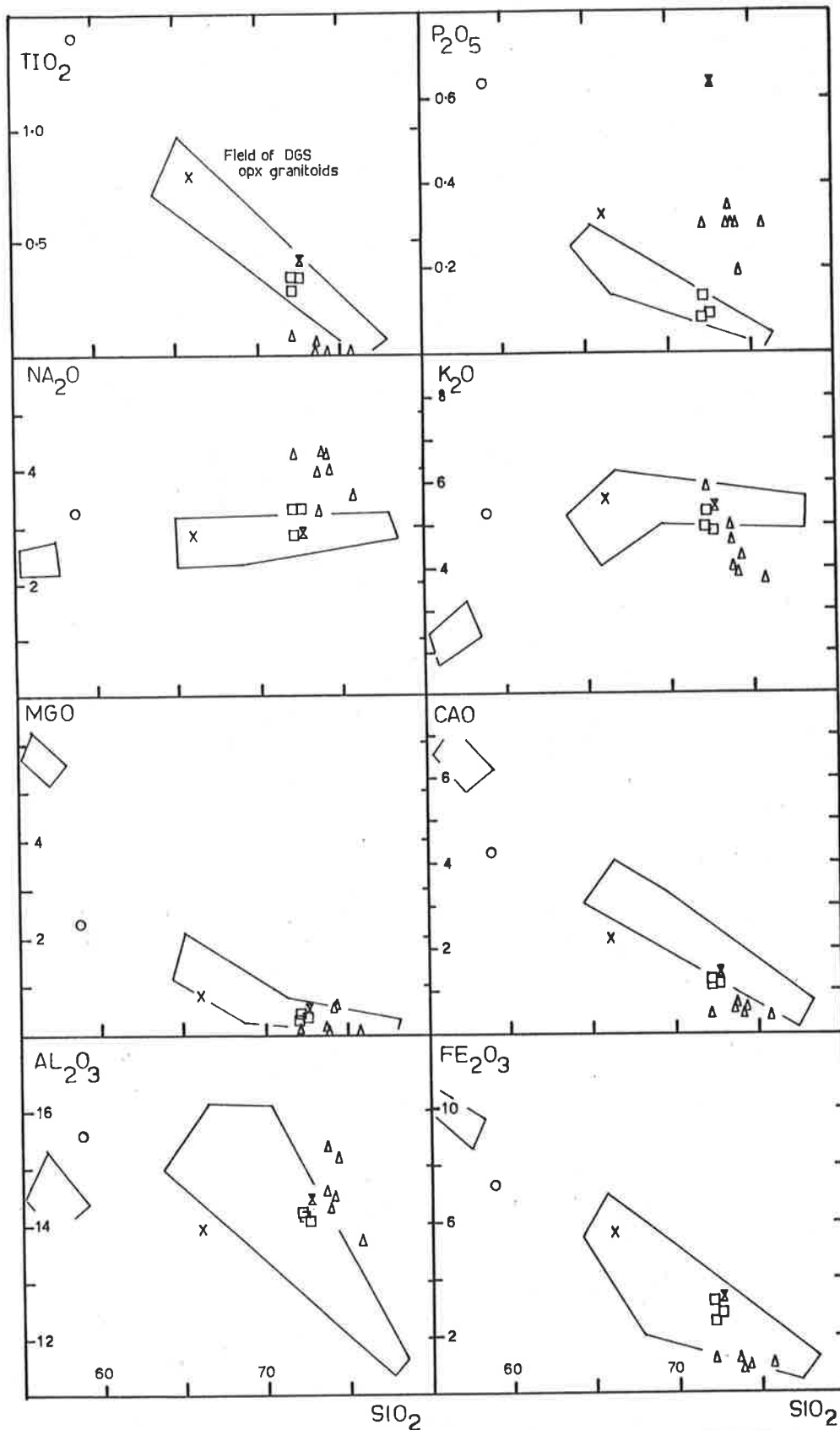


FIGURE 4.5 Major element variation diagrams for the Moody Granitoid Suite. Symbols as in Figures 4.2 & 4.4.

Nb and Y are transitional towards A-type the moderately high Ba and Sr argue for I-type. Data for key elements such as Ga, Ni and Cr are not available for the MGS adamellites. The transitional nature of the adamellites will be discussed further in Chapter 7.

A similar comparison for the YWL (Table 4.3) is inconclusive, values for Ba, Sr, Zr, Y and Sc all being extremely low and not typical of any of the granitoid types. The mineralogical and geochemical indicators mentioned above however, argue in favour of an S-type origin.

These observations suggest that the two groups of granitoid rocks within the MGS may have fundamentally different petrogeneses.

4.3.2 Major element geochemistry

Although the data are meagre for some of the rock types, the major element geochemistry of the MGS shows the following features (Appendix Table 4.1; Table 4.4; Fig. 4.5),

- (1) SiO_2 range from ca. 59% to ca. 76%
- (2) regular elemental variation with respect to SiO_2 in adamellites and CHS, for most elements, but,
- (3) disparate element variation between YWL and other granitoids.

For the adamellites and CHS,

- (4) the distributions of most elements are similar to those of the DGS non-cumulate opx-granitoids, although CaO is slightly depleted,

whereas for the YWL,

- (5) there is an absolute enrichment of Al_2O_3 , Na_2O and P_2O_5
- and (6) an absolute depletion of CaO, K_2O and TiO_2 , with respect to the DGS opx-granitoids.

These data suggest that the adamellites and CHS have had a petrogenetic history broadly similar to the DGS, but that the YWL has had a different origin.

4.3.3 Trace element geochemistry

The differences between the YWL and other granitoids of the MGS are confirmed by the trace element data (Appendix Table 4.2; Table 4.4; Fig. 4.6). The most noticeable deviation occurs for Y, where the YWL is depleted by a factor of ca. 4 with respect to the other granitoids.

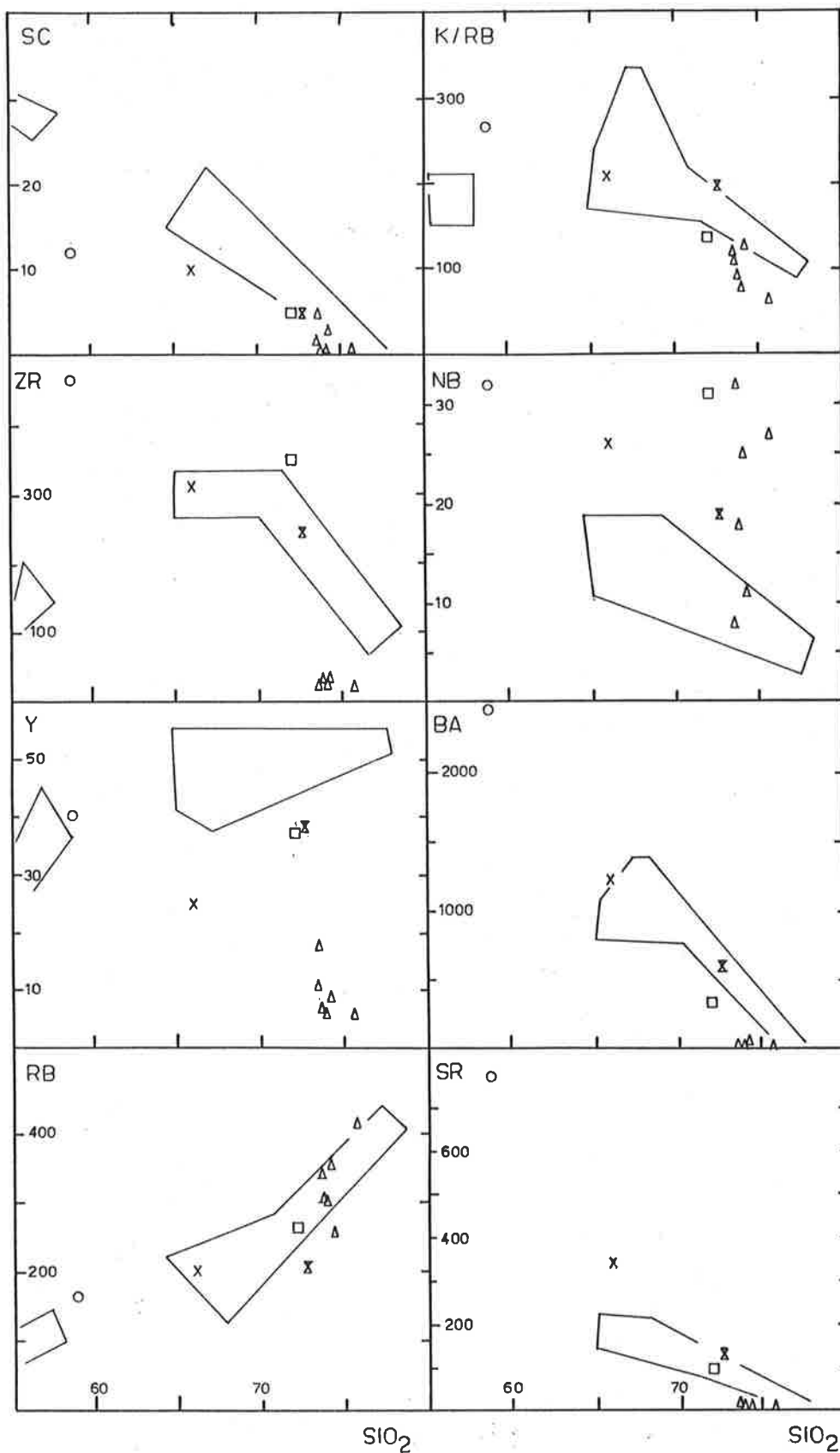


FIGURE 4-6 Trace element variation diagrams for the Moody Granitoid Suite. Symbols as in Figures 4.2 & 4.4.

The distribution patterns for Rb, Sr, Ba, Zr, Sc and K/Rb in the MGS are similar to the corresponding DGS patterns although the absolute levels tend to deviate markedly especially in the CHS and MOA. In the CHS in particular Sr, Ba, Nb and Zr are enriched whereas Sc is depleted relative to the DGS. In the YWL all trace elements other than Rb and Nb tend to be depleted with respect to the DGS.

4.3.4 REE geochemistry

The REE in the MGS clearly distinguish the YWL from the other granitoids (Appendix Table 4.2; Table 4.4; Fig. 4.7). Whereas the adamellites and CHS have strongly fractionated patterns with $(Ce/Y)_N$ ca. 20, the YWL have relatively flat patterns with $(Ce/Y)_N$ ca. 1 to 2. Also the absolute levels of concentration are markedly different from those in the adamellites and CHS, the latter having Ce_N ca. 250-500 times chondritic, whereas the YWL has Ce_N ca. 5-7 times and Y_N ca. 3-4 times chondritic.

Moreover with respect to the DGS field (Fig. 4.7) the adamellites have $(La/Sm)_N$ ca. 4.5 - 6.3 and $(Yb/Gd)_N$ ca. 0.24 - 0.45 and are therefore more fractionated than the DGS opx-granitoids, which in particular, have relatively unfractionated HREE. In this regard the adamellites and CHS are more similar to the CGS.

The adamellites and CHS have a pronounced negative Eu anomaly which increases from CHS to MTA. As the Eu anomaly increases it is notable that the HREE become less fractionated and the patterns become slightly concave up.

4.3.5 Discussion

(1) Adamellites and CHS

The CHS and adamellites have I-type petrological and geochemical features, and their geochemical coherence suggests that they are comagmatic. In contrast to the DGS which was shown to be a crystal fractionated suite of progressively more siliceous granitoids (Chapter 2), the MGS has been shown to comprise progressively more mafic intrusive pulses (Coin 1976; 1980). Within the spectrum of bulk rock compositional changes there exist systematic mineralogical compositional changes which suggest that the suite represents a progressive partial fusion series (cf. discussion in Chapter 2). It is thus likely that the MTA represents an early generated silicic magma whereas the CHS represents a later generated mafelsic magma which has intruded the earlier intrusive phases.

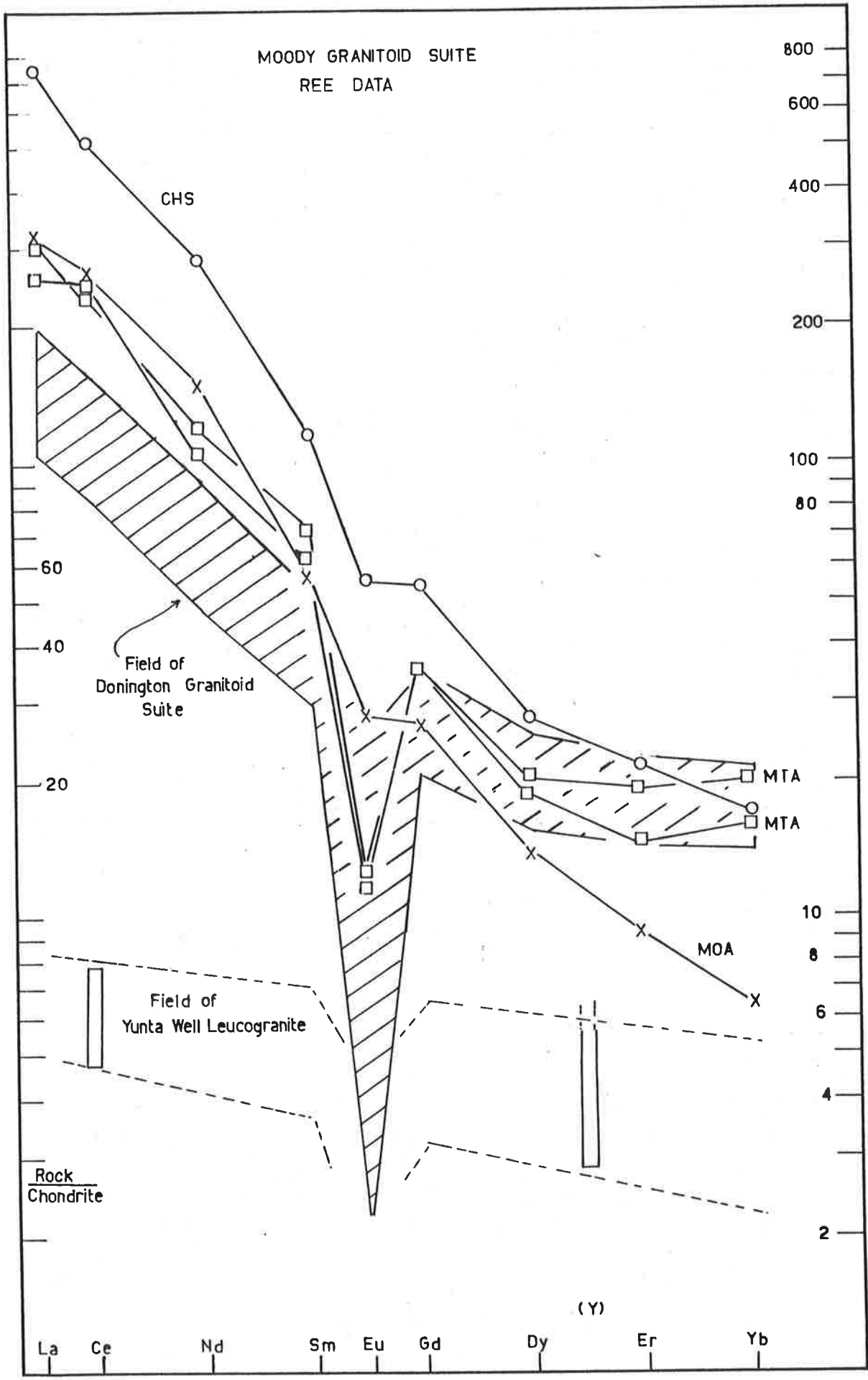


FIGURE 4-7

The concave up HREE pattern and large Eu anomaly for MTA, in contrast to the linear HREE fractionation and small Eu anomaly for CHS and MOA suggest a marked change in either the residual minerals, or their behaviour, occurred during partial melting.

In particular it is probable that the MTA magma developed in equilibrium with residual plagioclase and amphibole, whereas the CHS does not show the pronounced signature expected from these minerals. A physical model to account for these features may be proposed.

The I-type granitoid outcrop pattern is zonal (Fig. 4.1) suggesting an intrusive model involving unmixing of more silicic adamellite magma and emplacement ahead of a rising segregating diapir. Residual mafelsic granitoid thus may intrude earlier segregated and emplaced adamellite in the sequence observed. In this way the bulk I-type suite may have geochemical characteristics more typical of the CHS e.g. linear fractionated HREE but the MTA, segregated during emplacement may show the effect of residual hornblende e.g. concave up HREE.

The petrogenesis of the MGS I-type granitoids will be discussed more fully in Chapter 7 in comparison with the other I-type suites of this study.

(2) Yunta Well Leucogranite

As noted above, the YWL is quite different from the CHS and the adamellites and has S-type characteristics. It is the only S-type granitoid so far recognised in the present author's study area. Its common association in the field with abundant pegmatites of similar petrology (Coin 1976), and the location of the main body of the YWL within the highest metamorphic grade Hutchison Group metasediments suggest that the YWL developed by partial melting of the surrounding or subjacent Hutchison Group (regional-aureole type of White et al. 1974). The muscovite leucogranite would probably have been near water-saturated and unable to move far from its source region (White et al. 1974) without freezing. It is probable that elevation of isotherms ahead of the ascending I-type plutons may have provided the heat impetus for melting the Hutchison Group in this area to produce the YWL.

(3) Regional spatial considerations

The outcrop of the Moody Granitoid Suite is structurally far to the west of the outcrop of the DGS and CGS (Fig. 1.1). In addition

they were apparently emplaced into different prevailing P-T conditions, viz

DGS ca. 8 Kbar at 800° - 900° C
and MGS ca. 3 Kbar at 490° - 650° C

Furthermore the two outcrop areas are on opposite sides of the Kalinjala Mylonite Zone (KMZ) which here is separating a major orthogneiss terrain in the east containing only I-type granitoids from a metasedimentary terrain in the west containing I- and S-type granitoids.

Hence it is suggested here that the KMZ may represent a major crustal boundary separating two crustal blocks of markedly different petrogenetic histories. This question will be examined in more detail in Chapters 5 and 7.

4.4 RB-SR GEOCHRONOLOGY

The Rb-Sr geochronological investigation was initiated,

- (1) to date the time of emplacement of the MGS,
 - (2) to constrain the age of high-grade metamorphism and D_3 tectonism,
 - (3) to examine the distinction between the I- and S-type plutonic rocks
- and (4) to aid in characterising crustal evolution in this portion of the Gawler orogenic domain.

The initial observation of Coin (1976;1980) that the MGS comprises two distinct episodes of magma emplacement has been confirmed by the geochemical study outlined above. There has been recognised

- (1) an early, foliated, syn- D_3 , S-type Yunta Well Leucogranite
- and (2) a later, massive, late to post- D_3 , I-type suite of adamellites and the Chinmina Syenite.

Previous studies of I- and S-type granitoids have suggested that IR differences exist (e.g. Chappell & White 1974), although this simple conclusion has been challenged by subsequent authors (e.g. Flood & Shaw 1977).

4.4.1 Results

(1) Yunta Well Leucogranite

These leucogranites have very high Rb/Sr ratios averaging ca. 32.5 (Table 4.5), a feature which makes the calculated age relatively

TABLE 4.5

Moody Granitoid Suite
Rb-Sr Analytical Data.

Sample	Rb ppm	Sr ppm	Rb/Sr	$^{87}\text{Rb}/^{86}\text{Sr}$	$^{87}\text{Sr}/^{86}\text{Sr}$ *
Chirmina Syenite (CHS) 350-829	164	774	0.21	0.6125	0.721931
Moreenia Adamellite (MOA) 350-839	201	340	0.59	1.7211	0.749770
Moody West Adamellite (MWA) 350-849	206	132	1.56	4.5839	0.824887
Moody Tank Adamellite (MTA) 350-801A	263	97	2.71	8.0221	0.903916
350-802G	258	99	2.61	7.6597	0.895752
W1	-	-	-	7.8697	0.900200
W2	-	-	-	7.9086	0.901000
W3	-	-	-	8.5740	0.916000
Yunta Well Leucogranite (YWL)					
350-858	308	23	13.4	43.274	1.75490
350-857	257	15	17.1	57.768	2.11308
350-854	300	8.2	36.6	140.671	4.09175
350-853	303	7.3	41.5	166.743	4.73631
350-851	356	6.6	53.9	248.579	6.69755

* All $^{87}\text{Sr}/^{86}\text{Sr}$ data normalised to E & A $^{87}\text{Sr}/^{86}\text{Sr} = 0.70800$.

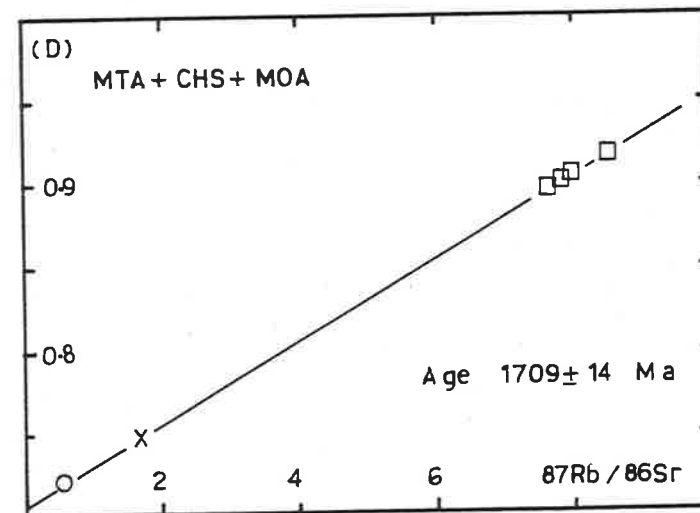
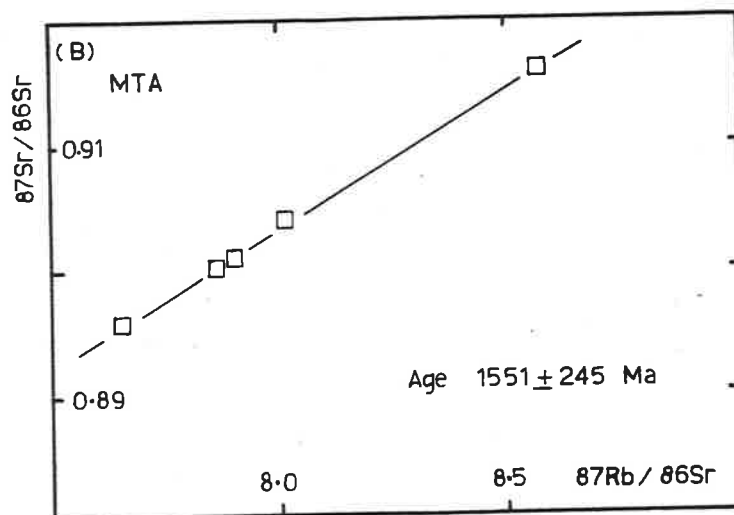
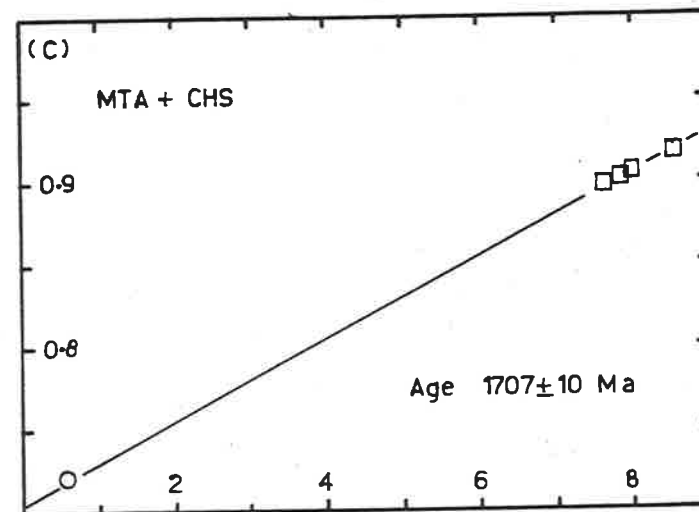
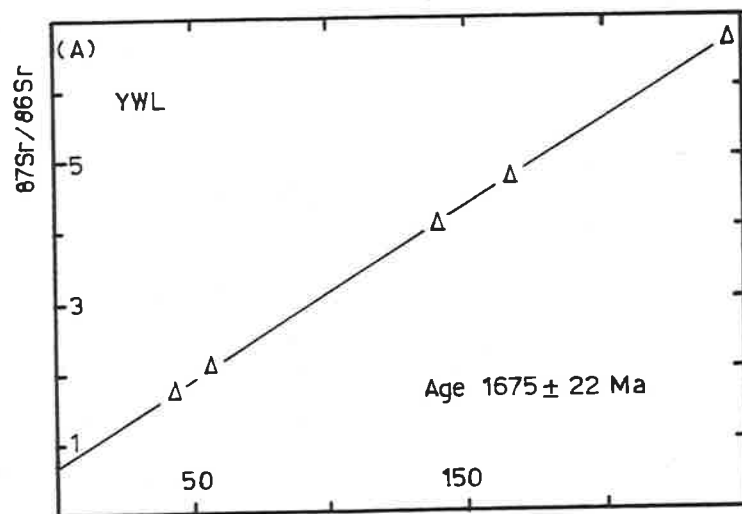


Figure 4.8 Isochron diagrams for the Moody Granitoid Suite. Symbols as in Figures 4.2 and 4.4.

insensitive to the IR, in much the same way that a mica age is insensitive to IR. The five total rock samples define a perfect-fit isochron (Fig. 4.8) with MSWD of 0.54 and calculated Model 1 age of 1675 ± 22 Ma (Regression 1, Table 4.6). However, due to the long extrapolation to the $^{87}\text{Sr}/^{86}\text{Sr}$ axis the calculated IR of 0.7163 ± 233 (Regression 1, Table 4.6) is very imprecise.

The simplest interpretation of this perfect-fit isochron is that it represents the emplacement age of the YWL.

(2) Moody Tank Adamellite

The limited range of Rb/Sr ratio for the MTA (Table 4.5) allows only imprecise estimates of both age and IR. Two samples analysed by the present author have been supplemented by three from Webb (1978).

The five total-rock samples define a perfect-fit isochron (Fig. 4.8) with MSWD of 0.07 and calculated Model 1 age of 1551 ± 245 Ma and IR of 0.7251 ± 278 (Regression 2, Table 4.6). This imprecise result cannot be distinguished from that of the YWL at the 95% confidence level.

The apparent elevated IR is suggestive of some updating, so that the calculated age is viewed with caution.

(3) Chinmina Syenite

Reconnaissance Rb-Sr analyses by XRF revealed that the CHS has a low and uniform Rb/Sr ratio, so only one total-rock sample was analysed (Table 4.5).

Assuming that the CHS and MTA are comagmatic (see above), the data for these two rock-types were regressed together. The resulting six point isochron is a perfect-fit (Fig. 4.8), with MSWD of 0.94, a calculated Model 1 age of 1707 ± 10 Ma and IR of 0.7069 ± 5 (Regression 3, Table 4.6). This combined result is indistinguishable at the 95% confidence level from the imprecise result for the MTA alone, but the age range is different from that given by the YWL regression.

(4) Moreenia Adamellite

On the basis of reconnaissance XRF only one total rock sample of the Moreenia Adamellite was chosen for isotopic analysis (Table 4.5). The results regressed with the MTA and CHS data produce a near-perfect isochron (Fig. 4.8), with MSWD of 1.97; and following the criteria of Brooks et al. (1972) a Model 1 calculated age of 1709 ± 14 Ma and

Table 4.6: Moody Granitoid Suite -
Rb-Sr isochron regression groups.

Regression number	Grouping	MSWD*	Model	Age (Ma)	IR
1.	YWL	0.54(5)	1	1675± 22	0.7163±233
2.	MTA	0.07(5)	1	1551±245	0.7251±278
3.	MTA + CHS	0.94(6)	1	1707± 10	0.7069± 5
4.	MTA+CHS+MOA	1.97(7)	1	1709± 14	0.7070± 4

*number in brackets refers to number of samples regressed.

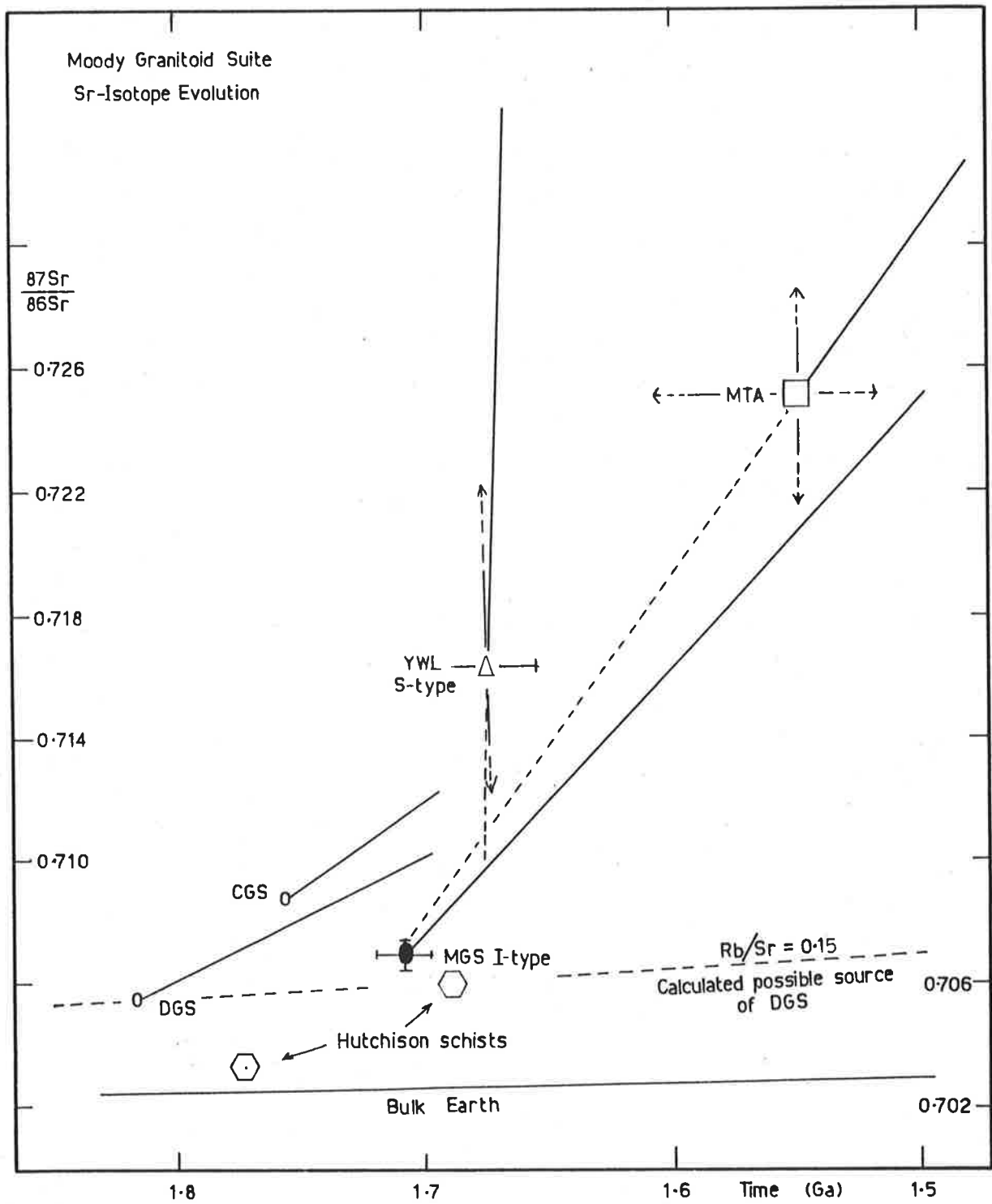


Figure 4.9

Sr-isotope evolution diagram for the Moody Granitoid Suite, compared with possible model source rocks.

IR of 0.7070 ± 4 results (Regression 4, Table 4.6). This combined result is indistinguishable from the result for MTA alone and the combined MTA and CHS result, which is strong confirming evidence for the comagmatism of the adamellites and CHS, and suggests that the I-type granitoids were emplaced at 1709 ± 14 Ma with IR of 0.7070 ± 4 .

4.4.2 Discussion

(1) Resolution of I-type and S-type granitoids

On the basis of the data presently available it is not possible, at the 95% confidence level, to distinguish the calculated ages and IR's of the I-type and S-type granitoids of the MGS. This is due primarily to the imprecision of the calculated isochron IR and age for the YWL caused by its very high Rb/Sr ratio and resultant long extrapolation to the $^{87}\text{Sr}/^{86}\text{Sr}$ axis.

However, the precise I-type result fixes the minimum emplacement age of the YWL at 1709 ± 14 Ma since the adamellites and CHS have been shown by Coin (1976; 1980) to post-date the YWL.

(2) Timing of D_3

The intrusion of the I-type granitoids of the MGS has been suggested to be late- to post- D_3 , which suggests a minimum age for D_3 of 1709 ± 14 Ma. This is in agreement with the conclusions drawn from the emplacement age for the CGS (Chapter 3) which suggested an age for D_3 of less than 1757 ± 14 Ma.

However, it is in distinct contrast to the conclusion of Parker et al. (1981) and Rutland et al. (1981), that D_2 is 1650 ± 35 Ma, based on a preferred isochron age for the syn- D_2 Middlecamp Granite. The present author has proposed that this lower age may date D_3 tectonism and metamorphism (Chapter 3).

Pooling all the estimates of the age of D_3 currently available to the present author (Table 4.7) allows a best estimate of 1697 ± 12 Ma.

(3) Petrogenesis of the I-type granitoids

Comparison of the age and IR of the MGS I-type granitoids with the I-type DGS and CGS (Fig. 4.9) shows that the MGS IR is too low to be derived from DGS or CGS material at ca. 1710 Ma. Moreover, as with the DGS and CGS, the MGS cannot be derived from older Archaean

Table 4.7: Estimates of timing of D₃

Fisherman's Point Granite Gneiss 2 DGS	1632±96 Ma
Colbert Alkali Feldspar Granite Gneiss two-point join	1624±190 Ma
Middlecamp Granite	1635±86
Moody Granitoid Suite I-type granitoids	1709±14 Ma
Moody Granitoid Suite S-type granitoids	1675±22 Ma

*Pooled age 1697±12 Ma.

*calculated after method of Paradine & Rivett (1960).

crust of the type represented by the Sleaford Complex or its equivalents (Fig. 4.9).

However, source material similar to that proposed for the DGS and CGS would also be suitable for the MGS I-type granitoids (Fig. 4.9).

The petrogenesis of the MGS I-type granitoids will be examined in more detail in Chapter 7, in conjunction with the other granitoid suites.

(4) Petrogenesis of the S-type granitoids

It is difficult to speculate on the nature of the YWL protolith because the imprecision of the calculated isochron IR does not adequately constrain the isotopic nature of the source of the granitoid.

Isotopic data for the Hutchison Group of metasediments, in particular metapelitic schists, when plotted on Fig. 4.9, and compared with the isotope evolution curve for YWL, do not discount derivation of YWL from the enclosing schists.

4.5 SUMMARY

The Moody Granitoid Suite comprises an early, syn-D₃ foliated S-type granitoid, the Yunta Well Leucogranite, and a later, massive, late- to post-D₃ suite of adamellites and Chinmina Syenite of I-type. The I-type granitoids have been emplaced at 1709 ± 14 Ma with IR of 0.7070 ± 4 and carry hydrated ferromagnesian silicates. The S-type granitoid is of similar age but with an imprecisely determined IR.

The YWL and associated pegmatites and migmatites were probably derived by partial melting at or about their present position from the enclosing Hutchison Group pelitic metasediments at ca. 10 km depth. Partial melting was probably associated with the breakdown of muscovite to sillimanite, and was of near-minimum melt type.

The I-type granitoids were probably derived by progressive partial melting and diapiric ascent through the crust. The advance of isotherms ahead of hot I-type diapir into the Hutchison Group metasediments at the exposed level may have contributed to the partial melting of the YWL.

The Moody Granitoid Suite is unique in the present author's study area in containing S-type granitoid material. The Kalinjala

Mylonite Zone apparently bounds the eastward extent of the Hutchison Group and S-type plutonism in southeastern Eyre Peninsula.

CHAPTER 5.MASSENA BAY GNEISSES.5.1 INTRODUCTION

The Massena Bay Gneisses (MBG) has not been defined as a separate rock-unit by previous authors. Thomson (1980) implicitly included it in the Lincoln Complex (Table 1.1) presumably as his "granitic gneisses", "migmatites", or "quartzofeldspathic gneiss relics of older basement complexes reworked by Kimban tectonism".

The present author has briefly defined and described the MBG and its geological relationships to the other rock units of the study area in Chapter 1. At least in part metasedimentary, but predominantly orthogneissic (see below), the MBG predates D_1 and appears to be intruded by the DGS. Although within the MBG in the present study area metapelites are scarce and poorly layered, on Yorke Peninsula (Fig. 1.1) Richardson (1978) has recognised abundant, well-layered metapelite gneisses in rocks correlated by the present author with the MBG. Furthermore he recognised gabbroic intrusives with rounded mafic xenoliths, similar in many respects to the QGNG of the DGS (Chapter 2), which were emplaced prior to the D_1 deformation. These field relationships suggest to the present author that the MBG comprises a pre- D_1 , pre-DGS layered sequence.

This stratigraphic position is apparently similar to that of the Hutchison Group (Tables 1.1, 1.2, 1.4).

However, the dominant rock types within the MBG are biotite quartzofeldspathic gneisses and hornblende + biotite quartzofeldspathic gneisses, atypical of the Hutchison Group (Coin 1976; Glen et al. 1977; Parker & Lemon 1982) suggesting that the MBG is distinct from the Hutchison Group. In addition, Rb-Sr isotopic data (see below), do not allow the MBG gneisses to be reworked basement. The present author's contention in this chapter is that the MBG comprises a recognisable pre-DGS layered sequence, approximately coeval with, but petrogenetically distinct from the Hutchison Group.

Two main outcrop areas will be described, the Massena Bay locality (Fig. 5.1), and the Cape Donington locality (Fig. 1.2, Fig. 2.1), supplemented by observations at Boston Point (Fig. 1.2). These will be compared with the observations of the Yorke Peninsula MBG outcrops of Pedler (1976) and Richardson (1978). In addition the relationship of the Hutchison Group to the MBG will be further explored.

Table 5.1 Massena Bay Gneisses - modal and textural summary

Rock unit	major chemicals	texture
Quartzofeldspathic gneisses (QF)	Qtz + plag + ksp _{ar} + biot + hbl _{nd} + Fe-Ti oxide (+ musc + epidote)	foliated inequigranular to seriate polygonal to interlobate
Garnet + sillimanite	Qtz + plag + biot + gt + Fe-Ti oxide + sillimanite	foliated inequigranular to seriate polygonal to interlobate
Calc-silicate gneisses	Qtz + plag + cpx + hbl _{nd} + scapolite + gt + Fe-Ti oxide	inequigranular to seriate polygonal to interlobate
Granite gneisses	Qtz + plag + ksp _{ar} + biot + Fe-Ti oxide	inequigranular to seriate polygonal to interlobate
Amphibolites	plag + opx + cpx + hbl _{nd} + biot + Fe-Ti oxide + Qtz	inequigranular to seriate polygonal (to interlobate)
Migmatite leucosomes	Qtz + plag + ksp _{ar} + biot	seriate to inequigranular polygonal to interlobate

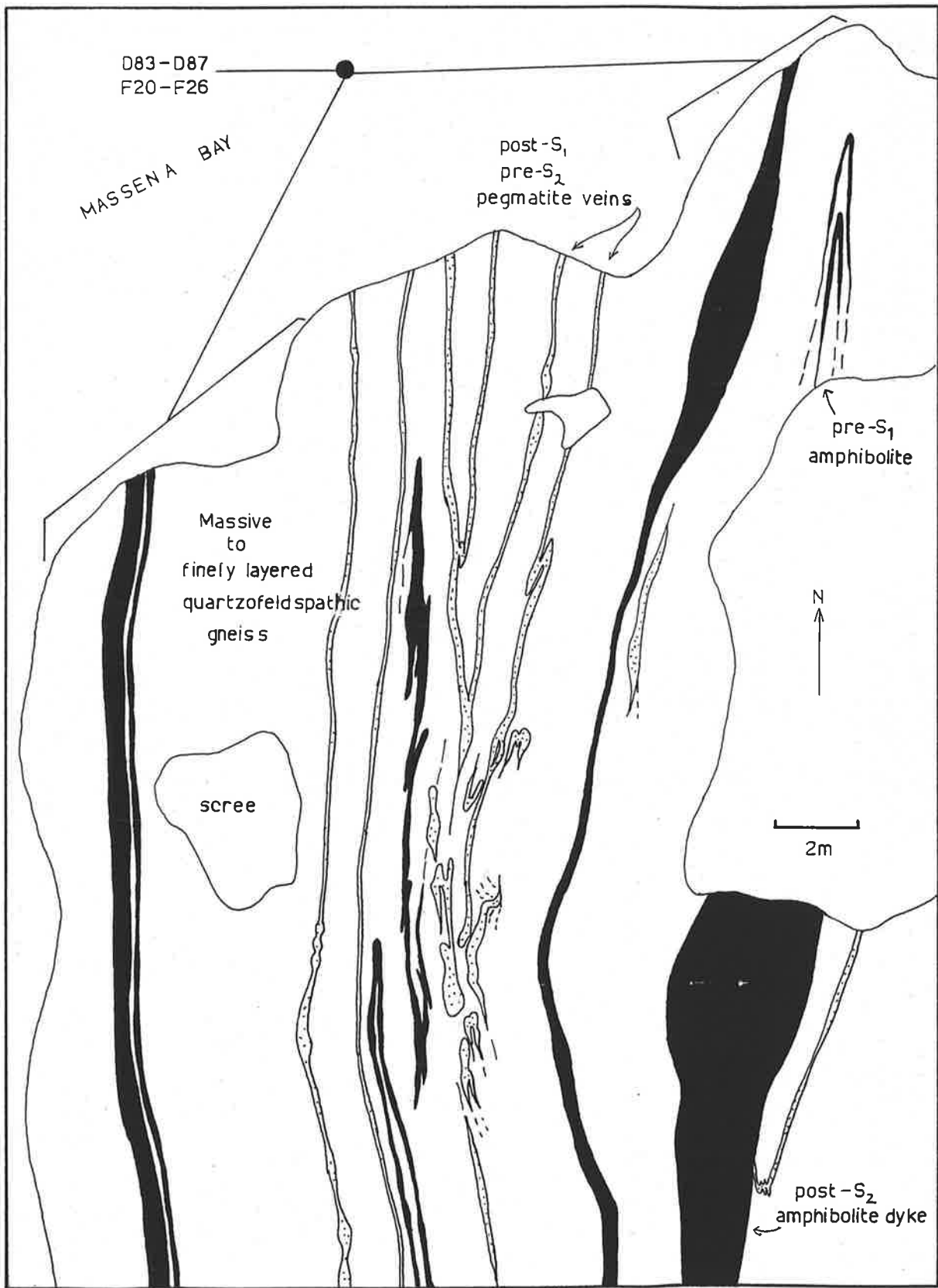


Figure 5.1

Small area on south side of Massena Bay (see Fig. 1.2) mapped in detail and sampled for Rb-Sr total-rock dating of massive quartzofeldspathic (QF) gneisses.

5.2 PETROGRAPHY AND MINERAL CHEMISTRY

There are six main lithological groups present in the MBG in the study area, viz

- (1) quartzofeldspathic, biotite hornblende gneisses (QF)
- (2) garnet + sillimanite gneisses
- (3) calc-silicate gneisses
- (4) granitic gneisses
- (5) amphibolitic "dykes"
- (6) pegmatitic veins.

Of these the QF gneisses comprise the bulk (ca. 75%), with the amphibolitic "dykes" comprising the bulk of the remainder, (ca. 15%). The granitic gneisses will be discussed briefly in this chapter. They are considered by the present author to be part of the DGS, although Flook (1975) suggested them to be granitised metasediments.

Each of these lithological groups will now be described in turn.

5.2.1 Quartzofeldspathic Gneisses

(1) Massena Bay locality

These grey coloured, medium to coarse grained gneissic rocks outcrop mainly on the Bolingbroke Peninsula (Fig. 1.2) and in scattered outcrops further south. One major foliation is present, which is defined primarily by biotite and which is attributed to D_{1-2} (Chapter 1). Hornblende porphyroblasts are common, as are thin (up to 5mm), often diffuse, migmatitic veins concordant with and containing S_{1-2} and forming a layering (Fig. 1.6). Thicker, coarse grained, sharply discordant pegmatitic veins are also common (Fig. 1.6).

The microscopic rock texture is inequigranular to seriate, polygonal to interlobate, and the major mineral assemblages are detailed in Table 5.1. Common accessory minerals are zircon, sphene, apatite and allanite. Locally muscovite, epidote and clinozoisite may replace plagioclase and biotite extensively.

Although S_{1-2} fabrics are well-developed in most specimens, there is considerable evidence for subsequent recrystallisation. S_{1-2} quartz ribbons have developed new quartz sub-grains which may also exhibit undulose extinction, either as a result of late D_2 strain and recrystallisation or D_3 tectonism.

The hornblende porphyroblasts are commonly poikiloblastic with respect to sub-randomly oriented rounded quartz inclusions, and apparently pre-date fabric development (Fig. 1.9). Specimen 515-D87

exhibits one large hornblende poikiloblast which has been dismembered during the development of S_{1-2} .

In thin section, the migmatitic veins are seen to be coarser-grained than the host, more leucocratic and only poorly foliated.

(2) Boston Point locality

In the outcrop of QF gneisses on Boston Point (Fig. 1.2), rare mafic inclusions up to 5 cm long are interpreted to be xenoliths, suggesting that the QF gneiss host is a meta-igneous rock.

(3) Yorke Peninsula outcrops

Inspection of specimens collected by Pedler (1976), and a reconnaissance survey of his study area reveal that these gneisses display marked similarities to the QF gneisses at Massena Bay. Specimen 510-100 contains common hornblende poikiloblasts, although here the quartz inclusions show more of a tendency to be sub-parallel within some of the poikiloblasts (Fig. 1.9).

Pedler (1976) has however described extensive local patches of retrograde D_3 epidote which are not observed in the present study area.

5.2.2. Garnet + sillimanite gneisses

(1) Cape Donington locality

These purple to grey coloured, medium to fine grained rocks occur in intimate association with calc-silicate gneisses and granitic gneisses. The layering on the meso-scale is discontinuous and has the appearance of being either sedimentary layering disrupted and transposed during S_{1-2} fabric development or intensely flattened xenoliths within pre-tectonic granitoid. This point will be examined in more detail below in discussion of the granitic gneisses.

In thin section the rock is inequigranular to seriate, polygonal to interlobate and contains the major mineral assemblages summarised in Table 5.1. Apatite and zircon are common accessory minerals.

The garnet porphyroblasts contain abundant inclusions of biotite, opaque oxide and some quartz, which may be in random orientation or in some examples sub-parallel to the elongation axis of porphyroblasts in the S_{1-2} layer parallel fabric (Fig. 1.9). It is suggested that garnet growth occurred, at least in part, pre- D_1 .

Plagioclase porphyroblasts tend to be rounded and often contain a number of small euhedral green spinel inclusions, which are suggested to have exsolved from the plagioclase host.

The S_{1-2} fabric is, in part, defined by quartz ribbons which have subsequently been recrystallised into strain free sub-grains. In one specimen, the quartz ribbon fabric is folded with new quartz ribbons in an axial planar orientation (Fig. 1.9). In addition the quartz ribbon fabric often wraps around the plagioclase and garnet porphyroblasts (Fig. 1.9).

Sillimanite occurs as euhedral porphyroblasts which are generally parallel to the S_{1-2} fabric but may also be inclined to it.

Retrogressive alteration of plagioclase to sericite, and biotite to chlorite is locally common and may be associated with the intrusion nearby of later granitoids.

5.2.3 Calc-silicate gneisses

Cape Donington locality

These green coloured, medium to fine grained rocks occur intimately interlayered with the garnet + sillimanite gneisses at this locality. The layering of each is discontinuous on the meso-scale. Scattered outcrops of these calc-silicate rocks occur elsewhere in the study area, either as rare interlayers within layered gneisses or more commonly as xenoliths within later granitoid gneisses (e.g. in QGNG at Cape Donington).

In thin section, the rock is inequigranular to seriate, polygonal to interlobate, and contains the major mineral assemblages summarised in Table 5.1. In addition sphene may be abundant in some micro-layers whereas clinozoisite, zircon, apatite, allanite and Fe - Ti oxide may be present in accessory to minor proportions.

A prominent fabric is often lacking, except where quartz ribbons are present or where amphibole defines a lineation. The S_{1-2} fabric, where present, is layer parallel.

Local patches of retrogressive alteration of plagioclase to sericite are common.

5.2.4 Granitic Gneisses

Cape Donington locality

This rock type is buff coloured and medium to coarse grained. It occurs interlayered on the meso-scale with garnet + sillimanite

gneisses and calc-silicate gneisses, where it is strongly deformed, but also occurs in adjacent outcrops where it is less strongly deformed. In the less deformed outcrops xenolithic blocks of metasediment similar to the garnet + sillimanite and calc-silicate gneisses are present.

In thin section the texture is inequigranular to seriate, polygonal to interlobate, and the major mineral assemblages are summarised in Table 5.1. Large grains of plagioclase and orthoclase microperthite within the gneisses are interpreted to be relict igneous phenocrysts. Euhedral zircon and apatite are present as accessory minerals and sphene may be present as coronas surrounding and probably replacing Fe - Ti oxide grains.

The dominant fabric is defined by biotite and quartz ribbons and is folded by F_3 folds. Hence the main fabric is interpreted to be S_{1-2} . The fabrics in the granitic gneisses are entirely similar to those in the interlayered garnet + sillimanite and calc-silicate gneisses.

The granitic gneisses are interpreted by the present author as deformed and metamorphosed intrusive igneous rocks. It is suggested that metasedimentary xenolithic blocks of garnet + sillimanite and calc-silicate gneisses were caught up in the granitoid magma and subsequently deformed in D_{1-2} along with the granitic gneiss. Intense flattening of xenoliths contributed to the development of fine scale discontinuous layering in the metasedimentary gneisses.

This interpretation is supported by the Rb-Sr dating of the granitic gneiss (Chapter 2) which suggests it is part of the Donington Granitoid Suite.

In contrast, Flock (1975) suggested that the granitic gneiss was developed by in situ granitisation of the metasedimentary gneisses which he considered to be a remnant of a layered sedimentary succession. The present author finds little evidence to support the granitisation model at this locality.

5.2.5 Amphibolitic "dykes"

Massena Bay locality

Amphibolitic "dykes" were emplaced prior to the first deformation in the MBG but after the development of the migmatitic veins (Chapter 1). They are distinct from the late tectonic dolerite dykes (DK2; Table 1.4) but may overlap in time the early pre- to syn- metamorphic mafic dykes (DK1; Table 1.4). Indeed some of the "dykes" in the

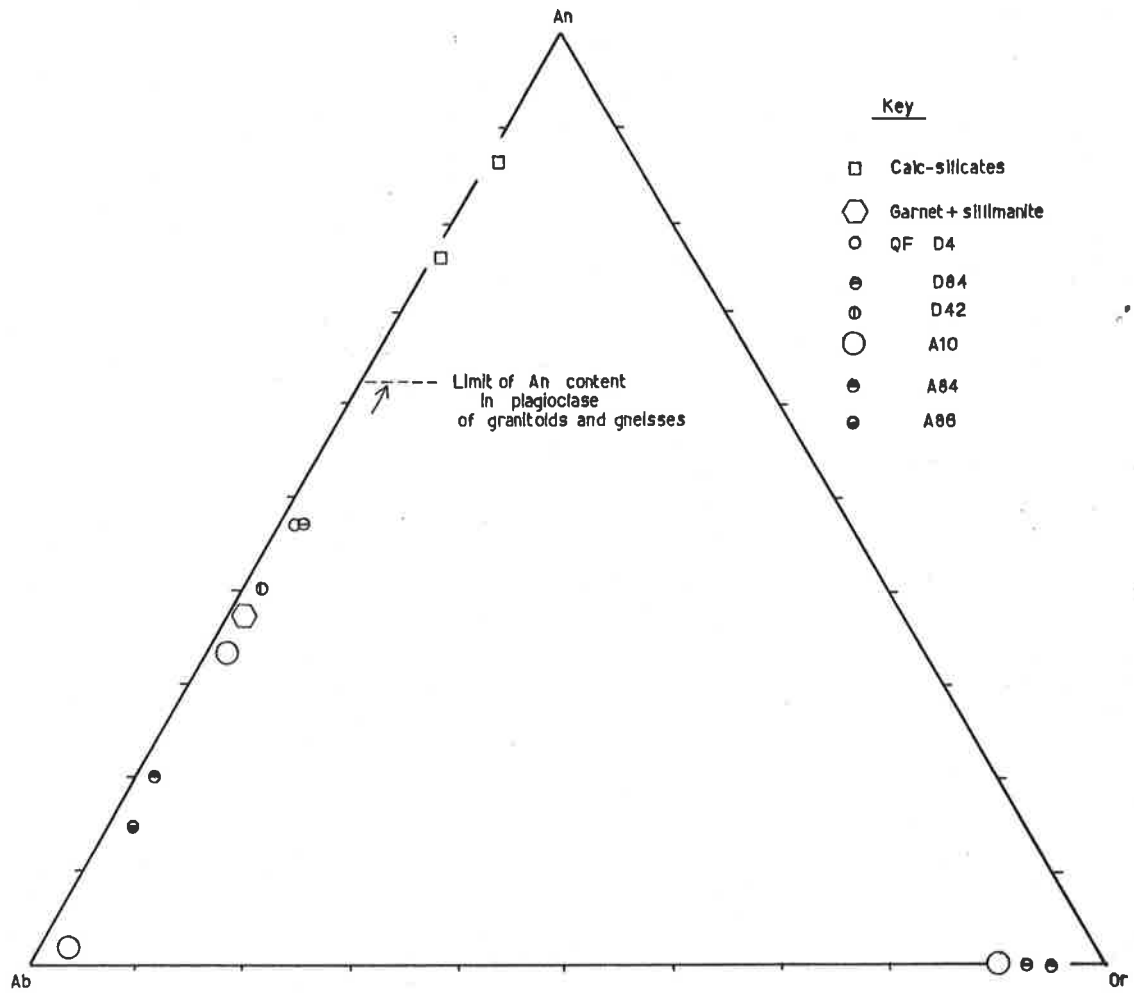
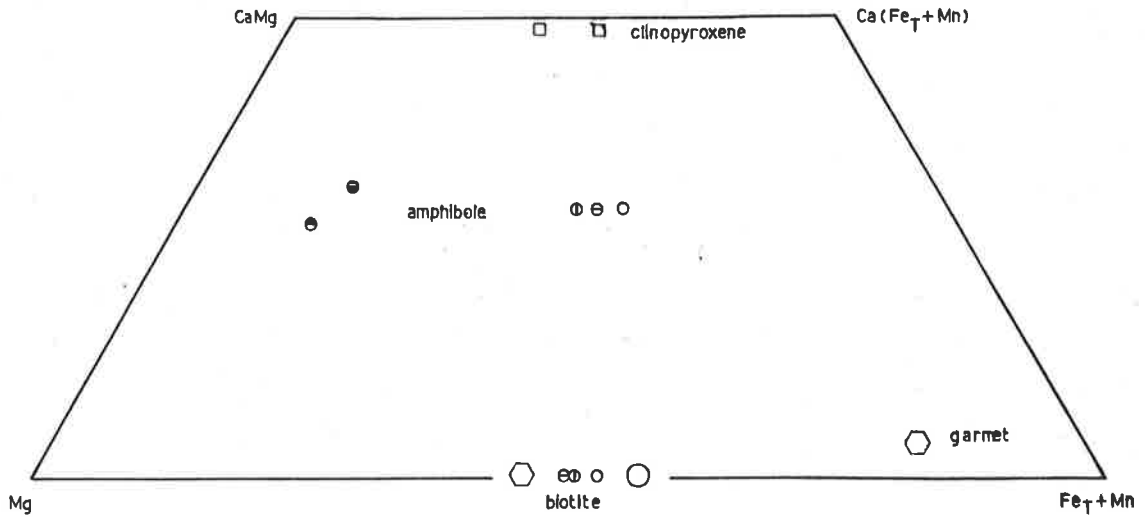


Figure 5.2 Ferromagnesian and feldspar mineral compositions of various units within the Massena Bay Gneisses.

MBG preserve granulite facies assemblages although most of the thin "dykes" are amphibolitic.

The amphibolitic "dykes" contain S_{1-2} fabrics and are tectonically semi-concordant. They are dark coloured and medium to coarse grained and contain the major mineral assemblages detailed in Table 5.1.

In thin section those "dykes" preserving orthopyroxene are inequigranular to seriate, polygonal, but also tend to contain patches of relict igneous doleritic texture and primary igneous pyroxene and plagioclase. Amphibole may also be present in these "dykes".

The more common amphibolite "dykes" are inequigranular to seriate and polygonal to interlobate. Quartz is common and may form quartz ribbons exhibiting sub-grain development and recrystallisation. Garnet porphyroblasts are present in some specimens. Some hornblende and garnet porphyroblasts are poikiloblastic with respect to randomly oriented plagioclase and quartz inclusions, and may be manifesting pre-tectonic metamorphism.

In some specimens there is extensive alteration of plagioclase to sericite and clinozoisite, and sphene coronas surrounding and replacing the opaque oxides may be present.

5.2.6 Mineral Chemistry

Electron microprobe analyses referred to in this section are tabulated in Appendix Table 3.1.

(1) Feldspars

The calc-silicate gneisses contain calcic (An_{76} & An_{87}) plagioclases (Fig. 5.2). These are well outside the range of the QF gneiss plagioclases (Fig. 5.2) and exceed the most calcic plagioclase in the I-type granitoids and granitoid gneisses described in previous chapters (Fig. 5.2).

Within the QF gneisses coexisting plagioclase and alkali feldspar are generally in textural equilibrium and calculated feldspar temperatures (after Powell & Powell 1977) range from 455°C to 567°C (Table 5.2) in the vicinity of Massena Bay. Retrograde QF gneisses within the DGS near North Shields, approaching the Kalinjala Mylonite Zone (Fig. 1.2) yield a calculated temperature of ca. 345°C (Table 5.2). The higher temperatures apparently are reflecting the similar metamorphic history of the DGS granite gneisses and the MBG away from the immediate vicinity of the KMZ.

Table 5.2: Massena Bay Gneisses geothermometry

Method	T ^o C	Comments
biot +Kspar + mag Wones & Eugster (1965)	820-870	-log a _{0₂} = 13-15 at 2 Kbar
gt + biot Ferry & Spear (1978)	565	
mag+ilm Powell & Powell (1977)	580	-log a _{0₂} = 18.1
plag + Kspar Powell & Powell (1977)	345-567	at 8 Kbar

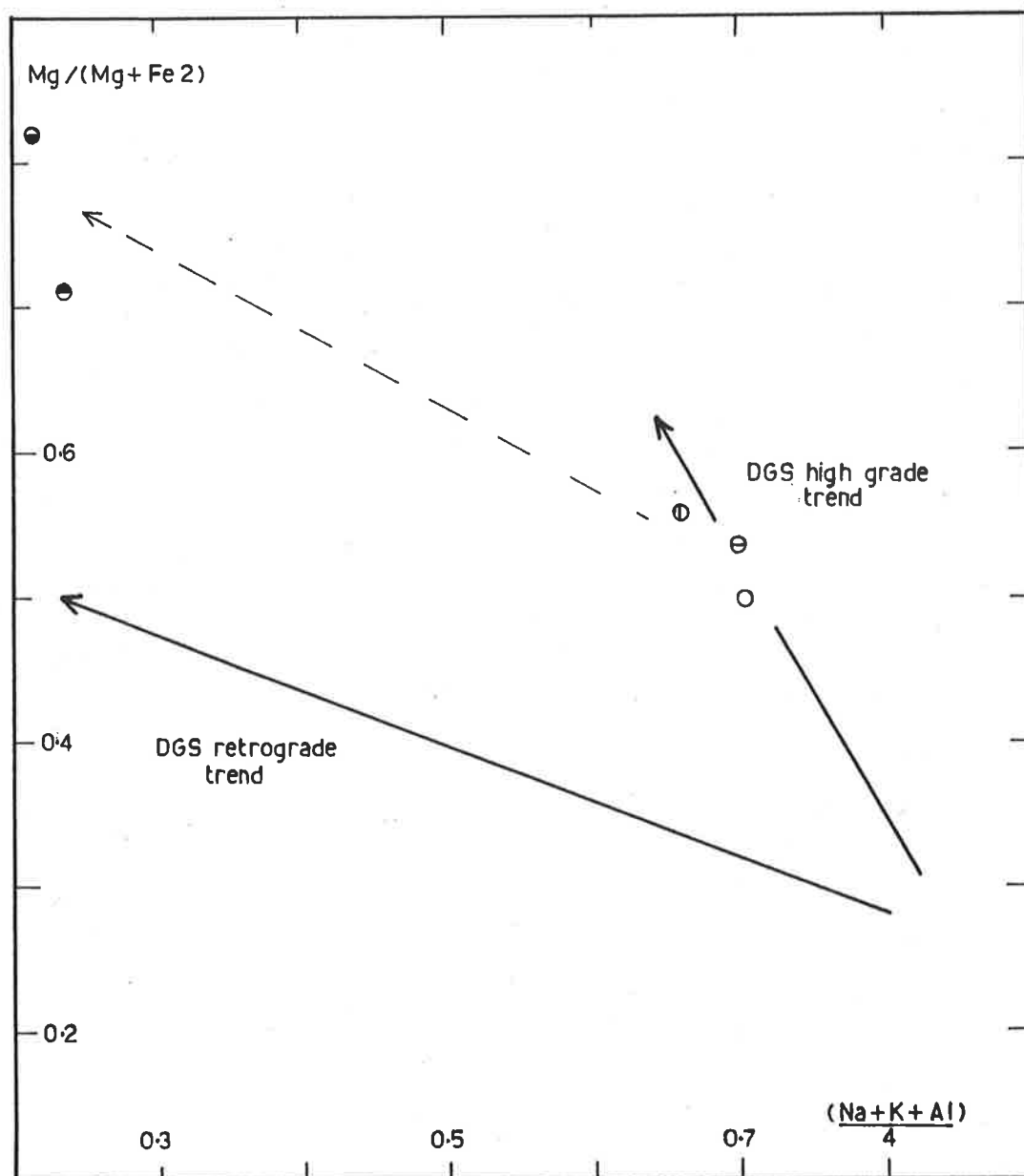


Figure 5.3

Amphiboles within the QF gneisses of the Massena Bay Gneisses. Symbols as in Figure 5.2.

(2) Amphiboles

Amphiboles in the QF gneisses range from magnesian hastingsitic hornblende and magnesian hastingsite in the higher grade rocks near Massena Bay, to actinolite and silicic edenite in the retrograde rocks near North Shields (classification after Leake 1978). Amphiboles in the higher grade rocks are very similar in composition to amphiboles in the DGS high-grade granite gneisses (Figs. 5.2, 5.3) and amphiboles in the retrograde QF gneisses show a similar trend to retrograde amphiboles in the DGS gneisses (Figs. 5.2, 5.3).

These features testify to the similar metamorphic history experienced by the DGS and MBG.

(3) Biotites

Biotites within the QF gneisses and garnet + sillimanite gneisses show a restricted range of compositions (Figs. 5.2, 5.4). Using the criteria of Wones & Eugster 1965, the biotites suggest equilibration temperatures of ca. 820° - 870° C at $\log a_{O_2}$ between ca. -13 to -15 (Table 5.2).

(4) Opaque oxides

Coexisting magnetite and ilmenite have been analysed in one specimen of QF gneiss (A10; Appendix Table 3.1). The calculated temperature of equilibration is ca. 580° C at $\log a_{O_2} = -18.1$ (Table 5.2; Fig. 5.4; calculated after method of Powell & Powell 1977).

(5) Others

Scapolite, grossular garnet and clinopyroxene are present in some calc-silicates at Cape Donington (Appendix Table 3.1; Fig. 5.2) and almandine garnet is present in the garnet + sillimanite gneiss also at Cape Donington (Appendix Table 3.1; Fig. 5.2).

The coexisting garnet and biotite in the garnet + sillimanite gneiss yields a calculated temperature of ca. 565° C (after the method of Ferry & Spear 1978; Table 5.2).

(6) Summary

Apart from the retrograde QF gneisses at North Shields, the majority of the MBG samples showing high-grade metamorphic textures appear to have equilibrated at ca. 450° - 600° C. Biotite compositions suggest possible initial crystallisation at higher temperature ca. 800° - 900° C.

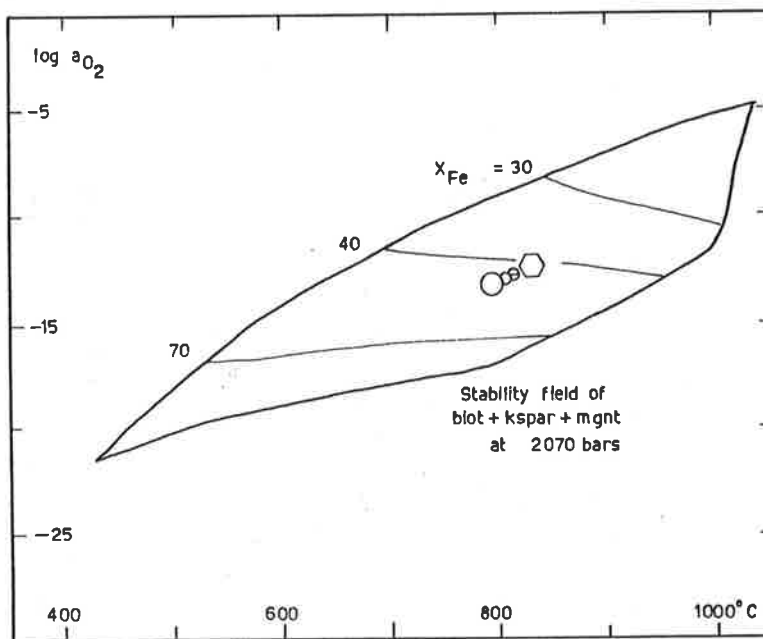
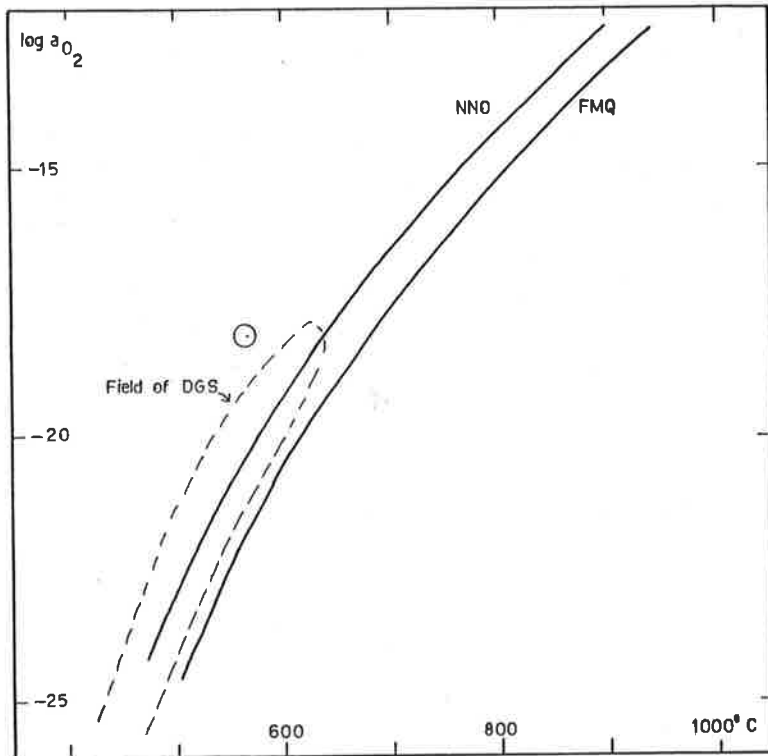


Figure 5.4 Upper: Coexisting magnetite and ilmenite temperature - $\log a_{O_2}$ plot of QF gneiss.
 Lower: Biotites in the Massena Bay Gneisses compared with the data of Wones & Eugster (1965)

5.2.7 Discussion

The microtextural and mineralogical evidence presented above suggests that the gneisses of the MBG at both the Massena Bay and Cape Donington localities have experienced a similar tectonothermal history, involving at least local granulite facies. In addition, there are many similarities to the DGS metamorphic history. Moreover, lithological and textural similarities suggest the layered gneisses of southern Yorke Peninsula constitute an extension of the MBG. Outcrops of the MBG thus extend over a present day width of at least 120 km.

Migmatitic veins, predating D_1 , are common in the QF gneisses, and pre- S_1 poikiloblasts of garnet and hornblende occur in rocks of suitable composition. These observations suggest that a period of metamorphism and possibly in situ partial melting was initiated prior to the first deformation. A similar pre- D_1 growth of poikiloblasts has been reported over large areas of the Gawler domain (Glen et al. 1977).

D_{1-2} metamorphism culminated at least locally in granulite facies, although most rocks now show only parageneses of the amphibolite facies. Mineral chemical data indicate a concentration of calculated temperatures in the range $455^\circ - 580^\circ\text{C}$, although there is some evidence of former temperatures as high as $820^\circ - 870^\circ\text{C}$ in the QF gneisses. The lower temperatures are similar to proposed D_3 conditions in the DGS whereas the higher temperatures are consistent with the D_{1-2} granulite facies in the DGS (Chapter 2).

The local preservation of granulite facies assemblages occurs only in the inner portions of metabasaltic "dykes" whereas the surrounding QF gneisses show no present trace of granulite facies. This observation could be interpreted to mean either

- (1) all the gneisses have experienced granulite facies and have been heterogeneously retrogressed,
- or (2) all the gneisses have experienced the same P-T conditions, but initial differences in H_2O content resulted variously in granulite facies and amphibolite facies assemblages.

Retrogression is a feature ubiquitous in the DGS where it has been particularly localised adjacent to the Kalinjala Mylonite Zone (KMZ) and has been attributed to influx of retrogressive fluids along the KMZ (Chapter 2). It was also pointed out in Chapter 2 that such retrogression may be more pervasively and ubiquitously distributed

prior to localisation along shear zones (Beach 1980). Hence it is possible that an early granulite facies metamorphism (M_1) of the MBG gave place to almost pervasive yet heterogeneous retrogression ((1) above). The presence of S_{1-2} fabrics in the QF gneisses defined by hornblende and biotite suggest the retrogression occurred prior to or during D_{1-2} , similar to the DGS (Chapter 2).

D_3 mineral assemblages are of amphibolite facies, although greenschist facies retrogressive epidote, clinozoisite, sericite, muscovite and chlorite are locally abundant. On Yorke Peninsula much retrogressive epidote has been attributed to D_3 (Pedler 1976).

Although granulite facies assemblages are preserved locally and D_3 retrogression is also localised, suggesting only limited migration of chemical components, the four phases of migmatite and pegmatitic segregations recognised (Table 1.4) "may involve metre (or larger) scales of material transport" (Etheridge et al. 1983). Such chemical mobility has important implications for geochemical and isotopic interpretations (see below).

5.3 GEOCHEMISTRY

5.3.1 Introduction

The MBG has been suggested above to constitute a pre- D_1 layered succession, the major component of which is the probably metavolcanic QF gneisses. As far as can be discerned within the study area, this unit of metavolcanic rocks registers the earliest Kimban orogenic silicic magmatic activity, and so affords the opportunity of placing constraints on the geochemistry of earliest Kimban magmatism.

To this end a small suite of representative QF gneisses were collected from Massena Bay (Fig. 5.1). Care was taken to avoid as much as possible migmatitic or pegmatitic veining in favour of homogeneous QF gneiss.

In addition a few samples of finely interlayered, and mixed, garnet + sillimanite and granitic gneiss were collected from Cape Donington, as well as some calc-silicate gneisses from Cape Donington and Cape Euler (Fig. 1.2).

Although it has been suggested above that the metamorphism was essentially isochemical on the outcrop scale, there is a likelihood that the individual specimens have experienced open system behaviour (which is recognised in the Rb-Sr systematics (see below)). Hence geochemical interpretation must be tempered by this constraint.

Table 5.3: Geochemical comparison of the average QF gneiss of the Massena Bay Gneisses with selected I-type granitoids.

	1	2	3	4	5
SiO ₂	64.78	68.33	64.42	68.48	72.50
Fe/(Fe+Mg) *	0.56	0.70	0.70	0.50	0.64
Al ₂ O ₃ /(Na ₂ O+K ₂ O+CaO) *	0.94	0.96	0.91	0.92	1.03
K ₂ O/Na ₂ O**	1.0	1.8	2.0	1.3	1.2
(La) _N	121	190	219	98	105
(Ev) _N	17	25	26		
(Yb) _N	12	21	20		
Ba	623	915	1113	985	577
Sr	209	147	175	435	165
Zr	176	305	357	181	147
Nb	12	16	21	11	9
Y	27	41	49	19	29
Sc	18	13	15	9	9
Ni	22	21		17	6
(La/Yb) _N	10	10	11		
(La/Sm) _N	4.0	3.7	3.6		
(Yb/Gd) _N	0.59	0.62	0.46		
(Eu/Eu*) _N	0.66	0.57	0.50		
Shaw D.F.	1.63				

*molar ratio

**wt.% ratio

1. QF gneisses, Average of 8.
2. FGG1, Donington Granitoid Suite, Average of 7.
3. hornblende granite, Colbert Granitoid Suite, Average of 4.
4. Moonbi I-types, Average of 10 (Chappell 1978).
5. Bega I-types, Average of 48 (Collins et al. 1982).

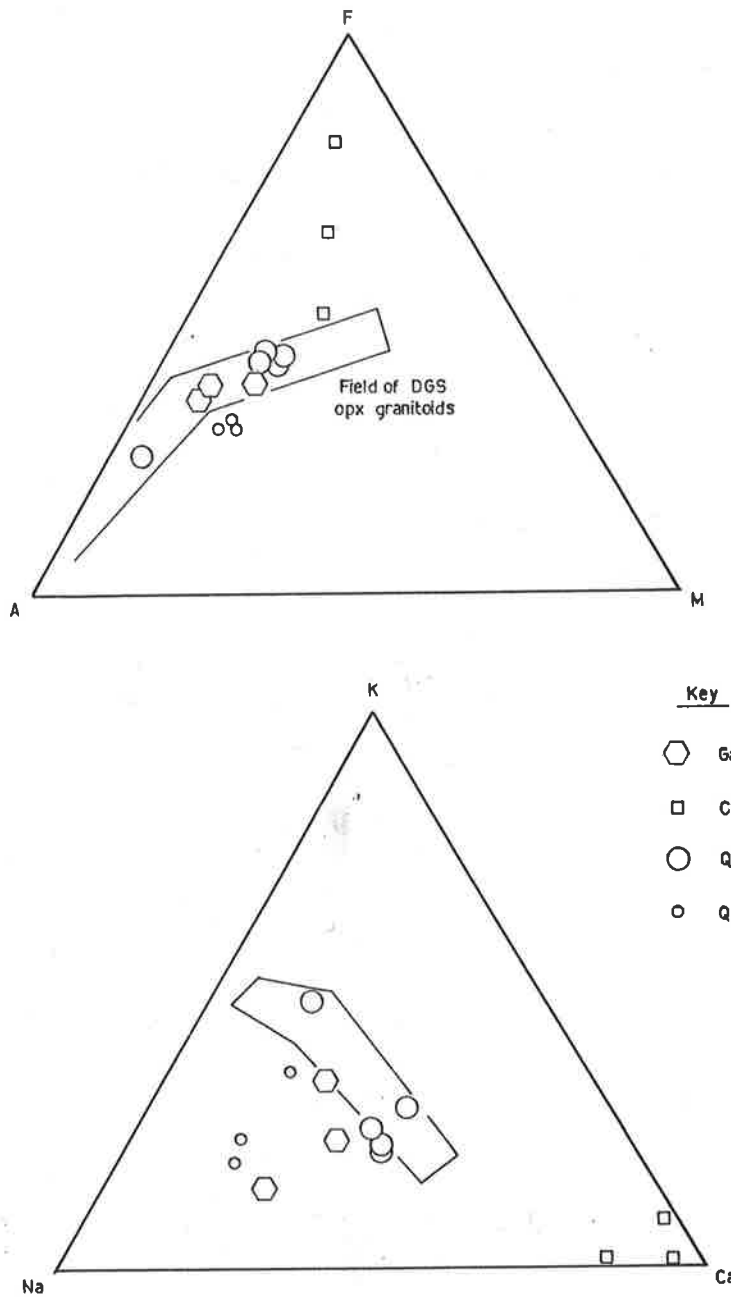


Figure 5-5 AFM and K-Na-Ca diagrams for the Massena Bay Gneisses.

The chief aim of this section is to establish a geochemical comparison with the granitoids of the present study area, to enable integration of geochemical trends with time in a crustal evolutionary model (Chapter 7).

All the major and trace element geochemical data are presented in Appendix Table 5.1. The Massena Bay data are supplemented by a few from the Yorke Peninsula gneisses (Pedler 1976).

5.3.2 Geochemical classification of the gneiss groups

(1) Calc-silicate gneisses

The calc-silicate gneisses contain high Ca contents and generally low contents of K, Na and Mg so that they plot away from the fields of the other gneisses on the AFM and K-Na-Ca diagrams (Fig. 5.5). This probably reflects the low content of detrital feldspar, clays and dolomite in the original sediments, in favour of calcite and quartz. The calc-silicate gneisses will be discussed no further in this chapter.

(2) Garnet + sillimanite gneisses

The garnet + sillimanite gneiss material is finely interlayered with granitic gneiss, so that the three samples analysed do not adequately represent the bulk composition of garnet + sillimanite gneiss. Partly for this reason the garnet + sillimanite gneisses plot near the fields of the QF gneisses and of the DGS on the AFM and K-Na-Ca diagrams. Specimen B74 however is more closely representative of garnet + sillimanite gneiss and its high normative corundum testifies to its aluminous metapelitic composition (Appendix Table 5.1). No further discussion of the garnet + sillimanite gneisses will be included in this chapter.

(3) Quartzofeldspathic hornblende-biotite gneisses

The major element geochemical data for the QF gneisses allows the calculation of the discriminant function (DF) of Shaw (1972). These are positive (Table 5.3) for all samples, strengthening the conclusion drawn above on petrographic grounds that the QF gneisses are probably metavolcanic rocks.

The low normative corundum or the presence of diopside in the norm (Appendix Table 5.1), and the molar $\text{Al}_2\text{O}_3/(\text{Na}_2\text{O} + \text{K}_2\text{O} + \text{CaO})$ values less than 1.1 (Table 5.3) suggest that the metavolcanic QF

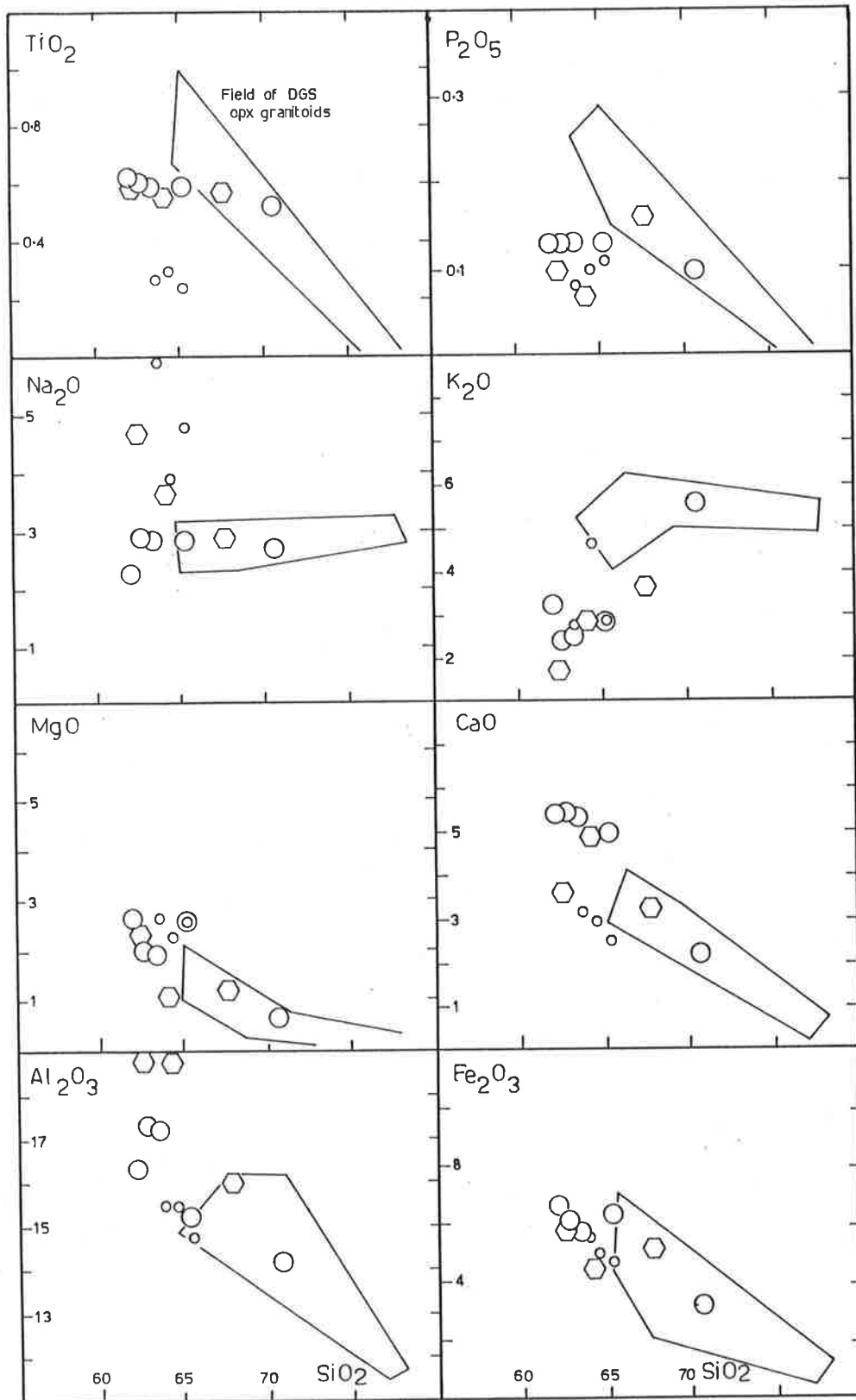


Figure 5.6 Major element variation diagrams for the Massena Bay Gneisses. Symbols as in Figure 5.5.

gneisses are I-type, according to the model of Chappell & White (1974). With respect to all the geochemical indicators tabulated in Table 5.3, the QF gneisses are more closely similar to East Australian orogenic I-type granitoids than the granitoids of the present study.

The QF gneisses define a coherent, sub-linear trend on the AFM diagram (Fig. 5.5) although the Yorke Peninsula (YP) gneisses are displaced slightly away from the Eyre Peninsula (EP) field. The AFM trend is similar to that of the DGS and of calc-alkaline igneous rocks.

The features such as high $\text{Fe}/(\text{Fe} + \text{Mg})$, high K_2O and $\text{K}_2\text{O}/\text{Na}_2\text{O}$, high Zr, Nb and LREE, and low CaO and Ni, transitional towards A-type or anorogenic magmatism and observed in the earlier described granitoids, are not present in the QF gneisses.

5.3.3 Major element geochemistry of the QF gneisses

Much scatter is evident on the K-Na-Ca diagram (Fig. 5.5) which mainly reflects the $\text{K}_2\text{O}/\text{Na}_2\text{O}$ variation within the Yorke Peninsula (YP) samples. The YP rocks analysed, in particular specimen 42, (Appendix Table 5.1), are migmatitic and probably do not closely represent the original bulk rock composition. For this reason the interpretations below place more weight on the Eyre Peninsula (EP) data.

The major element variation diagrams for the QF gneisses (Fig. 5.6) show coherent, sub-linear trends for most elements, which tend to be sub-parallel to the fields of the DGS opx-granitoids. However, in detail some elements are displaced above or below the DGS fields. As a first order conclusion it is suggested that the broadly similar SiO_2 range, the similar levels of major elements $\text{Fe}_2\text{O}_3\text{TOTAL}$, MgO, CaO and Na_2O for Eyre Peninsula samples argue for a broadly similar primary petrogenesis of DGS and QF magma.

However whereas the field, petrographic and mineralogical evidence for the DGS argued in favour of fractional crystallisation within the suite as the major cause of lithological diversity, it is not possible to unambiguously assign the variation in chemical composition within the QF gneisses to fractional crystallisation or partial melting processes. Bearing in mind these uncertainties it is nevertheless suggested that

- (1) the Al_2O_3 decrease with increasing SiO_2 probably reflects either crystal fractionation of plagioclase, or residual plagioclase during partial melting

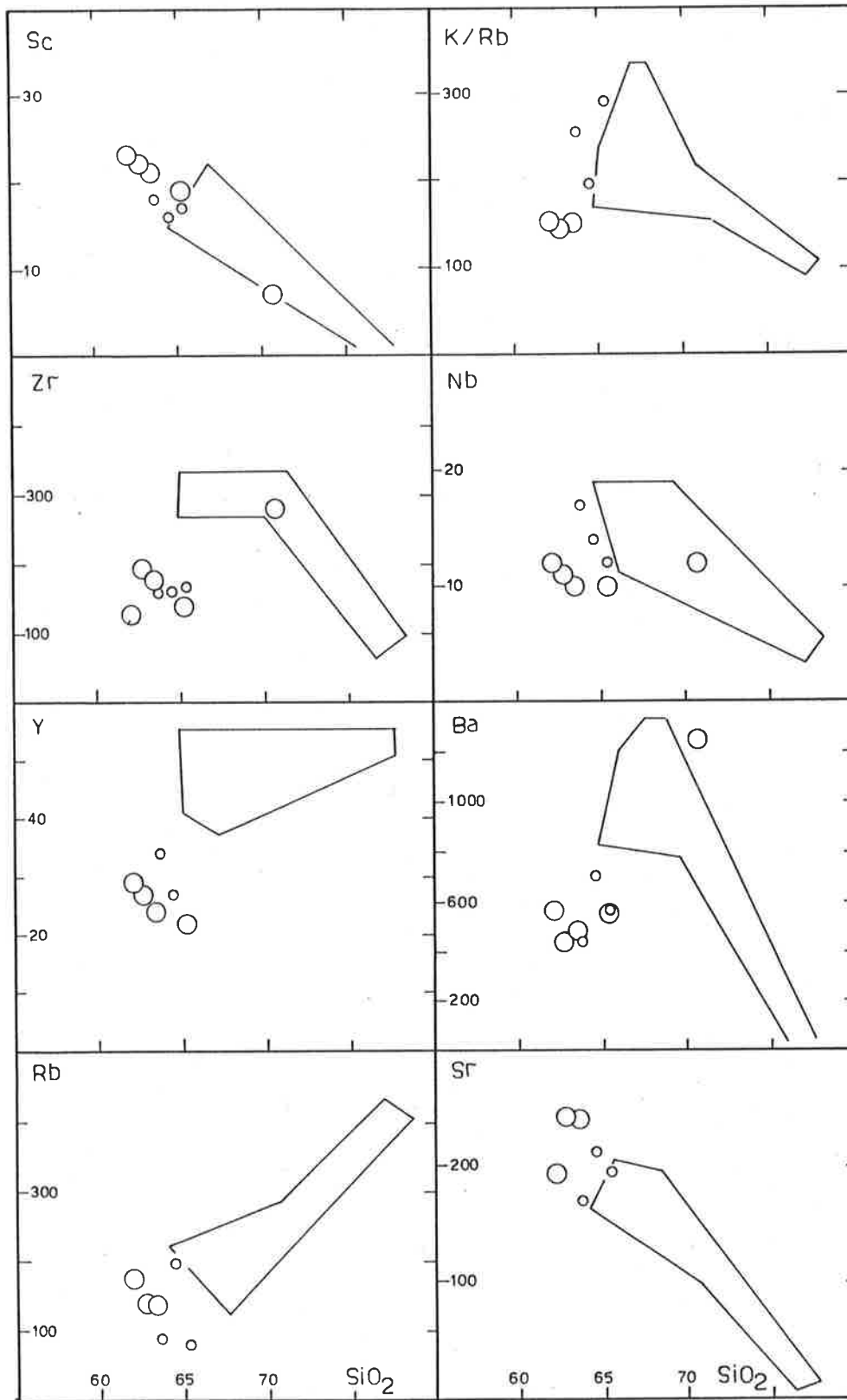


Figure 5-7 Trace element variation diagrams for the Massena Bay Gneisses. Symbols as in Figure 5.5.

- (2) the decrease in MgO, $\text{Fe}_2\text{O}_3^{\text{Total}}$ with increasing SiO_2 probably reflects the crystallisation of minerals such as pyroxene, biotite, magnetite or hornblende or their occurrence in the residue
- (3) the decrease in CaO probably reflects fractionating or residual plagioclase or clinopyroxene
- (4) the increasing K_2O suggests biotite or alkali feldspar are not prominent fractionating or residual minerals
- (5) the approximately constant Na_2O in Eyre Peninsula samples suggests sodic feldspar does not play a prominent role in fractionating or residual minerals
- (6) the approximately constant TiO_2 and P_2O_5 contents of Eyre Peninsula samples suggests that ilmenite, titanomagnetite, or apatite are not prominent fractionating or residual minerals.

Hence the compositional variation within the Eyre Peninsula QF gneisses is attributed to either fractional crystallisation of a combination of relatively calcic plagioclase, pyroxene or hornblende or the presence of these minerals in the residue of partial melting. In this way, the QF gneisses are broadly similar to the I-type granitoid suites of the study area.

Moreover, the broadly similar levels of most major elements in the I-type suites suggest a broadly similar source rock composition and petrogenetic history. This will be developed more in discussion in Chapter 7.

5.3.4 Trace element geochemistry

The trace element data of Appendix Table 5.2 are depicted in Fig. 5.7 where it can be seen that the elements Rb, Sr, Nb, Sc, Ni and K/Rb are similar to the DGS abundances, whereas Y, Ba and Zr are significantly depleted. For most elements the Yorke Peninsula and Eyre Peninsula samples show similar distribution patterns, tending to confirm their relationship.

When the trace element variation within the QF gneisses is considered in conjunction with the major element data,

- (1) the increasing K_2O and Ba (with respect to SiO_2) suggests biotite and K-feldspar are not major crystallisates nor residual minerals.

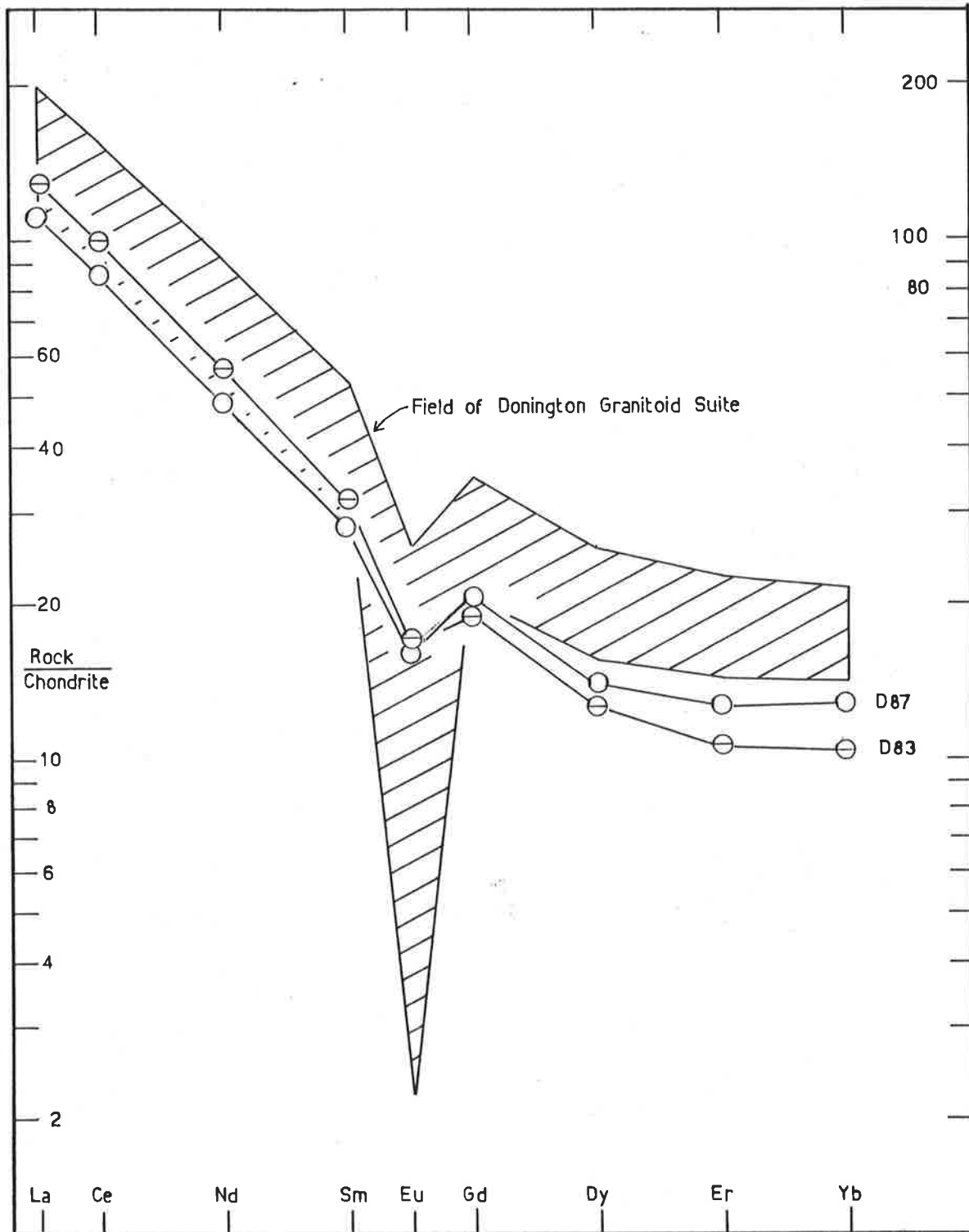


Figure 5.8 Chondrite-normalised REE for two QF gneisses of the Massena Bay Gneisses.

5.3.5 REE geochemistry

To further characterise the QF gneisses and to facilitate comparison with other rock suites, the REE from two samples from Eyre Peninsula were analysed (Appendix Table 5.2; Fig. 5.8).

Both samples have steeply fractionated REE patterns with $(La/Yb)_N$ of 8.5 and 12.5 respectively (Table 5.3). The LREE patterns of both are almost parallel with $(La/Sm)_N$ of 3.0 and 4.0 respectively, but the HREE show a crossover relationship with the higher SiO_2 sample having $(Yb/Gd)_N$ of 0.50, the less siliceous specimen a ratio of 0.68 (Table 5.3). This suggests that the variation of REE within the QF gneisses requires a mineral in the residue of partial melting or crystallising from the melt capable of accepting HREE but not LREE. Clinopyroxene, amphibole and garnet are minerals of this type and each has been ascribed importance in various granitoid petrogeneses (Barker & Arth 1976; Arth & Hanson 1975; Barker et al. 1976).

Both samples have prominent negative Eu anomalies with $(Eu/Eu^*)_N$ ca. 0.7, and which is slightly greater in the less siliceous sample (Table 5.3) suggesting that plagioclase is either a crystallising mineral in the melt or a residual mineral during partial melting.

The QF gneisses occupy similar LREE fields as the DGS opx-granitoids, but the HREE are depleted with respect to the DGS (Fig. 5.8).

5.3.6 Discussion and summary

The brief presentation of major and trace element geochemical characteristics of the MBG has demonstrated the distinction of the metasedimentary gneisses from the metavolcanic QF gneisses.

The QF gneisses have been suggested to be calc-alkaline and I-type, and to have major element and trace element geochemistry broadly similar to the DGS opx-granitoids, other than K_2O , TiO_2 , P_2O_5 , Ba, Y, Zr and HREE which, for comparable SiO_2 contents, are all relatively depleted. This has been suggested to indicate a broadly similar petrogenesis for the QF gneisses and DGS. This point will be re-examined in more detail in Chapter 7.

5.4 RB-SR GEOCHRONOLOGY OF QF GNEISSES

5.4.1 Introduction

A Rb-Sr total rock isotopic study of the QF gneisses was initiated with the following aims,

- (1) to constrain the age of emplacement of the QF gneisses
- (2) to determine the isotopic character of the QF protolith
- (3) to facilitate geochemical comparison with other volcanic and plutonic rock suites of the Gawler orogenic domain
- (4) to place constraints on the timing of regional crustal evolutionary processes.

The QF gneisses were sampled at Massena Bay, within the area of Fig. 5.1. A small area ca. 20m x 5m was chosen, containing near homogeneous QF gneiss and relatively free of discordant post- D_1 pegmatitic veins. However the conclusion of Etheridge et al. (1983) concerning the inevitability of material transport over metres during migmatite formation suggests that considerable caution must be exercised in the interpretation of Rb-Sr isotopic total rock dating studies of these high grade metamorphic rocks.

Various workers, e.g. Lanphere et al. (1964), Pidgeon & Compston (1965), Nunes & Steiger (1974) and Majoribanks & Black (1974), have demonstrated the migration of Sr over distances of at least one metre during high-grade metamorphism. Conversely, Krogh & Davis (1973) have shown that in some circumstances even during high-grade metamorphism, Sr isotopes may not equilibrate over small (cm^3) volumes of rock. However, Roddick & Compston (1977) conclude that interpretation can be facilitated by an analysis of the regional versus local variation in Rb/Sr, and hence $^{87}\text{Sr}/^{86}\text{Sr}$, prior to metamorphism. A pre-metamorphic age may be preserved if regional variations in Rb/Sr (and hence $^{87}\text{Sr}/^{86}\text{Sr}$) exist on a scale larger than the supposed scale of isotopic homogenisation, whereas the metamorphic age could be recorded if the total range of Rb/Sr variation exists on a local scale that is less than the supposed scale of Sr isotopic homogenisation.

Thus assuming migration of Sr-isotopes to be less than a few metres in extent, total-rock sampling of the QF gneisses may be expected to yield a pre-metamorphic age provided

- (1) total-rock samples are dispersed by more than ca. 2 metres
- (2) a wide range in Rb/Sr exists between samples.

An additional complication would be introduced by the emplacement of discordant pegmatite veins if the pegmatite material was derived

Table 5.4: OF gneisses of the Massena Bay Gneisses
Rb-Sr isotopic data.

Sample	Rb ppm	Sr ppm	Rb/Sr	$^{87}\text{Rb}/^{86}\text{Sr}$	$^{*87}\text{Sr}/^{86}\text{Sr}$
<u>Massena Bay</u>					
515-D83	138	241	0.573	1.658	0.75005
515-D85	140	243	0.576	1.673	0.75039
515-D86	141	245	0.576	1.669	0.75079
515-D87	175	193	0.907	2.641	0.77209
515-F20	133	252	0.528	1.537	0.74470
515-F26	142	245	0.580	1.686	0.74734
515-F22	146	240	0.608	1.762	0.75042
515-F24	149	243	0.613	1.783	0.75061
515-F21	149	238	0.626	1.826	0.75138
515-F23	155	168	0.923	2.701	0.76828
<u>**Yorke Peninsula</u>					
76-22	82	194	0.423	1.223	0.73750
76-24	88	179	0.491	1.417	0.74204
76-28	77	136	0.568	1.644	0.75232
76-27	148	183	0.809	2.358	0.76444
76-41	165	157	1.051	3.068	0.78532
76-30A	148	125	1.184	3.451	0.78810
76-29	174	127	1.370	4.003	0.80440
76-44	213	146	1.459	4.269	0.81227
76-35	280	150	1.867	5.467	0.83718

*normalised to E&A $^{87}\text{Sr}/^{86}\text{Sr} = 0.70800$

**data from Pedler (1976).

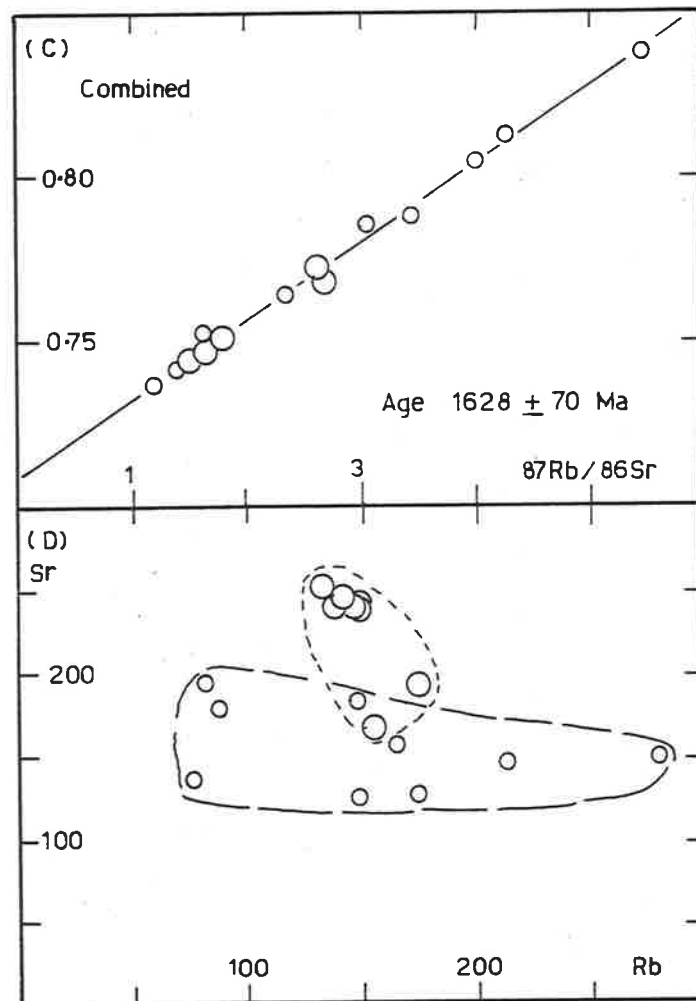
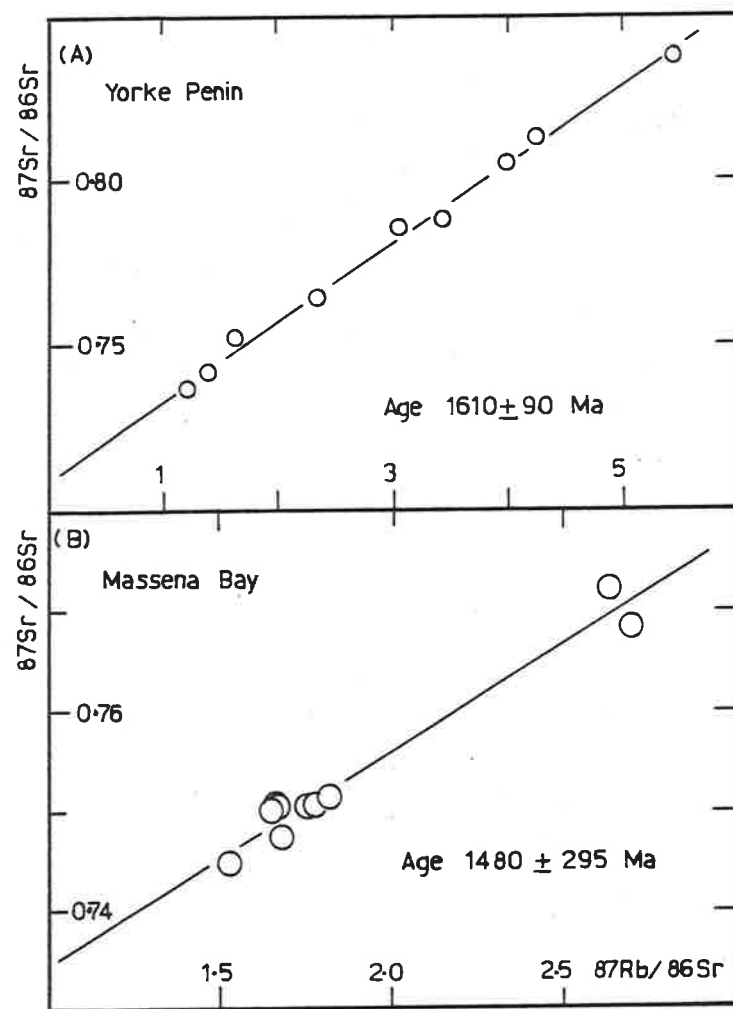


Figure 5.9 Isochron and Rb vs Sr diagrams for the QF gneisses of the Massena Bay Gneisses. Symbols as in Figure 5.5.

from outside of the QF gneisses. The Rb-Sr isotope data may then record a mixing event or events. Most of the QF gneiss samples however fulfil condition (1), and are relatively free of pegmatite veins.

5.4.2 Previous dating of QF gneisses

In his study of the QF gneisses of southern Yorke Peninsula, Pedler (1976) attempted to date them using the Rb-Sr total rock method. He sampled two areas, each ca. 50m x 10m, and separated from one another by ca. 100m. Almost all his samples were separated by at least 2 metres. The analytical data are presented in Table 5.4 and Fig. 5.9.

Regression of all nine samples resulted in a poor fit to the isochron with MSWD = 105 and Model 3 solution age of 1610 ± 90 Ma with IR of 0.7116 ± 40 (regression 1, Table 5.5). Arbitrary rejection of data points and recombination of sub-groups by Pedler resulted in a "pooled best-fit" age of 1636 ± 35 Ma with IR of 0.7091 ± 9 (regression 2, Table 5.5).

Pedler (1976) was unable to decide the significance of this date because it is much younger than the granite gneiss which intrudes the QF gneisses and which gave an isochron age of 1752 ± 66 Ma (regression 3, Table 5.5).

5.4.3 Rb-Sr geochronology of QF gneisses, Massena Bay

5.4.3.1 Results

Four reconnaissance samples of the QF gneisses (labelled D in Table 5.4) were subsequently supplemented by six samples labelled F in Table 5.4). Specimens D83 and D85 were prepared from one block of rock ca. 6kg, but all the others came from separate blocks of rock.

It is apparent that the Rb/Sr ratio between D83 and D85 varies by less than 1% (Table 5.4) suggesting homogeneity of Rb/Sr over the volume of the 6kg block of rock (ca. 2 litres). Moreover the Rb/Sr ratio over the whole Massena Bay suite of QF gneisses ranges between 0.53 and 0.92 with the average (0.65) being nearer to the lower Rb/Sr. This situation is in contrast to the outcrops on Yorke Peninsula sampled by Pedler (1976) where the range of Rb/Sr is much greater, viz from 0.42 to 1.9 (Table 5.4; Fig. 5.9) although the variation is similarly homogeneously distributed.

Table 5.5: QF gneisses of the Massena Bay Gneisses - Rb-Sr isochron regressions.

Regression number	Rock grouping and locality	MSWD*	Model	Age (Ma)	IR
1.	**Yorke Peninsula	105 (3)	3	1610± 90	0.7116± 40
2.	**Yorke Peninsula best-fit, pooled.			1636± 35	0.7091± 9
3.	**Yorke Peninsula granite gneiss.	8.5 (10)	2	1752± 66	0.7114±211
4.	Massena Bay	78 (10)	2	1480±295	0.7134± 70
5.	Massena Bay +Yorke Peninsula	89 (19)	4	1628± 70	0.7101± 30

*number in brackets refers to number of samples regressed.

**from Pedler (1976).

The ten total-rock Massena Bay samples of this study produce a scatter of points on the isochron diagram (Fig. 5.9). Regression of these data produce a Model 2 solution with MSWD of 77, and calculated age of 1480 ± 295 Ma and IR of 0.7134 ± 70 (Regression 4, Table 5.5). This result is indistinguishable from the result for the QF gneisses on Yorke Peninsula.

Combining of the ten Massena Bay data points and the nine Yorke Peninsula points (Fig. 5.9) results in an MSWD of 89 and calculated Model 4 age of 1628 ± 70 Ma and IR of 0.7101 ± 30 (Regression 5, Table 5.5). This result is indistinguishable from the separate locality results, although the indicated age is closer to that of the Yorke Peninsula samples (Regression 1, Table 5.5) due to the higher Rb/Sr ratio of these samples controlling the isochron slope. The Model 4 solution suggests detailed Rb/Sr and IR geochemical differences exist at the two localities.

The indicated ages tend to be much lower than the age of the DGS opx-granitoids (1841 ± 7 Ma) that intrude the QF gneisses. This confirms the conclusion drawn by Pedler (1976) that the Yorke Peninsula QF gneisses give a younger calculated age than the granite gneiss (1752 ± 66 Ma) that intrudes them.

5.4.3.2 Discussion

(1) Significance of dates

Field relations and reliable geochronological data from granitoids intruding the QF gneisses suggest the calculated ages of the latter are spuriously young. This strongly suggests that the isotopic systems within the QF gneisses have been disturbed at some time after initial emplacement. The question remains as to whether the calculated ages, although imprecise, register specific isotopic events or whether the ages are meaningless "mixed" ages.

The combined QF age of 1628 ± 70 Ma is similar to the age of the Middlecamp Granite cited by Rutland et al. (1981) as 1650 ± 35 Ma and believed by them to be syn- D_2 . However, the present author has disputed the dating of D_2 (Chapters 3,4) and suggested that D_3 may have occurred at ca. 1697 ± 12 Ma. It is thought likely that the combined QF age registers D_3 tectonothermal effects, which especially on Yorke Peninsula have been shown to be retrogressive (Pedler 1976).

The thorough-going isotopic homogenisation on the scale of sampling which may be envisaged as necessary to produce this updating

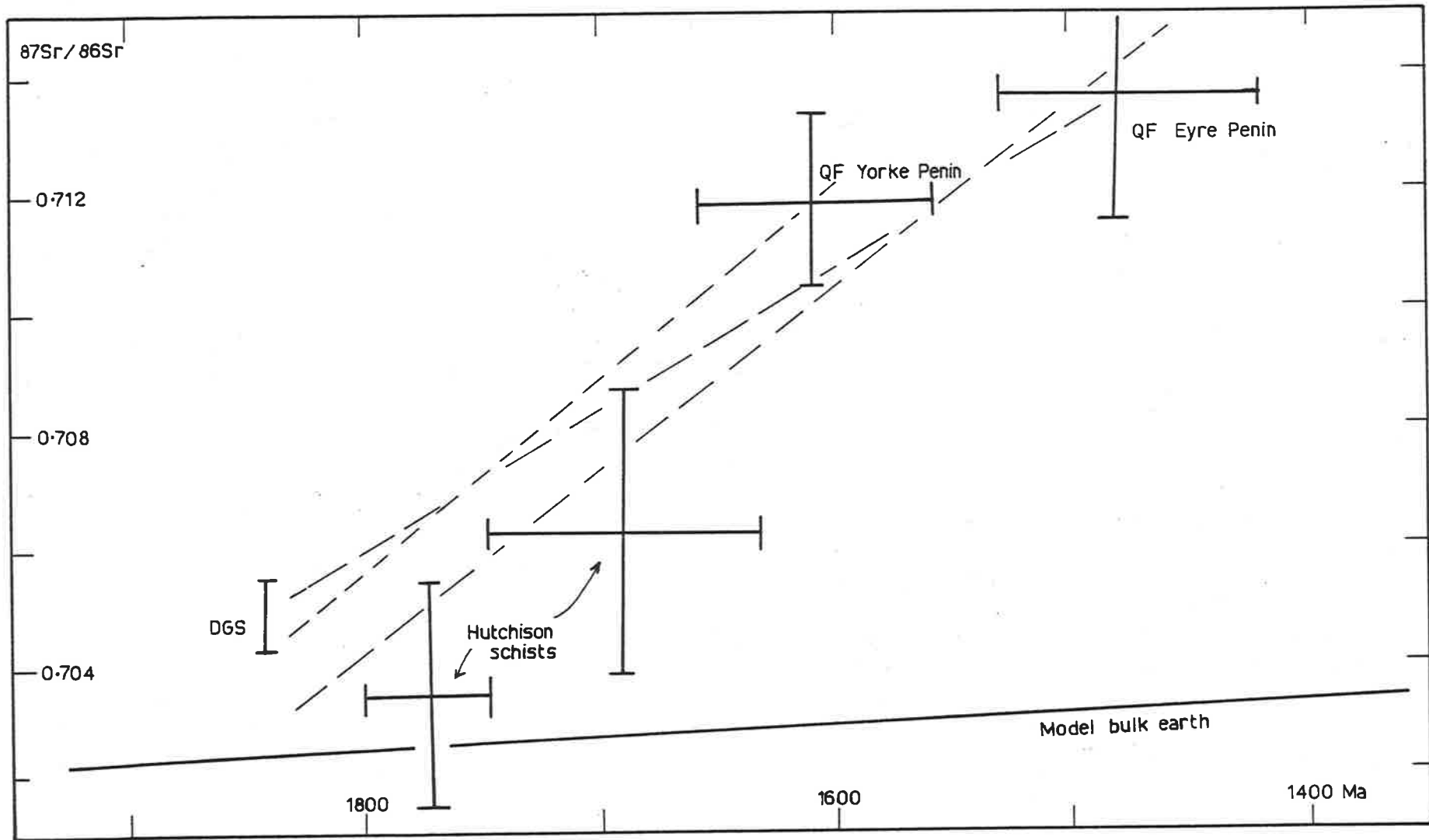


Figure 5.10

Sr-isotope evolution diagram for QF gneisses of the Massena Bay Gneisses compared with other Gawler domain rock units (see text).

may be simulated by the near-resetting of small sub-volumes, each representative of the bulk outcrop variations, which has the net effect of appearing to reset the whole outcrop (Roddick & Compston 1977). Both the Yorke Peninsula and Massena Bay localities have the bulk variation in Rb/Sr, and $^{87}\text{Sr}/^{86}\text{Sr}$ homogeneously distributed over the outcrop, suggesting the sub-volume resetting model of Roddick & Compston may be appropriate.

It is possible also that the isotopic scatter may be a cumulative effect of any or all of the four periods of migmatite and pegmatite generation and emplacement, and of a possible original mixed population of volcanic and sedimentary components, so that the age calculated above may be a meaningless mixed "age".

(2) Sr-isotope evolution

Despite the uncertainty in interpretation of the ages of the QF gneiss isochrons, it is instructive to consider the evolution of Sr-isotopic composition.

It has been suggested above that Sr-isotope migration may be limited to a few metres. If it is assumed, however, that on the larger, ca. 10m^2 , outcrop scale there has been no net loss or gain of Rb, Sr, or ^{87}Sr , it is possible to average the $^{87}\text{Rb}/^{86}\text{Sr}$ and $^{87}\text{Sr}/^{86}\text{Sr}$ at each outcrop and calculate Sr-isotope evolution curves. This has been done (Appendix Table 1.2) and plotted in Fig. 5.10.

Although the Yorke Peninsula gneisses have a higher average Rb/Sr than the Massena Bay samples, the two curves intersect at ca. 1750 Ma at $^{87}\text{Sr}/^{86}\text{Sr}$ ca. 0.705 (Fig. 5.10). The curve for the Yorke Peninsula gneisses is similar to that for the DGS (Fig. 5.10), and given the crudity of the calculations, it is suggested that the DGS and QF gneisses share a similar IR of ca. 0.705 at ca. 1800 Ma.

Furthermore, if the bulk outcrops of the MBG have experienced no net loss of Rb, Sr or ^{87}Sr calculated bulk earth model ages for the two outcrops are closely similar at between 1810 Ma and 1880 Ma. If however, the early retrogressive event proposed for the QF gneisses was similar in geochemical character to that seen in the granite gneisses of the DGS (Chapter 2) a net increase in Rb/Sr may have occurred. This would allow the primary accretion age of the QF gneiss protolith to be significantly older than 1810 Ma - 1880 Ma, more in keeping with its apparent stratigraphic position. Speculation of this nature is difficult to constrain adequately on the basis

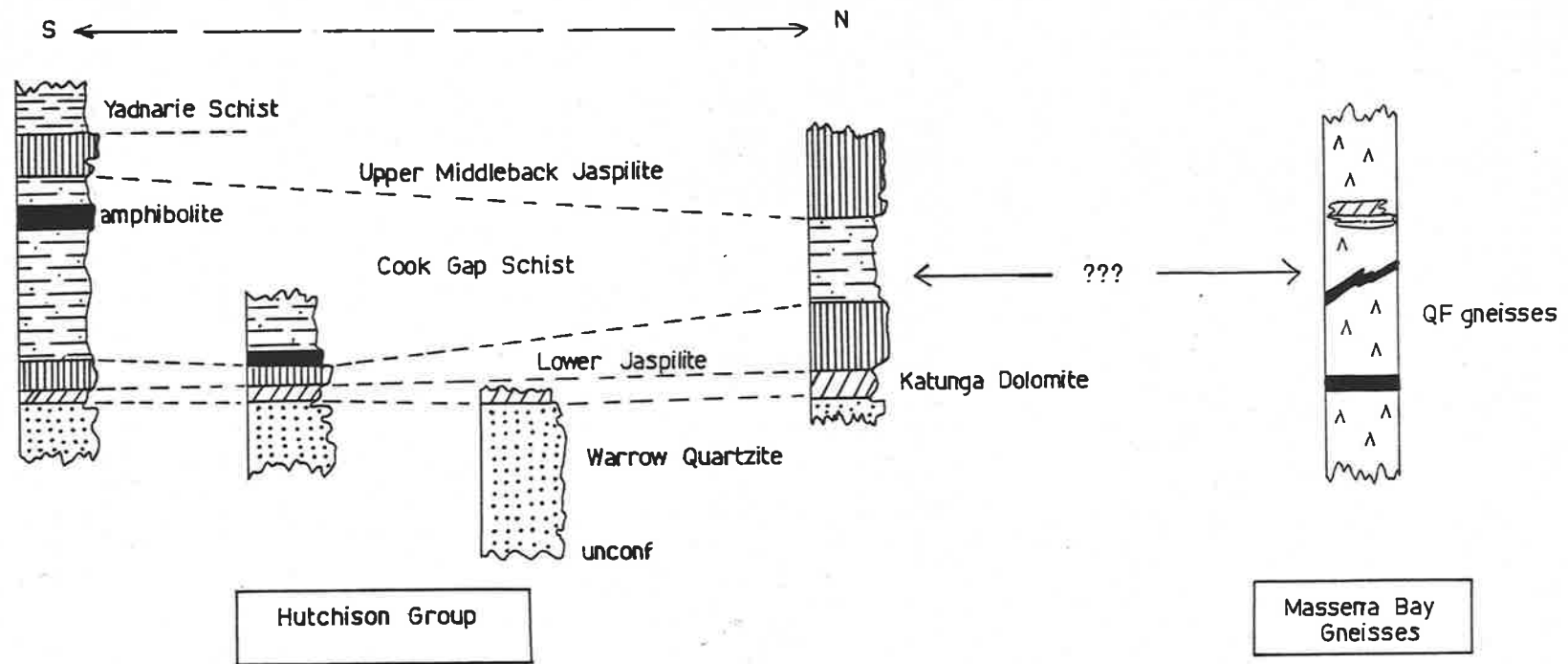


Figure 5.11 Schematic stratigraphic comparison of the Hutchison Group (after Parker & Lemon 1982) and the Massena Bay Gneisses.

of the data presently at hand. Zircon U-Pb dating of the QF gneisses may help to resolve the uncertainty as to their primary accretion age.

The relationship of the QF gneisses to the DGS and to the other I-type granitoids of the Gawler orogenic domain will be discussed further in Chapter 7.

5.4.4 Summary

The main conclusions to be derived from the Sr-isotope systematics of the QF gneisses are,

- (1) on both Yorke Peninsula and Eyre Peninsula the apparent isochron ages of QF gneisses are younger than granites which intrude them
- (2) the Rb-Sr isotope systems have been updated on the scale of sampling, possibly by D_3 retrogressive metamorphism
- (3) reconstruction of Sr-isotope evolution curves suggests that the QF gneiss protolith may be derived from a source similar to that of the DGS.

5.5 COMPARISON WITH THE HUTCHISON GROUP

5.5.1 Stratigraphy

A major conclusion of the previous sections of this chapter is that the MBG represents a layered sequence established prior to the early Kimban emplacement of the DGS at 1841 ± 7 Ma. It is suggested then that the MBG lies in an equivalent stratigraphic position to the Hutchison Group (as most recently defined by Parker & Lemon 1982).

However, the MBG and Hutchison Group are lithologically very dissimilar (Fig. 5.11), although some points in common do exist. For example, the Cook Gap Schist contains early Kimban interlayered amphibolites of probable metabasaltic origin (Parker & Lemon 1982). The composition of the Hutchison Group amphibolites is very similar to the major element composition of the dykes intruding the DGS (see Fig. 5.12; Appendix Table 6.7 data from Parker 1978).

Apart from the amphibolites, the Hutchison Group is believed to consist almost entirely of clastic and chemical metasedimentary rocks (Parker & Lemon 1982) whereas the dominant QF gneiss component of the MBG is thought to be metavolcanic by the present writer.

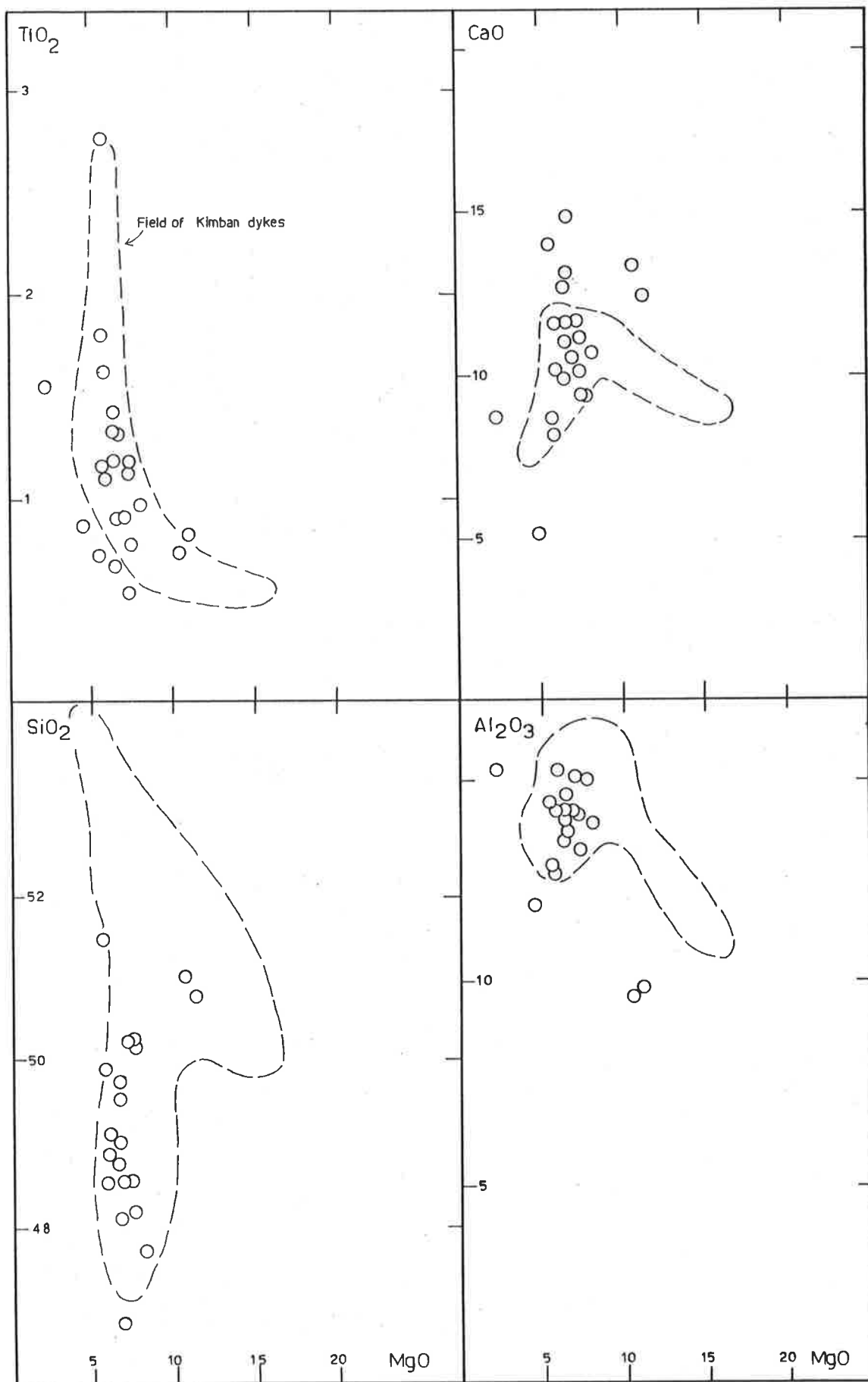


Figure 5-12

Comparison of the major element composition of Hutchison Group amphibolites (after Parker 1978) and Gawler domain Proterozoic metatholeiite dykes.

5.5.2 Metamorphism

The petrography of some metabasaltic "dykes" within the MBG indicates the local attainment of granulite facies conditions. Granulite facies mineral assemblages in the DGS to the south of Cape Donington suggest local metamorphism at temperatures in excess of 800°C and pressure in excess of 8 Kb. The QF gneisses at Massena Bay may have initially crystallised at in excess of 800°C . In contrast Coin's (1976) estimates of maximum metamorphic conditions in the Hutchison are $490^{\circ} - 650^{\circ}\text{C}$ and ca. 3 Kb. If the P-T conditions estimated for the early granulite facies metamorphism in the DGS and MBG are accepted to be similar it is apparent that there is a marked difference in metamorphism between the Hutchison Group and the MBG. Coin (1976) also noted the lithological and metamorphic contrast across the intervening Kalinjala Mylonite Zone.

These features suggest a deeper burial and consequently more pronounced subsequent uplift of the MBG interlayered metavolcanics and metasediments in the Massena Bay area, compared with the Hutchison Group.

5.5.3 Isotopic constraints

Two schist units within the Hutchison Group have been dated by the Rb-Sr method, and the ages and IR's are reported in Parker & Lemon (1982) as 1773 ± 25 Ma, 0.7033 ± 28 and 1688 ± 76 Ma, 0.7061 ± 42 . Parker & Lemon (1982) conclude that these ages date metamorphic events.

These isotopic data are of considerable interest in the light of the contention by Parker & Lemon (1982) that the Hutchison Group basal Warrow Quartzite, later Cook Gap Schist and Yadnarie Schist are clastic sediments derived from Archaean basement to the south and west. No published isotopic data exist for the Warrow Quartzite. Parker & Lemon's (1982) sedimentological and stratigraphical evidence for their model is geologically reasonable. However, Webb (1978) concluded that the low IR's of the schist units (above) preclude an Archaean crustal provenance.

Comparison of the isotopic data for Hutchison Group schist units with that of the QF gneisses (Fig. 5.10) shows that these suites appear to constitute a common Sr-isotope system, with an apparent Rb/Sr ratio ca. 0.8, within which local metamorphic and/or retrogressive events have reset the Rb-Sr total-rock isochrons at different times

in the different localities. Hence it is suggested that the QF gneisses and Hutchison Group schists, as well as being of similar stratigraphic age, may be genetically related.

A possible scenario is that the QF gneisses represent an easterly, contemporaneous volcanic source of detritus for the Hutchison Group which was deposited to the west in a shallow basin constructed on Archaean crust. Only a minimal contribution to the schistose sediments from the older Archaean crust is allowed by the isotopic data.

This model is in contrast to the contention by Parker & Lemon (1982) that the Hutchison Group Schists have a westerly provenance of Archaean age.

The ultimate source of metavolcanic QF gneisses will be discussed more fully in Chapter 7.

5.6 SUMMARY OF CONCLUSIONS

The Massena Bay Gneisses,

- (1) are a unit of mixed metasedimentary and mainly metavolcanic rocks not previously described
- (2) form a pre-Kimban lithostratigraphic unit of similar age to the Hutchison Group
- (3) have experienced the full Kimban tectonothermal history including local granulite facies, and retrogression
- (4) have Rb-Sr total-rock isotopic systems that have been updated by retrogressive metamorphism
- (5) contain quartzofeldspathic, metavolcanic gneisses which show geochemical and isotopic similarities to the DGS
- (6) are possibly the source of much of the detritus which comprises the Hutchison Group clastic sediments.

CHAPTER 6.BASALTIC AND ULTRAMAFIC ROCKS.6.1 INTRODUCTION

The Proterozoic basaltic and subordinate ultramafic rocks to be discussed in detail in this chapter occur as discordant to semi-concordant dykes. These are distinct from the less common, tectonically concordant boudins and blocks of amphibolite and basic granulite, of uncertain age, which are treated only cursorily. Data collected by the present author have been supplemented by the data of Bradley (1972) after close scrutiny of Bradley's samples to distinguish dykes of undoubted Proterozoic age from rocks of uncertain, possibly much older, age.

Previous petrographic investigations on southern Eyre Peninsula have described two groups of basaltic dykes, viz,

- (1) those showing appreciable or complete metamorphic recrystallisation (DK1 of the present author)
- and (2) those showing good preservation of primary igneous texture and mineralogy (DK2 of the present author).

The DK2 dykes may manifest amphibolite facies (Tilley 1921c; Flock 1975; Bradley 1972) or granulite facies (Tilley 1921c; Bradley 1972; Fanning 1975) mineral assemblages. Petrographic studies by the present author support the subdivision of the Proterozoic dykes into these two main groups.

On the basis of palaeomagnetic data Giddings & Embleton (1976) also recognised two main groups of Proterozoic basaltic dykes from the southern Gawler domain, with widely divergent relative magnetic pole positions. Furthermore they cited unpublished Sr-isotopic data which suggest that the two groups of dykes were emplaced at 1700 ± 100 Ma and 1500 ± 200 Ma respectively. It is thought likely by the present author that these two groups correspond to the two petrographic groups above.

In the following sections of this chapter the DK1 and DK2 dykes will be examined in detail, the nature of Kimban metamorphism will be discussed, and the geochemistry and petrogenesis of the basaltic magmas will be investigated.

Table 6.1 Tholeiitic dykes - petrographic modal and textural summary*

Category and examples	Mineralogy	Texture	Comments
<u>DK1 dykes</u>			
1A (B26)	plag + opx + cpx + biot + Fe-Ti oxide	equigranular to inequigranular polygonal	emplaced prior to metamorphic peak px-granulite facies
1B (B32)	plag + opx + cpx + amph + biot + Fe-Ti oxide	equigranular to inequigranular polygonal often foliated	emplaced prior to metamorphic peak hb-granulite facies
1C (A85)	plag + amph + cpx + biot + Qtz + Fe-Ti oxide	equigranular to inequigranular polygonal often foliated	emplaced prior to metamorphic peak amphibolite facies often as boudins
<u>DK2 dykes</u>			
2A (B69)	plag + opx + cpx + ol + biot + Fe-Ti oxide (+ kspar)	sub-ophitic to intergranular	late metamorphic some of cores in px phenocrysts
2B (B16)	plag + opx + cpx + ol + biot + Fe-Ti oxide + gt (+ kspar)	sub-ophitic to intergranular	late metamorphic minor granular recrystallisation some coronal gt
2C	plag + opx + cpx + amph + ol + biot + Fe-Ti oxide	sub-ophitic to intergranular	late metamorphic common granular recrystallisation common conversion of px to amph
2D (B36)	plag + opx + cpx + amph + biot + ol + Fe-Ti oxide + gt	sub-ophitic to intergranular	late metamorphic common patches of recrystallisation extensive conversion of px to amph some coronal gt
2E (B1)	plag + opx + cpx + amph + biot + Fe-Ti oxide	sub-ophitic to intergranular	late metamorphic local contact retrogression plag sericitised extensive conversion of px to amph
2F (D1)	plag + opx + cpx + amph + biot + Fe-Ti oxide	sub-ophitic to intergranular	late metamorphic local alteration in fault zones plag altered and turbid

* refer also to Figure 6.1

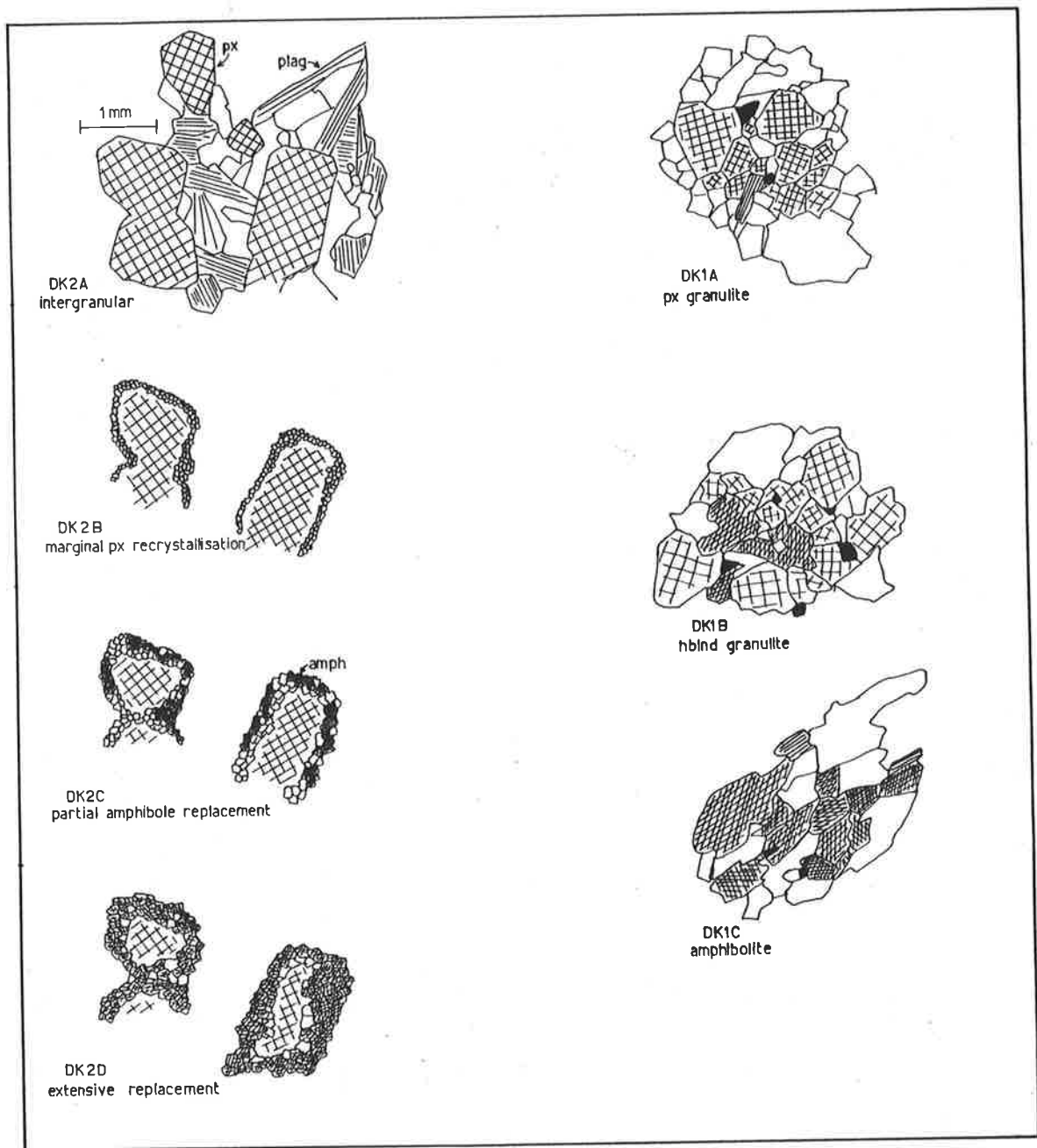


Figure 6.1

Schematic representation of main texture categories of Gawler domain Proterozoic tholeiitic dykes. DK1A, DK1B, DK1C and DK2A were taken from rock specimens. DK2B, DK2C and DK2D are schematic and modified from DK2A.

6.2 PETROGRAPHY AND MINERAL CHEMISTRY

6.2.1 Petrography of DK2 dykes

DK2 dykes outcrop as structurally late, discordant dykes, 0.5 to 1 metre thick. The majority are medium to coarse grained and holocrystalline, although a small proportion show fine-grained, chill characteristics. In general the narrower dykes tend to be finer grained.

Detailed petrographic studies by the present author allow further sub-divisions of this group, based on the degree of metamorphic recrystallisation manifested and the nature of the minerals present (Table 6.1; Fig. 6.1). The main features to emerge may be summarised as follows.

- (1) Olivine is a rare mineral in dyke rocks and is never seen in contact with plagioclase.
- (2) Basaltic dykes contain phenocrysts of opx and cpx, some of which show rare relict cores of olivine.
- (3) Ultramafic rocks are rare, but consist dominantly of cumulate pyroxene, some of which contains rare relict cores of olivine.
- (4) Apatite, Fe-Ti oxide, alkali feldspar, biotite and quartz may occur interstitial to the main minerals.

These observations suggest that the main minerals of the DK2 dykes were crystallised from the magma at considerable depth where the stability field of olivine is decreased in favour of pyroxene, possibly ca. 10 Kbar (Ringwood 1975). Furthermore the apatite, Fe-Ti oxide and biotite crystallised late from the liquid.

- (5) The pyroxene recrystallisation and replacement textures vary widely from unaltered to near complete recrystallisation and replacement.
- (6) Metamorphic minerals in dykes range from pyroxene through green-brown amphibole to blue-green amphibole.
- (7) The Cape Donington to Cape Colbert section shows the full spectrum of metamorphic facies variation in secondary minerals, with dykes of categories 2A, 2B, 2C and 2D (see Table 6.1) often outcropping within a few metres of each other.

These observations suggest that not only was there considerable regional variation in late metamorphic conditions but that the range from pyroxene granulite facies to amphibolite facies was manifested on the outcrop scale. This apparent range in some instances corresponds to the localised narrow zonal effects of the late D_3 deformation (Chapter 1), and in others reflects the regional D_{1-2} retrogressive zonation adjacent to the Kalinjala Mylonite Zone (Chapters 1 and 2). In this way late narrow deformation zones promoted recrystallisation and the recrystallised assemblages reflect the relative degree of hydration of the country rock. The interrelationships of recrystallisation, hydration and deformation is most obvious however in DK1 dykes (see below).

The presence of pristine doleritic and only slightly recrystallised and altered metabasaltic dyke rocks allows the possibility of preservation of primary igneous geochemical composition (see later).

- (8) Chilled, fine-grained dykes such as B58 and B52 allow the possibility of preservation of original liquid compositions.
- (9) Subordinate category 2E was erected for dykes from McLaren Point where local specialised lower grade contact retrogressive metamorphism associated with late granitoid intrusion is manifested by blue-green amphibole development, often overprinting earlier textures (e.g. D123 of Category 2D). This feature has been described also in granitoids of the DGS at this locality (Chapter 2).
- (10) At North Shields on the frontal scarp of the Lincoln Uplands (Fig. 1.2) probable late uplift related to faulting has resulted in localised alteration of plagioclase and pyroxene and the erection of subordinate category 2F.
- (11) The Boston Point and Spalding Cove localities have country rock and dykes tending not to manifest hydrated secondary mineral assemblages.

These observations illustrate the local and regional metamorphic facies variations referred to above.

- (12) Two distinct primary mineralogical types can be recognised within DK2 dykes,
- (a) dykes containing minor interstitial Fe-Ti oxide (and apatite)
- and (b) dykes containing pyroxene phenocrysts exsolving abundant Fe-Ti oxide (and abundant interstitial apatite).

These mineralogical differences are reflected in the bulk rock geochemistry of the dykes (see later), and the phenocrysts with exsolved Fe-Ti oxide in the latter group suggest the high-TiO₂ in these rocks is not due to cumulate ilmenite.

- (13) One specimen (B36, Table 6.1) from Spalding Cove exhibits some recrystallised aggregates, in place of the dominant primary cpx phenocrysts, which assume two distinct mineral assemblages, viz,
- (a) garnet + opx + cpx (+ biotite + ilmenite)
- and (b) amphibole + opx + cpx (+ biotite + ilmenite).

The textural relationships suggest that some of the garnet formed as early coronas around the cpx, and was subsequently incorporated in garnet + opx + cpx polygonal equigranular aggregates as opx was exsolved from the relict cpx phenocrysts during recrystallisation. Some of the garnet contains vermicular pyroxene. The pargasitic amphibole occurs to the exclusion of garnet in some patches, but no clear corona textures are present, the opx + cpx + amphibole forming polygonal equigranular aggregates. One other specimen north of Carcase Rock (Fig. 1.2) shows similar, less well developed textures.

Similar garnet textures were observed by Tilley (1921c) in metabasaltic dykes on Boston Island (Fig. 1.2).

Also in specimen B36 is rare olivine, which shows coronas of cpx in contact with plagioclase. The dominant ferromagnesian phenocryst phase however is cpx. No free quartz is present in the rock.

These textures are interpreted to suggest early recrystallisation from the melt of cpx and plagioclase and some olivine phenocrysts which on consolidation and cooling to the prevailing geotherm formed the coronas described above (cf. Griffin & Heier 1973). Cooling apparently took place under garnet granulite conditions.

6.2.2 Petrography of DK1 dykes

DK1 dykes outcrop mainly as dykes but also as more equivocal boudins or blocks in the granitoid gneiss country rocks. All have been recrystallised during early Kimban metamorphism, some show fold structures, and most of the amphibole bearing dykes show tectonite fabrics.

Other features to emerge from the detailed petrographic studies are as follows, (Table 6.1; Fig. 6.1).

- (1) No olivine is present in the metamorphic mineral assemblages but rather opx + cpx + plag, suggesting intermediate pressure of metamorphism ca. 10 Kbar (Green & Ringwood 1967a; Ringwood 1975).
- (2) A geographical distribution of metamorphic facies variation is evident in DK1 rocks, px-granulite facies being dominant at Spalding Cove and Boston point, whereas Kirton Point and Massena Bay manifest mainly amphibolite facies, although rare hornblende granulites and pyroxene granulites do outcrop at the latter two localities. Similar variations are present in the host rocks. Evidence has been presented in Chapter 1 and Chapter 2 that local retrogression of the host DGS occurred in a zone ca. 5 km wide adjacent to the Kalinjala Mylonite Zone, prior to or during D_1 , by influx of fluids along the mylonite zone. Regionally, the granulite and amphibolite facies gneisses otherwise crystallised during D_{1-2} at similar pressure and temperature conditions. The deformation along the mylonite zone is thought both to be crucial to the passage of fluids and to be aided by the hydraulic fracturing associated with them (cf. Etheridge et al. 1983).
- (3) Some amphibolites at Kirton Point are veined by the granitoid country rocks, which led Flook (1975) to propose that the granitoids intruded the amphibolite. However Cooper et al. (1976) proposed that intrusion of amphibolite precursor into granitoid caused partial melting of granitoid at some contacts and back-veining into the amphibolite. Parker et al.

(1981) suggested that at least some of the amphibolites pre-date granitoid intrusion. No firm conclusions as to the primary age of the amphibolites were stated.

The present author notes that the presence of scarce meta-basaltic xenoliths in the DGS granitoids (Chapter 2) suggests that some of the amphibolites may predate the granitoids. However, field relationships show that most of the amphibolites are pre-metamorphic dyke intrusions.

- (4) There are DK1 dykes containing abundant Fe-Ti oxide as well as dykes containing minor Fe-Ti oxide, demonstrating that neither of these mineralogical (geochemical) types is unique to either early or late Kimban basaltic magmatism. The dykes containing abundant Fe-Ti oxide are however, volumetrically subordinate.

6.2.3 Mineral Chemistry

In order to delineate the metamorphic conditions of recrystallisation of the subsolidus assemblages and to constrain the original magmatic conditions, a number of specimens from each of the two groups of dykes were analysed by electron microprobe. All the analytical data are tabulated in Appendix Table 6.1 and a summary of calculations based on various geothermometers and geobarometers is presented in Table 6.2.

6.2.3.1 Mineral chemistry of DK2 dykes

- (1) Specimen B69 - category 2A

This metadolerite contains opx and cpx phenocrysts with moderate exsolution and so the analysed compositions most probably reflect sub-solidus conditions. Analysis of opx phenocrysts shows that exsolution is not complete and considerable Ca is present but the recrystallised granular opx has much lower Ca (Appendix Table 6.1). The calculated pyroxene temperatures for this specimen are ca. 868° - 898°C (Table 6.2).

- (2) Specimen B36 - category 2D

The textures and mineral assemblages in this specimen (see above) allow the calculation of a temperature and pressure of equilibration of the garnet + opx + cpx aggregates. The temperature

Table 6.2 Metabasaltic dyke rocks, calculated pressure and temperature of equilibration of coexisting phases

Method and Source	Specimen	T°C	P Kbar	Comments
Opx+Cpx Wood and Banno (1973)	B69	879-898		Recrystallised polygonal pyroxene or exsolved relict phenocryst No garnet present
	A113	858		
	B26	890		
	B32	826		
	B36	870		
		830-882		Bradley (1972), mineral separates
	B36	1032-1038		Recrystallised polygonal pyroxene with garnet
Opx+Cpx Wells (1977)	B69	868-889		As above
	A113	910		
	B26	959		
	B32	879		
	B36	915		
		960-885		Bradley (1972), mineral separates
	B36	1160-1186		As above
Plag + Kspar Powell & Powell (1977)	B69	618	(8)	B69 averaged zoned plagioclase phenocrysts
	A113	526	(8)	
	B32	523	(8)	
Mag + Ilm Powell & Powell (1977)	B36	446-569		- log a _{O2} 20.2 - 27.7
Opx+Gt Harley & Green (1982)	B36	(1038)	20.8	low mole fraction of Al in opx = 0.0325
		(870)	15.5	
Cpx+Plag+Qtz Ellis (1980)	A113	(858)	7.2	
	B32	(826)	4.4	
	B26	(890)	8.3	

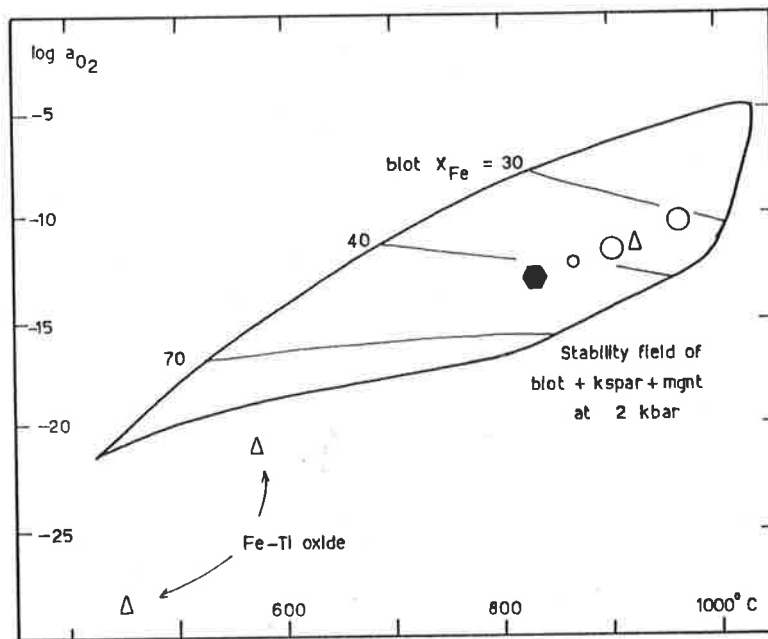
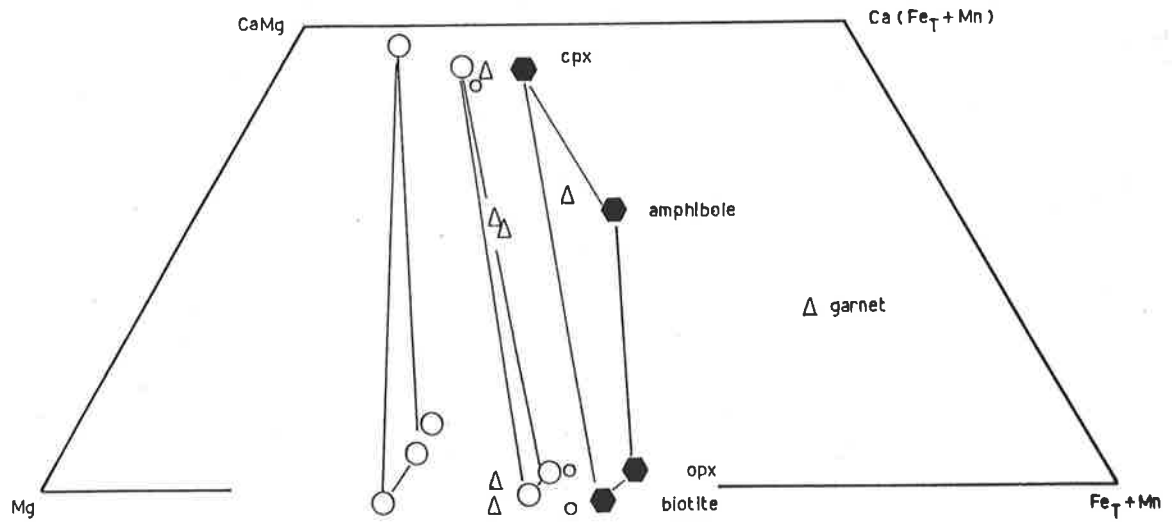


Figure 6.2

Upper: Ferromagnesian mineral compositions
 Lower: Fe-Ti oxide T-log aO₂ and biotite
 compositional data compared with
 the data of Wones & Eugster (1976).

Key

- Group A dolerite
- " px granulite
- △ Group B dolerite
- B32 hblnd granulite

calculated by two different geothermometers are ca. 1035°C and ca. 1170°C (Table 6.2). The calculated pressure is ca. 20 Kb (Table 6.2), but this calculation is less reliable at low mole fractions of Al in opx (Harley & Green 1982) so that this pressure estimate is not well constrained.

In this same specimen the coexisting exsolved aggregates of magnetite and ilmenite allow the calculation of a temperature of equilibration of 446°C - 569°C at oxygen fugacities of $-\log a_{O_2} = 20.2 - 27.7$. These conditions are similar to those deduced for subsolidus recrystallisation of the plutonic granitoids of this study (Fig. 6.2) and suggest that the opaque oxides were open to subsolidus equilibration to lower temperatures than the silicate minerals.

(3) Specimen A113 - category 2C

This specimen has much relict igneous petrographic character, but also many areas of extensively recrystallised (and equilibrated?) aggregates of opx + cpx + plag + Kspar + quartz. These aggregates allow the calculation of pressure and temperature of equilibration. The coexisting pyroxenes and coexisting feldspars geothermometers produce calculated temperatures of ca. 858°C - 910°C and ca. 526°C respectively, and the cpx + plag + quartz geobarometer produces a calculated pressure of 7.2 Kbar (Table 6.2).

The pyroxene temperatures are very similar to the calculated temperatures for B69, but the feldspar temperature is significantly lower. This suggests that the feldspar solvus allows equilibration to lower temperature than the pyroxenes.

The calculated pressure is much lower than that calculated for the opx + garnet assemblages but probably is to be preferred in view of the uncertainty of the latter calculation. Moreover the equilibration of plagioclase at lower than the metamorphic peak temperature suggests the lower calculated pressure may also represent post-peak conditions.

6.2.3.2 Mineral chemistry of DK1 dykes

(1) Specimen B26 - category 1A

This pyroxene granulite has a well-developed, apparently equilibrium polygonal equigranular metamorphic texture and the opx and cpx compositions are typical of granulite facies metamorphic

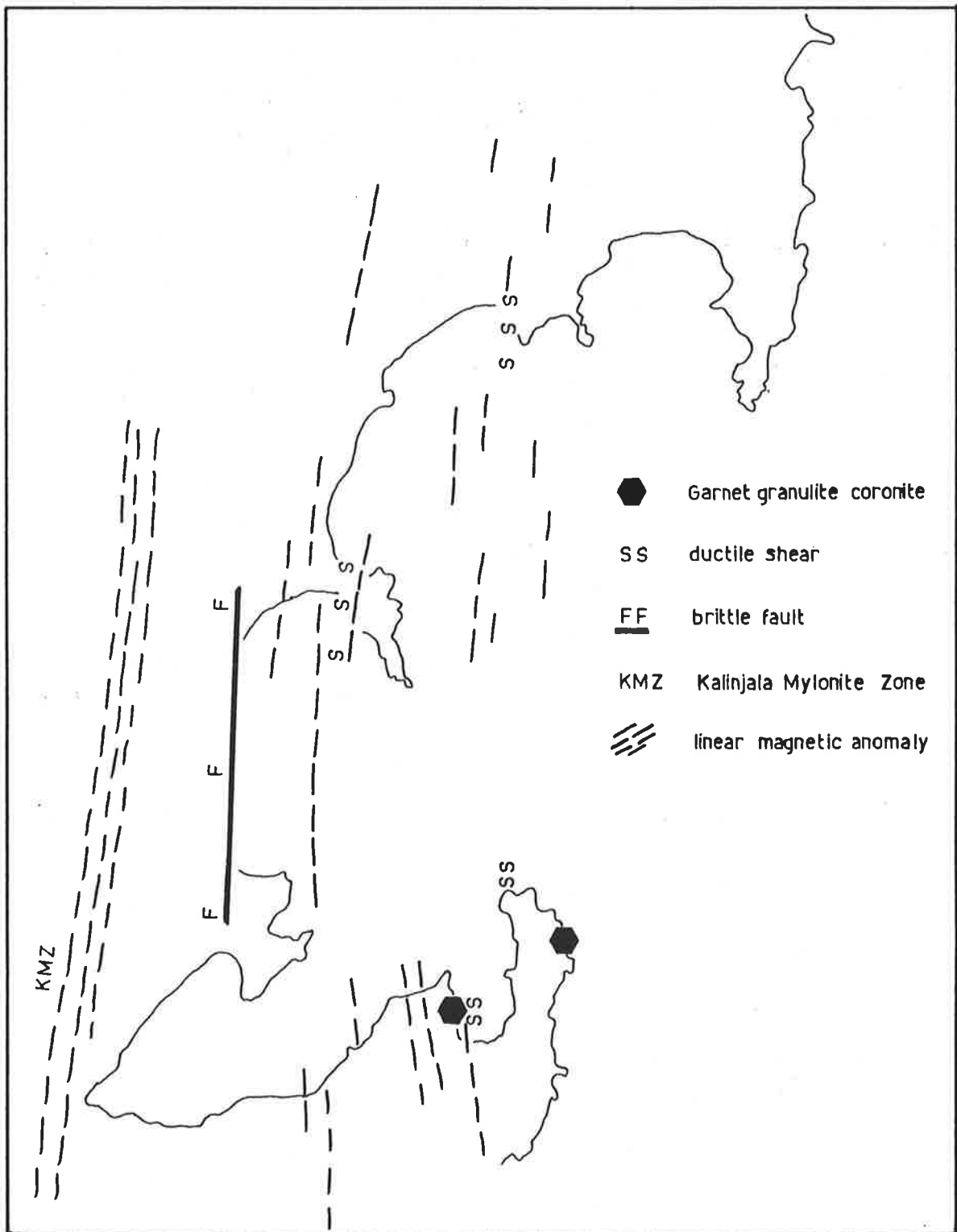


Figure 6.3 Garnet granulite coronite localities, known ductile shear zones and brittle faults in relation to linear magnetic anomalies in the present study area.

rocks (e.g. Weaver et al. 1978; Fig. 6.2). The calculated pyroxene temperature of ca. 890° - 959° C (Table 6.2), is similar to that of the other specimens. Furthermore the calculated pressure from the cpx + plag + quartz assemblages is ca. 8.3 Kbar (Table 6.2) which is similar to that for specimen A113 (and for the DGS; Chapter 2).

(2) Specimen B32 - category 1B

This hornblende granulite is similar to B26 with the addition of amphibole to the mineral assemblage. The calculated pyroxene temperature of ca. 826° - 879° C (Table 6.2) is in accord with the other specimens. However its cpx + plag + quartz pressure of ca. 4.4 Kbar (Table 6.2) and the calculated temperature of equilibration of the feldspars at ca. 523° C (Table 6.2) are low, similar to specimen A113, and probably reflect plagioclase equilibration to post-metamorphic peak conditions.

(3) Bradley (1972) separated bulk pyroxene fractions from pyroxene and hornblende granulites and analysed them by XRF techniques. Coexisting pyroxene temperatures calculated by the present author from Bradley's data are 830° - 882° C (Table 6.2) and are consistent with the microprobe data calculations.

6.2.4 Constraints on Kimban metamorphism

The majority of metabasaltic dyke rocks examined in this study show evidence of having been emplaced and variably recrystallised in the intermediate pressure pyroxene granulite or hornblende granulite facies of metamorphism (Green & Ringwood 1967a). Adjacent to the Kalinjala Mylonite Zone however amphibolite facies assemblages are common, some of which may be retrogressed granulites and may coexist with subordinate relict granulites. Elsewhere garnet granulite corona textures are present in a few localities west of Kalinjala at Spalding Cove, Boston Island and north of Carcase Rock (Fig. 6.3; Fig. 1.2).

These observations suggest that a widespread granulite facies metamorphism occurred, with coexisting apparently retrograde amphibolite facies conditions adjacent to the Kalinjala, and local preserved relics of garnet granulite facies. The zonation of facies is parallel to the major Kalinjala zone and subsidiary

parallel zones, and parallel to the major linear magnetic anomalies of the area some of which correspond to known faults or shear zones (Fig 6.3); this suggests that in particular the local garnet granulite assemblages may have been exposed as a result of differential uplift along parallel shear zones or faults coincident with the magnetic anomalies. The garnet corona textures originally may have resulted from essentially isobaric cooling to the prevailing geotherm, after igneous crystallisation and prior to uplift (Griffin & Heier 1973).

The mineral chemical calculations suggest that the dykes may have equilibrated at ca. 830° - 960° C at pressures ca. 7.2 - 8.3 Kbar with some lower grade adjustment at ca. 4-5 Kbar. The garnet granulites may initially have equilibrated at a minimum of ca. 1030 C and at pressure well in excess of 8 Kbar, but very probably not as high as the figure of 20.8 Kbar which was calculated using the unreliable, low-Al pyroxene system. These metamorphic conditions are precisely those expected when large amounts of hot mafic magma are intruded into the lower crust (underplated), disturbing and elevating the local geotherm, and subsequently cooling to the prevailing steady-state geotherm (e.g. Wells 1980).

6.3 GEOCHEMISTRY

6.3.1 Sampling and alteration

It is well known that during hydrothermal alteration and metamorphism of basaltic volcanic rocks significant chemical redistribution, so as to mask the primary igneous geochemical character, may occur (e.g. Frey et al. 1974; Wood et al. 1979; Sun & Nesbitt 1978a). The volcanic terrains investigated by these authors are not directly comparable to the deep crustal environment of the basaltic dykes of the present study.

Elliott (1973) and Field & Elliott (1974) showed that the transition from dolerite dyke to amphibolite may not be isochemical. In particular they suggested K_2O , P_2O_5 , Fe_2O_3 , Rb and maybe Zr may be increased, whereas CaO and FeO may be decreased. They also suggested TiO_2 , total Fe, MgO, MnO, Na_2O , Al_2O_3 , Sr and Ba are probably static, although some scatter may be induced. Weaver & Tarney (1981c) illustrated similar chemical changes associated with amphibolisation of dolerite dykes.

However Green et al. (1972) demonstrated that the REE are relatively immobile during prograde metamorphism. Bradley (1972)

in his study of southern Eyre Peninsula basaltic dykes, demonstrated that retrogressive rehydration of pyroxene granulites to amphibole-rich assemblages resulted in marked disturbance of elements such as K, Rb and Ba, whereas the geochemistry of mafic granulites and little metamorphosed dolerites is apparently undisturbed and reflects the primary igneous character. Bradley further suggested that the average K_2O content of unaltered Gawler domain basaltic dyke rocks is ca. 0.6%, and that rocks with greater than 1.5% K_2O are altered.

To minimise the effects of these complications the present author has preferred to examine in detail only essentially unaltered dolerites and pyroxene granulites. Data from slightly altered metadolerites, hornblende granulites and a few amphibolites are included for comparison.

Suites of basaltic dyke rocks were selected from the DK1 and DK2 groups described above. Care was taken to include both Fe-Ti oxide-poor and Fe-Ti oxide-rich specimens. These were supplemented by samples analysed by Bradley (1972) and Pedler (1976) which could be demonstrated to be of DK1 or DK2 type.

6.3.2 Basaltic geochemical groups and approach to their interpretation

6.3.2.1 Introduction

Bradley (1972) showed that the basaltic dyke rocks of Southern Eyre Peninsula are of continental tholeiitic character and are divisible into two main types,

- (1) abundant tholeiitic basalts
- (2) less abundant picritic tholeiites or "pyroxenites".

Furthermore he suggested, on the basis of the pioneering experimental petrological studies of Hawaiian olivine tholeiite (Green & Ringwood 1967b), that it is possible to model some of the pyroxenites as crystal-enriched liquids from an olivine tholeiite parental liquid, whereas others could not be so modelled and hence more likely represent picritic tholeiitic liquid compositions.

The knowledge of phase and melting relations in the basaltic system has increased greatly of recent years, as has the sophistication of major and trace element geochemical interpretation, so that a more detailed interpretation of the Eyre Peninsula basaltic dyke rocks is now possible.

(1) The model pyrolite source of basaltic magmas (see discussion by Ringwood 1975; Frey et al. 1978) is now well established, despite dissent by O'Hara (e.g. 1968); volumes of experimental melting results at various P, T and p_{H_2O} conditions are available in support (see e.g. Green 1973; Jaques & Green 1980; Ringwood 1975; and references in these). It is clear that tholeiitic magmas result from relatively high degrees of partial melting of model pyrolite, leaving residual mineral assemblages dominated by olivine and orthopyroxene, with lesser amounts of other minerals such as clinopyroxene and garnet possibly present. The presence or absence of these minerals is controlled by factors such as the P-T at the site of melting, the extent of melting, and the nature and amount of fluids such as H_2O and CO_2 in the source rock. The detailed major element compositions of basaltic melts will sensitively reflect the interplay of these factors.

(2) Similarly the content in the melt of compatible trace elements such as Ni, Cr, Sc and V will be dependent on these factors.

(3) For the incompatible trace elements it has been proposed that the upper mantle pyrolite source has relative abundance ratios similar to chondritic meteorites and absolute abundance levels ca. 2x chondritic (see discussion in Ringwood 1975). This model has been substantially confirmed for high degree partial melts such as Archaean komatiites and some tholeiites (e.g. Nesbitt & Sun 1976). However, it has been shown by many studies that incompatible trace element distributions in the upper mantle peridotite sources of basaltic magmas are globally, and even often locally, heterogeneous (e.g. in MORB, Sun et al. 1979; Wood et al. 1979; in tholeiites of continental areas, Frey et al. 1978; Sheraton & Black 1981; Weaver & Tarney 1981b). It is not possible to explain these apparent heterogeneities solely on the basis of residual mineralogy at the site of melt production, but a two-stage history is often invoked, involving either an early melt extraction and consequent depletion or an early enrichment in a component which is itself enriched in incompatible elements (component B of Frey & Green 1974). The incompatible trace element content of primary mantle liquids should be a faithful indicator of the trace element character of the upper mantle peridotite source.

(4) Crystal fractionation, or accumulation during ascent, may considerably modify the major and trace element compositions of a basalt, so that meaningful conclusions as to the physical and chemical conditions at the site of melting can only be drawn if essentially unmodified mantle liquids are studied. It is possible to discern liquid compositions on the basis of petrographic criteria such as chill textures. In addition a primary mantle liquid can be identified on the basis of geochemical criteria such as high $Mg/(Mg + Fe)$, and high content of compatible trace elements such as Ni, Cr and Sc (Frey et al. 1978).

(5) Combining these interpretational steps it is ideally possible to allocate tholeiitic liquids to a P, T, pH_2O petrogenetic grid for a given locality and hence to formulate models of upper mantle geothermal and geochemical evolution.

Adopting this approach it is possible to refine the petrogenetic interpretations of Bradley (1972). The addition of data from certain key samples collected by the present author has greatly facilitated this refinement.

6.3.2.2 Definition of basaltic geochemical groups A, B and C

Because regularities in the partitioning of major and trace elements between melt and residual mineral phases impress specific characteristics on the derivative melts, and because the basaltic rocks of this study exhibit a wide diversity of compositions particularly with regard to trace elements, it is possible to distinguish a number of different geochemical groups and to interpret these in terms of specific petrogenetic processes.

On the basis of the less mobile elements Ti, Zr and Y (Pearce & Cann 1973) it is possible to define three separate geochemical groups within the Proterozoic metadolerites and mafic granulites of the present study (Appendix Tables 6.3, 6.4 and 6.5) viz

Group A	Ti/Zr	av. 50	Zr/Y	av. 4.5
Group B		83		3.8
Group C		98		2.7

The detailed interpretation of these differences is given below; it suffices here to draw attention to these three groups.

It is worthy of note that DK1 and DK2 dykes occur in each of these three groups, suggesting that they do not represent unique

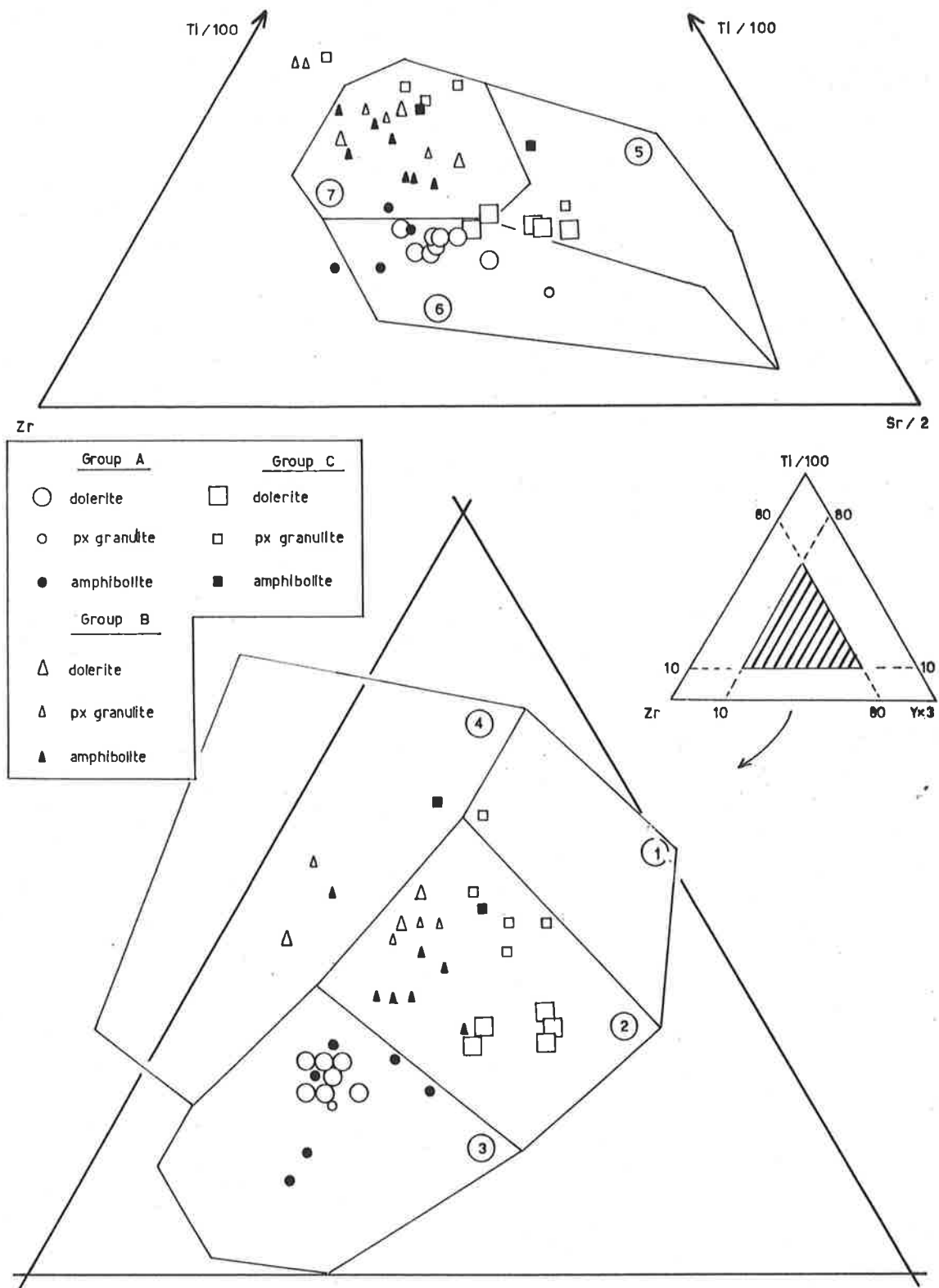


Figure 6.4

Ti-Zr-Y and Ti-Zr-Sr plots of tholeiitic dykes of the present study. Outlined fields are after Pearce & Cann (1973) and refer to modern volcanics of known geotectonic settings.

- (1) = low K tholeiite
- (2) = ocean floor basalt
- (3) = calc-alkali basalt
- (4) = within plate basalt
- (5) = (1)
- (6) = (3)
- (7) = (2)

stages in development of the Kimban orogenic cycle. In addition both Group A and Group C contain Bradley's picrites as well as the more common tholeiites.

Pearce & Cann (1973) used triangular plots involving Ti, Zr and Y in an attempt to delineate the fields appropriate to basalts of different modern geotectonic regimes. On their criteria only a few of the Group B and C specimens plot in the field of within-plate basalts (Fig. 6.4). Most plot in the fields of island arc calc-alkaline or low-K tholeiites or ocean-floor tholeiites. These differences will be discussed further below.

6.3.3 Geochemistry of Group A basaltic rocks

6.3.3.1 Primary liquids

The tholeiites and picritic tholeiites of Group A display a wide range in chemical composition, from olivine-normative to quartz-normative types (Appendix Tables 6.2, 6.3). Samples B58, B60 and B69 have Mg numbers in or close to the range 68-72 (Appendix Table 6.2) appropriate for liquids which have equilibrated with upper mantle olivine (Roeder & Emslie 1970; Frey et al. 1978). They also have high compatible trace element contents (Ni = 289 - 526 ppm; Cr = 1119 - 2401 ppm; Sc = 31 - 37 ppm; Appendix Table 6.3). This strongly suggests that they were derived from upper mantle peridotite with little or no subsequent modification (Frey et al. 1978). In addition, B58 exhibits good petrographic evidence for its likely origin as a chilled liquid (Section 6.2) so that it almost certainly represents a primary liquid. However B60 and B69 are coarse-grained and do not unequivocally represent liquid compositions but their geochemical coherence with B58 suggests their primary or near-primary liquid status.

6.3.3.2 Cumulates

Bradley (1972) crudely modelled the composition of 739 (Appendix Table 6.2) as a crystal enriched partial cumulate rock consisting of 27% olivine, 7% opx and 66% parent melt, using experimental data from a Hawaiian olivine tholeiite at 9 Kbar (Green & Ringwood 1967b). However he was unable to model satisfactorily the compositions of 785 and 786 on a similar basis, but none the less suggested that their high normative opx contents (ca. 50% - 60%, Appendix Table 6.2) may indicate origins as higher pressure (greater than 13 Kb) crystal enriched picritic tholeiites.

Table 6.3 Geochemical least squares modelling of selected major elements in simulation of compositions of ultramafic rocks 739, 785 and 786 as crystal cumulates.

(a) Accumulation of 739 from B58 liquid

Composition data	B58	Ol	739	739*	Residual
SiO ₂	49.99	39.87	47.19	47.07	-0.12
Al ₂ O ₃	11.05	-	8.19	8.01	-0.18
Fe ₂ O ₃ Total	11.35	15.53	11.77	12.44	0.67
MgO	15.86	45.38	23.94	23.81	-0.13
CaO	9.04	0.25	6.38	6.62	0.24
Model proportions	B58		0.725		
		Ol	0.275		
Sum of squares of residuals = 0.58					

(b) Accumulation of 786 from B69 liquid

Composition data	B69	Opx	Cpx	786	786*	Residual
SiO ₂	51.10	52.35	52.80	52.00	51.43	-0.57
Al ₂ O ₃	13.63	1.20	1.96	5.83	6.54	0.71
Fe ₂ O ₃ Total	10.70	23.25	7.21	16.52	17.09	0.57
MgO	10.60	21.49	14.78	15.79	16.41	0.62
CaO	10.07	3.39	23.08	6.32	6.98	0.66
Model proportions	B69			0.428		
		Opx		0.526		
		Cpx		0.039		
Sum of squares of residuals = 1.96						

(c) Accumulation of 785 from B69 liquid

Composition data	B69	Opx	785	785*	Residual
SiO ₂	51.10	52.49	53.33	52.44	-0.89
Al ₂ O ₃	13.63	1.24	5.95	6.74	0.79
Fe ₂ O ₃ Total	10.70	23.85	16.47	18.28	1.81
MgO	10.60	22.76	17.62	17.62	0.00
CaO	10.07	1.58	3.85	5.36	1.51
Model proportions	B69		0.443		
		Opx	0.568		
Sum of squares of residuals = 6.98					

- Explanatory Notes :
- (1) all compositional data in wt. %
 - (2) least squares modelling after Bryan et al., 1969
 - (3) Opx, Cpx phenocryst data from B69
 - (4) Ol data from Deer et al., (1966) for composition Fo 86
 - (5) 739 = observed composition
739* = estimated model composition

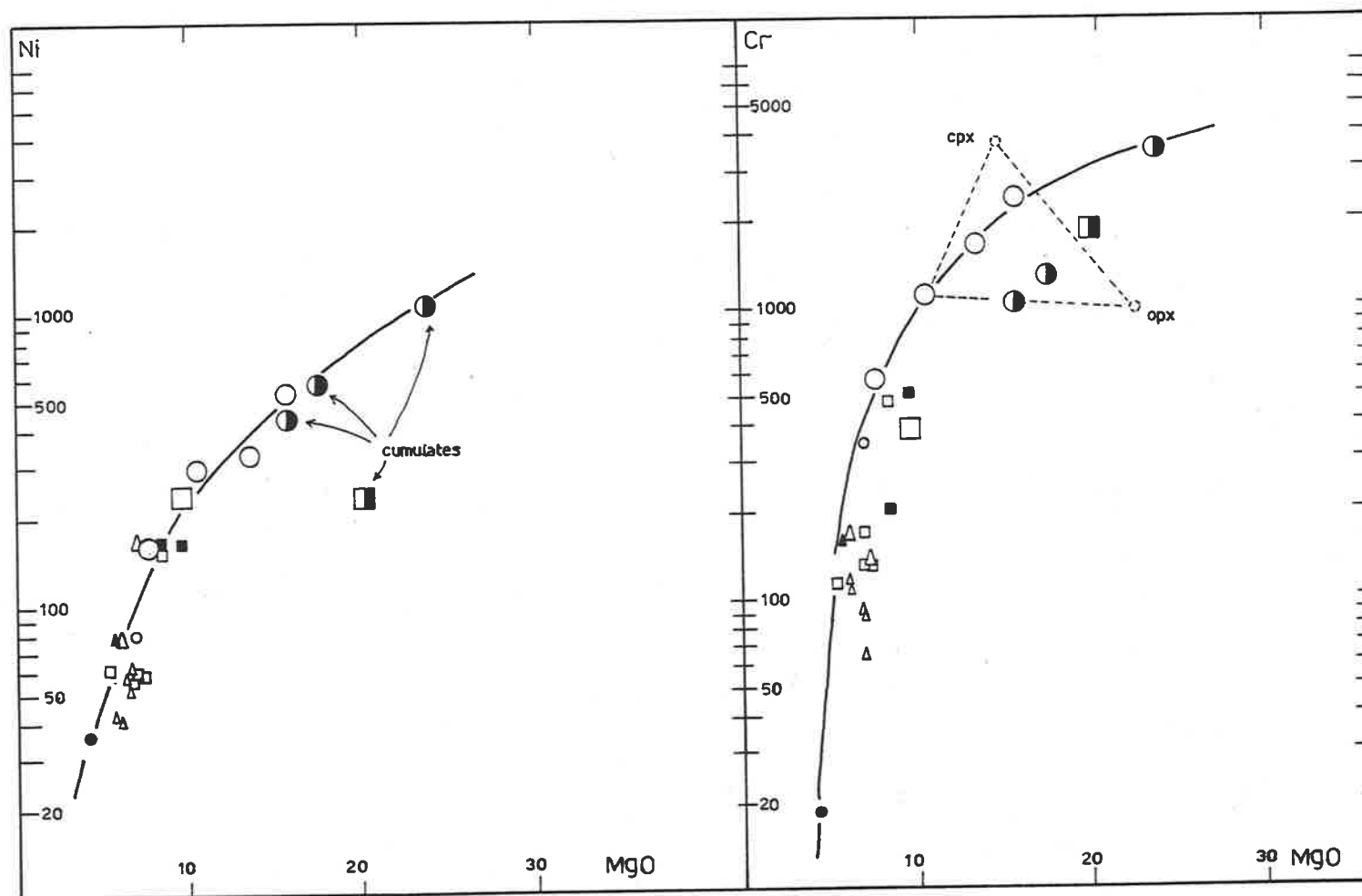


Figure 6.5

MgO-Ni and MgO-Cr diagrams for tholeiitic dykes of the present study.
 Symbols as in Figure 6.4.

The present author has modelled the compositions of the ultramafic rocks using the compositions of primary or near primary Group A liquids B58 and B69 and the opx and cpx phenocrysts in B69 (Appendix Table 6.1) supplemented by an olivine of composition Fo86 from Deer et al. (1966).

A satisfactory model fit for 739 is achieved by adding ca. 28% olivine to liquid B58 and a reasonable fit for 786 is achieved by adding ca. 53% opx and ca. 4% cpx to liquid B69 (Table 6.3). However only a very poor fit is achieved for 785 by adding ca. 57% opx to liquid B69 (Table 6.3). In all cases the modelling is hampered by the lack of knowledge of the pyroxene phenocryst compositions prior to exsolution, spot microprobe data only being available. However the modelling suggests that only in the most magnesian (ca. 16% MgO) liquids is olivine a major fractionating phase, and that in less magnesian liquids (ca. 11% MgO) orthopyroxene predominates over olivine. The presence of rare olivine cores in pyroxene phenocrysts is probably representative of such a compositional change in the liquids.

The prominence of liquidus orthopyroxene increases with elevated pressure in tholeiitic melts e.g. (Green & Hibberson 1970) and suggests pressure of fractionation for most of these samples in excess of ca. 13 Kbar. It is not clear whether the fractionation and accumulation occurred prior to emplacement at greater depth or whether it occurred during emplacement in narrow dyke conduits.

Qualitative interpretation of the MgO-Cr relations (Fig. 6.5) is in accord with the suggestion that opx is the dominant cumulate mineral in 785 and 786 but olivine in 739.

6.3.3.3 Fractionated rocks

Specimens B16 and B26 have Mg number, Ni, and Cr (Appendix Tables 6.2, 6.3) too low to be primary upper mantle liquids and almost certainly have suffered extensive crystal fractionation. Major element modelling demonstrates that it is possible to derive these compositions from a near-primary liquid of B69 type by fractionation of the phenocryst phases observed in B69 (Table 6.4). Good fit models show that fractionation of opx, cpx and plagioclase in the ratio 3:1:3 produce residual liquids of B16 and B26 compositions after ca. 85% and ca. 92% crystallisation respectively. It is notable that extended fractionation of these minerals produces only minimal SiO₂ enrichment.

Table 6.4 Geochemical least squares modelling of selected major elements in simulation of compositions of fractionated tholeiitic liquids B16 and B26.

(a) Fractionation of B69 liquid to B16

Composition data	B16	Opx	Cpx	Plag	B69	B69*	Residual
SiO ₂	51.83	52.35	52.80	52.63	51.10	51.22	0.12
Al ₂ O ₃	14.92	1.20	1.96	29.89	13.63	13.47	-0.16
Fe ₂ O ₃ Total	10.69	23.25	7.21	-	10.70	10.53	-0.17
MnO	0.17	0.32	-	-	0.17	0.13	-0.04
MgO	7.66	21.49	14.78	-	10.60	10.52	-0.08
CaO	10.31	3.39	23.08	12.01	10.07	9.91	-0.16
Na ₂ O	2.28	0.20	0.30	4.55	2.00	2.06	0.06
Model proportions				B16	0.127		
				Opx	0.354		
				Cpx	0.131		
				Plag	0.365		
Sum of squares of residuals					= 0.10		

(b) Fractionation of B69 liquid to B26

Composition data	B26	Opx	Cpx	Plag	B69	B69*	Residual
SiO ₂	52.89	52.35	52.80	52.63	51.10	51.23	0.13
Al ₂ O ₃	15.13	1.20	1.96	29.89	13.63	13.47	-0.16
Fe ₂ O ₃ Total	10.67	23.25	7.21	-	10.70	10.46	-0.24
MnO	0.17	0.32	-	-	0.17	0.13	-0.04
MgO	7.04	21.49	14.78	-	10.60	10.58	-0.02
CaO	9.88	3.39	23.08	12.01	10.07	9.87	-0.20
Na ₂ O	2.47	0.20	0.30	4.55	2.00	2.07	0.07
Model proportions				B26	0.076		
				Opx	0.372		
				Cpx	0.139		
				Plag	0.388		
Sum of squares of residuals					= 0.15		

Explanatory notes as for Table 6.3 plus

- (1) Plag composition data from specimen B69.

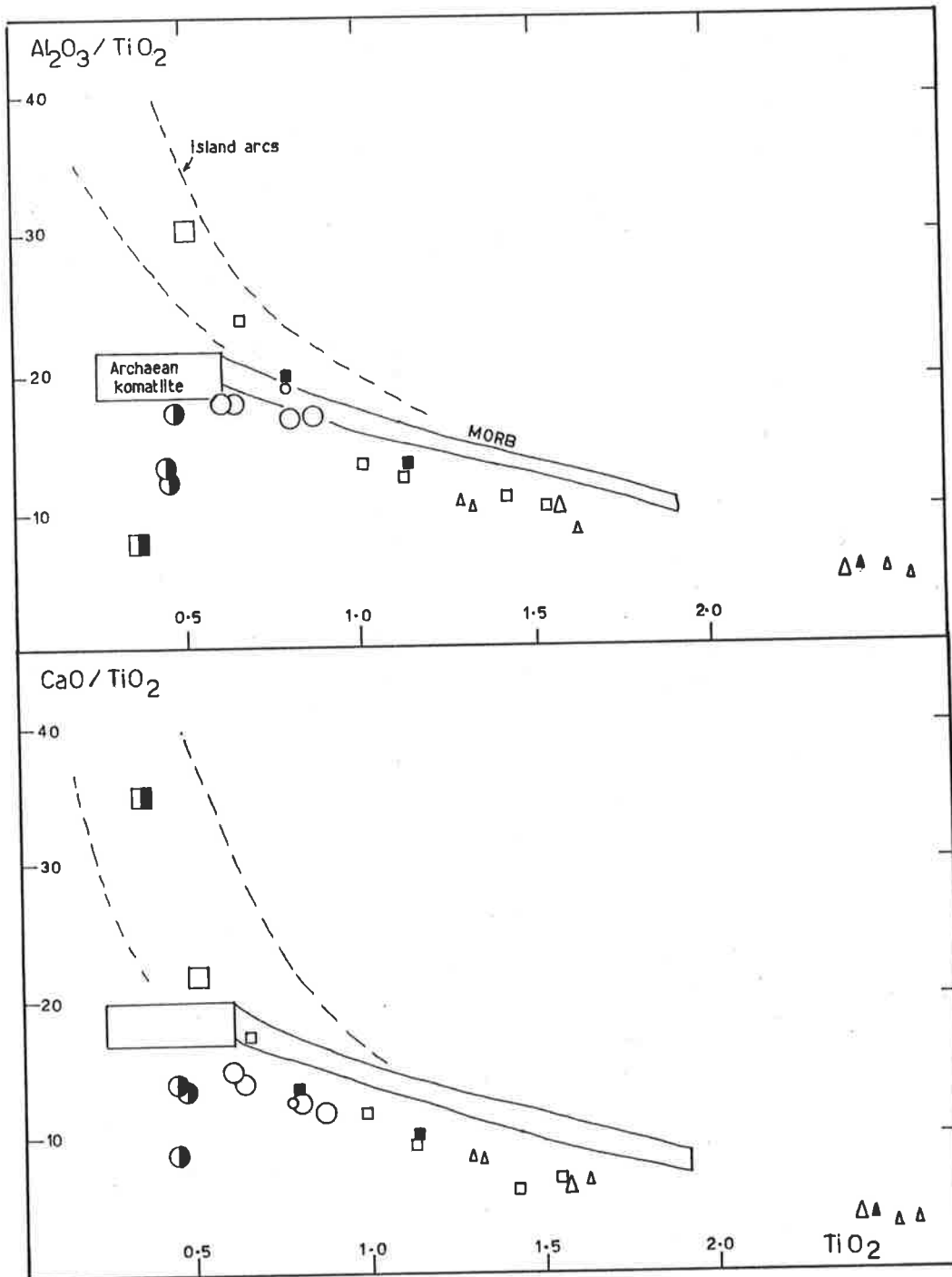


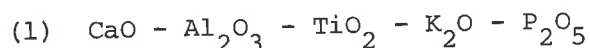
Figure 6-6

Al_2O_3/TiO_2-TiO_2 and CaO/TiO_2-TiO_2 diagrams for tholeiitic dykes of the present study. Outlined and labelled fields are after Purvis et al. (1979). Symbols as in Figure 6.4.

The modelling also confirms the observation in the preceding section that, in all but the most magnesian liquids, orthopyroxene is favoured over olivine as the dominant liquidus ferromagnesian phase in the tholeiitic liquids of Group A. Once again a pressure of fractionation in excess of ca. 13 Kbar is favoured.

6.3.3.4 Geochemistry of primary and near-primary liquids

Although petrogenetic information is best obtained from primary liquid compositions, the near-primary and fractionated liquids and cumulate rocks will be included in the following discussion where appropriate.



The interpretation of the interrelationship between CaO, Al_2O_3 and TiO_2 is based on the belief that at the high degrees of melting represented by tholeiitic liquids, Ti is completely incompatible so that all of the Ti enters the melt (Nesbitt et al. 1979). This has been disputed by Frey et al. (1978) who have shown experimentally that residual peridotite minerals retain some Ti, and by Pearce & Norry (1979) who have calculated non-zero partition coefficients for Ti for these ferromagnesian minerals (Appendix Table 6.6). Nevertheless the plots of Ti vs. Zr, Y and Nb for Archaean komatiites and tholeiites (Nesbitt & Sun 1976) and Group A tholeiites (Figs. 6.7, 6.8) suggest that Ti is close to incompatible, if not perfectly so.

Ideally progressive single stage melting of a chondritic pyrolite source will first show a high concentration of TiO_2 in the melt, but low concentrations of CaO and Al_2O_3 due to residual Ca- and Al-bearing minerals. The CaO/TiO_2 and $\text{Al}_2\text{O}_3/\text{TiO}_2$ ratios in the melt increase with progressive melting as the Ca- and Al-bearing minerals are consumed and TiO_2 becomes more dilute (Nesbitt et al. 1979). Limiting values for these ratios are reached when no residual Ca- or Al-bearing minerals remain, at which stage the $\text{CaO}/\text{Al}_2\text{O}_3$ ratio in the melt will be 0.82, the chondritic value. This feature is demonstrated in Figure 6.6 and applies well to Archaean komatiites, and MORB. However the rocks of Group A show a systematic tendency relative to komatiites and MORB to have lower CaO/TiO_2 and $\text{Al}_2\text{O}_3/\text{TiO}_2$ ratios for all TiO_2 contents (Fig. 6.6).

These lower ratios may reflect the presence in the residue of a mineral or minerals holding back CaO and to a lesser extent Al_2O_3 . However in the case of B58, which has the chondritic value for $\text{CaO}/\text{Al}_2\text{O}_3$ (Fig. 6.6), both CaO and Al_2O_3 must be held back equally to buffer the $\text{CaO}/\text{Al}_2\text{O}_3$ ratio if the chondritic model is valid. Alternatively the source of Group A tholeiites may be depleted in CaO and Al_2O_3 (equally) or enriched in TiO_2 .

To test the possibility of a residual mineral controlling the CaO/TiO_2 and $\text{Al}_2\text{O}_3/\text{TiO}_2$ in this way it is necessary to consider the possible residual minerals and their likely effects on the individual ratios. Minor residual phases in pyrolite at the relatively high degrees of melting required for tholeiitic magmas may be plagioclase, clinopyroxene or garnet depending largely on the pressure in the source. The lack of significant Eu anomalies (especially in B69, Fig. 6.9) and the low $\text{CaO}/\text{Al}_2\text{O}_3$ ratios (ca. 0.4) in plagioclase argue against residual plagioclase alone. Although the fractionated HREE (Fig. 6.9) with $(\text{Yb}/\text{Gd})_N$ averaging 0.74 may allow the possibility of either garnet or clinopyroxene involvement, the more depleted CaO relative to Al_2O_3 favours residual clinopyroxene. This may be further tested by trace element modelling using elements such as Sc which are favoured by clinopyroxene, and not plagioclase.

An estimate of the degree of melting of the pyrolite source is required to adequately construct partial melting models. K_2O , P_2O_5 and possibly TiO_2 (see above) are regarded as completely incompatible in pyrolite residues for all but the smallest degrees of partial melting, so that their concentration in the melt should be directly dependent on the degree of partial melting (Frey et al. 1978). The pyrolite model compositions of K_2O and P_2O_5 are not well established but Frey et al. (1978) used Ringwood's (1966) original estimates which are quite different from Ringwood's (1975) preferred average. Furthermore the original estimate of TiO_2 in pyrolite, which was based on a Hawaiian tholeiite derivative liquid, is now considered inappropriate for most environments so that Frey et al. (1978) used a value of 0.3% - 0.4%.

Results of calculations using these different pyrolite compositions (Table 6.5) show that although the pyrolite K_2O of Ringwood (1966) gives reasonable estimates of 19% - 25% partial melting for the tholeiites of this study, the TiO_2 and P_2O_5 require unrealistically high partial melting percentages. Ringwood's (1975) average values

produce reasonable estimates of 17% - 32% partial melting using P_2O_5 and TiO_2 but K_2O requires unrealistically low (3% - 4%) partial melts. The modified TiO_2 content of Frey et al. (1978) requires 37% - 48% partial melting of the pyrolite source, still probably too high.

These results suggest that the K_2O , P_2O_5 and TiO_2 contents of the pyrolite source of Group A tholeiites are heterogeneously different from the model compositions. In detail, P_2O_5 and TiO_2 are probably depleted with respect to, but K_2O approximately similar to, the oceanic source of Hawaiian tholeiites. In addition the Group A source probably differed similarly from that suggested by Frey et al. (1978) for the S.E. Australian basalts. This serves to illustrate the conclusion, more fully investigated below, that although a pyrolite upper mantle model composition may be appropriate for the major mineral forming compatible elements such as Mg, Fe, Ca, Al etc., the likelihood of the heterogeneity of incompatible minor elements appears to be inescapable. However, the K_2O , TiO_2 and P_2O_5 partial melting calculations (and phase petrological considerations) may be taken to suggest a possible range of partial melting from ca. 15% to 35%.

Compatible trace element model calculations, involving Sc, V and Y and based on a model pyrolite source similar to that calculated by Frey et al. (1978), suggest that 20% - 35% partial melting leaving a residue of only olivine and opx may account for B58, and that 10% - 25% partial melting leaving a similar residue with ca. 5% cpx as well may account for B60 and B69 (Table 6.6). If 5% garnet is substituted for the cpx in the residue, using the partition coefficients favoured by Frey et al. (1978), it is not possible however, to match the Sc content of B60 and B69 at any level of partial melting (Table 6.6). Similarly qualitative interpretation of MgO - Cr relations (Fig. 6.5) suggests that once the level of MgO in the melt has reached ca. 15%, e.g. B58, the Cr in the melt is no longer controlled by residual cpx, whereas at lower MgO, e.g. B60 and B69, control of Cr by residual cpx is likely (Nesbitt & Sun 1976). The key conclusion of this discussion is that B60 and B69 compatible element geochemistry suggests the presence of a small but significant proportion of residual clinopyroxene (rather than garnet), whereas B58 has neither of these but more probably olivine + opx alone. This suggests, furthermore, that the melts of Group A segregated at shallow mantle depths at pressures less

Table 6.5 Calculated fraction of partial melt from various model pyrolite sources for primary and near-primary basaltic liquids of this study.

	Pyrolite 1	Pyrolite 2	Pyrolite 3	B58	B60	B69	B36	B52
Mg No (FeTot)				73	71	66	48	63
K2O wt. %	0.13	0.02	0.13	0.53	0.67	0.69	0.76	0.51
% melt Pyr. 1 & 3				25	19	19	17	25
% melt Pyr. 2				3	3	3	3	4
P2O5 wt. %	0.06	0.02	0.06	0.08	0.08	0.12	0.16	0.08
% melt Pyr. 1 & 3				75	75	50	38	75
% melt Pyr. 2				25	25	17	13	25
TiO2 wt. %	0.7	0.2	0.30	0.62	0.65	0.81	1.58	0.52
% melt Pyr. 1				113	108	86	44	135
% melt Pyr. 2				32	31	25	13	38
% melt Pyr. 3				48	46	37	19	58

Explanatory notes -:

- (1) Pyrolite 1 after Ringwood (1966)
- (2) Pyrolite 2 average after Ringwood (1975)
- (3) Pyrolite 3 after Frey et al. (1978)

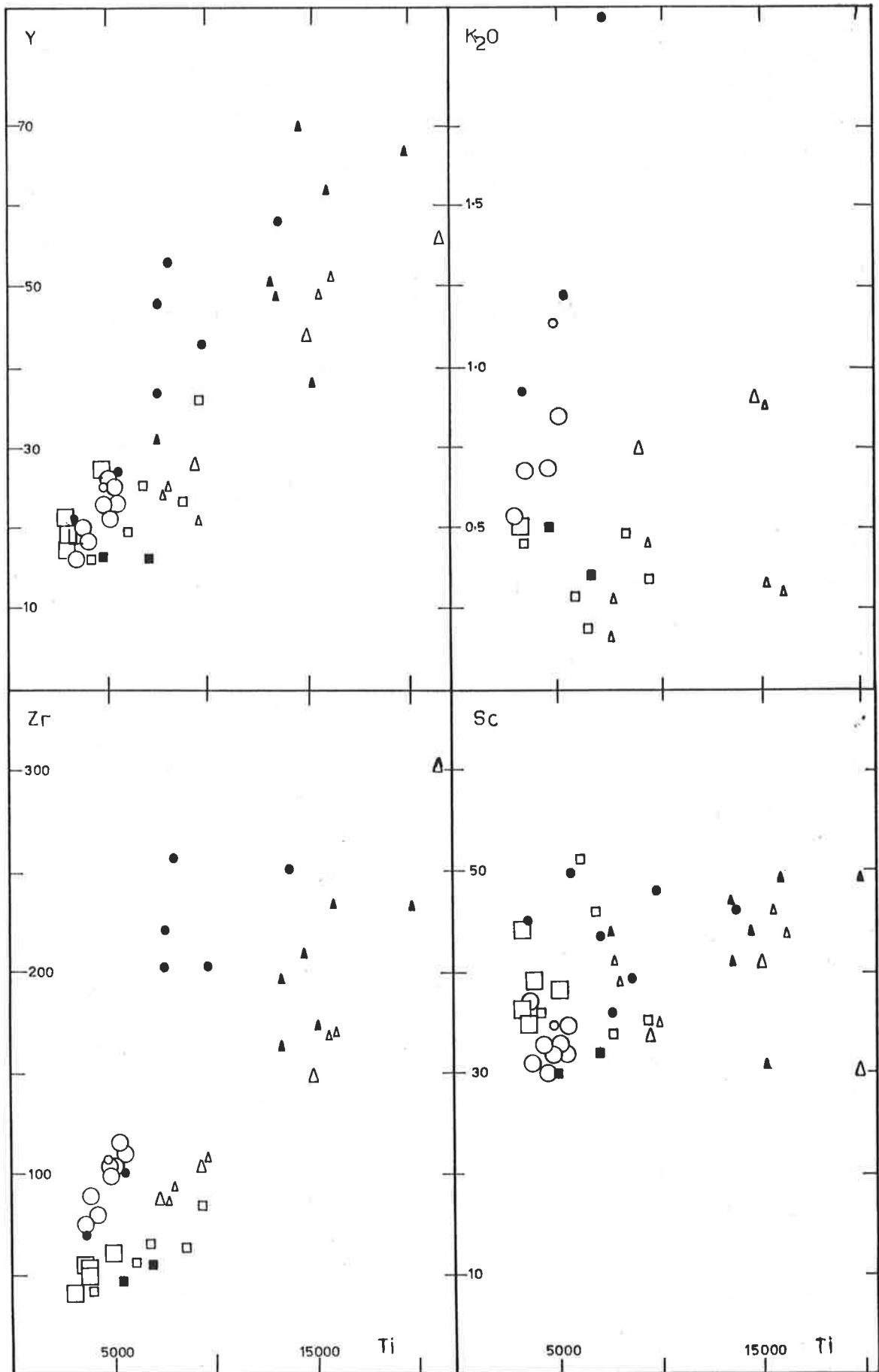


Figure 6.7 Ti-Zr, Ti-Y, Ti-K₂O, Ti-Sc diagrams for tholeiitic dykes of the present study. Symbols as in Figure 6.4.

than the garnet stability limit (ca. 60 km; Green 1973) and that the low CaO/TiO_2 and $\text{Al}_2\text{O}_3/\text{TiO}_2$ ratios of B58 (and possibly therefore also the other samples) are not due to the presence of residual cpx or garnet. Hence it is suggested that the Group A pyrolite source for B58 and the other samples has been relatively enriched in TiO_2 with respect to chondrites. The alternative explanation that CaO and Al_2O_3 have been depleted by a previous melt extraction fails because TiO_2 would be relatively more depleted by such a process (e.g. Sun & Nesbitt 1978b).

(2) Ti - Zr - Y - Nb - Sc - V

Nesbitt & Sun (1976) demonstrated that for most pairs of these trace elements, Archaean komatiitic and tholeiitic volcanics produce collinear arrays passing through the origin, with chondritic relative ratios. These relationships were interpreted as indicating that the elements have behaved incompatibly during partial melting and that the upper mantle source itself had chondritic relative abundances at that time.

Group A tholeiites have collinear arrays passing through the origin for element pairs among Ti, Zr, Y and Nb (Fig. 6.7, 6.8) suggesting that these elements are incompatible, but the plots of Zr-Sc and Zr-V (Fig. 6.8) clearly demonstrate that Sc and V have behaved compatibly. This graphically illustrates the calculations in the preceding section which suggest the presence of a small proportion of clinopyroxene in the residue of Group A primary liquids (Table 6.6).

Although Ti, Zr, Nb and Y have apparently behaved incompatibly in the source of Group A tholeiites, ratios such as Ti/Zr ca. 50, Ti/Y ca. 208 and Zr/Y ca. 4.5 (Appendix Table 6.4) deviate markedly from the chondritic values, of 110, 275 and 2.5 respectively, and indicate that relative to Ti both Zr and Y are enriched to different degrees in the melt. The Zr/Nb ratio is approximately chondritic (ca. 16; Appendix Table 6.4) and suggests that both Zr and Nb are enriched in the melt relative to Ti to a similar degree. Since all of these elements have behaved incompatibly it is probable that the source of Group A tholeiites was enriched in these trace elements heterogeneously relative to Ti, prior to or at the time of partial melting.

Furthermore, it was concluded above on the basis of the $\text{CaO}-\text{Al}_2\text{O}_3-\text{TiO}_2$ relations that Ti itself was relatively enriched in the

Table 6.6 Calculated Sc, V and Y contents in mantle derived melts, assuming varying degrees of melting and a range of residual mineral assemblages.

	Residue			% melt	Sc ppm	V ppm	Y ppm
A.	ol	opx		20	37.3	245	25.9
	80	20		25	35.4	215	20.8
				30	33.7	191	17.4
				40	30.7	157	13.1
B.	ol	opx	cpx	10	31.8	262	47.0
	70	25	5	15	30.8	230	32.6
				20	29.8	205	24.9
				25	28.9	185	20.2
C.	ol	opx	garnet				
	70	25	5	1	25.8		
				5	25.4	387	
				10	25.1	317	
				15	24.7	269	25
				20	24.4	233	20
				B58	37	231	16
				B60	31	238	20
				B69	32	235	23
				Mantle	20	75	5.25

Explanatory notes :- (1) Assumed mantle composition after Frey et al. (1978)

(2) Partition coefficients used after Frey et al. (1978)

	ol	opx	cpx	gar
Sc	0.25	1.1	3.1	6.5
V	0.09	0.3	1.5	0.27
Y	0.002	0.009	0.20	1.4

(3) Calculations assume equilibrium batch melting of Schilling & Winchester (1967)

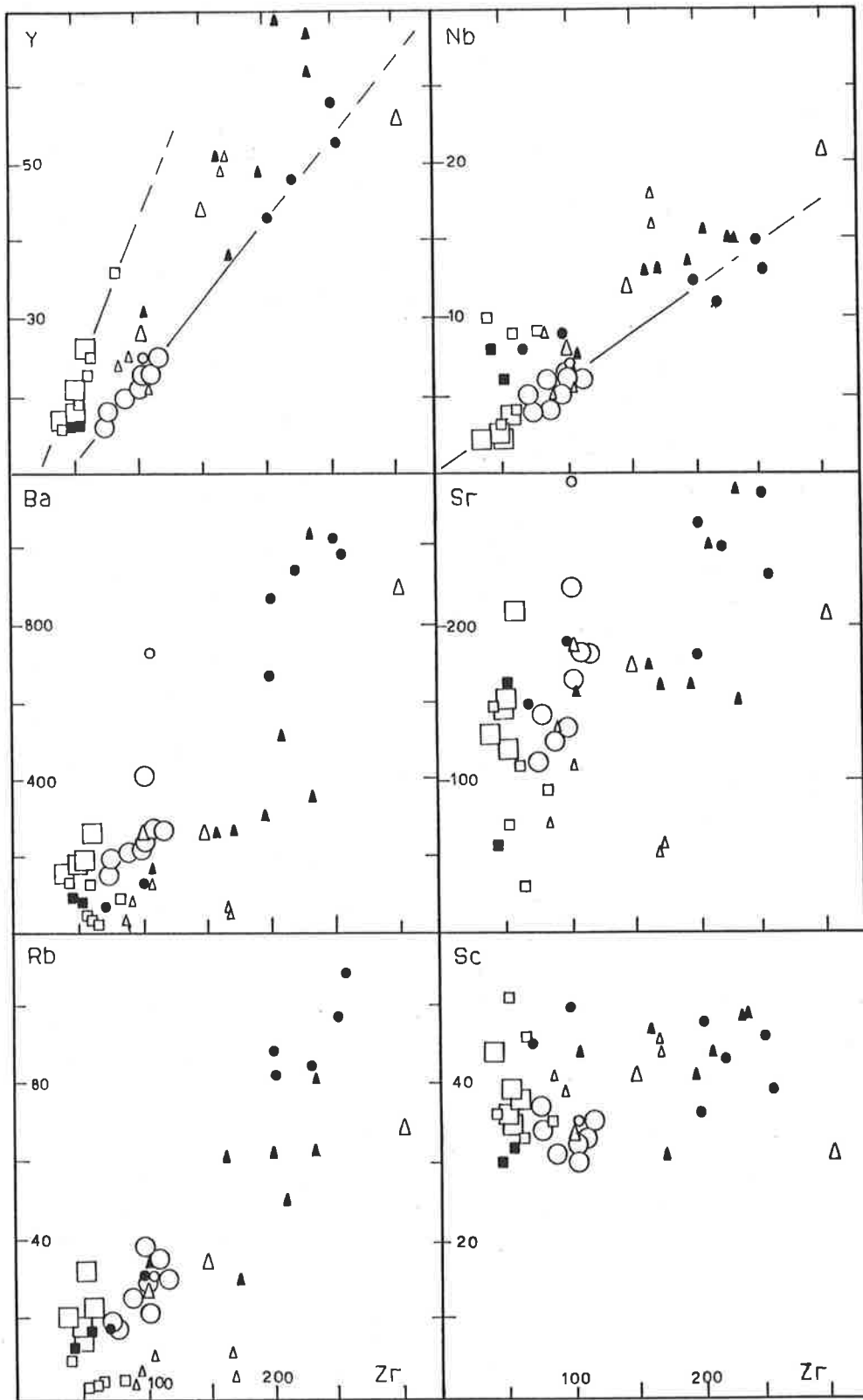


Figure 6.8 Zr-Y, Zr-Nb, Zr-Ba, Zr-Sr, Zr-Rb, Zr-Sc diagrams for tholeiitic dykes of the present study. Symbols as in Figure 6.4.

source with respect to the chondritic value.

(3) Rare earth elements

The REE contents of Group A tholeiitic rocks are all greater than 9X chondritic and with marked LREE enrichment over HREE (Fig. 6.9). The LREE are steeply fractionated with $(La/Sm)_N$ ca. 2.78 but HREE are only moderately fractionated with $(Yb/Gd)_N$ ca. 0.77 (Appendix Table 6.4).

Simple partial melt modelling of REE by Sun & Nesbitt (1978a) has demonstrated that for olivine + opx + cpx residues, even with the most favourable partition coefficients and up to 15% residual cpx, it is not possible to raise the $(La/Sm)_N$ ratio of the melt by more than 10% over that of its source. Similar calculations by the present author based on the residues in Table 6.6 confirm their conclusion (Table 6.7), and in addition show that the presence of residual garnet apparently also would be unable to raise the $(La/Sm)_N$ significantly in the melt, and moreover would severely fractionate the HREE (calculated $(Yb/Gd)_N$ ca. 0.57). The inescapable conclusion is that the LREE enriched and fractionated character of the Group A tholeiitic rocks is inherited from their source, which therefore did not have relative chondritic REE, and is not due to the presence of residual cpx (nor garnet).

Moreover, although the data in some cases are sparse the apparent collinear arrays passing through the origin for P, K, Zr, Rb, Sr and Ba with respect to Ce (Fig. 6.10) are sufficient to show these elements to be coherent and incompatible and not to be held back in residual phases such as apatite or phlogopite (Sun & Hanson 1975).

(4) Discussion

The tholeiitic liquids of Group A are here suggested to have resulted from large degrees of melting (15% - 35%) of a variably trace element enriched upper mantle source leaving a residue dominated by olivine and orthopyroxene, with a small amount of clinopyroxene possibly residual for B60 and B69 but not for B58. Extensive trace element studies of mid-ocean ridge tholeiitic basalts (MORB) by Sun et al. (1979), and Wood et al. (1979) have shown that the trace elements may be arranged in a relative order of incompatibility, (modified slightly by the present author) which

Table 6.7: Calculated model elemental fractionations produced by partial melting of an upper mantle pyrolite source with model elemental ratios equal to unity, leaving residues of olivine + opx ± cpx ± garnet.

Residue	% melt	Ratio in melt						
		(La/Sm) _N	(Yb/Gd) _N	Ti/Zr	Ti/Y	Zr/Y	Zr/Nb	Rb/Sr
ol opx 80 20	25	1.01	0.98	0.94	1.03	1.10	1.07	1.01
ol opx cpx 70 25 5	20	1.03	1.01	0.89	1.09	1.23	1.11	1.15
	30							1.02
ol opx cpx gt 70 20 5 5	20	1.05	0.58					
ol opx gt 70 25 5	20	1.02	0.57					

Note: (1) Kd's after Frey et al. (1978), Appendix Table 6.6.

(2) calculations assume equilibrium batch melting of Schilling & Winchester (1967).

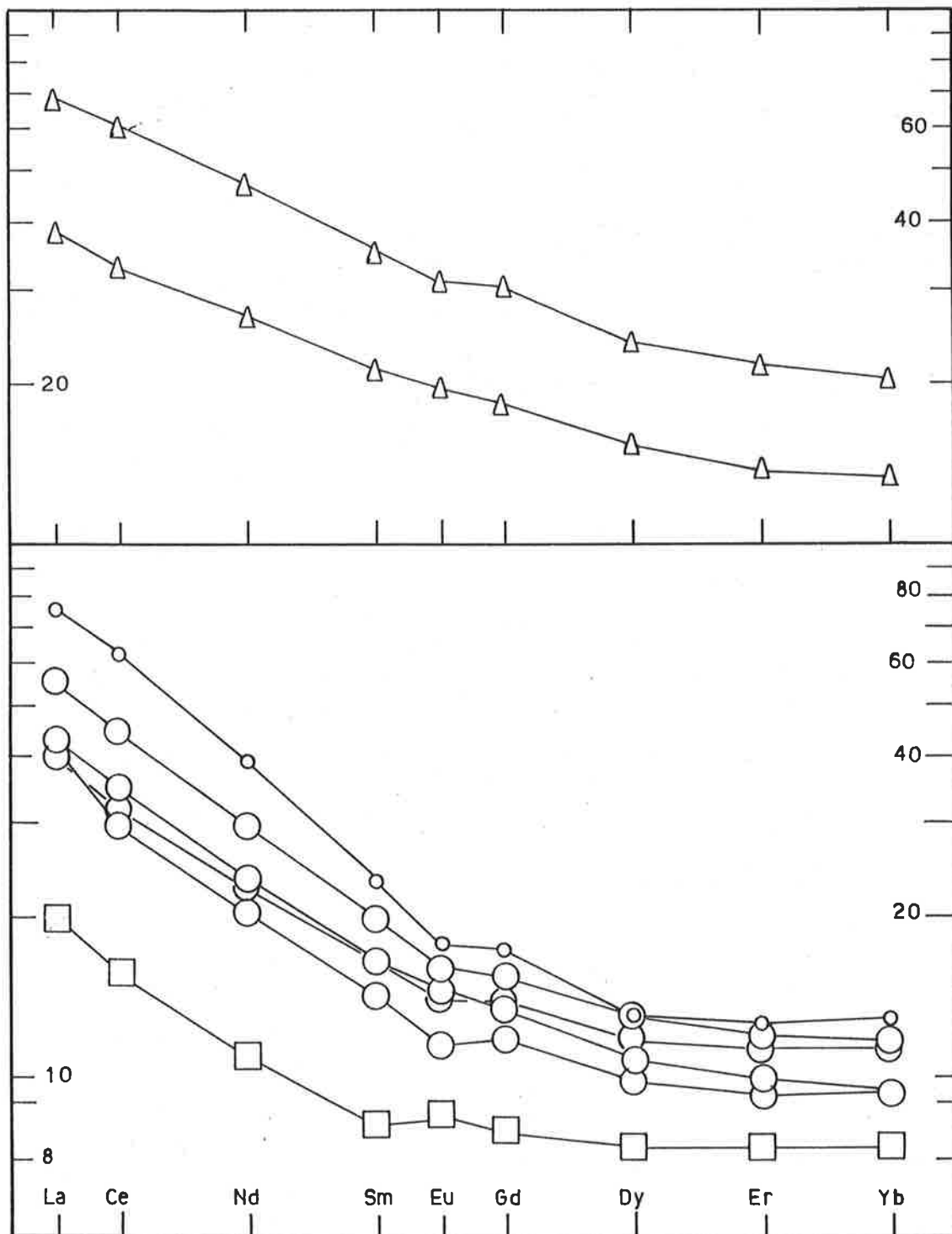


Figure 6.9 Chondrite-normalised REE plots for tholeiitic dykes of the present study. Symbols as in Figure 6.4.

may be expected to apply to most tholeiitic source areas. A number of tholeiitic rocks from diverse geological settings are plotted in Fig. 6.11, viz,

1. Two MORB (482/2, Sun et al. 1979; 413-1, Wood et al. 1979).
2. Two continental tholeiites from Victoria.
(69-1018 & T-14, Frey et al. 1978)
3. Two komatiites (STPK) from Western Australia.
(SD4/193 & 331/144/42, Sun & Nesbitt 1978a).

These rocks confirm the general order of incompatibility and highlight a number of points, e.g.

1. The Zr to Yb region of the plot is a smooth curve for all of the examples demonstrating the coherence of these trace elements,
2. Sc and V are coherent with Zr to Yb for the STPK rocks but are relatively depleted for the tholeiitic rocks, reflecting the role of clinopyroxene in the formation of the latter,
3. The alkali elements K, Rb, Ba in the least altered rocks form a relatively smooth pattern (e.g. Victorian tholeiite 69-1018) and are coherent with the La to P region of the curve, although the slope of the curve decreases towards Rb and Ba. The MORB show a similar pattern, although with more scatter, but the slope reverses for Rb and Ba.
4. P may be anomalous e.g. STPK; however the role of P in the upper mantle is poorly understood (see e.g. Nesbitt & Sun 1976; Thompson 1975b; Beswick & Carmichael 1978).
5. Sr may be anomalously depleted, probably due to "low" pressure fractionation of plagioclase.
6. Nb data, although scarce, indicate that it is generally coherent with the La to Rb region of the plot.

Comparison of Group A primary liquids with the above examples illustrates marked dissimilarities (Fig. 6.12), notably prominent Ti, P, Sr and Nb anomalies. Of these the most unexpected is the relative depletion of Ti in the Group A liquids, resulting in the decoupling of e.g. Ti and Zr. Although the Sr feature may possibly be attributed to some plagioclase fractionation, and the P abundances are apparently erratic, the decoupling of Ti

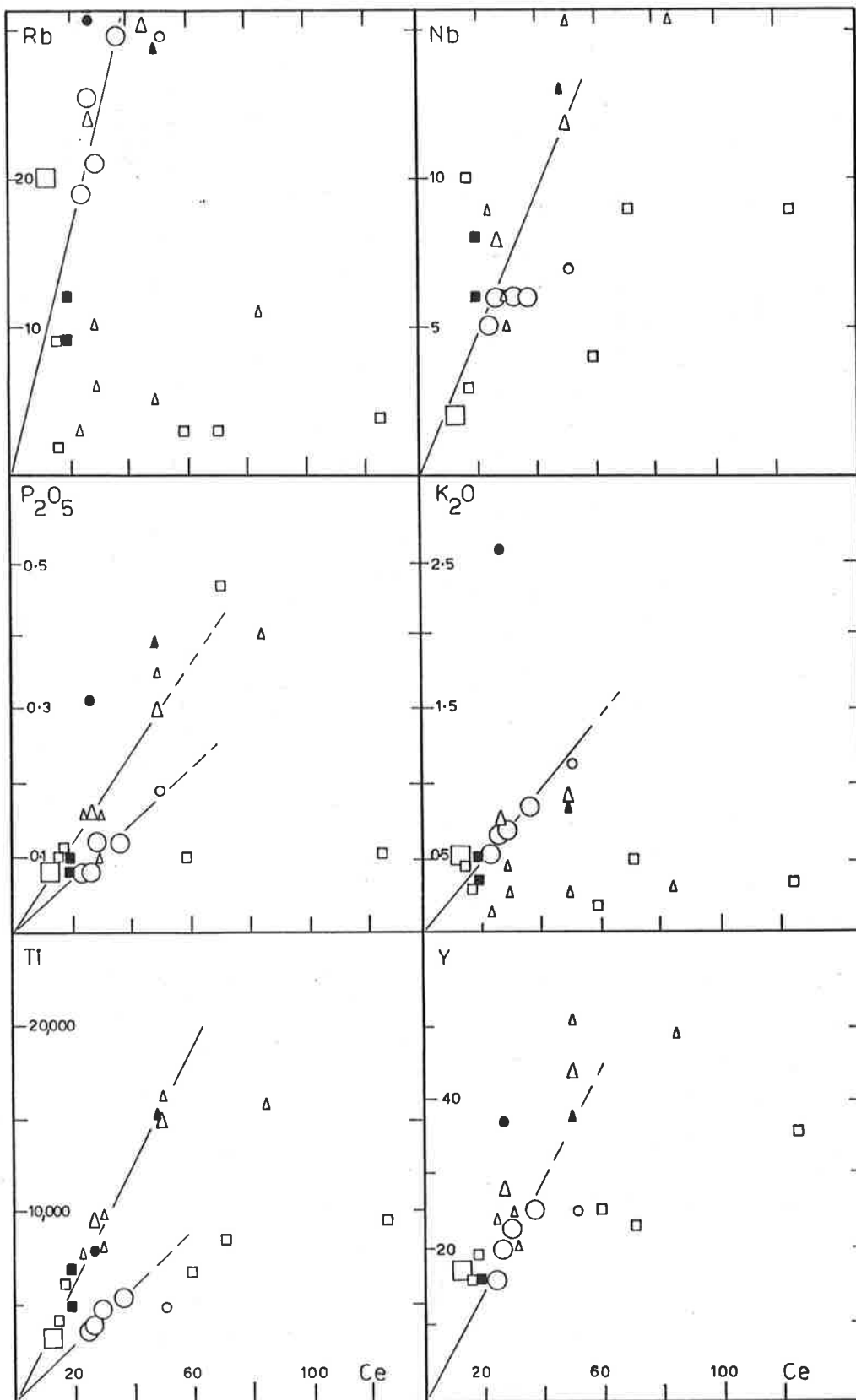


Figure 6.10

Ce-Ti, Ce-Y, Ce- P_2O_5 , Ce- K_2O , Ce-Rb, Ce-Nb diagrams for tholeiitic dykes of the present study. Symbols as in Figure 6.4.

from Zr (and the MREE) and the Nb anomaly are not immediately explicable.

Partition coefficient data for Ti and Zr (Pearce & Norry 1979) indicate that no combination of the common residual minerals of tholeiitic liquids can effectively fractionate these two elements. Similarly the presence of a residual Ti-mineral such as ilmenite is discounted for tholeiitic liquids by abundant experimental data (see e.g. Green 1973). Indeed, as has been noted above, it is not possible to ascribe the more incompatible element (e.g. Rb to Zr including LREE) enrichment pattern to anything other than the probable enriched nature of the source of the tholeiitic liquids. The conclusion then is that the elemental distribution pattern of Group A primary liquids reflects the elemental enrichment pattern of their source and not the residual mineralogy.

Closer scrutiny of the Group A data (Fig. 6.12) indicates a natural division into two groups of elements, each of which shows a subparallel correlated trend of decreasing degree of both enrichment and incompatibility, viz

1. Rb, Ba, K, La, Ce, Nd, Zr, Sm, Eu, Gd, Dy, Y, Er, Yb
2. Nb, Sr, P, Ti, Sc, V

Although within these two groups there is a similar trend of relative enrichment e.g. Yb to Rb and V to Nb, between the two groups there is a 3X difference in absolute enrichment, the former being more enriched than the latter. The arguments above suggest that this enrichment pattern is characteristic of the source. It remains to explain how the source of these tholeiitic liquids can be enriched in trace elements and what sort of enrichment process is possible to decouple trace elements such as Ti and Zr and Ba and Nb.

(5) Trace element enrichment processes

Two main methods of enriching an upper mantle source of basaltic liquids in trace elements have been proposed, viz

1. intrusion of low degree melt from a deep mantle source e.g. alkali basalt (Sun & Hanson 1975),
- or 2. metasomatism by fluid component (component B of Frey & Green 1974).

For very low degrees of partial melting these two possibilities may merge e.g. in the case of volatile-rich kimberlitic melts. The dynamic melting model of Langmuir et al. (1977), involving

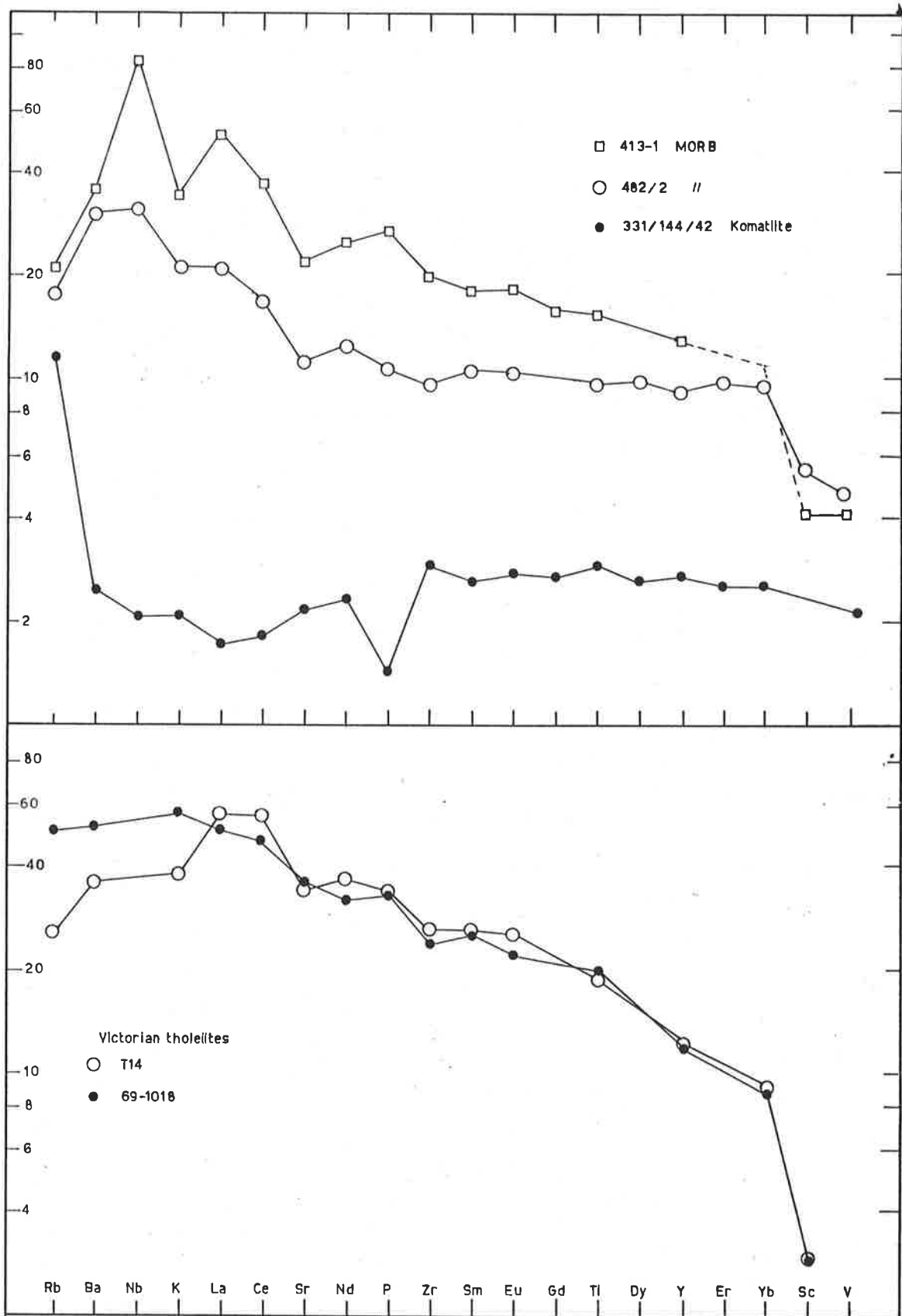


Figure 6.11

Extended REE normalised plots for typical komatiite, MORB and Victorian Cainozoic tholeiites. Data from Sun et al. (1979), Wood et al. (1979), Sun & Nesbitt (1978) and Frey et al. (1978).

variable partial melting and partial melt retention processes in an ascending diapir and variable incorporation into later melts, may be approximated by the former case above, for the purposes of this present discussion.

The trace element character of some kimberlite, basanite and olivine melilitite examples are plotted on Fig. 6.13 and may be compared with Group A tholeiites. The distinctive Ti and Nb anomalies of Group A are lacking in these rock-types. Similarly there is a marked difference in the Rb, Ba and K relationships where for instance, Group A has $(Rb/Ba)_N$ greater than 1 but the others have a ratio less than 1. Hence it is unlikely melts of this type could be responsible for the enrichment of the upper mantle source of Group A tholeiites.

The enriching component of the Group A source must be depleted in Ti and Nb relative to the surrounding trace elements, and probably reflects a source area for the enriching component where a Ti-rich (and Nb-rich?) mineral is stable and in equilibrium with melt or volatile-rich component.

Further discussion of this proposed metasomatic process is presented in Chapter 7 in particular with regard to its likely expression within the continental crust.

(7) Significance of minor non-incompatibility of Ti, Zr, Nb and Y

Many of the above arguments have relied on the near complete incompatibility of Ti, Zr, Nb and to a lesser extent Y. Pearce & Norry (1979) and Frey et al. (1978) have disputed this assumption.

Recalculation of models A and B of Table 6.7 using the Kd's suggested by Pearce & Norry (1979) shows that the ratios Ti/Zr, Ti/Y and Zr/Nb may be fractionated by up to ca. 10% with respect to these same ratios in the source of Group A tholeiites. Zr/Y may be fractionated by up to ca. 23% for tholeiites B60 and B69 but only ca. 10% for B58. These deviations cannot account for the difference between Group A tholeiites and a model "normal" chondritic upper mantle.

The conclusion remains that Group A tholeiites have been derived from an enriched upper mantle source.

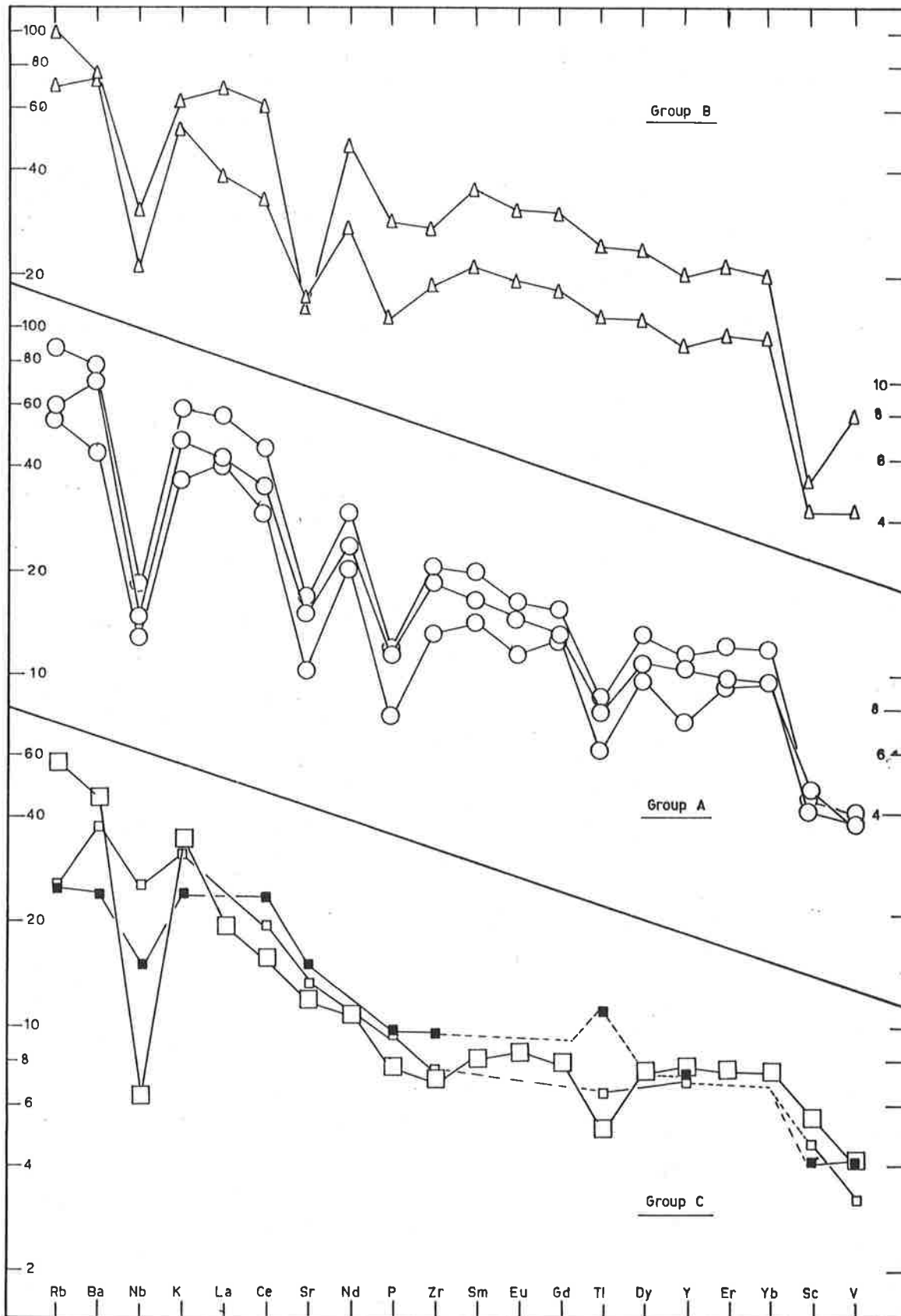


Figure 6.12 Extended REE normalised plots of tholeiitic dykes of the present study. Symbols as in Figure 6.4.

(8) Relationship of amphibolised dykes to pyroxenic dykes

Cursory examination of the data available for amphibolitic dykes of Group A (Appendix Table 6.5) shows that for the compatible elements MgO, Cr, and Ni (Fig. 6.5) the limited data are coherent with the dolerites and pyroxene granulites. The incompatible elements Ti, Zr, Y and Nb of the amphibolites are coherent with the dolerites and pyroxene granulites trends (Figs. 6.7, 6.8). However whereas the Yorke Peninsula samples (Pedler 1976) contain similar abundance levels of these elements as the dolerites and pyroxene granulites, the amphibolites from the present author's immediate study area are absolutely enriched by a factor of 2X or more. If Ti is assumed to be immobile during amphibolisation (Field & Elliott 1974) Zr may be enriched in the amphibolites.

Rb and Zr correlate almost perfectly in the amphibolites and pyroxenic rocks (Fig. 6.8); Ba is markedly enriched relative to Zr in the amphibolites (Fig. 6.8).

These features will be discussed further below.

6.3.4 Geochemistry of Group B basaltic rocks

6.3.4.1 Introduction

Group B basaltic dykes show textures manifesting both DK1 and DK2 types and apparently have been emplaced both early and late in the Kimban Orogeny. Most are moderately coarse grained with intergranular to ophitic textures so that none of the specimens analysed can be unequivocally shown to represent a liquid composition. Although all are hypersthene normative tholeiites, most of the specimens have little or no normative olivine (Appendix Table 6.2). In addition the Mg numbers are all low (40 - 55), Cr is low (66 - 170 ppm) and Ni is low (41 - 169 ppm) suggesting that no primary or near-primary compositions are represented (Appendix Tables 6.2, 6.3).

Although no certainty exists that the compositions of the analysed specimens represent liquids the interpretation below is based on that assumption. Numerous differences exist between Group B and Group A basaltic rocks, and these will be discussed largely by comparison with Group A data.

The initial discussion of the geochemistry of Group B tholeiites rests, as before, on dolerites and pyroxene granulites.

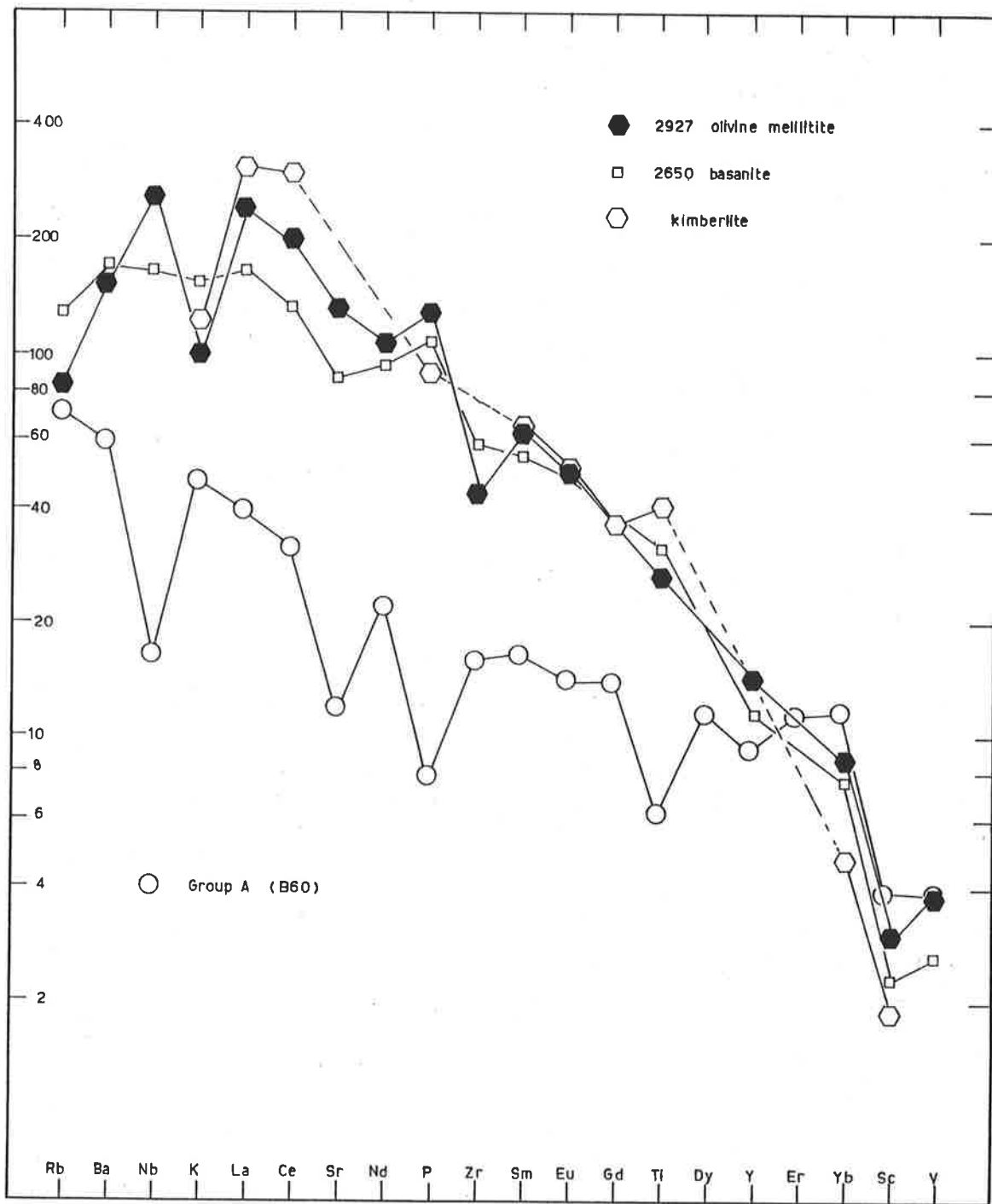


Figure 6.13

Extended REE normalised plots of kimberlite, basanite and olivine melilitite compared with a tholeiitic dyke of Group A (this study). Data from Frey et al. (1978) and

6.3.4.2 Geochemistry of fractionated liquids

(1) MgO vs. CaO - Al₂O₃ - TiO₂ - Cr

The limited geochemical diversity within this group shows out on plots of MgO against the elements CaO, Al₂O₃, TiO₂ (Fig. 6.14) and Cr (Fig. 6.5) where tight clusters of data points result. In general, compared with Group A, the least fractionated Group B samples take up where the most fractionated Group A samples end. Qualitatively the trends on the MgO-CaO and MgO-Al₂O₃ diagrams suggest fractionation of clinopyroxene and plagioclase as the major geochemical controls.

Texturally B36 and B82, although preserving much relict igneous texture, including pyroxene phenocrysts with exsolution lamellae, also display corona textures and subsolidus recrystallised aggregates. Hence it was not possible to test the above fractionation model quantitatively using compositions of igneous phases. However, the textural evidence suggests that the aggregates of

(a) cpx + opx + garnet,

and (b) cpx + amphibole (+ biotite),

in B36 replace clinopyroxene phenocrysts, so that it may be possible to model the igneous assemblage using the plagioclase phenocrysts plus (a) or (b) assuming essentially isochemical subsolidus recrystallisation. The two models in Table 6.8 are very good fits and suggest that B82 may be derived from B36 by ca. 45% - 80% fractionation of plagioclase and clinopyroxene in the ratio ca. 2:1. The apparent petrographic and geochemical dominance of cpx over olivine suggests a high pressure fractionation, in the range of ca. 8-16 Kbar, as suggested by Thompson (1975a) for an olivine tholeiite (59-P-13) which is similar to B36. Furthermore, the subsolidus stability field of garnet in 59-P-13, although not well controlled by the experimental data, suggests the emplacement and cooling of B36 may have occurred closer to the upper pressure limit rather than the lower (Thompson 1975a).

Hence it is concluded that the geochemical diversity within Group B tholeiites may be attributed to deep crustal fractionation of clinopyroxene and plagioclase. However detailed geochemical discontinuities in the major elements between Group B and Group A tholeiites (esp. Fig. 6.14; MgO - SiO₂) suggest that these two groups are unrelated. This is further suggested by the contrasting

Table 6.8 Geochemical least squares modelling of selected major elements in simulation of composition of fractionated liquid B82.

(a) Fractionation of B36 liquid to B82 liquid

Composition data	B82	Plag	Opx	Cpx ¹	Gar	B36	B36*	Residual
SiO ₂	47.54	52.19	51.76	52.14	38.44	47.33	47.38	0.05
Al ₂ O ₃	13.43	30.16	1.46	2.20	21.87	16.16	16.14	-0.02
Fe ₂ O ₃ Total	17.40	-	28.96	17.94	30.72	15.49	15.47	-0.02
MgO	6.06	-	19.92	15.58	4.90	7.21	7.12	-0.09
MnO	0.23	-	0.20	-	0.92	0.21	0.23	0.02
CaO	9.09	12.31	0.41	13.28	6.79	9.70	9.66	-0.04
Na ₂ O	2.32	4.53	-	0.51	0.21	2.25	1.93	-0.32
Model proportions					B82	0.200		
					Plag	0.290		
					Opx	0.079		
					Cpx	0.219		
					Gar	0.188		

Sum of squares of residuals = 0.12

(b) Fractionation of B36 liquid to B82 liquid

Composition data	B82	Plag	Cpx ²	Parg	Biot	B36	B36*	Residual
SiO ₂	47.54	52.19	50.87	39.64	35.45	47.33	47.33	0.00
Al ₂ O ₃	13.43	30.16	3.61	13.88	15.13	16.16	16.16	0.00
Fe ₂ O ₃ Total	17.40	-	11.75	17.49	18.58	15.49	15.49	0.00
MgO	6.06	-	12.75	9.28	12.50	7.21	7.21	0.00
MnO	0.23	-	-	-	-	0.21	0.13	-0.08
CaO	9.39	12.31	21.11	11.53	0.13	9.70	9.70	0.00
Na ₂ O	2.32	4.53	0.53	2.17	0.05	2.25	2.27	0.02
Model proportions					B82	0.553		
					Plag	0.143		
					Cpx	0.053		
					Parg	0.139		
					Biot	0.152		

Sum of squares of residuals = 0.01

- Explanatory notes:
- (1) Composition data in wt. %
 - (2) Mathematical modelling after Bryan et al. (1969)
 - (3) Plag composition average of phenocrysts
 - (4) Ferromagnesian mineral assemblages represent different domains in subsolidus coronas and aggregates.

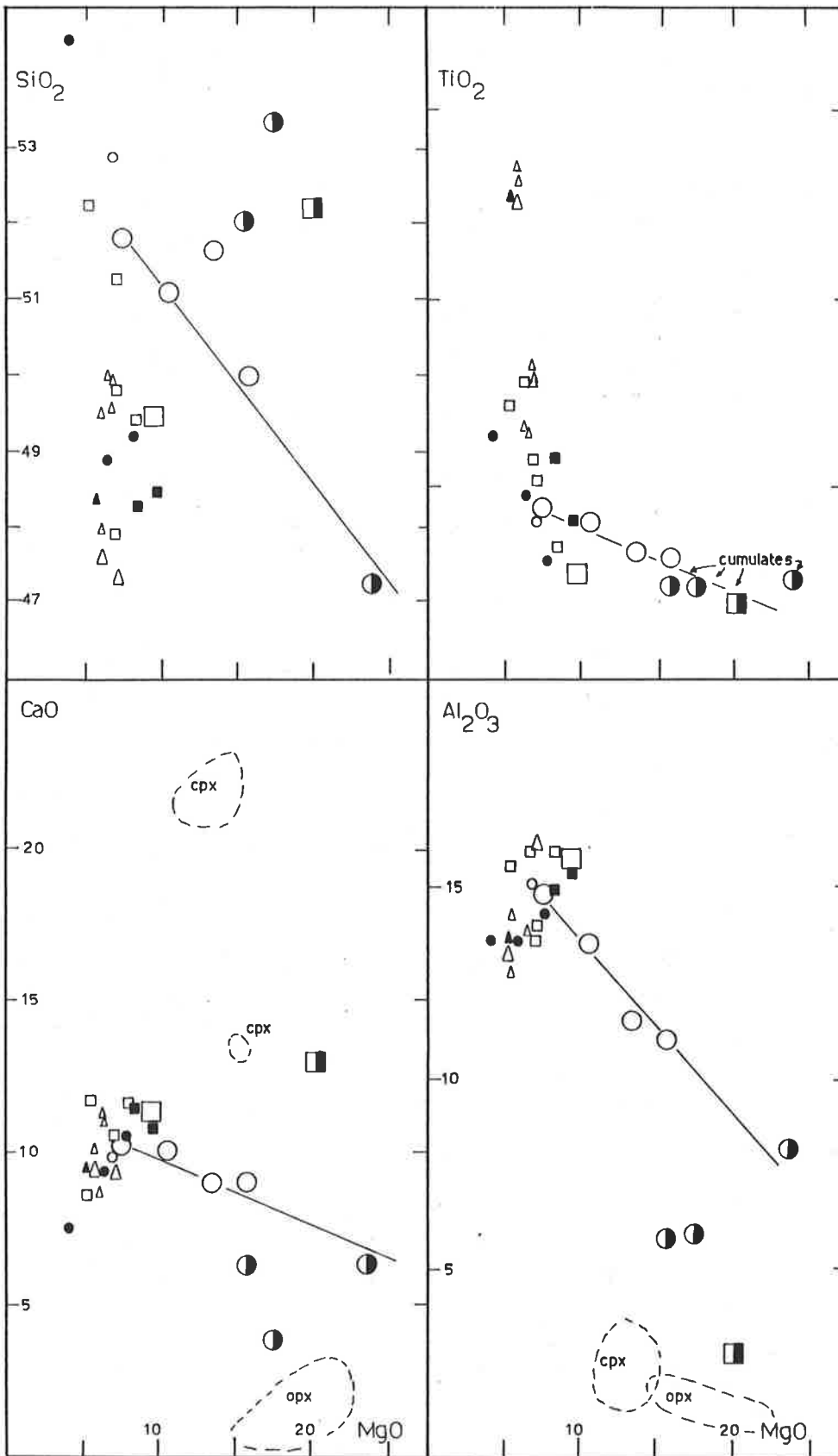
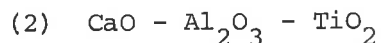


Figure 6.14

MgO-CaO, MgO-Al₂O₃, MgO-SiO₂ and MgO-TiO₂ diagrams for tholeiitic dykes of the present study. Symbols as in Figure 6.4. Fields outlined by broken lines represent analysed phenocrysts.

modelled crystallisates for Group A (opx + cpx + plag) and Group B (cpx + plag), (cf. Tables 6.8 and 6.14).



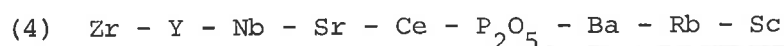
The fractionated rocks of Group B show CaO/TiO₂ and Al₂O₃/TiO₂ ratios less than MORB (Fig. 6.6) similar to Group A, but in this case the fractionating phases clinopyroxene and plagioclase are responsible for depletion of CaO and Al₂O₃ so that no deductions concerning the source character are possible. The analysed specimens fall into two sub-groups, one at ca. 1.5% TiO₂ and the other at ca. 2.5% TiO₂.



With respect to TiO₂ - P₂O₅ there is significant scatter, the lower TiO₂ sub-group having TiO₂/P₂O₅ ca. 10 but the higher TiO₂ sub-group showing decreased TiO₂/P₂O₅ ratios (Appendix Table 6.4). The ratio of 10 is that deduced by Nesbitt & Sun (1976) to be typical of "normal" upper mantle sources of Archaean basaltic and ultramafic liquids and suggests the less fractionated Group B tholeiites may have derived from a "normal" source, but that the more fractionated liquids have crystallised a Ti-phase, possibly the clinopyroxene (as witnessed by the exsolved ilmenite, see above).

The Ti-Zr and Ti-Y plots (Fig. 6.7) are approximately collinear and pass through the origin suggesting these elements are incompatible. However the respective ratios are not chondritic (Fig. 6.7) and suggest Group B liquids are relatively enriched in Zr and depleted in Y over Ti. The Ti-Sc (and Ti-V) plot (Fig. 6.7) clearly exhibits the compatible nature of Sc (and V) and probably reflects control by clinopyroxene fractionation.

The Ti-K₂O plot (Fig. 6.7) suggests that the dolerites and pyroxene granulites may have very different K₂O contents (see Zr-Rb and Zr-Ba relations below).



The Zr-Y plot of the dolerites and pyroxene granulites of Group B (Fig. 6.8) shows a coherent collinear trend passing through the origin. However the Zr-Rb, Zr-Sr, Zr-Ba and to a lesser extent

Zr-Nb plots (Fig. 6.8) clearly differentiate the dolerites from the pyroxene granulites. Sc and Sr are buffered at an almost constant level in the dolerites, probably by clinopyroxene and plagioclase fractionation. However Rb, Ba, and Sr appear to be depleted in the pyroxene granulites, whereas Nb may be enriched.

The Ce - P_2O_5 data (Fig. 6.10) show considerable scatter, but the approximate trend possibly could be interpreted to rule out apatite fractionation as the cause of P_2O_5 variation.

(5) REE

The REE patterns of B36 and B82 (Fig. 6.9) are parallel although B82 is enriched in all REE elements by a factor of ca. 1.5 over B36, probably reflecting its more evolved nature. The patterns are LREE enriched and fractionated with $(La/Sm)_N$ ca. 1.88 and La_N ca. 40 - 70 times chondritic, and have moderately fractionated HREE with $(Yb/Gd)_N$ ca. 0.69 (Appendix Table 6.4). Both samples have only very small Eu anomalies, which suggests that the melts may have been relatively oxidised as the prominent plagioclase fractionation modelled above would otherwise be expected to generate a negative Eu anomaly in B82 (see below).

Relative to Group A tholeiites the Group B basalts are much less steeply fractionated, although the La contents are very similar (Fig. 6.9). This relationship precludes derivation of Group B REE patterns from Group A by crystal fractionation unless the fractionating mineral assemblage has partition coefficients for La and Ce ca. 1.0 and for Er and Yb less than 1.0. Minerals with such K_d 's are generally present only as accessory phases (see e.g. Campbell & Gorton 1980) and not likely to contribute greatly. For this reason, and for others above, it is concluded that Group B tholeiites have an origin distinct in detail from Group A.

(6) Extended REE plots

Following the reasoning applied to Group A tholeiites, the extended REE plots of Group B tholeiites (Fig. 6.12) show a number of distinctive features, highlighting their distinct petrogenesis. Almost no Ti anomaly is present in Group B tholeiites. Zr tends to be more depleted relative to the

surrounding elements than in Group A, but otherwise the patterns are similar in shape (with pronounced P, Nb, Sc, V, and Sr anomalies), although different in slope. The Sr anomaly increases markedly for the more fractionated B82, no doubt reflecting plagioclase fractionation and further contrasting the absence of a Eu anomaly.

Although not unequivocal, the patterns are interpreted to reflect the presence of heterogeneous sources for the tholeiites of this study. The enriched character of the tholeiites is interpreted to reflect the enriched nature of the source and hence the enriching component. The Nb, P, Sr (?), Zr (?), Sc and V relative depletions reflect either the enriching component (e.g. probably Nb, P & Zr) or the residual phases at the site of melting (e.g. probably Sc and V in cpx) and the fractionating phases during emplacement (e.g. Sc and V in cpx).

The lack of Ti anomaly must be accounted for in any combination of these factors.

(7) Trace element model of crystal fractionation

Using the partition coefficient data in Appendix Table 6.6 and the major element model of Table 6.8 it is possible to model the fractionation of trace elements in B36 using the equations in Arth (1976). This is presented in Table 6.9 and shows that the model B, based on fractionation of 45% of cpx and plagioclase in the ratio 1:2 duplicates the pattern of B82 closely. These calculations suggest that the model of variation of major and trace elements within Group B by fractionation of cpx and plagioclase is appropriate and furthermore that the combination of these minerals is unable to vary the relative shape of the extended trace element pattern scarcely at all and hence the pattern is representative of the original more primitive Group B liquid and probably of its upper mantle source.

(8) Petrogenetic summary

The within suite variation in Group B tholeiites can be accounted for by extensive fractionation of plagioclase and cpx at pressures in the lower crustal range 8 - 16 Kbar. The primary magma was apparently relatively oxidised with a high

Table 6.9: Calculated model normalised elemental abundances in Group B tholeiites following crystal fractionation of plagioclase + cpx.

initial liquid B36		model derived liquids		derived liquid B82
		(A) 20% liquid	(B) 55% liquid	
Rb	69	309	120	100
Ba	74	286	122	76
Nb	21	98	37	31
K	53	218	89	63
La	39	172	67	69
Cl	33	143	57	61
Sr	17	11	15	16
Nd	27	118	47	47
Zr	19	88	33	27
Sm	21	92	37	36
Eu	20	62	30	31
Gd	18	78	31	30
Ti	15	63	26	24
Dy	15	64	26	24
Y	13	47	21	20
Er	14	58	23	22
Yb	13	56	23	20
Sc	4.3	4.1	4.2	5.2
V	4.5	10.1	6.1	6.5

- Notes: (1) crystallisate = 0.67 plag + 0.33 cpx
(2) Kd's from Appendix Table 6.6
(3) Calculations utilise fractional crystallisation expression from Arth (1976).

$\text{Eu}^{3+}/\text{Eu}^{2+}$ ratio. This elevated ratio may have been promoted by a relatively high H_2O content in the magma.

The trace element characteristics, by analogy with Group A, suggest the source of Group B had been heterogeneously enriched.

The pyroxene granulites apparently were depleted in K, Rb, Ba and Sr, but enriched in Nb during metamorphism.

(9) Relationship of amphibolised dykes to pyroxenic dykes

Comparison of the Group B amphibolites with the dolerites and pyroxene granulites, shows that (relative to Ti) Zr and Y are enriched in the amphibolites (Fig. 6.7) and (relative to Zr) Rb, Ba and possibly Sr are also enriched (Fig. 6.8). Furthermore the enriched elements are displaced towards the fields of Group A amphibolites.

These relationships will be discussed more fully below.

6.3.5 Geochemistry of Group C basaltic rocks

6.3.5.1 Introduction

Only one of the specimens in Group C analysed for the major elements (B52, Appendix Table 6.2) was collected by the present author; all other major element data are from Bradley (1972). Specimen B52 is a chilled DK2 dyke and probably represents an original liquid composition. Bradley's specimens are DK1 dykes now manifesting hornblende granulite and pyroxene granulite facies assemblages and cannot be unequivocally interpreted as liquid compositions.

The present author has also analysed four other DK2 dolerites of Group C for the trace elements Ti, Zr, Y, Nb, Sc, Rb, Sr and Ba (Appendix Table 6.5).

All Group C rocks are hypersthene normative, and may contain up to ca. 5% normative olivine (Appendix Table 6.2). Their geochemistry will be interpreted in terms of liquid compositions, except for ultramafic 756 which is modelled below as a cumulate.

6.3.5.2 Primary and near-primary liquids

Specimens B52 and 742 have high Mg numbers (63 and 66 respectively; Appendix Table 6.2) and moderate Ni (234 ppm and 162 ppm; Appendix Table 6.3) and Cr (382 ppm and 507 ppm; Appendix Table 6.3) contents, and may represent primary or near-primary upper mantle liquids.

Specimens 744 and 1396 also have moderately high Mg numbers and Ni and Cr contents and may represent only moderately fractionated liquids.

It is possible to infer the geochemical character of the source of these liquids, assuming the liquid compositions have been only moderately modified by fractionation.

6.3.5.3 Cumulate rocks

Ultramafic specimen 756 has been crudely modelled by Bradley (1972) on the basis of accumulation of opx and cpx from a parental olivine tholeiite (opx, cpx and Hawaiian olivine tholeiite of Green & Ringwood, 1967b). A cumulate model, specific to Group C liquids and phenocrysts, is not able to be calculated as no compositional data for Group C phenocrysts exist. However, qualitative interpretation of the $MgO - Al_2O_3$ and $MgO - CaO$ relations (Fig. 6.14) suggests an origin for 756 similar to 785 and 786 of Group A involving pyroxene enriched cumulates.

An approximate model for 756 based on B52 liquid and phenocrysts from B69 of Group A (Table 6.10) shows that a poor fit may be obtained by mixing ca. 15% liquid with cpx, opx and olivine in the ratio ca. 3:1:1.

6.3.5.4 Fractionated rocks

The other Group C tholeiites are considerably fractionated, having Mg numbers as low as 47, Ni and Cr decreased by ca. 4X, and quartz in the norms (Appendix Table 6.2 and 6.3). The $MgO - CaO$ and $MgO - Al_2O_3$ plots (Fig. 6.14) show two distinct trends within Group C tholeiites, although the MgO range is small. Specimen 1351 falls at the extreme of a trend towards decreasing Al_2O_3 at almost constant CaO, whereas specimen 1354 falls at the extreme of a trend towards decreasing CaO at almost constant Al_2O_3 . Qualitative interpretation of these trends suggests that the former may be dominated by plagioclase fractionation and the latter by clinopyroxene fractionation.

Although, as above, no phenocryst data exist for Group C tholeiites these two trends have been modelled by fractionation of B69 phenocrysts (of Group A) from B52 liquid (Table 6.10). The poor fit models suggest

Table 6.10 Geochemical least squares modelling of selected major elements in simulation of compositions of ultramafic rock 756 and fractionated liquids 1351 and 1354.

(a) Accumulation of 756 from B52 liquid

Composition data	B52	Ol	Cpx	Opx	756	756*	Residual
SiO ₂	49.46	39.87	52.80	52.35	52.21	51.24	-0.97
Al ₂ O ₃	15.79	-	1.96	1.20	2.87	3.48	0.61
Fe ₂ O ₃ Total	11.28	15.53	7.21	23.25	10.67	12.37	1.70
MgO	9.68	45.38	14.78	21.49	20.20	20.46	0.26
CaO	11.33	0.25	23.08	3.39	12.97	14.44	1.47
Model proportions				B52	0.140		
				Ol	0.157		
				Cpx	0.526		
				Opx	0.196		
Sum of squares of residuals = 6.43							

(b) Fractionation of B52 liquid to 1351 liquid

Composition data	1351	Ol	Cpx	Plag	B52	B52*	Residual
SiO ₂	49.88	39.87	52.80	52.63	49.46	49.67	0.21
Al ₂ O ₃	13.70	-	1.96	29.89	15.79	15.39	-0.40
Fe ₂ O ₃ Total	13.87	15.53	7.21	-	11.28	11.05	-0.23
MnO	0.23	-	-	-	0.16	0.16	0.00
MgO	7.12	45.38	14.78	-	9.68	9.58	-0.10
CaO	11.71	0.25	23.08	12.01	11.33	11.01	-0.32
Na ₂ O	2.62	-	0.30	4.55	1.65	2.70	1.05
Model proportions				1351	0.674		
				Ol	0.096		
				Cpx	0.028		
				Plag	0.204		
Sum of squares of residuals = 1.48							

(c) Fractionation of B52 liquid to 1354 liquid

Composition data	1354	Ol	Cpx	Plag	B52	B52*	Residual
SiO ₂	52.27	39.87	52.80	52.63	49.46	50.26	0.81
Al ₂ O ₃	15.63	-	1.96	29.89	15.79	14.71	-1.08
Fe ₂ O ₃ Total	13.39	15.53	7.21	-	11.28	10.07	-1.21
MnO	0.19	-	-	-	0.16	0.11	-0.05
MgO	5.39	45.38	14.78	-	9.68	9.39	-0.29
CaO	8.58	0.25	23.08	12.01	11.33	10.13	-1.20
Na ₂ O	2.99	-	0.30	4.55	1.65	2.59	0.94
Model proportions				1354	0.570		
				Ol	0.097		
				Cpx	0.129		
				Plag	0.186		
Sum of squares of residuals = 5.68							

Explanatory notes: (1) All composition data in wt. %

(2) Least squares modelling after Bryan et al. (1969).

- (a) 1351 may be derived by ca. 33% fractionation of plagioclase, olivine and cpx in the ratio of ca. 6:3:1
- and (b) 1354 may be derived by ca. 45% fractionation of plagioclase, cpx and olivine in the ratio of ca. 9:6:5.

The chief difference between these two models is the enhanced role of cpx in the fractionating assemblage in the latter.

The prominent role of olivine in these calculated models is in contrast to the models calculated for Group A tholeiites (Table 6.3) and Group B tholeiites (Table 6.4) and, if real and not a function of the inappropriateness of phenocryst data used, suggests a possible shallower depth of fractionation and emplacement, possibly less than 8 Kbar (Thompson 1975a; Green & Ringwood 1967a). If this is so, the observations that Group C tholeiites outcrop adjacent to dykes of Groups A and B and that Group C tholeiites are of both DK1 and DK2 types and hence were emplaced both during and after metamorphism, suggest that the geothermal gradient and exhumation temporal evolution must have been, in detail, complex (see below).

6.3.5.5 Geochemistry of Group C tholeiites

(1) CaO - Al₂O₃ - TiO₂

There are a number of striking features of the interrelationships of CaO - Al₂O₃ - TiO₂ within Group C basaltic liquids, immediately apparent from Figure 6.6. In the first instance the TiO₂ content of B52 is a minimum for all non-cumulate rocks of Groups A, B and C. Moreover, whereas most of Group C liquids have CaO/TiO₂ and Al₂O₃/TiO₂ ratios less than chondritic analogous to Groups A and B, samples B52 and 742 have corresponding ratios greater than or equal to chondritic, and hence plot in fields characteristic of island arc and ophiolitic basalts (Nesbitt et al. 1979). A detailed argument concerning the significance of CaO/TiO₂ and Al₂O₃/TiO₂ ratios greater than chondritic in ophiolites has been presented by Sun & Nesbitt (1978b). They suggest that as Ti is incompatible during moderate to high degree partial melting of the upper mantle, whereas Ca and Al may be held back, the elevated ratios are most likely to represent a previous event of depletion of Ti (and other

incompatible elements) by melt extraction from the source prior to the partial melting event which produced the ophiolitic basalts. Not all of the incompatible elements are likely to be removed from the source since it is probable that a proportion of the melt will be retained in the residue (e.g. Langmuir et al. 1977). This point will be returned to below; it suffices here to suggest that the source of Group C basaltic liquids had experienced a TiO_2 depletion event prior to the melting event producing the observed liquids.

(2) Ti - Zr - Y - Nb - Sc - V - P - Sr

The two anomalous samples above, B52 and 742, as well as having the lowest Ti contents of all Group C liquids, are low in other incompatible elements such as Zr and Y (Appendix Table 6.3). However 742 has among the highest Nb, P and Sr contents of Group C (Appendix Tables 6.2, 6.3). These and other other anomalies result in apparent curved distribution on some inter-element plots such as Ti-Zr, Ti-Y (Fig. 6.7) and broad scatters of data points on others such as Zr-Nb (Fig. 6.8).

Considering for example the Ti-Zr distribution, (Fig. 6.7) the two likely primary or near primary liquids B52 and 742 have closely similar Ti and Zr contents. Using the partition coefficient data of Pearce & Norry (1979) and calculating vectors (Table 6.11)

corresponding to the major element models of Table 6.10 which successfully account for the extremes of major element composition, it is possible to show that the Ti-Zr data of the other Group C samples cannot be explained by crystal fractionation from B52 or 742 parental liquids. The conclusion is that the range in Ti/Zr ratios (Appendix Table 6.4) of Group C liquids must represent at least in part an initial variation in the melts and hence probably in the source. This conclusion may be applied similarly to the scattered plots such as Zr-Nb (Fig. 6.8) which also show a wide range in ratio unable to be explained by crystal fractionation from a single parental magma.

Thus Group C tholeiites are suggested to result from partial melting of a heterogeneous source to produce a number of different liquid batches which were emplaced independently. This is not unlikely in view of the two different temporal groups represented in Group C.

Table 6.11: Calculated model elemental ratios in fractionated liquids of Group B compared with the observed range in ratios.

	initial liquid	model derived liquids		observed derived liquids	
	B52	1351'	1354'	1351	1354
Ti/Zr	80	79	76	111	138
Ti/Y	183	184	189	322	373
Zr/Y	2.3	2.3	2.5	2.9	2.7
Zr/Nb	16	19	19	18	7

- Notes: (1) Fractional crystallisation models (cf. Table 6.10)
 $B52 = 0.65 (1351') + 0.35 (0.30 \text{ ol} + 0.10 \text{ cpx} + 0.60 \text{ plag})$
 $B52 = 0.55 (1354') + 0.45 (0.25 \text{ ol} + 0.30 \text{ cpx} + 0.45 \text{ plag})$
- (2) Simple fractional crystallisation calculations after Arth (1976).
- (3) K_d 's from Appendix Table 6.6.

Furthermore the ratios of Ti/Zr, Zr/Y and Ti/Y although varying have approximately chondritic averages for the majority of the specimens (Appendix Table 6.4) suggesting that the source of these had relative chondritic ratios.

(3) Rare earth elements

As can be seen from Figure 6.9 and Appendix Table 6.3, B52 has the lowest REE contents of all the basaltic rocks of this study. Whereas the HREE are almost unfractionated $(Yb/Gd)_N = 0.95$ (Appendix Table 6.4), the LREE are strongly enriched and fractionated $(La/Sm)_N = 2.40$ (Appendix Table 6.4); a marked discontinuity in slope is observed in the MREE. The extended REE plot (Fig. 6.12) indicates a marked Ti anomaly and Nb anomaly as in Group A, virtually no Sr anomaly in distinct contrast to Groups A and B, and small P and Zr anomalies. The flat region of the curve between P and Yb explains why, although Ti is anomalous (ratios involving Ti show this) ratios such as Zr/Y are almost chondritic. Furthermore the large Nb anomaly explains why Zr/Nb is nearly chondritic.

The low overall REE and the CaO/TiO_2 , and Al_2O_3/TiO_2 ratios greater than chondritic suggest a depletion of trace elements in the source of B52, so it is strange that the LREE are relatively enriched, as any depletion process normally depletes LREE also (e.g. MORB, Sun et al. 1979). It is possible by analogy with Group A that an enriching component generally similar to that proposed for the Group A source may have reintroduced a LREE enriched (but Ti and Nb depleted and Sc, V depleted) component into a previously depleted source area.

The extended REE plots (and partial plots) of the other Group C tholeiites show that not all have the Ti anomaly, but in essence the P to Yb (including Ti) region of curve is flat (Fig. 6.2). Hence for these specimens ratios involving Ti are essentially chondritic. An Sr anomaly appears in the more evolved rocks due to plagioclase fractionation but otherwise there is an abrupt change from flat P to Yb (or Y in a partial pattern) to steeply fractionated LREE and K, Rb and Ba. The Nb anomaly is of varying magnitude.

These observations suggest that the source of Group C tholeiites had flat HREE and that there was no residual mineral such as garnet during partial melting capable of fractionating the HREE. This does not preclude the presence of residual cpx which has partition

coefficients for the HREE which are almost constant (Frey et al. 1978). Indeed the Sc and V depletions (Fig. 6.12) suggest that cpx is a residual phase at some stage in the development of Group C tholeiites. Hence it is likely that the tholeiite liquids segregated at shallower than ca. 60 km depth in the upper mantle.

(4) Petrogenetic summary

Considerable variation in key elemental ratios within Group C tholeiites suggests that they represent a heterogeneous group of liquids. Variation in major elements can be modelled on the basis of fractionation from primary liquids of solid phases dominated by plagioclase, olivine and varying proportions of cpx.

Near primary liquids suggest that the source of some of the liquids had experienced a depletion event (probably a partial melting event) resulting in TiO_2 depletion, prior to an episode of enrichment in LREE and other trace elements. Less primitive liquids apparently may lack the Ti-depletion, suggesting some were derived from more "normal" upper mantle which did not experience a depletion but which nonetheless was enriched prior to tholeiitic liquid extraction.

The enriching component was probably a fluid or fluid-rich melt (cf. Group A discussion) generated in contact with residual minerals retaining Ti (e.g. for B52) and Nb. It is possible that the influx of the enriching fluid into previously depleted, refractory peridotite may have encouraged melting by depression of the solidus (cf. discussion on ophiolitic basalts; Sun & Nesbitt 1978b). Melting of the enriched-depleted source of Group C tholeiites was apparently at depths less than 60 km in contact with stable residual cpx, but not garnet.

(5) Relationship of dolerites to pyroxene granulites

Although the major elements (Fig. 6.14) and for instance, Zr-Y and Zr-Sc (Fig. 6.8) do not differentiate the dolerites of DK2 from the pyroxene granulites of DK1, element pairs such as Ti-Zr (Fig. 6.7) Zr-Nb, Zr-Sr, Zr-Rb and Zr-Ba (Fig. 6.8) show markedly distinct distributions. The Ti-Zr variation was interpreted above to infer marked source heterogeneity. However the possibility is raised here that metamorphism in the granulite facies might equally account for the variations.

Ti, Zr, and Y are generally considered to be immobile during metamorphism of basaltic rocks (e.g. Pearce & Cann 1973). Zr and Y are coherent for the dolerites and pyroxene granulites and their distribution may be interpreted in terms of igneous processes. If these two are assumed to have been immobile during the granulite facies metamorphism, then relative to Zr (and Y), Ti and Nb and possibly Ce have been enriched in the pyroxene granulites and Ba, Rb, Sr and probably K_2O have been depleted. Alternatively if Ti has been immobile Zr and Y have been depleted slightly and Ba, Rb, Sr and K_2O more strongly depleted, but the apparent Nb enrichment is more equivocal.

The Group B dolerites and pyroxene granulites suggest that Ti is immobile and correlates well with Nb, Sr, Y, (Fig. 6.7). However similar K_2O , Rb, Ba and probably Sr depletions are observed in the granulites.

These results suggest that during the pyroxene granulite facies metamorphism elemental mobility occurred, especially net depletions of K_2O , Rb, Ba and Sr. Net enrichments are difficult to define but possibly Ce and Nb have been enriched.

(6) Relationship of hornblende granulites to other rocks

Two hornblende granulites (742 and 1396; Appendix Table 6.2) are included in Group C. Bradley (1972) interpreted them to be due to retrogression of pyroxene granulites. Geochemically they tend to be transitional between the dolerites and pyroxene granulites, which suggests they may more likely be "prograde" hornblende granulites.

6.3.6 Summary of enrichment history of sources of Group A, B and C

Despite the fractionated nature of many Group B and Group C rocks it is possible to compare elemental distribution patterns among the three Groups A, B and C. Reference to the extended REE plots (Fig. 6.12) clearly indicates the proposed order of incompatibility of elements is generally appropriate, so that anomalous elemental abundances must be explicable in terms of process and response. Groups A, B and C are clearly dissimilar in absolute abundances, slopes and shapes and with respect to elemental anomalies, and these features presumably represent differences in detailed petrogenesis.

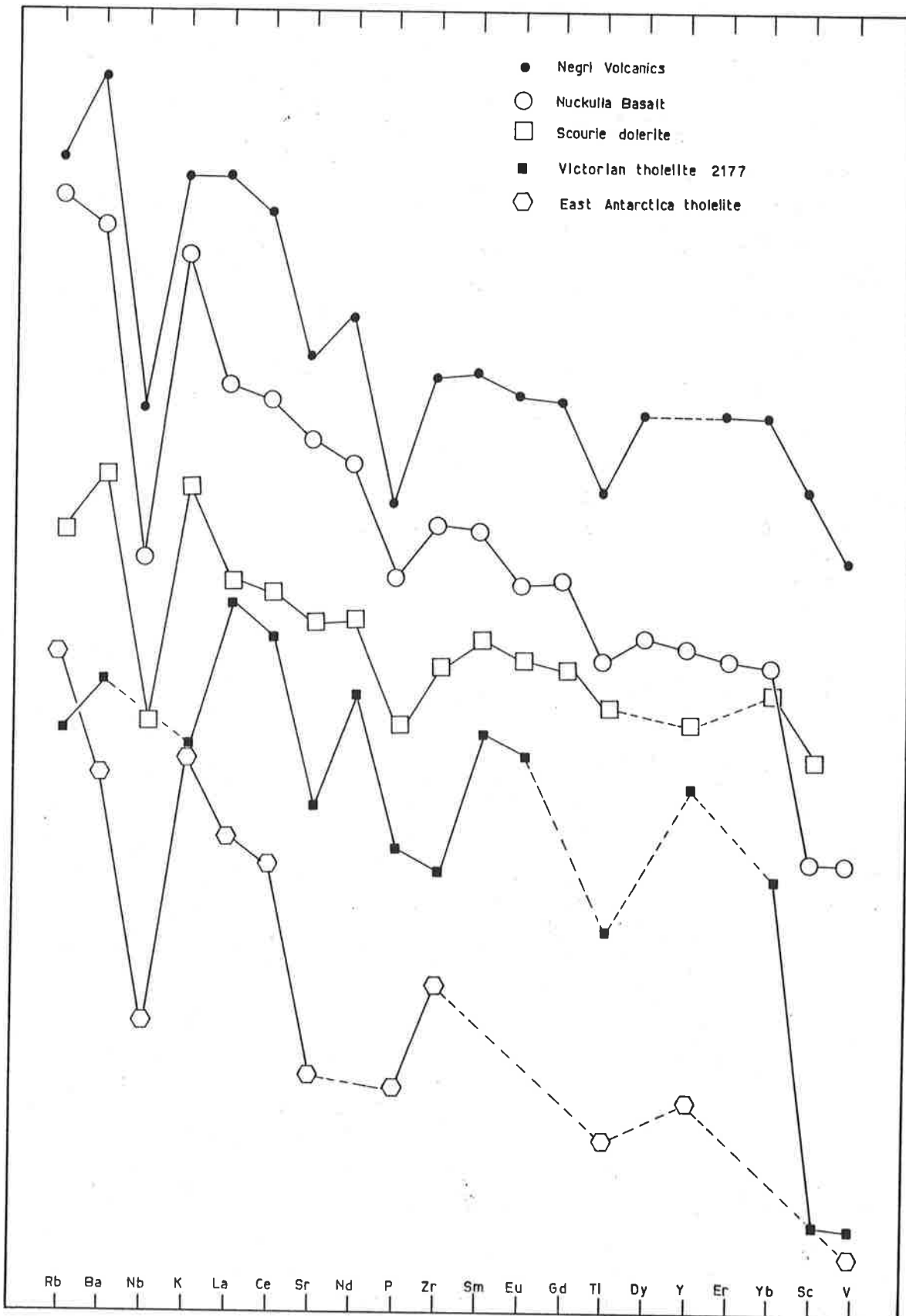


Figure 6-15

Extended REE normalised plots of tholeiites of various ages showing similar anomalous geochemical features to dykes of this present study. (Vertical scale not absolute).

The thrust of arguments concerning Group A and extended to Groups B and C is that the upper mantle source has been enriched in the relatively more incompatible elements, more so than in the less incompatible elements. Moreover marked anomalies in Nb, Ti, Sc and V and possibly Sr and P suggest that these elements are held back to some extent in the residue at the source of the enriching component. Decoupling, during this process, of normally coherent elements such as Ti from Zr and Ti from MREE suggests that residual minerals, at the source of the enriching component, must contain the less enriched element as an essential structural constituent (cf. Sun & Hanson 1975).

A more detailed discussion of the nature and origin of the enriching component will be presented in Chapter 7.

6.3.7 Comparable basaltic rock suites

Tholeiitic rocks enriched in LREE and other incompatible trace elements have been reported from many age provinces and tectonic settings. A brief comparative summary will be presented here to facilitate interpretation of a general model to account for such geochemical characteristics.

(1) Gawler Range Volcanics (GRV)

The Nuckulla basalts and Kokatha basalts of the GRV comprise part of an extensive post-tectonic, bimodal subaerial volcanic suite erupted ca. 200 km north of the present study area at ca. 1.5 Ga. (Giles 1980a,b; Branch 1978; Compston et al. 1966). As such they allow an interesting comparison between the orogenic basaltic magmatism of the present study, and subsequent post-tectonic magmatism. A more complete discussion will be included in Chapter 7.

The Nuckulla basalt has a very similar extended REE plot to that of the Group A tholeiites of this study (Fig. 6.15) although there apparently is no Sr anomaly. Furthermore the Nuckulla is relatively uniformly enriched in all trace elements, possibly due in part to its evolved nature.

(2) Scourie dyke suite, NW Scotland

These 2.4 Ga. largely tholeiitic dykes all show P and Nb anomalies and in some cases small Ti anomalies (Fig. 6.15) which Weaver & Tarney (1981b) attributed to their upper mantle source.

which they concluded had been enriched up to 500 Ma earlier.

(3) East Antarctic dykes

Sheraton & Black (1981) reported 2.4 Ga and 1.2 Ga dyke suites in East Antarctica which have similar geochemical characteristics to the dykes of the present study (Fig. 6.15). These authors suggest the earlier group reflect mantle enrichment immediately prior to their generation ($IR = 0.7020 \pm 8$) whereas the elevated IR of the younger group (0.7041 ± 5) allows the possibility that they were generated from a long-term enriched source (perhaps the same source as the earlier group).

(4) Negri volcanics, Pilbara region

Sun & Nesbitt (1978a) described Archaean basalts which are similar in many respects to Group A tholeiites (Fig. 6.15). Unpublished experimental work of these authors and geochemical interpretation led them to propose that the Negri volcanics were derived from shallow melting of a LREE-enriched upper mantle.

(5) Gondwanaland tholeiites

Kyle (1980) has interpreted the LREE enrichment and elevated $IR = 0.7115 \pm 12$ of Jurassic tholeiites from Antarctica and Tasmania in terms of a heterogeneously, long-term enriched upper mantle source.

(6) Victorian tholeiites

Cainozoic tholeiite 2177 from Victoria (Frey et al. 1978) shows a similar anomaly pattern to Group A tholeiites of this study (Fig. 6.15).

(7) Project FAMOUS tholeiites

In contrast to the studies reported above, Langmuir et al. (1977) attribute the variation in geochemistry of LREE-enriched to LREE-depleted modern MORB in the FAMOUS area, to dynamic melting of a homogeneous mantle source. Some FAMOUS MORB have Ti- anomalies. However Langmuir et al. (1977) suggested the constancy of La/Ce, Zr/Nb, K/Ba and $87Sr/86Sr$ precluded source heterogeneity in the FAMOUS area.

(8) Newfoundland (?) oceanic volcanics

In similar vein to Langmuir et al. (1977), Strong & Dostal (1980) attributed the 0.75 Ga (?) oceanic tholeiites of S.E. Newfoundland, some of which have LREE enrichment and Ti, Nb and P anomalies, to dynamic melting of a single homogeneous source region. The mantle source was suggested to have chondritic relative REE abundances.

(9) Discussion

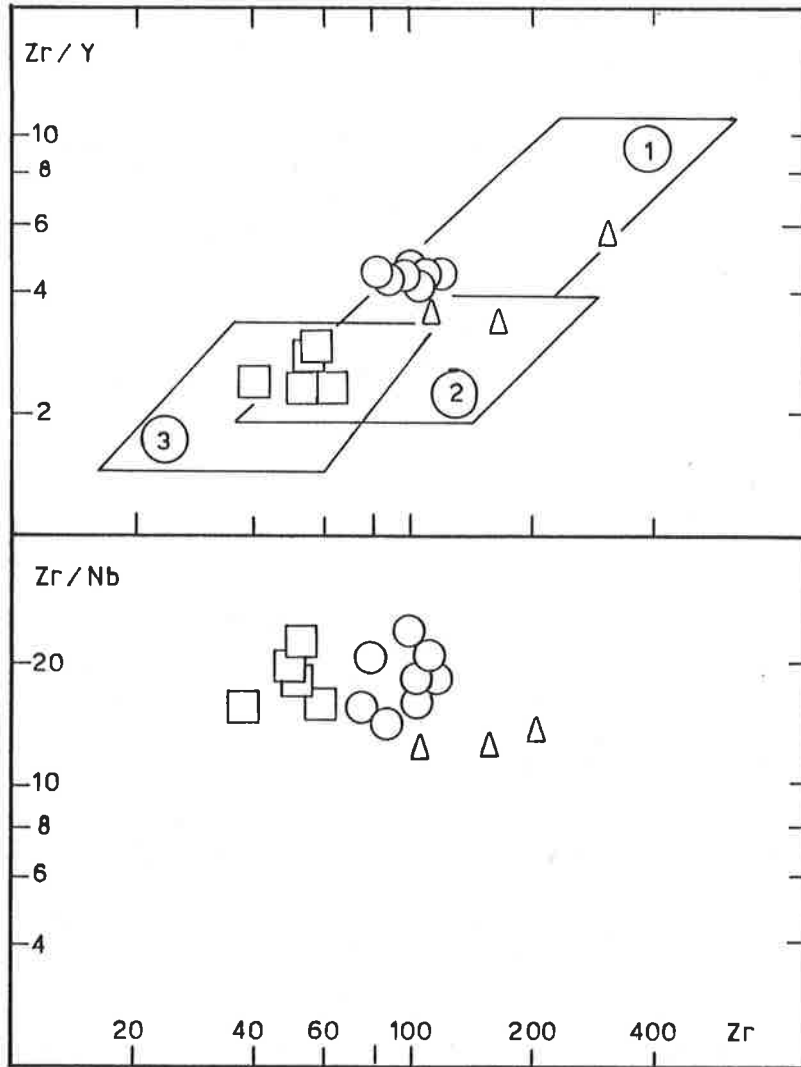
LREE-enriched tholeiitic volcanics and intrusives with $Ti + Nb + P$ etc. anomalies have been reported from continental and oceanic environments of widely ranging age from the Archaean to the modern day. Most studies have ascribed the suites to enriched mantle sources.

The alternative dynamic melting model predicts a progressive temporal depletion in LREE, and a relative constancy of La/Ce, Zr/Nb K/Ba and $87Sr/86Sr$, features which are not observed in the Gawler domain tholeiites (e.g. Appendix Table 6.4). For this reason it is difficult to escape the conclusion that the Gawler domain tholeiites have been derived from a heterogeneous, enriched upper mantle source.

6.3.8 Retrogression of dolerites to amphibolites

Some DK1 dykes of Groups A and B in particular show amphibolite facies assemblages apparently coeval with pyroxene granulites and hornblende granulites. The primary fractionating ferromagnesian minerals of Groups A and B are dominated by pyroxenes and the dykes were almost certainly emplaced at considerable depth in the crust. Following initial high-temperature crystallisation the dykes have been suggested to have cooled near-isobarically to the prevailing local P, T and pH_2O conditions. It has furthermore been suggested above (Chapter 1, 2 and Section 6.2) that influx of fluids adjacent to the Kalinjala Mylonite Zone has produced the amphibolisation of mafic dykes and granitoid gneisses. This amphibolisation process has been shown briefly to be accompanied by geochemical changes.

If Ti is considered immobile (Pearce & Cann 1973; Field & Elliott 1974), Zr and Y are relatively enriched in the amphibolites over the dolerites (Fig. 6.7) in Groups A and B. Relative to Zr,



- ① within plate
- ② MORB
- ③ Island arc

Figure 6.16 Zr-Zr/Y and Zr-Zr/Nb diagrams for unaltered tholeiitic dolerite dykes of the present study, compared to the fields of modern volcanics of known geotectonic settings (after Pearce & Norry 1979).

Ba and Rb tend to be enriched but Nb coherent with Zr in the amphibolites (Fig. 6.8). This order of enrichment is similar to the order of incompatibility of minor elements on the extended REE plots (Fig. 6.11). Furthermore the Group B amphibolites tend to be displaced towards the Group A amphibolites (especially Zr-Rb, Fig. 6.8; Ti-Y, Fig. 6.7). These relationships suggest to the present author that the retrogressive fluid had a similar geochemical character to the enriching component in the Group A tholeiite mantle source. It is thus considered most likely that the retrogressive fluid emanated from the mantle (cf Weaver & Tarney 1981b; Drury 1973) and may reflect mantle outgassing.

Group A amphibolites on Yorke Peninsula are not enriched over the tholeiites. Retrogressive fluid enrichment is thus apparently regionally spatially located adjacent to the Kalinjala Mylonite Zone. The mylonite zone apparently has acted as a conduit for the channelling of mantle derived retrogressive fluids.

6.3.9 Tectonic environment of Groups A, B and C tholeiites

Following Pearce & Cann's (1973) attempt to distinguish the tectonic environments of modern basaltic volcanics on the basis of their immobile trace element contents, it has been shown that continental tholeiites are not discriminated (Holm 1982). Most continental tholeiites plot in the fields of ocean-floor basalts or calc-alkali basalts (Holm 1982) as do the tholeiites of Groups A, B and C. However, Pearce & Norry (1979) have shown that useful petrogenetic information can nonetheless be derived from the elements Ti, Zr, Y, and Nb. The following discussion is based on discussion in Pearce & Norry (1979).

(1) Zr/Y ratio

The Zr/Y - Y plot (Fig. 6.16) shows that the Groups A, B and C data define a trend towards source enrichment, whereas the subhorizontal distributions within Groups B and C are consistent with fractional crystallisation.

(2) Zr/Nb ratio

Pearce & Norry's Kd data show that this ratio is insensitive to the degree of partial melting, and hence its variation is most likely to reflect source heterogeneity. Their observed tenfold difference in Zr/Nb between the most enriched and most depleted lavas (Fig. 6.16) cannot be modelled on melting processes. Rather

Table 6.12 Rb-Sr isotopic data for selected basaltic dykes

Sample	87Rb/86Sr	87Sr/86Sr
(a) <u>Group A - petrographic category 1</u>		
B58	0.4912	0.71577 ± 6
B69	0.3684	0.71318 ± 6
B16	0.4773	0.71544 ± 34
(b) <u>Group A - petrographic category 2</u>		
B26	0.2713	0.71087 ± 4
(c) <u>Group B - petrographic category</u>		
B36	0.3695	0.71230 ± 5
(d) <u>Group C - petrographic category</u>		
B52	0.4453	0.71246 ± 15

Calculated isochron for Group A petrographic category 1

MSWD = 0.05 Model 1 1463 ± 1400 Ma 0.70544 ± 90

Calculated isochron for all Group A specimens

MSWD = 0.37 Model 1 1539 ± 251 Ma 0.70493 ± 145

Explanatory notes:- (1) 87Sr/86Sr precision ± 20m

(2) 87Rb/86Sr precision ± 0.5% (20m)

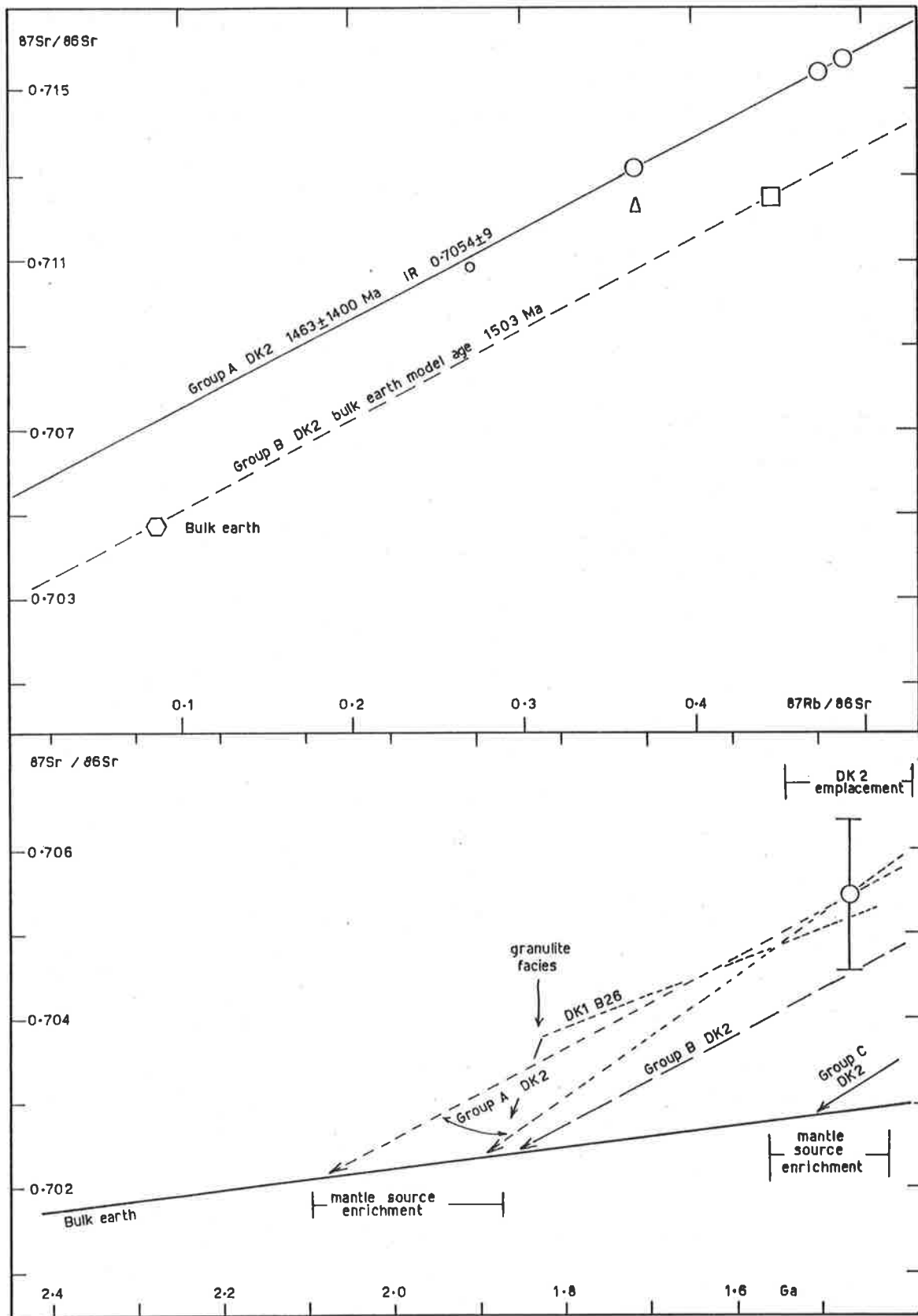


Figure 6.17

Isochron diagram and Sr-isotope evolution diagram for tholeiitic dolerite dykes of present study. Symbols as in Figure 6.4.

fluid transfer in the upper mantle may be required.

The simple conclusion of this section is that the Pearce & Cann (1973) approach is not a reliable indicator of tectonic environment. Information can be derived however from the elements Ti, Zr, Y and Nb which is helpful to define petrogenetic processes; but these processes cannot be uniquely linked to geotectonic environments.

More detailed discussion of the tectonic environment of the basaltic melts of this study will be presented in Chapter 7.

6.4 SR-ISOTOPE GEOCHEMISTRY

6.4.1 Introduction

Giddings & Embleton (1976) have cited unpublished Sr-isotopic data which suggest that the two groups of basaltic dykes distinguished by them on the basis of their palaeomagnetic measurements, may have been emplaced at 1700 ± 100 Ma and 1500 ± 200 Ma respectively. It is thought likely by the present author that these two groups correspond to DK1 and DK2 dykes respectively.

In order to investigate the possible age and Sr-isotopic relationships of both DK1 and DK2 dykes and geochemical groups A, B and C above, a few selected specimens have been analysed (Table 6.12) and are discussed below.

6.4.2 Group A basaltic dykes

6.4.2.1 DK2 dykes

Two near-primary specimens (B58 and B69) and one evolved rock (B16) were analysed (Table 6.12) and plotted on an isochron diagram (Fig. 6.17). A perfect fit line with a calculated age of ca. 1463 Ma is obtained though it is based on only a limited range in Rb/Sr ratio and is thus imprecise. This indicated age is similar to the younger age reported by Giddings & Embleton (1976).

The calculated IR of 0.70544 ± 90 also is imprecise due to the extrapolation to the $^{87}\text{Sr}/^{86}\text{Sr}$ axis by a factor of ca. 3X the total variation in Rb/Sr ratio, but is well-enough defined to demonstrate that the Group A tholeiites at ca. 1500 Ma were enriched in $^{87}\text{Sr}/^{86}\text{Sr}$ relative to an upper mantle source representative of the model bulk earth (Fig. 6.17). Bulk earth model ages for the near primary B58 and B69 are 1896 Ma and 2081 Ma respectively. Partition coefficient data (Frey et al. 1978) show that the fractionation of

Rb/Sr ratio in melt over residue for a 70 ol + 25 opx + 5 cpx residue (Table 6.7) after ca. 30% partial melting is less than 3%. An ol + opx residue produces even smaller Rb/Sr fractionation in the melt. Hence the model ages are likely to represent the age of the production of the mixed source of Group A tholeiites from an assumed bulk earth composition. Hence enrichment of this mantle source is likely to have occurred early in the Kimban Orogeny, perhaps associated with the initiation of mantle outgassing from deep in the mantle.

6.4.2.2 DK1 dykes

One specimen (B26) of fractionated liquid from this category was analysed (Table 6.12, Fig. 6.17). This sample plots very close to the isochron defined by the three DK2 samples, and the four samples define a perfect fit isochron (MSWD = 0.37) of calculated age 1539 ± 251 Ma and IR of 0.70493 ± 145 (Table 6.12).

The poor precision in the calculated age allows the possibility that rocks of quite different crystallisation ages may be collinear within experimental error. The uncertainty spans the whole period of the Kimban Orogeny, ca. 1900 Ma to ca. 1400 Ma (Thomson 1980). Thus if the mafic granulite (B26) behaved as an open system at some stage during this period it may still appear to fit well on the short isochron plot.

Of more interest is the very similar $^{87}\text{Sr}/^{86}\text{Sr}$ ratios shown by the granulite and the dolerites. The coherent geochemistry of Group A dolerites and granulite suggests a very similar source composition enriched in trace elements such as Rb and Sr (see above). The Sr-isotope evolution of all four Group A tholeiites is depicted in Figure 6.17. Calculations (above) demonstrate that the Rb/Sr of the melt is very likely to represent closely the ratio of the source (unless modified by fractional crystallisation of e.g. plagioclase or fractionation by granulite facies metamorphism (cf Heier 1973)). The three dolerites intersect the bulk earth model curve between ca. 1880 Ma and 2070 Ma but the basic granulite (B26) intersects at ca. 2300 Ma. The Rb/Sr ratio of B26 is much lower than that of the dolerites and probably reflects Rb depletion during granulite facies. If this conclusion is accepted then calculation of the Rb/Sr ratio of B26 prior to metamorphism may be attempted. On the basis of the major element model for B26 (Table 6.4) by fractionation of plag + opx + cpx from B69, and

using the K_d 's of Arth (1976; Appendix Table 6.6) a Rb/Sr in B26 liquid of ca. 1 may be calculated. If metamorphism is assumed to have occurred at ca. 1800 Ma a Sr-isotope evolution curve for the B26 liquid may be plotted (Fig. 6.17). This intersects the bulk earth curve at ca. 1900 Ma, within the range of dolerite intersections.

This allows an interpretation of Rb-Sr systematics of Group A as follows :-

- (1) bulk earth reservoir up to ca. 2000 Ma
- (2) generation of enriched upper mantle reservoir
ca. 2000 Ma; Rb/Sr ratio ca. 0.15
- (3) enriched source melting ca. 1800 Ma and
emplacement of DK1 dykes; IR ca. 0.703,
Rb/Sr ca. 0.2 - 1.0; followed by Rb
depletion in granulite facies producing
Rb/Sr ca. 0.05 - 0.10
- (4) melting of the same or a similar enriched
source ca. 1500 Ma and emplacement of DK2
dykes; IR ca. 0.7045 - 0.7055 and Rb/Sr of
ca. 0.15 - 0.25.

Such an interpretation suggests that relatively long-lived mantle heterogeneities existed in the mantle underlying the Gawler domain during this interval of Earth history. Furthermore it appears that the enriched sources were established from a pre-existing bulk earth model reservoir at the beginning of the Kimban Orogeny and do not represent older Archaean pre-history.

6.4.3 Group B basaltic dykes

One specimen only (B36) of Group B least fractionated tholeiite has been analysed (Table 6.12; Fig. 6.17). Relative to Group A tholeiites it has lower present day $^{87}\text{Sr}/^{86}\text{Sr}$ but a similar Rb/Sr ratio. The specimen is a DK2 dyke and has suffered no Rb depletion by metamorphism, but is fractionated so that its Rb/Sr ratio is probably higher than its source. Nonetheless its bulk earth model age ca. 1850 Ma is not far removed from those of Group A. Hence it is suggested that Group B tholeiites represent partial

melts of an enriched source which was developed at a similar time to the Group A source (ca. 2000 Ma), with a lower Rb/Sr ratio.

6.4.4 Group C basaltic dykes

Only one specimen (B52, Table 6.12) from Group C has been analysed. Interpreted above as a near primary liquid and intruded late this specimen was possibly generated in the same melting episode as Group A DK2 dykes.

Its Rb/Sr ratio is similar to that of Group A but present day $^{87}\text{Sr}/^{86}\text{Sr}$ is much lower at 0.71246 ± 15 . The bulk earth model age calculated at 1503 Ma is very similar to the isochron age for Group A.

However, the Sr-isotope evolution curve (Fig. 6.17) illustrate its very different isotopic history.

If emplaced at ca. 1500 Ma, B52 must have been derived from an almost unmodified model bulk earth reservoir. However, its trace element, especially LIL-element, geochemistry (see above) suggests that the source of B52 had been enriched. These two constraints suggest that the enrichment must have occurred at or near the time of partial melting. This suggests a two-stage enrichment for the Proterozoic sub-continental mantle in this area.

Furthermore the geochemistry of B52 has been interpreted to suggest that the enriched source had experienced a previous depletion event (see above). The bulk earth, essentially unmodified, IR of B52 then constrains the time of this depletion to be very close to the time of partial melting as well.

Alternatively the bulk earth model IR could be the fortuitous result of depletion and enrichment changes in Rb/Sr ratio at unspecified times which exactly cancelled each other and restored, at ca. 1500 Ma, a bulk earth IR value. This alternative is unable to be ruled out on the basis of the meagre data but is considered highly improbable.

6.4.5 Summary

The Sr-isotope data confirm the geochemical conclusion that Group A and Group B tholeiites have been derived from distinct, modified, enriched upper mantle sources. The enrichment occurred at ca. 2000 Ma early in the Kimban Orogeny and was not a relic of Archaean pre-history or mantle evolution.

Group C tholeiites appear to have been derived from a source having an unmodified bulk earth model Sr-isotopic composition, late in the Kimban Orogeny. This constrains the depletion and subsequent re-enrichment processes which have occurred in the Group C source, to have taken place close to the time of melt generation.

Two events of mantle enrichment are therefore proposed in the Kimban Orogeny between ca. 2000 Ma and ca. 1400 Ma, resulting in a Gawler domain heterogeneous Proterozoic sub-continental mantle.

CHAPTER 7.EARLY TO MIDDLE PROTEROZOIC CRUSTAL EVOLUTION.7.1 INTRODUCTION

Of recent years much attention has been directed towards an understanding of the Earth's recent geological history and the formulation of plate tectonic concepts, as well as the unravelling of the Earth's distant past in the Archaean cratons. Comparatively little attention was paid for many years to the intervening Proterozoic Era. A fundamental question relating to Proterozoic crustal evolution is to what extent new crust has been formed from the upper mantle or, conversely, to what extent Proterozoic crustal rocks represent reworked Archaean sial.

Many authors have suggested that the Earth's crust and upper mantle have become irreversibly and episodically differentiated over geological time and that as a consequence the continents have grown with time. Plate tectonic concepts have been applied to suggest that continental growth has taken place largely by the accretion of island arcs (Taylor & White 1966; Taylor 1967; Taylor & McLennan 1979; and review of Ringwood 1975) or calc-alkaline batholiths of Cordilleran fold belts (Windley & Smith 1976; Tarney 1976; Tarney & Windley 1979). Some authors have recognised in isotope age data the episodic nature of crustal growth (Hurley & Rand 1969; Moorbath 1977, 1978). In such an interpretation, major Precambrian periods of juvenile addition of sialic crust from the mantle or mantle-derived precursors are thought to have occurred in the Precambrian at 3.8 - 3.5 Ga, 2.8 - 2.6 Ga and 1.9 - 1.6 Ga (Moorbath 1978). The last of these is coincident with the Kimban Orogeny of this present study. Proponents of this model usually favour the permanence of continental crust and do not favour the recycling of large amounts of sial into the mantle.

Such a model does not rule out the likelihood that the newly formed sial may undergo internal metamorphic, anatectic and geo-chemical differentiation over a period of tens of millions of years to produce a multistage complexity, but does deny the possibility of production of vast amounts of juvenile calc-alkaline material from much older continental crust (e.g. Moorbath 1978).

An alternative crustal accretion process, particularly relevant to intracontinental (or intraplate) environments has been proposed by Wass & Hollis (1983) who note that xenoliths in continental basalts often require a substantially basaltic lower crust (cf. Griffin et al. 1979; Arculus & Smith 1979). They suggest that successive ultramafic and mafic intrusions may be emplaced deep in the lower continental crust, thickening the crust by underplating, and subsequently metamorphosed in the granulite and eclogite facies. Wyborn & Page (1983) suggested that granitoid magmas may be derived by remelting of such underplated mafic material.

In the light of these considerations, it is important to establish whether the Proterozoic terrain which is the subject of this thesis does in fact represent the addition of island arc or Cordilleran calc-alkaline material or material of another kind. This question will be examined below.

An alternative view of Earth history, championed especially by Armstrong (e.g. 1968, 1982), has proposed that the Earth suffered an early, major, planetary differentiation into primitive core, mantle, crust and surface fluids. A tectonic regime, similar in kind to modern plate tectonics, is envisaged to have existed within the Earth since at least ca. 3.9 Ga and to have continuously recycled large amounts of continental sial back into the mantle by sediment subduction. In this model the continents are not considered to have grown significantly in volume since ca. 3.9 Ga, although a progressive cratonisation and decreasing rate of recycling is envisaged.

Both the continent growth and no-growth schools integrate their interpretations essentially into a near-Uniformitarian plate tectonic scheme. Still other authors (e.g. Wynne-Edwards 1976; Kroner 1977; Glikson 1976) have proposed that significant secular variations in tectonic style have occurred. In this interpretative scheme the Proterozoic is suggested to be distinct in tectonic style from both the Archaean and Phanerozoic, and to involve largely ensialic, intracontinental or intracratonic mobile belts of rift-valley type.

In this chapter I will seek to draw together the petrological, petrochemical, age and Sr-isotopic data for the granitoid gneisses and metabasaltic dykes of the present study and to answer the following questions :-

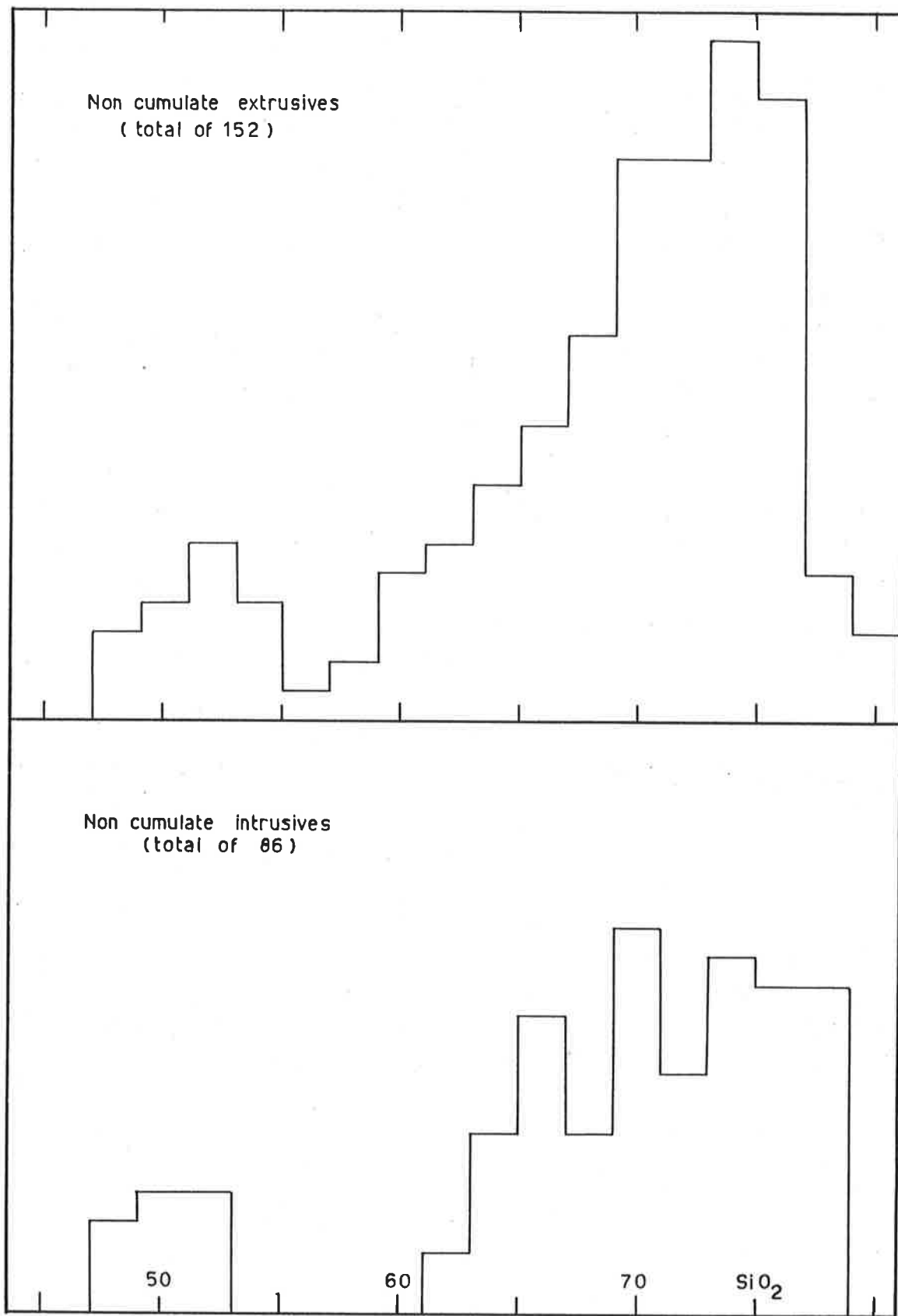


Figure 7.1 Histograms of SiO₂ contents of Gawler domain non-cumulate intrusive and extrusive magmatic rocks.

1. Does the Early to Middle Proterozoic of the study area represent a marginal plate tectonic setting or an intracontinental ensialic orogen?
2. Is there a large addition of juvenile sial at this time?
3. How does the study area relate to the Gawler domain as a whole?
4. What implications do the conclusions of this study have for global Proterozoic interpretation?

To this end the rock suites described and characterised in previous chapters, will be compared with each other, and with the well-documented 1.5 Ga Gawler Range Volcanic province (Fig. 1.1; Giles 1980a,b; Branch 1978) to assess the temporal evolution of the Gawler domain. Then a model will be erected to account for the variation, which will be tested against the various tectonic and petrogenetic schemes above, and assessed on the basis of occurrences of Proterozoic terrains on the Australian and other continents.

7.2 PETROGENESIS OF BASALTIC AND GRANITOID MAGMAS OF THE STUDY AREA AND GAWLER RANGE VOLCANICS

7.2.1 Bimodal magmatism

The histogram of SiO_2 contents of the non-cumulate rocks of the study area reveals a marked bimodality (Fig. 7.1). A similar trend is apparent for the Gawler Range Volcanics (Fig. 7.1). This feature has been considered to be typical of anorogenic cratonic magmatism (Emslie 1978; Christiansen & Lipman 1972; Lipman et al. 1972; Martin & Piwinski 1972) in contrast to the orogenic regions of dominant calc-alkaline intermediate magmatism. This conclusion is not surprising for the post-tectonic platform cover Gawler Range Volcanics, but more notable for the rocks of the present study area, many of which were emplaced during the Kimban Orogeny. It is suggested here that the Early to Middle Proterozoic magmatic rocks of the present study area may not be related to a simple calc-alkaline subduction environment analogous to modern Cordillera or island arcs, but to reflect a significant rifting component (e.g. Emslie 1978).

A tectonic model to account for the evolution of the present study area will be examined in more detail in a later section of this chapter. This section will enlarge upon the petrogenesis of

the mafic and silicic components of the bimodal suite of magmas.

7.2.2 Petrogenesis of basaltic magmas

(1) Basaltic dykes of the study area

Detailed arguments have been presented in Chapter 6 which seek to describe the nature of igneous mineralogical, geochemical and Sr-isotopic variation within the basaltic dykes of the study area. These will not be duplicated here, but a summation of the chief conclusions and some further discussion will be presented.

The tholeiitic liquids have been concluded to have been derived by high degree partial melting at depths less than ca. 60 km of a pyrolite upper mantle which had suffered variable enrichment in many trace elements. The enriching component for Groups A and B tholeiites apparently was generated early in the Kimban Orogeny and altered an upper mantle source region in which the Sr-isotopes previously evolved similarly to the model bulk earth. A third group (C) of tholeiites was apparently derived from a mantle source which may have evolved similarly to the model bulk earth until late in the Kimban Orogeny, but which immediately before partial melting experienced first a depletion and then a re-enrichment process. These conclusions suggest that the Proterozoic basaltic magmatism tapped a mantle source which itself had not previously been involved in magma generation nor enrichment processes.

The characteristics of the enriching component are variable for the three individual geochemical groups of basaltic dykes, but two important characteristics are,

- (1) decoupling of Ti and Zr, apparently reflecting a residual Ti mineral at the source of the enriching component
- and (2) relative depletion of Nb.

(2) Basaltic volcanics of the Gawler Range Volcanics

In Chapter 6 these tholeiitic volcanics were briefly compared with the basaltic dykes of the study area and shown to be very similar in many key geochemical characteristics. In particular the Ti-Zr, and Nb relationships are closely similar to the dykes.

Giles (1980a,b) proposed that the basaltic volcanics were derived by hydrous, shallow melting of variably enriched pyrolite upper mantle. However, he also proposed that the basaltic

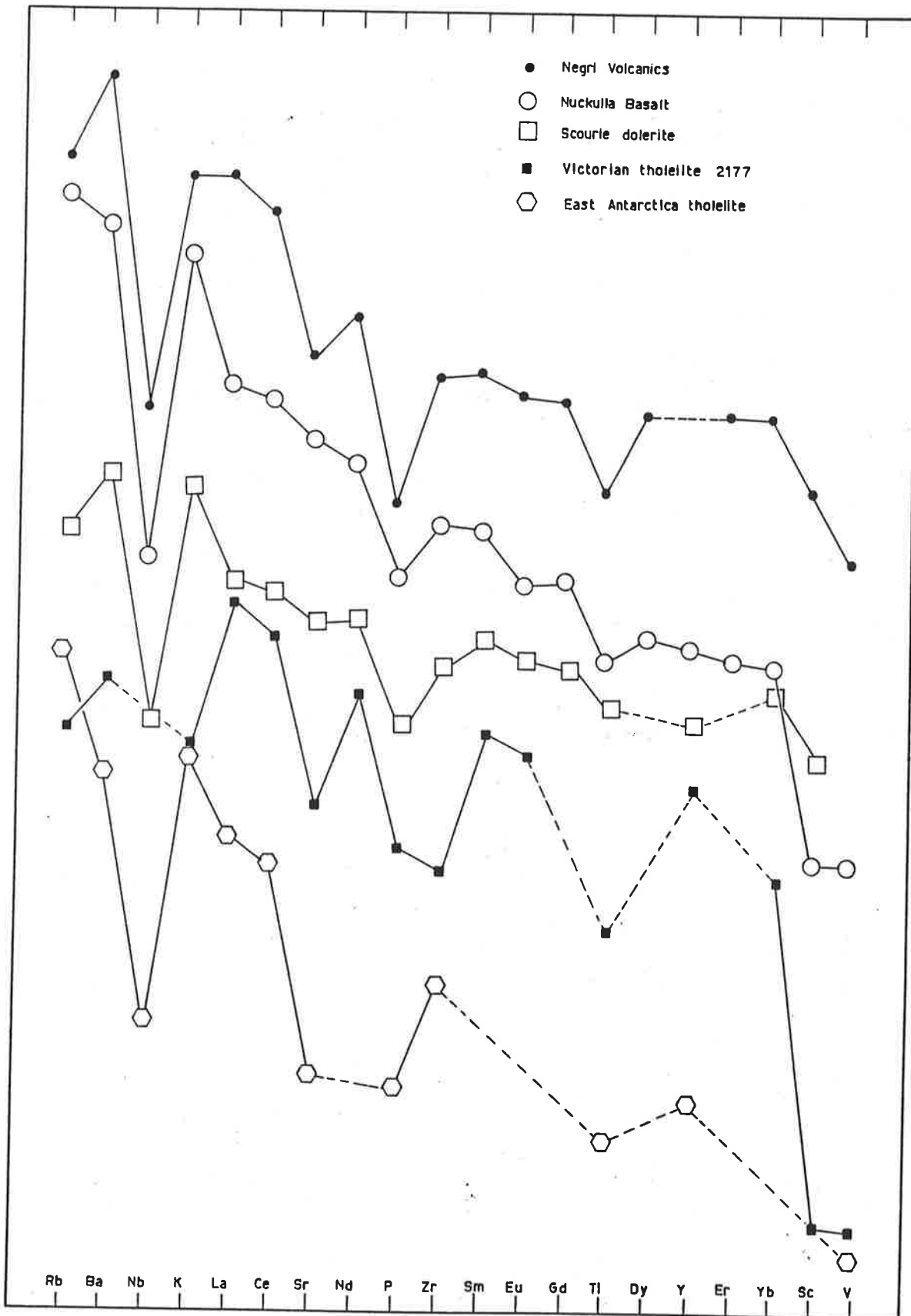


Figure 6-15

Figure 7-2

Extended REE normalised plots of tholeiites of various ages showing similar anomalous geochemical features to dykes of this present study. (Vertical scale not absolute).

volcanism was reflecting melting in a long-lived Proterozoic low velocity zone (LVZ) or layered upper mantle, that may have been formed initially in the Archaean. The Sr-isotopic data for the basaltic dykes of the present study do not allow such a long-lived enriched source for either the early (DK1) or late (DK2) dykes, and it is therefore suggested here that such a situation is unlikely for the GRV. Indeed it is probable that the post-metamorphic (DK2) dolerite dykes and the basalts of the GRV are of the same age and may manifest the same source and melting event.

It is most significant that the orogenic granulite DK1 dykes and the post-tectonic DK2 dolerite dykes of the present study area as well as the basaltic GRV show such similar geochemistry. This strongly suggests that the petrogenetic processes involved in their generation are not specific to any particular stage in the development of the Kimban Orogeny but were apparently occurring throughout, and hence are more likely to represent a specific ongoing process rather than a unique tectonic event or environment. The specific process will be discussed more fully below.

(3) Geochemically analogous tholeiites

In Chapter 6 a brief comparison was presented between the Gawler domain tholeiitic volcanic and dyke rocks and geochemically analogous continental tholeiitic rocks of Archaean to Cainozoic age. All of the other suites show the Nb anomaly and many show the Ti anomaly characteristic of Group A tholeiites of the present study, as well as LREE enrichment (Fig. 7.2). In each of these other studies, these distinctive characteristics were attributed to the LREE enriched nature of the upper mantle source of the tholeiitic liquids. A number of authors attributed the LREE enrichment to metasomatism of the upper mantle by hydrous fluids (e.g. Sheraton & Black 1981; Weaver & Tarney 1981b) which were rich in LREE and other trace elements, especially LIL-elements.

The Nb anomaly also was attributed by Weaver & Tarney (1981b) to the stabilisation of rutile by high pO_2 in the presence of H_2O in the metasomatised upper mantle source of the tholeiitic liquids. They noted the likely role of H_2O in the upper mantle in the vicinity of subduction zones in island arcs or possibly back-arc basins.

(4) Discussion of subcontinental mantle metasomatism

Earlier proponents of the metasomatism of subcontinental upper mantle sources of tholeiitic liquids favoured a hydrous fluid (e.g. Weaver & Tarney 1981b). Inspection of the phase relations in pyrolite at pressures in excess of 30 kb with 0.2% H₂O shows that ilmenite is a super solidus phase up to 150°C above the solidus (Green 1973). Incipient volatile-rich melts at this depth will have residual ilmenite and so may be depleted in Ti and possibly Nb. Also at these melting conditions phlogopite and garnet and clinopyroxene are stable supersolidus phases (Green 1973) so that the resulting melt would be LREE enriched but HREE, Sc, V, K, Rb and Ba depleted. The expected K, Rb and Ba depletion is not observed in Group A tholeiites of this study. However, under H₂O-saturated conditions at similar depth phlogopite disappears from the residual assemblage immediately above the solidus, but ilmenite may coexist with cpx + garnet up to 40°C above the solidus (Green 1973). An initial melt generated under H₂O-saturated conditions would be K, Rb and Ba as well as LREE enriched.

If such a low degree partial melt from relatively deep in the subcontinental mantle were able to rise to shallower depths less than ca. 60 km, it would be able to significantly enrich the upper mantle pyrolite in LREE, K, Rb, and Ba but retain a marked Ti and Nb depletion.

However such a melt is incapable of rising without almost immediately freezing due to release of its volatiles (Bailey 1983). It is thus suggested that a low degree partial melt at depth in the mantle under H₂O saturated conditions, migrating to the immediately overlying upper mantle froze and released its fluid phase which had similar enriched trace element character and was able to similarly enrich the upper mantle source of tholeiites

It is unusual to speculate on the likelihood of water-saturated, subcontinental mantle at depths of ca. 90 km, however it is possible that such an area need not be large or laterally continuous (cf. LVZ model of Green & Liebermann 1976) but could be confined to the head of one ascending mantle diapir, and may possibly represent some deep mantle degassing.

It is furthermore possible to speculate that the P anomaly in some tholeiites may similarly be due to residual apatite in the source of the low degree melt or fluid phase proposed above.

However, residual apatite would require the melting process to occur in disequilibrium because the high partition coefficients for e.g. REE in apatite suggest that the REE would otherwise be reequilibrated and retained in the source.

An alternative disequilibrium melting process, proposed by Campbell & Gorton (1980) and named flash melting, explains the LREE enrichment in basaltic melts such as alkali basalt and kimberlite by melting immediately above the pyrolite solidus (and rapid extraction of melt) of LREE enriched accessory phases, so that the resultant melt has a REE content essentially reflecting the character of the accessory phase. This model has numerous possible variations and could account for the highly discriminating nature of the enriching component in the tholeiite source.

Bailey (1982, 1983) has summarised a wealth of information concerning volatile activity in the mantle and proposed a model to account for upper mantle heterogeneity. Rather than the H₂O-saturated system discussed briefly above, he discussed the dominant role of CO₂ in mantle volatile processes. In essence he noted the grazing incidence of normal continental shield geotherms with the vapour-present solidus for kimberlite at depths between 150 and 200 km. From this he suggested an interpretation of kimberlite activity whereby volatiles migrating up the continental geotherm or some lithospheric weakness cause first metasomatism and then incipient melting in the zone of grazing incidence. On steeper geotherms the first formed melt can rise without freezing and penetrate further above the solidus and grow in volume. At the same time the vapour solubility will decrease with falling pressure, and the rising melt will exsolve vapour, resulting in further melting of the surrounding rocks. Mafic melts may result and finally segregate from their residual minerals at shallower depths ca. 70 - 90 km. These melts will retain the LIL-element signature of the metasomatising fluid.

Wass & Rogers (1980) and Menzies & Wass (1983) also comment on the role of CO₂ in sub-continental mantle metasomatism. They suggest it is a necessary precursor to continental alkaline volcanism and relate it to rifting.

Newton et al. (1980) point out the decrease in CO₂ solubility in basaltic melts at shallower mantle depths, and note the

variability in H_2O/CO_2 possible at different P-T. This has consequence for lower crustal CO_2 flux and the driving out of H_2O from the lower crust (see later - KMZ, tectonics).

The presence of CO_2 -rich fluid inclusions in the opx-granitoids of the DGS (Chapter 2) points to the role of CO_2 in the petrogenesis of at least some magmatic rocks in the present study area.

(5) Specific origins of Group A, B and C

The phase relations of H_2O -saturated and H_2O -undersaturated pyrolite at moderately deep (greater than ca. 90 km) upper mantle conditions (Green 1973) shows that it is possible for such minerals as ilmenite to hold Ti in the residue of very low degree partial melts or aqueous fluids, thus allowing the production of a Ti-depleted fluid-rich component. The present author suggests that this component may ascend and metasomatise shallower mantle source areas. In such a residual ilmenite-bearing assemblage it is also necessary for Groups A and B to have a P-, and a Sr- bearing mineral and for all three Groups a Nb-bearing mineral and for Groups B and C possibly a Zr- bearing mineral. It is most likely that the production of the fluid-rich phase occurred quickly and not necessarily in equilibrium with the residual assemblage because if, for instance, residual apatite accounts for the P-anomaly in Groups A and B it would also be expected to hold back much of the REE if equilibrium was maintained. An analogous process to the disequilibrium flash melting of Campbell & Gorton (1980) is possible.

Moreover the petrogenesis of Group C liquids B52 and 742 seems to require a complicated depletion-enrichment-melting process in the source, a sequence which may well be accommodated in a dynamic evolving upper mantle, where continual upward migration of selectively trace element enriched fluids into melting or previously melted upper mantle source regions may re-enrich and trigger new partial melting events.

The fluid-rich melting conditions suggested in the above account may account for the stability of deeper mantle residual minerals capable of generating the Nb anomaly. It is considered possible by the present author that the proposed fluid-rich conditions may stabilise rutile in preference to ilmenite and that Nb may be retained in residual rutile (partition coefficient

for Nb in rutile = 16; Pearce & Norry 1979). It is noteworthy that Nb anomalies are not present in MORB but are common in island arc basalts, perhaps reflecting the contrasting role of fluids in these tectonic settings.

Giles (1980a,b) also concluded that the GRV tholeiites were derived by moderate degrees of partial melting of shallow upper mantle hydrous pyrolite which had been heterogeneously enriched in many LIL-elements. The residual mineralogy was suggested to be dominated by olivine and opx with a small proportion of cpx. A mantle diapir was believed responsible for the partial melting event.

(6) Concluding statement

The abundant tholeiitic dyke magmatism of the study area testifies to a major Proterozoic disturbance within the sub-continental lithosphere. Pronounced mantle metasomatism, probably linked to mantle degassing of, in particular, CO₂ and H₂O, is suggested to have occurred in at least two episodes. Elsewhere on Gondwanaland similar mantle metasomatic events have been proposed at ca. 2.8(?) Ga (Sun & Nesbitt 1978), ca. 2.4 Ga (Sheraton & Black 1981), ca. 170 Ma (Kyle 1980) and in the Cainozoic (Menzies & Wass 1983). The two latest of these were associated with the rifting and break-up of the Gondwanaland continent. Mantle metasomatism has elsewhere been proposed to be associated with continental rifting environments (e.g. Weaver & Tarney 1981b; Bailey 1983).

7.2.3 Petrogenesis of granitoid magmas

(1) Granitoid magmatism of the study area

The silicic magmatic rocks of the study area show a younging sequence from

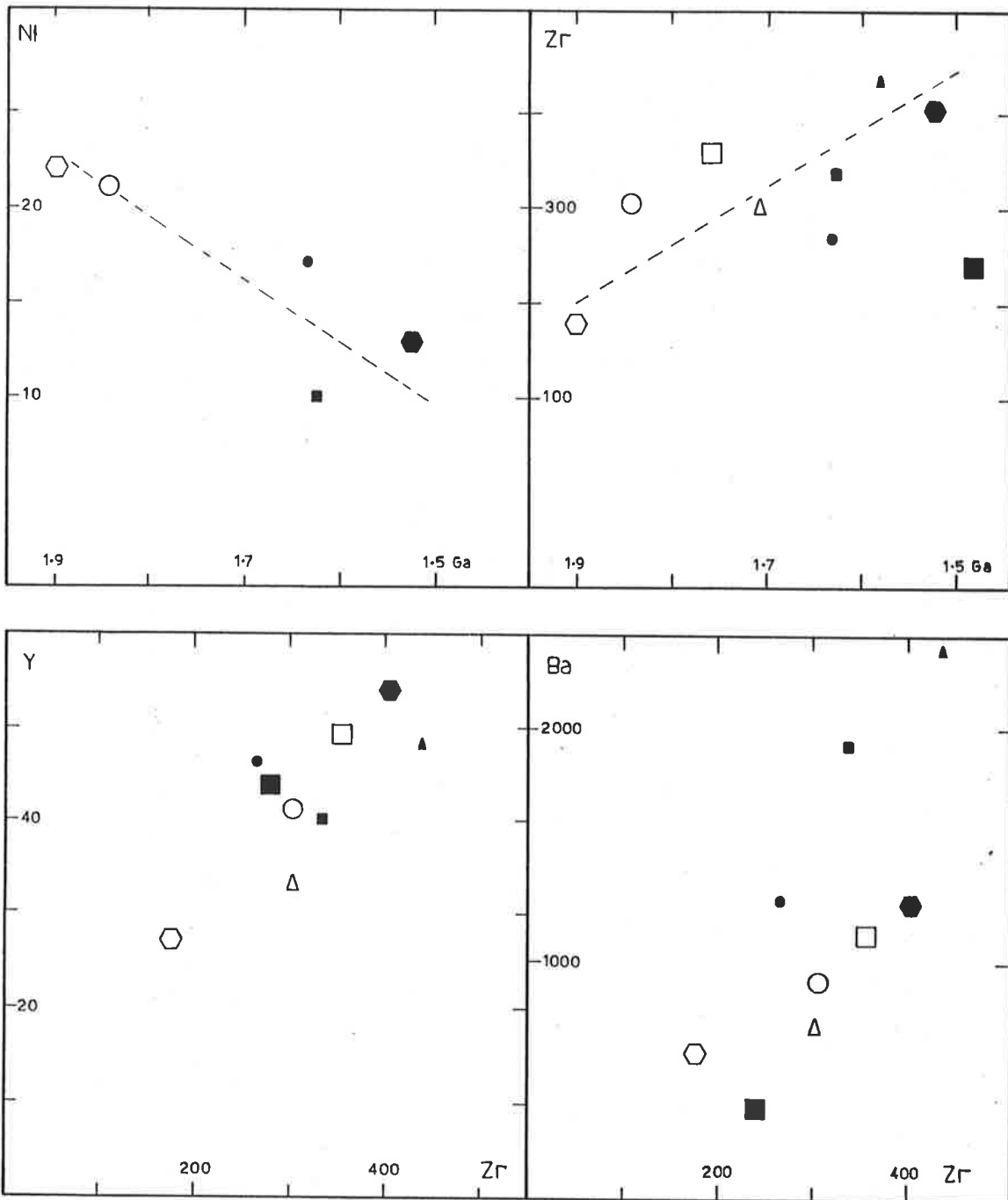
- (1) Massena Bay Quartzofeldspathic gneisses (MBG QF)
- to (2) Donington Granitoid Suite (DGS)
- to (3) Colbert Granitoid Suite (CGS)
- to (4) Moody Granitoid Suite (MGS).

All of these have been suggested in previous chapters to be similar in many respects to I-type granitoids (except the Yunta Well Leucogranite of the MGS which is probably S-type), although perhaps transitional towards A-type. In contrast to the DK1 and DK2

Table 7.1 Geochemical comparison of I-type granitoids of present study and selected volcanics of the Gawler Range Volcanics (GRV) and Central Australian Volcanics (CAV).

	1	2	3	4	5	6	7	8	9	10	11
Age (Ma)	1841	1841+7	1757+14	1709+14	1630(?)	1630(?)		1525(?)	1480(?)	1630(?)	1100(?)
SiO ₂	64.78	68.33	64.42	71.10	64.02	65.98	65.28	66.97	75.81	60.12	67.28
TiO ₂	0.47	0.65	1.03	0.44	1.12	0.72	1.01	0.81	0.21	1.25	0.87
Al ₂ O ₃	15.74	14.67	14.89	14.17	14.30	16.33	15.00	14.21	12.20	15.74	13.02
Fe ₂ O ₃ T	5.44	4.58	6.15	3.53	6.65	4.48	6.15	6.03	1.70	8.49	7.62
MnO	0.08	0.07	0.08	0.06	0.16	0.12	0.16	0.11	0.03		
MgO	2.16	0.97	1.30	0.50	1.80	1.52	2.00	0.93	0.21	2.93	0.69
CaO	3.99	2.82	3.32	1.47	2.97	0.87	2.22	2.55	0.67	4.41	2.69
Na ₂ O	3.52	2.83	2.72	3.05	4.09	4.77	3.12	3.60	3.76	3.79	3.90
K ₂ O	3.36	5.07	5.38	5.23	3.98	4.72	4.51	4.48	5.22	3.57	4.40
P ₂ O ₅	0.11	0.16	0.30	0.25	0.56	0.31	0.36	0.23	0.03	0.43	
Fe/(Fe+Mg)	0.56	0.70	0.70	0.78	0.65	0.60	0.61	0.76	0.80	0.59	0.85
Al ₂ O ₃ /(Na ₂ O+K ₂ O+CaO)	0.94	0.96	0.91	1.06	0.87	1.12	1.07	0.92	0.93	0.87	0.81
K ₂ O/Na ₂ O	0.95	1.8	2.0	1.6	0.97	0.99	1.4	1.2	1.4	0.94	1.1
Sr	209	147	175	190	320	432	338	185	59	308	
Ba	623	915	1113	725	1261	1932	3250	1253	390	1000	
Zr	176	305	357	302	264	337	439	402	239	294	
Nb	12	16	21	25	17	16	15	21	22	13	
Y	27	41	49	33	46	40	48	54	44	42	
Sc	18	13	15	7	17	11	17	13	4		
V		4			105		79	39			
Ni	22	21			17	10		13			
Cr		12	6				14				
(La)N	121	190	219	324		203	163	216	229		
(Eu)N	17	25	26	19		35	37	32	6.4		
(Yb)N	12	21	20	15		14	18	24	29		
(La/Sm)N	4.0	3.7	3.6	5.5		3.7	3.0	3.8	4.3		
(Yb/Gd)N	0.59	0.62	0.46	0.36		0.44	0.50	0.59	0.77		

1. QF MBG Av. of 8
2. FGG1 DGS Av. of 7
3. hornblende granite CGS Av. of 4
4. adamellites MGS Av. of 5
5. Childera Dacite GRV Av. of 5 (Giles 1980)
6. Bunburn Dacite GRV Av. of 9 (Giles 1980)
7. Wyeela Dacite GRV Av. of 2 (Giles 1980)
8. Yardea Dacite GRV Av. of 3 (Giles 1980)
9. Hiltaba Granite GRV Av. of 3 (Giles 1980)
10. Andesite GRV (Giles 1980)
11. dacite CAV (Giles 1980)



- | | | |
|------------|-------------------|-------------------|
| ○ MBG QF | △ MGS adamellites | ▲ Wyeela Dacite |
| ○ DGS FGG1 | ● Chlidera Dacite | ● Yardea Dacite |
| □ CGS | ■ Bunburn Dacite | ■ Hiltaba Granite |

Figure 7.3 Comparison of selected geochemical indicators in the I-type granitoids of the present study with selected Gawler Range Volcanics and the Hiltaba Granite (after Giles 1980).

basaltic dyke rocks, the granitoids show clear temporal geochemical variations (Table 7.1; Figs. 7.3, 7.4, 7.5, 7.6).

There is significant variation in the range of SiO_2 contents in the four suites (Fig. 7.4), but the minimum SiO_2 content of the I-type non-cumulate granitoid rocks is closely similar at ca. 62% to 65%. The suites plot in almost coincident fields on an AFM diagram (not shown), although marked variation in the $\text{K}_2\text{O}/\text{Na}_2\text{O}$ ratio is apparent (Table 7.1). This variation in alkali elements is also noticeable on the $\text{K}_2\text{O}-\text{SiO}_2$ plot (Fig. 7.4) where a progressive enrichment at similar SiO_2 level is noted from MBG QF through DGS to CGS. In addition the $\text{P}_2\text{O}_5-\text{SiO}_2$ plot (Fig. 7.4) shows a clear enrichment in P_2O_5 from MBG QF through to MGS, and the $\text{TiO}_2-\text{SiO}_2$ plot (Fig. 7.4) suggests TiO_2 enrichment from MBG QF to CGS. The K_2O and TiO_2 plots also illustrate the deviation of the MGS I-type from the progressive enrichment trends towards the respective fields of the MGS S-types. Most of the other major elements, especially MgO , $\text{Fe}_2\text{O}_{3\text{total}}$ and CaO show more nearly coincident fields on the variation diagrams (Fig. 7.4).

The most significant variations can be seen in the plot of SiO_2-Nb (Fig. 7.5), which very clearly illustrates a progressive enrichment from MBG QF through to MGS I-types similar to P_2O_5 . The SiO_2-Y and SiO_2-Zr plots (Fig. 7.5) show enrichments from MBG QF to CGS but as in the case of K_2O and TiO_2 the MGS I-types deviate towards the fields of the MGS S-types. Rb, Sr and Ba fields show considerable overlap and are not displayed, but the $\text{Sc}-\text{SiO}_2$ is almost constant, similar to MgO , $\text{Fe}_2\text{O}_{3\text{total}}$ and CaO .

The REE have very similar LREE slopes for the four I-type suites (Table 7.1; Fig. 7.6) with $(\text{La}/\text{Sm})_{\text{N}}$ ranging from 4.0 to 5.5. However there is a very clear increase in absolute level of enrichment of LREE from MBG QF through to MGS I-types with La_{N} ranging from ca. 121 to ca. 324 (Table 7.1). The HREE slopes for MBG QF and DGS are similar and relatively unfractionated with $(\text{Yb}/\text{Gd})_{\text{N}}$ ranging from ca. 0.59 to ca. 0.62 (Table 7.1; Fig. 7.6). The absolute level of HREE enrichment increases from MBG QF to DGS with Yb_{N} ranging from ca. 12 to ca. 21 (Table 7.1; Fig. 7.6). However an abrupt change in slope occurs in CGS and in some of the MGS I-types where $(\text{Yb}/\text{Gd})_{\text{N}}$ ranges from ca. 0.36 to ca. 0.46 (Table 7.1; Fig. 7.6). This observation strongly suggests either an abrupt change in the minerals controlling the HREE fractionation

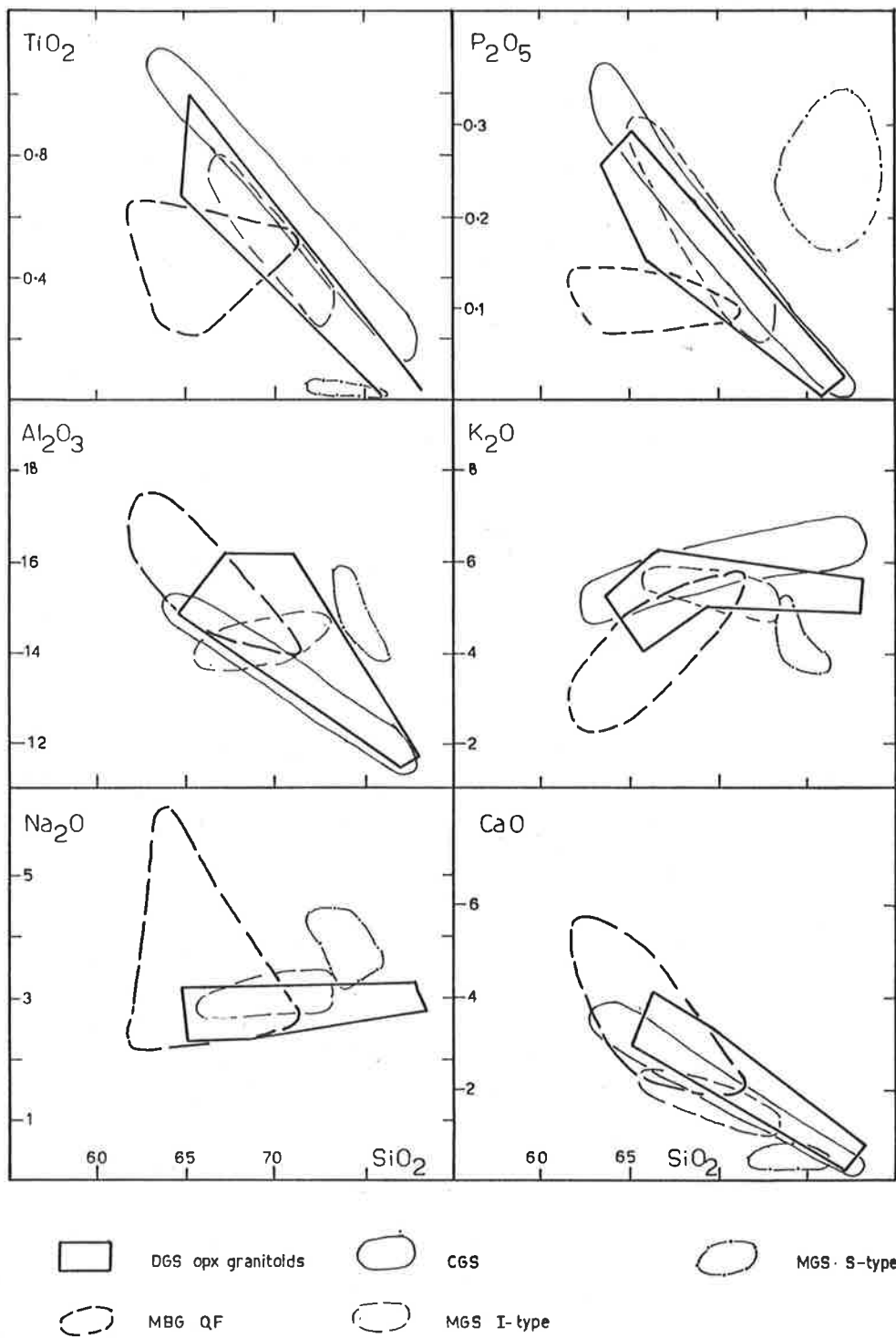


Figure 7.4 Comparison of the major element variation diagrams of the granitoids of the present study.

in the I-type granitoids between the production of DGS and CGS, or a marked change in source character. Regardless of which of these possibilities is favoured, the REE geochemistry of the I-type granitoids shows a clear temporal evolution from MBG QF to MGS.

Although the generally similar minimum SiO_2 contents and the similar levels of the elements such as Fe, Mg, Ca, Al and Sc in the I-type granitoids may argue for a similar degree of melting of a similar bulk source, the progressive enrichment trends for K, P, Ti, Zr, Nb, Y and REE in the granitoids argue for progressively higher levels of these elements in their source or sources.

It is noteworthy that the least evolved liquids in each suite, when compared with the extended REE plots of a representative Group A basaltic dyke (Fig. 7.7), show a trace element character similar to the basaltic magmas of the study area. This strongly suggests that the enriching component of the upper mantle source of basaltic magmas is somehow linked to the crustal source of granitoid magmas. This suggestion will be reexamined below.

(2) Silicic volcanics of the Gawler Range Volcanics and Hiltaba Granite

The 1.5 Ga Gawler Range Volcanics (GRV) have been studied in great detail by Giles (1980 a,b) and in lesser detail by Branch (1978).

Their major element geochemistry is very similar to the granitoids of the present study area, except that the least evolved liquids have SiO_2 contents as low as ca. 58%, and K_2O and P_2O_5 may be enriched over the granitoids (Fig. 7.8; Table 7.1). Trace elements such as Rb, Y, Nb, Sc and V are generally similar to the granitoids, but Sr and Ba tend to be ca. 2X enriched in the GRV and Zr scatters to higher abundances in the GRV (Table 7.1; Fig. 7.9).

Significantly the REE in the GRV and associated Hiltaba Granite show patterns with both steeply fractionated and only moderately fractionated HREE similar to the granitoids of the present study area (Fig. 7.6). It is suggested here that the ultimate cause of this variation is probably similar in both areas, and it is noted that whereas the two different types of REE

Comparison of some trace element variation diagrams of the granitoids of the present study. Symbols as in Figure 7.4.

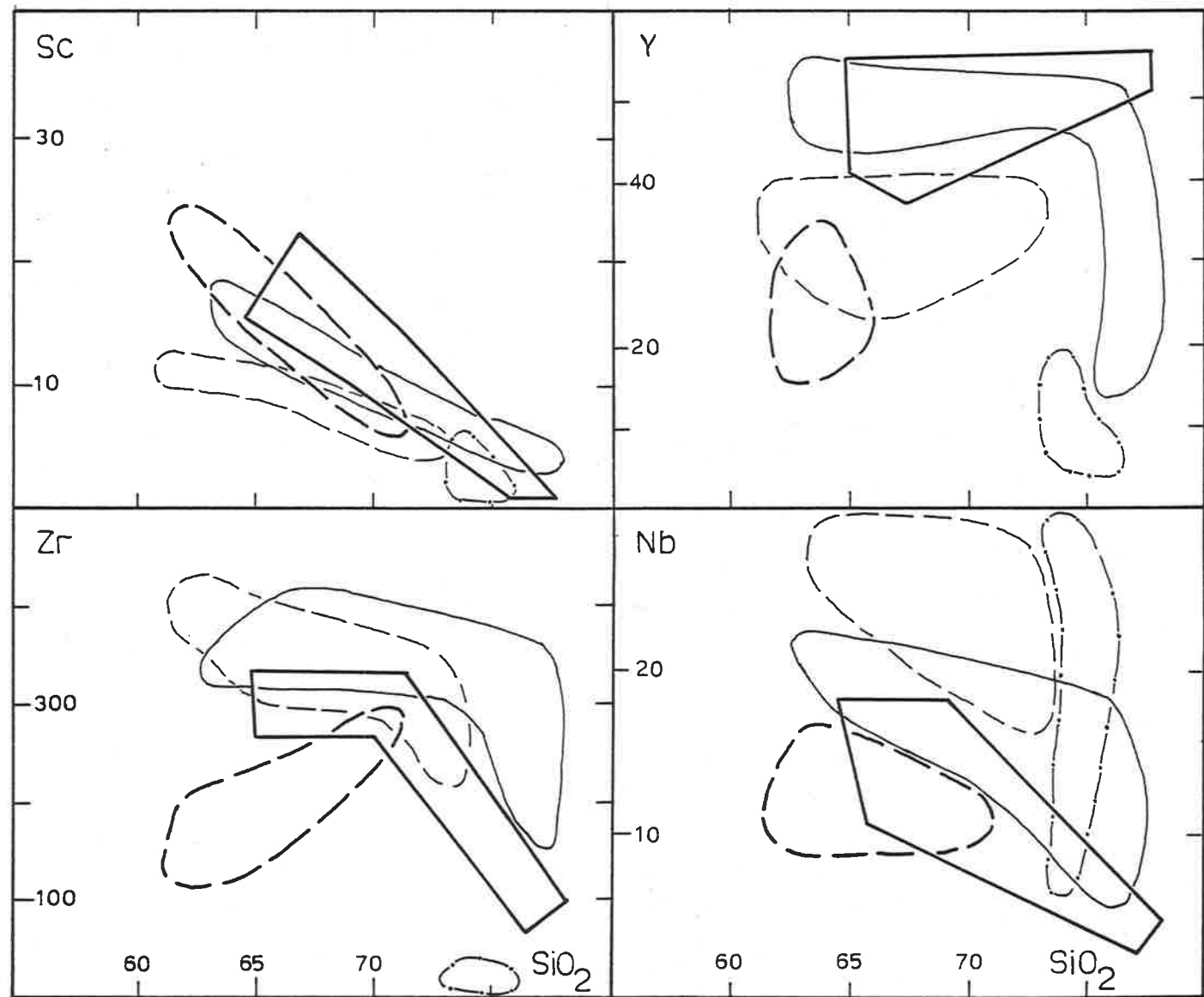


Figure 7.5

pattern in the granitoids apparently reflect a temporal control, the GRV patterns are approximately coeval. In addition it is noted that the close similarity between the Kimban Orogeny granitoids of the present study and the post-orogenic GRV suggests that the processes responsible for the development of these magmas are not critically dependent on the presence or absence of active orogenesis. This conclusion is similar to that drawn for the basaltic rocks that specific processes were acting in this Proterozoic segment of the earth that may occur in diverse tectonic environments.

Giles (1980a,b) interpreted the GRV in terms of a post-orogenic continental environment under the influence of a mantle diapir. He proposed that the mantle diapir supplied the heat to partially melt the lower crust which he furthermore suggested was of basic - to - intermediate granulite. He also attributed the pronounced enrichment of the silicic rocks in e.g. Zr and REE, to the breakdown under high temperature lower crustal melting conditions of refractory accessory minerals such as zircon. He concluded that the plutono-volcanic episode of the GRV and Hiltaba Granite was "fundamentally different from continental accretion through calc-alkaline magmatism."

The origin of the GRV will be discussed further below in conjunction with the granitoids of the present study, following a brief review of models for the production of silicic magmas.

(3) Petrogenetic models of derivation of silicic magmas

Much of the historical discussion of the origins of granitoid magmas has carried the implicit notion that granitoids were at some stage liquid. This is no doubt true in some cases, although most granitoid magmas probably contain a significant solid component (e.g. restite; Chappell & White 1974; White & Chappell 1977). However the granitoids of this study, and the GRV were largely liquid magmas and the following discussion is based on this premise unless specifically stated otherwise.

A number of possible modes of origin of granitoids have been discussed in the literature. The major groups of possible origins will be examined in turn.

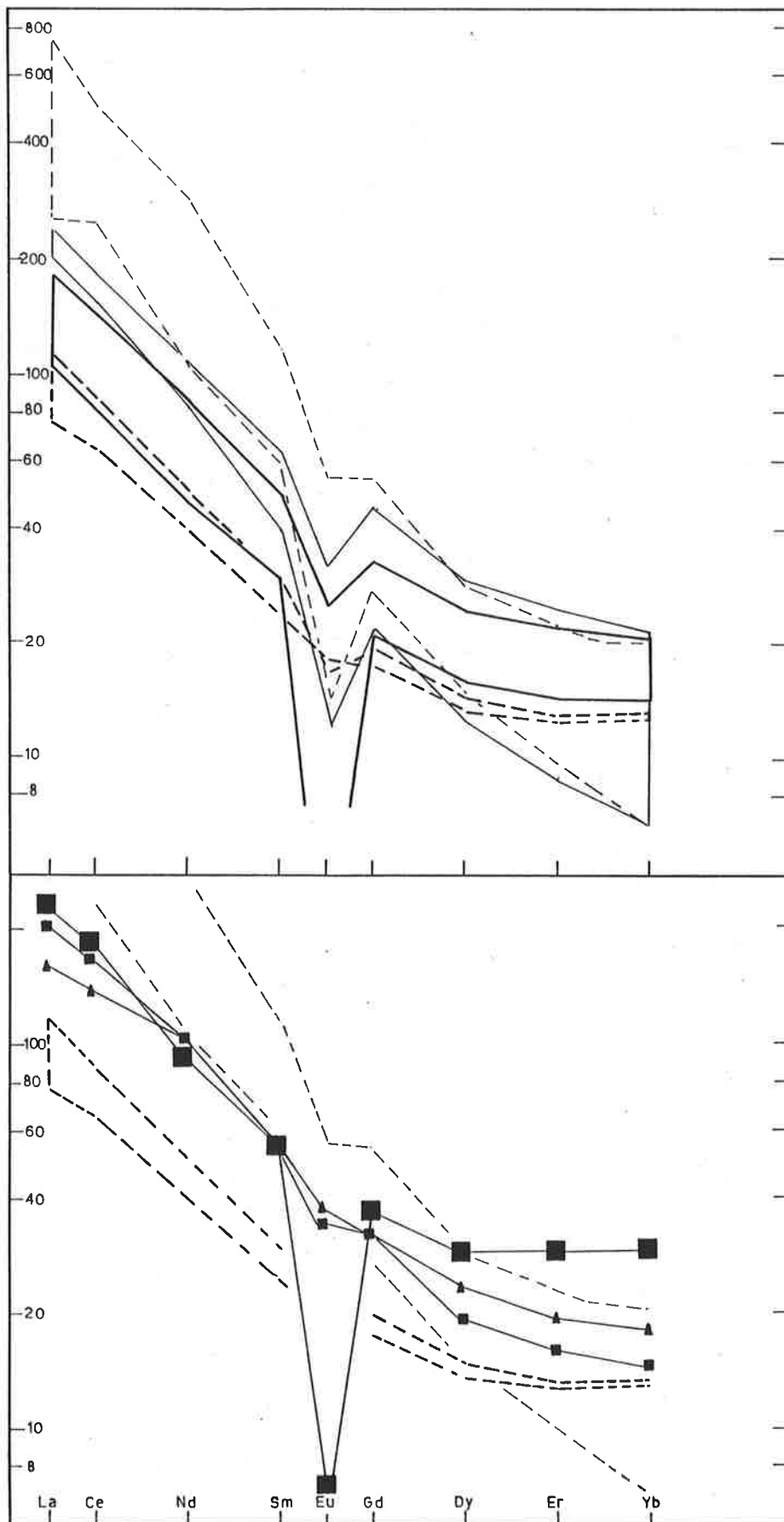


Figure 7.6 Comparison of chondrite normalised REE plots of the granitoids of the present study and selected Gawler Range Volcanics and the Hiltaba Granite (after Giles 1980). Symbols as in Figures 7.3 & 7.4.

(a) Crystal fractionation of basaltic magma to silicic magma

Various studies from diverse geological settings have proposed that crystal fractionation of basaltic magma has resulted in the production of granitoid magma (e.g. Zielinski 1975; Price & Sinton 1978; Thorpe et al. 1977).

In the light of the suggestion that large volumes of basaltic magma underplated the Proterozoic crust of the Gawler domain (see below) and underwent protracted crystal fractionation, it is worthy of further consideration here whether large volumes of silicic magma may have been derived from fractionation of this basaltic magma. To increase the SiO_2 content of residual liquids during basalt fractionation requires the crystallisation of minerals of SiO_2 content considerably lower than that of the basaltic liquid itself e.g. olivine, garnet, amphibole, magnetite or ilmenite. Giles (1980b) was able to successfully model a 60% SiO_2 andesite by fractionation of a 52.8% SiO_2 basalt in the GRV by separation of 47% of an assemblage of 0.53 amphibole + 0.41 plag + 0.06 magnetite. When coupled with the closely similar extended REE plots for Gawler domain basaltic and silicic rocks this modelling seems to argue in favour of a fractionated basalt parentage.

However, the compatible trace elements such as Ni, Cr, V and Sc in fractionated basaltic suites quickly tend to zero (e.g. Taylor et al. 1969; Zielinski 1975; Giles 1980b; Condie 1981) and do not allow the generation of residual silicic liquids of the present study and the GRV with their appreciable Ni, Cr, Sc and V contents (Table 7.1). Furthermore the petrographic evidence, and the modelling of the within suite variation in the major elements of the basaltic rocks of the study area argue for fractionation dominated by pyroxene ferromagnesian minerals, without amphibole and without appreciable magnetite or ilmenite (see Chapter 6). This fractionation style does not produce significant SiO_2 enrichment (see also Thompson 1975a).

In addition there is a marked absence of magmatic rocks of non-cumulate origin in the Gawler domain which bridge the SiO_2 gap between the basaltic and silicic rocks (Fig. 7.1).

Hence it is concluded that basalt fractionation has not been responsible for the generation of the abundant silicic magmas of the Early to Middle Proterozoic of the Gawler domain.

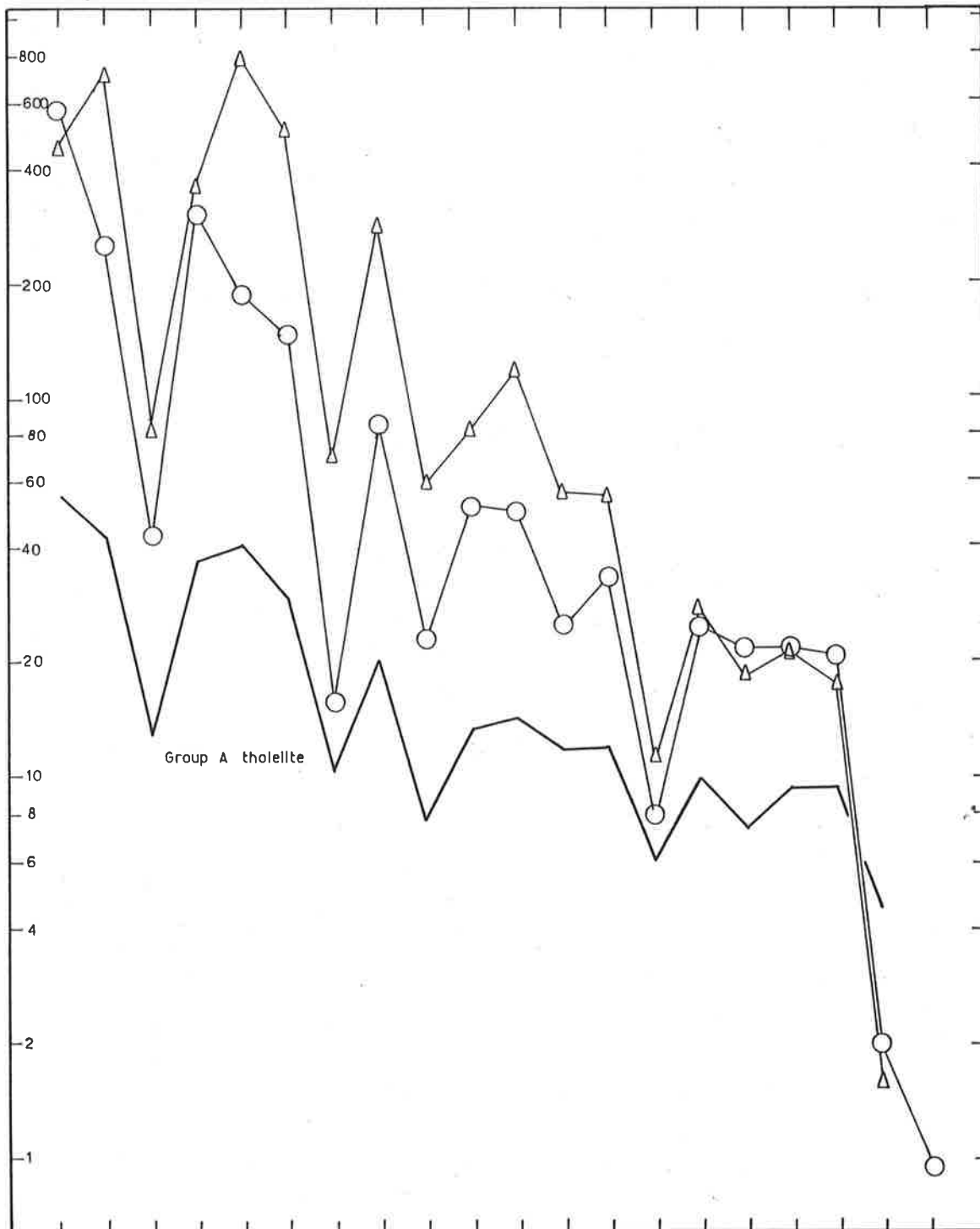


Figure 7.7

Comparison of extended REE plots of selected granitoids of the present study and a representative Group A tholeiite of the present study. Symbols as in Figure 7.3.

(b) Mixing of basaltic and silicic liquids

A general model for the production of calc-alkaline andesite and dacite involving mixing of basaltic and rhyolitic magmas within the crust has been proposed by Eichelberger (1978). He recognised abundant petrographic, geochemical and isotopic indications of disequilibrium in andesitic rocks which he attributed to mixing of basaltic liquid and its phenocrysts with rhyolitic liquid and its phenocrysts in large magma chambers at intermediate crustal depths.

The main objection to any notion of mixing of magmas in the Gawler subdomain is the prominent SiO_2 gap observed in both the granitoids of the present study and the post-orogenic GRV (Fig. 7.1). Furthermore there is no petrographic evidence for such a process, in contrast to the calc-alkaline andesites. Indeed the geochemical variation within, for instance, the DGS can be perfectly modelled on the basis of the phenocryst phases observed which show no evidence of disequilibrium. In addition Giles (1980b) has noted no petrographic evidence in the GRV in favour of this mode. The silicic and basaltic liquids of the Gawler subdomain are thus suggested to have had quite distinct origins, and not to have mixed to any appreciable extent.

Eichelberger (1978) also noted that bimodal magmatism is favoured in tensional tectonic environments where decreased efficiency of mixing at intermediate crustal depths occurs due to the escape of magmas.

(c) Hybridisation of silicic liquid by solid mafic material

The model of origin of the silicic magmas by mixing of more silicic liquids and solid mafic material (e.g. de Albuquerque 1971) may be rejected for similar reasons to the mixing of basic and silicic liquids and phenocrysts. Disequilibrium textures and mineral chemistry of liquids and enclosed "phenocrysts" would be expected, but is not observed.

These considerations lead to the more likely and preferred model of origin for the silicic magmas by partial melting processes.

(d) Partial melting model of the petrogenesis of silicic magmas

A consensus based on experimental petrology has apparently been reached in recent years that direct mantle derivation of silicic

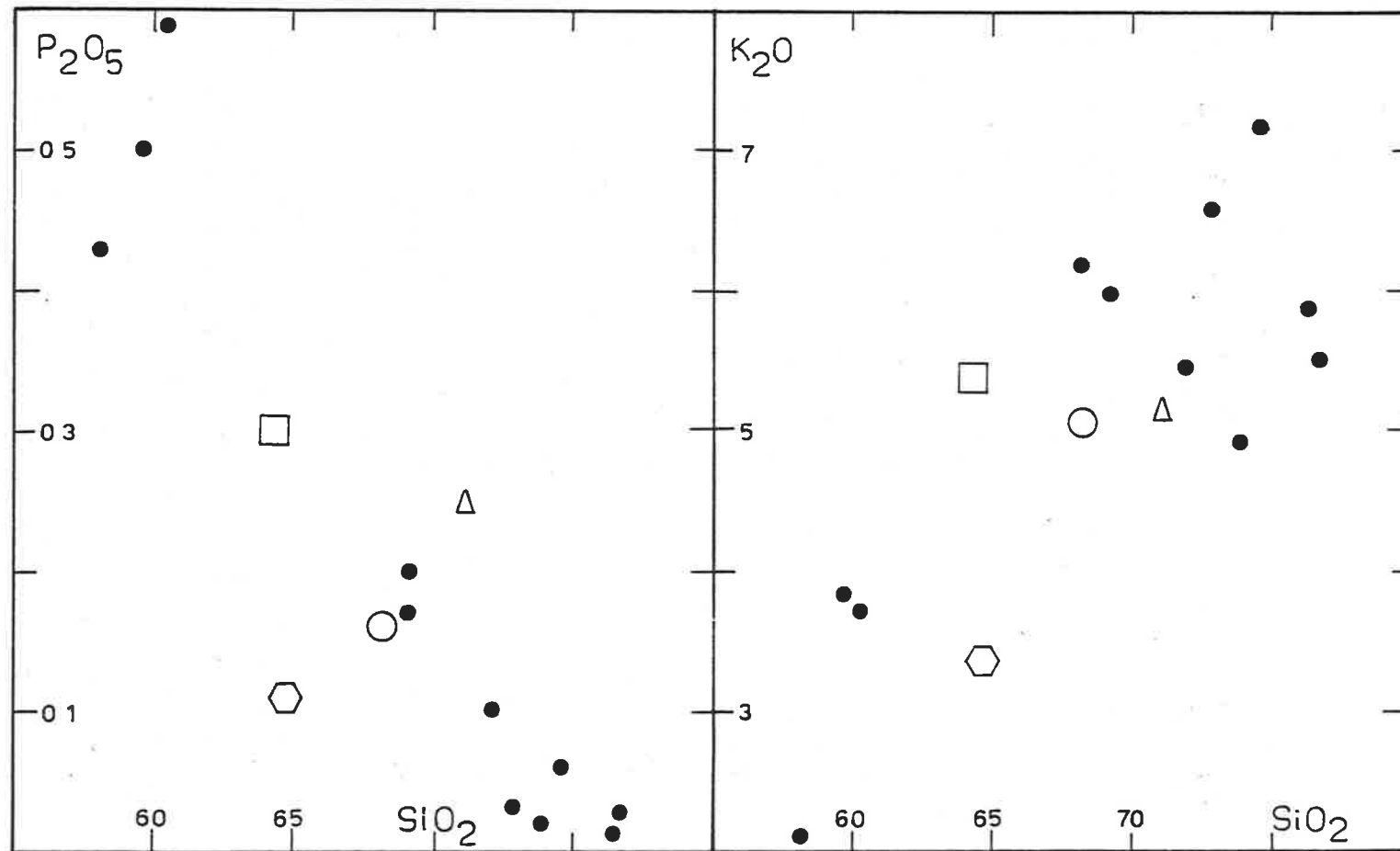


Figure 7.8

SiO_2 - P_2O_5 and SiO_2 - K_2O comparison of I-type granitoids of the present study and various Gawler Range Volcanics (after Giles 1980). Symbols as in Figure 7.3.

● various GRV

(and intermediate) liquids is not possible (e.g. Wyllie et al. 1976; Wyllie 1977; White & Chappell 1977). The conclusion of these authors is that all true granites are crustal in origin, and hence silicic magmas formed by partial melting are at least second-stage mantle derivatives.

Most of the least evolved liquids of the present study and the GRV are relatively silicic (granodioritic-dacitic) and cannot be simple mantle-derived primary liquids. A crustal origin is indicated. Limiting the source of the silicic magmas to the crust poses the question as to the specific nature of the Gawler domain crustal source.

(4) Nature of the crustal source of the silicic magmas

The initial $87\text{Sr}/86\text{Sr}$ ratios of the granitoids of the present study and of the GRV (Compston et al. 1966; Webb 1978) are too low to allow derivation of the silicic magmas from typical upper crustal rocks or Gawler domain older high-grade gneisses (e.g. see Chapter 2). A presumably deep-level, relatively unradiogenic crustal source is required. Furthermore the crustal source must be capable of yielding liquids with ca. 58% - 60% SiO_2 for the GRV and 62% - 65% SiO_2 for the granitoids of the present study. This constraint limits the bulk composition of the source to be intermediate to basic as the level of melting otherwise required for a siliceous source is unrealistically high (e.g. up to 50% partial melting, Condie 1978). The presence of mainly metabasic xenoliths (although not common) within the granitoids of the study area is consistent with this conclusion. The xenoliths are probably residual source material of the granitoids.

The nature of the lower crust has been the subject of considerable debate, much of which centres around the interpreted crustal accretionary mechanisms. Taylor & McLennan (1979) modelled the composition of the lower crust by assuming it comprised the residue from an accreted average island arc andesite after extraction of 2/3 average upper crust (Table 7.2).

Tarney & Windley (1977, 1979) criticised the Taylor andesite model of crustal growth and proposed that the Archaean high-grade gneiss terrains such as the Lewisian of Scotland constitute more likely candidates for typical lower crustal rocks. They propose

Table 7.2 Estimated compositions of model lower crust

	1	3	3	4	5	6	7
SiO ₂	54.0	61.5	63.1	59.7	61.2	52.89	47.33
Al ₂ O ₃	19.0	15.5	16.5	16.8	15.6	15.13	16.16
Fe ₂ O ₃	10.0	6.5	5.2	6.3	5.9	10.67	15.49
MnO						0.17	0.21
MgO	4.1	3.5	3.5	5.4	3.4	7.04	7.21
CaO	9.5	5.9	5.0	5.7	5.6	9.88	9.70
Na ₂ O	3.4	4.0	4.1	3.9	4.4	2.47	2.25
K ₂ O	0.6	1.0	2.1	1.4	1.0	1.13	0.76
TiO ₂	0.9	0.56	0.8	0.95	0.5	0.80	1.58
P ₂ O ₅						0.19	0.16
Rb	20	10	71		12	30	24
Sr	425	495	435		569	320	188
Ba	175	645	655		757	728	258
Y	20				9	25	28
Zr	30	165	100		202	107	105
Nb	4					7	8
Ni		69	45		58	79	169
Cr		90	31		88	345	141
La	9.5	20	27		22	24	12
Ce	17	40	66		44	51	27
Nd	8.0				18.5	23.3	16.2
Sm	2.8	2.5	5.7		3.3	4.5	4.1
Eu	1.1	1.0	1.4		1.18	1.28	1.41
Gd	3.1					4.5	4.8
Dy	3.4					4.2	4.9
Er	2.0					2.7	2.9
Yb	1.9	0.7	1.6		1.2	2.7	2.8
Rb/Sr	.047	.020	.16		.021	.094	.13

1. Estimate based on average andesite (Taylor & McLennan 1979).
2. Estimate based on Lewisian granulites (Condie 1981).
3. Average high-grade gneiss (Condie 1981).
4. Calculated refractory gneiss (Condie 1981).
5. Average Lewisian granulite (Weaver & Tarney 1980).
6. Mafic granulite B26 (this study).
7. Mafic garnet granulite coronite B36 (this study).

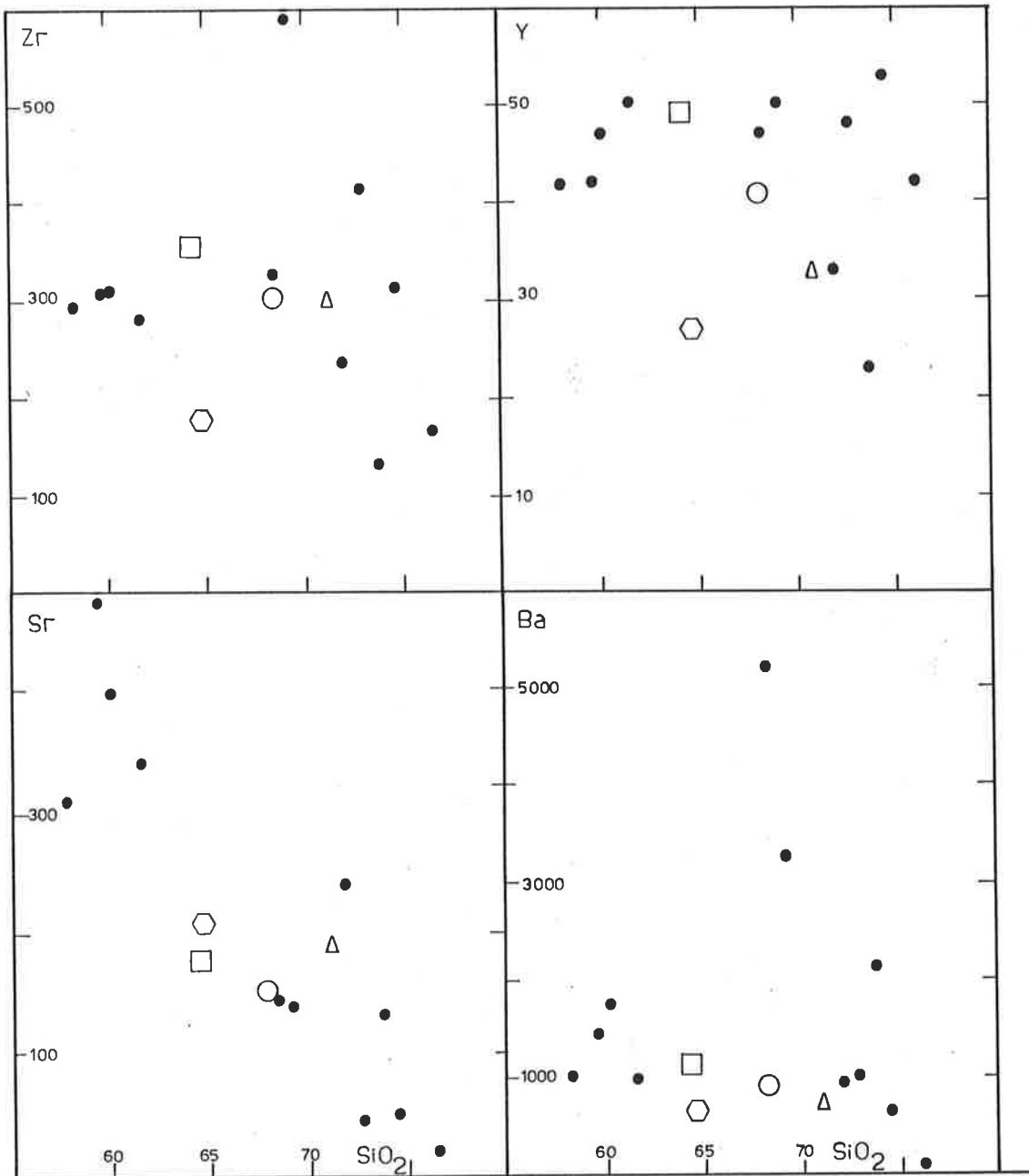


Figure 7-9

SiO₂-Zr, SiO₂-Y, SiO₂-Sr, and SiO₂-Ba comparison of I-type granitoids of the present study and various Gawler Range Volcanics (after Giles 1980). Symbols as in Figures 7.3 & 7.8.

that the distinctive geochemical features are not representative of residues after melt extraction but that they simply reflect the primary processes of Cordilleran crustal generation involving residual or fractioning garnet or hornblende in the genesis of the primary trondhjemitic melts making up the new crust. In addition Hamilton et al. (1979), Weaver & Tarney (1980) and Newton et al. (1980) propose that the K, Rb, U and Th depleted nature of Lewisian type lower granulite crust is not due to granitoid melt extraction but due to CO₂-fluid flushing of the lower crust. In this view of the lower crust it may constitute a fertile source of later granitoid magmas (given the necessary P, T, pH₂O conditions). Average Lewisian granulite gneiss is included in Table 7.2.

Condie (1981) noted that the Archaean granite-greenstone terrains and high-grade gneiss terrains are essentially bimodal in composition, but that the high-grade gneisses have been well-mixed possibly during partial melting and granite extraction or deformation in the lower crust, so that they have an overall intermediate bulk composition. He suggested that most of the lower crust must have been involved in the production of late Archaean K-granites, so that Archaean terrains are underlain by depleted crust. However, Condie proposed that such depleted crust is capable of yielding further granite magmas provided that some elements, such as Rb, are replenished. The lower crustal estimate of Condie based on Lewisian-like high-grade gneisses is included in Table 7.2, as well as an estimate of gneiss residual after granitoid melt extraction.

Wass & Hollis (1983) proposed that there is evidence for abundant lower continental crustal accretion (underplating) of mafic to ultramafic eclogitic to granulitic material in many areas. Wyborn & Page (1983) proposed that Early Proterozoic I-type granitoids throughout Australia were derived by remelting such material.

Lower crustal estimated compositions of Taylor & McLennan (1979), Weaver & Tarney (1980), Condie (1981) and a basaltic rock from the present study area (following the reasoning of Wass & Hollis 1983) are presented in Table 7.2. These are modelled below as possible sources of the silicic magmas of the present study and of the GRV.

(5) Major element testing of the models

Following the model of Wyborn & Page (1983), the I-type granitoids of this study have been modelled as melts derived from

basic granulites of the type represented by the meta-tholeiites of this study. A measured Group A pyroxene granulite (B26) and its analysed minerals have been tested as the source and residual mineral assemblage. The major element models are a perfect fit, and suggest the granitoids may have been derived by 10% - 15% partial melting of Proterozoic meta-tholeiite leaving a residue comprising ca. 45% plag + 25% cpx + 20% opx + 8% biot + 1% Fe-Ti oxide (Table 7.3). Similar calculations indicate that the silicic volcanics of the Gawler Ranges and Central Australia may have been derived in a similar manner from similar source rocks (Table 7.4).

The calculated model residue contains a higher proportion of residual biotite than may normally be expected in lower crustal mafic granulites, although Wass & Hollis (1983) reported up to 25% biotite in the mode of southeastern Australian mafic granulites and eclogites.

In addition, to assess the possible role of garnet and amphibole in the petrogenesis of the I-type granitoids from the basic granulitic sources, further modelling of B26 granulite + hornblende + garnet and of B36 metatholeiite + garnet + pargasite, (using compositions of minerals actually observed), was undertaken. This model suggest that neither hornblende or garnet was prominent in the relatively silicic B26 type source (Table 7.5), but pargasite and garnet may have constituted up to 20% each of the B36 type source (Table 7.5). Biotite is not required in the garnet + pargasite B36 type model residue.

Similar calculations indicate that the silicic volcanics of the Gawler Ranges and Central Australia (CAV) may also be accounted for in a similar way (Table 7.6).

These calculations, based on the major elements only, suggest that it is possible to derive the I-type granitoids and silicic volcanics by partial melting in the lower crust of accreted biotite-bearing pyroxene granulite and (hornblende + garnet)-poor pyroxene granulite or garnet + pargasite granulite.

Major element modelling of this type, however, does not always provide a unique solution. For instance, Giles (1980b) modelled the GRV andesites (60% SiO₂) and dacites (62% SiO₂) and Central Australian dacites (67% SiO₂) as partial melts of the basic lower crustal estimate of Taylor & McLennan (1979), leaving a residue

Table 7.3 Partial melt least squares modelling of basic pyroxene granulite source to produce I-type melts of the present study.

(a) Model partial melt MBG QF = D87 from basic granulite = B26

	B26	B26*	Residual	Component	Weight Fraction
SiO ₂	52.89	52.89	0.00	D87	0.14
Al ₂ O ₃	15.13	15.11	-0.02	cpx	0.23 (0.27)
Fe ₂ O ₃ T	10.67	10.67	0.00	opx	0.16 (0.19)
MgO	7.04	7.04	0.00	plag	0.39 (0.46)
CaO	9.88	9.88	0.00	biot	0.07 (0.08)
Na ₂ O	2.47	2.56	0.09	ilm	0.01 (0.01)
TiO ₂	0.80	0.80	0.00	Sum of squares of	
K ₂ O	1.13	1.16	0.03	residuals = 0.01	

(b) Model partial melt FGGL DGS = B143 from basic granulite = B26

	B26	B26*	Residual	Component	Weight Fraction
SiO ₂	52.89	52.88	-0.01	B143	0.10
Al ₂ O ₃	15.13	15.10	-0.03	cpx	0.24 (0.27)
Fe ₂ O ₃ T	10.67	10.67	0.00	opx	0.17 (0.19)
MgO	7.04	7.06	0.02	plag	0.42 (0.46)
CaO	9.88	9.88	0.00	biot	0.07 (0.08)
Na ₂ O	2.47	2.68	0.21	ilm	0.01 (0.01)
TiO ₂	0.80	0.80	0.00	Sum of squares of	
K ₂ O	1.13	1.18	0.05	residuals = 0.05	

(c) Model partial melt CGS = B112B from basic granulite = B26

	B26	B26*	Residual	Component	Weight Fraction
SiO ₂	52.89	52.88	-0.01	B112B	0.10
Al ₂ O ₃	15.13	15.10	-0.03	cpx	0.24 (0.26)
Fe ₂ O ₃ T	10.67	10.67	0.00	opx	0.18 (0.20)
MgO	7.04	7.06	0.02	plag	0.42 (0.47)
CaO	9.88	9.88	0.00	biot	0.06 (0.07)
Na ₂ O	2.47	2.68	0.21	ilm	0.01 (0.01)
TiO ₂	0.80	0.80	0.00	Sum of squares of	
K ₂ O	1.13	1.18	0.05	residuals = 0.05	

(d) Model partial melt of MGS Av, adamellite from basic granulite = B26

	B26	B26*	Residual	Component	Weight Fraction
SiO ₂	52.89	52.88	-0.01	MGS	0.08
Al ₂ O ₃	15.13	15.10	-0.08	cpx	0.24 (0.26)
Fe ₂ O ₃ T	10.67	10.67	0.00	opx	0.17 (0.19)
MgO	7.04	7.06	0.02	plag	0.43 (0.47)
CaO	9.88	9.89	0.01	biot	0.07 (0.08)
Na ₂ O	2.47	2.69	0.22	ilm	0.01 (0.01)
TiO ₂	0.80	0.80	0.00	Sum of squares of	
K ₂ O	1.13	1.18	0.05	residuals = 0.05	

- Notes (1) Calculations after method of Bryan et al. 1969
 (2) B26 = measured composition
 B26* = estimated model composition
 (3) all composition data in wt. %
 (4) bracketted weight fractions = residue
 (5) Mineral compositions used are from B26 :-

	cpx	opx	plag	biot	ilm
SiO ₂	52.13	50.57	54.66	34.75	
Al ₂ O ₃	1.61	1.32	28.64	14.58	
Fe ₂ O ₃ T	12.75	32.01		20.95	52.86
MgO	13.15	17.84		10.98	
CaO	21.02	0.51	10.53	0.48	
Na ₂ O	0.27	0.16	5.46	0.08	
TiO ₂	0.04	0.10		5.49	48.59
K ₂ O			0.29	8.74	

dominated by plagioclase, pyroxenes and magnetite. Although most major elements agree closely, a major discrepancy exists for K_2O which is a factor of ca. 2X enriched in the observed melts over the calculated melts. Giles was unable to account for this discrepancy. In addition the I-type granitoids of the present study can be modelled for 10% - 20% melting of the Taylor & McLennan lower crustal estimate leaving a residue composed of ca. 66% plagioclase, 16% cpx, 13% opx and 5% Fe-Ti oxide (Table 7.7). It is noteworthy that it is possible to model closely the granitoids from a source of this type without significant mismatch in K_2O and yet without residual biotite, which is necessary for the metatholeiite granulite source above.

However, no satisfactory model of production of the I-type granitoids from residual high-grade gneisses of Condie (1981) was possible on any combination of residual minerals. This may reflect the inappropriate choice of mineral compositions. However because of the relatively silicic nature of the high-grade gneiss source (ca. 59.7% SiO_2) derivation of liquids with ca. 62% SiO_2 such as the MBG QF would require unrealistically high proportions of partial melting perhaps as high as 50% - 60% (cf. Condie 1978).

It is not possible to discriminate between these varied possibilities on the basis of the major element modelling. Indeed on geological and geophysical grounds it is highly likely that the Early to Middle Proterozoic lower continental crust in this area was a complex mixture of Archaean and Proterozoic refractory and fertile, basic, intermediate and siliceous material (cf. Smithson & Brown 1977) so that each may have contributed to some extent. However, it is attempted below to constrain more closely the likely granitoid source material on the basis of trace element models.

However, in summary, it is apparent that ca. 10% - 20% partial melting of a basic to intermediate source, with a pyroxene + plagioclase-rich residue, is required.

(6) Trace element testing of the models

Knowing the trace element contents of the I-type granitoids (Table 7.1) it is possible on the basis of the calculated major element models above, to calculate the trace element contents of the model sources and to compare them with the known or estimated compositions of the respective source rocks. The models are

Table 7.4 Partial melt least squares modelling of basic pyroxene granulite source to produce silicic melts of the Gawler Range Volcanics and Central Australian Volcanics.

(a) Model partial melt GRV andesite from basic granulite = B26

	B26	B26*	Residual	Component	Weight Fraction	B26	B26*	Residual	Component	Weight Fraction
SiO ₂	52.89	52.87	-0.02	andesite	0.14	52.89	52.84	-0.05	dacite	0.12
Al ₂ O ₃	15.13	15.10	-0.03	cpx	0.24 (0.27)	15.13	15.12	-0.01	cpx	0.26
Fe ₂ O ₃ T	10.67	10.67	0.00	opx	0.16 (0.19)	10.67	10.67	0.00	opx	0.15
MgO	7.04	7.09	0.05	plag	0.40 (0.46)	7.04	7.17	0.13	plag	0.40
CaO	9.88	9.89	0.01	biot	0.06 (0.07)	9.88	9.91	0.03	biot	0.07
Na ₂ O	2.47	2.79	0.32	ilm	0.01 (0.01)	2.47	2.94	0.47	ilm	0.01
TiO ₂	0.80	0.80	0.00	Sum of squares of		0.80	0.80	0.00	Sum of squares of	
K ₂ O	1.13	1.19	0.06	residuals = 0.11		1.13	1.17	0.04	residuals = 0.24	

(c) Model partial melt Central Australian dacite from basic granulite = B26

	B26	B26*	Residual	Component	Weight Fraction
SiO ₂	52.89	52.87	-0.02	dacite	0.09
Al ₂ O ₃	15.13	15.10	-0.03	cpx	0.24
Fe ₂ O ₃ T	10.67	10.67	0.00	opx	0.17
MgO	7.04	7.08	0.04	plag	0.43
CaO	9.88	9.89	0.01	biot	0.08
Na ₂ O	2.47	2.76	0.29	ilm	0.01
TiO ₂	0.80	0.80	0.00	Sum of squares of	
K ₂ O	1.13	1.19	0.06	residuals = 0.09	

Notes: (1) as for Table 7.3

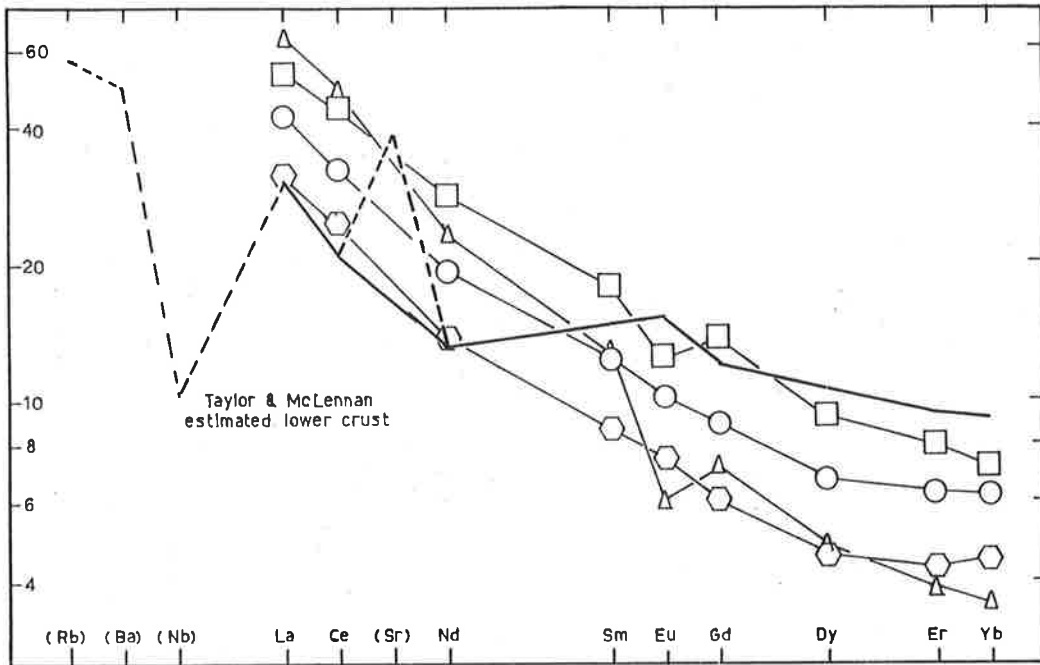


Figure 7-10 Calculated extended REE plots of sources of I-type melts of the present study based on the lower crustal estimate of Taylor & McLennan (1979) and compared with their estimate. Symbols as in Figure 7.3.

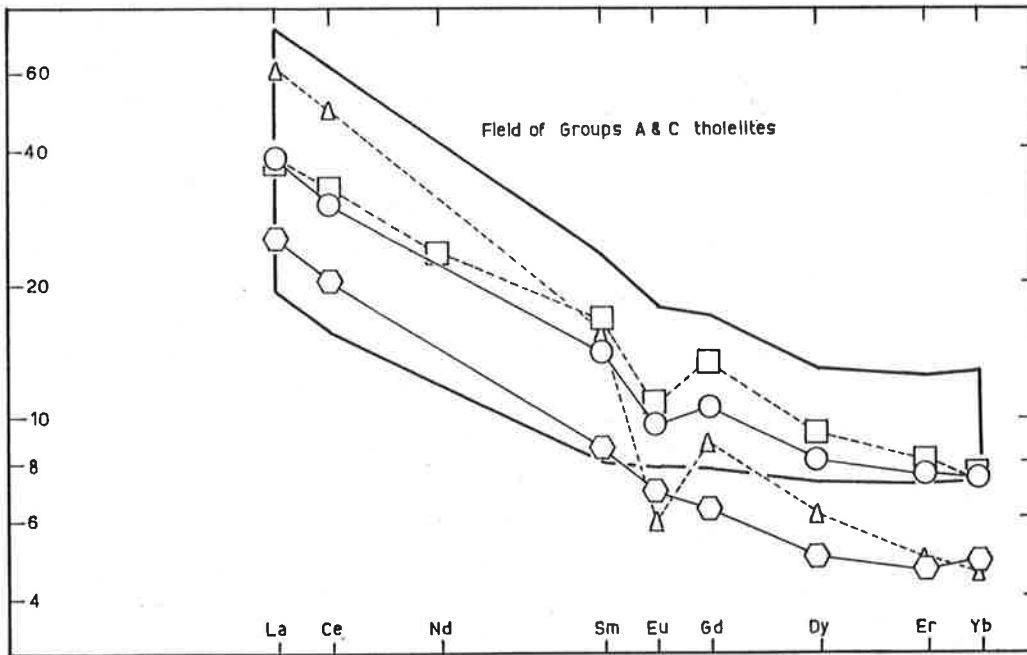


Figure 7-11 Calculated REE plots of sources of I-type melts of the present study based on the B26 pyroxene granulite model, and compared with the field of Groups A & C tholeiite dykes. Symbols as in Figure 7.3.

calculated assuming batch melting and using the formula of Schilling & Winchester (1967) and the mineral/melt distribution coefficients in Appendix Table 6.6.

The calculated source REE patterns suggest that the Taylor & McLennan (1979) type lower crustal source is not suitable having a $(La/Yb)_N$ too low at ca. 3.3 and almost flat REE from Nd to Yb, whereas the calculated model sources required for the I-type granitoids are more steeply and uniformly fractionated (Fig. 7.10, Appendix Table 7.1).

The calculated REE patterns for the sources of the MBG QF and DGS I-type granitoids, based on the B26 pyroxene granulite major element models, correspond well with the fields of Group A and C tholeiites of the present study (Fig. 7.11). However similarly calculated patterns for the CGS and MGS granitoids have HREE more steeply fractionated than known Gawler domain tholeiites (Fig. 7.11). When the REE patterns of the sources of the CGS and MGS are calculated based on the B26 granulite + 8% hornblende + 2% garnet model residue they more closely correspond to the fields of Group A, B and C tholeiites (Fig. 7.12). These results suggest that it is possible to derive the I-type granitoids from pyroxene granulite source rocks of the type known from the Gawler domain, but that the two younger suites require a partly hydrated and garnetiferous source. However the calculated model REE patterns of the sources for the CGS and MGS based on the B36 granulite + garnet + pargasite type source, even for the lowest available distribution coefficients for garnet, show a HREE slope with $(Yb/Gd)_N$ ca. 2 which is quite unlike any common crustal rock (Fig. 7.13). Hence on the basis of REE alone, a pyroxene + hornblende + garnet granulite of B26 type is the most favoured candidate as source of the I-type granitoids.

Furthermore, the extended REE plots of the calculated model B26 pyroxene granulite and pyroxene granulite + hornblende + garnet sources are closely similar in shape to the tholeiite fields, (Fig. 7.14) except Rb, but dissimilar to the Taylor & McLennan model lower crust (Fig. 7.10). In particular the Taylor & McLennan source shows a pronounced positive Sr anomaly when compared to the calculated I-type granitoid sources.

Finally and more conclusively the compatible trace elements Ni, Cr, Sc and V, have large bulk distribution coefficients for each of the modelled sources and residual mineral assemblages, and hence constrain the levels of these elements in the calculated

Table 7.5 Partial melt least squares modelling of basic (amphibole + garnet + pyroxene) granulite source to produce I-type melts of the present study.

(a) Model partial melt MBG QF = D87 from (amph + gt) granulite = B26

	B26	B26*	Residual	Component	Weight Fraction
SiO2	52.89	52.88	-0.01	D87	0.15
Al2O3	15.13	15.13	-0.00	cpx	0.22
Fe2O3T	10.67	10.68	0.01	opx	0.15
MgO	7.04	7.05	0.01	plag	0.38
CaO	9.88	9.89	0.01	biot	0.07
Na2O	2.47	2.56	0.09	amph	0.04
TiO2	0.80	0.57	-0.23	gt"	-0.01
K2O	1.13	1.28	0.15		
				Sum of squares of residuals = 0.08	

(b) Model partial melt MBG QF = D87 from (parg + gt) granulite = B36

	B36	B36*	Residual	Component	Weight Fraction
	47.33	47.33	0.00	D87	0.10
	16.16	16.21	0.05	cpx"	0.20
	15.49	15.45	-0.04	opx"	0.06
	7.21	7.27	0.06	plag"	0.25
	9.70	9.70	0.00	ilm	0.02
	2.25	1.96	-0.29	parg"	0.20
	1.58	1.62	0.04	gt"	0.16
	0.76	0.79	0.03		
				Sum of squares of residuals = 0.10	

(c) Model partial melt FGGL DGS = B143 from (parg + gt) granulite = B36

	B36	B36*	Residual	Component	Weight Fraction
SiO2	47.33	47.33	0.00	B143	0.08
Al2O3	16.16	16.19	0.03	cpx"	0.21
Fe2O3T	15.49	15.46	-0.03	opx"	0.06
MgO	7.21	7.25	0.04	plag"	0.27
CaO	9.70	9.69	-0.01	ilm	0.02
Na2O	2.25	2.02	-0.23	parg"	0.19
TiO2	1.58	1.61	0.03	gt"	0.17
K2O	0.76	0.80	0.04		
				Sum of squares of residuals = 0.06	

(d) Model partial melt CGS = B112B from (parg + gt) granulite = B36

	B36	B36*	Residual	Component	Weight Fraction
	47.33	47.33	0.00	B112B	0.07
	16.16	16.20	0.04	cpx"	0.22
	15.49	15.46	-0.03	opx"	0.07
	7.21	7.25	0.04	plag"	0.28
	9.70	9.69	-0.01	ilm	0.02
	2.25	2.00	0.25	parg"	0.17
	1.58	1.62	0.04	gt"	0.17
	0.76	0.80	0.04		
				Sum of squares of residuals = 0.07	

(e) Model partial melt MGS Av. adamellite from (parg + gt) granulite + B36

	B36	B36*	Residual	Component	Weight Fraction
SiO2	47.33	0.00		MGS	0.07
Al2O3	16.20	0.04		cpx"	0.21
Fe2O3T	15.46	-0.03		opx"	0.06
MgO	7.25	0.04		plag"	0.27
CaO	9.69	-0.01		ilm	0.02
Na2O	2.01	0.24		parg"	0.19
TiO2	1.61	0.03		gt"	0.17
K2O	0.80	0.04			
				Sum of squares of residuals = 0.06	

Notes: (1) as for Table 7.3

(2) Mineral compositions from B36 :-

	cpx"	opx"	plag"	parg"	gt"
SiO2	52.14	51.76	52.19	39.72	38.44
Al2O3	2.20	1.46	30.16	14.07	21.87
Fe2O3T	17.94	28.96	-	17.48	30.73
MgO	15.58	19.92	-	9.53	4.90
CaO	13.28	0.41	12.31	11.52	6.79
Na2O	0.51	-	4.53	2.21	0.21
TiO2	-	-	-	3.41	-
K2O	-	-	0.22	2.04	-

(3) other minerals from B26; Table 7.3

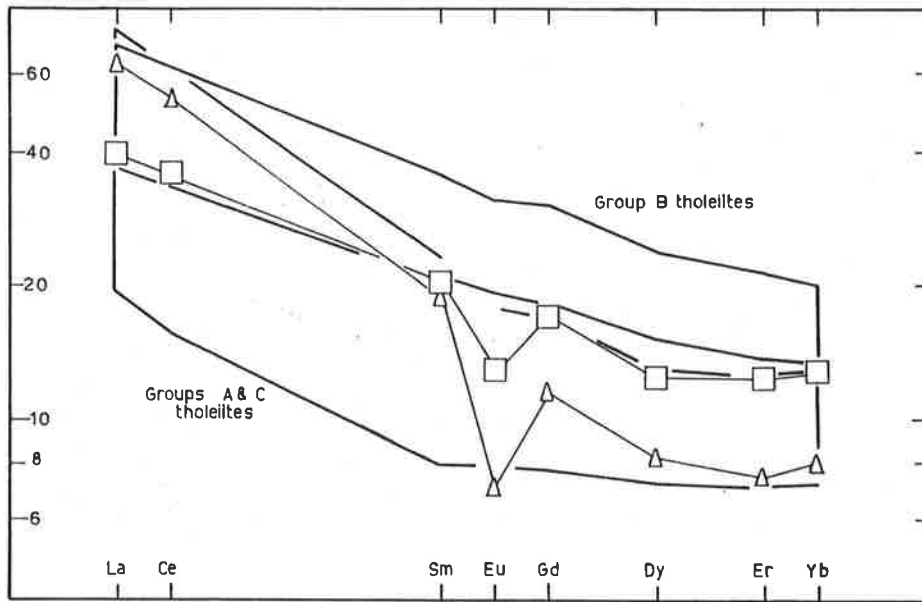


Figure 7.12 Calculated REE plots of sources of selected I-type melts of the present study based on the B26 (amph + gt) granulite model, and compared with the fields of Groups A, B & C tholeiite dykes. Symbols as in Figure 7.3.

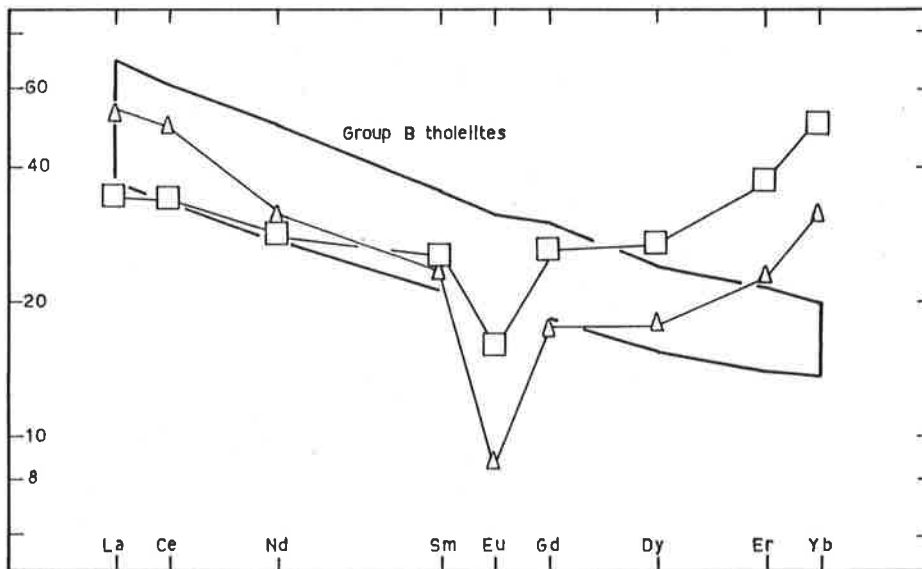


Figure 7.13 Calculated REE plots of sources of selected I-type melts of the present study based on the B36 (parg + gt) granulite model, and compared with the field of Group B tholeiite dykes. Symbols as in Figure 7.3.

sources for whatever model favoured to be moderately high (Table 7.8). Comparison of the calculated sources with proposed sources suggests strongly that only a basic source has high enough compatible trace element levels to produce the I-type granitoids. Hence the favoured source for the I-type granitoids is of a basic pyroxene granulite or pyroxene granulite with minor hornblende and/or garnet.

These conclusions may be extended to the silicic volcanics of the Gawler Range and Central Australia, because of their many similarities to the I-type granitoids.

(7) Temporal evolution

The calculated sources of the I-type granitoids show the same progressive enrichment in e.g. REE as the granitoids themselves, although whereas the granitoids show different degrees of fractionation of the HREE, the calculated sources have parallel HREE (Figs. 7.12). This suggests that although minor variations in the residual mineralogy may account for the different degree of fractionation of the HREE in the derivative partial melts the different and evolving levels of REE in the model sources may represent a progressive absolute enrichment of the granitoid source with time. This enrichment pattern is of similar character to the enriching component proposed for the upper mantle source of basaltic liquids, although no clear temporal trend could be discerned within the tholeiites of the present study. However, the younger basalts of the Gawler Ranges (Giles 1980) are progressively enriched in incompatible trace elements compared with the tholeiite dykes of the present study (Fig. 7.2).

Hence I propose that the lower crustal meta-basaltic, under-plated source of the I-type granitoids has, with time, suffered a progressive increase in incompatible trace elements, probably by both the transfer of enriched basaltic melt and mantle-derived fluids. This process is here suggested to account for the apparent transitional A-type character of the I-type granitoids.

Jahn et al. (1979) also suggested that some granitic rocks enriched in alkali elements were derived from granulites metasomatised shortly prior to the melting event.

However Giles (1980 a,b) explained the temporal enrichment in Zr, LREE etc. between GRV and CAV in quite a different way.

Table 7.6 Partial melt least squares modelling of (amphibole + garnet) granulite source to produce silicic melts of the Gawler Range Volcanics and the Central Australian Volcanics.

(a) Model partial melt GRV andesite from (parg + gt) granulite = B36

	B36	B36*	Residual	Component	Weight Fraction
SiO ₂	47.33	47.33	0.00	andesite	0.11
Al ₂ O ₃	16.16	16.18	0.02	cpx"	0.21
Fe ₂ O ₃ T	15.49	15.47	-0.02	opx"	0.05
MgO	7.21	7.22	0.01	plag"	0.26
CaO	9.70	9.70	-0.00	ilm	0.02
Na ₂ O	2.25	2.11	-0.14	parg"	0.18
TiO ₂	1.58	1.60	0.02	gt"	0.17
K ₂ O	0.76	0.80	0.04		
				Sum of squares of residuals = 0.02	

(b) Model partial melt Bunburn dacite from (parg + gt) granulite = B36

	B36	B36*	Residual	Component	Weight Fraction
	47.33	47.33	0.00	dacite	0.10
	16.16	16.16	0.00	cpx"	0.25
	15.49	15.49	0.00	opx"	0.03
	7.21	7.21	0.00	plag"	0.25
	9.70	9.70	0.00	ilm	0.02
	2.25	2.21	-0.04	parg"	0.17
	1.58	1.58	0.00	gt"	0.18
	0.76	0.78	0.02		
				Sum of squares of residuals = 0.01	

(c) Model partial melt Central Australian dacite from (parg + gt) granulite = B36

	B36	B36*	Residual	Component	Weight Fraction
SiO ₂	47.33	47.33	0.00	dacite	0.07
Al ₂ O ₃	16.16	16.18	0.02	cpx"	0.20
Fe ₂ O ₃ T	15.49	15.47	-0.02	opx"	0.07
MgO	7.21	7.22	0.01	plag"	0.27
CaO	9.70	9.70	0.00	ilm	0.02
Na ₂ O	2.25	2.12	-0.13	parg"	0.21
TiO ₂	1.58	1.60	0.02	gt"	0.16
K ₂ O	0.76	0.80	0.04		
				Sum of squares of residuals = 0.02	

Notes: (1) as for Table 7.5

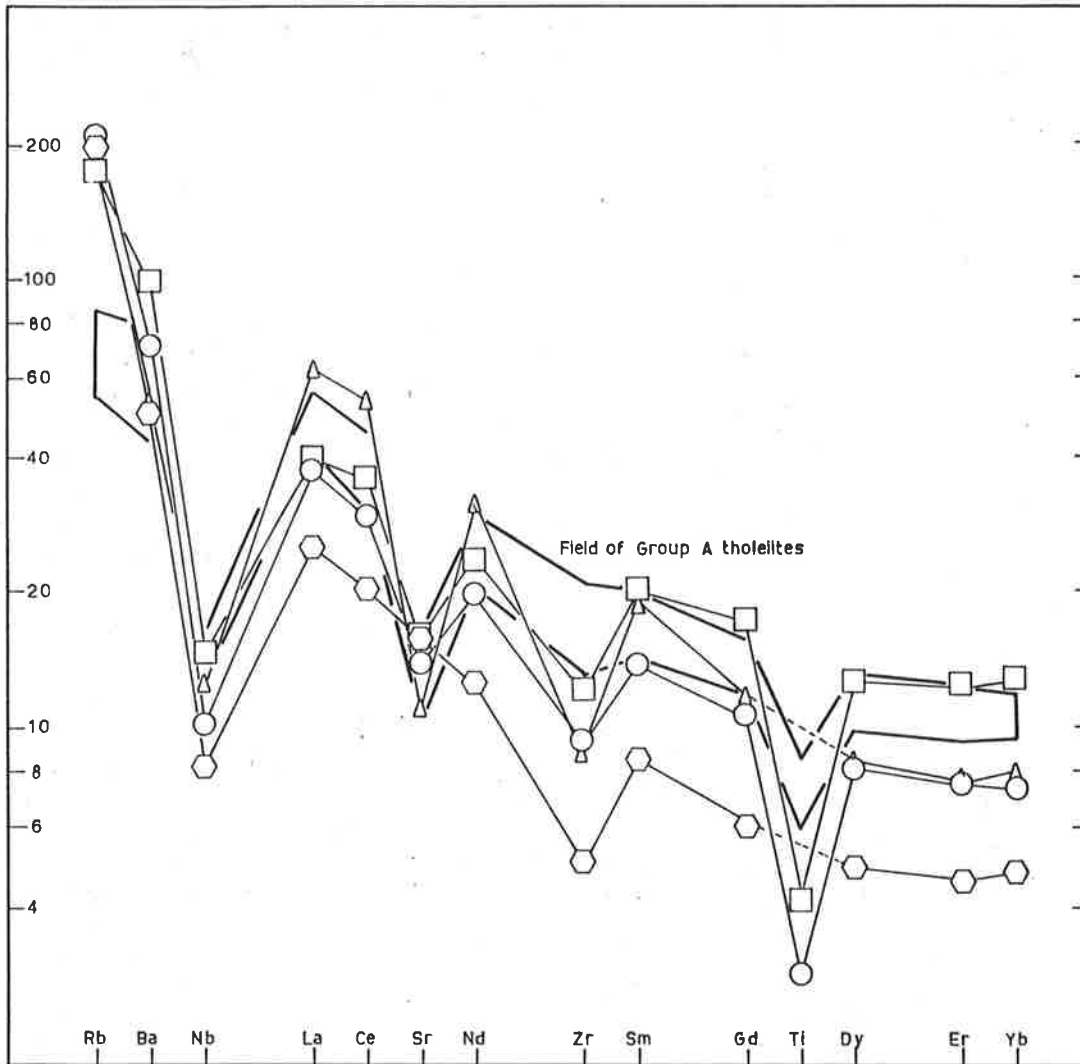


Figure 7.14

Calculated extended REE plots of preferred sources of the I-type melts of the present study compared with the field of Group A tholeiite dykes. Symbols as in Figure 7.3.

In line with suggestions by Vorma (1976) and Emslie (1978), Giles suggested that post-tectonic heating of the lower granulite crust under the influence of mantle diapirism, resulted in the breakdown of normally refractory accessory minerals such as zircon, liberating much Zr, REE etc. into the melts. It is difficult to envisage however, how such a mechanism could account for the associated very high concentrations of Rb, Ba and other elements unrelated to the refractory accessory minerals. Hence the present author favours the temporal enrichment of the source of the melts in these trace elements as outlined above.

Furthermore it is apparent that the I-type granitoid (and volcanic) geochemistry can be attributed to partial melting of juvenile accreted fertile mafic material without recourse to refractory lower crustal (possibly older) granulites.

7.3 CONSTRAINTS IMPOSED BY ISOTOPIC DATA

7.3.1 Sr-isotopic constraints on the source of the I-type melts

A previous crude calculation in Chapter 2 suggested the source of the DGS may have had a Rb/Sr ratio ca. 0.15 and hence may have separated from the bulk earth reservoir at ca. 2.4 Ga, assuming a simple two-stage model. Although this is approximately the age of the Sleaford Complex basement to the Early Proterozoic sequences in the Gawler domain, the exposed Sleaford Complex and its northerly equivalent the Mulgathing Complex have Rb/Sr ratios much greater than 0.15 (Appendix Table 1.2). Hence, if Sleaford Complex material comprises the source of the I-type granitoids there must necessarily exist a subjacent, relatively Rb depleted and extensive source.

However, a number of factors suggest the Sleaford Complex is not the granitoid source.

- (1) The siliceous Sleaford Complex would require ca. 50% partial melting to generate the silicic I-type granitoids (cf. Condie 1978).
- (2) A basic granulite is favoured as the model source of I-type granitoids (see above).
- (3) "Normal" lower Archaean crust has Rb/Sr much lower than 0.15, e.g. Taylor & McLennan (1979) estimate 0.047 and Weaver & Tarney (1980) suggest 0.021 based on Lewisian granulites.

Hence although reworking of Archaean sialic crust to produce younger

Table 7.7 Partial melt least squares modelling of Taylor & McLennan model lower crustal source to produce representative I-type melt of the present study.

Model partial melt MBG QF = D87

	T & M source	T & M source*	Residual	Component	Weight fraction
SiO ₂	54.00	53.98	-0.02	D87	0.20
Al ₂ O ₃	19.00	19.03	0.03	cpx	0.13 (0.16)
Fe ₂ O ₃ T	10.00	10.00	0.00	opx	0.11 (0.13)
MgO	4.10	4.16	0.06	plag	0.54 (0.66)
CaO	9.50	9.52	0.02	ilm	0.01 (0.02)
Na ₂ O	3.40	3.45	0.05	mag	0.03 (0.04)
TiO ₂	0.90	0.90	0.00		
K ₂ O	0.60	0.79	0.19		
				Sum of squares of residuals = 0.04	

- Notes: (1) as for Table 7.3
- (2) Magnetite composition from B26
- mag = Fe₂O₃T 96.44
- TiO₂ 2.22

granitoids has been favoured in the past by many workers, it does not seem to be favourable for the Gawler domain Proterozoic I-type granitoids and volcanics.

The basic granulite sources modelled above have calculated Rb/Sr ratios ranging from 0.36 - 0.52 (Appendix Table 7.1). These ratios are critically dependent on the presence of residual biotite in the model and on the Kd for biotite used in the calculations. Arth (1976) suggested a Kd = 3.06 for Rb in basaltic phlogopite and this value was used in calculating the above ratios. However Arth's Kd data for phlogopite and biotite in basalts, andesites, dacites and rhyolites indicate that Ba usually has a Kd much greater than for Rb. Hence the basaltic phlogopite Kd for Rb is probably overestimated and should be less than unity. Recalculation of the model source Rb/Sr ratios based on a Kd = 1 results in a range from 0.25 - 0.37 (Appendix Table 7.1). These are likely to be slightly too high. However, the calculated normalised Rb abundances and Rb/Sr ratios are similar to the meta-tholeiites of the study area (Fig. 7.14). If these lower calculated Rb/Sr ratios characterised the granitoid sources for the period of their existence, they could not have separated from the bulk earth reservoir more than ca. 600 Ma prior to the granitoid melt extraction events, and so probably evolved during the early stages of the Kimban Orogeny in the Early Proterozoic.

Similar arguments and calculations may be applied to the GRV and CAV (Fig. 7.15; see below).

Rb-Sr isotope systematics of the tholeiitic dyke rocks of the study area (Chapter 6) indicated that

- (1) upper mantle source areas of tholeiitic liquids were metasomatised and enriched in Rb/Sr at ca. 2.0 Ga and ca. 1.5 Ga,
 - (2) the Rb/Sr ratios of enriched sources and derived tholeiitic liquids were ca. 0.13 - 0.17,
- and (3) evolved tholeiitic liquids may have Rb/Sr ratios as high as ca. 1.0.

Sheraton & Black (1981) have also demonstrated that similar mantle enrichment processes occurred at ca. 2.4 Ga in Antarctic rocks which in the Early Proterozoic along with the Gawler domain comprised part of the Gondwanaland super continent. An extensive development of granulite facies metamorphism and granitoids occurred in the

Table 7.8 Calculated Ni and Cr abundances in model sources of I-type melts of the present study, compared with various proposed source rocks.

<u>Model pyroxene granulite source (B26)</u>			<u>Ni ppm</u>	<u>Cr ppm</u>
(this study)	MBG QF	(D87)	108	
	DGS FGGS	(B143)	88	177
	CGS	(B112B)		67
<u>Model garnet granulite source (B36)</u>				
(this study)	CGS	(B112B)		100
<u>Model Taylor & McLennan source</u>				
(this study)	MBG QF	(D87)	67	
	DGS FGGL	(B143)	56	116
	CGS	(b112B)		40
<hr/>				
Tholeiite dykes - Gawler domain (measured values)				
			41-256	66-2401
Andesite model lower crust - Taylor & McLennan (1979)				
			5-42	5-130
High-grade gneiss (Condie 1981)			40-50	20-35
Lewisian granulite (Weaver & Tarney 1980)			58	88

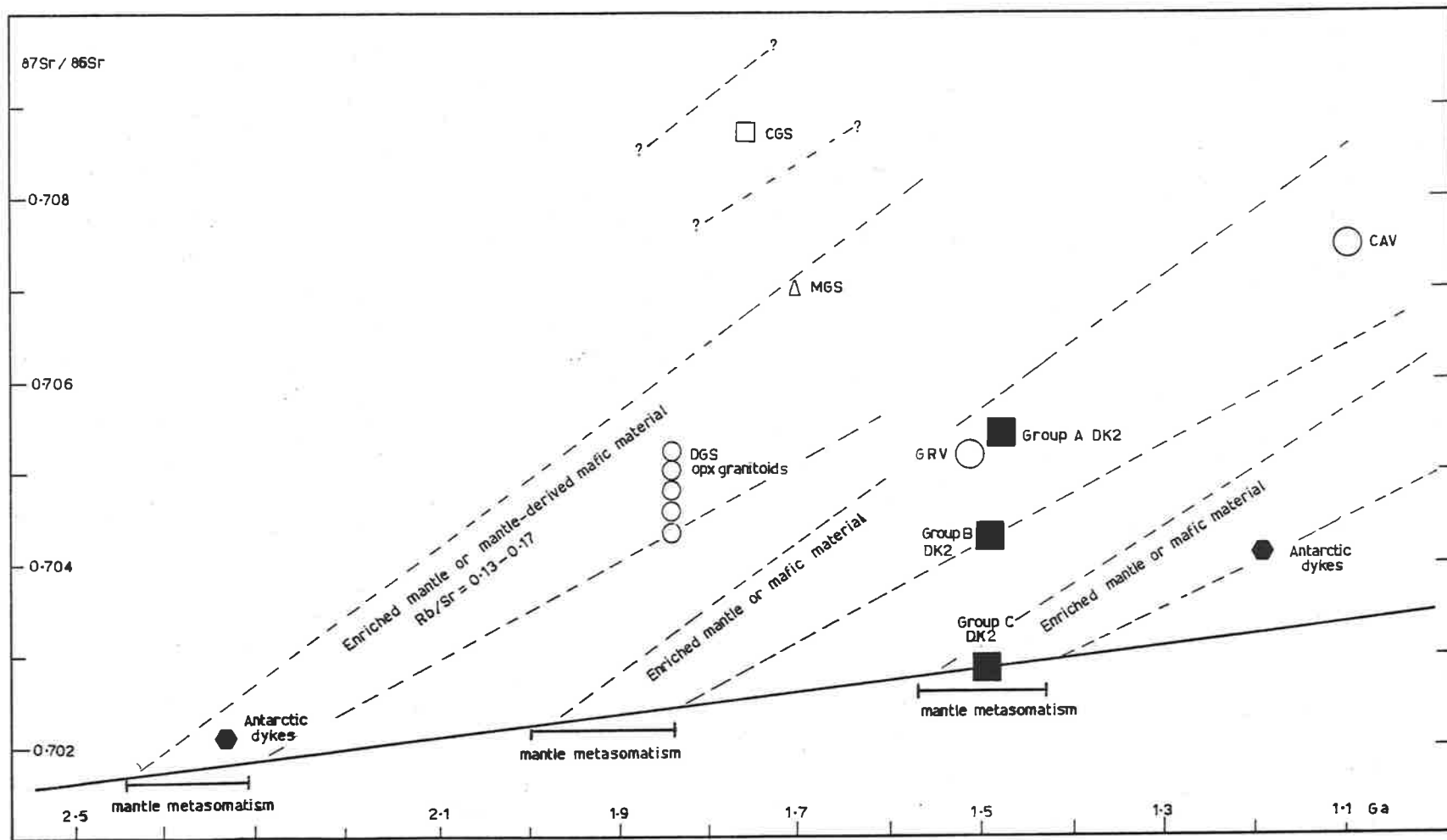


Figure 7.15

Sr-isotope evolution of model sources of I-type melts of the present study and of the Gawler Range Volcanics (GRV) and Central Australian Volcanics (CAV).

Gawler domain at ca. 2.4 Ga (Cooper et al. 1976; Webb & Thomson 1977; Daly et al. 1978) and may be another expression of this broad Gondwana event.

Sr-isotope evolution curves (Fig. 7.15) indicate that the CAV could have been generated at ca. 1.1 Ga (Gray 1971) from a tholeiite source generated at ca. 1.5 Ga from a mantle source enriched at ca. 2.0 Ga, or from a tholeiite derived from a bulk earth reservoir at ca. 2.0 Ga. The GRV could have been derived from a similar source to that of the CAV. The DGS, CGS and MGS (and probably the MBG QF) could also have been derived from a tholeiite source separated from an upper mantle reservoir at ca. 2.4 Ga and enriched in Rb shortly prior to partial melting or from a tholeiite source separated at ca. 2.0 Ga from a mantle source enriched at ca. 2.4 Ga (Fig. 7.15). Age and IR data for the granitoids intruding the Sleaford Complex suggest they too may have been derived from a tholeiite source generated at ca. 2.4 Ga from upper mantle enriched shortly prior to partial melting (Fig. 7.15).

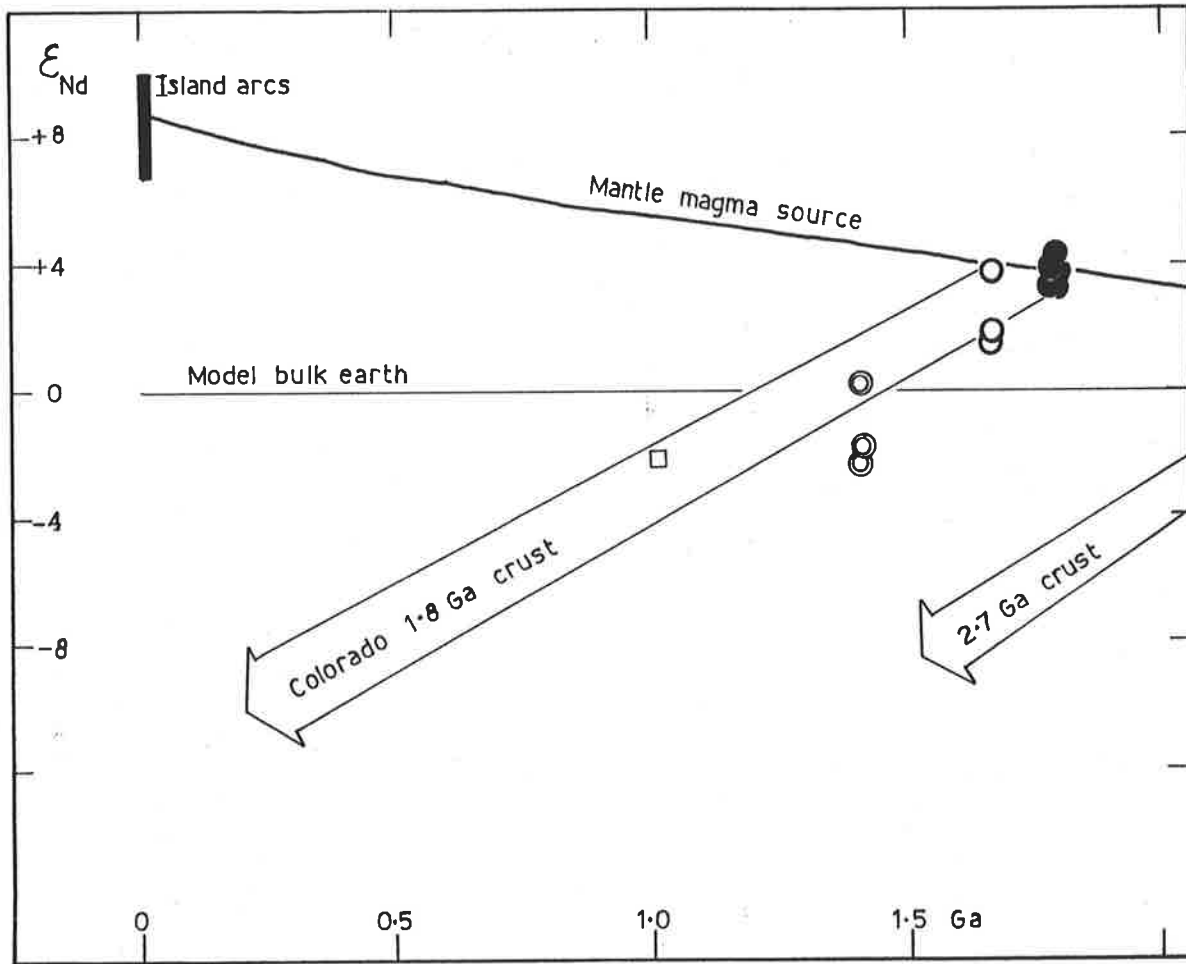
Thus a relatively simple isotopic model is favoured which closely couples upper mantle and lower crustal events, but which does not require the pre-existing Archaean sialic crust to have been actively involved in melt generation. Rather an enriched upper mantle source is envisaged to have been created at ca. 2.4 Ga, and shortly after, partially melted to yield enriched tholeiitic melts with Rb/Sr ca. 0.1 - 0.25 but bulk earth $87\text{Sr}/86\text{Sr}$. These melts intruded and underplated the lower sialic crust and formed a fertile source of anatectic silicic I-type magma.

The apparent episodicity and sequence of events may be due to a necessary rise in the prevailing geotherm in the lower crust to a level above the solidus of the underplated basaltic material either through radioactive heat build-up or mantle diapiric upwelling (see later discussion on tectonic development).

7.3.2 Sm-Nd isotopic constraints on magma sources

Germane to the question of the nature of Proterozoic orogenesis, and whether or not Proterozoic orogens represent new additions to the crust or recycled sialic crust is an examination of the body of data on Nd and Sr isotopes published in the last decade.

Data from Archaean to Recent volcanics and plutonic rocks suggest that for the early portion of Earth history prior to ca.



- metatholeiites
- Sherman & Silver Plume (GSP-1)
- Boulder Creek
- Pike's Peak

Figure 7.16

Large arrows show ϵ_{Nd} evolution for typical Colorado crust, and typical 2.7 Ga crust. The curve labelled 'mantle magma source' connects the average ϵ_{Nd} of the 1.8 Ga samples with the average for modern oceanic island arcs. The Colorado crust seems to have been derived solely from the mantle at 1.8 Ga (after DePaolo 1981).

2.7 Ga the bulk of the mantle reservoir had a chondritic Sm-Nd character, but that by melt extraction processes leading to crust formation a large mantle reservoir depleted in Nd over Sm was established by ca. 2.7 Ga (e.g. Weaver & Tarney 1980; Hamilton et al. 1979). However, McCulloch & Compston (1981) have shown that 2.8 Ga greenstones were derived from a depleted mantle source and suggest that mantle differentiation may have occurred (and been subsequently preserved) as early as 4.0 Ga.

Other studies have shown that long term time-integrated LREE enriched as well as depleted mantle reservoirs have existed within the Earth (e.g. Menzies & Murthy 1980; Carter et al. 1978).

These processes have led to a correlation between Nd isotopic composition and Sr isotopic composition for mantle derived melts which may be observed in modern oceanic and continental tholeiites and alkali basalts (e.g. De Paolo 1979).

If the mantle correlation between Nd and Sr isotopic composition is due to the extraction of continental crust, it is possible to deduce the Rb-Sr and Sm-Nd character of bulk continental crust (De Paolo 1979), and hence through ratios such as K/Rb, K/U, Th/U (Hamilton et al. 1979) to deduce the distribution of radioactive heat producing elements throughout the crust. These considerations have led Weaver & Tarney (1980) to propose that the Lewisian lower granulite and middle to upper amphibolite facies crustal segments represent typical Archaean crustal development in the root zones of ancient Cordilleran orogens, and to discount the andesite crustal accretion model of Taylor (e.g. Taylor & McLennan 1979). These conclusions are important to the consideration of the petrogenetic model for the Gawler domain silicic magmatic rocks enunciated above.

De Paolo (1981) has reported Sm-Nd isotopic data for a segment of Proterozoic crustal rocks in Colorado, U.S.A. Due to the presumed chondritic bulk earth Sm/Nd ratios of unmodified mantle equal to unity, and the tendency for mantle magmatism to generate melts with Sm/Nd less than unity, leaving a residual depleted mantle with Sm/Nd greater than unity, and the tendency for subsequent crustal processes to preserve the Sm/Nd ratio of the newly formed crust, it is possible with this technique to deduce the age at which a crustal segment first separated from the mantle. Furthermore it is possible to deduce whether a crustal rock of known age has come more or less directly from a mantle source at that time or whether it has

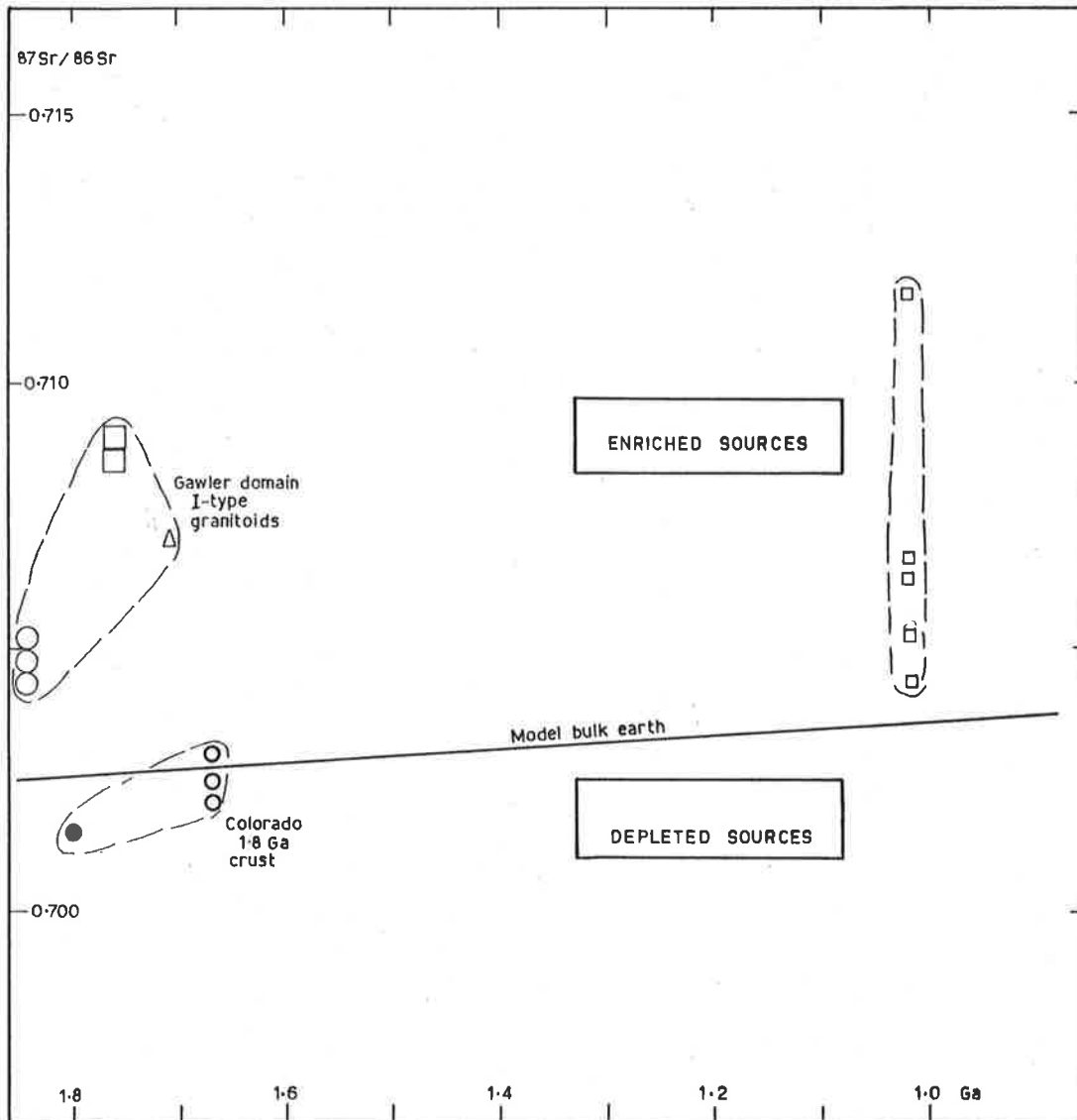


Figure 7.17

Comparison of Sr-isotopes of I-type melts of the present study with 1.8 Ga Colorado crustal rocks and 1.0 Ga Pikes Peak batholith granitoids. Symbols as in Figures 7.3 and 7.16.

experienced prior crustal history and hence may represent remelted sial. De Paolo's results (Fig. 7.16) demonstrate these possibilities and have led him to conclude that, in the Colorado rocks,

- (1) the Sm-Nd isotopic system is resistant to gross redistribution in crustal metamorphic processes
- (2) a major suite of 1800 Ma metavolcanics shows no evidence of influence from the adjacent Archaean continental crustal rocks, but were apparently derived in toto from the mantle at 1800 Ma
- (3) the mantle source was depleted (i.e. had Sm/Nd greater than the chondritic value)
- (4) comparison with modern oceanic island arcs suggests that a similar source of 1800 Ma crust and island arcs has existed in the mantle since the Archaean
- (5) subsequent granitoid intrusives in Colorado at 1670 Ma, 1430 Ma and 1415 Ma were derived by remelting of the 1800 Ma crust, rather than the mantle or older Archaean crust.

These rocks studied by De Paolo have been dated by Rb/Sr methods and hence invite comparison with the rocks of the present study.

7.3.3 Comparison of Sr-isotopes between Colorado and Gawler domain Proterozoic rocks

The initial ratios of the rock units studied by De Paolo are plotted against their isochron age on the Sr-isotope evolution diagram (Fig. 7.17) along with those of the present study. Relative to the model bulk earth Sr-isotope evolution, it is apparent that the 1800 Ma gneisses and 1670 Ma intrusives from Colorado are consistent with mantle sources depleted in Rb.

The 1000 Ma Colorado intrusives had been interpreted previously (Barker et al. 1975) to have resulted from a complex process of interaction and mixing of mantle derived basaltic melts and crustal rocks and melts. The wide range in IR's (Fig. 7.17) is consistent with such an interpretation.

However, comparison with the Sr-isotope data for the Gawler domain granitoids and silicic volcanics shows a fundamental difference, a source with a time integrated enrichment in Rb over the model bulk earth being required. Evidence has been presented above that the basaltic dyke rocks also were derived from Rb (and other LIL-element, including LREE) enriched source areas, which

may have been enriched up to 800 Ma prior to melt generation and extraction. The dominant geochemical cycle seems to be volatile fluxing of LIL-elements to upper mantle regions, followed by transfer of these elements to the lower crust by underplating of basaltic melt and subsequent impress of these characteristics on silicic melts derived from melting of the accreted underplated basaltic material. Within such a scheme, the present author finds little scope in the Gawler domain for the long-term depleted mantle source of Colorado and oceanic-island-arc-type proposed by De Paolo.

More generally speaking, De Paolo & Wasserburg (1979) have also shown the existence of an enriched upper mantle source region at 2700 Ma for the Stillwater complex, and oceanic volcanics show that both enriched and depleted mantle sources coexist at present (Carter et al. 1978). It seems probably then that long-lived, contemporaneous enriched and depleted mantle sources may be maintained within the Earth.

There exists abundant evidence for long-lived upper mantle heterogeneities, especially LREE and Rb enrichment, under the continents even in the Proterozoic (Kyle 1980; Sheraton & Black 1981; also the Hf isotope evidence of Patchett et al. 1981) and certainly in the modern day (e.g. Carter et al. 1978; Menzies & Murthy 1980).

This allows many possible isotopic scenarios for crust generation and coupled mantle-crust evolution, and also argues against efficient mantle convective mixing, or may be simply a natural consequence of heterogeneous recycling of surface materials back into the mantle via subduction (e.g. Armstrong 1982; Fyfe 1978). Such a view may favour the possibility in the Proterozoic that although most orogenesis was essentially ensialic, within plates, involving accretion from below by underplating and ductile spreading above hot-spots, elsewhere at plate margins subduction processes analogous to those of the modern day may have been recycling continent derived sediment and volatiles from the ocean back into the mantle.

7.3.4 Concluding statement

The Sr-isotope character of Gawler domain silicic magmatic rocks, although superficially suggestive of involvement of older Archaean sial, when compared with Nd-isotopic data from other areas, is more suitably interpreted in the framework of derivation by remelting of juvenile mafic material of Proterozoic age.

Analysis of Sm-Nd isotopes of Gawler domain basaltic and silicic rocks would be a most powerful addition to the data of the present study.

7.4 PROTEROZOIC TECTONIC MODELS

7.4.1 Introduction

A major aim of this study is to comment on the likely processes occurring in Proterozoic orogenesis. To this end the tectonic pattern of the study area will be examined, followed by a comparison with previous regional studies of the Gawler domain and a consideration of Proterozoic orogenic belts on a global scale. In this way, it is hoped to contribute to the debate concerning the question of whether or not juvenile sial has been created in large amounts in the interval following the Archaean.

7.4.2 Tectonic pattern of the study area

The study area is within the Cleve subdomain (Parker & Lemon 1982) of the Gawler domain of the Arunta-Gawler Province (Rutland 1976). Within the Cleve subdomain Archaean sialic basement is overlain by Early Proterozoic metasedimentary rocks (Hutchison Group) and both have been highly metamorphosed and interfolded with granitic gneisses (Lincoln Complex) during the interval ca. 1.8 Ga to 1.5 Ga (Rutland et al. 1981). The Hutchison Group consists of a thin (ca. 2 km) sequence of shallow water, mature quartzites, calc-silicates, pelitic schists, dolomite, iron formation and quartzofeldspathic gneisses with associated amphibolites of probable metatholeiitic origin (Parker & Lemon 1982). There is no stratigraphic reason to propose the existence of oceanic crust in the Cleve subdomain at this time.

In Chapter 5 it was proposed that the quartzofeldspathic gneisses (QF) of the Massena Bay Gneisses (MBG) occupy a similar stratigraphic position to the Hutchison Group, but are dominated by metaigneous rocks, probably metavolcanics, and possibly served as a coeval volcanogenic source for much of the sediment in the adjacent Hutchison Group. The metavolcanics of the QF and associated amphibolite dykes or sills comprise a bimodal magmatic suite and lack intermediate composition magmas. The lack of calc-alkaline andesite argues against subduction related, plate marginal tectonics for the Cleve subdomain (Martin & Piwinski 1972).

Furthermore, the structural analyses of the present study and of Parker & Lemon (1982), Richardson (1978), Glen et al. (1977), Cooper et al. (1976) and Rutland et al. (1981) show clearly that the early foliation in the metamorphic rocks was layer parallel and flat-lying. Such a pattern is unlikely to be related to the stress field associated with subductive, plate marginal tectonics but is more consistent with extensional ductile tectonics (e.g. Park 1981; Pulvertaft 1973).

In addition, evidence derived from the basaltic dyke rocks (Chapter 6) may be taken to suggest that the geothermal gradient represented by the pyroxene and garnet granulites was transient and a disturbed situation resulting from extensive underplating of the crust by basaltic melts (cf. Wells 1980). Unusual tectonic stability may be proposed to have allowed near-isobaric cooling to the prevailing geotherm, manifested by garnet coronal textures (cf. Ellis 1980).

Such features are more consistent with an ensialic intra-continental hot-spot mode of orogenesis (e.g. Fyfe 1978; Wynne-Edwards 1976; Rossiter & Ferguson 1980). This model will be enunciated more fully below following a review of the Arunta-Gawler Province and the Proterozoic geology of other continents.

7.4.3 Tectonic review of the Arunta-Gawler Province

Rutland et al. (1981) and Glen et al. (1977) compared the Gawler, Willyama and Musgrave domains of the Arunta-Gawler Province, and Rutland (1976) reviewed the Proterozoic domains of the Australian continent as a whole. Rossiter & Ferguson (1980) in addition, have reviewed the Proterozoic domains of the northern half of the Australian continent.

The general consensus of these reviews is that the Early Proterozoic sequences were deposited in long troughs, fault bounded and apparently due to extensional tectonics or rifting. Some of the troughs were non-volcanogenic and apparently floored by sialic crust, but Rossiter & Ferguson propose that some, e.g. the Halls Creek and Pine Creek domains, rifted sufficiently to form ocean basins. In any case, the dominant bimodal volcanism or plutonism and hence the lack of calc-alkaline intermediate rocks argues against the involvement of plate marginal subduction zones, in favour of rifting. In concert with the prominence of rifting Rossiter & Ferguson (1980) and Katz (1976) recognised the importance

of fundamental strike-slip faults in the distribution of these domains.

Although recognising the importance of extensional tectonics and crustal thinning in these domains, compressional stages of deformation also have been emphasised (e.g. Rutland 1976).

Subsequent to active orogenesis in these domains, thin continental sedimentary sequences and subaerial volcanics (e.g. Gawler Range Volcanics), which remain essentially undisturbed to the present day, are common. There can be no doubt that these deposits accumulated on cratonic sialic crust. Rossiter & Ferguson (1980) have linked the basaltic and silicic magmatism in all these domains to the activity of mantle plumes (Anderson 1975) and their interaction with the overlying lithosphere. Giles (1980 a,b) also has invoked mantle plumes to initiate basic and silicic volcanism in the Gawler Ranges and other Proterozoic domains. The general conclusion to be drawn from the above review is that the Proterozoic geology of Australia is not in a framework of plate marginal subduction related tectonics but is of continental interior (or perhaps marginal) rifting type, probably initiated and sustained by mantle plumes.

The prominence of rifting tectonics in the Proterozoic of Australia led Rutland (1976) to assert that "active continental margins ... analogous to those of the present day are absent from (both the Archaean and) Proterozoic provinces of Australia."

7.4.4 Brief review of global Proterozoic tectonics

(1) Ensimatic rifting

A number of localities exist throughout the world where there exists good evidence that Proterozoic volcanic and sedimentary sequences were deposited on oceanic crust. Strong et al. (1978) and Strong & Dostal (1980) proposed for the Avalon Zone of eastern Newfoundland that the abundance of Proterozoic pillow lavas and mafic pyroclastics argue for an oceanic environment associated with ensimatic rifting. Strong & Dostal, however, further suggested that the rifting was aborted for some reason and the small ocean closed up again.

In many other localities the importance of rifting and aulacogen formation in the Proterozoic is recognised (e.g. Coronation geosyncline and East Arm and Bathurst aulacogens; Circum-Ungava geosyncline and Labrador Trough; references cited in Wynne-Edwards

1976) but the volcanic and sedimentary sequences are believed to have been deposited on sialic crust and hence to be ensialic (e.g. Wynne-Edwards 1976).

(2) Subduction-related orogenesis

Katz (1972) asserted that remnant paired metamorphic belts associated with eugeosynclinal and island arc elements of Precambrian age are recognisable in Ceylon and other parts of Gondwanaland. Torske (1977,1976) described a zonation in lithological associations in southern Norway including abundant calc-alkaline andesite which he suggested was derived from a long-lived Cordilleran orogen dating from ca. 1750 Ma to 850 Ma. More spectacularly, Lewry (1981) has proposed a complex tectonic pattern for the Early Proterozoic of northern Saskatchewan involving multiple collisions of island arcs and microcontinents with associated abundant intermediate calc-alkaline volcanic and plutonic rocks.

Taylor & McLennan (1979) defended the model of growth of continental crust by accretion of island arcs.

(3) Intracontinental ensialic orogenesis

Sutton & Watson (1974) argued strongly that the bulk of Early Proterozoic orogenic areas showed a contrasting and probably fundamentally different style of intracontinental tectonism from the Archaean and Late Proterozoic. A similar thesis has been proposed by e.g. Wynne-Edwards (1976), Glikson (1976), Bridgewater et al. (1973), Kroner (1977), Fyfe (1978) and others. The common areas of post-orogenic or anorogenic bimodal magmatism of Proterozoic age have been considered to be of intracontinental rift type (e.g. Emslie 1978). Complexes of this latter type may consist of essentially flat-lying volcanics (e.g. Gawler Ranges, Giles 1980a,b) or granitic rocks of the rapakivi-anorthosite association (e.g. Vorms 1976), or both.

Glikson (1976) has reviewed the initiation and evolution of Proterozoic mobile belts on the major continents and concurred with McConnell (1972) and Windley (1973) in emphasising the close spatial relationship of subsequent Phanerozoic rift structures and the earlier mobile belts, leading to an ensialic rift model. The rift valley model is capable of explaining the evolution of ensialic mobile belts in terms of subsidence of down faulted troughs and

associated advection of subjacent mantle diapirs (Glikson 1976). The following features are a natural consequence of this model (after Glikson 1976)

- (a) common epicontinental and continental-type sediments, especially quartzite
- (b) the scarcity of deposits typical of modern oceanic, island arc or cordilleran environments such as ophiolites, andesites, turbidites and melange-type sediments
- (c) abundance of bimodal continental-type tholeiites and silicic rocks
- (d) the major boundary faults and shear zones within mobile belts
- (e) the common occurrence of alkaline intrusions.

Glikson extended this model to imply Proterozoic ensialic circum-cratonic mobile belts without the existence of much oceanic crust, and suggested this may be consistent with the expanding Earth hypothesis.

Many workers favour an origin of the silicic magmas, in such an ensialic rift model, by melting of the lower sialic crust. The heat for such melting is thought to be supplied by mantle diapirism (e.g. Wynne-Edwards 1976; Giles 1980 a,b) or by ponding and differentiation of sub-crustal basaltic magma (e.g. Barker et al. 1975; Emslie 1978). Wynne-Edwards (1976) further suggested that it was possible in the mobile belts to recognise an early stage of crustal attenuation which led him to propose ductile spreading of sialic crust over the hot-spot. In his millepede model of ductile plate tectonics he proposed that the common mylonite shear zones represented transformal shear zones analogous to transform faults on the modern ocean floor. He also suggested that the transformal shear zones acted as conduits for metal-rich exhalative fluids leading to ore deposit formation within, or adjacent to, the zones. Sawkins (1976) developed this theme with relation to Cu, Pb and Zn deposits.

Fyfe (1978) in a more theoretical and general discussion of plate tectonic and hot-spot related tectonics concluded that the role of fluids in the crust was of major importance. He emphasised the likelihood of ponding of basaltic melts at the Moho and the associated release of much heat and vapour into the overlying crust with expected consequences of reactivation and melting of sialic

crust. The vapour influx could account for the retrogression observed in many granulite terrains and retrograde shear zones (e.g. Beach & Tarney 1978; Etheridge & Cooper 1981). Fyfe concluded that "dense magma injection at the base of the light continental crust is an obvious method of producing tectonic processes inside a continental plate by decoupling continental crust at the Moho interface."

Rossiter & Ferguson (1980) have applied a hot-spot related rifting model to the northern Australian Proterozoic orogenic areas and concluded that mantle plumes located adjacent to the old continental margin resulted in fault bounded trough deposition, often on newly generated oceanic crust, and rifting of continental blocks away from the margin on major transcurrent zones. An important facet of their model is the possibility of episodic activity associated with the mantle plumes due to depletion and subsequent replenishment of radioactive heat in the uranium-rich plumes (Anderson 1975).

Wynne-Edwards (1976) favoured similar hot-spot related rifting, but preferred to accept an ensialic association for most Proterozoic orogens. He suggested that Proterozoic sialic crust may have been more ductile than Phanerozoic lithospheric crust so that considerable ensialic ductile spreading and thinning may have occurred in the Proterozoic without brittle failure to produce oceanic basins. He envisaged relatively fixed mantle hot-spots (cf. Kroner 1977) over which the crust passed, resulting in migratory metamorphism and magmatism. Such fixed heat sources are consistent with the chemical plumes proposed by Anderson (1975) and required in the modern oceans for island chains such as Hawaii.

Wyborn & Page (1983) argued that in the Australian Early Proterozoic a plume-related rifting or extension event(s) took place, with associated accretion of large volumes of basic material to the base of the crust, now represented by residual positive gravity anomalies. The geochemical and Rb/Sr isotopic constraints imposed by I-type granitoids of the Mount Isa inlier, believed by Wyborn & Page to be typical of the other I-type granitoids, suggest that the granitoids were derived by partial melting of this accreted basic material.

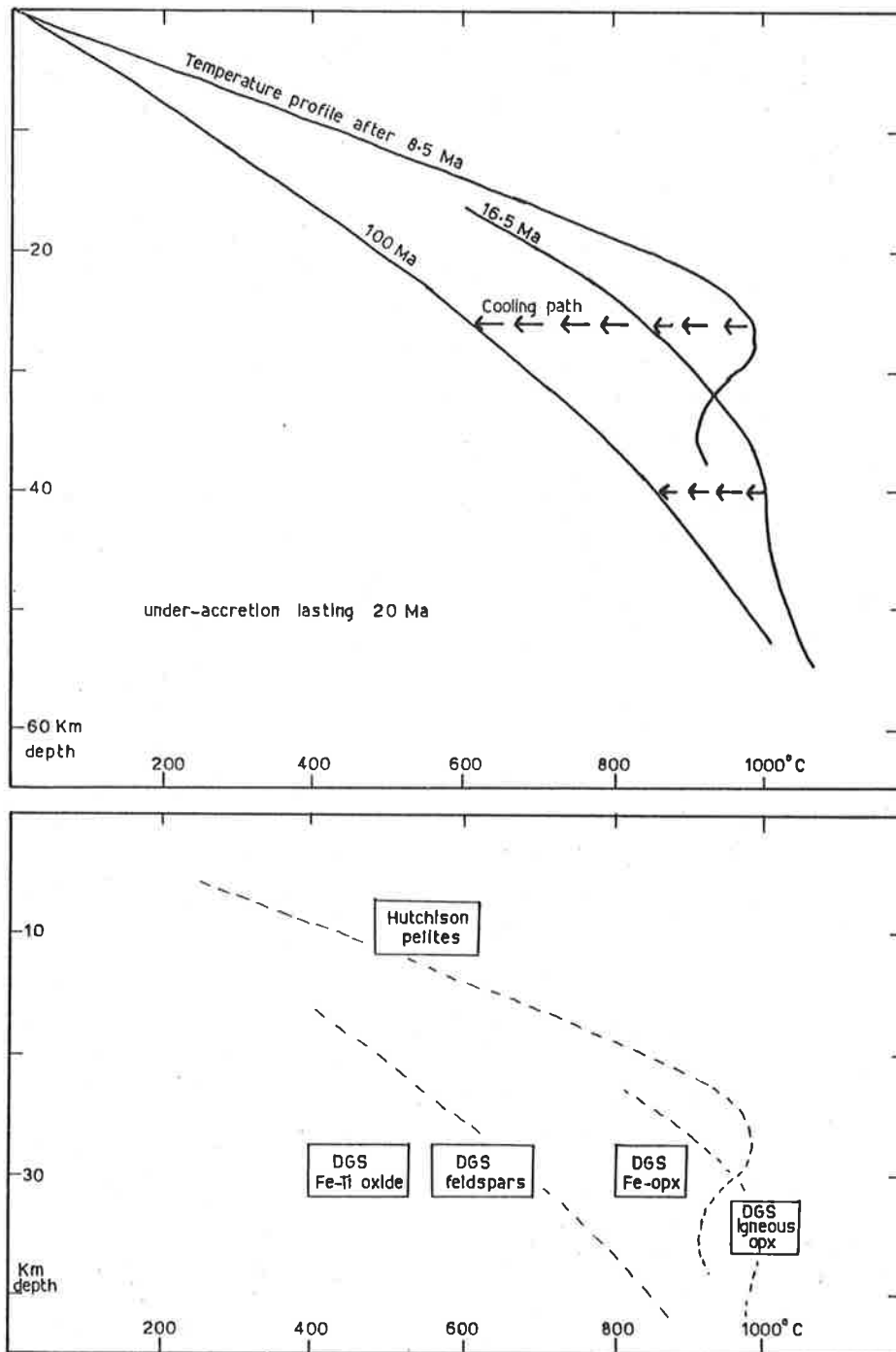


Figure 7-18

Model temperature profiles and cooling paths in crust undergoing under-accretion (after Wells 1980) compared with some P-T estimates from the present study and from the Hutchison Group (after Coin 1976).

7.4.5 Brief review of models of crustal development

Ancient terrains of both Archaean and Proterozoic age are commonly metamorphosed into the granulite and amphibolite facies. Newton et al. (1980) argued that newly accreted crust, if residing at depths of 25 - 40 km at elevated temperatures would suffer widespread melting by intrinsic heat production unless the radioactive heat producing elements were removed within 50 - 100 Ma after accretion. An upward transport of K, U, Th, and Rb by fluids has been proposed by Newton et al. (1980), Hamilton et al. (1979) and Weaver & Tarney (1980), leaving residual depleted lower granulite crust which has otherwise normal major and trace element composition. Newton et al. (1980) and Glassley (1982) have emphasised the role of CO₂-rich fluids in these lower crustal processes consistent with the observed CO₂ fluid inclusions in granulites (Touret 1971). This lower granulite crust is viewed as being stable in terms of tectonothermal mobility. Newton et al. (1980) emphasised mantle outgassing as the source of CO₂ and in some cases utilised a hot-spot model and basaltic underplating of continental crust which cools to garnet granulites or amphibole eclogite or garnet amphibolite.

Bailey (1983), Menzies & Wass (1983) and Wass & Rogers (1977) also comment on the role of CO₂ in the subcontinental mantle. They suggest that mantle metasomatism by CO₂-rich deep mantle fluids (manifesting continuing mantle degassing) is a precursor to rift-related mafic continental magmatism. Bailey (1983) in particular, strongly challenged the upwelling mantle, active rift mechanism repeatedly invoked in the studies reviewed above, in favour of a passive lithospheric extensional mechanism. He suggested the volatile fluxing or outgassing mechanism could better explain the localised magmatism in the narrow rift zones and the common observation that rift zones abort abruptly.

Wells (1980) modelled the thermal state with time of a profile through continental crust as accretion within or below the crust occurs. In all of the various models he presented, the overall thermal profiles are markedly convex towards the temperature axis, "a feature which is typical of crustal segments undergoing extensive magmatic addition." Such geotherms may even become partly inverted (Fig. 7.18). When underplating ceases the opportunity for near-isobaric cooling and subsequent isostatic uplift exists. "With

modest erosion rates the post-tectonic, post-accretion, conductive relaxation of the thermal profiles follows near isobaric cooling patterns, of the kind preserved in mineral assemblages described in some granulite terrains" (Wells 1980; cf. Ellis 1980).

7.4.6 A specific tectonic model for the present study area

The present author finds the arguments presented in favour of the ensialic rifting model to be most attractive. It is suggested here that a deep mantle chemical plume of the type described by Anderson (1975) may have underlain the Cleve subdomain in the Early Proterozoic (cf. Rossiter & Ferguson 1980). Such a chemical plume is a fertile source of radioactive heat but not of chemical components, the low melting fraction presumably having been extracted earlier in earth history, and does not necessarily entail widespread mantle upwelling (Anderson 1975). The hot asthenospheric plume is mainly envisaged to have disturbed the configuration of the base of the lithosphere and to have precipitated a lithospheric tectonic (and anatectic) response. This is favoured by the present author as the geochemical and isotopic compositions of the basaltic rocks (Chapter 6) do not favour an old chemically anomalous source in the plume itself for the tholeiitic melts, but a more normal bulk earth reservoir. It is here suggested, though, that incipient melting deep in the lithosphere as the rising sub-continental geotherms intersected the pyrolite solidus may have occurred in the presence of moderately high fluid activities (CO_2 and H_2O in particular) possibly a function of outgassing of the deep mantle, and possibly focussed by the chemical plume (cf. Bailey 1983). This incipient fluid-rich melt is suggested to be the ultimate metasomatic source of the enriching component of the upper mantle tholeiite melt sources.

The early response of Proterozoic sialic crust to the plume activity, enhanced by the underplating of basaltic melt to the base of the crust and possible decoupling of crust and mantle (e.g. Fyfe 1978), was ductile spreading and thinning and the formation of upper crustal shallow depositional troughs. Deposition of the Hutchison Group (Chapter 5) is envisaged to have occurred in this shallow environment.

Ductile spreading may also account for the early S_1 fabric in the study area being flat-lying and layer-parallel and only rarely

seen to be associated with F_1 folds (Chapter 1). Rise of geotherms and transfer of much heat to the lower crust by basaltic melt and fluid-rich trace element enriched component, produced the transient disturbed elevated geotherms described above. Partial melting of the early accreted basic material resulted in I-type granitoid melts such as the MBG QF and DGS. Continued evolution of this granitoid source by addition of fluid enriching component is suggested to account for the temporal evolution seen in the I-type granitoid chemical composition.

The Kalinjala Mylonite Zone, although now largely expressed as a D_3 structure, has been suggested above to have been an active zone of retrogressive metasomatic fluid flow and deformation in D_1 and D_2 as well, and to constitute a fundamental crustal weakness. Large mylonitic zones may intersect the mantle (Beach 1976) and this, coupled with the geochemical character of the retrogressive fluids (Chapters 2 and 6), suggests that the Kalinjala may have acted as a channel way for the passage of mantle derived fluids of the type responsible for the metasomatism of the upper mantle source of basalts (Chapter 6). In this way the Kalinjala has many of the characteristics of the transformal shear zones of Wynne-Edwards (1976). Furthermore it has been noted above (Chapter 5) that the Kalinjala is a stratigraphic and metamorphic discontinuity and as such has exercised a strong control over the geology of the study area.

The locus of granitoid magmatic activity tends to have been displaced to the north with time from the DGS to the MGS to the GRV (Fig. 1.1). This may support the concept of southward migration of the sialic crust over a relatively fixed mantle hot-spot (cf. Wynne-Edwards 1976). Cooling of the crust as it moved away from the heat source may account for the isobaric cooling proposed for some of the metatholeiitic rocks and may have contributed to the decline in ductile spreading within the crustal rocks in favour of a compressional crustal thickening against the cratonic foreland, in this case the Archaean Coultas subdomain (Fig. 1.1). This thickening could also account for the isostatic uplift and erosion within the Cleve subdomain prior to and following D_3 (Rutland et al. 1981), thus resulting in the GRV resting unconformably on the high-grade gneisses.

Production of the subaerial GRV without apparent high-grade metamorphism suggests that although similar melting conditions existed at the base of the crust below the GRV at ca. 1.5 Ga, the geotherms had not risen as high, nor had the crust in this segment thinned as much with basin rifting, perhaps reflecting faster spreading or a decline in heat production or more brittle fracturing allowing upward migration of melts.

These observations suggest that the model of Giles (1980 a,b) for the extreme enrichment of the GRV (and CAV) silicic volcanics in LIL-elements such as Zr etc., whereby his proposed extreme elevated temperatures, dry lower crustal conditions and high fO_2 led to the decomposition of refractory accessory minerals such as zircon etc., is not appropriate. It is difficult to envisage these minerals decomposing at ca. 1.5 Ga for the GRV in the absence of high-grade metamorphism in the Cleve subdomain, but not decomposing to the same or greater extent in the source of the DGS or MBG QF at ca. 1.8 Ga in the presence of granulite facies metamorphism. However, it is considered here that the ensialic hot-spot tectonic model outlined above is well able to explain the geochemical similarities between the orogenic granitoids and post-orogenic GRV in terms of an evolving, migrating, metasomatised source region, better indeed than Giles's model or subduction related tectonic models.

It is important to note that although crustal growth by accretion of island arc andesite is not favoured in this model, the sub-crustal basaltic accretion and subsequent partial melting of this accreted material, does constitute a crustal accretionary process. However, it is also important to note that the hot-spot tectonic model adopted, despite allowing crustal accretion in this manner, does not require nor favour the extensive creation of oceanic crust nor subducting plate marginal processes, but allows intraplate ensialic tectogenesis.

7.5 CONCLUDING DISCUSSION

The questions posed at the beginning of this chapter concerning the nature of Gawler domain Proterozoic orogenies and its implications for world wide interpretation may now be addressed.

- (1) In the Early to Middle Proterozoic the study area developed by rifting continental crust over a mantle hot-spot; the area was intracontinental not continent marginal.
- (2) Juvenile sialic crust was created at this time by a complex addition of underplated basaltic melt and subsequent infracrustal emplacement of I-type granitoid melts derived from remelting of this underplated material. Bimodal magmatism resulted there being no hint of growth of continental crust in the study area by accretion of subduction related calc-alkaline andesite or tonalite.
- (3) The Gawler domain is well portrayed by the sequence of mantle, subcrustal, lower crustal and upper crustal events discernible in the study area.
- (4) Although areas of continental marginal orogenesis do exist in the Early Proterozoic globally, the dominant pattern is apparently one of intracontinental ensialic orogenesis. Magmatism is commonly bimodal and of a similar type to that observed in the study area. It is suggested that a close examination and comparison of high-crustal pressure igneous and metamorphic trends within associated basaltic and silicic rocks in other Proterozoic terrains may reveal similar relationships to those suggested for the present study area. In this regard it is noted that Vorms (1976) has commented on the geochemical similarity with respect to certain key elements of basaltic and granitoid rocks in the rapakivi massifs of Finland.

The dominance of intracontinental mobile belts developed within sialic crust, without the development of major ocean basins, may be related to the enhanced ductility of continental lithosphere in the Proterozoic in contrast to more brittle Phanerozoic lithosphere (e.g. Wynne-Edwards 1976).

7.6 SUGGESTIONS FOR FURTHER WORK

Much of the evidence for mantle metasomatism is provided by the LIL-element enriched nature of basaltic dyke rocks, and their elevated IR's, which were argued to be primary and to reflect their

mantle source. Assessment of the isotopic state of equilibrium of the minerals within the dolerites would serve to confirm or dispute this conclusion (cf. Patchett et al. 1979), and place this major portion of thesis on a firmer footing.

By analogy a similar test applied to the phenocrysts in the granitoid rocks (although most have been metamorphosed) would help to assess the emplacement and subsolidus history of the granitoids.

In the light of the powerful combined application of Nd and Sr isotopes in many geological situations, analysis of the basaltic and granitoid rocks would be illuminating. In addition a coupled Sr-Nd study of the Archaean basement rocks of the Gawler domain would provide a useful counterpoint to the conclusions of this study.

O and H isotope studies would also serve to delineate any radiogenic isotope and geochemical features attributable to water-rock interaction. Furthermore, in the light of the retrogressive model applied to the Kalinjala Mylonite Zone an O and H isotope study may enable the source of water to be constrained and hence to comment on the applicability of the present author's model.

REFERENCES CITED

- Albuquerque CAR de (1971) Petrochemistry of a series of granitic rocks from northern Portugal. Bull Geol Soc Am 82: 2783-2798
- Anderson DL (1975) Chemical plumes in the Mantle. Bull Geol Soc Am 86: 1593-1600
- Arculus RJ, Smith D (1979) Eclogite, pyroxenite and amphibolite inclusions in the Sullivan Buttes latite, Chino Valley, Yavapai County, Arizona. In: Boyd FR, Meyer HOA (eds.) The Mantle Sample: Inclusions in Kimberlites and Other Volcanics., Am Geophys Union, Washington DC: 309-317
- Armstrong RL (1968) A model for the evolution of strontium and lead isotopes in a dynamic earth. Rev Geophys 6: 175-199
- Armstrong RL (1981) Radiogenic isotopes: the case for crustal recycling on a near-steady-state no-continental-growth Earth. Phil Trans R Soc Lond A 301: 443-472
- Arriens P (1975) Geochronological study of some Proterozoic rocks in Australia. Abstr I Aust Geol Conv, "Proterozoic Geology, Geol Soc Aust:
- Arth JG (1976) Behaviour of trace elements during magmatic processes - A summary of theoretical models and their applications. Jour Research US Geol Surv 4: 41-47
- Arth JG, Barker F (1976) Rare-earth partitioning between hornblende and dacitic liquid and implications for the genesis of trondhjemitic - tonalitic magmas. Geology 4: 534-536
- Arth, JG, Hanson GN (1975) Geochemistry and origin of the early Precambrian crust of northeastern minnesota. Geochim Cosmochim Acta 39 : 325-362
- Bailey DK (1982) Mantle metasomatism - continuing chemical change within the Earth. Nature 296: 525-530
- Bailey DK (1983) The chemical and thermal evolution of rifts. Tectonophys 94: 585-597
- Barker DS (1978) Magmatic trends on alkali-iron-magnesium diagrams. Am Mineral 63: 531-534
- Barker F, Arth JG (1976) Generation of trondhjemitic - tonalitic liquids and Archean bimodal trondhjemite - basalt suites. Geology 4: 596-600
- Barker F, Arth JG, Peterman ZE, Friedman I (1976) The 1.7 to 1.8 - b.y. - old trondhjemites of southwestern Colorado and northern New Mexico: Geochemistry and depths of genesis. Geol Soc Am Bull 87 : 189-198.
- Barker F, Wones DR, Sharp WN, Desborough GA (1975) The Pikes Peak batholith, Colorado Front Range, and a model for the origin of the gabbro - anorthosite - syenite - potassic granite suite. Precambrian Res 2: 97-160
- Bateman PC, Chappell BW (1979) Crystallization, fractionation, and solidification of the Tuolumne Intrusive Series, Yosemite National Park, California. Bull Geol Soc Am 90: 465-482
- Beach A (1974) Amphibolisation of Scourian granulites. Scott J Geol 10: 35-43

- Beach A (1976) The interrelations of fluid transport, deformation, geochemistry and heat flow in early Proterozoic shear zones in the Lewisian complex. *Phil Trans R Soc Lond A* 280: 569-604
- Beach A (1980) Retrogressive metamorphic processes in shear zones with special reference to the Lewisian complex. *J Struct Geol* 2: 257-263
- Beach A, Fyfe WS (1972) Fluid transport and shear zones at Scourie, Sutherland: evidence of overthrusting? *Contrib Mineral Petrol* 36: 175-180
- Beach A, Tarney J (1978) Major and trace element patterns established during retrogressive metamorphism of granulite facies gneisses, NW Scotland. *Precambrian Res* 7: 325-348
- Beswick AE, Carmichael ISE (1978) Constraints on mantle source compositions imposed by phosphorus and the rare-earth elements. *Contrib Mineral Petrol* 67: 317-330
- Bhattacharyya C (1977) The present status of the charnockite problem with special reference to the progress of research on charnockite and orthophroxene-bearing granulites of India. *Ind J Earth Sci, S Ray Volume* 195-223
- Binns RA (1962) Metamorphic pyroxenes from the Broken Hill district, New South Wales. *Mineral Mag* 33: 320-338
- Black LP (1977) A Rb-Sr geochronological study in the Proterozoic Tennant Creek Block, Central Australia. *BMR J Aust Geol Geophys* 2: 111-122
- Black LP, Bell TH, Rubenach MJ, Withnall IW (1978) Geochronology of discrete structural - metamorphic events in a multiply deformed Precambrian terrain. *Tectonophys* 54: 103-137
- Bohlen SR, Essene EJ (1978) Igneous pyroxenes from metamorphosed anorthosite massifs. *Contrib Mineral Petrol* 65: 433-442
- Bradley GM (1972) The geochemistry of a medium pressure granulite terrain at southern Eyre Peninsula, Australia. Ph.D. Thesis, Aust Natl Univ (unpubl)
- Bradley GM (1980) Metamorphism of the Archaean and Proterozoic basement at southern Eyre Peninsula, South Australia. *J Geol Soc Aust* 27: 50-51
- Branch CD (1978) Evolution of the Middle Proterozoic Chandabooka caldera, Gawler Range acid volcano-plutonic province, South Australia. *J Geol Soc Aust* 25: 199-216
- Bridgwater D, Escher A, Watterson J (1973) Tectonic displacements and thermal activity in two contrasting Proterozoic mobile belts from Greenland. *Phil Trans R Soc Lond A* 273: 513-533
- Brooks C, Hart SR, Wendt I (1972) Realistic use of two-error regression treatments as applied to Rubidium-Strontium data. *Revs Geophys Space Phys* 10: 551-577
- Brown GM (1972) Pigeonitic pyroxenes: A review. *Geol Soc Am Mem* 132: 523-534
- Bryan WB, Finger LW, Chayes F (1969) Estimating proportions in petrographic mixing equations by least squares approximation. *Science* 163: 426-427

- Buddington AF, Lindsley DH (1964) Iron-Titanium oxide minerals and synthetic equivalents. *J Petrol* 5: 310-357
- Burwash RA, Krupicka J (1969) Cratonic reactivation in the Precambrian basement of western Canada. I. Deformation and chemistry. *Can J Earth Sci* 6 : 1381-1396
- Campbell IH, Gorton MP (1980) Accessory phases and the generation of LREE - enriched basalts - A test for disequilibrium melting. *Contrib Mineral Petrol* 72: 157-163
- Carmichael ISE (1967) The iron-titanium oxides of salic volcanic rocks and their associated ferromagnesian silicates. *Contrib Mineral Petrol* 14: 36-64
- Carter SR, Evensen NM, Hamilton PJ, O'Nions RK (1978) Continental volcanics derived from enriched and depleted source regions: Nd- and Sr- isotope evidence. *Earth Planet Sci Lett* 37: 401-408
- Chappell BW (1978) Granitoids from the Moonbi district, New England batholith, Eastern Australia. *J Geol Soc Aust* 25: 267-283
- Chappell BW, White AJR (1974) Two contrasting granite types. *Pacific Geol* 8: 173-174
- Cherry ME, Trembath LT (1978) The pressure quench formation of rapakivi texture. *Contrib Mineral Petrol* 68: 1-6
- Christiansen RL & Lipman PW (1972) Cenozoic volcanism and plate tectonic evolution of the Western United States II. Late Cenozoic. *Phil Trans R Soc A* 271: 249-284
- Clarke NG (1976) Structural analysis of the Port Neill mylonite zone and its country rocks, Port Neill, South Australia. BSc (Hon) thesis, Univ of Adelaide (unpubl)
- Coin CDA (1976) A study of the Precambrian rocks in the vicinity of Tumby Bay, South Australia. PhD thesis, Univ of Adelaide (unpubl)
- Coin CDA (1980) The geology of the Proterozoic rocks of lower Eyre Peninsula in the vicinity of Tumby Bay. *J Geol Soc Aust* 27: 49-50
- Coish RA, Taylor LA (1979) The effects of cooling rate on texture and pyroxene chemistry in DSDP Leg 34 basalt: a microprobe study. *Earth Planet Sci Lett* 42: 389-398
- Collerson KD, Fryer BJ (1978) The role of fluids in the formation and subsequent development of early continental crust. *Contrib Mineral Petrol* 67: 151-167
- Collerson KD, Kerr A, Compston W (1981) Geochronology and evolution of late Archaean gneisses in northern Labrador : An example of reworked sialic crust. *Spec Publs Geol Soc Aust* 7 : 205-221
- Collins WJ, Beams SD, White AJR, Chappell BW (1982) Nature and origin of A-type granites with particular reference to southeastern Australia. *Contrib Mineral Petrol* 80: 189-200
- Compston W, Arriens P (1968) The Precambrian geochronology of Australia. *Can J Earth Sci* 5: 561-583

- Compston W, Chappell BW (1979) Sr-isotope evolution of granitoid source rocks. in. McElhinny MW (ed) The Earth : its origin, structure and evolution. Academic Press, London
- Compston W, Crawford AR, Bofinger VM (1966) A radiometric estimate of the duration of sedimentation in the Adelaide geosyncline, South Australia. J Geol Soc Aust 13: 229-276
- Condie KC (1978) Geochemistry of Proterozoic granitic plutons from New Mexico, USA. Chem Geol 21: 131-149
- Condie KC (1981) Geochemical and isotopic constraints on the origin and source of Archaean granites. Spec. Publs Geol Soc Aust 7: 469-479
- Cooper JA, Fanning CM, Flock MM, Oliver RL (1976) Archaean and Proterozoic metamorphic rocks on Southern Eyre Peninsula, South Australia. J Geol Soc Aust 23: 287-292
- Daly S, Benbow MC, Blissett AH (1980) Archaean to Early Proterozoic geology of the northwestern Gawler Craton. J Geol Soc Aust 27: 47-48
- Daly S, Webb AW, Whitehead SG (1978) Archaean to early Proterozoic banded iron formations in the Tarcoola region, South Australia. Trans R Soc S Aust 102: 141-149
- Deer WA, Howie RA, Zussman J (1966) An introduction to the rock-forming minerals. Longman Group Ltd London 528pp.
- DePaolo DJ (1979) Implications of correlated Nd and Sr isotopic variations for the chemical evolution of the crust and mantle. Earth Planet Sci Lett 43: 201-211
- DePaolo DJ (1981) Neodymium isotopes in the Colorado Front Range and crust-mantle evolution in the Proterozoic. Nature 291: 193-196
- DePaolo DJ, Wasserburg GJ (1979) Sm-Nd age of the Stillwater complex and the mantle evolution curve for neodymium. Geochim. Cosmochim Acta 43: 999-1008
- Dickinson DR, Gibson IL (1972) Feldspar fractionation and anomalous Sr^{87}/Sr^{86} ratios in a suite of peralkaline silicic rocks. Bull Geol Soc Am 83: 231-240
- Drury SA (1973) The geochemistry of Precambrian granulite facies rocks from the Lewisian complex of Tiree, Inner Hebrides, Scotland. Chem Geol 11: 167-188
- Eichelberger JC (1978) Andesitic volcanism and crustal evolution. Nature 275: 21-27
- Elliott RB (1973) The chemistry of gabbro/amphibolite transitions in south Norway. Contrib Mineral Petrol 38: 71-79
- Ellis DJ (1980) Osumilite - sapphirine - quartz granulites from Enderby Land, Antarctica: P-T conditions of metamorphism, implications for garnet-cordierite equilibria and the evolution of the deep crust. Contrib Mineral Petrol 74: 201-210
- Emmermann R (1977) A petrogenetic model for the origin and evolution of the Hercynian granite series of the Schwarzwald. N Jb Miner Abh 128: 219-253

- Emslie RF (1978) Anorthosite massifs, rapakivi granites, and late Proterozoic rifting of North America. *Precambrian Res* 7: 61-98
- Etheridge MA, Cooper JA (1981) Rb/Sr isotopic and geochemical evolution of a recrystallized shear (mylonite) zone at Broken Hill. *Contrib Mineral Petrol* 78: 74-84
- Etheridge MA, Wall VJ, Vernon RH (1983) The role of the fluid phase during regional metamorphism and deformation. *J metamorphic Geol* 1: 205-226
- Eugster HP, Wones DR (1962) Stability relations of the ferruginous biotite, annite. *J Petrol* 3: 82-125
- Fanning CM (1975) Petrology, structure and geochronology of some high grade metamorphic rocks at Fishery Bay and Cape Carnot, Southern Eyre Peninsula. B.Sc. (Hons) thesis, University of Adelaide, (unpubl)
- Fanning CM, Oliver RL, Cooper JA (1981) The Carnot Gneisses, southern Eyre Peninsula. *Q Geol Notes, Geol Surv S Aust* 80, 7-12
- Ferry JM, Spear FS (1978) Experimental calibration of the partitioning of Fe and Mg between biotite and garnet. *Contrib Mineral Petrol* 66: 113-117
- Field D, Elliott RB (1974) The chemistry of gabbro/amphibolite transitions in south Norway. *Contrib Mineral Petrol* 47: 63-76
- Flood RH, Shaw SE (1977) Two S-type granite suites with low initial $87\text{Sr}/86\text{Sr}$ ratios from the New England batholith, Australia. *Contrib Mineral Petrol* 61: 163-173
- Flood MM (1975) The geology and geochronology of high grade metamorphic rocks at Kirton Point and Cape Donington, Southern Eyre Peninsula. B.Sc. (Hons) thesis, Univ. Adelaide (unpubl.)
- Frey FA, Bryan WB, Thompson G (1974) Atlantic Ocean floor: Geochemistry and petrology of basalts from Legs 2 and 3 of the Deep-Sea Drilling Project. *J Geophys Res* 79: 5507-5527
- Frey FA, Green DH (1974) The mineralogy, geochemistry and origin of lherzolite inclusions in Victorian basanites. *Geochim Cosmochim Acta* 38: 1023 - 1059
- Frey FA, Green DH, Roy SD (1978) Integrated models of basalt petrogenesis: a study of quartz tholeiites to olivine melilitites from southeastern Australia utilizing geochemical and experimental petrological data. *J Petrol* 19: 463-513
- Fyfe WS (1978) The evolution of the earth's crust: modern plate tectonics to ancient hot spot tectonics? *Chem Geol* 23: 89-114
- Giddings JW, Embleton BJJ (1976) Precambrian palaeomagnetism in Australia II: Basic dykes from the Gawler Block. *Tectonophys.* 30: 109-118
- Giles CW (1980a) The origin of the Middle Proterozoic Gawler Range Volcanics in the Lake Everard area, South Australia. *J Geol Soc Aust* 27: 52
- Giles CW (1980b) A comparative study of Archaean and Proterozoic felsic volcanic associations in southern Australia. Ph.D. thesis, Univ Adelaide (unpubl)

- Gill JB (1978) Role of trace element partition coefficients in models of andesite genesis. *Geochim Cosmochim Acta* 42: 709-724
- Glassley W (1982) Fluid evolution and graphite genesis in the deep continental crust. *Nature* 295: 229-231
- Glen RA, Laing WP, Parker AJ, Rutland RWR (1977) Tectonic relationships between the Proterozoic Gawler and Willyama Orogenic Domains, Australia. *J Geol Soc Aust* 24: 125-150
- Glikson AY (1976) Archaean to early Proterozoic shield elements; relevance of plate tectonics. *Geol Assoc Can, Sp Paper* 14: 489-516
- Gray CM (1971) Strontium isotopic studies on granulites. PhD thesis, Aust Nat Univ (unpubl)
- Gray CM, Compston W (1978) A rubidium - strontium chronology of the metamorphism and prehistory of central Australian granulites. *Geochim Cosmochim Acta* 42: 1735-1747
- Green DH (1973a) Experimental melting studies on a model upper mantle composition at high pressures under water-saturated and water-undersaturated conditions. *Earth Planet Sci Lett* 19: 37-53
- Green DH (1973b) Contrasted melting relations in a pyrolite upper mantle under mid-oceanic ridge, stable crust and island arc environments. *Tectonophys* 17: 285-297
- Green DH, Hibberson WO (1970) Experimental duplication of conditions of precipitation of high pressure phenocrysts in a basaltic magma. *Phys Earth Planet Int* 3: 247-254
- Green DH, Liebermann RC (1976) Phase equilibria and elastic properties of a pyrolite model for the oceanic upper mantle. *Tectonophys* 32: 61-92
- Green DH, Ringwood AE (1967a) An experimental investigation of the gabbro to eclogite transformation and its petrological implications. *Geochim Cosmochim Acta* 31: 767-833
- Green DH, Ringwood AE (1967b) The genesis of basaltic magmas. *Contrib Mineral Petrol* 15: 103-190
- Green TH (1969a) Experimental fractional crystallization of quartz diorite and its application to the problem of anorthosite origin. *NY State Mus & Sci Serv Mem* 18: 23-29
- Green TH (1969b) High pressure experimental studies on the origin of anorthosite. *Can J Earth Sci* 6: 427-440
- Green TH (1972) Crystallisation of calc-alkaline andesite under controlled high-pressure conditions. *Contrib Mineral Petrol* 34: 150-166
- Green TH, Brunfelt AO, Heier KS (1972) Rare-earth element distribution and K/Rb ratios in granulites, mangerites and anorthosites, Lofoten - Vesteraalen, Norway. *Geochim Cosmochim Acta* 36: 241-257
- Griffin WL, Carswell DA, Nixon PH (1979) Lower-crustal granulites and eclogites from Lesotho, southern Africa. In: Boyd FR, Meyer HOA (eds). *The Mantle Sample: Inclusions in Kimberlites and Other Volcanics*, Am Geophys Union, Washington DC: 59-86

- Griffin WL, Heier KS (1973) Petrological implications of some corona structures. *Lithos* 6: 315-335
- Hamilton PJ, Evensen NM, O'Nions RK, Tarney J (1979) Sm-Nd systematics of Lewisian gneisses: implications for the origin of granulites. *Nature* 277: 25-28
- Hanson GN (1978) The application of trace elements to the petrogenesis of igneous rocks of granitic composition. *Earth Planet Sci Lett* 38: 26-43
- Harley SL & Green DH (1982) Garnet-orthopyroxene barometry for granulites and peridotites. *Nature* 300: 697-701
- Heier KS (1973) A model for the composition of the deep continental crust. *Fortschr Miner* 50: 174-187
- Hewins RH (1975) Pyroxene geothermometry of some granulite facies rocks. *Contrib Mineral Petrol* 50: 205-209
- Hibbard MJ (1965) Origin of some alkali feldspar phenocrysts and their bearing on petrogenesis. *Am J Sci* 263: 245-261
- Higgins NC, Kawachi Y (1977) Microcline megacrysts from the Green Lake granodiorite, eastern Fiordland, New Zealand. *NZ J Geol Geophys* 20: 273-286
- Himmelberg GR, Ford AB (1977) Iron-titanium oxides of the Dufek intrusion, Antarctica. *Am Mineral* 62: 623-633
- Hine R, Williams IS, Chappell BW, White AJR (1978) Contrasts between I - and S - type granitoids of the Kosciusko Batholith. *J Geol Soc Aust* 25: 219-234
- Holm RE (1982) Non-recognition of continental tholeiites using the Ti-Y-Zr diagram. *Contrib Mineral Petrol* 79: 308-310
- Hubbard FH, Whitley JF (1978) Rapakivi granite, anorthosite and charnockitic plutonism. *Nature* 271: 439-440
- Hurley PM, Rand JR (1969) Pre-drift continental nuclei. *Science* 163: 1229-1242
- Ishii T, Takeda H (1974) Inversion, decomposition and exsolution phenomena of terrestrial and extraterrestrial pigeonites. *Mem Geol Soc Japan* 11: 19-36
- Jaffe HW, Robinson P, Tracy RJ (1978) Orthoferrosilite and other iron-rich pyroxenes in microperthite gneiss of the Mount Marcy area, Adirondack Mountains. *Am Mineral* 63: 1116-1136
- Jahn B-M, Sun SS, Nesbitt RW (1979) REE distribution and petrogenesis of the Spanish Peaks igneous complex, Colorado. *Contrib Mineral Petrol* 70: 281-298
- Jaques AL, Green DH (1980) Anhydrous melting of peridotite at 0-15 Kb pressure and the genesis of tholeiitic basalts. *Contrib Mineral Petrol* 73: 287-310
- Johns RK (1961) Geology and mineral resources of southern Eyre Peninsula. *Geol Surv S Aust Bull* 37

- Katz HB (1972) Paired metamorphic belts of the Gondwanaland Precambrian and Plate Tectonics. *Nature* 239: 271-273
- Katz MB (1976a) Lineament tectonics of the Willyama Block and its relationship to the Adelaide Aulacogene. *J Geol Soc Aust* 23: 275-285
- Katz MB (1976b) Broken Hill - A Precambrian hot spot? *Precambrian Res* 3: 91-106
- Kerrick DM (1969) K-feldspar megacrysts from a porphyritic quartz monzonite, central Sierra Nevada, California. *Am Mineral* 54: 839-847
- Kranck EH (1969) Anorthosites and rapakivi, magmas from the lower crust. *NY State Mus Sci Serv Mem* 18: 93-98
- Krogh TE (1973) A low contamination method for hydrothermal decomposition of zircon and extraction of U and Pb for isotopic age determinations. *Geochim Cosmochim Acta* 37: 485-494
- Krogh TE (1982) Improved accuracy of U-Pb zircon ages by the creation of more concordant systems using an air abrasion technique. *Geochim Cosmochim Acta* 46: 637-649
- Krogh TE, Davis GL (1973) The effect of regional metamorphism on U-Pb systems in zircon and a comparison with Rb-Sr systems in the same whole-rock and its constituent minerals. *Carnegie Inst Washington Yb* 72: 601-610
- Kröner A (1977) The Precambrian geotectonic evolution of Africa: Plate accretion versus plate destruction. *Precambrian Res* 4: 163-213
- Kyle PR (1980) Development of heterogeneities in the subcontinental mantle: evidence from the Ferrar Group, Antarctica. *Contrib Mineral Petrol* 73: 89-104
- Langmuir CH, Bender JF, Bence AE, Hanson GN (1977) Petrogenesis of basalts from the FAMOUS area, Mid-Atlantic Ridge. *Earth Planet Sci Lett* 36: 133-156
- Lanphere MA, Wasserburg GJ, Albee AL, Tilton GR (1964) Redistribution of strontium and rubidium isotopes during metamorphism, World Beater Complex, Panamint Range California IN Craig E et al (eds) *Isotopic and Cosmic Chemistry*. North Holland Publishing Co. Amsterdam 269-320
- Leake BE (1978) Compiler, Nomenclature of amphiboles. *Mineral Mag* 42: 533-563
- Leelanandam C (1967) Chemical study of pyroxenes from the charnockitic rocks of Kondapalli (Andhra Pradesh). *Mineral Mag* 36: 153-179
- Lewry JF (1981) Lower Proterozoic arc-microcontinent collisional tectonics in the western Churchill Province. *Nature* 294: 69-72
- Lipman PW, Prostka HJ, Christiansen RL (1972) Cenozoic volcanism and plate-tectonic evolutions of the Western United States. 1 Early and Middle Cenozoic *Phil Trans R Soc Lond* 271: 217-248
- Loiselle MC, Wones DR (1979) Characteristics and origin of anorogenic granites. *Geol Soc Am Abstr Progr* 11: 468
- Marjoribanks RW, Black LP (1974) Geology and geochronology of the Arunta Complex, north of Ormiston Gorge, Central Australia. *J Geol Soc Aust* 21: 291-300

- Martin RF, Piwinski AJ (1972) Magmatism and tectonic settings. *J Geophys Res* 77: 4966-4975
- Mason BH, Moore CB (1982) Principles of geochemistry. John Wiley & Sons, Inc.
- McCarthy TS, Cawthorn RG (1980) Changes in initial $87\text{Sr}/86\text{Sr}$ during protracted fractionation in igneous complexes. *J Petrol* 21: 245-264
- McConnell RB (1972) Geological development of the rift system of eastern Africa. *Bull Geol Soc Am* 83: 2549-2572
- McCulloch MT, Compston W (1981) Sm-Nd age of Kambalda and Kanowna greenstones and heterogeneity in the Archaean mantle. *Nature* 294: 322-327
- Menzies MA, Wass Sy (1983) CO_2 - and LREE-rich mantle below eastern Australia: a REE and isotopic study of alkaline magmas and apatite-rich mantle xenoliths from the southern Highlands Province, Australia. *Earth Planet Sci Lett* 65: 287-302
- Menzies MM, Murthy VR (1980) Enriched mantle: Nd and Sr isotopes in diopsides from kimberlite nodules. *Nature* 283: 634-636
- Moorbath S (1977) Ages, isotopes and evolution of Precambrian continental crust. *Chem Geol* 20: 151-187
- Moorbath S (1978) Age and isotope evidence for the evolution of continental crust. *Phil Trans R Soc Lond A* 288: 401-413
- Moore AC (1970) Descriptive terminology for the textures of rocks in granulite facies terrains. *Lithos* 3: 123-127
- Mortimer GE, Cooper JA, Oliver RL (1980) Petrological and petrochemical evolution of the 1.82 b.y. Donington Granitoid Suite of the southeast Eyre Peninsula. *J Geol Soc Aust* 27: 50
- Nesbitt RW, Sun SS (1976) Geochemistry of Archaean spinifex-textured peridotites and magnesian and low magnesian tholeiites. *Earth Planet Sci Lett* 31: 433-453
- Nesbitt RW, Sun SS, Purvis AC (1979) Komatiites: geochemistry and genesis. *Canad Mineral* 17: 165-186
- Newton RC, Smith JV, Windley BF (1980) Carbonic metamorphism, granulites and crustal growth. *Nature* 288, 45-50
- Nilsen O (1973) Petrology of the Hylligen gabbro complex Sor-Trondelag, Norway. *Norsk Geol Tidsskr* 53: 213-231
- Nowgorodov PG, Shkodzinsky VS (1974) Experiments on melting of granite in $\text{H}_2\text{O}-\text{CO}_2$ mixtures and some problems of granite formation. *Geochim Int* 11: 522-531
- Nunes PD, Steiger RH (1974) U-Pb zircon and Rb-Sr and U-Th-Pb whole-rock study of a polymetamorphic terrain in the Central Alps, Switzerland. *Contrib Mineral Petrol* 47: 255-280
- O'Hara MJ (1968) The bearing of phase equilibria studies in synthetic and natural systems on the origin and evolution of basic and ultrabasic rocks. *Earth Sci Rev* 4: 69-133

- Oliver RL, Schultz PK (1968) Colour in charnockites. *Min Mag* 36: 1135-1138
- Ormaasen DE (1977) Petrology of the Hopen mangerite - charnockite intrusion, Lofoten, north Norway. *Lithos* 10: 291-310
- Ormaasen DE, Raade G (1978) Heat generation versus depth of crystallization for Norwegian monzonitic rocks. *Earth Planet Sci Lett* 39: 145-150
- Paradine CG, Rivett BHP (1960) *Statistical methods for technologists*. English Universities Press, London
- Park RG (1981) Origin of horizontal structure in high-grade Archaean terrains. *Spec Publs Geol Soc Aust* 7: 481-490
- Parker AJ (1978) Structural, stratigraphic and metamorphic geology of Lower Proterozoic rocks in the Cowell/Cleve district, eastern Eyre Peninsula. Ph.D thesis, University of Adelaide, (unpubl)
- Parker AJ (1980) The Kalinjala Mylonite Zone, eastern Eyre Peninsula. *Q Geol Notes, Geol Surv S Aust* 76: 6-11
- Parker AJ, Fanning CM, Flint RB (1981) Archaean to Middle Proterozoic geology of the Southern Gawler Craton South Australia; Excursion guide. *Geol Surv S Aust* 77 p
- Parker AJ, Lemon NM (1982) Reconstruction of the Early Proterozoic stratigraphy of the Gawler Craton, South Australia. *J Geol Soc Aust* 29: 221-238
- Patchett PJ, Kouvo O, Hedge CE, Tatsumoto M (1981) Evolution of continental crust and mantle heterogeneity: evidence from Hf isotopes. *Contrib Mineral Petrol* 78: 279-297
- Patchett PJ, van Breemen O, Martin RF (1979) Sr isotopes and the structural state of feldspars as indicators of post-magmatic hydrothermal activity in continental dolerites. *Contrib Mineral Petrol* 69: 65-73
- Peacock MA (1931) Classification of igneous rocks. *J Geol* 39: 54-67
- Pearce, JA, Cann JR (1973) Tectonic setting of basic volcanic rocks. *Earth Planet Sci Lett* 19: 290-300
- Pearce JA, Norry MJ (1979) Petrogenetic implications of Ti, Zr, Y and Nb variations in volcanic rocks. *Contrib Mineral Petrol* 69: 33-47
- Pedler AD (1976) The Geology and geochronology of high grade metamorphic rocks between Point Yorke and Meteor Bay, southern Yorke Peninsula. BSc (Hons) thesis, Univ of Adelaide (unpubl)
- Philpotts AR (1966) Origin of the anorthosite - mangerite rocks in southern Quebec. *J Petrol* 7: 1-64
- Pidgeon RT, Compston W (1965) The age and origin of the Cooma granite and its associated metamorphic zones, New South Wales. *J Petrol* 6: 193-222
- Powell M, Powell R (1977) Plagioclase - alkali - feldspar geothermometry revisited. *Min Mag* 41: 253-256
- Powell R, Powell M (1977) Geothermometry and oxygen barometry using coexisting iron-titanium oxides: a reappraisal. *Min Mag* 41: 257-263

- Price RC, Sinton JM (1978) Geochemical variations in a suite of granitoids and gabbros from Southland, New Zealand. *Contrib Mineral Petrol* 67: 267-278
- Propach G (1976) Models of filter differentiation *Lithos* 9: 203-209
- Pulvertaft TCR (1973) Recumbent folding and flat-lying structure in the Precambrian of northern West Greenland. *Phil Trans R Soc Lond A273*: 535-545
- Richardson SM (1978) Structural analysis of the gneisses at Corny Point, southern Yorke Peninsula. BSc (Hons) thesis, Univ of Adelaide (unpubl)
- Ringwood AE (1966) The chemical composition and origin of the Earth. In: *Advances in Earth Science* (ed) PM Hurley MIT Press, Cambridge, Massachusetts.
- Ringwood AE (1975) Composition and petrology of the Earth's mantle. McGraw-Hill Inc, 618 pp
- Robinson P, Ross M, Nord GL, Smyth JR, Jaffe HW (1977) Exsolution in augite and pigeonite; fossil indicators of lattice parameters at high temperature and pressure. *Am Mineral* 62: 857-873
- Roddick JC, Compston W (1977) Strontium isotopic equilibration: A solution to a paradox. *Earth Planet Sci Lett* 34: 238-246
- Roeder PL, Emslie RF (1970) Olivine-liquid equilibrium. *Contrib Mineral Petrol* 29: 275-289
- Ross M, Huebner JS (1975) A pyroxene geothermometer based on composition - temperature relationships of naturally occurring orthopyroxene, pigeonite and augite (abstr) Extended abstracts, Int Conf Geothermometry Geobarometry, Penn State Univ.
- Ross M, Huebner JS, Dowty E (1973) Delineation of the one atmosphere augite - pigeonite miscibility gap for pyroxenes from Lunar basalt 12021. *Am Mineral* 58: 619-635
- Rossiter AG, Ferguson J (1980) A Proterozoic tectonic model for northern Australia and its economic implications. *Proceeding of the International Uranium Symposium on the Pine Creek Geosyncline, 1980*: 209-232
- Rutland RWR (1976) Orogenic evolution of Australia. *Earth-Sci: Rev* 12: 161-196
- Rutland RWR (1981) Structural framework of the Australian Precambrian. In: Hunter DR (ed) *Precambrian of the Southern Hemisphere, Developments in Precambrian geology* 2: 1-32
- Rutland RWR, Parker AJ, Pitt GM, Preiss WV, Murrell B (1981) The Precambrian of South Australia. In: Hunter DR (ed) *Precambrian of the Southern Hemisphere, Developments in Precambrian Geology* 2: 309-360
- Sawkins FJ (1976) Metal deposits related to intracontinental hotspot and rifting environments. *J Geol* 84: 653-671
- Schilling JG, Winchester JW (1967) Rare-earth fractionation and magmatic processes. In: *Mantles of the Earth and terrestrial planets* (Runcorn SK ed): 267-283, Interscience Publishers, John Wiley and Sons, London

- Shaw DM (1972) The origin of the Apsley Gneiss, Ontario. *Can J Earth Sci* 9: 18-35
- Sheraton JW, Black LP (1981) Geochemistry and geochronology of Proterozoic tholeiite dykes of East Antarctica: evidence for mantle metasomatism. *Contrib Mineral Petrol* 78: 305-317
- Smith D (1971) Stability of the assemblage iron-rich orthopyroxene - olivine - quartz. *Am J Sci* 271: 370-382
- Smith D (1972) Stability of iron-rich pyroxene in the system CaSiO_3 - FeSiO_3 - MgSiO_3 . *Am Mineral* 57: 1413 - 1428
- Smithson SB, Brown SK (1977) A model for the lower continental crust. *Earth Planet Sci Lett* 35: 134-144
- Smithson SB, Decker ER (1973) K, U and Th distribution between dry and wet facies of a syenitic intrusion and the role of fluid content. *Earth Planet Sci Lett* 19: 131-134
- Smithson SB, Heier KS (1971) K, U and Th distribution between normal and charnockitic facies of a deep granitic intrusion. *Earth Planet Sci Lett* 12: 325-336
- Streckeisen A (1976) To each plutonic rock its proper name. *Earth-Sci Rev* 12: 1-33
- Strong DF, Dostal J (1980) Dynamic melting of Proterozoic upper mantle: evidence from rare earth elements in oceanic crust of eastern Newfoundland. *Contrib Mineral Petrol* 72: 165-173
- Strong PG, O'Brien SJ, Taylor SW, Strong PG, Wilton DH (1978) Aborted Proterozoic rifting in eastern Newfoundland. *Can J Earth Sci* 15: 117-131
- Sun S-S, Hanson GN (1975) Origin of Ross Island basanitoids and limitations upon the heterogeneity of mantle sources for alkali basalts and nephelinites. *Contrib Mineral Petrol* 52: 77-106
- Sun S-S, Nesbitt RW (1978a) Petrogenesis of Archaean ultrabasic and basic volcanics: Evidence from rare earth elements. *Contrib Mineral Petrol* 65: 301-325
- Sun S-S, Nesbitt RW (1978b) Geochemical regularities and genetic significance of ophiolitic basalts. *Geol* 6: 689-693
- Sun S-S, Nesbitt RW, Sharaskin AY (1979) Geochemical characteristics of Mid-Ocean Ridge basalts. *Earth Planet Sci Lett* 44: 119-138
- Sutton J, Watson JV (1974) Tectonic evolution of continents in early Proterozoic times. *Nature* 247: 433-435
- Tarney J (1976) Geochemistry of high-grade gneisses with implications as to the origin and evolution of the Precambrian crust. In: Windley BF (ed) *The Early History of the Earth*. Wiley, London: 405-418
- Tarney J, Windley BF (1977) Chemistry, thermal gradients and evolution of the lower continental crust. *J Geol Soc Lond* 134: 153-172

- Tarney J, Windley BF (1979) Continental growth, island arc accretion and the nature of the lower crust - a reply to SR Taylor & SM McLennan. *J Geol Soc Lond* 136: 501-504
- Taylor SR (1967) The origin and growth of continents. *Tectonophys* 4: 17-34
- Taylor SR, Kaye M, White AJR, Duncan AR, Ewart A (1969) Genetic significance of Co, Cr, Ni, Sc and V content of andesites. *Geochim Cosmochim Acta* 33: 275-286
- Taylor SR, McLennan SM (1979) Discussion on "Chemistry, thermal gradients and evolution of the lower continental crust" by J Tarney & BF Windley. *J Geol Soc Lond* 136: 497-500
- Taylor SR, White AJR (1966) Trace element abundances in andesites. *Bull Volcanol* 29: 177-194
- Thompson RN (1975a) Primary basalts and magma genesis. II Snake River Plain, Idaho, USA. *Contrib Mineral Petrol* 52: 213-232
- Thompson RN (1975b) Is upper mantle phosphorous contained in sodic garnet? *Earth Planet Sci Lett* 26: 417-424
- Thomson BP (1969) The Precambrian crystalline basement in Parkin LW (ed) *Handbook of South Australian geology*, S Aust Geol Surv, Adelaide
- Thomson BP (1980) Compiler, Geological map of South Australia, 1: 1 000 000 scale. S Aust Dept Mines and Energy
- Thorpe RS, Potts PJ, Sarre MB (1977) Rare earth evidence concerning the origin of granites of the Isle of Skye, northwest Scotland. *Earth Planet Sci Lett* 36: 111-120
- Tilley CE (1920) The metamorphism of the Precambrian dolomites of Southern Eyre Peninsula, South Australia. *Geol Mag* 57: 449-462, 492-500
- Tilley CE (1921a) The graphite rocks of Sleaford Bay, South Australia. *Econ Geol* 16: 184-198
- Tilley CE (1921b) Precambrian para-gneisses of Southern Eyre Peninsula, South Australia. *Geol Mag* 58: 251-259; 305-312
- Tilley CE (1921c) The granite gneisses of southern Eyre Peninsula (South Australia) and their associated amphibolites. *Quart J Geol Soc Lond* 77: 75-134
- Tobi AC (1971) The nomenclature of the charnockitic rock suite. *N Jb Miner Mon* 5: 193-205
- Torske T (1976) Metal provinces of a Cordilleran-type orogen in the Precambrian of south Norway. *Geol Assoc Can Spec Pap* 14: 597-613
- Torske T (1977) The South Norway Precambrian Region - a Proterozoic cordilleran - type orogenic segment. *Norsk Geol Tidsskr* 57: 97-120
- Touret J (1971) Les facies granulite en Norvege Meridionale II Les fluides inclusions. *Lithos* 4: 423-426
- Tuttle OF, Bowen NL (1958) Origin of granites in the light of experimental studies in the system $\text{NaAlSi}_3\text{O}_8 - \text{KAlSi}_3\text{O}_8 - \text{SiO}_2 - \text{H}_2\text{O}$. *Geol Soc Am Mem* 74

- Vorma A (1976) On the petrochemistry of rapakivi granites with special reference to the Laitila massif, southwestern Finland. Bull Geol Surv Finland 285
- Wass SY, Hollis JD (1983) Crustal growth in south-eastern Australia - evidence from lower crustal eclogitic and granulitic xenoliths. J Metamorphic Geol 1: 25-45
- Wass SY, Rogers NW (1980) Mantle metasomatism - precursor to continental alkaline volcanism. Geochim Cosmochim Acta 44: 1811-1823
- Weaver BL, Tarney J (1980) Continental crust composition and nature of the lower crust: constraints from mantle Nd-Sr isotope correlation. Nature 286: 342-346
- Weaver BL, Tarney J (1981a) Lewisian gneiss geochemistry and Archaean crustal development models. Earth Planet Sci Lett 55: 171-180
- Weaver BL, Tarney J (1981b) The Scourie Dyke Suite: Petrogenesis and geochemical nature of the Proterozoic sub-continental mantle. Contrib Mineral Petrol 78: 175-188
- Weaver BL, Tarney J (1981c) Chemical changes during dyke metamorphism in high-grade basement terrains. Nature 289: 47-49
- Weaver BL, Tarney J, Windley BF, Sugavanam EB, Rao VV (1978) Madras granulites: geochemistry and P-T conditions of crystallisation. In: Windley BF, Naqvi SM (eds) Archaean Geochemistry: 177-204 Elsevier, Amsterdam
- Webb AW (1978) Geochronology of the younger granites of the Gawler Craton and its northwest margin. Aust Mineral Develop Lab, Rept 1215 (unpubl)
- Webb AW (1980) A geochronological investigation of the tectono-magmatic history of the Gawler Craton. J Geol Soc Aust 27: 45-46
- Webb AW, Thomson BP (1977) Archaean basement rocks in the Gawler Craton, South Australia. Search 8: 34-36
- Wells PRA (1977) Pyroxene thermometry in simple and complex systems. Contrib Mineral Petrol 62: 129-139
- Wells PRA (1980) Thermal models for the magmatic accretion and subsequent metamorphism of continental crust. Earth Planet Sci Lett 46: 253-265
- Wheeler EP II (1965) Fayalitic olivine in northern Newfoundland - Labrador. Can Mineral 8: 339-346
- White AJR, Chappel BW (1977) Ultrametamorphism and granitoid genesis. Tectonophys 43: 7-22
- White AJR, Chappell BW, Cleary JR (1974) Geologic setting and emplacement of some Australian Palaeozoic batholiths and implications for intrusive mechanisms. Pacific Geol 8: 159-171
- Whitney JA (1975) The effects of pressure, temperature, and X_{H_2O} on phase assemblages in four synthetic rock compositions. J Geol 83, 1-31

- Whitney JA, Stoimer JC (1976) Geothermometry and geobarometry in epizonal granitic intrusions: a comparison of iron-titanium oxides and coexisting feldspars. *Am Mineral* 61: 751-761
- Wilson AF (1976) A normalizing procedure for comparing chemical variations in pyroxenes in mafic granulites. *Contrib Mineral Petrol* 55: 131-138
- Windley BF (1973) Crustal development in the Precambrian. *Phil Trans R Soc Lond A* 273: 321-341
- Windley BF (1981) Phanerozoic granulites. *J Geol Soc Lond* 138: 745-751
- Windley BF, Smith JV (1976) Archaean high-grade complexes and modern continental margins. *Nature* 260: 671-675
- Wones DR, Eugster HP (1965) Stability of biotite: experiment, theory and application. *Am Mineral* 50: 1228-1272
- Wood BJ (1975) The influence of pressure, temperature and bulk composition on the appearance of garnet in orthogneiss - an example from South Harris, Scotland. *Earth Planet Sci Lett* 26: 299-311
- Wood BJ, Banno S (1973) Garnet-orthopyroxene and orthopyroxene - clinopyroxene relationships in simple and complex systems. *Contrib Mineral Petrol* 42: 109-124
- Wood DA, Tarney J, Varet J, Saunders AD, Bougault H, Joron JL, Treuil M, Cann JR (1979) Geochemistry of basalts drilled in the North Atlantic by IPOD Leg 49: implications for mantle heterogeneity. *Earth Planet Sci Lett* 42: 77-97
- Wright TL (1974) Presentation and interpretation of chemical data for igneous rocks. *Contrib Mineral Petrol* 48: 233-248
- Wyborn LAI, Page RW (1983) Chemical and isotopic constraints on the source regions of the Kalkadoon and Ewen Batholiths, Mount Isa Inlier and their implications for Early Proterozoic crustal evolution in Australia. *Geol Soc Aust Abstr Ser* 9: 191
- Wyllie PJ (1977) Crustal anatexis: an experimental review. *Tectonophys* 43: 41-71
- Wyllie PJ, Huang W-L, Stern CS, Maaloe S (1976) Granitic magmas: possible and impossible sources, water contents, and crystallization sequences. *Can J Earth Sci* 13: 1007-1019
- Wynne-Edwards HR (1976) Proterozoic ensialic orogenesis: The millipede model of ductile plate tectonics. *Am J Sci* 276: 927-953
- Zielinski RA (1975) Trace element evaluation of the petrogenesis of a suite of rocks from Reunion Island, Indian Ocean. *Geochim Cosmochim Acta* 39: 713-734

...000...

APPENDIX A1 EXPERIMENTAL TECHNIQUES(1) RB-SR GEOCHRONOLOGYIntroduction

The techniques of Rb-Sr total-rock dating employed in this laboratory have been described by Cooper et al. (1978). However, in detail, some deviations from their method have been adopted for this study.

Sample selection and preparation

Sampling of a rock unit for dating usually involved choosing an area as geologically simple as possible and of dimensions ca. 20m x 20m. Surface collected rock samples weighing between 1kg and 4kg were taken using sledge hammers. Usually the samples were separated by 1m to 5m.

In the laboratory weathered skins were removed from the large rock samples and 1kg to 2kg aliquots free from alteration were prepared for crushing. These were broken down to 3 mm or less in a jaw crusher. A 100-150g split was then crushed to 200 mesh size in a Sieb Technic Mill.

Determination of Rb and Sr contents

Approximate measures of the Rb and Sr contents were made using a Siemens SRS 1 fully automatic X-ray fluorescence spectrometer.

For more accurate determinations of those samples chosen for analysis the procedures of Chappell et al. (1969) were generally followed. Three powder presses of each sample were taken and each was analysed three times using an enriched reference standard. The standard was calibrated against the reference standard NBS 70A (522 ppm Rb and 65.3 ppm Sr.). Intertail, selftail, and U, Th, and Pb inter-element effects were precalibrated for the machine and monitored and corrected for each particular sample. The Mo Compton peak was also measured to correct for variable mass absorption effects (Reynolds 1967) so that Rb and Sr ppm levels reported are not biased by this factor.

For the accurate determination of samples with low Sr-contents the isotope dilution method (Compston et al. 1965) was generally followed. A mixed $^{85}\text{Rb} + ^{84}\text{Sr}$ spike was used.

Sr-isotope ratio measurement

Sr isotope ratio measurements were made using a modified Thomson TSN 205 S, 30 cm radius of curvature mass spectrometer with a Cary 401 vibrating reed electrometer, automatic peak-switcher (designed by E. Penikis of A.N.U., Canberra), Hewlett Packard 5326 B digital voltmeter and Digital PDP 8E computer (with 12K storage). All ratios were corrected for variable mass discrimination by normalizing $^{88}\text{Sr}/^{86}\text{Sr}$ to 8.3752.

For part of the time of accumulation of the data in this study replicate analyses of the Eimer and Amend Sr standard gave 0.70825 ± 0.00004 (2 standard deviations of mean, 15 analyses). Following instrumental modification, later replicate analyses of the Sr standard gave 0.70802 ± 0.00005 (2 standard deviations of mean, 10 analyses). All measured $^{87}\text{Sr}/^{86}\text{Sr}$ ratios have been normalized to a value of Eimer and Amend Sr standard of 0.70800.

Regression analysis of isochrons

Replicate analyses and reproducibility of the nine separate measurements on each sample in the XRF technique suggest 1 standard deviation errors may be assigned to the $^{87}\text{Rb}/^{86}\text{Sr}$ measurement of $\pm 0.4\%$ for XRF results and $\pm 0.5\%$ for isotope dilution measurements. Similarly, 1 standard deviation errors in $^{87}\text{Sr}/^{86}\text{Sr}$ ratios have been assigned at $\pm 0.015\%$.

Final regression analyses were made using the method of McIntyre et al. (1966), allowing for the modifications of Brooks et al. (1972). Ages and tests of significance are at the 95% confidence level. The ^{87}Rb decay constant used is $1.42 \times 10^{-11} \text{ a}^{-1}$.

References

Brooks C, Hart SR, Wendt I (1972).

Realistic use of two-error regression treatments as applied to rubidium-strontium data. *Revs Geophys Space Phys* 10 : 551-577.

Chappell BW, Compston W, Arriens PA, Vernon MJ (1969).

Rubidium and strontium determinations by X-ray fluorescence spectrometry and isotope dilution below the part per million level. *Geochim Cosmochim Acta* 33 : 1002-1006.

Compston W, Lovering JF, Vernon MJ (1965).

The rubidium-strontium age of the Bishopville aubrite and its component enstatite and feldspar. *Geochim*

Cosmochim Acta 29 : 1085-1099.

Cooper JA, Nesbitt RW, Platt JP, Mortimer GE (1978).

Crustal development in the Agnew region, Western Australia, as shown by Rb/Sr isotopic and geochemical studies. Precambrian Res 7 : 31-59.

McIntyre GA, Brooks C, Compston W, Turek A (1966).

The statistical assessment of Rb-Sr isochrons. J Geophys Res 71 : 5459-5468.

Reynolds RC (1967).

Estimation of mass absorption coefficients by Compton scattering : improvements and extension of the method. Am. Min 52 : 1493-1502.

(2) ZIRCON U-PB GEOCHRONOLOGY

Sample selection and preparation

A surface collected, unweathered samples ca. 30 kg in weight was used for separation of zircons.

This was crushed to less than 500 microns grain size and zircon extracted using conventional Wilfley Table, heavy liquids and electromagnetic techniques. The zircon concentrate was divided first into size and then magnetic fractions.

Zircon fraction selection

The size and magnetic fractions obtained above were routinely examined under a binocular microscope and further purified by hand-picking to remove any impurities or to select in favour of particular zircon grain types. Grain modifying techniques such as air-abrasion (Krogh 1982) were applied in some instances. Final zircon fractions of 5-10 mg were boiled in aqua regia for several hours and rinsed many times in pure water prior to dissolution.

Chemical procedures and isotope ratio measurement and calculation

The chemical analysis procedures for U and Pb content and Pb isotopic ratios were adapted from those of Krogh (1973). A mixed $^{208}\text{Pb}/^{235}\text{U}$ spike was used. Blank levels were 2 nanograms of Pb of modern isotopic composition and 0.01 nanograms of U. A TSN 206 S mass-spectrometer with a 30 cm radius of curvature magnet, Hall probe control, automatic peak switching and on-line computer was used for the isotope ratio measurements. Uncertainties in the $^{206}\text{Pb}/^{238}\text{U}$ and $^{207}\text{Pb}/^{206}\text{U}$ ratios are 0.6-0.8%, at the 95% confidence level. Similarly uncertainties in the $^{207}\text{Pb}/^{206}\text{Pb}$ ratios are about 0.1%. Concordia - discordia analyses were made following Ludwig (1980). Constants utilized in the age calculations are $\lambda^{238}\text{U} = 0.155125 \times 10^{-9}\text{a}^{-1}$, $\lambda^{235}\text{U} = 0.984850 \times 10^{-9}\text{a}^{-1}$, $^{238}\text{U}/^{235}\text{U} = 137.88$. Common lead corrections were made using the isotopic compositions predicted by the Cumming & Richards (1975) lead-evolution model.

The uncertainties quoted for the intercepts between regression lines and concordia are the 95% confidence limits, and involve the appropriate Student's *t* multiplier.

References

Cumming GL, Richards JR (1975).

Ore lead isotope ratios in a continuously changing Earth. Earth Planet Sci Lett 28 : 155-171.

Krogh TE (1973).

A low contamination method for hydrothermal decomposition of zircon and extraction of U and Pb for isotopic age determination. Geochim Cosmochim Acta 37 : 485-494.

Krogh TE (1982).

Improved accuracy of U-Pb zircon ages by the creation of more concordant systems using an air abrasion technique. Geochim Cosmochim Acta 46 : 637-649.

Ludwig KR (1980).

Calculation of uncertainties of U-Pb isotopic data. Earth Planet Sci Lett 46 : 212-220.

(3) MAJOR AND TRACE ELEMENT GEOCHEMISTRY

Introduction

The aliquots of pulverised rock used for Rb-Sr geochemical investigations (and rock powder prepared in an entirely similar manner for rocks not dated) were used in the analysis of major and trace elements.

Major and trace elements

All of the major and trace element data (excluding Na₂O and REE) reported in this study were determined by X-ray fluorescence techniques. The methods of Norrish & Chappell (1967), Mastins et al. (1972) and Nesbitt et al. (1976) have been adopted.

Determination of Na₂O was by flame photometric techniques.

All of these techniques have been compiled in a single volume by Nesbitt & Stanley (1980).

References

Mastins H, Jones JB, Nesbitt RW (1972).

X-ray mass absorption applied to mineral and rock analysis. J. Geol Soc Aust 19 : 217-224.

Nesbitt RW, Mastins H, Stolz GW, Bruce DR (1976).

Matrix corrections in trace-element analysis by X-ray fluorescence : an extension of the Compton scattering technique to long wavelengths. Chem Geol 18 : 203-213.

Nesbitt RW, Stanley JL (eds) (1980).

Compilation of analytical geochemistry reports 1973-1979, Research Report 3, Centre for Precambrian Research, University of Adelaide.

Norrish K, Chappell BW (1976).

X-ray fluorescence spectrography. In : J. Zussman (ed), Physical methods in determinative mineralogy, Academic Press, New York, N.Y.

(4) REE GEOCHEMISTRY

An isotope dilution, mass-spectrometric technique, introduced to Adelaide University isotope geology unit by S.S. Sun, was utilised for the analysis of REE.

All but four of the naturally occurring REE can be analysed by isotope dilution. Pm has no stable isotopes and does not occur in nature. Pr, Tb, Ho and Tm have only one stable isotope each and as a consequence cannot be analysed by isotope dilution.

Sm and Nd have neither interfering elements nor oxide. If Ba is separated from the sample, Eu is also easily analysed. All of the other REE however, have other REE or rare earth oxide interferences, and therefore good chemical separation is necessary for their analysis. It is sufficient to separate the REE into a heavy REE fraction

light REE fraction

a Ce fraction free of Nd

and a La fraction free of Ce and Ba.

After the rock plus SPIKE solution is digested in acids, the solution is passed through two cation exchange columns. In the first column the major elements, Ba and Sr, are removed with 2N HNO₃, and then the REE are collected as a group with 6N HNO₃.

The various REE fractions are separated on the second column using 3N HCl. 4 or 5 fractions are collected which are then run separately in the Mass Spectrometer where isotopic abundances are obtained as ratios of two isotopes for each element.

Comparative analysis

Results for two international standards and duplicates of one specimen from the present author's study area are tabulated below along with the chondrite normalising factors utilised in data presentation.

	BCR-1	GSP-1	B143	B143	Chondrite
La	25.2	93.4	58.5	62.5	0.315
Ce	54.0	241	120	123	0.813
Nd	30.9	107	50.9	53.9	0.597
Sm	6.50	14.2	9.58	10.2	0.192
Eu	1.95	1.64	1.77	1.84	0.0722
Gd	6.84	7.31	8.60	9.13	0.259
Dy	6.30	3.79	7.93	8.25	0.325
Er	3.64	1.77	4.62	4.87	0.213
Yb	3.34	1.32	4.32	4.50	0.208

APPENDIX A2 RECONNAISSANCE FLUID INCLUSION STUDY OF SOME
PYROXENE GRANITOIDS OF THE DONINGTON SUITE.

A short fluid inclusion study was undertaken of Ferro-hypersthene granitoids FGG1 and FGG2 of the Donington Granitoid Suite (Chapter 2). The study concentrated on the observation of possible primary inclusions in quartz which contain undissolved CO₂ as a separate phase. The percentage CO₂ was estimated and the CO₂ liquid/gas homogenization was observed allowing an estimate of the CO₂ density, and thus a pressure/temperature curve could be assigned for the inclusion formation.

The identification of inclusions necessitates the solidification of the inclusion contents to enable observation of the triple point melting. Unfortunately it thereby eliminates the positive identification of inclusions which, due to super-cooling effects, remain fluid below their triple point. The primary nature of the observed inclusion is necessarily a subjective identification, however the factors considered are: isolation of inclusion, inclusion shape, relationships between inclusions, and inclusion/grain relationships. The percentage CO₂ fill is likewise a subjective observation but identification charts have been published (Roedder 1967; p. 563), to aid in this decision.

The density calculation is done by observing the homogenization of the CO₂ phases; the homogenization temperature can then be used in conjunction with the Pressure vs Temperature, density isograd graph (Hollister 1981). The density thus calculated can then be transferred to the appropriate percentage fill (at 40°C) Pressure vs Temperature, density isograd graph (Swanenberg 1980) to give the appropriate Pressure/Temperature curve.

The four samples provided are identified as B144, B150, B152 and AB109. Of these only the last provided inclusions which could be positively identified as containing CO₂. The CO₂ inclusions observed in AB109 have contents of 80% to 95% CO₂ at 40°C. These same inclusions show CO₂(g-l) homogenization temperatures ranging from 7.1°C to 12.9°C. These temperatures correspond to densities of .87 to .89 g/cc CO₂. The resulting curve can be followed from about 220°C at 1 Kb to 700°C at 10 Kb. It is likely that these CO₂ rich inclusions originally formed at magmatic temperatures in excess of 700°C and pressure in excess of 10 Kb.

The other three sections contained numerous inclusions similar in appearance to those of AB109 at room temperature, however, prolonged cooling of them produced no change.

Sections examined by E. Bleys,
Department of Economic Geology,
University of Adelaide.

References

Hollister LS (1981).

Information intrinsically available from fluid inclusions in Short Course in Fluid Inclusions : Applications to Petrology.

Editors: Hollister, L.S. and Crawford, M.L.

Mineralogical Association of Canada, pp. 1-12.

Roedder E (1967).

Fluid inclusions of samples of ore fluids in

"Geochemistry of Hydrothermal ore deposits."

Ed. by H.L. Barnes, Pennsylvania State

University, Ch. 12, pp. 515-566

Swanenberg HEC (1980).

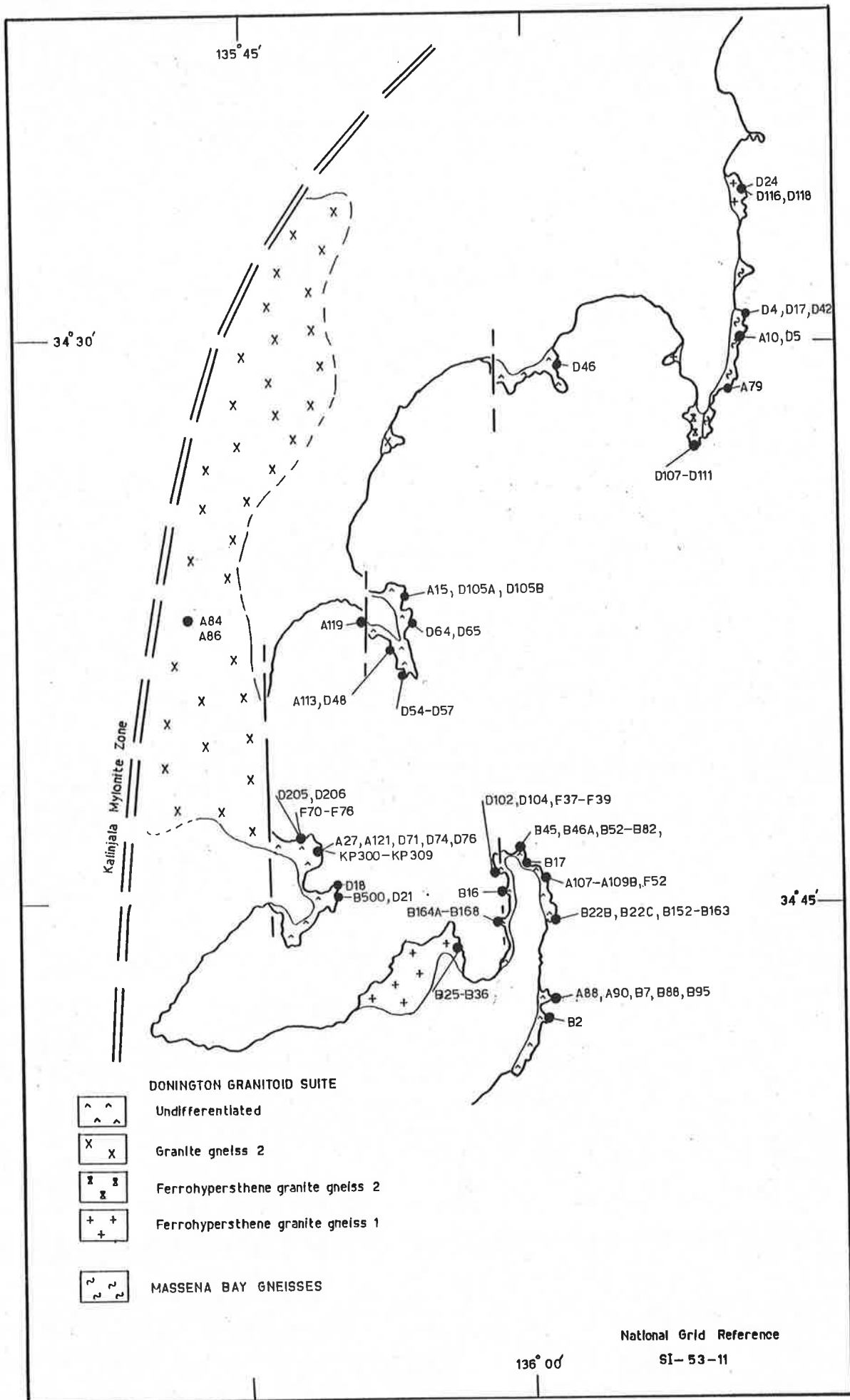
Fluid inclusions in high-grade metamorphic rocks

from S.W. Norway in Geologica Ulcraiectina,

University of Utrecht. No. 25. pp. 1-47 (in Eng.).

APPENDIX A3 SAMPLE LOCATIONS

Sample locations are plotted on the accompanying map in this Appendix and on Figs. 2.1, 3.1, 4.1 and 5.1. Location names appear on Figure 1.2. Unless otherwise indicated all specimen numbers have the prefix 515-.



Appendix Table 1.1 Previously published Rb-Sr analytical data for Sleaford Complex, Mulgathing Complex and Lincoln Complex rocks of the Gawler orogenic domain.

Sample	87Rb/86Sr	87Sr/86Sr	Sample	87Rb/86Sr	87Sr/86Sr
<u>SLEAFORD COMPLEX</u>			<u>SLEAFORD COMPLEX</u>		
Augen Gneiss Cooper et al. (1976)			Whidbey Granite Webb & Thomson (1977)		
466-C252	1.513	0.7578	74-1077	3.1655	0.8043
466-C250	2.242	0.7860	74-1078	3.6308	0.8259
466-C260	2.440	0.7931	74-1103	13.823	1.1722
466-C262*	2.484	0.7958	74-1105	5.6781	0.8950
466-C263*	2.548	0.7974	74-1106	6.4892	0.9180
466-C256	2.634	0.7988	74-1107	1.6771	0.7572
466-C259	2.694	0.8024	74-1108	2.8342	0.7974
466-C261	2.766	0.8031	74-1140	2.2658	0.7820
466-C253	2.781	0.8032	74-1142	2.9268	0.8053
466-C254	2.921	0.8079	74-1168	1.7164	0.7667
466-C257	2.972	0.8102	74-1187	4.3353	0.8482
466-C251	3.017	0.8096	74-1227	3.9294	0.8432
466-C255	3.284	0.8220	74-1228	6.5345	0.9243
			74-1229	10.126	1.0531
Average	2.638		74-1232	3.637	0.8271
			Average	4.851	
<u>Leucogneiss Cooper et al. (1976)</u>					
466-J1	0.880	0.7387			
466-J3	0.929	0.7432			
466-J2	1.133	0.7460			
466-J5	1.170	0.7468			
466-J7	1.227	0.7507			
466-J6	1.610	0.7683			
466-J8	1.671	0.7709			
Average	1.231				

Sample	87Rb/86Sr	87Sr/86Sr	Sample	87Rb/86Sr	87Sr/86Sr
<u>MULGATHING COMPLEX</u>			<u>MULGATHING COMPLEX</u>		
Iron formation Daly et al. (1978)			Iron formation Daly et al. (1978)		
76-1728	0.2025	0.7114	76-1454	0.7245	0.7284
76-1735	1.0631	0.7405	76-1455	1.8019	0.7675
76-1733	1.1969	0.7444	76-1459	0.8416	0.7307
76-1731	1.4503	0.7535	76-1447	2.0173	0.7739
76-1729	1.6632	0.7612	76-1448	2.1941	0.7772
76-1721	1.8329	0.7687	76-1450	2.4706	0.7930
76-1749	1.9265	0.7718	76-1456	2.8549	0.8025
76-1723	2.0376	0.7753	76-1458	3.8386	0.8192
76-1718	2.0638	0.7754	76-1451	3.9949	0.8459
76-1722	2.3449	0.7846			
76-1748	2.6388	0.7962	Average	2.304	
Average	1.675				
<u>Tarcoola granites Webb & Thomson (1977)</u>			<u>Glenloth Granite Webb & Thomson (1977)</u>		
76-47	2.5023	0.7860	72-391	6.544	0.9204
76-48	3.3726	0.8135	72-396	3.294	0.8052
76-49	2.6424	0.7875	75-1938	1.270	0.7457
76-50	1.8738	0.7699	75-1939	1.482	0.7509
76-107	2.2944	0.7801	75-1941	0.7084	0.7256
76-108	3.3932	0.8141	75-1942	0.821	0.7302
76-109	2.6101	0.7864	75-1943	0.8866	0.7329
76-110	1.8796	0.7700	75-1944	0.3922	0.7162
Average	2.571		75-1945	0.3569	0.7147
			Average	1.751	

Sample	87Rb/86Sr	87Sr/86Sr	Sample	87Rb/86Sr	87Sr/86Sr
<u>LINCOLN COMPLEX</u>			<u>SYN-TECTONIC GRANITES</u>		
Snapper Point Granite Gneiss			Middlecamp Granite Webb (1978)		
Cooper et al. (1976)			P281	1.941	0.7562
468-309	2.2342	0.76248	P282	2.571	0.7697
468-300	5.6052	0.84998	P283	5.162	0.8324
468-302	7.4165	0.8983	P285	0.738	0.7273
468-304	7.5305	0.90073	P286	2.352	0.7661
468-308	7.7035	0.90804	P289	1.415	0.7462
468-306	9.5444	0.95241	<hr/>		
468-305	9.9891	0.96057	Average	2.363	0.7663
468-303	10.0660	0.96785	<hr/>		
468-307	10.327	0.97374	Narridy Creek Granite Webb (1978)		
<hr/>			P274	34.912	1.5499
Average	7.824		P276	46.701	1.8245
<hr/>			P277	44.777	1.7916
<u>SYN-TECTONIC GRANITES</u>			P279	41.889	1.6940
Carpa Granite Webb (1978)			P280	41.299	1.7058
P269	2.923	0.7829	<hr/>		
P270	3.319	0.7920	Average	41.916	1.7132
P271	3.108	0.7878	<hr/>		
P272	1.939	0.7591	<hr/>		
<hr/>			<u>MASSENA BAY GNEISSES</u>		
Average	2.822	0.7805	Quartzofeldspathic gneisses		
<hr/>			Pedler (1976)		
76-22	1.223	0.73750	76-22	1.223	0.73750
76-24	1.417	0.74204	76-24	1.417	0.74204
76-28	1.644	0.75232	76-28	1.644	0.75232
76-27	2.358	0.76444	76-27	2.358	0.76444
76-41	3.068	0.78532	76-41	3.068	0.78532
76-30A	3.451	0.78810	76-30A	3.451	0.78810
76-29	4.003	0.80440	76-29	4.003	0.80440
76-44	4.269	0.81227	76-44	4.269	0.81227
76-35	5.467	0.83718	76-35	5.467	0.83718
<hr/>			<hr/>		
Average	2.989	0.78040	<hr/>		
<hr/>			<hr/>		

Appendix Table 1.2 Calculated Sr-isotope evolution curves for rock units of the Gawler orogenic domain

Rock Unit	Isochron Age (Ma)	IR	Ave. 87Rb/86Sr	Calculated 87Sr/86Sr						
				2600Ma	2400Ma	2200Ma	2000Ma	1800Ma	1600Ma	1400Ma
¹ Sleaford Complex Augen Gneiss	2587 ₊₁₃₀	0.7015 ₊₄₃	2.638	0.70101	0.70851	0.71604	0.72358	0.73115	0.73873	0.74634
¹ Sleaford Complex Leucogneiss	2778 ₊₅₆₃	0.7026 ₊₁₀₂	1.231	0.70572	0.70923	0.71275	0.71627	0.71981	0.72336	0.72692
² Mulgathing Complex Iron formation	2417 ₊₅₉	0.7036 ₊₁₅	1.675	0.70163	0.70400	0.70877	0.71355	0.71834	0.72315	0.72796
² Mulgathing Complex Iron formation	2488 ₊₁₃₀	0.7014 ₊₃₈	2.304	0.69774	0.70428	0.71084	0.71742	0.72402	0.73064	0.73727
³ Sleaford Complex Whidbey Granite	2356 ₊₅₀	0.7029 ₊₃₇	4.851	0.68612	0.69987	0.71366	0.72748	0.74135	0.75526	0.76920
³ Glenloth Granite	2300 ₊₃₃	0.7028 ₊₆	1.751	0.69536	0.70032	0.70529	0.71028	0.71528	0.72029	0.72532
³ Tarcoola granites	2233 ₊₄₃	0.7031 ₊₈	2.571	0.68974	0.79701	0.70431	0.71162	0.71896	0.72631	0.73369
Massena Bay Gneisses Quartzofeldspathic										
⁴ Eyre Peninsula		0.75361*	1.893	0.68499	0.69018	0.69539	0.70061	0.70584	0.71109	0.71635
⁵ Yorke Peninsula		0.78073*	2.989	0.67239	0.68058	0.68880	0.69704	0.70530	0.71359	0.72190
⁴ Donington Granitoid Suite	1841 ₊₇	0.7041	2.823	0.67384	0.68178	0.68975	0.69773	0.70574	0.71378	0.72183
opx-granitoids		0.7053		0.67504	0.68298	0.69095	0.69893	0.70694	0.71498	0.72303
⁴ Colbert Granitoid Suite hornblende granite gneiss	1757 ₊₁₄	0.7087 ₊₁₀	4.031	0.66073	0.76206	0.78342	0.69481	0.70624	0.71770	0.72919
⁴ Moody Granitoid Suite I-type granitoids	1709 ₊₁₄	0.7070 ₊₄	6.053	0.63090	0.64790	0.66494	0.68204	0.69918	0.71638	0.73362
S-type granitoids	1675 ₊₂₂	0.7163 ₋₂₃₃	131.4					0.48327	0.85632	1.23042
Moody Tank Adamellite	1551 ₊₂₄₅	0.7251 ₊₂₇₈	8.007	0.60671	0.62915	0.65165	0.67421	0.69684	0.71953	0.74229
⁴ Donington Granitoid Suite possible source		0.7041**		0.69946	0.70068	0.70190	0.70312	0.70435	0.70558	0.70682
		0.7053**	0.433	0.70066	0.70188	0.70310	0.70432	0.70555	0.70678	0.70902
⁴ Mafic dykes B58		0.71577 ₊₆ *	0.491	0.69797	0.69932	0.70067	0.70202	0.70338	0.70474	0.70610
B69		0.71318 ₊₆ *	0.368	0.69984	0.70085	0.70186	0.70288	0.70389	0.70491	0.70594
B16		0.71544 ₊₃₄ *0.477	0.69815	0.69946	0.70077	0.70208	0.70340	0.70472	0.70605	
B26		0.71087 ₊₄ *	0.271	0.70105	0.70179	0.70253	0.70328	0.70403	0.70478	0.70554
B36		0.71230 ₊₅ *	0.370	0.69889	0.69903	0.70092	0.70194	0.70296	0.70399	0.70502
B52		0.71246 ₊₁₅ *0.445	0.69633	0.69755	0.69877	0.69999	0.70123	0.70246	0.70370	
⁶ Bulk Earth		0.7047*	0.08560	0.70160	0.70183	0.70207	0.70230	0.70254	0.70278	0.70302

Notes:

- 1 data from Cooper et al. (1976)
- 2 data from Daly et al. (1978)
- 3 data from Webb & Thomson (1977)
- 4 data from this thesis
- 5 data from Pedler (1976)
- 6 data from Collerson et al. (1981)

* ratio at present day
 ** IR of granitoid isochron

Appendix Table 2.1 Donington Granitoid Suite, mineral analytical data and structural formulae.

(a) Clinopyroxenes and Orthopyroxenes (Calculated after Jaffe et al., 1978)

Specimen* Rock Type	B200(4) QGNG	D18(1) GG1	B200(2) QGNG	B29(4) FGG1	B34(1) FGG1	Al09(4) FGG2	B152(2) EAGG
SiO2	52.49	51.97	51.97	48.55	46.58	48.90	46.25
TiO2	-	-	-	0.15	2.33	0.03	0.14
Al2O3	1.17	1.20	0.82	0.52	0.58	0.58	0.67
Cr2O3	0.28	-	-	0.04	-	0.03	-
FeOTotal	10.06	12.97	27.87	37.90	37.09	37.32	46.33
MnO	0.10	0.61	0.72	0.94	0.77	0.72	1.20
MgO	13.34	10.41	19.00	10.82	11.64	11.56	4.51
CaO	22.27	22.56	0.44	0.69	0.55	0.62	0.29
Na2O	0.30	0.69	0.09	0.41	0.36	0.25	0.56
Total	100.01	100.42	100.01	100.02	99.90	100.01	99.94

Structural formula calculated on basis of 6 oxygens

Si	1.964	1.965	1.947	1.953	1.873	1.959	1.945
Al(4)	0.036	0.035	0.037	0.025	0.028	0.027	0.033
Al(6)	0.016	0.019	-	-	-	-	-
Ti	-	-	-	0.005	0.070	0.001	0.004
Cr	0.008	-	-	0.001	-	0.001	-
Fe3	0.035	0.067	0.077	0.092	0.118	0.071	0.118
Fe2	0.280	0.343	0.812	1.183	1.130	1.180	1.511
Mn	0.003	0.019	0.023	0.032	0.026	0.024	0.043
Mg	0.744	0.587	1.080	0.649	0.698	0.690	0.283
Ca	0.893	0.914	0.018	0.030	0.024	0.027	0.013
Na	0.022	0.051	0.007	0.032	0.028	0.019	0.046

(b) Biotites

Specimen* Rock Type	B200(3) QGNG	B29(2) FGG1	Al09(2) FGG2	D18(1) GG1	B88(4) GG1	Al07(1) GG1	D24(1) GG1	D71(2) GG2	B164(2) GG2	B158(1) AGG
SiO2	35.93	36.12	36.41	38.02	34.81	35.47	34.43	35.59	36.37	37.12
TiO2	4.32	4.40	4.40	4.46	2.83	2.75	4.52	3.04	3.74	4.34
Al2O3	14.23	12.19	14.42	13.20	14.15	15.40	13.67	14.72	13.57	15.17
FeOTotal	17.76	21.72	22.61	19.33	25.94	27.08	28.62	25.42	24.67	26.04
MnO	-	-	-	0.13	0.16	0.23	0.17	0.13	0.17	0.49
MgO	12.75	9.95	8.54	11.23	7.07	5.11	5.94	7.75	7.77	2.94
CaO	-	-	0.08	-	0.11	0.10	-	-	-	0.08
Na2O	-	0.09	0.11	0.19	0.35	0.39	-	-	0.28	0.66
K2O	9.66	9.50	8.96	9.59	9.09	9.18	9.08	9.77	9.53	8.03
Total	94.65	93.97	95.53	96.15	94.51	95.71	96.43	96.42	96.10	94.88

Structural formula calculated on basis of 22 oxygens

Si	5.507	5.695	5.623	5.752	5.568	5.610	5.468	5.556	5.672	5.834
Ti	0.498	0.522	0.511	0.507	0.341	0.327	0.539	0.357	0.438	0.513
Al	2.570	2.265	2.624	2.354	2.668	2.871	2.558	2.708	2.494	2.809
FeOTotal	2.277	2.864	2.920	2.446	3.471	3.582	3.800	3.319	3.218	3.422
Mn	-	-	-	0.017	0.022	0.031	0.023	0.017	0.023	0.065
Mg	2.914	2.338	1.966	2.533	1.687	1.204	1.407	1.803	1.807	1.687
Ca	-	-	0.013	-	0.019	0.017	-	-	-	0.014
Na	-	0.026	0.033	0.056	0.108	0.118	-	-	0.084	0.201
K	1.889	1.910	1.766	1.851	1.854	1.852	1.839	1.946	1.897	1.610

(c) Amphiboles (calculated after Leake, 1978)

Specimen* Rock Type	B200(2) QGNG	B29(3) FGG1	B34(1) FGG1	D18(1) GG1	A88(1) GG1	A88(1) GG1
SiO2	42.58	40.23	38.58	43.91	36.82	40.03
TiO2	1.29	1.26	1.97	1.22	0.54	0.75
Al2O3	10.84	11.01	11.54	9.25	11.60	10.72
Cr2O3	0.25	-	-	-	0.16	-
FeOTotal	16.39	21.42	24.25	19.21	25.09	25.59
MnO	-	0.07	-	0.36	0.48	0.46
MgO	11.09	7.37	5.65	10.01	4.20	5.20
CaO	11.53	10.55	10.71	11.78	10.65	10.98
Na2O	1.34	1.99	1.95	1.74	1.38	1.70
K2O	1.39	1.92	2.44	1.25	1.53	1.64
Total	96.70	95.82	97.09	98.74	92.45	97.07

Structural formula calculated on basis of 23 oxygens

T8	Si	6.380	6.293	6.089	6.559	6.089	6.286
	Al(4)	1.620	1.707	1.911	1.441	1.917	1.714
	Al(6)	0.293	0.323	0.236	0.188	0.342	0.270
	Ti	0.146	0.148	0.234	0.138	0.068	0.089
	Cr	0.030	-	-	-	0.022	-
C5	Fe3	0.584	0.507	0.447	0.414	0.796	0.655
	Fe2	1.470	2.295	2.753	1.986	2.671	2.707
	Mn	-	0.009	-	0.046	0.068	0.061
	Mg	2.477	1.719	1.329	2.228	1.035	1.218
	Ca	1.878	1.790	1.830	1.906	1.922	1.876
B2	Na	0.122	0.210	0.170	0.094	0.078	0.124
	Na	0.273	0.401	0.432	0.414	0.372	0.401
A0-1	K	0.270	0.388	0.497	0.243	0.328	0.334

Amphiboles continued

Specimen* Rock Type	A88(1) GG1	A88(1) GG1	D24(1) GG1	D71(1) GG2	D77(1) GG2	B164(3) GG2
SiO2	49.53	43.65	40.66	40.22	39.61	38.95
TiO2	-	0.41	1.77	1.03	2.09	1.09
Al2O3	2.97	7.36	10.86	12.05	10.42	11.64
Cr2O3	0.11	-	-	-	-	0.03
FeOTotal	21.04	23.42	25.33	24.81	22.70	25.48
MnO	0.53	0.48	0.56	0.41	0.33	0.41
MgO	9.56	7.25	5.04	5.40	5.97	5.06
CaO	11.27	10.70	10.77	11.57	11.11	10.95
Na2O	0.72	1.18	1.80	1.53	1.64	1.97
K2O	0.31	0.86	1.58	1.83	1.55	2.07
Total	96.04	95.31	98.57	98.85	95.42	97.65

Structural formula calculated on basis of 23 oxygens

T8	Si	7.539	6.801	6.295	6.199	6.296	6.157
	Al(4)	0.461	1.199	1.705	1.801	1.704	1.843
	Al(6)	0.071	0.153	0.277	0.388	0.220	0.325
	Ti	-	0.048	0.206	0.120	0.232	0.130
	Cr	0.013	-	-	-	-	0.004
C5	Fe3	0.393	0.774	0.534	0.482	0.440	0.486
	Fe2	2.286	2.278	2.746	2.716	2.429	2.807
	Mn	0.068	0.064	0.073	0.054	0.058	0.056
	Mg	2.169	1.684	1.164	1.240	1.619	1.191
	Ca	1.855	1.820	1.809	1.933	1.914	1.869
B2	Na	0.145	0.180	0.191	0.067	0.086	0.131
	Na	0.070	0.182	0.356	0.395	0.360	0.478
A0-1	K	0.060	0.175	0.317	0.364	0.305	0.420

(d) Plagioclases

Specimen* Rock Type	QGNG		QGNG B200 Traverse					Rim	FGG1	FGG1	FGG2
	B200(14)	Rim							B34(1)	B29(b)	Al09(10)
SiO2	53.90	55.05	50.81	52.70	54.10	50.82	53.06	52.76	55.37	57.98	57.80
Al2O3	29.44	28.58	32.24	29.90	29.28	31.89	29.95	30.15	28.38	26.49	26.80
CaO	11.00	10.09	12.56	11.89	11.06	12.70	11.83	11.97	10.07	7.87	8.03
Na2O	5.25	5.75	4.13	4.95	5.21	4.12	4.89	4.76	5.89	7.20	6.94
K2O	0.34	0.38	0.26	0.41	0.36	0.30	0.27	0.23	0.29	0.32	0.37
Total	99.93	99.85	100.00	99.85	100.01	99.83	100.00	99.87	100.00	99.86	99.94

Structural formula calculated on basis of 32 oxygens

Si	9.748	9.938	9.225	9.578	9.775	9.250	9.611	9.570	9.976	10.400	10.359
Al	6.276	6.081	6.900	6.405	6.236	6.841	6.394	6.446	6.027	5.600	5.661
Ca	2.132	1.952	2.443	2.316	2.141	2.477	2.296	2.327	1.944	1.512	1.542
Na	1.841	2.013	1.454	1.744	1.825	1.454	1.717	1.674	2.058	2.504	2.412
K	0.078	0.088	0.060	0.095	0.083	0.070	0.062	0.053	0.067	0.073	0.085
An	52.6	48.2	61.7	55.7	52.9	61.9	56.3	57.4	47.8	37.0	38.2
Ab	45.4	49.7	36.7	42.0	45.1	35.3	42.1	41.3	50.6	61.2	59.7
Or	2.0	2.1	1.6	2.3	2.0	1.8	1.6	1.3	1.6	1.8	2.1

Plagioclases continued

Specimen* Rock Types	FGG2	FGG2	EAGG	GG1	GG1	GG1	GG1	GG2	GG2	GG2	AGG
	Al09 Rim	Al09 Core	B152	A88 (1)	Al07 (5)	D18 (1)	D24 (1)	D77 (2)	D71 (1)	B164 (4)	B158 (2)
SiO2	58.79	56.90	63.65	59.80	60.99	64.58	61.03	62.58	59.99	60.58	62.33
Al2O3	26.09	27.23	22.78	25.83	24.59	23.01	25.38	23.98	25.94	24.74	23.77
CaO	7.37	8.86	3.44	6.97	5.69	3.36	5.94	4.88	6.89	5.86	4.12
Na2O	7.40	6.46	9.87	7.76	8.33	9.49	8.31	8.38	7.50	8.41	9.45
K2O	0.36	0.38	0.27	0.29	0.37	0.38	0.18	0.42	0.28	0.38	0.28
Total	100.01	99.83	100.01	99.93	99.97	100.82	100.84	100.24	100.60	99.97	99.95

Structural formula calculated on basis of 32 oxygens

Si	10.509	10.232	11.253	10.561	10.851	11.300	10.762	11.053	10.625	10.796	11.054
Al	5.497	5.772	4.747	5.443	5.157	4.746	5.275	4.992	5.415	5.196	4.969
Ca	1.412	1.707	0.652	1.335	1.085	0.630	1.122	0.924	1.308	1.119	0.783
Na	2.565	2.253	3.383	2.690	2.874	3.220	2.841	2.870	2.576	2.906	3.250
K	0.082	0.087	0.061	0.066	0.084	0.085	0.040	0.095	0.063	0.086	0.063
An	34.8	42.2	15.9	32.6	26.8	16.0	28.0	23.8	33.1	27.2	19.1
Ab	63.2	55.7	82.6	65.8	71.1	81.8	71.0	73.8	65.3	70.7	79.3
Or	2.0	2.1	1.5	1.6	2.1	2.2	1.0	2.4	1.6	2.1	1.6

(e) Alkali Feldspars

Specimen* Rock Type	QGNG B200(1)	FGG1 B29(6)	FGG1 B34(2)	FGG2 A109(6)	EAGG B152(6)	GG1 A88(6)	GG1 A107(3)
SiO ₂	63.94	65.01	65.26	64.87	65.00	64.75	64.92
Al ₂ O ₃	19.61	18.77	18.89	18.84	18.58	18.77	18.64
CaO	0.12	0.02	0.05	0.11	0.00	-	0.05
Na ₂ O	0.73	1.44	2.07	1.59	1.07	0.85	1.14
K ₂ O	15.39	14.77	13.72	14.59	15.36	15.63	15.25
Total	99.79	100.01	99.99	100.00	100.01	100.01	100.00

Structural formula calculated on basis of 32 oxygens

Si	11.813	11.953	11.952	11.929	11.976	11.944	11.961
Al	4.270	4.068	4.078	4.084	4.035	4.081	4.048
Ca	0.024	0.004	0.010	0.022	-	-	0.010
Na	0.262	0.513	0.735	0.567	0.382	0.304	0.407
K	3.628	3.464	3.206	3.423	3.610	3.678	3.585
An	0.6	0.1	0.3	0.5	-	-	0.2
Ab	6.7	12.9	18.6	14.1	9.6	7.6	10.2
Or	92.7	87.0	81.1	85.4	90.4	92.4	89.6

Alkali Feldspars continued

Specimen* Rock Type	GG1 D18(1)	GG1 D24(1)	GG2 D77(1)	GG2 D71(1)	GG2 B164(3)	AGG B158(4)
SiO ₂	64.32	64.52	63.36	64.01	65.01	64.98
Al ₂ O ₃	18.66	18.87	18.43	18.89	18.81	18.62
CaO	0.10	0.00	-	-	0.04	-
Na ₂ O	1.13	1.33	0.26	0.12	1.83	1.02
K ₂ O	15.33	15.13	16.44	16.85	14.31	15.39
Total	99.54	99.85	98.49	99.87	100.00	100.01

Structural formula calculated on basis of 32 oxygens

Si	11.924	11.911	11.923	11.889	11.941	11.972
Al	4.077	4.106	4.088	4.136	4.072	4.044
Ca	0.020	-	-	-	0.008	-
Na	0.406	0.476	0.095	0.043	0.652	0.364
K	3.626	3.563	3.947	3.993	3.353	3.617
An	0.5	-	-	-	0.2	-
Ab	10.0	11.8	2.4	1.1	16.2	9.1
Or	89.5	88.2	97.6	98.9	83.6	90.9

(f) Oxides (calculated after Carmichael, 1967)

Specimen* Rock Type	B200(5) QGNG	B29(2) FGG1	B34(1) GGG1	B152(4) EAGG	A88(5) GG1	B200(1) QGNG	B29(3) FGG1	B152(4) EAGG	A88(2) GG1
SiO ₂	1.16	1.90	1.13	1.71	0.85	2.33	1.70	1.25	0.34
TiO ₂	0.30	1.36	1.13	1.20	0.29	49.25	48.14	49.14	49.11
Al ₂ O ₃	1.28	1.19	1.27	1.53	0.59	0.94	0.92	0.53	0.32
Cr ₂ O ₃	1.46	0.34	0.76	0.04	0.17	-	0.07	-	-
Fe ₂ O ₃	64.32	59.76	64.03	63.43	67.07	0.32	3.21	3.24	6.33
FeO	32.14	33.50	33.32	34.58	31.98	42.65	43.38	43.61	41.57
MnO	-	-	-	-	-	3.68	1.29	1.46	2.57
MgO	0.89	0.64	0.70	0.69	0.68	0.64	0.59	0.38	0.31
CaO	0.14	0.18	0.18	0.06	0.03	0.17	0.21	0.02	0.05
Total	101.65	98.87	102.52	103.24	101.66	99.98	99.51	99.63	100.60
Hm						1.7	7.3	3.9	6.4
Ilm						98.3	92.7	96.1	93.6
Ulv	5.2	11.1	7.3	9.2	4.0				
Mt	94.8	88.9	92.7	90.8	96.0				
T C**	433	612		536	507				
-logaO ₂ **	26.88	18.20		21.65	21.21				

Notes: (1) * Rock type designations after Table 2.1; number in brackets refers to number of analyses averaged.

(2) ** Temperature and oxygen fugacity calculations after Powell & Powell (1977)

Appendix Table 2.2 Donington Granitoid Suite major element geochemical data and CIPW Normative mineralogy.

	Quartz gabbronorite gneiss			B204	B202
	B203	B201	B205		
SiO2	55.53	55.96	56.41	57.12	57.22
Al2O3	14.64	14.78	15.09	14.50	14.17
Fe2O3T	10.14	9.93	9.70	9.65	9.63
MnO	0.15	0.15	0.15	0.15	0.14
MgO	5.91	5.95	5.71	5.58	5.53
CaO	6.93	6.94	7.02	6.38	6.29
Na2O	2.38	2.47	2.47	2.55	2.35
K2O	2.20	2.21	2.17	2.52	2.80
TiO2	0.84	0.80	0.75	0.79	0.81
P2O5	0.22	0.20	0.22	0.20	0.21
Total	98.95	99.39	99.69	98.68	99.15
LOI	0.33	0.44	0.30	0.33	0.40
CIPW Norms					
Q	8.32	8.18	8.94	9.20	9.98
C	-	-	-	-	-
OR	13.00	13.06	12.82	14.84	16.55
AB	20.14	20.90	20.90	21.51	19.89
AN	22.79	22.72	23.68	20.61	19.85
DI	WO 4.24	4.35	4.05	4.02	4.17
	EN 2.50	2.58	2.39	2.33	2.45
	FS 1.53	1.54	1.47	1.50	1.52
HY	EN 12.22	12.24	11.83	11.52	11.32
	FS 7.47	7.31	7.24	7.41	7.00
MT	3.89	3.81	3.73	3.49	3.70
IL	1.60	1.52	1.42	1.50	1.54
AP	0.51	0.46	0.51	0.46	0.49

Ferrohypersthene granite gneiss 1

	B143	B144	B25	B145	D118	D111	D116	*Bradley
SiO2	65.37	66.66	66.68	69.22	69.80	70.12	70.48	65.80
Al2O3	14.92	14.71	14.90	14.47	14.01	15.68	14.03	15.11
Fe2O3T	6.09	5.38	5.76	3.92	4.60	2.09	4.20	5.94
MnO	0.10	0.09	0.08	0.06	0.07	0.03	0.05	0.08
MgO	1.57	1.23	1.39	0.88	0.67	0.48	0.56	1.31
CaO	3.37	3.06	3.28	2.44	2.40	2.87	2.27	3.59
Na2O	2.98	2.93	2.91	2.83	2.64	2.87	2.64	2.93
K2O	4.43	4.75	4.76	5.28	5.36	5.53	5.41	4.46
TiO2	0.87	0.77	0.81	0.60	0.54	0.41	0.53	0.85
P2O5	0.24	0.19	0.23	0.14	0.12	0.12	0.11	0.26
Total	99.93	99.76	100.80	99.82	100.20	100.20	100.30	100.33
LOI	0.09	0.59	0.30	0.20	0.40	0.47	0.20	
CIPW Norms								
Q	20.19	21.85	21.28	25.03	26.50	25.07	27.50	
C	-	-	-	-	-	0.04	-	
OR	26.18	28.07	28.13	31.20	31.68	32.68	31.97	
AB	25.22	24.79	24.62	23.95	22.34	24.29	22.34	
AN	14.25	12.96	13.54	11.19	10.55	13.45	10.46	
DI	WO 0.37	0.41	0.51	-	0.24	-	0.04	
	EN 0.17	0.17	0.22	-	0.08	-	0.01	
	FS 0.21	0.24	0.29	-	0.17	-	0.03	
HY	EN 3.74	2.89	3.24	2.19	1.59	1.20	1.38	
	FS 4.63	4.02	4.26	3.02	3.64	1.46	3.38	
MT	2.33	2.06	2.20	1.51	1.77	0.80	1.61	
IL	1.63	1.46	1.54	1.14	1.03	0.78	1.01	
AP	0.56	0.44	0.53	0.33	0.28	0.28	0.26	

Granite Gneiss 2 continued

	KP300	KP307	B500	D205	B168	B164D	B164E	B164B	B163
SiO2	73.48	74.39	75.71	75.79	68.04	70.94	73.34	74.98	76.65
Al2O3	13.43	13.00	12.09	12.52	15.46	13.93	13.90	13.25	12.45
Fe2O3T	1.44	1.89	2.39	1.97	3.48	3.41	1.75	0.72	1.03
MnO	0.02	0.03	0.02	0.03	0.04	0.05	0.02	0.01	0.01
MgO	0.36	0.34	0.44	0.26	0.65	0.72	0.34	0.19	0.17
CaO	1.22	1.33	1.92	1.18	2.12	1.97	1.27	0.55	1.04
Na2O	2.52	2.73	2.52	2.89	3.48	2.83	2.54	2.10	2.60
K2O	6.26	5.66	4.41	5.33	6.23	5.87	7.12	8.15	5.60
TiO2	0.23	0.27	0.34	0.21	0.43	0.44	0.21	0.07	0.18
P2O5	0.05	0.05	0.06	0.03	0.08	0.09	0.04	0.01	0.02
Total	99.01	99.69	99.89	100.21	100.01	100.25	100.53	100.03	99.75
LOI	0.33	0.39	0.25	0.25	0.34	0.11	0.15	0.15	0.27
CIPW Norms									
Q	31.36	32.95	38.83	35.03	17.65	25.89	27.59	29.80	37.21
C	0.41	0.08	-	-	-	-	-	-	0.27
OR	37.00	33.45	26.06	31.50	36.69	34.65	42.01	48.09	33.01
AB	21.32	23.10	21.32	24.45	29.35	23.92	21.46	17.74	21.94
AN	5.73	6.27	8.65	5.45	8.14	7.96	5.49	2.65	5.02
DI	-	-	0.20	0.09	0.76	0.51	0.23	-	-
WO	-	-	0.08	0.03	0.28	0.20	0.08	-	-
EN	-	-	0.13	0.07	0.50	0.32	0.15	-	-
FS	-	-	0.07	0.62	1.34	1.59	0.76	0.47	0.42
HY	0.90	0.85	1.02	0.62	1.34	1.59	0.76	0.47	0.42
EN	1.09	1.49	1.73	1.60	2.45	2.57	1.35	0.64	0.78
FS	0.55	0.72	0.91	0.75	1.26	1.23	0.63	0.26	0.37
MT	0.44	0.51	0.65	0.40	0.81	0.83	0.40	0.13	0.34
IL	0.44	0.51	0.65	0.40	0.81	0.83	0.40	0.13	0.34
AP	0.12	0.12	0.14	0.07	0.19	0.21	0.09	0.02	0.05

Alkali feldspar granite gneiss

	B161A	B22C	B159B	B154B	B154A	B22B
SiO2	77.20	77.42	77.64	77.93	78.10	78.81
Al2O3	11.94	12.11	12.24	12.17	12.27	12.05
Fe2O3T	0.64	0.50	0.48	0.45	0.54	0.60
MnO	0.01	0.01	0.01	0.00	0.02	0.01
MgO	0.15	0.04	0.21	0.00	0.09	0.05
CaO	0.71	0.73	0.73	0.73	0.73	0.72
Na2O	2.97	2.92	3.00	2.94	2.92	3.01
K2O	5.44	5.65	5.56	5.45	5.40	5.47
TiO2	0.07	0.07	0.08	0.07	0.08	0.07
P2O5	0.00	0.00	0.01	0.00	0.00	0.00
Total	99.12	99.44	99.96	99.73	100.11	100.80
LOI	0.24	0.30	0.27	0.06	0.26	0.23
CIPW Norms						
Q	37.19	36.96	36.80	38.23	38.50	38.59
C	-	-	-	0.13	0.34	-
OR	32.15	33.29	32.77	32.19	31.03	32.33
AB	25.13	24.63	25.32	24.86	24.64	25.47
AN	3.18	3.24	3.50	3.55	3.50	3.21
DI	0.14	0.15	0.02	-	-	0.15
WO	0.06	0.03	0.01	-	-	0.03
EN	0.08	0.13	0.00	-	-	0.13
FS	0.31	0.07	0.51	0.02	0.22	0.09
HY	0.45	0.28	0.37	0.37	0.44	0.38
EN	0.25	0.18	0.17	0.16	0.20	0.23
FS	0.13	0.13	0.15	0.13	0.15	0.13
MT	-	-	0.02	0.02	0.02	-
IL	-	-	0.02	0.02	0.02	-
AP	-	-	0.02	0.02	0.02	-

Notes:

- (1) All oxide abundances in wt%
- (2) Sample locations as in Table 2.4
- (3) CIPW Norms calculated for FeO = 0.75 Fe2O3Total
- (4) * BRADLEY Average of 4 analyses from Bradley (1972)
- (5) ** EXPT Composition of granite used in experiments by Nowgorodov & Shkodzinsky (1974).

Appendix Table 2.3 Donington Granitoid Suite trace element geochemical data

	(a) Quartz gabbro-norite gneiss						(b) Ferrohypersthene granite gneiss 2				
	B203	B201	B205	B204	B202	B67	D108	A109B	A109A	D107	B46A
Rb	97	102	97	130	117	201	185	147		193	204
Sr	229	231	240	219	217	167	171	174		179	151
Ba	506	500	522	605	655	365	1176	1178	1281		1030
Y	32	31	30	43	34	149	40	43			31
Zr	138	168	138		380	78	315		300		316
Nb	12	12	10		12	29	15		11		15
Sc	28	29	28		28	45	19	14	13		12
V	169	157	157		154			53	53		53
Ni	107	111	104		99		18			19	
Cr								16	19	23	12
La			33.1				49.3				
Ce			67.1				101				
Nd			28.5				45.4				
Sm			5.64				8.56				
Eu			1.46				1.70				
Gd			5.35				8.17				
Dy			5.13				6.45				
Er			3.03				3.58				
Yb			2.94				3.14				

	(c) Ferrohypersthene granite gneiss 1							(d) Eulitic alkali feldspar granite gneiss		
	B143	B144	B25	B145	D118	D116	D111	*Bradley	B153	B152
Rb	201	223	207	238	251	255		188	397	413
Sr	171	155	167	140	126	121		181	12	12
Ba	885	985	878	1004	888	847		865	5	6
Y	47	53	47	43	44	52		36	53	52
Zr	288	316		305	307	311		268	100	118
Nb	17	18		17	15	15		15	5	6
Sc	16	14	15	12	11	11		14	1	1
V	58	49	56	31	27	26		44	0	0
Ni	22	20	21	20				12		11
Cr	16	17		7	10	11	12	23		0
La	58.5							42		
Ce	120							92.5		
Nd	50.9			47.9				43.5		33.8
Sm	9.58			9.00				8.5		5.74
Eu	1.77			1.52				1.85		0.163
Gd	8.60			8.02				7.95		6.45
Dy	7.93			7.50				8.95		7.13
Er	4.62			4.39				4.0		4.33
Yb	4.32			4.09				3.8		4.02
Ga								18		
Pb								27		
Li								25		
U								2		
Co								10		

* Average of 4 specimens from Bradley (1972)

	(e) Granite Gneiss 1						(f) Granite Gneiss 2 - Fishermans Point				
	B111	B103	B106	B101	B109	A88	B168	B164D	B164E	B164B	B163
Rb	261	296	274	299		235	361	323	370	414	
Sr	121	101	85	70		131	108	100	103	99	
Ba	610	652	505	474	506	901	670	647	689	788	279
Y	24	36	19	25		45	45	51	28	13	39
Zr	330	222	267			318	231	217	300	316	140
Nb	16	13	18			17	18	16	11	15	10
Sc	6	9	2		12	12	9	10	6	3	4
Cr							10	11		2	

	(g) Granite gneiss 2 - Kirton Point							(h) Alkali feldspar granite gneiss						
	A121	D206	KP309	D21	KP300	DP307	B500	D205	B161A	B22C	B159B	B154B	B154A	B22B
Rb	244	273	84	293	285	301	263	371	413	448	437	442	440	425
Sr	129	113	109	109	147	88	79	59	11	10	12	11	10	11
Ba	835	689		722	1093	575	439	246	6	3	9	5	5	8
Y	43	45	32	41	7	41	37	51	21	12	17	15	18	18
Zr	228	227	76	172	130	169	151	174	129	92	114	148	137	122
Nb	16	16	24	15	4	14	13	14	5	6	8	7	9	8
Sc	11	11		7	1	5	6	4	1	2	1	1	1	2
V	38						20							
Ni	17	17						13	12					
Cr	12			10			6			3		0	0	
La							60.8				9.9		38.8	
Ce							129			17.1	13.8		70.3	
Nd							37.0			4.03	3.9		20.9	
Sm							6.17			0.731	0.88		3.7	
Eu							1.00			0.130	0.15		0.15	
Gd							5.41			0.818	0.99		2.8	
Dy							5.30			1.35	1.84		2.5	
Er							3.31			1.45	1.64		1.4	
Yb							3.19			2.05	2.05		1.4	

- Notes: (1) All elemental abundances in ppm.
(2) No value presented indicates not analysed.
Zero value presented indicates below detection limit.
(3) *BRADLEY average of 4 analyses from Bradley (1972)

Appendix Table 3.1 Colbert Granitoid Suite, Moody Granitoid Suite and Massena Bay Gneisses, mineral analytical data and calculated structural formulae.

(a) Plagioclases

	Colbert Suite		Moody Granitoid Suite				Massena Bay Gneisses	
	B114(3)	B135(6)	I-type 830(5)	C4(4)	S-type 858(7)	851(5)	857(5)	Quartzofeldspathic D42(2) D84(4)
SiO2	59.57	57.77	60.44	61.89	66.00	66.79	65.96	57.09 54.71
Al2O3	25.43	26.71	25.06	23.95	21.19	20.77	21.17	26.99 28.37
CaO	6.64	8.08	6.03	4.87	1.48	0.92	1.54	8.63 10.35
Na2O	7.81	6.97	8.13	8.97	11.08	11.32	11.13	6.77 6.00
K2O	0.33	0.43	0.34	0.33	0.24	0.20	0.20	0.31 0.40
Total	99.78	99.96	100.00	100.01	100.00	100.00	100.00	99.79 99.83

Structural formulae based on 32 oxygen atoms

Si	10.649	10.359	10.760	10.987	11.608	11.718	11.603	10.269	9.906
Al	5.359	5.645	5.259	5.012	4.393	4.295	4.389	5.722	6.054
Ca	1.272	1.552	1.150	0.925	0.279	0.173	0.290	1.663	2.008
Na	2.707	2.423	2.806	3.088	3.779	3.851	3.796	2.361	2.106
K	0.075	0.098	0.077	0.075	0.054	0.045	0.045	0.071	0.092
An	31.4	38.1	28.5	22.6	6.8	4.3	7.0	40.6	47.7
Ab	66.8	59.5	69.6	75.5	91.9	94.6	91.9	57.7	50.1
Or	1.8	2.4	1.9	1.9	1.3	1.1	1.1	1.7	2.2

Plagioclases continued

	Massena Bay Gneisses continued				Calc-silicate		Gn-sill	
	Quartzofeldspathic continued				A86(2)	D65(4)	B65B(3)	B74(4)
	A10(3)	A10(1)	D4(3)	A84(1)				
SiO2	58.66	67.15	55.35	72.88	63.41	48.65	45.62	57.87
Al2O3	26.03	20.13	28.26	23.32	22.47	32.88	34.81	26.73
CaO	7.26	0.50	10.00	4.29	3.32	15.63	17.62	7.90
Na2O	7.69	11.65	5.96	9.22	9.59	2.60	1.42	7.08
K2O	0.33	0.45	0.34	0.29	0.41	0.14	0.15	0.29
Total	99.97	99.88	99.91	100.76	99.19	99.89	99.61	99.86

				B74	A84	A86	D65	B65B
Si	10.499	11.806	9.986	10.374	11.135	11.294	8.907	8.432
Al	5.491	4.172	6.009	5.648	4.867	4.717	7.095	7.583
Ca	1.392	0.094	1.933	1.517	0.814	0.634	3.066	3.489
Na	2.669	3.972	2.085	2.461	3.166	3.312	0.923	0.509
K	0.075	0.101	0.078	0.066	0.066	0.093	0.033	0.035
An	33.7	2.3	47.2	37.5	20.1	15.7	76.2	86.5
Ab	64.5	95.3	50.9	60.8	78.3	82.0	22.9	12.6
Or	1.8	2.4	1.9	1.6	1.6	2.3	0.8	0.9

(b) Alkali feldspars

	Moody Suite						
	Colbert Suite		I-type		S-type	↓	
	B114(6)	B135(3)	830(2)	C4(7)	858(4)	85(3)	857(3)
SiO ₂	64.79	64.12	64.65	64.67	64.57	64.36	64.61
Al ₂ O ₃	18.73	19.53	19.04	18.78	18.70	18.94	18.65
CaO	0.02	0.56	-	-	-	-	-
Na ₂ O	1.09	1.33	1.14	0.81	0.42	0.52	0.34
K ₂ O	15.38	14.46	14.88	15.74	16.32	16.18	16.40
Total	100.01	100.00	99.71	100.00	99.99	100.00	100.00

Structural formulae on basis of 32 oxygen atoms

Si	11.944	11.800	11.920	11.937	11.942	11.903	11.952
Al	4.070	4.236	4.138	4.086	4.077	4.129	4.067
Ca	0.004	0.110	-	-	-	-	-
Na	0.389	0.475	0.408	0.290	0.151	0.186	0.122
K	3.617	3.395	3.500	3.706	3.851	3.818	3.870
An	0.1	2.8	-	-	-	-	-
Ab	9.7	11.9	10.4	7.3	3.8	4.6	3.1
Or	90.2	85.3	89.6	92.7	96.2	95.4	96.9

Alkali feldspars continued

Massena Bay Gneisses

Quartzofeldspathic

	D42(2)	D84(3)	A10(2)	D4(2)	A84(1)
SiO ₂	64.73	64.65	64.78	64.86	64.48
Al ₂ O ₃	18.92	18.81	18.94	18.68	18.57
CaO	0.07	-	-	-	0.10
Na ₂ O	0.96	0.70	1.05	0.95	0.50
K ₂ O	15.29	15.71	15.24	15.37	16.36
Total	99.95	99.87	100.00	99.85	99.66
Si	11.927	11.941	11.928	11.964	11.939
Al	4.109	4.095	4.111	4.062	4.053
Ca	0.014	-	-	-	0.020
Na	0.343	0.251	0.375	0.340	0.180
K	3.594	3.702	3.580	3.617	3.865
An	0.3	-	-	-	0.5
Ab	8.7	6.3	9.5	8.6	4.4
Or	91.0	93.7	90.5	91.4	95.1

(c) Amphiboles calculated after method of Leake (1978)

	Colbert Suite		Moody Suite	Massena Bay Gneisses				
	B114(2)	B135(3)	830(2)	Quartzofeldspathic D42(2)	D84(2)	D4(2)	A84(3)	A86(5)
SiO ₂	39.91	40.11	43.13	42.54	41.57	41.39	55.36	51.29
TiO ₂	1.29	1.46	1.31	1.04	1.00	0.97	-	-
Al ₂ O ₃	12.36	11.65	9.81	11.01	11.68	11.82	3.21	3.45
Cr ₂ O ₃	0.06	-	-	-	-	0.13	0.04	0.05
FeO ^T	24.24	20.80	18.11	18.81	19.30	20.56	6.91	8.03
MnO	0.36	0.36	0.37	0.32	0.40	0.45	0.20	0.35
MgO	6.13	7.77	10.45	9.92	9.21	8.59	18.33	17.09
CaO	11.43	11.04	11.53	11.79	11.64	11.64	11.88	14.07
Na ₂ O	1.78	1.79	1.73	1.42	1.39	1.36	0.91	1.05
K ₂ O	1.94	1.90	1.50	1.45	1.60	1.68	0.39	0.24
Total	99.50	96.88	97.94	98.29	97.77	98.57	97.23	95.62

Structural formulae on basis of 23 oxygen atoms

T ₈	Si	6.089	6.192	6.009	6.350	6.262	6.218	7.785	7.587
	Al(4)	1.911	1.808	1.611	1.650	1.738	1.782	0.215	0.413
	Al(6)	0.311	0.310	-	0.287	0.336	0.311	0.317	0.189
	Ti	0.148	0.170	0.137	0.116	0.113	0.110	-	-
	Cr	0.007	-	-	-	-	0.015	0.004	0.006
C ₅	Fe ₃	0.590	0.536	1.550	0.605	0.634	0.693	-	-
	Fe ₂	2.504	2.148	1.479	1.744	1.797	1.890	0.817	1.520
	Mn	0.046	0.047	0.044	0.040	0.051	0.057	0.024	0.044
	Mg	1.394	1.787	2.170	2.207	2.068	1.923	3.842	3.769
	Ca	1.895	1.850	1.874	1.914	1.908	1.906	1.790	2.202
	Na	0.534	0.543	0.509	0.417	0.412	0.403	0.248	0.297
	K	0.383	0.379	0.290	0.280	0.312	0.328	0.070	0.045
	Mg/Mg+Fe ₂	0.36	0.45	0.59	0.56	0.54	0.50	0.82	0.71

(d) Opaque oxides calculated after method of Carmichael (1967)

	Colbert Granitoid Suite		Moody Suite		Massena Bay Gneisses QF			
	B114(2)	B114(1) B135	B135(4)	830(4) 830(2)	A10(2)	A10(1)		
SiO ₂	0.58	0.93	1.04	1.24	0.84	0.52	1.30	0.95
TiO ₂	0.22	49.50	0.72	37.21	0.12	49.88	0.12	46.21
Al ₂ O ₃	1.13	0.63	1.08	1.03	0.86	0.20	0.87	0.40
Cr ₂ O ₃	0.26	-	0.23	0.14	0.20	-	0.05	-
Fe ₂ O ₃	68.97	2.90	65.07	27.21	68.02	8.34	61.83	10.50
FeO	32.37	43.61	32.43	31.62	30.60	40.63	30.51	39.74
MnO	-	1.46	-	1.98	-	4.61	-	2.69
MgO	0.69	0.30	0.76	0.53	0.82	0.18	0.71	0.29
CaO	0.12	-	0.10	0.29	0.13	-	-	-
Total	104.34	99.33	101.43	101.25	101.59	104.36	95.39	100.79

Mt	97.3		04.1		06.6		94.48	
Ulv	2.7		5.9		3.4		5.52	
Ilm		96.3		72.8		92.1		89.51
Hm		3.7		27.2		7.9		10.49
T C	440		704		512		579	
-log _a O ₂	24.63		13.10		20.55		18.10	

(e) Clinopyroxenes calculated after
method of Jaffe et al. (1978)

(f) Garnets

	Massena Bay Gneisses calc - silicates		Moody Suite S-type			Massena Bay Gneisses Gnt- Sillimanited		Calc- silicate
	D65(5)	B65B(2)	858(2)	851(4)	857(2)	B74(3)	B65B(4)	
SiO2	50.45	49.85	35.69	35.72	35.78	36.71	37.78	
TiO2	0.03	-	-	-	-	0.03	0.33	
Al2O3	2.20	1.98	21.72	21.11	21.32	21.59	12.68	
Cr2O3	0.27	0.22	0.19	-	-	-	0.21	
FeOT	13.77	17.13	31.77	33.58	32.83	35.56	15.19	
MnO	0.58	0.33	9.06	7.75	7.89	0.79	0.48	
MgO	9.23	7.42	1.19	0.81	1.31	4.04	0.29	
CaO	22.90	22.78	0.35	0.25	0.36	1.28	32.95	
Na2O	0.57	0.30	-	-	0.48	-	-	
Total	100.00	100.00	100.00	99.21	99.97	100.00	99.90	

Structural formulae based
on 6 oxygen atoms

Structural formulae based on 12 oxygen atoms

Si	1.927	1.935	Si	2.925	2.958	2.937	2.948	3.072
Al(4)	0.073	0.065	Al	0.075	0.042	0.063	0.052	-
Al(6)	0.026	0.026	Al	2.023	2.019	2.000	1.991	1.215
Ti	0.001	-	Cr	0.012	-	-	-	0.014
Cr	0.008	0.007	Ti	-	-	-	0.002	0.020
Fe3	0.079	0.055	Mg	0.145	0.100	0.160	0.484	0.035
Fe2	0.361	0.502	Fe2	2.178	2.326	2.254	2.388	1.033
Mn	0.019	0.011	Mn	0.629	0.544	0.549	0.054	0.033
Mg	0.525	0.429	Ca	0.031	0.022	0.032	0.110	2.871
Ca	0.938	0.948	Na	-	-	0.076	-	-
Na	0.043	0.023						

(g) Biotites

	Colbert Suite		Moody Suite			Massena Bay Gneisses Quartzofeldspathic				garnet- sill.
	B114(2)	B135(3)	830(2)	C4(3)	858(2)	D42(2)	D84(2)	A10(1)	D4(2)	B74(4)
SiO2	35.68	35.94	37.47	34.16	34.62	36.72	36.60	36.23	36.41	34.86
TiO2	4.11	4.20	2.81	2.46	1.23	3.46	3.23	2.39	3.30	4.03
Al2O3	15.26	13.89	14.06	18.55	19.52	15.77	15.58	17.61	15.95	16.84
Cr2O3	-	-	-	-	-	-	-	-	-	-
FeOT	24.48	20.58	18.10	25.12	24.59	19.74	19.56	18.81	20.13	17.49
MnO	0.18	-	0.18	-	0.32	0.22	0.18	0.28	0.26	-
MgO	8.16	10.42	13.59	5.69	3.84	10.81	10.85	8.03	10.17	11.32
CaO	0.06	-	-	0.05	0.08	0.06	-	-	-	-
Na2O	0.21	0.25	0.10	0.29	0.38	0.19	0.08	0.18	0.25	-
K2O	9.50	9.46	9.75	9.53	8.80	9.94	9.69	8.89	9.63	9.36
Total	97.64	94.74	96.06	95.85	93.38	96.89	95.77	92.42	96.08	93.89

Structural formulae based on 22 oxygen atoms

Si	5.465	5.577	5.650	5.340	5.510	5.536	5.570	5.654	5.540	5.362
Al(4)	2.535	2.423	2.350	2.660	2.490	2.464	2.430	2.346	2.460	2.638
Al(6)	0.220	0.118	0.149	0.758	1.172	0.338	0.365	0.893	0.401	0.415
Ti(6)	0.473	0.490	0.318	0.289	0.147	0.392	0.370	0.281	0.378	0.466
FeT	3.136	2.671	2.283	3.284	3.273	2.489	2.490	2.455	2.562	2.250
Mn	0.023	-	0.023	-	0.043	0.028	0.023	0.037	0.034	-
Mg	1.863	2.410	3.055	1.326	0.911	2.429	2.462	1.868	2.307	2.596
Ca	0.010	-	-	0.008	0.014	0.010	-	-	-	-
Na	0.062	0.075	0.029	0.088	0.117	0.056	0.024	0.055	0.074	-
K	1.856	1.873	1.876	1.901	1.787	1.912	1.882	1.770	1.869	1.837

(h) Muscovites and others

	Moody Suite				Massena Bay	Gnenisses
	I-type C4 (1)	858 (5)	S-type 851 (3)	857 (2)	Quartzo- feldspathic A10 (2)	Scapolite in calcilic B65B (2)
SiO ₂	45.96	44.47	44.56	44.84	44.47	45.30
TiO ₂	0.51				0.71	
Al ₂ O ₃	33.62	34.95	34.94	35.30	32.80	27.66
Cr ₂ O ₃						0.16
FeO*	1.90	1.58	1.65	1.64	3.30	0.09
MnO						
MgO	0.91	0.63	0.49	0.55	0.83	0.19
CaO						18.22
Na ₂ O	0.30	0.49	0.57	0.53	0.50	3.10
K ₂ O	10.88	10.48	10.73	10.58	10.47	0.19
Total	94.09	92.60	92.94	93.44	93.07	94.90

Notes: (1) Number in brackets after specimen number refers to number of analyses averaged.

(2) Temperature and oxygen activities calculated from opaque oxide data after method of Powell & Powell (1977).

Appendix Table 3.2 Colbert Granitoid Suite - Major element geochemical data and CIPW Norms

	Colbert Hornblende Granite Gneiss				Colbert Alkali Feldspar Granite Gneiss				
	B112B	B112A	B109	B135	B129B	A119	B125A	B130A	A90
SiO2	63.35	63.66	63.75	66.90	76.01	76.08	76.83	77.16	77.24
Al2O3	14.99	14.95	15.08	14.55	12.06	11.72	12.35	11.47	11.85
Fe2O3Total	6.43	6.56	6.48	5.12	1.69	1.99	1.66	1.12	1.62
MnO	0.09	0.08	0.08	0.05	0.02	0.04	0.01	0.01	0.02
MgO	1.32	1.39	1.43	1.07	0.20	0.25	0.07	0.07	0.15
CaO	3.56	3.62	3.70	2.41	0.75	0.76	0.55	0.46	0.58
Na2O	2.75	2.77	2.97	2.38	2.18	2.67	2.25	2.42	2.08
K2O	5.32	5.23	4.94	6.02	6.59	6.06	6.77	6.17	6.85
TiO2	1.08	1.10	1.09	0.84	0.25	0.30	0.24	0.16	0.25
P2O5	0.33	0.35	0.30	0.23	0.02	0.03	0.02	0.01	0.02
Total	99.22	99.71	99.82	99.57	99.77	99.90	100.75	99.05	100.66
LOI	0.41	0.40	0.61	0.38	0.40	0.27	0.43	0.24	0.30
CIPW NORMS									
Q	16.54	16.89	16.64	22.00	35.49	34.92	35.84	37.90	36.81
C	-	-	-	0.29	0.03	-	0.37	-	-
OR	31.31	30.78	29.02	35.44	38.79	35.72	39.84	36.38	40.36
AB	23.17	23.35	24.98	20.06	18.37	22.53	18.96	20.43	17.55
AN	12.79	12.86	13.15	10.41	3.58	2.09	2.59	2.21	2.74
DI WO	1.11	1.15	1.31	-	-	0.62	-	-	-
EN	0.44	0.47	0.55	-	-	0.18	-	-	-
FS	0.67	0.69	0.77	-	-	0.47	-	-	-
HY EN	2.83	2.98	2.99	2.65	0.50	0.44	0.17	0.17	0.37
FS	4.33	4.40	4.24	3.98	1.36	1.16	1.33	0.91	1.29
MT	2.32	2.37	2.33	1.85	0.61	0.72	0.60	0.41	0.59
IL	2.04	2.08	2.06	1.59	0.47	0.57	0.45	0.30	0.47
AP	0.76	0.81	0.69	0.53	0.05	0.07	0.05	0.02	0.05

Appendix Table 3.3 Colbert Granitoid Suite - Trace element geochemical data.

	Colbert Hornblende Granite Gneiss				Colbert Alkali Feldspar Granite Gneiss				
	B112B	B112A	B109	B135	B129B	A119	B125A	B130A	A90
Rb	198	197	196	235	277	312	276	300	342
Sr	184	183	187	145	57	48	54	28	22
Ba	-	1133	1144	1063	711	387	743	267	84
Y	52	53	46	46	16	50	19	32	27
Zr	333	339	343	411	235	263	226	173	335
Nb	22	22	21	17	7	18	10	12	11
Sc	-	17	15	13	4	5	5	5	4
Ti	-	6197	5768	5039	1384	1977	1519	1170	1550
Cr*	10	4	-	5	0	-	0	0	-
La		62.2		75.2			62.3		
Ce		136		-			123		
Nd		62.8		60.6			47.7		
Sm		12.0		10.9			7.66		
Eu		2.07		1.71			0.857		
Gd		11.8		9.38			3.9		
Dy		9.46		8.11			3.98		
Er		5.24		4.36			1.81		
Yb		4.46		3.66			1.37		

Appendix Table 4.1 Moody Granitoid Suite:
Major element geochemical data and CIPW Norms.

	CHS		Moody Tank Adamellite			MWA
	829	839	801(4)	241	801(6)	849
SiO2	58.88	66.04	72.10	72.14	72.57	72.66
Al2O3	15.57	13.93	14.23	14.15	14.07	14.46
Fe2O3Total	7.33	5.68	3.24	2.53	2.83	3.38
MnO	0.12	0.10	0.05	0.05	0.04	0.06
MgO	2.31	0.81	0.37	0.46	0.37	0.48
CaO	4.28	2.26	1.19	1.29	1.19	1.43
Na2O	3.27	2.87	3.31	2.87	3.31	2.91
K2O	5.28	5.60	4.94	5.32	4.86	5.42
TiO2	1.40	0.79	0.35	0.29	0.35	0.42
P2O5	0.63	0.32	0.08	0.13	0.09	0.63
Total	100.10	98.91	100.53	99.57	100.25	99.19
LOI	1.03	0.51	0.57	0.34	0.57	0.62
CIPW Norms						
Q	7.30	20.61	29.59	30.88	30.59	31.47
C	-	-	1.46	1.63	1.41	2.70
OR	30.88	32.93	29.03	31.33	28.56	31.83
AB	27.39	24.16	27.85	24.20	27.85	24.47
AN	12.09	8.54	5.35	5.53	5.29	2.96
DI	2.03	0.22	-	-	-	-
WO	1.01	0.07	-	-	-	-
EN	0.07	0.16	-	-	-	-
FS	4.68	1.94	0.92	1.14	0.92	1.19
HY	4.46	4.56	2.84	2.22	2.41	2.89
EN	2.63	2.05	1.17	0.91	1.02	1.22
FS	2.63	1.49	0.66	0.55	0.66	0.79
MT	1.45	0.74	0.18	0.30	0.21	1.46
IL						
AP						

	Yunta Well Leucogranite						
	419	854	858	853	851	857	856
SiO2	72.16	75.39	73.67	73.83	74.12	74.31	75.73
Al2O3	14.17	14.60	15.38	14.33	14.53	15.20	13.76
Fe2O3Total	1.26	1.30	1.19	0.93	1.00	0.98	1.09
MnO	0.04	0.12	0.03	0.07	0.06	0.14	0.08
MgO	0.16	0.06	0.19	0.06	0.58	0.63	0.06
CaO	0.50	0.61	0.73	0.53	0.52	0.63	0.46
Na2O	4.29	3.98	3.30	4.32	4.30	3.99	3.57
K2O	5.90	5.02	4.66	4.00	3.89	4.28	3.83
TiO2	0.09	0.03	0.07	0.03	0.03	0.03	0.03
P2O5	0.30	0.30	0.34	0.30	0.30	0.19	0.30
Total	99.79	100.17	100.33	99.04	99.94	100.82	99.16
LOI	0.92	0.56	0.77	0.64	0.61	0.44	0.35
CIPW Norms							
Q	23.39	29.82	34.95	32.33	32.39	32.27	39.76
C	0.53	2.22	4.36	2.63	3.00	3.30	3.72
OR	34.53	29.50	27.33	23.49	22.85	25.18	21.97
AB	35.97	33.49	27.71	36.32	36.16	33.61	30.10
AN	0.51	1.06	1.39	0.66	0.61	1.87	0.32
DI	-	-	-	-	-	-	-
WO	-	-	-	-	-	-	-
EN	-	-	-	-	-	-	-
FS	-	-	-	-	-	-	-
HY	0.39	0.15	0.47	0.15	1.44	1.56	0.15
EN	1.22	1.51	1.16	1.03	1.09	1.22	1.22
FS	0.45	0.47	0.43	0.33	0.36	0.35	0.39
MT	0.17	0.06	0.13	0.06	0.06	0.06	0.06
IL	0.69	0.69	0.78	0.69	0.69	0.44	0.70
AP							

Appendix Table 4.2 Moody Granitoid Suite

Trace element geochemical data

	CHS 829	MOA 839	MTA 8014	MWA 849	854	Yunta Well 858	853	Leucogranite 851	857	856
Rb	164	201	263	206	343	308	303	356	257	416
Sr	774	340	97	132	8	23	7	7	15	8
Ba	2471	1229	340	606	3	28	2	1	55	2
Y	40	25	37	38	11	18	7	6	9	6
Zr	464	311	349	247	25	26	33	30	35	25
Nb	32	26	31	19	8	32	18	25	11	27
Sc	12	10	5	5	2	5	1	1	3	1
La	236	104	102	101						
Ce	418	212	191	204				6	4	
Nd	169	90.7	71.1	70.2						
Sm	22.9	11.4	13.7	11.3						
Eu	4.03	2.05	0.915	1.14						
Gd	14.3	6.95	9.27	7.93						
Dy	8.89	4.52	6.20	6.24						
Er	4.66	2.00	3.13	3.22						
Yb	3.64	1.35	3.35	2.80						

Appendix Table 5.1 Massena Bay Gneisses Major element geochemical data and CIPW norms

	Quartzofeldspathic Gneisses							"Interlayered Gneisses"			
	D87	D85	D83	D17	D46	42*	46B*	22*	B74	B78	B77
SiO2	62.16	62.79	63.52	65.33	70.71	63.75	64.56	65.42	62.59	64.24	67.73
Al2O3	16.33	17.31	17.24	15.21	14.19	15.48	15.43	14.73	18.81	18.75	16.00
Fe2O3T	6.66	6.17	5.76	6.35	3.25	5.64	5.01	4.68	5.87	4.53	5.17
MnO	0.10	0.07	0.07	0.09	0.04	0.07	0.07	0.09	0.06	0.05	0.07
MgO	2.63	2.00	1.92	2.58	0.63	2.65	2.28	2.56	2.31	1.10	1.22
CaO	5.39	5.44	5.32	4.95	2.20	3.17	2.94	2.53	3.62	4.86	3.27
Na2O	2.27	2.90	2.85	2.84	2.70	5.90	3.89	4.77	4.70	3.67	2.89
K2O	3.23	2.44	2.52	2.84	5.58	2.76	4.65	2.87	1.73	2.89	3.67
TiO2	0.62	0.61	0.59	0.59	0.52	0.27	0.30	0.24	0.61	0.56	0.57
P2O5	0.13	0.13	0.13	0.13	0.10	0.08	0.10	0.11	0.10	0.07	0.16
Total	99.03	99.86	99.92	100.91	99.92	99.77	99.23	98.00	100.40	100.72	100.75
LOI	1.58	0.93	1.08	0.75	0.36				1.30	1.18	0.78
CIPW Norms											
Q	18.97	19.81	21.08	21.96	27.14	7.48	13.18	16.00	15.36	18.22	26.44
C	-	0.32	0.46	-	-	-	-	-	2.86	0.92	1.71
OR	19.09	14.42	14.89	16.78	32.98	16.31	27.48	16.96	10.22	17.08	21.69
AB	19.21	24.54	24.12	24.03	22.85	49.92	32.92	40.36	39.77	31.05	24.45
AN	24.83	26.14	25.54	20.37	10.12	7.61	10.91	10.31	17.31	23.65	15.18
DI	0.44	-	-	1.39	0.06	3.17	1.26	0.64	-	-	-
WO	0.22	-	-	0.72	0.02	1.68	0.66	0.36	-	-	-
EN	0.21	-	-	0.64	0.04	1.40	0.56	0.26	-	-	-
FS	6.32	4.98	4.78	5.71	1.55	4.92	5.01	6.02	5.75	2.74	3.04
HY	5.83	5.50	5.10	5.11	2.54	4.11	4.25	4.35	5.17	3.85	4.53
EN	2.41	2.24	2.09	2.30	1.18	2.04	1.82	1.70	2.13	1.64	1.87
FS	1.18	1.16	1.12	1.12	0.99	0.51	0.57	0.46	1.16	1.06	1.08
MT	0.30	0.30	0.30	0.30	0.23	0.19	0.23	0.26	0.23	0.16	0.37
IL											
AP											

Calc - silicates and "quartzites"

	D27	D105B	D65	D105A	D64	A79	D57
SiO2	54.11	70.20	76.60	69.50	72.44	74.62	76.61
Al2O3	19.70	12.30	10.56	11.95	13.84	13.33	11.76
Fe2O3T	4.71	2.55	3.46	3.77	3.27	1.47	1.79
MnO	0.32	0.06	0.07	0.09	0.05	0.02	0.02
MgO	1.73	0.22	0.75	1.53	0.28	0.26	0.17
CaO	15.97	14.15	6.74	5.89	1.86	1.29	0.87
Na2O	0.33	0.32	1.31	1.33	2.91	2.51	2.04
K2O	2.20	0.04	0.10	5.39	5.27	6.02	6.24
TiO2	0.50	0.26	0.37	0.50	0.36	0.32	0.35
P2O5	0.27	0.12	0.10	0.10	0.06	0.03	0.04
Total	99.83	100.22	100.05	99.94	100.33	99.86	99.88
LOI	3.67	0.66	0.13	0.15	0.19	0.78	0.26

* Gneisses of Massena Bay Type, from Yorke Peninsula; after Pedler (1976).

Appendix Table 5.2 Massena Bay Gneisses
trace element analytical data.

Sample	Quartzofeldspathic			Gneisses				
	D87	D85	D83	D17	D46	42*	46B*	22*
Rb	175	140	138			90	197	82
Sr	193	243	241			170	212	194
Ba	563	433	480	550	1249	439	703	566
Y	29	27	24	22		34	27	
Zr	129	194	177	140	280	160	161	168
Nb	12	11	10	10	12	17	14	12
Sc	23	22	21	19	7	18	16	17
Ni	28	21	21		18			
La	35		41					
Ce	70		81					
Nd	29		34					
Sm	5.5		6.1					
Eu	1.2		1.2					
Gd	4.9		5.4					
Dy	4.5		4.2					
Er	2.7		2.3					
Yb	2.7		2.2					

	Calc-silicates and quartzites						
	D27	D105B	D65	D105A	D64	A79	D57
Ba		4		1460	1017		472
Y		26		38			
Zr				151	276		236
Nb				24	14		11
Sc		7		11	8		5

Notes: (1) Elemental abundances in ppm
(2) * denotes sample data from Pedler (1976)

Appendix Table 6.1 Basaltic dyke and metabasaltic dyke mineral analytical data and structural formulae.

(a) Clinopyroxenes (calculated after Jaffe et al., 1978)

Specimen * Texture Category	B69(2) 2A	Al13(5) 2C	B36(2) 2D	B36(4) 2D	B36(1)** 2D	B26(4) 1A	B32(4) 1B
SiO2	52.80	52.34	50.50	50.87	52.14	52.13	51.11
TiO2	0.08	-	0.18	0.28	-	0.04	0.08
Al2O3	1.96	1.36	3.04	3.61	2.20	1.61	1.70
Cr2O3	0.53	0.29	0.27	0.29	-	0.28	0.27
FeTotal	6.49	10.61	16.98	10.57	16.14	11.47	13.74
MnO	-	0.03	0.20	-	-	0.04	0.08
MgO	14.78	13.20	14.80	12.75	15.58	13.15	11.09
CaO	23.08	21.81	13.64	21.11	13.28	21.02	21.52
Na2O	0.30	0.36	0.40	0.53	0.51	0.27	0.39
Total	100.02	100.00	100.01	100.01	99.85	100.00	99.98

Mineral formula calculated on basis of 6 oxygens

Si	1.949	1.960	1.901	1.900	1.955	1.957	1.941
Al(4)	0.051	0.040	0.099	0.100	0.045	0.043	0.059
Al(6)	0.033	0.020	0.036	0.059	0.052	0.028	0.017
Ti	0.002	-	0.005	0.008	-	0.001	0.002
Fe3	0.020	0.037	0.074	0.055	0.030	0.024	0.060
Cr	0.015	0.009	0.008	0.009	-	0.008	0.008
Mg	0.814	0.737	0.831	0.710	0.781	0.736	0.628
Fe2	0.181	0.295	0.461	0.276	0.476	0.336	0.377
Mn	-	0.001	0.006	-	-	0.001	0.003
Ca	0.913	0.875	0.551	0.845	0.534	0.846	0.876
Na	0.022	0.026	0.029	0.039	0.037	0.020	0.029
Mg/Mg+Fe2	0.82	0.71	0.64	0.72	0.65	0.69	0.62

(b) Orthopyroxenes (calculated after Jaffe et al., 1978)

Specimen Texture Category	B69(2) 2A	B69(2) 2A	Al13(4) 2C	B36(5)** 2D	B26(5) 1A	B32(3) 1B
SiO2	52.35	52.49	51.12	51.76	50.57	49.29
TiO2	-	-	0.03	-	0.10	0.11
Al2O3	1.20	1.24	1.07	1.46	1.32	2.03
Cr2O3	0.15	0.14	-	-	-	-
FeOTotal	20.92	21.46	28.64	26.06	28.80	32.54
MnO	0.32	0.34	0.51	0.20	0.53	0.51
MgO	21.49	22.76	17.96	19.92	17.84	14.96
CaO	3.39	1.58	0.52	0.41	0.51	0.77
Na2O	0.20	-	0.16	-	0.16	0.30
Total	100.02	100.01	100.01	99.81	99.83	100.51

Structural formula calculated on basis of 6 oxygens

Si	1.944	1.946	1.959	1.961	1.942	1.911
Al(4)	0.053	0.054	0.041	0.039	0.058	0.089
Al(6)	-	-	0.007	0.026	0.002	0.004
Ti	-	-	0.001	-	0.003	0.003
Fe3	0.070	0.051	0.045	0.013	0.063	0.103
Cr	0.004	0.004	-	-	-	-
Mg	1.190	1.258	1.025	1.125	1.020	1.864
Fe2	0.581	0.614	0.873	0.813	0.862	0.952
Mn	0.010	0.011	0.017	0.006	0.017	0.017
Ca	0.135	0.063	0.021	0.017	0.021	0.032
Na	0.014	-	0.012	-	0.012	0.023
Mg/Mg+Fe2	0.67	0.67	0.54	0.58	0.54	0.48

(c) Biotites

Specimen Texture Category	B69(3) 2A	A113(4) 2C	B36(3) 2C	B26(3) 1A	B32(3) 1B
SiO2	37.15	36.11	35.45	34.75	35.75
TiO2	5.29	4.96	5.68	5.49	5.25
Al2O3	14.41	14.99	15.13	14.58	14.08
Cr2O3	0.29	0.10	-	0.23	0.34
FeOTotal	12.54	17.61	16.72	18.85	19.92
MnO	-	-	-	-	-
MgO	15.48	11.77	12.50	10.98	10.56
CaO	0.39	0.12	0.13	0.48	0.18
Na2O	-	0.09	0.05	0.08	0.07
K2O	0.55	9.29	9.65	8.74	9.43
Total	95.10	95.03	95.31	94.18	95.58

Structural formula calculated to 22 Oxygens

Si	5.517	5.489	5.373	5.380	5.486
Ti	.591	.567	.647	.639	.606
Al	2.522	2.686	2.703	2.660	2.547
Cr	.034	.012	-	.028	.041
Fe Total	1.557	2.239	2.119	2.441	2.556
Mn	-	-	-	-	-
Mg	3.427	2.667	2.824	2.534	2.416
Ca	.062	.020	.021	.080	.030
Na	-	.027	.015	.024	.021
K	1.809	1.802	1.866	1.726	1.846

(d) Amphiboles (calculated after Leake, 1978)

Specimen Texture Category	B36(4) 2D	B36(3)** 2D	B32(3) 1B
SiO2	39.72	39.64	40.95
TiO2	3.41	3.43	1.82
Al2O3	14.07	13.88	11.80
Cr2O3	0.09	0.04	0.21
FeOTotal	15.73	15.74	18.82
MnO	-	-	0.04
MgO	9.53	9.28	8.73
CaO	11.52	11.53	11.31
Na2O	2.21	2.17	1.63
K2O	2.04	1.96	1.92
Total	98.31	97.57	97.23

Structural formula calculated on basis of 23 oxygens

T8 Si	5.983	6.025	6.250
Al (4)	2.017	1.975	1.750
Al (6)	0.481	0.512	0.372
Ti	0.386	0.392	0.209
Cr	0.011	0.005	0.026
C5 Fe3	-	-	0.341
Fe2	1.982	1.988	2.061
Mn	-	-	0.005
Mg	2.140	2.103	1.986
Ca	1.859	1.874	1.865
B2 Na	0.141	0.126	0.135
Na	0.504	0.512	0.351
A0-1 K	0.392	0.379	0.377

(e) Garnet

Specimen Texture Category	B36(4)** 2D
SiO2	38.44
Al2O3	21.87
FeOTotal	27.64
MnO	0.92
MgO	4.90
CaO	6.79
Na2O	0.21
Total	100.76

Structural formula based on 12 oxygen atoms

Si	2.991
Al	2.006
Total	4.997
Fe2	1.799
Mn	0.061
Mg	0.568
Ca	0.566
Na	0.032
Total	3.026

(f) Plagioclases and Alkali feldspars

Specimen Texture Category	B69(7) 2A	A113(4) 2C	B36(6) 2D	B26(6) 1A	B32(6) 1B	B69(2) 2A	A113(2) 2C	B32(1) 1B
SiO ₂	52.63	54.59	52.19	54.66	56.49	64.37	64.43	64.74
Al ₂ O ₃	29.89	28.87	30.16	28.64	27.26	18.80	18.97	18.75
CaO	12.01	10.56	12.31	10.53	9.02	0.23	0.11	-
Na ₂ O	4.55	5.57	4.53	5.46	6.39	0.96	0.72	0.82
K ₂ O	0.26	0.33	0.22	0.29	0.35	15.21	15.41	15.55
Total	99.34	00.92	99.41	99.57	99.51	99.57	99.63	99.86

Mineral formula calculated on basis of 32 oxygens

Si	9.593	9.861	9.520	9.898	10.198	11.916	11.915	11.951
Al	6.422	6.147	6.485	6.113	5.801	4.102	4.135	4.080
Ca	2.346	2.044	2.406	2.043	1.745	0.046	0.022	-
Na	1.608	1.951	1.602	1.917	2.237	0.345	0.258	0.294
K	.060	.076	.051	.067	.081	3.592	3.636	3.662
An	58.4	50.2	59.3	50.7	43.0	1.1	0.6	-
Ab	40.1	47.9	39.5	47.6	55.1	8.7	6.6	7.4
Or	1.5	1.9	1.2	1.7	1.9	90.2	92.8	92.6

(g) Oxides (calculated after Carmichael, 1967)

Specimen Texture Category	B69(3) 2A	A113(3) 2C	B36(3) 2D	B36(4) 2D	B36(2)** 2D	B26(3) 1A	B32(2) 1B
SiO ₂	-	1.10	-	1.15	-	0.86	0.66
TiO ₂	49.10	50.93	50.29	2.22	51.95	48.59	50.35
Al ₂ O ₃	0.56	0.47	0.56	2.29	0.23	0.62	0.48
Cr ₂ O ₃	0.28	0.18	0.08	1.73	-	0.23	0.12
Fe ₂ O ₃	7.30	-	4.33	59.01	0.70	5.06	2.16
FeO	40.83	45.70	43.09	33.68	45.31	43.01	44.82
MnO	0.43	0.43	0.72	-	0.33	1.03	0.72
MgO	1.88	0.77	1.01	0.92	0.69	0.67	0.50
CaO	-	-	-	-	-	-	-
Total	100.38	99.58	100.08	101.31	99.58	100.07	99.81
Hm	7.9	0.7	5.0		1.0	5.9	2.9
Ilm	92.1	99.3	95.0		99.0	94.1	97.1
Ulv				10.4			
Mt				89.6			
T ^o C			569	569	446		
log ₁₀ a _{O₂}			-20.2	-20.2	-27.7		

- Notes: (1) * Number in brackets after specimen number denotes number of analyses averaged.
- (2) ** Analysed in 1983 on University of Adelaide microprobe; all others analysed 1978 on Australian National University microprobe.
- (3) All elemental oxide values in wt. %.
- (4) Temperature and oxygen activities calculated after method of Powell & Powell (1977).

Appendix Table 6.2 Major element geochemical data and CIPW normative mineralogy of cumulate ultramafic rocks and basaltic dyke rocks.

	GROUP A							
	739*1	785*1	786*1	B58 ^{2D}	B60 ^{1A}	B69 ^{1A}	B16 ^{1B}	B26 ^{1A}
SiO ₂	47.19	53.33	52.00	49.99	51.66	51.10	51.83	52.89
TiO ₂	0.48	0.45	0.46	0.62	0.65	0.81	0.88	0.80
Al ₂ O ₃	8.19	5.95	5.83	11.05	11.61	13.63	14.92	15.13
Fe ₂ O ₃ Total	11.77	16.47	16.52	11.35	11.20	10.70	10.69	10.67
MnO	0.18	0.27	0.28	0.17	0.18	0.17	0.17	0.17
MgO	23.94	17.62	15.79	15.86	13.59	10.60	7.66	7.04
CaO	6.38	3.85	6.32	9.04	9.01	10.07	10.31	9.88
Na ₂ O	0.96	1.16	1.20	1.29	1.68	2.00	2.28	2.47
K ₂ O	0.48	0.67	0.68	0.53	0.67	0.69	0.84	1.13
P ₂ O ₅	0.08	0.11	0.15	0.08	0.08	0.12	0.12	0.19
Total	99.65	99.88	99.28	99.99	100.33	99.90	99.70	100.35
LOI				0.14	-0.03	-1.42	-1.49	-0.10
Mg.No.	83	68	65	73	71	66	59	57
CIPW Norm								
Q	-	3.27	1.89	-	-	-	1.90	2.42
OR	2.84	3.96	4.02	3.13	3.96	4.08	4.96	6.68
AB	8.12	9.82	10.15	10.92	14.22	16.92	19.29	20.90
AN	16.62	9.05	8.51	22.80	22.16	26.18	28.00	26.86
DI WO	6.06	3.90	9.13	8.99	9.19	9.60	9.34	8.73
EN	4.48	2.54	5.78	6.27	6.23	6.25	5.58	5.06
FS	0.99	1.09	2.77	1.97	2.25	2.69	3.28	3.27
HY EN	20.18	41.34	33.54	24.24	25.47	19.09	13.50	12.47
FS	4.45	17.74	16.10	7.62	9.19	8.21	7.95	8.07
OL FO	24.49	-	-	6.30	1.51	0.74	-	-
FA	24.49	-	-	2.18	0.60	0.35	-	-
MT	3.41	4.78	4.79	3.29	3.25	3.10	3.10	3.09
IL	0.91	0.85	0.87	1.18	1.23	1.54	1.67	1.52
AP	0.19	0.26	0.35	0.19	0.19	0.28	0.28	0.44
GROUP B								
	B36 ^{2D}	1374 ^{*1A}	1371 ^{*1A}	1166 ^{*1A}	1346 ^{*1A}	743 ^{*1A}	B82 ^{2D}	1397 ^{*1B}
SiO ₂	47.33	49.93	49.95	49.57	49.49	47.97	47.54	48.34
TiO ₂	1.58	1.64	1.30	1.33	2.62	2.69	2.50	2.54
Al ₂ O ₃	16.16	13.86	13.81	13.56	14.36	12.91	13.43	13.87
Fe ₂ O ₃ Total	15.49	15.10	15.05	15.49	17.70	18.22	17.40	16.53
MnO	0.21	0.22	0.23	0.24	0.26	0.27	0.23	0.25
MgO	7.21	6.94	6.81	6.77	6.06	6.05	6.06	5.85
CaO	9.70	11.01	10.96	10.72	8.76	10.13	9.39	9.66
Na ₂ O	2.25	1.91	2.37	2.52	0.84	1.52	2.32	2.38
K ₂ O	0.76	0.45	0.15	0.27	0.33	0.29	0.91	0.89
P ₂ O ₅	0.16	0.10	0.16	0.16	0.40	0.35	0.30	0.39
Total	100.85	101.16	100.79	100.53	100.82	100.40	100.08	100.70
Mg.No.	48	48	55	53	40	40	41	44
CIPW Norms								
Q	-	2.16	1.03	-	10.48	4.89	-	0.26
OR	4.49	2.66	0.89	1.60	1.95	1.71	5.38	5.26
AB	19.04	16.16	20.05	12.32	7.11	12.86	19.63	20.14
AN	31.75	27.92	26.60	24.89	34.44	27.55	23.55	24.54
DI WO	6.40	10.88	11.16	11.38	2.67	8.53	8.80	8.70
EN	3.32	5.64	5.66	5.68	1.26	3.95	4.16	4.17
FS	2.90	4.95	5.24	5.45	1.39	4.49	4.53	4.40
HY EN	7.44	11.65	11.30	10.57	13.83	11.12	9.70	10.40
FS	6.50	10.22	10.45	10.14	15.25	12.64	10.56	10.99
OL FO	5.04	-	-	0.42	-	-	0.86	-
FA	4.86	-	-	0.45	-	-	1.04	-
MT	4.49	4.38	4.36	4.49	5.13	5.28	5.05	4.79
IL	3.00	3.11	2.47	2.54	4.97	5.11	4.75	4.82
AP	0.37	0.23	0.37	0.37	0.93	0.81	0.70	0.91

Appendix Table 6.3A Trace element geochemical data for cumulate ultramafic rocks

	Group A			Group C	Normalising Value
	739 ^{*2}	785 ^{*2}	786 ^{*2}	756 ^{*2}	
Rb	15	37	32	1	0.35
Sr	77	85	80	75	11.0
Ba	128	175	178	26	3.5
Y	12	12	19	16	2.2
Zr	59	84	69	38	5.6
Nb	2	5	5	1	0.39
Ti	2878	2698	2758	2218	620
Sc	24	32	31	46	7.9
V	140	108	138	178	62
Ni	1059	563	431	228	-
Cr	3421	1284	1027	1838	-
Co	100	88	70	62	-
La	8	9	10	10	0.315
Ce	14	19	26	31	0.813
Nd				24	0.597
Sm				5	0.192
Eu				0.9	0.0722
Gd				3.8	0.259
Dy				3.2	0.325
Er				1.6	0.213
Yb				1.4	0.208

Appendix Table 6.3B Trace element geochemical data for basaltic dyke rocks

	Group A				
	B58 ^{2D}	B60 ^{2A}	B69 ^{2A}	B16 ^{2B}	B26 ^{1A}
Rb	19	25	21	30	30
Sr	112	126	165	182	320
Ba	151	209	241	273	728
Y	16	20	23	25	25
Zr	74	89	104	116	107
Nb	5	6	6	6	7
Ti	3717	3897	4856	5276	4796
Sc	37	31	32	35	35
V	231	238	235	256	228
Ni	526	326	289	160	79
Cr	2401	1655	1119	568	345
Co	-	-	-	-	-
La	12.9	12.3	13.5	17.5	23.9
Ce	23.8	25.5	28.5	36.5	50.9
Nd	12.1	13.4	14.1	17.6	23.3
Sm	2.71	3.19	3.16	3.83	4.48
Eu	0.831	1.01	1.06	1.17	1.28
Gd	3.05	3.60	3.44	4.03	4.47
Dy	3.19	3.77	3.51	4.22	4.22
Er	1.98	2.41	2.10	2.57	2.68
Yb	1.96	2.42	1.96	2.46	2.67

Appendix Table 6.3B continued

	Group B							
	B36 ^{2D}	1374 ^{*1A}	1371 ^{*1A}	1166 ^{*1A}	1346 ^{*1A}	743 ^{*1A}	B82 ^{2D}	1397 ^{*1B}
Rb	24	10	3	6	11	5	35	30
Sr	188	110	73	135	52	59	177	162
Ba	258	131	24	84	64	56	266	267
Y	28	21	24	25	49	51	44	38
Zr	105	107	86	93	169	170	150	174
Nb	8	6	9	5	18	16	12	13
Ti	9472	9832	7793	7973	15707	16127	14987	15227
Sc	34	35	41	39	46	44	41	31
V	269	318	274	295	363	365	405	340
Ni	169	62	55	58	41	41	79	79
Cr	141	66	91	94	110	119	170	162
Co	-	34	55	31	24	31	-	36
La	12.2	12	11	14	34	21	21.8	21
Ce	27.0	29	24	30	85	50	49.9	49
Nd	16.2	13	7	14	45	21	28.2	21
Sm	4.09						6.90	
Eu	1.41						2.24	
Gd	4.75						7.87	
Dy	4.93						7.78	
Er	2.93						4.61	
Yb	2.76						4.17	

	Group C							
	B52 ^{2D}	742 ^{*1B}	1396 ^{*1B}	744 ^{*1A}	1359 ^{*1A}	1351 ^{*1A}	1366 ^{*1A}	1354 ^{*1A}
Rb	20	12	9	9	3	2	4	3
Sr	130	58	164	148	30	71	93	109
Ba	160	99	85	134	18	43	91	127
Y	17	16	16	16	25	19	36	23
Zr	39	46	54	42	65	55	83	62
Nb	2	8	6	10	4	3	9	9
Ti	3117	4856	6984	4017	6834	6115	9352	8573
Sc	44	30	32	36	46	51	35	33
V	251	105	270	205	276	234	266	233
Ni	234	162	163	156	58	60	57	62
Cr	382	507	202	485	134	136	171	114
Co	-	49	42	60	35	60	27	27
La	6.15	6	5	5	20	55	63	29
Ce	12.8	19	19	16	59	17	185	71
Nd	6.45	11	7	8	24	8.9	72	31
Sm	1.56					2.8	11	
Eu	0.611					1.1	2.0	
Gd	2.03					2.8	9.7	
Dy	2.40					4.4	10	
Er	1.57					2.6	4.5	
Yb	1.54					2.3	3.9	

Footnotes for Appendix Tables 6.3A and 6.3B

- (1) element abundances in ppm
- (2) Normalising values from Sun et al. (1979).
- (3) Normalising values from Sun et al. (1979) for K = 120 ppm, P = 46 ppm.
- (4) * = analysis from Bradley (1972)
- (5) Superscripts; 1 = DK1 ; 2 = DK2

Appendix Table 6.4 Key elemental ratios for non-cumulate basaltic dyke rocks

(a) Group A							(b) Group B			
	B58	B60	B69	B16	B26	B36	1374*	1371*	1166*	1346*
TiO ₂ /P ₂ O ₅	7.75	8.13	6.75	7.33	4.21	9.9	16.4	8.1	8.3	6.6
CaO/TiO ₂	14.6	13.9	12.4	11.7	12.4	6.1	6.7	8.4	8.1	3.3
Al ₂ O ₃	17.9	17.9	16.8	17.0	18.9	10.2	8.5	10.6	10.2	5.5
CaO/Al ₂ O ₃	0.82	0.78	0.74	0.69	0.65	0.60	0.79	0.79	0.79	0.61
Ti/Zr	50	44	47	45	45	90	91	91	86	93
Ti/Y	232	195	211	211	192	338	468	325	319	321
Ti/Sc	100	126	152	151	137	279	281	190	204	341
Zr/Y	4.6	4.5	4.5	4.6	4.3	3.8	5.1	3.7	3.7	3.4
Zr/Nb	15	14	18	18	15	13	18	10	19	9
(La/Sm)N	2.89	2.36	2.59	2.79	3.26	1.82				
(Yb/Gd)N	0.80	0.83	0.71	0.76	0.75	0.72				
(Eu/Eu*)N										
(La/Ce)N	1.40	1.24	1.22	1.24	1.21	1.17	1.07	1.18	1.20	1.03
Rb/Sr	0.17	0.20	0.13	0.16	0.09	0.13	0.09	0.04	0.04	0.21
K/Rb	235	221	268	232	318	264	374	415	374	249
K/Ba	29	27	24	26	13	24.5	28.5	51.9	26.7	42.8
P ₂ O ₅ /Ce	34	31	42	33	37	59	34	67	53	47

(b) Group B continued

	743*	B82	1397*
TiO ₂ /P ₂ O ₅	7.7	8.3	6.5
CaO/TiO ₂	3.8	3.8	3.8
Al ₂ O ₃	4.8	5.4	5.5
CaO/Al ₂ O ₃	0.78	0.70	0.70
Ti/Zr	95	98	88
Ti/Y	316	341	401
Ti/Sc	367	366	491
Zr/Y	3.3	3.5	4.6
Zr/Nb	11	13	13
(La/Sm)N		1.93	
(Yb/Gd)N		0.66	
(Eu/Eu*)N			
(La/Ce)N	1.08	1.13	1.11
Rb/Sr	0.08	0.20	0.19
K/Rb	481	216	246
K/Ba	43.0	28.4	27.7
P ₂ O ₅ /Ce	70	60	80

(c) Group C

	B52	742*	1396*	744*	1359*	1351*	1366*	1354*
TiO ₂ /P ₂ O ₅	6.5	10.1	11.5	6.7	11.4	9.3	14.2	3.0
CaO/TiO ₂	21.8	13.4	10.0	17.3	9.4	11.5	6.6	6.0
Al ₂ O ₃	30.4	19.0	13.1	23.9	12.3	13.4	10.2	10.9
CaO/Al ₂ O ₃	0.72	0.70	0.76	0.72	0.76	0.85	0.64	0.55
Ti/Zr	80	106	128	96	105	111	113	138
Ti/Y	183	303	431	251	273	322	260	373
Ti/Sc	71	162	215	112	149	120	267	260
Zr/Y	2.3	2.9	3.4	2.6	2.6	2.9	2.3	2.7
Zr/Nb	16	6	9	4	16	18	9	7
(La/Sm)N		2.40				1.20	3.49	
(Yb/Gd)N		0.94				1.02	0.50	
(Eu/Eu*)N								
(La/Ce)N	1.24	0.82	0.68	0.81	0.87	0.84	0.88	1.05
Rb/Sr	0.15	0.21	0.05	0.06	0.10	0.03	0.04	0.03
K/Rb	212	346	323	424	498	1162	706	1328
K/Ba	26.5	42	34	28	83	54	31	31
P ₂ O ₅ /Ce	63	42	53	63	17	65	6	66

Appendix Table 6.5 (a) Mafic Dykes not analysed for major elements
Key trace element data

Sample	Zr*	Nb	Sr	Rb	Y	Ba	Sc	Ti
A15	104	6.5	227	28.7	25.2	408	30.0	5148
A27	257	13.1	233	109	53	987	38.6	8104
B2	79	3.8	143	16.2	18.4	197	33.9	4234
B7	60	3.7	210	22.2	26.1	264	37.8	5036
B17	303	21.4	209	68	56	901	30.6	21825
B44	61	2.8	80	15.5	12.4	124	25.1	3284
B45	234	14.6	288	81	62	1047	48.7	16059
B88	99	4.2	135	37.6	21.4	223	32.6	5057
B95	107	7.5	164	31.6	30.7	167	43.5	7730
D5	233	14.8	152	63	67	356	47.5	19861
D48	220	11.0	252	84	47.8	943	43.3	7716
D54	196	13.6	162	62	48.9	302	41.2	13447
D74	251	14.8	287	97	58	1030	45.6	13841
D76	203	12.3	267	82	43.0	871	47.8	9777
D102	53	3.0	154	14.4	18.7	198	36.2	3801
D104	110	5.2	184	34.7	23.0	277	33.2	5578
F37	209	15.6	254	50	70	512	43.6	14614
F38	51	2.7	151	16.8	21.2	197	39.1	3765
F39	163	13.0	176	61	51	268	47.1	13389
F52	54	2.4	119	31.5	18.4	198	35.1	3684

* All elemental abundances in ppm

Appendix Table 6.5 (b) Prior analyses of amphibolites from present study area.

	*69-782	**All	***86	***87
SiO ₂	54.55	49.96	49.22	48.89
TiO ₂	1.27	2.21	0.61	0.95
Al ₂ O ₃	13.69	13.90	14.40	13.68
Fe ₂ O ₃ Tot	12.41	15.46	12.86	15.37
MnO	0.18	0.22	0.22	0.27
MgO	4.18	5.24	7.74	6.50
CaO	7.52	9.03	10.61	9.40
Na ₂ O	2.94	2.79	2.49	2.44
K ₂ O	2.60	1.04	0.92	1.22
P ₂ O ₅	0.31	0.21	0.09	0.17
Total	99.65	100.06	99.16	98.89
Rb	88	37	17	31
Sr	181	210	150	190
Ba	673	496	70	131
Y	37	31	21	27
Zr	202		70	100
Nb			8	9
Ti	7614	13249	3657	5695
Sc	36		45	50
V	200			
Ni	36			
Cr	19			

* data from Bradley (1972)

** data from Flook (1975)

*** data from Pedler (1976)

Appendix Table 6-6 Partition coefficients

Arth 1976

—Partition coefficients for basaltic and andesitic rocks

	Olivine			Orthopyroxene			Clinopyroxene			Augite			Pigeon-ite	Hornblende			Phlogopite	Plagioclase			Garnet
	Avg	Low	High	Avg	Low	High	Avg	Low	High	Avg	Low	High		Avg	Low	High		Avg	Low	High	
	2 determinations			3 determinations			2 determinations			5 determinations			1 determination	4 determinations			1 determination	3 determinations			5 determinations
Ce	0.0000	0.0026	0.0090	0.024	0.0020	0.038	0.070	0.043	0.006	0.15	0.077	0.21	0.02	0.20	0.094	0.34	0.034	0.12	0.023	0.28	0.028
Nd	0.0000	0.003	0.010	0.033	0.000	0.058	0.12	0.065	0.18	0.31	0.17	0.43	0.05	0.33	0.10	0.50	0.032	0.081	0.23	0.20	0.068
Sm	0.0066	0.003	0.011	0.054	0.014	0.100	0.18	0.090	0.26	0.50	0.20	0.74	0.19	0.52	0.24	0.93	0.031	0.067	0.21	0.17	0.20
Eu	0.0068	0.005	0.010	0.054	0.023	0.079	0.18	0.091	0.20	0.51	0.27	0.75	0.068	0.50	0.20	1.1	0.030	0.055	0.17	0.19	0.27
Gd	0.0077	0.004	0.012	0.091	0.032	0.171	0.19	0.095	0.27	0.61	0.32	0.87	0.10	0.63	0.28	1.1	0.030	0.053	0.17	0.19	0.27
Dy	0.0090	0.000	0.014	0.15	0.054	0.203	0.21	0.105	0.31	0.68	0.50	1.0	0.23	0.64	0.31	1.0	0.030	0.055	0.10	0.19	0.317
Er	0.011	0.008	0.017	0.23	0.070	0.40	0.17	0.107	0.23	0.65	0.40	1.0	0.32	0.55	0.24	1.0	0.034	0.063	0.10	0.24	0.50
Yb	0.014	0.009	0.023	0.34	0.11	0.67	0.10	0.092	0.23	0.62	0.43	1.0	0.40	0.49	0.23	0.98	0.042	0.067	0.06	0.30	11.5
La	0.010	0.009	0.026	0.42	0.11	0.84	0.13	0.071	0.19	0.50	0.27	0.95	0.45	0.43	0.22	0.82	0.040	0.060	0.045	0.24	11.9
	2 determinations			2 determinations			3 determinations			3 determinations			3 determinations			3 determinations			3 determinations		
K	0.0088	0.0056	0.0081	0.014	0.009	0.010	0.011	0.0084	0.014	0.038	0.004	0.078	0.0034	0.00	0.33	1.40	0.000	0.017	0.010	0.30	0.015
Rb	0.0098	0.0081	0.011	0.022	0.015	0.020	0.015	0.014	0.015	0.031	0.015	0.030	0.0003	0.20	0.45	0.33	0.006	0.071	0.010	0.14	0.012
Sr	0.014	0.0094	0.019	0.017	0.010	0.024	0.012	0.078	0.15	0.12	0.003	0.15	0.0019	0.40	0.10	0.64	0.081	1.83	1.20	2.87	0.012
Ba	0.0099	0.0086	0.011	0.013	0.012	0.014	0.013	0.013	0.013	0.020	0.004	0.046	0.0004	0.42	0.10	0.73	1.09	0.23	0.05	0.59	0.023

—Partition coefficients for dacitic rocks

[Data represent one determination per mineral]

	Garnet	Ilmenite	Plagioclase	Hornblende
Ce	0.35	0.037	0.24	0.890
Nd	.53	.044	.17	2.80
Sm	2.66	.058	.13	3.99
Eu	1.50	.145	2.11	3.44
Gd	10.5	.082	.000	5.48
Dy	28.6	.097	.080	6.20
Er	42.8	.162	.084	5.94
Yb	39.9	.179	.077	4.80
La	29.6	.185	.002	4.53
K	.020		.263	
Rb	.0085	3.20	.048	
Sr	.015	.12	2.84	
Ba	.017	6.36	.36	

—Partition coefficients for rhyolitic rocks

[Figures in parentheses indicate number of determinations]

	Hypersthene (4)			Clinopyroxene (2)			Hornblende (3)			K-feldspar (1)	Ilmenite (1)	Phlogopite (1)	Apatite (4)			Zircon (2)			Plagioclase (4)		
	Avg	Low	High	Avg	Low	High	Avg	Low	High				Avg	Low	High	Avg	Low	High	Avg	Low	High
Ce	0.15	0.082	0.20	0.50	0.36	0.65	1.52	1.38	1.77	0.044	0.32	0.23	14.7	18.0	52.5	2.04	2.20	3.00	0.27	0.17	0.35
Nd	.22	.12	.35	1.11	.94	1.28	4.20	4.03	4.40	.025	.20	.34	57.1	27.4	81.1	2.20	1.97	2.43	.21	.12	.20
Sm	.27	.10	.38	1.07	1.52	1.81	7.77	7.1	8.1	.019	.20	.30	62.8	20.3	80.8	3.14	2.58	3.70	.13	.084	.16
Eu	.17	.093	.27	1.56	1.11	2.01	5.14	4.5	5.0	1.13	.24	.50	30.4	20.5	50.2	3.14	1.07	5.22	2.15	.90	2.81
Gd	.34	.23	.46	1.85	1.5	2.2	10.0	9.3	10.5	.011	.28	.35	50.3	27.2	78.0	12.0	10.0	14.0	.097	.00	.13
Dy	.46	.33	.55	1.93	1.22	2.63	13.0	12.5	13.5	.006	.29	.20	50.7	25.0	69.2	45.7	37.8	53.5	.064	.04	.08
Er	.65	.53	.73	1.80	1.07	2.25	12.0	10.8	14.0	.000	.36	.17	37.2	20.0	61.2	136	110	152	.055	.038	.072
Yb	.86	.78	.99	1.58	1.14	2.01	8.38	7.45	9.0	.012	.44	.17	23.0	13.1	37.0	270	242	200	.049	.03	.07
La	.90	.76	1.14	1.54	1.28	1.81	5.5	4.4	6.3	.006	.33	.21	20.2	11.2	30.2	323	281	306	.046	.03	.06
	Hypersthene (1)			Clinopyroxene (1)			Hornblende (1)												Plagioclase (1)		
K	.0023			.037			.081												.10		
Rb	.0027			.032			.014			0.34 (12)			2.24						.041		
Sr	.0085			.010			.022			3.87									.44		
Ba	.0029			.131			.044			6.12			0.7			15.3			.308		

Pearce and Norry 1979

Recommended mineral-liquid distribution coefficients for Ti, Zr, Y and Nb, Values in parentheses have been determined by interpolation or extrapolation from measured values

		ol	pl	cpx	opx	hbl	gt	mt	ap	phl
Basic	Ti	0.02	0.04	0.3	0.1	1.5	0.3	7.5	—	0.9
	Zr	0.01	0.01	0.1	0.03	0.5	0.3	(0.1)	—	(0.6)
	Y	0.01	0.03	0.5	0.2	1.0	2.0	(0.2)	—	0.03
	Nb	0.01	0.01	0.1	0.15	0.8	(0.1)	(0.4)	—	(1.0)
bi+zr										
Intermediate	Ti	0.03	0.05	0.4	0.25	3.0	(0.5)	9.0	—	1.5
	Zr	0.01	0.03	0.25	0.08	1.4	0.5	0.2	—	(1.2)
	Y	0.01	0.06	1.5	0.45	2.5	11.0	0.5	20	(1.2)
	Nb	0.01	0.025	0.3	0.35	1.3	—	1.0	—	(1.8)
Acid	Ti	(0.04)	0.05	0.7 ²	0.4	7.0	(1.2)	12.5	(0.1)	2.5
	Zr	(0.01)	0.1	0.6	0.2	4.0	1.2	0.8	(0.1)	2.0
	Y	(0.01)	0.1	4.0	1.0	6.0	35.0	2.0	40	2.0*
	Nb	(0.01)	0.06	0.8	0.8	4.0	—	2.5	(0.1)	3.0

Other values: $D_{Zr}^{ilm} = 0.28(\text{bas})$;
 $D_{Nb}^{ilm} = 0.8(\text{bas})$; $D_{Ti}^{ilm} \sim 50$
 $D_{Nb}^{rut} = 16(\text{bas})$
 $*D_Y^{bi-1} = 0.03$; $D_Y^{rut} = 60$

Gill 1978

Phenocryst/matrix partition coefficients from orogenic andesite whole rocks.

	Pl	Aug	Opx	Ol	Hb	Bt	Mt	Gar
K	.02-.20 ^{2,3,4†} .11**	.01-.03 ⁷ .02	.01-.02 ² .01	.01 ⁹	.33 ²	—	—	—
Rb	.02-.19 ² .07	.01-.04 ² .02	.01-.03 ² .02	.01 ⁹	.05 ²	3.3 ⁹	—	—
Sr	1.3-3.2 ^{2,3,4} 1.8	.06-.09 ^{2,3} .08	.01-.04 ^{2,3}	.01 ⁹	.19-.26 ^{2,3} .23	.12 ⁹	—	.02 ⁹
Ba	.05-.21 ^{2,3,4} .16	.01-.15 ^{2,3} .02	.01-.06 ^{2,3} .02	.01 ⁹	.08-.10 ^{2,3} .09	6.4 ⁹	—	.02 ⁹
Ce	.06-.30 ^{1,12} .20	.04-.51 ¹ .25	.03-.04 ¹ .03	.01 ⁹	.09 ¹	.04 ⁹	—	—
Sm	.03-.20 ^{1,12} .11	.09-.95 ¹ .57	.05-.10 ¹ .06	.01 ⁹	.34 ¹	.06 ⁹	—	1.3 ¹¹
Eu	.06-.73 ^{1,15} .31	.09-.68 ¹ .47	.06-.08 ¹ .07	.01 ⁹	.36 ¹	.14 ⁹	—	1.6 ¹¹
Yb	.02-.30 ¹ .07	.09-1.3 ¹ .76	.24-.67 ¹ .46	.01 ⁹	.46 ¹	.18 ⁹	—	56 ¹¹
Ni	—	3.5-8 ^{3,4} 6	5-9 ^{3,4} 8	—	7-8 ^{3,5} 8	13 ⁵	4-19 ^{4,7}	0.6 ¹⁰
Co	—	2-8 ^{3,4} 2	3-12 ^{3,4} 6	—	7-19 ^{3,5} 13	25 ⁵	6-11 ^{4,6} 8	2 ¹¹
Cr	—	10-70 ^{3,4} 30	7-23 ^{3,4} 13	—	23-36 ^{3,5} 30	17 ⁵	1-58 ^{4,7} 32	22 ¹⁰
V	—	0.9-10 ^{3,4} 1.1	0.5-7.2 ^{3,4} 1.1	—	10-45 ^{3,5} 32	50 ⁵	24-63 ^{4,6,7} 30	8 ¹⁰
Sc	—	2.5-17 ^{3,4} 3	1.4-7.5 ^{3,4} 3	—	12.5 ³	—	1-3 ⁴ 2	4 ¹¹

[†] Range of reported values

** Suggested value (a weighted mean)

Frey et al. 1978
Residual mantle minerals

REE partition coefficient sets

	<i>Set 1^(a)</i>				<i>Set 2^(b)</i>				<i>Set 3^(c)</i>	<i>Set 4^(d)</i>
	<i>cpx</i>	<i>opx</i>	<i>ol</i>	<i>gar</i>	<i>cpx</i>	<i>opx</i>	<i>ol</i>	<i>gar</i>	<i>gar</i>	<i>gar</i>
La	0.02	0.0005	0.0005	0.001	0.084	0.0021	0.0021	0.003	0.004	0.003
Ce	0.04	0.0009	0.0008	0.0033	0.166	0.004	0.0033	0.007	0.021	0.007
Nd	0.09	0.0019	0.0013	0.0184	0.382	0.0083	0.0055	0.033	0.087	0.033
Sm	0.14	0.0028	0.0019	0.0823	0.736	0.0147	0.0098	0.161	0.217	0.161
Eu	0.16	0.0036	0.0019	0.1333	0.753	0.0171	0.0088	0.284	0.320	0.284
Tb	0.19	0.0059	0.0019	0.2568	0.97	0.0303	0.0097	1.2	0.70	1.2
Ho	0.195	0.0089	0.0020	1.083	1.03	0.0468	0.0103	3.5	1.4	3.5
Yb	0.20	0.0286	0.0040	4.0	1.01	0.1443	0.0202	9.84	4.03	9.84
Lu	0.19	0.038	0.0048	7.0	0.95	0.19	0.0238	13	5.7	13

	<i>Set 5^(e)</i>				<i>Set 6^(f)</i>				<i>Set 7^(g)</i>			
	<i>cpx</i>	<i>opx</i>	<i>ol</i>	<i>gar</i>	<i>cpx</i>	<i>opx</i>	<i>ol</i>	<i>gar</i>	<i>cpx</i>	<i>opx</i>	<i>ol</i>	<i>gar</i>
La								0.18	0.026	0.0089	0.0035	
Ce	0.096	0.0014	0.0005	0.003	0.11	0.003	0.0006	0.003	0.256	0.0325	0.009	0.0083
Nd	0.18	0.0029	0.0009	0.019	0.14	0.005	0.0007	0.015	0.40	0.0508	0.010	0.039
Sm	0.26	0.005	0.0013	0.107	0.24	0.01	0.0012	0.096	0.57	0.079	0.0105	0.205
Eu								0.61	0.099	0.011	0.418	
Tb	0.31	0.0106	0.0016	1.27	0.48	0.032	0.0024	1.92	0.645	0.153	0.0128	1.6
Ho	0.28	0.0136	0.0014	2.57	0.51	0.051	0.0026	4.63	0.62	0.24	0.0152	5
Yb	0.23	0.0192	0.0011	4.20	0.54	0.09	0.0027	11.48	0.56	0.47	0.023	9.26
Lu								0.54	0.59	0.027	10	

cpx = clinopyroxene, opx = orthopyroxene, ol = olivine, gar = garnet.

Partition Coefficients

<i>Element</i>	<i>Garnet</i>	<i>Cpx</i>	<i>Opx</i>	<i>Olivine</i>
Sc	6.5	3.1	1.1	0.25
V	0.27	1.5	0.3	0.09
Co	2	1.2	2	6.5-1.3
Ni	0.8	4-2	5-3	35-3.8
Rb	0.02	0.05	0.02	0.01
Sr	0.014	0.165	0.016	0.016
Y	1.4	0.20	0.009	0.002
Ba, Zr, Hf	bulk solid/liquid P.C. arbitrarily set = 0.01			
Cu, Zn, Th, U	bulk solid/liquid P.C. arbitrarily set = 0.00 to 0.01			

Appendix Table 6.7 Hutchison Group amphibolites
(after Parker 1978)

Sample No. S.A.D.M. No.	A3 A31/75	A-3	C9 A32/75	161-1 A34/75	161-2	292-5 A38/75	292-6	292-7	424-5
SiO ₂	51.06	50.80	48.59	48.77	49.92	49.52	49.05	50.28	50.29
Al ₂ O ₃	9.59	9.87	18.02	14.60	12.93	13.70	13.48	15.08	14.15
Fe ₂ O ₃	2.39	10.18	.67	1.11	16.73	1.14	15.87	12.09	13.70
FeO	6.40		7.00	11.40		10.30			
MnO	.18		.16	.25		.25			
MgO	10.5	11.13	7.44	6.50	5.73	6.57	6.51	7.07	7.41
CaO	13.26	12.27	10.00	11.08	8.70	11.58	11.10	11.54	11.10
Na ₂ O	1.58	1.73	2.08	2.69	2.88	2.52	1.80	2.54	2.54
K ₂ O	1.39	1.71	2.03	.43	1.22	.54	.24	.31	.98
TiO ₂	.74	.83	.54	1.19	1.80	.91	1.34	.92	1.13
P ₂ O ₅	.18	.28	.02	.06	.15	.06	.11	.09	.16
H ₂ O ⁺	1.03		2.07	1.05		1.15			
H ₂ O ⁻	.13		.13	.11		.13			
Total	98.44	98.80	98.75	99.22	100.06	98.36	99.50	99.92	101.46
Loss on Ignition		1.13			1.33		1.37	1.45	1.59

Analyses with South Australian Department of Mines numbers were done by the Australian Mineral Development Laboratories. All other analyses were done at the University of Adelaide.

	424-6 A39/75	424-7 A40/75	452-1A A41/75	452-1B A42/75	452-3 A43/75	573-7	573-8	573-9 A44/75
SiO ₂	51.51	57.28	48.17	50.21	48.11	48.54	48.91	48.57
Al ₂ O ₃	14.38	15.19	13.25	14.97	14.20	12.65	15.24	14.25
Fe ₂ O ₃	.43	.70	.92	.60	.89	17.03	13.51	1.93
FeO	8.10	8.75	12.60	9.70	7.00			10.30
MnO	.24	.19	.26	.19	.20			.22
MgO	5.64	2.35	7.53	7.69	6.60	5.80	5.99	6.86
CaO	13.88	8.65	9.27	9.28	13.15	8.13	10.05	10.41
Na ₂ O	2.76	1.65	2.34	2.62	2.77	3.40	3.45	3.05
K ₂ O	.91	1.26	.88	1.12	1.07	.51	.66	.65
TiO ₂	.72	1.55	1.18	.78	.67	2.76	1.63	1.32
P ₂ O ₅	.09	.43	.04	.04	.11	.16	.14	.09
H ₂ O ⁺	1.01	1.18	1.62	2.04	4.30			1.13
H ₂ O ⁻	.07	.06	.10	.06	.16			.33
Total	99.75	99.23	98.16	99.30	99.24	98.98	99.58	99.10
Loss on Ignition						.87	.80	

	573-10A A45/75	573-12 A46/75	573-13	1128-4 A50/75	1225 A51/75	1250 A52/75
SiO ₂	59.17	47.70	49.77	49.68	49.14	46.80
Al ₂ O ₃	11.90	13.85	13.95	16.23	14.17	14.19
Fe ₂ O ₃	1.91	1.43	14.75	1.00	1.94	.65
FeO	8.20	10.30		8.80	8.70	8.95
MnO	.50	.34		.18	.20	.25
MgO	4.71	8.06	6.48	6.50	6.00	6.76
CaO	5.09	10.68	9.90	12.65	11.53	14.77
Na ₂ O	3.04	1.95	2.86	1.67	2.30	1.98
K ₂ O	.99	1.18	.79	.37	.84	.53
TiO ₂	.87	.80	1.43	.83	1.10	1.16
P ₂ O ₅	<.01	.05	.13	.05	.18	.21
H ₂ O ⁺	1.63	1.52		1.08	2.08	1.23
H ₂ O ⁻	.41	.18		.06	.36	.09
Total	98.41	98.22	100.06	99.10	98.54	97.57

Appendix Table 7.1 Normalised calculated model source abundances for I-type melts of the present study

Residue ⁽¹⁾ Sample	A ⁽²⁾		B ⁽²⁾		D	
	D87	B143	B112A	849	D87	B143
Rb (3)	196(125)	208(123)	175(132)	181(127)	120	97
Ba	51	72	99	52	52	66
Nb	8.2	10	14.5	12	7.6	7.6
La	25	38	40	63	32	43
Ce	20	30	36	53	24	32
Sr	16	14	15	11	21	19
Nd	13	20			14	19
Zr	5.0	9.3	12	8.8	5.1	7.6
Sm	8.5	14	20	19	8.7	12
Eu	6.8	9.7	13	7.1	7.5	10
Gd	6.2	10.4	17	11.4	6.0	8.9
Ti		2.8	4.2			4.4
Dy	4.9	8.1	12.4	8.2	4.6	6.7
Y	4.1	5.9	8.6	6.3	4.0	5.1
Er	4.6	7.5	12.2	7.5	4.3	6.3
Yb	4.8	7.4	12.7	8.0	4.5	6.2
Sc	3.9	2.7		1.4	2.8	2.0
V		4.1				1.6
Ni (4) ppm	108	88			67	56
Cr (4) ppm		177	70			116
Rb/Sr (3)	0.39(0.25)	0.48(0.28)	0.36(0.27)	0.52(0.37)		
(La/Sm)N	3.0	2.7	2.0	3.4	3.7	3.6
(Yb/Gd)N	0.78	0.71	0.74	0.70	0.75	0.70

Residue ⁽¹⁾ Sample	D		A		C	
	B112A	849	B112A	849	B112A	849
Rb (3)	127	88	205(121)	213(117)	103	103
Ba	100	42	92	49	88	46
Nb	13	7.6	13	11	15	13
La	54	64	38	60	34	54
Ce	45	49	33	48	34	50
Sr	20	15	15	11	12	8.8
Nd	28	23	23	26	28	31
Zr	12	5.7	11	7.8	14	10
Sm	19	13	16	15	26	24
Eu	13	6.0	11	5.9	16	8.6
Gd	14	7.2	13	8.9	26	17
Ti	5.6		3.4		6.0	
Dy	9.2	4.8	9.2	6.1	27	18
Y	6.9	3.8	6.5	4.7	17	12
Er	8.0	3.9	8.1	4.9	37	23
Yb	7.2	3.6	7.3	4.6	50	32
Sc		0.6		0.9		2.3
V						
Ni (4) ppm			16			
Cr (4) ppm	40				100	
Rb/Sr (3)			0.43(0.26)	0.63(0.35)	0.27	0.37
(La/Sm)N	3.0	4.9	2.3	3.9	1.3	2.3
(Yb/Gd)N	0.51	0.50	0.54	0.51	1.9	1.9

(1) Residual assemblages

- A. B26 px granulite A. 0.45 plag + 0.27 cpx + 0.19 opx + 0.08 biot + 0.01 ilm
 B. B26 (amph + gt) granulite 0.45 plag + 0.25 cpx + 0.15 opx + 0.08 amph + 0.05 biot
 + 0.02 gt + 0.01 ilm
 C. B36 (parg + gt) granulite 0.31 plag + 0.23 cpx + 0.07 opx + 0.18 parg + 0.18 gt
 + 0.02 ilm + mt
 D. Taylor & McLennan model 0.66 plag + 0.16 cpx + 0.13 opx + 0.05 ilm + mt

(2) Preferred model

(3) Figure in brackets calculated for $K_d^{biot/Rb} = 1.0$

(4) Ni and Cr abundances not normalised